



A11106 082979

NIST  
PUBLICATIONS

REFERENCE

NBSIR 83-2742

# Photonuclear Data - Abstract Sheets 1955 - 1982 Volume X (Germanium - Palladium)

---

U.S. DEPARTMENT OF COMMERCE  
National Bureau of Standards  
National Measurement Laboratory  
Center for Radiation Research  
Gaithersburg, MD 20899

August 1985



---

U.S. DEPARTMENT OF COMMERCE  
NATIONAL BUREAU OF STANDARDS





NBSIR 83-2742

**PHOTONUCLEAR DATA - ABSTRACT SHEETS**  
**1955 - 1982**  
**VOLUME X (GERMANIUM - PALLADIUM)**

E. G. Fuller, Henry Gerstenberg

U.S. DEPARTMENT OF COMMERCE  
National Bureau of Standards  
National Measurement Laboratory  
Center for Radiation Research  
Gaithersburg, MD 20899

August 1985

**U.S. DEPARTMENT OF COMMERCE, Malcolm Baldrige, *Secretary***  
**NATIONAL BUREAU OF STANDARDS, Ernest Ambler, *Director***



## TABLE OF CONTENTS

Table of Contents. . . . .	i
Introduction . . . . .	1
Germanium (Natural). . . . .	3
Germanium (A=70) . . . . .	7
Germanium (A=72) . . . . .	19
Germanium (A=73) . . . . .	29
Germanium (A=74) . . . . .	35
Germanium (A=76) . . . . .	47
Arsenic (A=75) . . . . .	59
Selenium (Natural) . . . . .	91
Selenium (A=74). . . . .	103
Selenium (A=76). . . . .	107
Selenium (A=77). . . . .	113
Selenium (A=78). . . . .	117
Selenium (A=80). . . . .	123
Selenium (A=82). . . . .	131
Bromine (Natural). . . . .	137
Bromine (A=79) . . . . .	145
Bromine (A=81) . . . . .	149
Krypton (Natural). . . . .	157
Krypton (A=82) . . . . .	161
Krypton (A=84) . . . . .	165
Rubidium (Natural) . . . . .	169
Rubidium (A=85). . . . .	173
Rubidium (A=87). . . . .	179

Strontium (Natural) . . . . .	185
Strontium (A=86) . . . . .	197
Strontium (A=87) . . . . .	203
Strontium (A=88) . . . . .	209
Strontium (A=89) . . . . .	231
Yttrium (A=89) . . . . .	235
Yttrium (A=90) . . . . .	295
Zirconium (Natural) . . . . .	303
Zirconium (A=89) . . . . .	319
Zirconium (A=90) . . . . .	323
Zirconium (A=91) . . . . .	407
Zirconium (A=92) . . . . .	421
Zirconium (A=94) . . . . .	427
Niobium (A=93) . . . . .	431
Molybdenum (Natural) ; . . . . .	469
Molybdenum (A=92) . . . . .	489
Molybdenum (A=94) . . . . .	521
Molybdenum (A=95) . . . . .	531
Molybdenum (A=96) . . . . .	535
Molybdenum (A=97) . . . . .	547
Molybdenum (A=98) . . . . .	555
Molybdenum (A=100) . . . . .	565
Ruthenium (Natural) . . . . .	583
Ruthenium (A=99) . . . . .	587
Ruthenium (A=101) . . . . .	591
Ruthenium (A=102) . . . . .	595
Rhodium (A=103) . . . . .	599

Palladium (Natural). . . . .	625
Palladium (A=104). . . . .	631
Palladium (A=105). . . . .	635
Palladium (A=106). . . . .	639
Palladium (A=108). . . . .	647
Palladium (A=110). . . . .	655
Definitions of Abbreviations and Symbols . . . . .	665





Photonuclear Data-Abstract Sheets  
1955-1982

I. Introduction

As used in connection with this collection of data-abstract sheets, the term photonuclear data is taken to mean any data leading to information on the electromagnetic matrix element between the ground state and excited states of a given nuclide. The most common types of reactions included in this compilation are:  $(e,e')$ ,  $(\gamma,\gamma)$ ,  $(\gamma,\gamma')$ ,  $(\gamma,n)$ ,  $(\gamma,p)$ , etc. as well as ground-state particle capture reactions, e.g.  $(\alpha,\gamma_0)$ . Two reactions which fit the matrix element criterion are not included in the compilation because of their rather special nature. These are heavy particle Coulomb excitation and the thermal neutron capture reaction  $(n,\gamma_0)$ . While the energy region of particular interest extends from 0 to 150 MeV, papers are indexed which report measurements in the region from 150 MeV to 4 GeV. Most of the experiments listed are concerned with the excitation energy range from 8 to 30 MeV, the region of the photonuclear giant resonance.

The hierarchical grouping of the photonuclear data-abstract sheets within the file is by: 1. Target Element, 2. Target Isotope, and 3. by the Bibliographic Reference Code assigned to the paper from which the data on the sheet were abstracted. In this file, colored pages are used to mark the beginning and end of the sheets for each chemical element. A brief historical sketch of the element is given on the divider sheet marking the start of each section; the information for this sketch was derived from references such as the Encyclopaedia Britannica. In those cases where the sheets for a given element make up a major part of a volume, colored pages are also used to delineate sections pertaining to the individual isotopes of the element. Each of the sections of the file, as delineated by two colored divider sheets, represents a 27 year history of the study of electromagnetic interactions in either a specific nuclide or a specific element.

The data-abstract sheets are filed under the element and/or isotope in which the ground-state electromagnetic transition takes place. For example, the abstract sheet for a total neutron yield measurement for a naturally occurring copper sample would appear in the elemental section of the copper file. On the other hand, a measurement of the  $^{62}\text{Cu}$  9.73 minute positron activity produced in the same sample by photons with energies below the three-neutron separation energy for  $^{65}\text{Cu}$  (28.68 MeV) would be filed with the sheets for  $^{63}\text{Cu}$ . Similarly a measurement of the ground-state neutron capture cross section in  $^{12}\text{C}$  would be filed under  $^{13}\text{C}$  while the corresponding ground-state alpha-particle capture cross section would be filed under  $^{16}\text{O}$ .

At the end of this volume there is a master list of the abbreviations that have been used in the index section of the abstract sheets. The listings are those used in the final published index, Photonuclear Data Index, 1973-1981, NBSIR 82-2543, issued in August 1982 by the U. S. Department of Commerce, National Bureau of Standards, Washington, DC 20234. In some cases two notations are entered for the same quantity. The second entry is the abbreviation that was used in one or more of the earlier published editions of the index.



# THE HISTORY OF THE UNITED STATES

## CHAPTER I

The first settlers of the United States were the English, who came to the continent in the early part of the seventeenth century. They found the land inhabited by the Indians, who were divided into many different tribes. The English settled in the eastern part of the continent, and the Indians in the western part. The English were at first at war with the Indians, but they soon became friendly. The English taught the Indians how to plant corn, and the Indians taught the English how to hunt. The English and the Indians lived together in peace for many years.

The English then moved to the western part of the continent, and the Indians moved to the eastern part. The English and the Indians were at war again, but they soon became friendly. The English taught the Indians how to plant corn, and the Indians taught the English how to hunt. The English and the Indians lived together in peace for many years.

The English then moved to the western part of the continent, and the Indians moved to the eastern part. The English and the Indians were at war again, but they soon became friendly. The English taught the Indians how to plant corn, and the Indians taught the English how to hunt. The English and the Indians lived together in peace for many years.

The English then moved to the western part of the continent, and the Indians moved to the eastern part. The English and the Indians were at war again, but they soon became friendly. The English taught the Indians how to plant corn, and the Indians taught the English how to hunt. The English and the Indians lived together in peace for many years.

## GERMANIUM

Z=32

Germanium—the element noted for its remarkable electrical properties has a metallic silver-gray color with properties somewhere between a metal and a nonmetal. D. I. Mendelēyev (1834-1907) predicted the existence and properties of a hypothetical element between silicon and tin which he called eka-silicon. Clemens Winkler (1838-1904), in 1886, analyzed the sulphide mineral argyrodite and found a previously unknown constituent to which he gave the name germanium after his native country. The argyrodite was a recently discovered mineral from an old silver mine near Freiberg. Winkler had determined that the argyrodite consisted of 75% silver and 18% sulfur; this left an unknown substance of about 7%. After toiling incessantly for four months, Winkler managed to precipitate the sulfide of the new element.

GE



11.5

REF. NO.

Synchrotron;  $C^{12}(\gamma, n)$  monitor

64 Co 2

JCC

REACTION	RESULT	EXCITATION ENERGY	SOURCE		DETECTOR		ANGLE
			TYPE	RANGE	TYPE	RANGE	
G, XN	ADY	THR - 80	C	80	5FD-1		4.31

Table 1

Element	Yield (36) aV cm <sup>-2</sup> mol MeV	60 NZ/A (mb MeV)	$\frac{\Sigma}{0}$ 30	$\frac{\Sigma}{0}$ 80	$\frac{\Sigma}{0} \frac{80}{0}$ 30 80	$E_m$ (MeV)	$\sigma_m$ (mb)
$^{24}Cr$	$33 \times 10^{-5}$	777	1.21	2.1	0.53	18.5	97
$^{25}Mn$	$108 \times 10^{-5}$	313	1.32	2.02	0.65	18.5	114
$^{26}Fe$	$68 \times 10^{-5}$	832	0.53	1.40	0.60	17.5	75
$^{27}Co$	$39 \times 10^{-5}$	573	1.03	1.32	0.59	17.5	92
$^{28}Ni$	$44 \times 10^{-5}$	379	0.53	1.07	0.51	13.5	56
$^{29}Cu$	$95 \times 10^{-5}$	947	1.06	1.99	0.53	17.5	93
$^{30}Zn$	$58 \times 10^{-5}$	975	0.94	1.63	0.55	17.5	36
$^{31}Ga$	$130 \times 10^{-5}$	1024	1.29	2.13	0.59	17.5	131
$^{32}Ge$	$136 \times 10^{-5}$	1064	1.35	2.29	0.59	17.5	138
$^{33}As$	$137 \times 10^{-5}$	1109	1.22	2.13	0.56	17.5	127

$$\frac{\Sigma_{30}}{\Sigma_0} = \frac{\int_0^{30} d(\gamma, xn) dE}{60 NZ/A}$$

Table 2

Element	maximum yield ( $\times 10^{-5}$ )	$\sigma_{-1}(T_n)$	$\sigma_{-1}(T_n) \times \frac{0}{1-0.01} \frac{NZ}{A} \left( \frac{A-1}{AZ} \right)^{1/2}$
$^{12}C$	4.0	3.54	2.13
$^{16}O$	3.2	4.03	1.92
$^{23}Na$	10.0	11.00	2.40
$^{26}Mg$	10.0	3.31	1.73
$^{28}Si$	13.0	12.02	2.60
$^{29}Si$	12.0	9.50	1.83
$^{31}P$	10.3	17.50	2.62
$^{32}S$	9.5	3.53	1.67
$^{35}K$	10.0	17.00	1.61
$^{35}Cl$	12.1	11.03	1.91
$^{54}Cr$	36	61.0	3.53
$^{55}Mn$	123	70.1	3.60
$^{56}Fe$	71	50.5	2.53
$^{57}Co$	54	65.5	2.64
$^{58}Ni$	46	31.2	1.53
$^{59}Co$	102	72.0	1.60
$^{60}Zn$	33	33.7	2.03
$^{61}Ga$	140	90.6	3.01
$^{62}Ge$	130	101.5	3.23
$^{63}As$	101	60.3	3.11

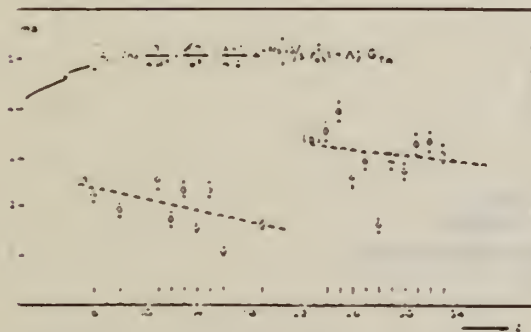


Fig. 2. Bremsstrahlung-weighted cross sections,  $\sigma_{-1}(T_n)$ , conveniently normalized, versus Z.

REF. G. Kraft, R. Kosiek, R. Mundhenke and J. Winter  
Nucl. Phys. A118, 25 (1968)

ELEM. SYM.	A	Z
Ge		32
REF. NO.		
68 Kr 2		egf

METHOD

REACTION	RESULT	EXCITATION ENERGY	SOURCE		DETECTOR		ANGLE
			TYPE	RANGE	TYPE	RANGE	
G,A	ABX	THR-33	C	33	SCD-D	4-11	90
				(32.5)			

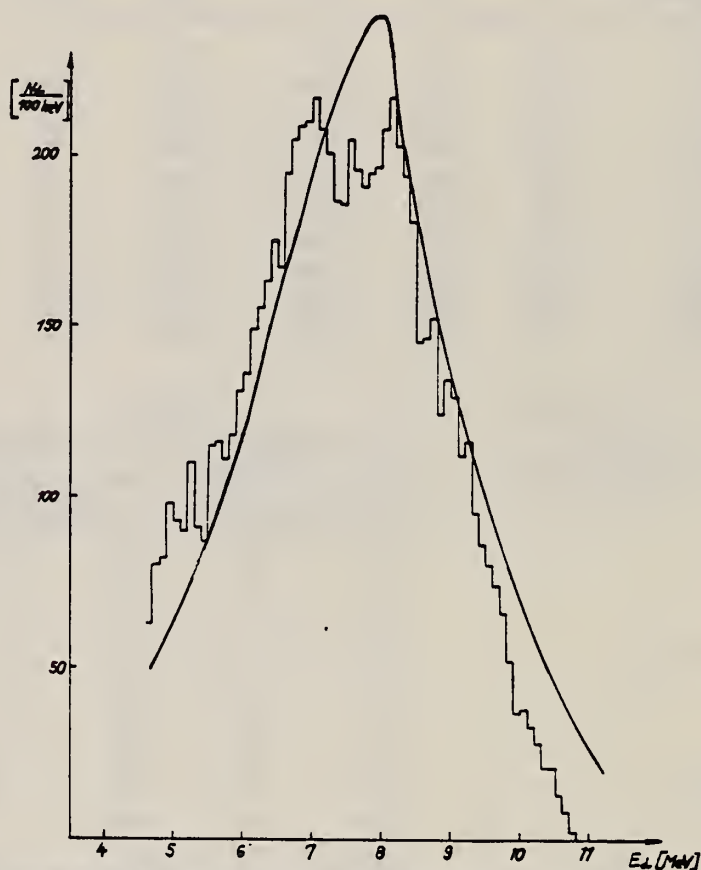


Fig. 3. Histogram: energy distribution of  $\alpha$ -particles from Ge. Curve: statistical-model calculation.

GE  
A=70

GE  
A=70

GE  
A=70





REP. O.A. Borello, J. Goldemberg, M.D.S. Santos  
An. Acad. Brasil. Cienc. 27, 413 (1955)

ELEM. SYM.	A	Z
Ge	70	32
REF. NO.		NVB
55 Bo 1		

METHOD Betatron

REACTION	RESULT	EXCITATION ENERGY	SOURCE		DETECTOR		ANGLE
			TYPE	RANGE	TYPE	RANGE	
G,N	ABX	12-21	C	12-21	ACT-I		4PI

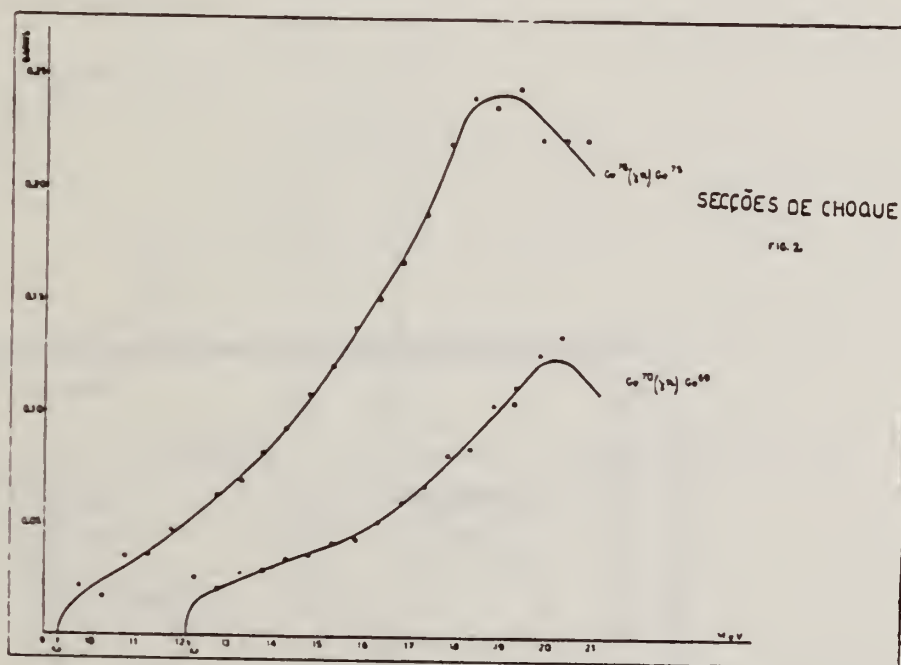


Fig. 2

Elemento	Threshold Limiar	$E_{max}$	$\sigma_{max}$	$\sigma_{int}$ até 21 Mev
$Ge^{70}$	$12,1 \pm 0,20$ Mev	20 Mev	0,125 barn	$0,59$ Mev $\times$ barn
$Ge^{76}$	$9,3 \pm 0,10$ Mev	18,9 Mev	0,243 barn	$1,5$ Mev $\times$ barn

M.D. DeSouza Santos, J. Goldemberg, R.R. Pieroni, E. Silva,  
 C.A. Borello, S.S. Villaca, J.L. Lopes  
 Int. Conf. Peaceful Uses of Atomic Energy II (UN, NY), 169 (1955)

ELEM. SYM.	A	Z
Ge	70	32

METHOD Betatron; neutron yield; radioactivity; r-chamber

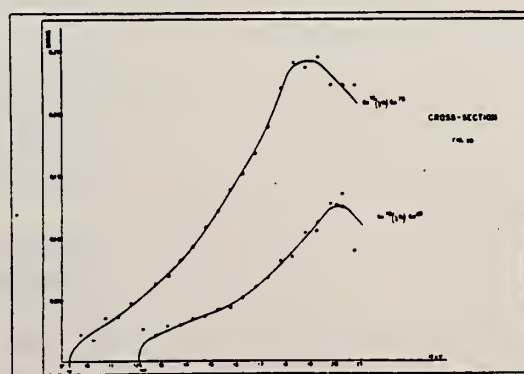
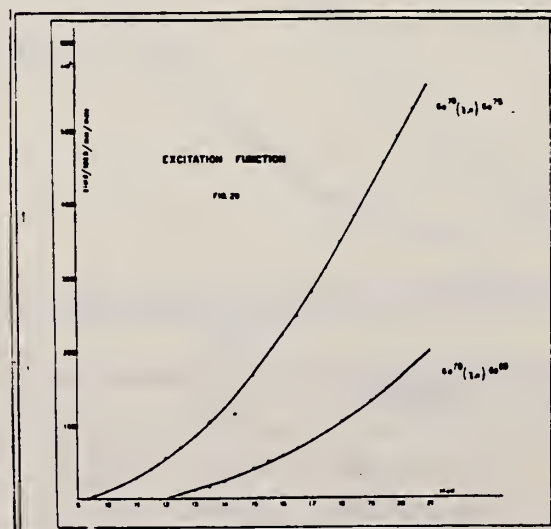
REF. NO.	EGF
55 De 1	

REACTION	RESULT	EXCITATION ENERGY	SOURCE		DETECTOR		ANGLE
			TYPE	RANGE	TYPE	RANGE	
G,N	ABX	9-21	C	9-21	ACT-I		4PI

$(\gamma, n)$  threshold =  $12.1 \pm 0.2$  MeV

THRESHOLD

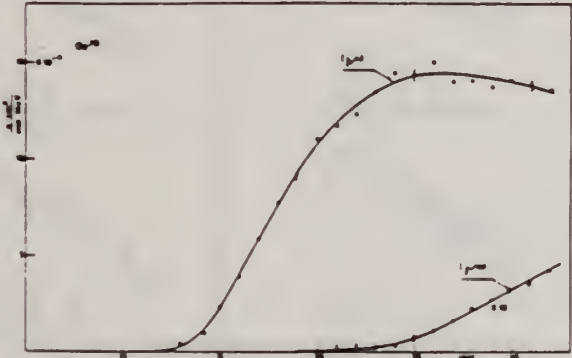
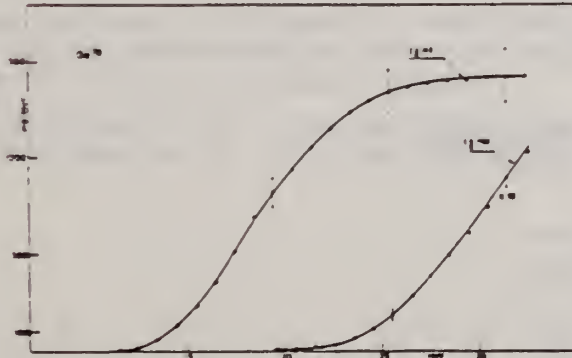
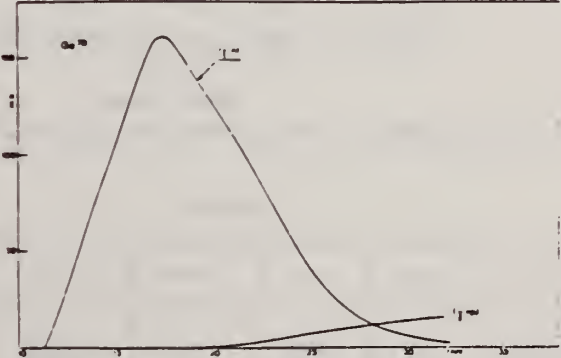
$$\int \sigma dE = 0.59 \text{ MeV-b}$$



44-45-473  
 (1,1) (1,0) (1,1)  
 10/10/55

Elem. Sym.	A	Z
Ge	70	32
Ref. No. 60 Fe 1		JHH

Method 31 MeV betatron; activation; NaI

Reaction	E or $\Delta E$	$E_0$	$\Gamma$	$\int \sigma dE$	$J\pi$	Notes
Bremss.						
$(\gamma, n)$	31					Annihilation radiation of $\beta^+$ from $Ge^{69}$
$(\gamma, np)$						Annihilation radiation of $\beta^+$ from $Ga^{68}$
 <p>Fig. 8 <math>(\gamma, n)</math>, <math>(\gamma, np)</math> excitation functions for <math>Ge^{68}</math></p>						
 <p>Fig. 9 Integrated cross sections deduced from the excitation functions of fig. 8</p>						
 <p>Fig. 10 Cross section for the two photoneuclear processes of fig. 8</p>						

REF. J.J. McCarthy, R.C. Morrison and H.J. Vander Molen  
Nucl. Phys. A213, 371 (1973)

ELEM. SYM.	A	Z
Ge	70	32
REF. NO.		
73 Mc 10		egf

METHOD			SOURCE		DETECTOR		ANGLE
REACTION	RESULT	EXCITATION ENERGY	TYPE	RANGE	TYPE	RANGE	
G,NP	ABX	17- 40	C	12- 42	ACT-I		4PI

$$\int^{40} \sigma dE = 39.3 \pm 5 \text{ MeV} \cdot \text{mb} \quad (\gamma, np)$$

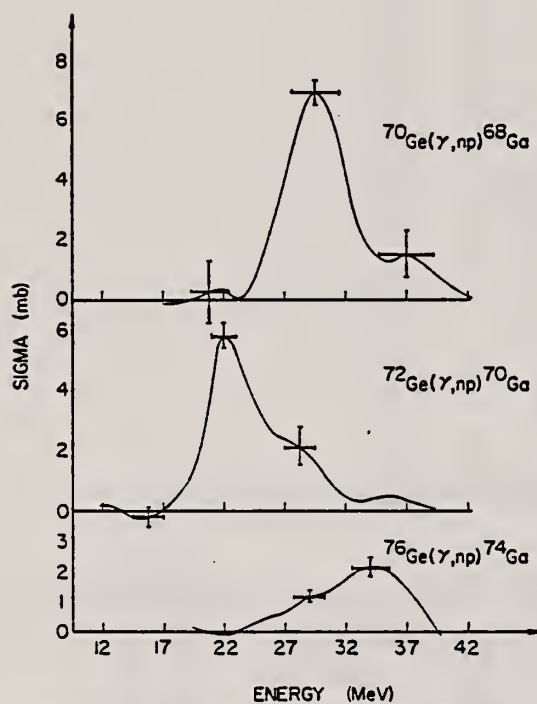


Fig. 5. Cross sections of  $^{70}\text{Ge}(\gamma, np)^{68}\text{Ga}$ ,  $^{72}\text{Ge}(\gamma, np)^{70}\text{Ga}$ , and  $^{76}\text{Ge}(\gamma, np)^{74}\text{Ga}$ .



REF.

A.M. Goryachev, G.N. Zalesnyi, and B.A. Tulupov  
 Izv. Akad. Nauk SSSR. Ser. Fiz. 39, 134 (1975)  
 Bull. Acad. Sci. USSR Phys. Ser. 39, 116 (1975)

ELEM. SYM.

A

Z

Ge

70

32

METHOD

REF. NO.

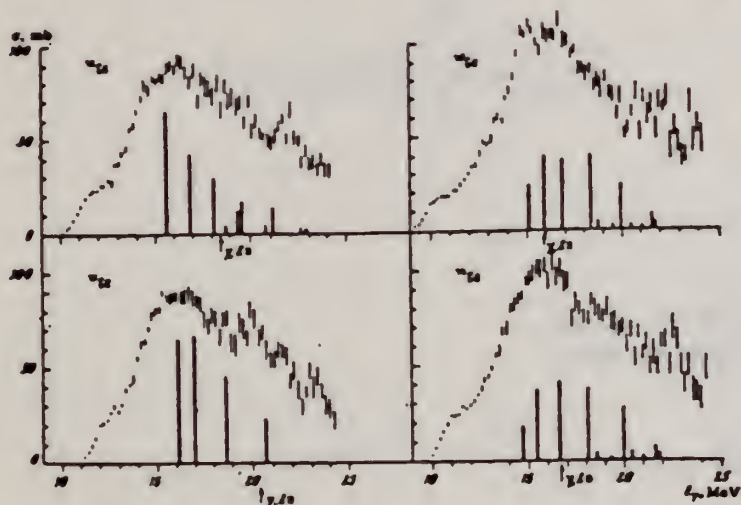
75 Go 1

hmg

REACTION	RESULT	EXCITATION ENERGY	SOURCE		DETECTOR		ANGLE
			TYPE	RANGE	TYPE	RANGE	
G,XN	ABX	11- 25	C	9- 25	BF3-I		4PI
$\sigma(G,SN)$ . Statistical theory used to obtain SN cross section from XN cross section.							

Table 2

Nuclide	$\lambda$	$E_2$ , MeV	$E_1$ , MeV	Nuclide	$\lambda$	$E_2$ , MeV	$E_1$ , MeV
$^{61}\text{Zn}$	0.25	0.99	18	$^{76}\text{Ge}$	0.25	0.562	18
$^{67}\text{Zn}$	0.23	1.04	18	$^{78}\text{Ge}$	0.33	0.559	18
$^{68}\text{Zn}$	0.2	1.08	18	$^{79}\text{Ge}$	0.3	0.818	18
$^{70}\text{Ge}$	0.21	1.04	18	$^{80}\text{Ge}$	0.25	0.654	18
$^{74}\text{Ge}$	0.25	0.835	18	$^{82}\text{Ge}$	0.2	0.653	18
$^{76}\text{Ge}$	0.3	0.6	18				

Fig. 2. The same as in Fig. 1, but for  $^{70,72,74,76}\text{Ge}$ .

Cross sections of photoneutron reactions.  
 The dipole photoabsorption forces are taken  
 from [6,7] (the solid black columns).

<sup>6</sup>M.G.Huber et al., Phys.Rev.155,1073(67)

<sup>7</sup>M.G.Huber et al., Phys.Rev.192,223(66).

Table 3

Nuclide	$\sigma$ , mb	Nuclide	$\sigma$ , mb	Nuclide	$\sigma$ , mb
$^{61}\text{Zn}$	$397 \pm 15$	$^{76}\text{Ge}$	$760 \pm 37$	$^{78}\text{Ge}$	$1021 \pm 52$
$^{67}\text{Zn}$	$579 \pm 27$	$^{79}\text{Ge}$	$872 \pm 41$	$^{80}\text{Ge}$	$1029 \pm 50$
$^{68}\text{Zn}$	$718 \pm 35$	$^{80}\text{Ge}$	$911 \pm 43$	$^{82}\text{Ge}$	$1067 \pm 53$
$^{70}\text{Ge}$	$751 \pm 37$	$^{82}\text{Ge}$	$930 \pm 50$		

\*Mean - square errors

Values given are for  $\sigma_0$  (24.2 MeV).

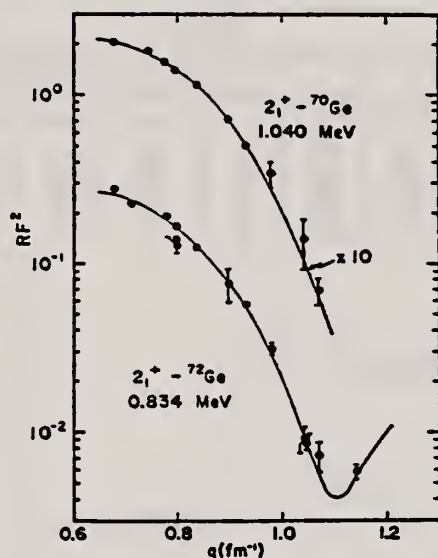
REF.

F. J. Kline, I. P. Auer, J. C. Bergstrom, and H. S. Caplan  
Nucl. Phys. **A255**, 435 (1975)

ELEM. SYM.	A	Z
Ge	70	32
REF. NO.		
75 K1 9		
egf		

METHOD

REACTION	RESULT	EXCITATION ENERGY	SOURCE		DETECTOR		ANGLE
			TYPE	RANGE	TYPE	RANGE	
E, E/	LFT	1, 2	D	84-120	MAG-D		DST



1.04, 2.562 MEV

Fig. 4. Plot of the converted form factors squared versus  $q$  for the  $2_1^+$  states in  $^{70,72}\text{Ge}$ . The solid lines are the results of fitting to the data with a DWBA program. Note that both the data and the curve for  $^{70}\text{Ge}$  have been multiplied by a factor of ten.

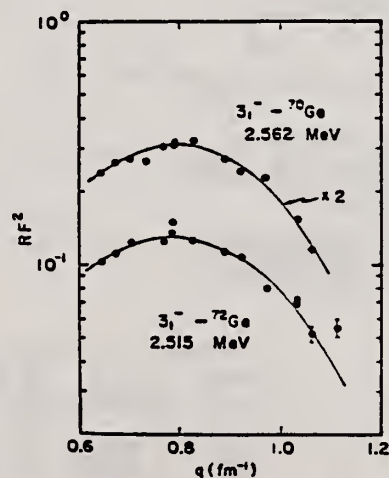


Fig. 5. Plot of the converted form factors squared versus  $q$  for the  $3_1^-$  states in  $^{70,72}\text{Ge}$ . The solid lines are the results of fitting to the data with a DWBA program. Note that both the data and the curve for  $^{70}\text{Ge}$  have been multiplied by a factor of two.

(over)

TABLE 3  
Parameters obtained from fits to the inelastic data

State	Nucleus	$c_w$ (fm)	$r_w$ (fm)	$B(EL, \omega)^\dagger$ (W.u.) <sup>a, b)</sup>	$\chi^2_{red}$
$2_1^+$	$^{70}\text{Ge}$	$4.22 \pm 0.14$	$2.41 \pm 0.26$	$19.7 \pm 1.2$	0.56
	$^{72}\text{Ge}$	$4.32 \pm 0.02$	$2.49 \pm 0.05$	$26.8 \pm 2.0$	5.2
$3_1^-$	$^{70}\text{Ge}$	$4.34 \pm 0.09$	$2.23 \pm 0.11$	$36 \pm 5$	12.4
	$^{72}\text{Ge}$	$3.84 \pm 0.12$	$2.80 \pm 0.11$	$37 \pm 7$	12.3

<sup>a)</sup> W.u. are Weisskopf single-particle units.

<sup>b)</sup> Uncertainties have been multiplied by  $\sqrt{\chi^2_{red}}$ .

TABLE 4  
Reduced transition probabilities

State	$B(EL, \omega)^\dagger$ (W.u.) <sup>a)</sup>		Work
	$^{70}\text{Ge}$	$^{72}\text{Ge}$	
$2_1^+$	$19.7 \pm 1.2$	$26.8 \pm 2.0$	present
	$20.5 \pm 1.1$	$22.3 \pm 1.4$	compilation <sup>b, c)</sup>
$3_1^-$	$36 \pm 5$	$37 \pm 7$	present
	21	22	Kregar and Elbek <sup>d)</sup>
	32	27	Curtis <i>et al.</i> <sup>e)</sup>
	27	23	Perey <i>et al.</i> <sup>f)</sup>
	21	17	Perey <i>et al.</i> <sup>g)</sup>

<sup>a)</sup> W.u. are Weisskopf single-particle units.

<sup>b)</sup> Ref. <sup>12)</sup>. <sup>c)</sup> Ref. <sup>13)</sup>. <sup>d)</sup> Ref. <sup>10)</sup>. <sup>e)</sup> Ref. <sup>9)</sup>. <sup>f)</sup> Ref. <sup>14)</sup>.

<sup>9)</sup> T.H. Curtis *et al.*, Phys. Rev. C1, 1418 (1970).

<sup>10)</sup> M. Kregar *et al.*, Nucl. Phys. A93, 49 (1967).

<sup>12)</sup> K.R. Alvar *et al.*, Nucl. Data Sheets 8, 1 (1972).

<sup>13)</sup> K.R. Alvar, Nucl. Data Sheets 11, 121 (1972).

<sup>14)</sup> C.M. Perey *et al.*, Phys. Rev. C2, 468 (1970).



REACTION	RESULT	EXCITATION ENERGY	SOURCE		DETECTOR		ANGLE
			TYPE	RANGE	TYPE	RANGE	
G,N	ABX	11- 40	C	10- 40	MOD-I		4PI
G,2N	ABX	20- 40	C	10- 40	MOD-I		4PI
G,NP	ABI	18- 40	C	10- 40	ACT-I		4PI

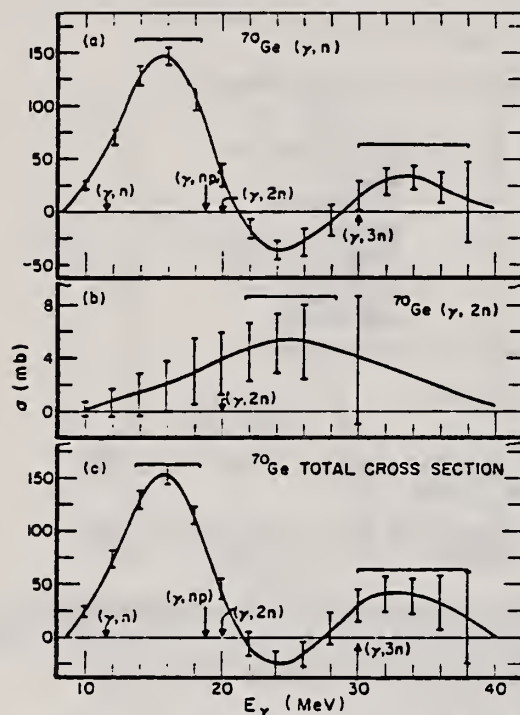


FIG. 4. (a) The  $(\gamma, n)$  cross section for  $^{70}\text{Ge}$ . (b) The  $(\gamma, 2n)$  cross section for  $^{70}\text{Ge}$ . (c) The total cross section  $\sigma[(\gamma, n) + (\gamma, 2n) + (\gamma, np) + (\gamma, p)]$  for  $^{70}\text{Ge}$ . The thresholds (arrows) are taken from Ref. 26.

TABLE II. Integrated cross sections.

Isotope	$(\gamma, p)$			Total
	$(\gamma, n)$	$(\gamma, 2n)$ (MeV mb)	$(\gamma, np)$	
$^{70}\text{Ge}$	1273(127) <sup>a</sup> 1464(290) <sup>b</sup>	60( 6)	40( 6)	1463(123)
$^{72}\text{Ge}$	1140(110)	420(40)	40(14)	1690(118)
$^{74}\text{Ge}$	1320(130)	360(40)	90(10)	35( 3) <sup>c</sup> 1805(126)
$^{76}\text{Ge}$	1077( 54) <sup>a</sup> 1067(106) <sup>b</sup>	710(70)	15( 3)	1892( 99)

<sup>a</sup> Result of the activation measurements.

<sup>b</sup> Result of the neutron counting measurements.

<sup>c</sup> Includes the contribution from the  $^{73}\text{Ge}(\gamma, p)$  reaction.

TABLE III. Lorentz fit parameters and integrated cross sections for total cross sections.

Isotope	$\sigma_0$	$\Gamma$	$E_0$	$\sigma_{LF}$	$\sigma_{int}$	$\sigma_{int} - \sigma_{LF}$	$D = 60NZ$	$\frac{\sigma_{int}}{D}$	$\frac{\sigma_{int} - \sigma_{LF}}{\sigma_{int}}$
	(mb)	(MeV)	(MeV)	$(\frac{1}{2}\pi)\sigma_0\Gamma$	(MeV mb)	(MeV mb)	(MeV mb)		
$^{70}\text{Ge}$	150	5.85	15.5	1390	1463	93	1040	1.41	0.06
$^{72}\text{Ge}$	150	5.90	17.9	1390	1690	300	1070	1.58	0.18
$^{74}\text{Ge}$	144	6.96	16.5	1580	1805	225	1090	1.66	0.12
$^{76}\text{Ge}$	120	8.20	16.7	1550	1892	342	1110	1.70	0.18

REF. P. Carlos, H. Beil, R. Bergere, J. Fagot, A. Lepretre,  
A. Veyssiere, G. V. Solodukhov  
Nucl. Phys. A258, 365 (1976)

ELEM. SYM.	A	Z
Ge	70	32
REF. NO.		egf
76 Ca 1		

METHOD

REACTION	RESULT	EXCITATION ENERGY	SOURCE		DETECTOR		ANGLE
			TYPE	RANGE	TYPE	RANGE	
G,N	ABX	11- 26	D	11- 26	MOD-I		4PI
G,2N	ABX	19- 26	D	11- 26	MOD-I		4PI

975+

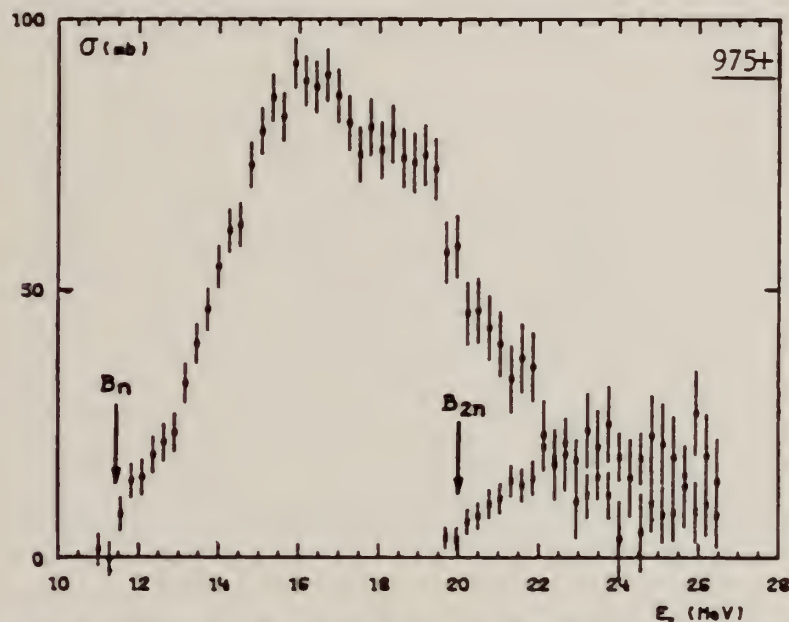


Fig. 3. Partial photoneutron cross sections [ $\sigma(\gamma, n) + \sigma(\gamma, pn)$ ] and  $\sigma(\gamma, 2n)$  for  $^{76}\text{Ge}$ . Arrows  $B_n$  and  $B_{2n}$  indicate theoretical threshold values for  $(\gamma, n)$  and  $(\gamma, 2n)$  reactions respectively. Data were not corrected for impurities.

TABLE 3

Integrated photoneutron cross sections and comparison with sum rules

Nucleus	$^{64}\text{Zn}$	$\left\{ \begin{matrix} ^{69}\text{Ga} \\ ^{71}\text{Ga} \end{matrix} \right\}$	$^{76}\text{Ge}$	$^{72}\text{Ge}$	$^{74}\text{Ge}$	$^{76}\text{Ge}$	$^{78}\text{As}$	$^{76}\text{Se}$	$^{78}\text{Se}$	$^{80}\text{Se}$	$^{82}\text{Se}$
$E_{\text{th}}$ (MeV)	29	26.5	26.5	26.5	26.5	26.5	26.5	26.5	26.5	26.5	26.5
$\sigma_{\text{ex}}$ (MeV · b)	0.75	0.91	0.78	0.94	1.02	1.12	1.09	1.01	1.06	1.11	1.13
$\frac{\sigma_{\text{ex}} A}{0.06 NZ}$	0.78	0.87	0.75	0.88	0.94	1	0.98	0.90	0.92	0.94	0.95
$B_n - B_p$ (MeV)	4.2	$\begin{pmatrix} 3.7 \\ 1.4 \end{pmatrix}$	3	1	-0.8	-2.6	3.3	1.7	0.1	-1.5	-3
$\sigma_{-10}$ (mb)	38	52	44	54	59	64	63	58	62	65	67
$\sigma_{-10} A^{-1}$ (mb)	0.15	0.18	0.15	0.18	0.19	0.20	0.20	0.18	0.19	0.19	0.19
$\sigma_{-20}$ (mb · MeV $^{-1}$ )	2.0	3.1	2.5	3.2	3.6	3.9	3.7	3.4	3.8	3.9	4.2
$\sigma_{-20} A^{-1}$ (μb · MeV $^{-1}$ )	1.9	2.6	2.1	2.6	2.8	2.9	2.8	2.5	2.7	2.6	2.7

FORM NBS-  
REV. 7-14-  
USCOMM-8

The notation used is defined in the text. The average experimental errors  $\Delta\sigma_{\text{ex}}/\sigma_{\text{ex}}$ ,  $\Delta\sigma_{-10}/\sigma_{-10}$  and  $\Delta\sigma_{-20}/\sigma_{-20}$  are approximately 8%.



GE  
A=72

GE  
A=72

GE  
A=72



Elem. Sym.	A	Z
Ge	72	32

Method Radioactive source; photon scattering; NaI spectrometer

Ref. No.  
56 Me 1 NVB

Reaction	E or $\Delta E$	$E_0$	$\Gamma$	$\int \sigma dE$	$J\pi$	Notes
$\text{Ge}^{72}(\gamma, \gamma)$	835 keV	835 keV			2 (excited)  0 (ground)	Mean life: $\tau = (4.6 \pm 1.2) 10^{-12}$ sec.

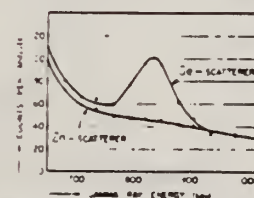


FIG. 2. Resonance fluorescence in  $\text{Ge}^{72}$ . Pulse-height distributions of the radiation scattered from zinc and germanium rings.



REF. J. J. McCarthy, R. C. Morrison and H. J. Vander Molen  
Nucl. Phys. A213, 371 (1973)

ELEM. SYM.	A	Z
Ge	72	32
REF. NO.		
73 Mc 10		egf

REACTION	RESULT	EXCITATION ENERGY	SOURCE		DETECTOR		ANGLE
			TYPE	RANGE	TYPE	RANGE	
G, NP	ABX	17- 40	G	12- 42	ACT-I		4PT

$$\int_{\gamma}^{40} \sigma dE = 38.9 \pm 14 \text{ MeV} \cdot \text{mb} \quad (\gamma, np)$$

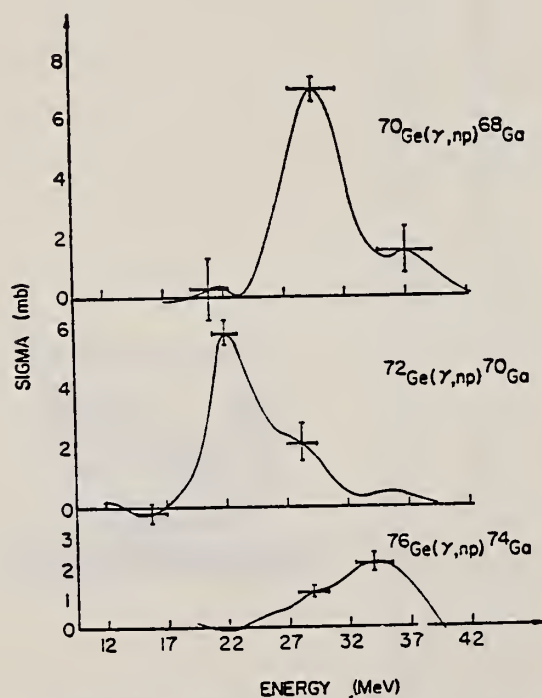


Fig. 5. Cross sections of  $^{70}\text{Ge}(\gamma, np)^{68}\text{Ga}$ ,  $^{72}\text{Ge}(\gamma, np)^{70}\text{Ga}$ , and  $^{76}\text{Ge}(\gamma, np)^{74}\text{Ga}$ .



REF.

A.M. Goryachev, G.N. Zalesnyi, and B.A. Tulupov  
 Izv. Akad. Nauk SSSR. Ser. Fiz. 39, 134 (1975)  
 Bull. Acad. Sci. USSR Phys. Ser. 39, 116 (1975)

ELEM. SYM.

A

Z

Ge

72

32

METHOD

REF. NO.

75 Go 1

nmg

REACTION	RESULT	EXCITATION ENERGY	SOURCE		DETECTOR		ANGLE
			TYPE	RANGE	TYPE	RANGE	
G,XN	ABX	11- 25	C	9- 25	BF3-I		4PI

$\sigma(G,SN)$ . Statistical theory used to obtain SN cross section from XN cross section.

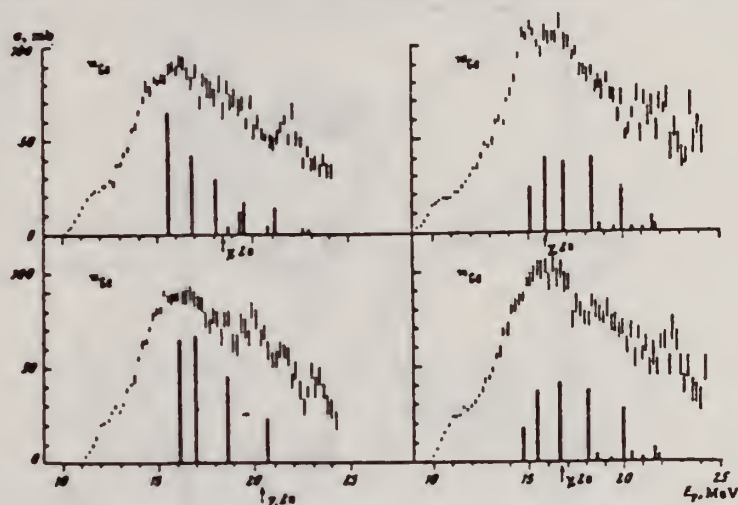


Fig. 2. The same as in Fig. 1, but for  $^{70,72,74,76}\text{Ge}$ .

Cross sections of photoneutron reactions.  
 The dipole photoabsorption forces are taken from [6,7] (the solid black columns).

<sup>6</sup>M.G. Huber et al., Phys. Rev. 155, 1073 (67)  
<sup>7</sup>M.G. Huber et al., Phys. Rev. 192, 223 (66).

Table 2

Nuclide	A	$E_2$ , MeV	$E_1$ , MeV	Nuclide	A	$E_2$ , MeV	$E_1$ , MeV
$^{70}\text{Zn}$	0.25	0.99	18	$^{70}\text{Ge}$	0.25	0.562	18
$^{72}\text{Zn}$	0.23	1.04	18	$^{72}\text{Ge}$	0.33	0.559	18
$^{74}\text{Zn}$	0.2	1.08	18	$^{74}\text{Ge}$	0.3	0.618	18
$^{76}\text{Zn}$	0.21	1.04	18	$^{76}\text{Ge}$	0.25	0.654	18
$^{70}\text{Se}$	0.25	0.865	18	$^{72}\text{Se}$	0.2	0.653	18
$^{74}\text{Se}$	0.3	0.8	18				

Table 3

Nuclide	$\sigma$ , mb	Nuclide	$\sigma$ , mb	Nuclide	$\sigma$ , mb
$^{70}\text{Zn}$	$397 \pm 19^*$	$^{70}\text{Ge}$	$760 \pm 37$	$^{70}\text{Se}$	$1021 \pm 52$
$^{72}\text{Zn}$	$570 \pm 27$	$^{72}\text{Ge}$	$872 \pm 41$	$^{72}\text{Se}$	$1029 \pm 50$
$^{74}\text{Zn}$	$718 \pm 35$	$^{74}\text{Ge}$	$911 \pm 43$	$^{74}\text{Se}$	$1167 \pm 53$
$^{76}\text{Zn}$	$751 \pm 37$	$^{76}\text{Ge}$	$930 \pm 50$		

\* Mean - square errors

Values given are for  $\sigma_0(24.2 \text{ MeV})$ .

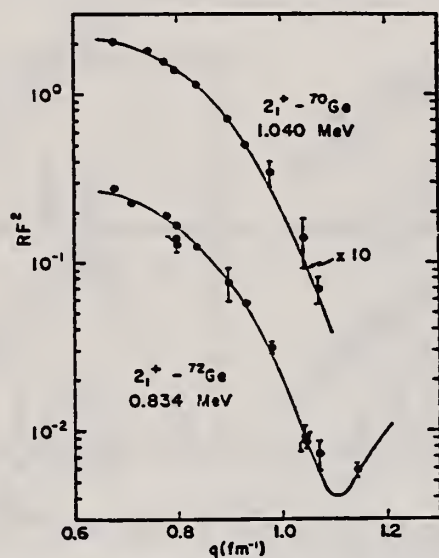
REF.

F. J. Kline, I. P. Auer, J. C. Bergstrom, and H. S. Caplan  
Nucl. Phys. A255, 435 (1975)

ELEM. SYM.	A	Z
Ge	72	32
REF. NO.		
75 K1 9		egf

METHOD

REACTION	RESULT	EXCITATION ENERGY	SOURCE		DETECTOR		ANGLE
			TYPE	RANGE	TYPE	RANGE	
E, E/	LFT	1, 2	D	84-120	MAG-D		DST



0.835, 2.515 MEV

Fig. 4. Plot of the converted form factors squared versus  $q$  for the  $2_1^+$  states in  $^{70,72}\text{Ge}$ . The solid lines are the results of fitting to the data with a DWBA program. Note that both the data and the curve for  $^{70}\text{Ge}$  have been multiplied by a factor of ten.

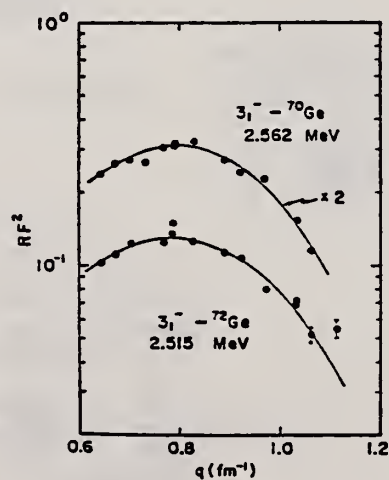


Fig. 5. Plot of the converted form factors squared versus  $q$  for the  $3_1^-$  states in  $^{70,72}\text{Ge}$ . The solid lines are the results of fitting to the data with a DWBA program. Note that both the data and the curve for  $^{70}\text{Ge}$  have been multiplied by a factor of two.

(over)

TABLE 3  
Parameters obtained from fits to the inelastic data

State	Nucleus	$c_w$ (fm)	$r_w$ (fm)	$B(EL, \omega)^\dagger$ (W.u.) <sup>a, b)</sup>	$\chi^2_{\text{par}}$
$2_1^+$	$^{70}\text{Ge}$	$4.22 \pm 0.14$	$2.41 \pm 0.26$	$19.7 \pm 1.2$	0.56
	$^{72}\text{Ge}$	$4.32 \pm 0.02$	$2.49 \pm 0.05$	$26.8 \pm 2.0$	5.2
$3_1^-$	$^{70}\text{Ge}$	$4.34 \pm 0.09$	$2.23 \pm 0.11$	$36 \pm 5$	12.4
	$^{72}\text{Ge}$	$3.84 \pm 0.12$	$2.80 \pm 0.11$	$37 \pm 7$	12.3

<sup>a)</sup> W.u. are Weisskopf single-particle units.

<sup>b)</sup> Uncertainties have been multiplied by  $\sqrt{\chi^2_{\text{par}}}$ .

TABLE 4  
Reduced transition probabilities

State	$B(EL, \omega)^\dagger$ (W.u.) <sup>a)</sup>		Work
	$^{70}\text{Ge}$	$^{72}\text{Ge}$	
$2_1^+$	$19.7 \pm 1.2$	$26.8 \pm 2.0$	present
	$20.5 \pm 1.1$	$22.3 \pm 1.4$	compilation <sup>b, c)</sup>
$3_1^-$	$36 \pm 5$	$37 \pm 7$	present
	21	22	Kregar and Elbek <sup>d)</sup>
	32	27	Curtis <i>et al.</i> <sup>e)</sup>
	27	23	Perey <i>et al.</i> <sup>f)</sup>
	21	17	Perey <i>et al.</i> <sup>f)</sup>

<sup>a)</sup> W.u. are Weisskopf single-particle units.

<sup>b)</sup> Ref. <sup>12)</sup>. <sup>c)</sup> Ref. <sup>13)</sup>. <sup>d)</sup> Ref. <sup>10)</sup>. <sup>e)</sup> Ref. <sup>9)</sup>. <sup>f)</sup> Ref. <sup>14)</sup>.

<sup>9)</sup> T.H. Curtis *et al.*, Phys. Rev. C1, 1418 (1970).

<sup>10)</sup> M. Kregar *et al.*, Nucl. Phys. A93, 49 (1967).

<sup>12)</sup> K.R. Alvar *et al.*, Nucl. Data Sheets 8, 1 (1972).

<sup>13)</sup> K.R. Alvar, Nucl. Data Sheets 11, 121 (1972).

<sup>14)</sup> C.M. Perey, R.J. Silva *et al.*, Phys. Rev. C2, 468 (1970).

## METHOD

REF. NO.

75 Mc 1

hmg

REACTION	RESULT	EXCITATION ENERGY	SOURCE		DETECTOR		ANGLE
			TYPE	RANGE	TYPE	RANGE	
G,N	ABX	10- 40	C	10- 40	MOD-I		4PI
G,2N	ABX	18- 40	C	10- 40	MOD-I		4PI
G,NP	ABI	19- 40	C	10- 40	ACT-I		4PI

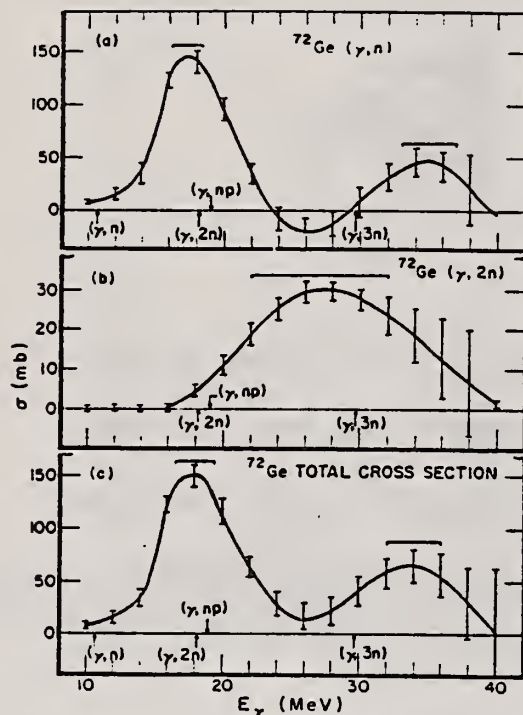


FIG. 3. The  $\sigma(\gamma, n)$  cross section for  $^{72}\text{Ge}$ . (b) The  $\sigma(\gamma, 2n)$  cross section for  $^{72}\text{Ge}$ . (c) The total cross section  $\sigma(\gamma, n) + \sigma(\gamma, 2n) + \sigma(\gamma, np) + \sigma(\gamma, p)$  for  $^{72}\text{Ge}$ .

TABLE II. Integrated cross sections.

Isotope	$(\gamma, p)$			Total
	$(\gamma, n)$	$(\gamma, 2n)$ (MeV mb)	$(\gamma, np)$	
$^{70}\text{Ge}$	1273(127) <sup>a</sup> 1464(290) <sup>b</sup>	60( 6)	40( 6)	1463(128)
$^{72}\text{Ge}$	1140(110)	420(40)	40(14)	1690(118)
$^{74}\text{Ge}$	1320(130)	360(40)	90(10)	35( 3) <sup>c</sup> 1805(136)
$^{76}\text{Ge}$	1077( 54) <sup>a</sup> 1067(106) <sup>b</sup>	710(70)	15( 3)	1892( 99)

<sup>a</sup> Result of the activation measurements.<sup>b</sup> Result of the neutron counting measurements.<sup>c</sup> Includes the contribution from the  $^{73}\text{Ge}(\gamma, p)$  reaction.

TABLE III. Lorentz fit parameters and integrated cross sections for total cross sections.

Isotope	$\sigma_0$ (mb)	$\Gamma$ (MeV)	$E_0$ (MeV)	$\sigma_{Lf}$ $(\frac{1}{2}\pi)\sigma_0\Gamma$ (MeV mb)	$\sigma_{Int}$ (MeV mb)	$\sigma_{Int} - \sigma_{Lf}$ (MeV mb)	$D = 60NZ$		
							$\frac{A}{D}$ (MeV mb)	$\frac{\sigma_{Int}}{D}$	$\frac{\sigma_{Int} - \sigma_{Lf}}{\sigma_{Int}}$
$^{70}\text{Ge}$	150	5.55	15.5	1380	1463	83	1040	1.41	0.06
$^{72}\text{Ge}$	150	5.90	17.9	1390	1690	300	1070	1.58	0.18
$^{74}\text{Ge}$	144	6.96	16.5	1580	1805	225	1090	1.66	0.12
$^{76}\text{Ge}$	120	8.20	16.7	1550	1892	342	1110	1.70	0.18



REF.

P. Carlos, H. Beil, R. Bergere, J. Fagot, A. Lepretre,  
A. Veyssiere, G. V. Solodukhov  
Nucl. Phys. A258, 365 (1976)

ELEM. SYM.

A

Z

Ge

72

32

METHOD

REF. NO.

76 Ca 1

egf

REACTION	RESULT	EXCITATION ENERGY	SOURCE		DETECTOR		ANGLE
			TYPE	RANGE	TYPE	RANGE	
G,N	ABX	10- 26	D	10- 26	MOD-I		4PI
G,2N	ABX	18- 26	D	10-26	MOD-I		4PI

978+

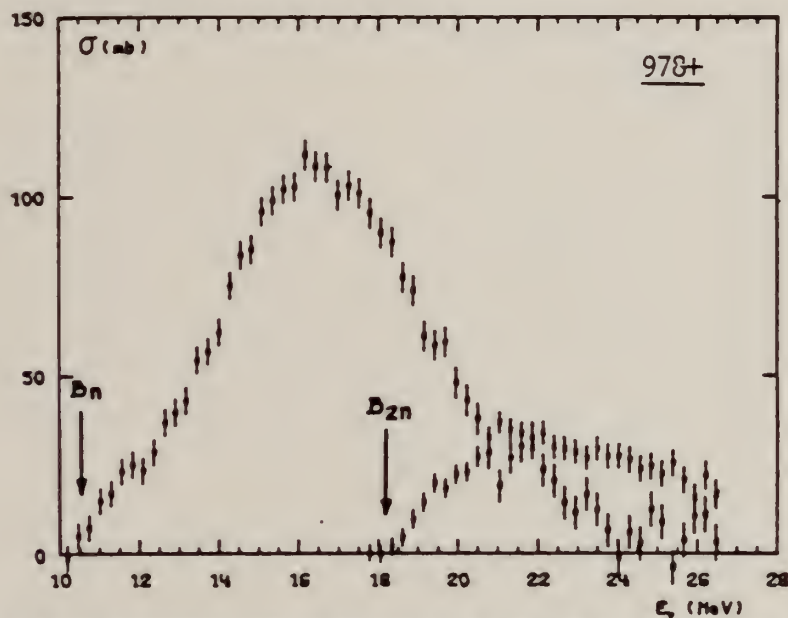


Fig. 4. Partial photoneutron cross sections [ $\sigma(\gamma, n) + \sigma(\gamma, pn)$ ] and  $\sigma(\gamma, 2n)$  for  $^{73}\text{Ge}$ . Arrows  $B_n$  and  $B_{2n}$  indicate theoretical threshold values for  $(\gamma, n)$  and  $(\gamma, 2n)$  reactions respectively.

TABLE 3

Integrated photoneutron cross sections and comparison with sum rules

Nucleus	$^{64}\text{Zn}$	$\begin{cases} ^{69}\text{Ga} \\ ^{71}\text{Ga} \end{cases}$	$^{70}\text{Ge}$	$^{73}\text{Ge}$	$^{74}\text{Ge}$	$^{76}\text{Ge}$	$^{78}\text{As}$	$^{76}\text{Se}$	$^{78}\text{Se}$	$^{80}\text{Se}$	$^{82}\text{Se}$
$E_{th}$ (MeV)	29	26.5	26.5	26.5	26.5	26.5	26.5	26.5	26.5	26.5	26.5
$\sigma_{00}$ (MeV · b)	0.75	0.91	0.78	0.94	1.02	1.12	1.09	1.01	1.06	1.11	1.13
$\frac{\sigma_{00}A}{0.06NZ}$	0.78	0.87	0.75	0.81	0.94	1	0.98	0.90	0.92	0.94	0.95
$B_n - B_p$ (MeV)	4.2	$\begin{cases} 3.7 \\ 1.4 \end{cases}$	3	1	-0.8	-2.6	3.3	1.7	0.1	-1.5	-3
$\sigma_{-10}$ (mb)	38	52	44	54	59	64	63	58	62	65	67
$\sigma_{-10}A^{-1}$ (mb)	0.15	0.18	0.15	0.18	0.19	0.20	0.20	0.18	0.19	0.19	0.19
$\sigma_{-20}$ (mb · MeV $^{-1}$ )	2.0	3.1	2.5	3.2	3.6	3.7	3.7	3.4	3.8	3.9	4.2
$\sigma_{-20}A^{-1}$ ( $\mu\text{b} \cdot \text{MeV}^{-1}$ )	1.9	2.6	2.1	2.6	2.8	2.9	2.8	2.5	2.7	2.6	2.7

FORM N35  
REV. 7-14  
USCOMM-N

The notation used is defined in the text. The average experimental errors  $\Delta\sigma_{00}/\sigma_{00}$ ,  $\Delta\sigma_{-10}/\sigma_{-10}$  and  $\Delta\sigma_{-20}/\sigma_{-20}$  are approximately 8%.

27





GE  
A=73

GE  
A=73

GE  
A=73



REF.

F. Heinrich, H. Wäffler, and M. Walter  
 Helv. Phys. Acta 29, 3 (1956)

ELEM. SIM.

Ge

73

32

METHOD

REF. NO.

56 He 2

EGF

REACTION	RESULT	EXCITATION ENERGY	SOURCE		DETECTOR		ANGLE
			TYPE	RANGE	TYPE	RANGE	
G,A	RLY	THR - 31	C	31	ACT-I		

Yield measured relative to ( $\gamma$ ,n) yield in  $^{63}\text{Cu}$ .

31 MeV bremsstrahlung yields

$$\frac{{}^{73}\text{Ge}(\gamma, \alpha)}{{}^{63}\text{Cu}(\gamma, n)} = (1.5 \pm 0.8) \times 10^{-2}$$

Method 22 MeV betatron; neutron counters

Ref. No.	EH
58 To 1	

Reaction	E or $\Delta E$	$E_0$	$\Gamma$	$\int \sigma dE$	$J\pi$	Notes
$\text{Ge}^{73}(\gamma, n)$	Bremss 22					$E_{th} = 6.5 \pm 0.16$

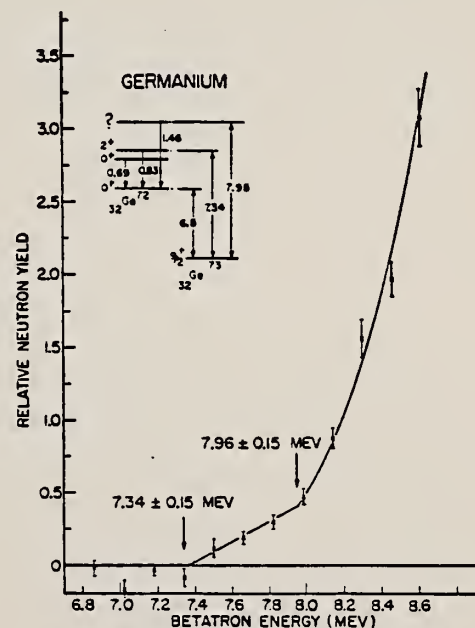


FIG. 4. Photoneutron yield from germanium as a function of betatron energy.

REF.

Y. Oka, T. Kato, K. Nomura, T. Saito and H. T. Tsai  
Bull. Chem. Soc. Japan 41, 2660 (1968)

ELEM. SYM.

A

Z

Ge

73

32

METHOD

REF. NO.

68 Ok 1

egf

REACTION	RESULT	EXCITATION ENERGY	SOURCE		DETECTOR		ANGLE
			TYPE	RANGE	TYPE	RANGE	
G, A	ABY	THR-20	C	20	ACT-I		4PI

TABLE 1. SUMMARY OF DATA ON  $(\gamma, \alpha)$  REACTIONS WITH 20 MeV BREMSSTRAHLUNG

Nuclide		$E_{th}$ (-Q, MeV)	Observed gamma-ray			Results obtained	
Parent (Natural abundance, %)	Product (Half-life)		Energy (MeV)	Branching ratio (%)	Type of multipole transition	$\mu\text{Ci/mg}^a$	Yield (mol <sup>-1</sup> ·R <sup>-1</sup> )
<sup>51</sup> V (99.75)	<sup>51</sup> Sc (3.4 d)	10.27	0.160	100	M1 + E2	$1.99 \times 10^{-3}$	$2.8 \times 10^3$
<sup>63</sup> Cu (30.9)	<sup>63</sup> Co (99 min)	6.75	0.068	99	M1 + E2	$7.23 \times 10^{-3}$	$9.7 \times 10^3$
<sup>71</sup> Ga (39.6)	<sup>71</sup> Cu (61 hr)	5.15	0.184	41	M1	$2.70 \times 10^{-3}$	$9.6 \times 10^3$
<sup>73</sup> Ge (7.67)	<sup>73</sup> Zn (14 hr)	5.89	0.435	100	M4	$1.11 \times 10^{-3}$	$5.0 \times 10^3$
<sup>81</sup> Br (49.48)	<sup>81</sup> As (39 hr)	6.46	0.246	2.81	M1 + E2	$1.97 \times 10^{-3}$	$4.3 \times 10^3$
<sup>109</sup> Ag (48.65)	<sup>109</sup> Rh (36 hr)	3.28	0.319 + 0.306	24.8	M1 + E2	$8.29 \times 10^{-4}$	$3.7 \times 10^3$
<sup>115</sup> In (95.77)	<sup>115</sup> Ag (7.6 d)	3.78	0.340	6	M1 + E2	$5.70 \times 10^{-4}$	$4.3 \times 10^3$

a) The value corrected at the end of 1 hr irradiation ( $9.4 \times 10^6$  R/min).

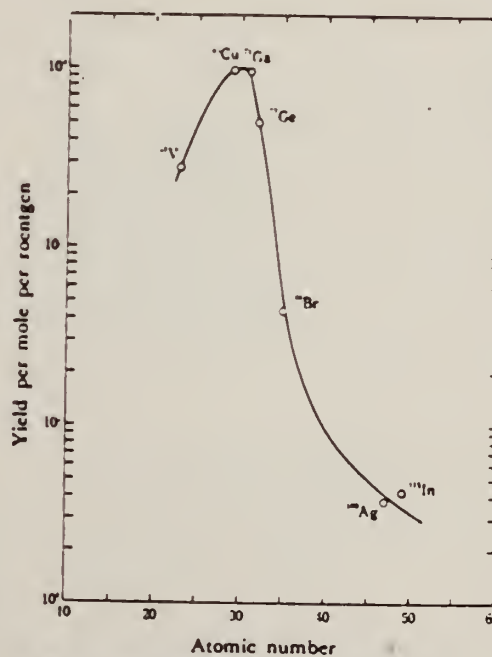


Fig. 1. The yield curve for  $(\gamma, \alpha)$  reaction with 20 MeV bremsstrahlung.





GE  
A=74

GE  
A=74

GE  
A=71



Method Radioactive source; photon scattering; NaI spectrometer

Ref. No.	
56 Me 1	NVB

Reaction	E or $\Delta E$	$E_0$	$\Gamma$	$\int \sigma dE$	$J\pi$	Notes
$\text{Ge}^{74}(\gamma, \gamma)$	596 keV	596 keV			<div>2 (excited)</div> <div>0 (ground)</div>	<p>Mean life:</p> <p><math>\tau = (1.9 \pm 0.3) 10^{-11}</math> sec.</p>

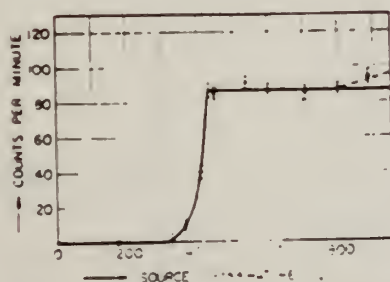


FIG. 3. Resonance fluorescence in  $\text{Ge}^{74}$ . Dependence of the resonance effect on the temperature of the arsenic source. The solid line represents the temperature dependence of the density of the  $\text{As}_4$ -vapor calculated on the basis of vapor pressure data,<sup>11</sup> and normalized to give the experimental value of the plateau. Above 800°C the dissociation of the  $\text{As}_4$  vapor causes an increase (dashed line) of the resonance fluorescence effect (see discussion in the last chapter).

FIG. 4. Angular distribution of the resonance radiation from the 596-kev level in  $\text{Ge}^{74}$ . The solid line represents the theoretical angular distribution for an excited state with spin 2 and a ground state with spin 0, corrected for the finite angular resolution. The differential cross section is given in arbitrary units.

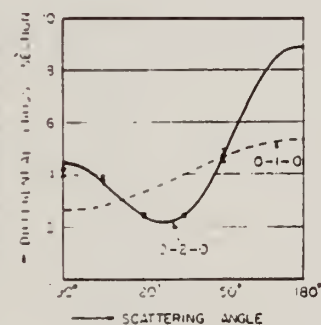


TABLE I. Observed and predicted ratios of the differential cross sections at 90° and 121°.

Spin of the 596-kev level	Theoretical ratio $d\sigma(90^\circ)/d\sigma(121^\circ)$	Experimental ratio
1	0.79	
2	2.04	
3	0.08	
		$2.2 \pm 0.3$

REF.			ELEM. SYM.			A	Z	
S. Costa, F. Ferrero, S. Ferroni and R. Malvano Proc. Paris Conference 1034 (1964)			Ge			74	32	
METHOD						REF. NO.		
100 MeV synchrotron						64 Co 3		
REACTION		RESULT	EXCITATION ENERGY		SOURCE		DETECTOR	
					TYPE		RANGE	
G,N		ABX	THR-80		C		10-80	

TABLE

ELEMENT	Yield (36 MeV) $\left(\frac{\text{n. cm}^2}{\text{mol. MeV}}\right) \times 10^8$	$\Sigma_0^{30}$	$\Sigma_0^{80}$	$\Sigma_0^{30}/\Sigma_0^{80}$	$\sigma_{-1}$ (mb)
<sup>24</sup> Cr .....	83	1.21	2.1	0.58	62
<sup>25</sup> Mn .....	108	1.52	2.33	0.65	76
<sup>26</sup> Fe .....	68	0.88	1.46	0.60	50
<sup>27</sup> Co .....	89	1.08	1.82	0.59	64
<sup>28</sup> Ni .....	44	0.55	1.07	0.51	34
<sup>29</sup> Cu .....	95	1.06	1.99	0.53	72
<sup>30</sup> Zn .....	88	0.94	1.68	0.56	66
<sup>31</sup> Ga .....	130	1.29	2.18	0.59	94
<sup>32</sup> Ge .....	139	1.35	2.29	0.59	101
<sup>33</sup> As .....	137	1.22	2.18	0.56	100

$\Sigma_0^b = \frac{A}{60 NZ} \int_0^b \sigma(E) dE$  is the integrated cross section measured in units of the classical dipole  $60 NZ/A$  mb. MeV.

REACTION	RESULT	EXCITATION ENERGY	SOURCE		DETECTOR		ANGLE
			TYPE	RANGE	TYPE	RANGE	
G,P	ABY	THR-20	C	20	ACT-I		4PI

TABLE I. SUMMARY OF DATA ON ( $\gamma, p$ ) REACTIONS WITH 20 MeV BREMSSTRAHLUNG

Parent (Natural abundance, %)	Nuclide	Residual (Half-life)	$S_p$ (MeV)	Observed $\gamma$ -ray			Yield determined	
				Energy (MeV)	Branching ratio (%)	Type of multipole transition	$\mu\text{Ci/mg}^a$	Yield/mol. R
$^{23}\text{Mg}$ (10.11)	$^{23}\text{Na}$ (15 hr)		12.06	1.37	100	E2	$1.48 \times 10^{-1}$	$1.7 \times 10^3$
$^{28}\text{Si}$ (4.71)	$^{28}\text{Al}$ (2.27 min)		12.33	1.78	100	E2	1.91	$2.8 \times 10^3$
$^{28}\text{Si}$ (3.12)	$^{28}\text{Al}$ (6.56 min)		13.59	1.28	93.8	E2 + M1	$6.51 \times 10^{-1}$	$1.5 \times 10^3$
$^{40}\text{Ca}$ (2.06)	$^{40}\text{K}$ (22.4 hr)		12.17	0.374	85	E2 + M1	$7.86 \times 10^{-3}$	$1.3 \times 10^3$
$^{47}\text{Ti}$ (7.32)	$^{47}\text{Sc}$ (84.1 d)		10.47	0.887	100	E2	$7.11 \times 10^{-4}$	$3.1 \times 10^3$
$^{47}\text{Ti}$ (73.99)	$^{47}\text{Sc}$ (3.4 d)		11.44	0.160	100	E2 + M1	$6.83 \times 10^{-3}$	$1.2 \times 10^3$
$^{48}\text{Ti}$ (5.46)	$^{48}\text{Sc}$ (1.8 d)		11.35	1.31	100	E2	$4.40 \times 10^{-3}$	$5.8 \times 10^3$
$^{52}\text{Cr}$ (9.55)	$^{52}\text{V}$ (3.8 min)		11.15	1.43	100	E2	$5.01 \times 10^{-1}$	$6.6 \times 10^3$
$^{54}\text{Fe}$ (2.17)	$^{54}\text{Mn}$ (2.58 hr)		10.57	1.81	23.5	E2 + M1	$8.10 \times 10^{-3}$	$2.1 \times 10^3$
$^{74}\text{Ge}$ (36.74)	$^{74}\text{Ga}$ (4.8 hr)		10.92	0.295	97	(E2)	$3.70 \times 10^{-1}$	$1.3 \times 10^3$
$^{77}\text{Se}$ (7.58)	$^{77}\text{As}$ (26.5 hr)		9.61	0.559	41	E2	$1.48 \times 10^{-3}$	$1.3 \times 10^3$
$^{87}\text{Sr}$ (7.02)	$^{87}\text{Rb}$ (19 d)		9.41	1.08	9	E2	$5.15 \times 10^{-4}$	$9.9 \times 10^3$
$^{114}\text{Cd}$ (12.26)	$^{114}\text{Ag}$ (3.2 hr)		9.74	1.39	35	E2	$1.91 \times 10^{-3}$	$2.1 \times 10^3$
$^{117}\text{Sn}$ (7.57)	$^{117}\text{In}$ (54 min)		9.58	1.27	84	E2	$9.80 \times 10^{-3}$	$6.9 \times 10^3$
$^{137}\text{Ba}$ (11.32)	$^{137}\text{Cs}$ (13 d)		8.67	0.830	100	E2	$1.68 \times 10^{-4}$	$2.2 \times 10^3$
$^{198}\text{Hg}$ (16.84)	$^{198}\text{Au}$ (2.7 d)		7.27	0.412	100	E2	$8.43 \times 10^{-4}$	$2.2 \times 10^3$

a) The value corrected at the end of 1 hr irradiation ( $9.4 \times 10^4$  R/min).

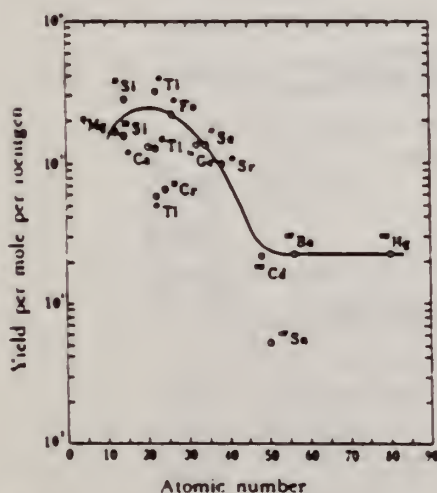


Fig. 2. The yield curve for the ( $\gamma, p$ ) reaction with 20 MeV bremsstrahlung.



ELEM. SYM.	A	Z
Ge	74	32
REF. NO.		
70 Mo 2		hmg

METHOD				REF. NO.	
				70 Mo 2	
REACTION	RESULT	EXCITATION ENERGY	SOURCE		ANGLE
			TYPE	RANGE	
G <sub>g</sub> G	ABX	6	D	6	DST
		(6.018)		(6.018)	

6 = 6.018, LFT

TABLE III. Summary of the results of spins, parities, and total widths of resonance levels excited by  $\gamma$  rays obtained from neutron capture in iron. Parities in parentheses are uncertain.

Isotope	Energy (MeV)	$\delta =  E_r - E_g $ (eV)	$J^\pi_0$	$J^\pi_r$	Transition	$\Gamma_0/\Gamma_\gamma$ ( $\pm 8\%$ )	$\Gamma_\gamma$ ( $10^{-3}$ eV)
<sup>50</sup> Cr	8.888	18 $\pm$ 1	0 <sup>+</sup>	1	...	0.90	750 $\pm$ 200
<sup>62</sup> Ni	7.646	14 $\pm$ 1	0 <sup>+</sup>	1 <sup>-</sup>	E1	0.64	480 $\pm$ 50
<sup>74</sup> Ge	6.018	4.5 $\pm$ 0.5	0 <sup>+</sup>	1 <sup>-</sup>	E1	0.19	120 $\pm$ 15
<sup>75</sup> As	7.646	7.4 $\pm$ 0.3	3/2 <sup>-</sup>	1/2 <sup>+</sup>	...	0.11	360 $\pm$ 100
<sup>109</sup> Ag	7.632	9 $\pm$ 1	1/2 <sup>-</sup>	3/2	...	0.7	2 $\pm$ 1
<sup>112</sup> Cd	7.632	4.8 $\pm$ 0.4	0 <sup>+</sup>	1 <sup>-</sup>	E1	0.55	86 $\pm$ 15
<sup>139</sup> La	6.018	8.2 $\pm$ 0.6	7/2 <sup>+</sup>	7/2 <sup>-</sup>	E1	0.50	51 $^{+14}_{-4}$
<sup>141</sup> Pr	7.632	11.4 $^{+0.3}_{-0.5}$	5/2 <sup>+</sup>	5/2 <sup>+</sup>	M1	0.46	72 $^{+24}_{-4}$
<sup>205</sup> Tl	7.646	9.3 $\pm$ 0.3	1/2 <sup>+</sup>	1/2 <sup>-</sup>	...	0.58	980 $\pm$ 90
<sup>208</sup> Pb	7.279	7.1 $\pm$ 0.3	0 <sup>+</sup>	1 <sup>+</sup>	M1	1.00	780 $\pm$ 60

TABLE IV. Effective elastic scattering cross section  $\langle\sigma_r\rangle = \sigma_0^r (\Gamma_0/\Gamma_\gamma) \psi(x_0, t_0)$ , where  $\delta$ ,  $J$ ,  $\Gamma_0$ ,  $\Gamma_\gamma$  were taken from Table III. The temperature of the scatterer was 300°K, while that of the iron  $\gamma$  source was 640°K.

Target	Resonance energy (MeV)	$\langle\sigma_r\rangle$ (mb)
<sup>50</sup> Cr	8.888	905
<sup>62</sup> Ni	7.646	569
<sup>74</sup> Ge	6.018	61
<sup>75</sup> As	7.646	4.4
<sup>109</sup> Ag	7.632	3.5
<sup>112</sup> Cd	7.632	193
<sup>139</sup> La	6.018	39
<sup>141</sup> Pr	7.632	20
<sup>205</sup> Tl	7.646	574
<sup>208</sup> Pb	7.279	5560



REACTION	RESULT	EXCITATION ENERGY	SOURCE		DETECTOR		ANGLE
			TYPE	RANGE	TYPE	RANGE	
G,G	LFT	6	D	6	SCD-D		DST
		(6.018)		(6.018)			

$$\Gamma_Y = 0.12 \text{ eV}, \Gamma_{\gamma}/\Gamma_Y = 0.19, \langle \sigma_r \rangle = 61 \text{ mb},$$

$$6=6.018, \text{J-PI, LFT}$$

$$\delta = 4.5 \text{ eV}$$

TABLE II. Most probable spins and parities of levels in  $^{14}\text{Ge}$  as found in the present work. Also listed are angular distribution coefficients  $A$  of the corresponding  $\gamma$  lines together with  $M2/E1$  mixing ratio.

Level energy (MeV)	$J^\pi$	$\gamma$ -line energy (MeV)	$A$	$\frac{x^2}{\frac{M2}{E1}}$
0.596	$2^+$	5.422	$0.044 \pm 0.010$	$(1.7^{+1.3}_{-1.1}) \times 10^{-4}$
1.206	$2^+$	4.812	$0.041 \pm 0.029$	$(0.2^{+1.3}_{-0.3}) \times 10^{-3}$
1.486	$0^+$	4.532	$0.506 \pm 0.076$	0
2.200	$2^+$	3.818	$0.140 \pm 0.040$	$(1.7^{+1.3}_{-1.1}) \times 10^{-4}$
2.229	$0^+$	3.789	$0.514 \pm 0.102$	0
6.018	$1^-$	6.018	$0.506 \pm 0.023$	0

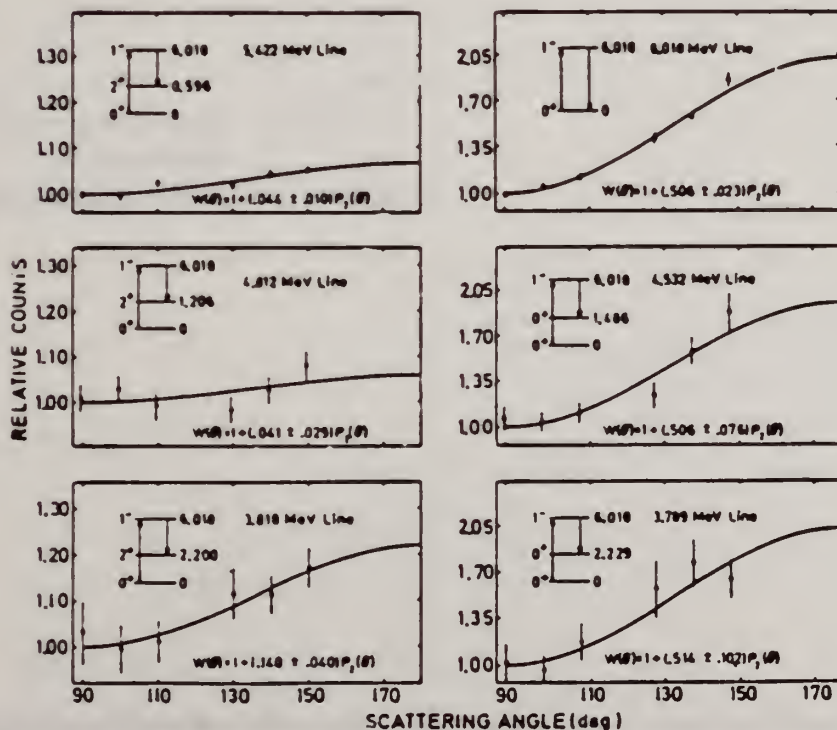


FIG. 4. Angular distribution of the elastic and some intense inelastic lines in  $^{14}\text{Ge}$  as measured using a 20-cm Ge(Li) detector. The solid lines have the form  $W(\theta) = 1 + AP_1(\cos\theta)$  and are least-square fits to the experimental distribution. In each case the corresponding  $\gamma$ - $\gamma$  cascade is indicated.

Ge

74

32

METHOD

REF. NO.

71 Mo 2

egf

REACTION	RESULT	EXCITATION ENERGY	SOURCE		DETECTOR		ANGLE
			TYPE	RANGE	TYPE	RANGE	
G,G/	LFT	6,8	D	6,8	SCD-D		DST

6.018, 7.632 MEV

Table 1

Summary of the experimental and theoretical decay properties of the resonance levels excited by nuclear photo-excitation.

Scatterer	Transition $1^- \rightarrow 2^+$ (keV)	A ( $1^- \rightarrow 2^+$ )	$\Gamma_\gamma$ (meV)	$\Gamma(M2)$ ( $\mu$ eV)	$\Gamma(M2)$ (W.u.)	$\delta^2(M2/E1)$ ( $\times 10^3$ )	$\delta^2(M2/E1)$ Weisskopf estimate ( $\times 10^6$ )
$^{74}\text{Ge}$	6018 $\rightarrow$ 2200	$0.14 \pm 0.04$	$120 \pm 15$	190	0.89	17 $\begin{smallmatrix} +23 \\ -12 \end{smallmatrix}$	3.2
$^{100}\text{Mo}$	6418 $\rightarrow$ 1064	$0.20 \pm 0.08$	$50 \pm 45$	110	0.079	46 $\begin{smallmatrix} +53 \\ -33 \end{smallmatrix}$	6.3
$^{112}\text{Cd}$	7632 $\rightarrow$ 617	$0.09 \pm 0.02$	$86 \pm 15$	36	0.006	3.6 $\begin{smallmatrix} +4.5 \\ -2.7 \end{smallmatrix}$	10.8
$^{186}\text{W}$	6418 $\rightarrow$ 122	$-0.011 \pm 0.014$	$46 \pm 35$	110	0.023	9.0 $\begin{smallmatrix} +5.4 \\ -4.1 \end{smallmatrix}$	8.7

REF. J.J. McCarthy, R. C. Morrison and H.J. Vander Molen  
Nucl. Phys. A213, 371 (1973)

ELEM. SYM.	A	Z
Ge	74	32

METHOD

REF. NO.

73 Mc 10

egf

REACTION	RESULT	EXCITATION ENERGY	SOURCE		DETECTOR		ANGLE
			TYPE	RANGE	TYPE	RANGE	
G,P	ABX	9- 40	C	9- 40	ACT-I		4PI

$$\int_0^{40} \sigma dE = 92 \pm 10 \text{ MeV} \cdot \text{mb}$$

( $\gamma, p$ )

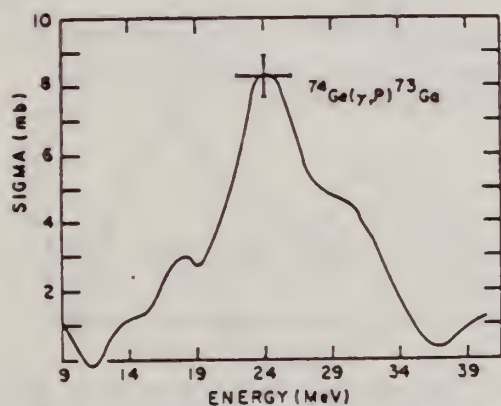


Fig. 3. Total cross section for the reaction  $^{74}\text{Ge}(\gamma, p)^{73}\text{Ga}$ .

REF.

A.M. Goryachev, G.N. Zalesnyi, and B.A. Tulupov  
 Izv. Akad. Nauk SSSR. Ser. Fiz. 39, 134 (1975)  
 Bull. Acad. Sci. USSR Phys. Ser. 39, 116 (1975)

ELEM. SYM.	A	Z
Ge	74	32

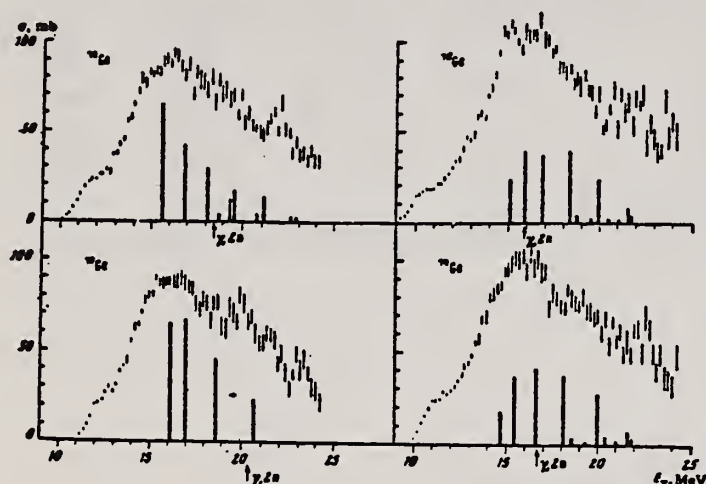
METHOD	REF. NO.	
	75 Go 1	hmg

REACTION	RESULT	EXCITATION ENERGY	SOURCE		DETECTOR		ANGLE
			TYPE	RANGE	TYPE	RANGE	
G,XN	ABX	10- 25	C	9- 25	BF3-I		4PI

$\sigma(G,SN)$ . Statistical theory used to obtain SN cross section from XN cross section.

Table 2

Nuclide	$\beta_0$	$E_2$ , MeV	$E_1$ , MeV	Nuclide	$\beta_0$	$E_2$ , MeV	$E_1$ , MeV
$^{64}\text{Zn}$	0.25	0.99	18	$^{76}\text{Ge}$	0.25	0.562	18
$^{66}\text{Zn}$	0.23	1.04	18	$^{78}\text{Ge}$	0.33	0.559	18
$^{68}\text{Zn}$	0.2	1.08	18	$^{80}\text{Ge}$	0.3	0.618	18
$^{70}\text{Ge}$	0.23	1.04	18	$^{82}\text{Ge}$	0.25	0.654	18
$^{72}\text{Ge}$	0.25	0.835	18	$^{84}\text{Ge}$	0.2	0.653	18
$^{74}\text{Ge}$	0.3	0.8	18				

Fig. 2. The same as in Fig. 1, but for  $^{70,72,74,76}\text{Ge}$ .

Cross sections of photoneutron reactions.  
 The dipole photoabsorption forces are taken  
 from [6,7] (the solid black columns).

<sup>6</sup>M.G.Huber et al., Phys.Rev.155,1073(67)  
<sup>7</sup>M.G.Huber et al., Phys.Rev.192,223(66).

Values given are for  $\sigma_0$  (24.2 MeV).

Table 3

Nuclide	$\sigma$ , mb	Nuclide	$\sigma$ , mb	Nuclide	$\sigma$ , mb
$^{64}\text{Zn}$	$397 \pm 19$	$^{72}\text{Ge}$	$760 \pm 37$	$^{76}\text{Ge}$	$1021 \pm 52$
$^{66}\text{Zn}$	$579 \pm 27$	$^{74}\text{Ge}$	$872 \pm 41$	$^{80}\text{Ge}$	$1029 \pm 50$
$^{68}\text{Zn}$	$718 \pm 35$	$^{76}\text{Ge}$	$911 \pm 43$	$^{82}\text{Ge}$	$1067 \pm 53$
$^{70}\text{Ge}$	$733 \pm 37$	$^{78}\text{Ge}$	$930 \pm 50$		

\*Mean - square errors



REACTION	RESULT	EXCITATION ENERGY	SOURCE		DETECTOR		ANGLE
			TYPE	RANGE	TYPE	RANGE	
G,N	ABX	10- 40	C	10- 40	MOD-I		4PI
G,2N	ABX	17- 40	C	10- 40	MOD-I		4PI
G,P	ABI	11- 40	C	10- 40	ACT-I		4PI
G,NP	ABI	20- 40	C	10- 40	ACT-I		4PI

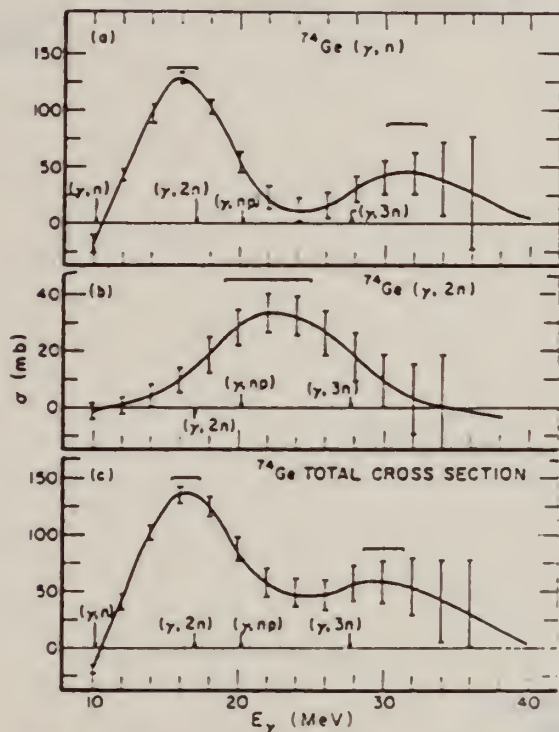


FIG. 6. (a) The  $(\gamma, n)$  cross section for  $^{74}\text{Ge}$ . (b) The  $(\gamma, 2n)$  cross section for  $^{74}\text{Ge}$ . (c) The total cross section  $\sigma[(\gamma, n) + (\gamma, 2n) + (\gamma, np) + (\gamma, p)]$  for  $^{74}\text{Ge}$ .

TABLE II. Integrated cross sections.

Isotope	$(\gamma, p)$			Total
	$(\gamma, n)$	$(\gamma, 2n)$	$(\gamma, np)$	
$^{70}\text{Ge}$	1273(127) <sup>a</sup> 1464(290) <sup>b</sup>	60(6)	40(6)	1463(123)
$^{72}\text{Ge}$	1140(110)	420(40)	40(14)	1690(119)
$^{74}\text{Ge}$	1320(130)	360(40)	90(10)	1905(136)
$^{76}\text{Ge}$	1077(54) <sup>a</sup> 1067(106) <sup>b</sup>	710(70)	15(3)	1892(99)

<sup>a</sup> Result of the activation measurements.

<sup>b</sup> Result of the neutron counting measurements.

<sup>c</sup> Includes the contribution from the  $^{73}\text{Ge}(\gamma, p)$  reaction.

TABLE III. Lorentz fit parameters and integrated cross sections for total cross sections.

Isotope	$f$ (mb)	$\Gamma$ (MeV)	$E_0$ (MeV)	$\sigma_{\text{L}}^{\text{fit}}$	$\sigma_{\text{int}}$ (McV mb)	$\sigma_{\text{int}} - \sigma_{\text{L}}^{\text{fit}}$ (McV mb)	$D = 60NZ$	$\frac{\sigma_{\text{int}}}{D}$	$\frac{\sigma_{\text{int}} - \sigma_{\text{L}}^{\text{fit}}}{\sigma_{\text{int}}}$
				$(\frac{1}{2}\pi)\sigma_0\Gamma$ (McV mb)			$\frac{A}{A}$ (McV mb)		
$^{70}\text{Ge}$	150	5.55	15.5	1390	1463	53	1040	1.41	0.06
$^{72}\text{Ge}$	150	5.90	17.9	1390	1690	300	1070	1.53	0.18
$^{74}\text{Ge}$	144	6.96	16.5	1560	1905	225	1090	1.66	0.12
$^{76}\text{Ge}$	120	3.20	16.7	1550	1892	342	1110	1.70	0.18

REF. P. Carlos, H. Beil, R. Bergere, J. Fagot, A. Lepretre,  
A. Veyssiere, G. V. Solodukhov  
Nucl. Phys. A258, 365 (1976)

ELEM. SYM.	A	Z
Ge	74	32
REF. NO.		egf
76 Ca 1		

METHOD

REACTION	RESULT	EXCITATION ENERGY	SOURCE		DETECTOR		ANGLE
			TYPE	RANGE	TYPE	RANGE	
G,N	ABX	10- 26	D	10- 26	MOD-I		4PI
G,2N	ABX	16- 26	D	10- 26	MOD-I		4PI

981+

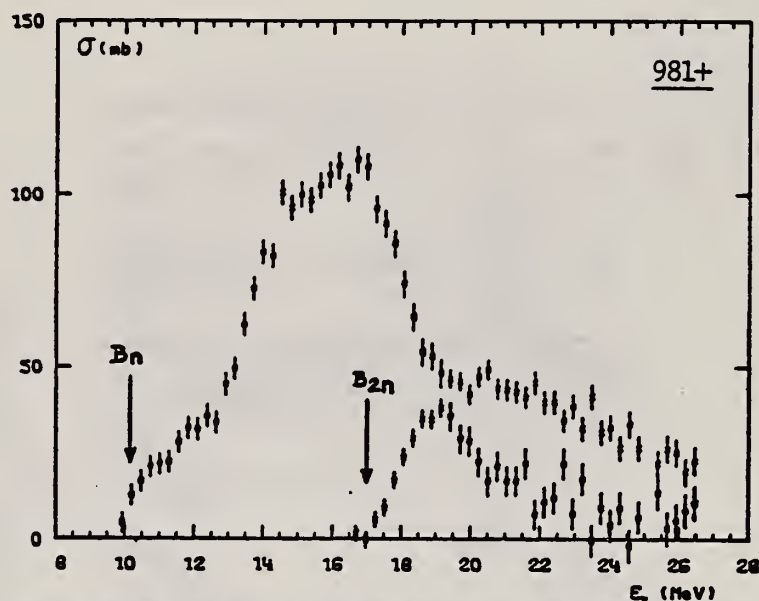


Fig. 5. Partial photoneutron cross sections [ $\sigma(\gamma, n) + \sigma(\gamma, pn)$ ] and  $\sigma(\gamma, 2n)$  for  $^{74}\text{Ge}$ . Arrows  $B_n$  and  $B_{2n}$  indicate theoretical threshold values for  $(\gamma, n)$  and  $(\gamma, 2n)$  reactions respectively.

TABLE 3  
Integrated photoneutron cross sections and comparison with sum rules

Nucleus	$^{64}\text{Zn}$	$\begin{Bmatrix} ^{69}\text{Ga} \\ ^{71}\text{Ga} \end{Bmatrix}$	$^{70}\text{Ge}$	$^{72}\text{Ge}$	$^{74}\text{Ge}$	$^{76}\text{Ge}$	$^{75}\text{As}$	$^{76}\text{Se}$	$^{78}\text{Se}$	$^{80}\text{Se}$	$^{82}\text{Se}$
$E_{\beta\beta}$ (MeV)	29	26.5	26.5	26.5	26.5	26.5	26.5	26.5	26.5	26.5	26.5
$\sigma_{00}$ (MeV · b)	0.75	0.91	0.78	0.94	1.02	1.12	1.09	1.01	1.06	1.11	1.13
$\frac{\sigma_{00}A}{0.06NZ}$	0.78	0.87	0.75	0.88	0.94	1	0.98	0.90	0.92	0.94	0.95
$B_n - B_p$ (MeV)	4.2	$\begin{Bmatrix} 3.7 \\ 1.4 \end{Bmatrix}$	3	1	-0.8	-2.6	3.3	1.7	0.1	-1.5	-3
$\sigma_{-1n}$ (mb)	38	52	44	54	59	64	63	58	62	65	67
$\sigma_{-1n}A^{-1}$ (mb)	0.15	0.18	0.15	0.18	0.19	0.20	0.20	0.18	0.19	0.19	0.19
$\sigma_{-2n}$ (mb · MeV $^{-1}$ )	2.0	3.1	2.5	3.2	3.6	3.9	3.7	3.4	3.8	3.9	4.2
$\sigma_{-2n}A^{-1}$ (μb · MeV $^{-1}$ )	1.9	2.6	2.1	2.6	2.8	2.9	2.8	2.5	2.7	2.6	2.7

FORM N35-  
(REV. 7-14-1)  
USCOMM-NE

The notation used is defined in the text. The average experimental errors  $\Delta\sigma_{00}/\sigma_{00}$ ,  $\Delta\sigma_{-1n}/\sigma_{-1n}$  and  $\Delta\sigma_{-2n}/\sigma_{-2n}$  are approximately 8%. 46



GE  
A=76

GE  
A=76

GE  
A=76

STATE OF NEW YORK

IN SENATE

JANUARY 19, 1906

REPORT

OF THE

COMMISSIONERS OF THE LAND OFFICE

IN RESPONSE TO A RESOLUTION

PASSED BY THE SENATE

APRIL 19, 1905

ALBANY:

THE STATE PRINTING OFFICE

1906

PRICE, 10 CENTS

PER COPY, 5 CENTS

BY MAIL, 10 CENTS

POSTAGE PAID BY ADDRESSEE

NEW YORK

REF.

O.A. Borello, J. Goldemberg, M.D.S. Santos  
An. Acad. Brasil. Cienc. 27, 413 (1955)

ELEM. SYM.

A

Z

Ge

76

32

METHOD

Betatron

REF. NO.

55 Bo 1

NVB

REACTION	RESULT	EXCITATION ENERGY	SOURCE		DETECTOR		ANGLE
			TYPE	RANGE	TYPE	RANGE	
G,N	ABX	9-21	C	9-21	ACT-I		4PI

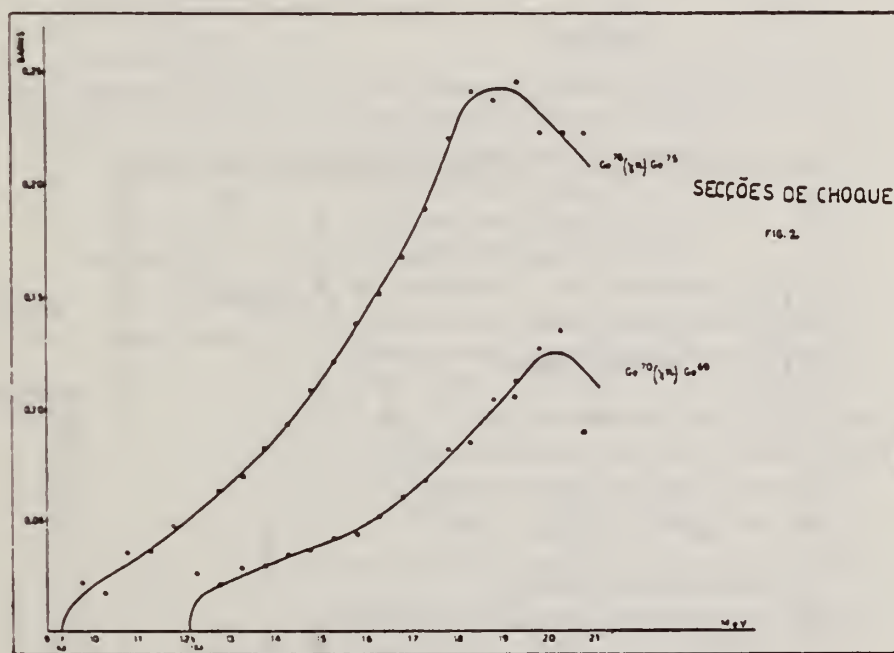


Fig. 2

Elemento	(Threshold) Limiar	$E_{max}$	$\sigma_{max}$	$\sigma$ int até 21 Mev
$Ge^{70}$	$12,1 \pm 0,20$ Mev	20 Mev	0,125 barn	0,59 Mev $\times$ barn
$Ge^{76}$	$9,3 \pm 0,10$ Mev	18,9 Mev	0,243 barn	1,5 Mev $\times$ barn

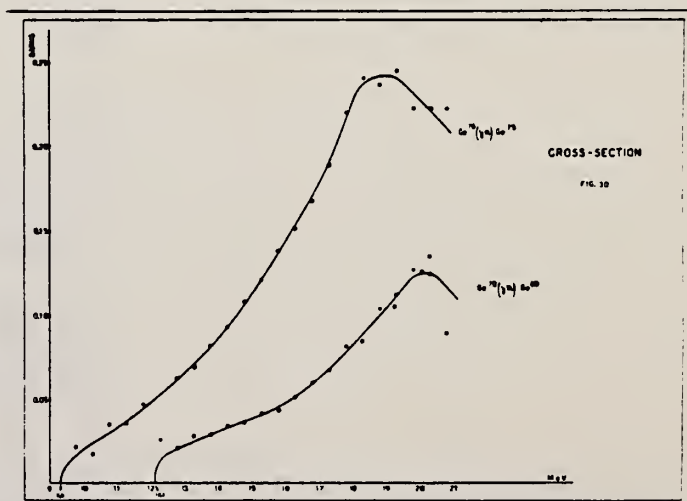
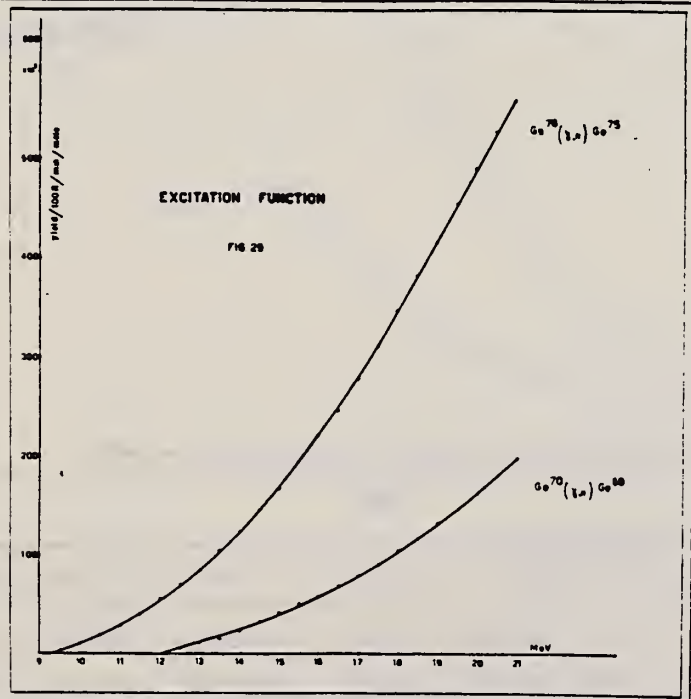
M.D. DeSouza Santos, J. Goldemberg, R.R. Pieroni, E. Silva,  
O.A. Borello, S.S. Villaca, J.L. Lopes  
Int. Conf. Peaceful Uses of Atomic Energy II (UN, NY), 169 (1955)

ELEM. SYM.	A	Z
Ge	76	32
REF. NO.		EGF
55 De 1		

METHOD Betatron; neutron yield; radioactivity; r-chamber

Reaction	RESULT	EXCITATION ENERGY	SOURCE		DETECTOR		ANGLE
			TYPE	RANGE	TYPE	RANGE	
G,N	ABX	9-21	C	9-21	ACT-I		4PI

$$\int \sigma dE = 0.59 \text{ MeV-b}$$



Method 30 MeV electron synchrotron; activation; NaI

Ref. No.	JHH
62 Ca 1	

Reaction	E or ΔE	E <sub>0</sub>	Γ	∫σdE	Jπ	Notes
Ge <sup>76</sup> (γ,n)	Bremss. 30					

TABLE 1  
Isomeric Ratios from (γ,n) reactions

Target Nucleus	J <sub>0</sub>	Residual Nucleus				Isomer ratio $r_1/(r_1 + r_2)$	σ		
		Ground state		Metastable state					
		Spin	Half-life	Spin	Half-life				
Co <sup>59</sup>	7/2 <sup>-</sup>	Co <sup>58</sup>	2 <sup>+</sup>	71.3d	5 <sup>+</sup>	9.2h	0.44 ± 0.02	3.2 ± 0.2	
Ge <sup>76</sup>	0 <sup>+</sup>	Ge <sup>75</sup>	1/2 <sup>-</sup>	82m	7/2 <sup>+</sup>	49s	0.48 ± 0.07	2.8 ± 0.5	
Se <sup>81</sup>	3/2 <sup>-</sup>	Se <sup>80</sup>	1 <sup>+</sup>	18m	5 <sup>-</sup>	4.4h	0.32 ± 0.02	6.5 ± 1.0	
Se <sup>96</sup>	0 <sup>+</sup>	Se <sup>95</sup>	9/2 <sup>+</sup>	64d	1/2 <sup>-</sup>	70m	0.36 ± 0.07	2.2 ± 0.4	
Se <sup>90</sup>	0 <sup>+</sup>	Se <sup>89</sup>	9/2 <sup>+</sup>	79h	1/2 <sup>-</sup>	4.4m	0.33 ± 0.10	2.8 ± 0.7	
Mo <sup>92</sup>	0	Mo <sup>91</sup>	9/2 <sup>+</sup>	15.7m	1/2 <sup>-</sup>	66s	0.46 ± 0.04	6 ± 2	
Ag <sup>107</sup>	1/2 <sup>-</sup>	Ag <sup>106</sup>	1 <sup>+</sup>	24m	6	9.3d	0.04 ± 0.02	2.0 ± 0.3	
Zn <sup>113</sup>	9/2 <sup>+</sup>	Zn <sup>112</sup>	1 <sup>+</sup>	14.5m	4 <sup>+</sup>	20.7m	0.8 ± 0.1	3.1 ± 0.7	
Cd <sup>116</sup>	0 <sup>+</sup>	Cd <sup>115</sup>	1/2 <sup>-</sup>	53h	11/2 <sup>+</sup>	43d	≤ 0.2	≤ 3	
Cd <sup>140</sup>	0 <sup>+</sup>	Cd <sup>139</sup>	3/2 <sup>+</sup>	140d	11/2 <sup>-</sup>	55s	0.08 ± 0.01	2.5 ± 0.2	
Hg <sup>198</sup>	0 <sup>+</sup>	Hg <sup>197</sup>	1/2 <sup>-</sup>	65h	13/2 <sup>+</sup>	24h	0.05 ± 0.01	3.4 ± 0.5	
						3/2 <sup>-</sup> 5/2 <sup>-</sup>			
Previous work									
Se <sup>81</sup> <sup>(10)</sup>	3/2 <sup>-</sup>	Se <sup>80</sup>	1 <sup>+</sup>	18m	5 <sup>-</sup>	4.4h	2 <sup>-</sup>	0.33	6.5
Se <sup>92</sup> <sup>(12)</sup>	0 <sup>+</sup>	Se <sup>91</sup>	1/2 <sup>-</sup>	18m	7/2 <sup>+</sup>	57m		0.5	3.0
Se <sup>90</sup> <sup>(11)</sup>	0 <sup>+</sup>	Se <sup>89</sup>	9/2 <sup>+</sup>	79h	1/2 <sup>-</sup>	4.3m		0.44 ± 0.06	4.5 ± 1
Zn <sup>113</sup> <sup>(23)</sup>	9/2 <sup>+</sup>	Zn <sup>112</sup>	1 <sup>+</sup>	72s	5 <sup>+</sup>	50d		0.85	3.0
							(T <sub>1/2</sub> = 2.5h)		

# REFERENCES

- 1) J. R. Huizenga and R. Vandenbosch, Phys. Rev. 120 (1960) 1505
- 2) T. Ericson, Advances in Physics, 2 (1960) 425
- 3) D. L. Allan, Nuclear Physics 24 (1961) 274
- 4) C. T. Hibdon, Phys. Rev. 114 (1959) 179
- 5) C. T. Hibdon, Phys. Rev. 122 (1961) 1235
- 6) T. Ericson, Nuclear Physics 11 (1959) 481
- 7) J. H. Carver and O. A. Jones, Nuclear Physics 19 (1960) 184
- 8) A. C. Douglas and W. Macdonald, Nuclear Physics 13 (1959) 382
- 9) T. Ericson and V. M. Serutinski, Nuclear Physics 2 (1958) 284
- 10) L. Katz, L. Pease and H. Moody, Can. J. Phys. 30 (1952) 476
- 11) L. Katz, R. G. Baker and R. Montalbetti, Can. J. Phys. 31 (1953) 250
- 12) E. Silva and J. Goldemberg, An. Acad. Brasil. Cienc. 28 (1956) 275
- 13) J. H. Carver and D. C. Peaslee, Phys. Rev. 120 (1960) 2155
- 14) J. M. Blatt and V. F. Weisskopf, "Theoretical Nuclear Physics" New York: Wiley (1952)
- 15) S. H. Vegors, L. L. Marsden and R. L. Heath, U.S. Atomic Energy Commission Report TDO-16370 (1958)
- 16) Nuclear Data Sheets, National Research Council, Washington (1960, up to and including Set 5)
- 17) R. Vandenbosch and J. R. Huizenga, Phys. Rev. 120 (1960) 1313
- 18) E. Weigold and R. Glover, Nuclear Physics (in press)
- 19) K. J. Le Couteur and D. W. Lang, Nuclear Physics 11 (1959) 32
- 20) T. D. Newton, Can. J. Phys. 34 (1956) 904
- 21) D. W. Lang, Nuclear Physics 26 (1961) 434
- 22) M. Z. Rose, "Internal Conversion Coefficients", Amsterdam: North Holland Publishing Co. (1958)
- 23) J. Goldemberg and L. Katz, Phys. Rev. 80 (1953) 308



REF. Y. Oka, T. Kato and A. Yamadera  
Bull. Chem. Soc. Japan 41, 1606 (1968)

ELEM. SYM.	A	Z
Ge	76	32

METHOD

REF. NO.	
68 Ok 2	egf

REACTION	RESULT	EXCITATION ENERGY	SOURCE		DETECTOR		ANGLE
			TYPE	RANGE	TYPE	RANGE	
G,N	ABY	THR-20	C	20	ACT-I		4PI

ISOMERIC YIELD

TABLE 1. THE PARTICULARS OF THE ( $\gamma$ ,n) REACTION PRODUCTS AND THE DATA OBTAINED WITH 20 MeV BREMSSTRAHLUNG

Nuclide		Half-life of product (sec)	Gamma-ray determined			Limit of detection ( $\mu$ g)	Yield ( $\text{mol}^{-1}\cdot\text{R}^{-1}$ )
Parent (Natural abundance, %)	Residual		Energy (MeV)	Branching ratio (%)	Photopeak activity (cpm/mg) <sup>a)</sup>		
<sup>24</sup> Mg(78.60)	<sup>23</sup> Mg	9.9	0.511	200	$2.04 \times 10^6$	0.49	$8.1 \times 10^6$
<sup>76</sup> Ge(7.67)	<sup>75m</sup> Ge	48	0.139	100	$6.37 \times 10^5$	1.6	$1.1 \times 10^6$
<sup>78</sup> Se(23.52)	<sup>77m</sup> Se	17	0.162	100	$1.82 \times 10^6$	0.55	$1.2 \times 10^6$
<sup>92</sup> Mo(15.86)	<sup>91m</sup> Mo	65	0.650	57	$2.22 \times 10^5$	4.5	$2.7 \times 10^6$
<sup>140</sup> Ce(88.48)	<sup>139m</sup> Ce	58	0.745	100	$1.06 \times 10^6$	0.95	$1.3 \times 10^6$
<sup>142</sup> Nd(27.13)	<sup>141m</sup> Nd	64	0.760	100	$3.19 \times 10^5$	3.1	$1.4 \times 10^6$
<sup>158</sup> Tb(100)	<sup>158m</sup> Tb	11	0.111	100	$2.56 \times 10^5$	3.8	$2.2 \times 10^6$

a) The value corrected at the end of one-minute irradiation with the dose rate of  $10^7$  R/min; Counting geometry is 20% with a 3"dia.  $\times$  3"NaI(Tl) detector.

REF.

J.J. McCarthy, R.C. Morrison and H.J. Vander Molen  
Nucl. Phys. **A213**, 371 (1973)

ELEM. SYM.

A

Z

Ge

76

32

METHOD

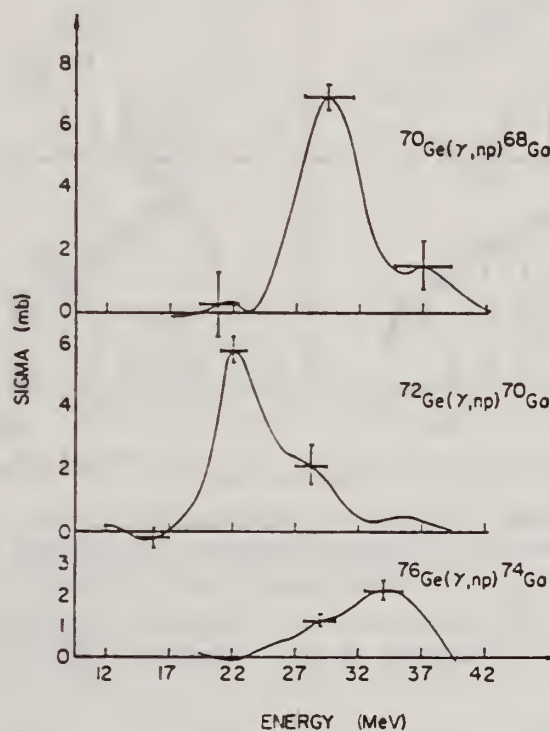
REF. NO.

73 Mc 10

egf

REACTION	RESULT	EXCITATION ENERGY	SOURCE		DETECTOR		ANGLE
			TYPE	RANGE	TYPE	RANGE	
G.NP	ABX	17- 40	C	12- 42	ACT-I		4PI

$$\int_{\gamma}^{40} \sigma dE = 15.2 \pm 3 \text{ MeV} \cdot \text{mb} \quad (\gamma, np)$$

Fig. 5. Cross sections of  $^{70}\text{Ge}(\gamma, np)^{68}\text{Ga}$ ,  $^{72}\text{Ge}(\gamma, np)^{70}\text{Ga}$ , and  $^{76}\text{Ge}(\gamma, np)^{74}\text{Ga}$ .

REF. A.M. Goryachev, G.N. Zalesnyi, and B.A. Tulupov  
Izv. Akad. Nauk SSSR. Ser. Fiz. 39, 134 (1975)  
Bull. Acad. Sci. USSR Phys. Ser. 39, 116 (1975)

ELEM. SYM.	A	Z
Ge	76	32

METHOD	REF. NO.	
	75 Go 1	hmg

REACTION	RESULT	EXCITATION ENERGY	SOURCE		DETECTOR		ANGLE
			TYPE	RANGE	TYPE	RANGE	
G, XN	ABX	9 - 25	C	9- 25	BF3-I		4PI

$\sigma(G, SN)$ . Statistical theory used to obtain SN cross section from XN cross section.

Table 2

Nuclide	$\beta_0$	$E_2$ , MeV	$E_1$ , MeV	Nuclide	$\beta_0$	$E_2$ , MeV	$E_1$ , MeV
$^{64}\text{Zn}$	0.25	0.99	18	$^{70}\text{Ge}$	0.25	0.562	18
$^{66}\text{Zn}$	0.23	1.04	18	$^{72}\text{Ge}$	0.33	0.579	18
$^{68}\text{Zn}$	0.2	1.08	18	$^{74}\text{Ge}$	0.3	0.616	18
$^{70}\text{Ge}$	0.23	1.04	18	$^{76}\text{Ge}$	0.25	0.654	18
$^{72}\text{Ge}$	0.25	0.835	18	$^{78}\text{Ge}$	0.2	0.633	18
$^{74}\text{Ge}$	0.3	0.6	18				

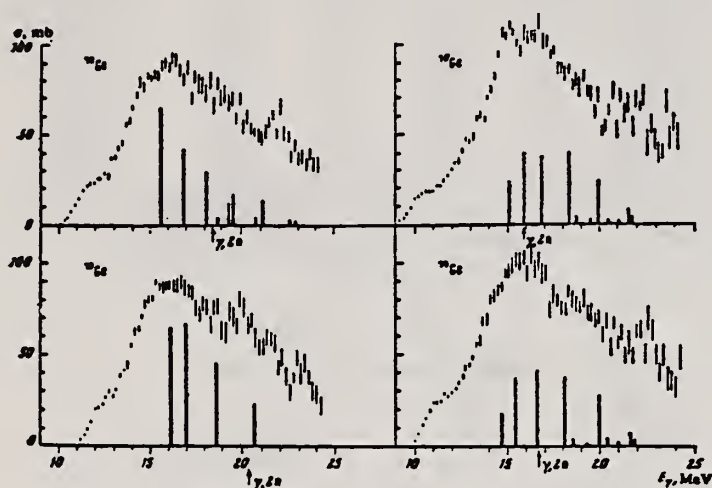


Fig. 2. The same as in Fig. 1, but for  $^{70,72,74,76}\text{Ge}$ .

Cross sections of photoneutron reactions.  
The dipole photoabsorption forces are taken  
from [6,7] (the solid black columns).

<sup>6</sup>M.G.Huber et al., Phys.Rev.155,1073(67)

<sup>7</sup>M.G.Huber et al., Phys.Rev.192,223(66).

[over]

Table 3

Nuclide	$\sigma$ , mb	Nuclide	$\sigma$ , mb	Nuclide	$\sigma$ , mb
$^{61}\text{Zn}$	$565 \pm 19$	$^{72}\text{Cu}$	$700 \pm 37$	$^{74}\text{Se}$	$1021 \pm 52$
$^{62}\text{Zn}$	$570 \pm 27$	$^{74}\text{Cu}$	$872 \pm 41$	$^{82}\text{Se}$	$1029 \pm 50$
$^{63}\text{Zn}$	$718 \pm 35$	$^{76}\text{Cu}$	$911 \pm 43$	$^{83}\text{Se}$	$1067 \pm 53$
$^{76}\text{Cu}$	$733 \pm 37$	$^{78}\text{Cu}$	$930 \pm 50$		

\*Mean - square errors

Values given are for  $\sigma_0$  (24.2 MeV).

ELEM. SYM.	A	Z
Ge	76	32
REF. NO.		
75 Mc 1		hmg

## METHOD

REACTION	RESULT	EXCITATION ENERGY	SOURCE		DETECTOR		ANGLE
			TYPE	RANGE	TYPE	RANGE	
G,N	ABX	9- 40	C	10- 40	MOD-I		4PI
G,2N	ABX	15- 40	C	10- 40	MOD-I		4PI
G,NP	ABI	20- 40	C	10- 40	ACT-I		4PI

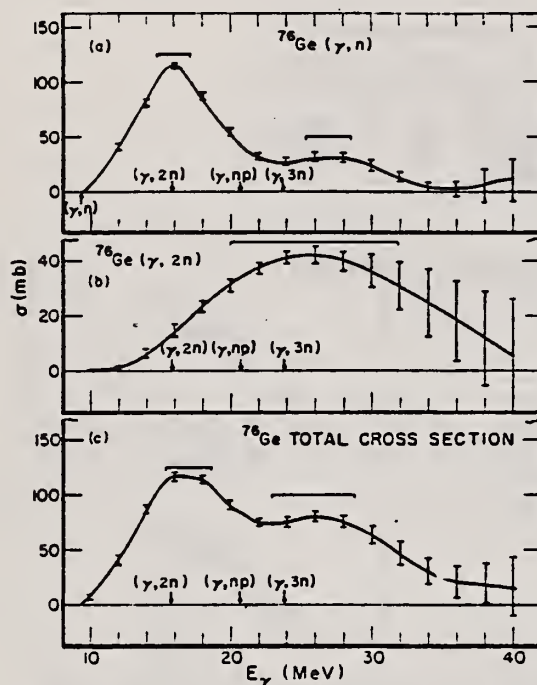


FIG. 7. (a) The  $(\gamma, n)$  cross section for  $^{76}\text{Ge}$ . (b) The  $(\gamma, 2n)$  cross section for  $^{76}\text{Ge}$ . (c) The total cross section  $\sigma[(\gamma, n) + (\gamma, 2n) + (\gamma, np) + (\gamma, p)]$  for  $^{76}\text{Ge}$ .

TABLE II. Integrated cross sections.

Isotope	$(\gamma, p)$				Total
	$(\gamma, n)$	$(\gamma, 2n)$	$(\gamma, np)$	$(\gamma, p)$	
$^{70}\text{Ge}$	1273(127) <sup>a</sup>	60(6)	40(6)	1464(290) <sup>b</sup>	1463(123)
$^{72}\text{Ge}$	1140(110)	420(40)	40(14)	1690(118)	
$^{74}\text{Ge}$	1320(130)	360(40)	90(10)	35(3) <sup>c</sup>	1805(136)
$^{76}\text{Ge}$	1077(54) <sup>a</sup>	710(70)	15(3)	1992(39)	
	1067(106) <sup>b</sup>				

<sup>a</sup> Result of the activation measurements.

<sup>b</sup> Result of the neutron counting measurements.

<sup>c</sup> Includes the contribution from the  $^{73}\text{Ge}(\gamma, p)$  reaction.

TABLE III. Lorentz fit parameters and integrated cross sections for total cross sections.

Isotope	$\sigma_0$ (mb)	$\Gamma$ (MeV)	$E_0$ (MeV)	$\sigma_{\text{LF}}$ $(\frac{1}{2}\pi)\sigma_0\Gamma$ (MeV mb)	$\sigma_{\text{int}}$ (MeV mb)	$\sigma_{\text{int}} - \sigma_{\text{LF}}$ (MeV mb)	$D = 60NZ$ $\frac{A}{\sigma_{\text{int}}}$ (MeV mb)	$\frac{\sigma_{\text{int}}}{D}$	$\frac{\sigma_{\text{int}} - \sigma_{\text{LF}}}{\sigma_{\text{int}}}$
$^{70}\text{Ge}$	150	5.85	15.5	1380	1463	52	1040	1.41	0.06
$^{72}\text{Ge}$	150	5.90	17.9	1390	1690	300	1070	1.58	0.18
$^{74}\text{Ge}$	144	6.96	16.5	1580	1805	225	1090	1.66	0.12
$^{76}\text{Ge}$	120	8.20	16.7	1550	1992	342	1110	1.70	0.18



REF. P. Carlos, H. Beil, R. Bergere, J. Fagot, A. Lepretre,  
A. Veyssiere, G. V. Solodukhov  
Nucl. Phys. A258, 365 (1976)

ELEM. SYM.	A	Z
Ge	76	32

METHOD

REF. NO.

76 Ca 1

egf

REACTION	RESULT	EXCITATION ENERGY	SOURCE		DETECTOR		ANGLE
			TYPE	RANGE	TYPE	RANGE	
G, N	ABX	8- 26	D	8- 26	MOD-I		4PI
G, 2N	ABX	16- 26	D	8- 26	MOD-I		4PI

984+

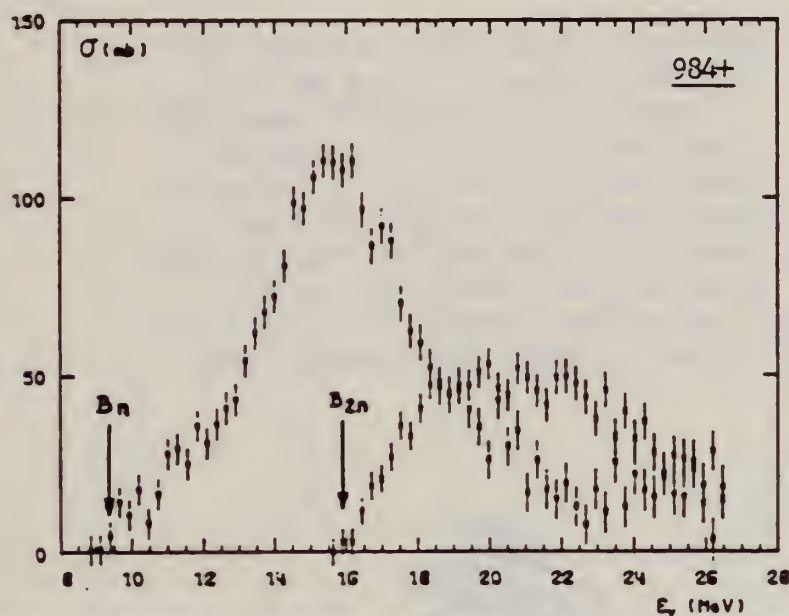


Fig. 6. Partial photoneutron cross sections [ $\sigma(\gamma, n) + \sigma(\gamma, pn)$ ] and  $\sigma(\gamma, 2n)$  for  $^{76}\text{Ge}$ . The rough data have been corrected for the presence of oxygen in the target but not for the 30 % impurities of other Ge isotopes. Arrows  $B_n$  and  $B_{2n}$  indicate theoretical threshold values for  $(\gamma, n)$  and  $(\gamma, 2n)$  reactions respectively.

TABLE 3

Integrated photoneutron cross sections and comparison with sum rules

Nucleus	$^{64}\text{Zn}$	$\begin{pmatrix}^{69}\text{Ga} \\ ^{71}\text{Ga} \end{pmatrix}$	$^{70}\text{Ge}$	$^{72}\text{Ge}$	$^{74}\text{Ge}$	$^{76}\text{Ge}$	$^{78}\text{As}$	$^{76}\text{Se}$	$^{78}\text{Se}$	$^{80}\text{Se}$	$^{82}\text{Se}$
$E_M$ (MeV)	29	26.5	26.5	26.5	26.5	26.5	26.5	26.5	26.5	26.5	26.5
$\sigma_{0n}$ (MeV · b)	0.75	0.91	0.78	0.94	1.02	1.12	1.09	1.01	1.06	1.11	1.13
$\frac{\sigma_{0n} A}{0.06 NZ}$	0.78	0.87	0.75	0.88	0.94	1	0.98	0.90	0.92	0.94	0.95
$B_n - B_p$ (MeV)	4.2	$\begin{pmatrix} 3.7 \\ 1.4 \end{pmatrix}$	3	1	-0.8	-2.6	3.3	1.7	0.1	-1.5	-3
$\sigma_{-1n}$ (mb)	38	52	44	54	59	64	63	58	62	65	67
$\sigma_{-1n} A^{-1/3}$ (mb)	0.15	0.18	0.15	0.18	0.19	0.20	0.20	0.18	0.19	0.19	0.19
$\sigma_{-2n}$ (mb · MeV $^{-1}$ )	2.0	3.1	2.5	3.2	3.6	3.9	3.7	3.4	3.8	3.9	4.2
$\sigma_{-2n} A^{-1/3}$ ( $\mu\text{b} \cdot \text{MeV}^{-1}$ )	1.9	2.6	2.1	2.6	2.8	2.9	2.8	2.5	2.7	2.6	2.7

FORM NBS-1  
REV. 7-14  
USCOMM-N

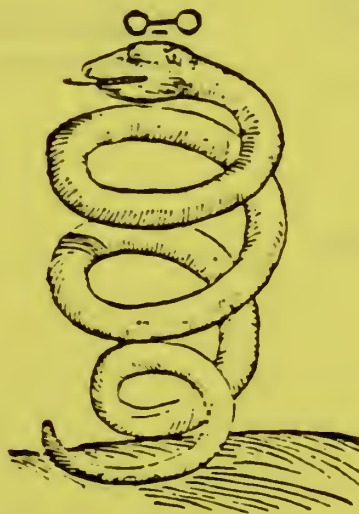
The notation used is defined in the text. The average experimental errors  $\Delta\sigma_{0n}/\sigma_{0n}$ ,  $\Delta\sigma_{-1n}/\sigma_{-1n}$  and  $\Delta\sigma_{-2n}/\sigma_{-2n}$  are approximately 8 %.



ARSENIC  
Z=33

"For smelter fumes have I been named.  
I am an evil, poisonous smoke . . .  
But when from poison I am freed,  
Through art and sleight of hand,  
Then can I cure both man and beast,  
From dire disease ofttimes direct them;  
But prepare me correctly, and take great care  
That you faithfully keep watchful guard over me;  
For else am I poison, and poison remain,  
That pierces the heart of many a one." (1)

As  
A=75



(2)

(1) Fr. Basilli Valentini chymische Schriften, Gottfried Liebezeit, Hamburg, 1694, part 2, p. 156.

(2) Seventeen-Century alchemistic symbol for arsenic.



REF.

T. T. Sugihara and I. Halpern  
Phys. Rev. 101, 1768 (1956)

ELEM. SYM.

A

Z

AS

75

33

METHOD

REF. NO.

56 Su 1

JOC

REACTION	RESULT	EXCITATION ENERGY	SOURCE		DETECTOR		ANGLE
			TYPE	RANGE	TYPE	RANGE	
G,N G,5N5P	RLY	THR-320	C	140,320	ACT-I		4PI
G,3N G,7N2P	ditto	ditto	ditto		ditto		ditto
G,N2P G,7N4P							
G,3N2P G,8N6P							
G,3N4P G,10N4P							
G,4N5P G,14N6P							
G,5N2P G,2P							

TABLE I. Relative yields of observed radionuclides from the irradiation of arsenic with x-ray spectra at 140 Mev and 320 Mev.<sup>a</sup>

Separated nuclide	Half-life <sup>b</sup>	Yield at 140 Mev (arbitrary units)	Yield at 320 Mev (arbitrary units)
As <sup>74</sup>	17.5 days	1050	1050
As <sup>73</sup>	26 hr	110	110
Ga <sup>73</sup>	5.0 hr	0.3	0.5
Ga <sup>72</sup>	14.3 hr	0.9	1.2
Ga <sup>70</sup>	20.3 min	8.4	9.5
Ga <sup>69</sup>	68 min	4.2	7.6
Ga <sup>68</sup>	9.45 hr	0.2	0.7
Cu <sup>67</sup>	58.5 hr	0.1	0.2
Cu <sup>66</sup>	12.80 hr	0.3	2.5
Cu <sup>64</sup>	3.33 hr	<0.1	0.6
Ni <sup>66</sup>	56 hr	<0.02	0.05
Ni <sup>64</sup>	2.56 hr	0.08	0.1
Co <sup>64</sup>	99.0 min	0.09	0.2
Co <sup>60</sup>	18.2 hr	<0.02	0.1

<sup>a</sup> The yields at both energies are normalized to the same flux of resonance-energy (17 Mev) photons.

<sup>b</sup> Hollander, Perlman, and Seaborg, Revs. Modern Phys. 23, 449 (1953).

TABLE III. Average cross sections. Average cross sections for the production of a number of nuclides from arsenic by photons from 140 Mev to 320 Mev.

Nuclide	$\bar{\sigma}$ (mb)	Integrated cross section (Mev-mb)
Ga <sup>73</sup>	0.02	3.6
Ga <sup>68</sup>	0.3	54
Ga <sup>69</sup>	0.05	9
Cu <sup>67</sup>	0.01	1.8
Cu <sup>66</sup>	0.2	36
Cu <sup>64</sup>	0.05	9
Ni <sup>66</sup>	0.002	0.4

TABLE II. Ratios of yields of some gallium isotopes from arsenic to the ( $\gamma, n$ ) yield.

Isotope	Reaction	50 Mev <sup>a</sup>	140 Mev	320 Mev
Ga <sup>73</sup>	( $\gamma, n$ )	$46 \times 10^{-4}$	$80 \times 10^{-4}$	$90 \times 10^{-4}$
Ga <sup>72</sup>	( $\gamma, n2p$ )	$2.4 \times 10^{-4}$	$9 \times 10^{-4}$	$12 \times 10^{-4}$
Ga <sup>70</sup>	( $\gamma, 2p$ )	$1.7 \times 10^{-4}$	$3 \times 10^{-4}$	$5 \times 10^{-4}$

<sup>a</sup> See reference 17.

<sup>17</sup> R. B. Holtzman and N. Sugarman, Phys. Rev. 87, 633 (1952).

<sup>18</sup> H. H. Hopkins, Jr., Phys. Rev. 77, 717 (1950).



Elem. Sym.	A	Z
As	75	33

Method Betatron; neutron yield; threshold detector

Ref. No.  
57 Fe 2  
NB

Reaction	E or $\Delta E$	$E_0$	$\Gamma$	$\int \sigma dE$	$J\pi$	Notes
As <sup>75</sup> ( $\gamma, n!$ )	Bremss. 14-30					R - ratio between area of second maximum in cross section and first maximum.  R = $0.6 \pm 0.12$

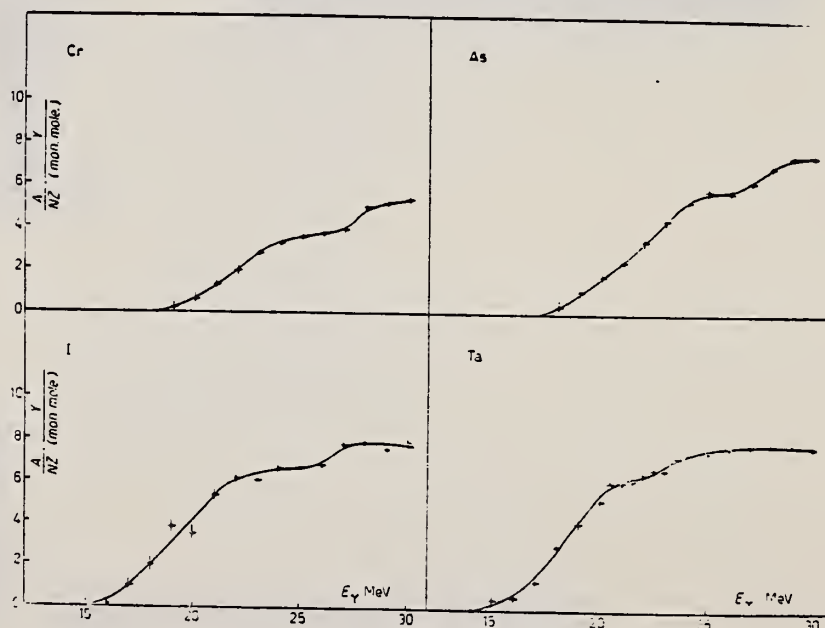


Fig. 1.

ELEM. SYM.	A	Z
As	75	33

METHOD					REF. NO.	
Betatron					58 Ch 2	NVB
REACTION	RESULT	EXCITATION ENERGY	SOURCE		DETECTOR	
			TYPE	RANGE	TYPE	RANGE
G, N	RLY	THR	C	THR	BF <sub>3</sub> -I	4PI

See 58 Ka 1 for cross sections.

THRESHOLD

TABLE I  
MEASURED PHOTONEUTRON THRESHOLDS

Reaction	Measured Q value, Mev.	Other Q values, Mev.	Method	Reference
As <sup>74</sup> ( $\gamma$ , n)As <sup>73</sup>	10.24 $\pm$ 0.08 (10.14 $\pm$ 0.10)	10.18 $\pm$ 0.19	Mass data	Wapstra (1955)
		10.3 $\pm$ 0.2	Threshold	Ogle <i>et al.</i> (1950)
		10.10 $\pm$ 0.20	Threshold	Sher <i>et al.</i> (1951)
		9.92 $\pm$ 0.07*	Mass data	Duckworth (unpublished)
			Q <sup>+</sup> value	Way <i>et al.</i> (1955)
		10.14 $\pm$ 0.07*	Mass data	Duckworth (unpublished)
			Q <sup>-</sup> value	Way <i>et al.</i> (1955)

\*Errors given are from mass values only, those of Q<sup>+</sup> and Q<sup>-</sup> values are not known.

METHOD Betatron; neutron cross section;  $\text{BF}_3$  counters; ion chamber monitor

REF. NO.

58 Ka 1

NVB

REACTION	RESULT	EXCITATION ENERGY	SOURCE		DETECTOR		ANGLE
			TYPE	RANGE	TYPE	RANGE	
G, XN	ABX	10-22	C	10-22	$\text{BF}_3\text{-I}$		4PI

# THRESHOLDS

Таблица 2

Пороги испускания фотонейтронов

Изотоп	$B_n, \text{Mэв}$	$B_{nn}, \text{Mэв}$	Изотоп	$B_n, \text{Mэв}$	$B_{nn}, \text{Mэв}$
V <sup>51</sup>	11,16	20,5	La <sup>139</sup>	8,81	16,1
Mn <sup>55</sup>	10,14	19,2	Pr <sup>141</sup>	9,46	17,6
Co <sup>59</sup>	10,44	18,6	Tb <sup>159</sup>	8,16	14,8
As <sup>75</sup>	10,24	18,1	Ho <sup>165</sup>	8,10	14,6
Y <sup>89</sup>	11,82	20,7	Tm <sup>169</sup>	8,00	14,7
Nb <sup>93</sup>	8,86	17,1	Lu <sup>175</sup>	7,77	14,2
Rh <sup>103</sup>	9,46	16,8	Ta <sup>181</sup>	7,66	13,8
J <sup>127</sup>	9,14	16,2	Au <sup>197</sup>	7,96	13,3
Cs <sup>133</sup>	9,11	16,5	Bi <sup>209</sup>	7,43	14,5

не приведены, поскольку они превышают 22 Мэв во всех случаях, кроме золота, для которого  $B_{nn}=21 \text{ Мэв}$ . Свойства сечений  $\sigma_s(\gamma)$  сведены в табл. 3.

Таблица 1

Изотоп	$E_{\text{порог}}, \text{Mэв}$	$\sigma_n(E_\gamma), \text{барн}$	$\Gamma, \text{Mэв}$	$\Sigma^{\text{в}}, \text{Mэв} \cdot \text{барн}$	$\gamma(22), 10^3 \text{ нейтрон}/100 \text{ р} \cdot \text{мэв}$
V <sup>51</sup>	18,4	0,062	5,2	0,33	1,62
Mn <sup>55</sup>	20,2	0,060	7,0	0,39	2,01
Co <sup>59</sup>	18,3	0,068	6,3	0,44	2,30
As <sup>75</sup>	16,4	0,090	9,5	0,74	4,25
Y <sup>89</sup>	17,1	0,172	5,2	0,93	5,32
Nb <sup>93</sup>	18,0	0,156	7,5	1,17	6,80
Rh <sup>103</sup>	17,5	0,160	9,4	1,40	8,28
J <sup>127</sup>	15,2	0,273	6,8	1,76	11,9
Cs <sup>133</sup>	16,5	0,238	7,7	1,59	10,7
La <sup>139</sup>	15,5	0,325	3,8	1,55	11,2
Pr <sup>141</sup>	15,0	0,320	4,9	1,93	13,1
Tb <sup>159</sup>	15,6	0,274	9,8	2,49	18,1
Ho <sup>165</sup>	13,5	0,305	8,9	2,52	18,7
Tm <sup>169</sup>	16,4	0,250	8,4	1,91	14,9
Lu <sup>175</sup>	16,0	0,225	8,4	1,90	23,0
Ta <sup>181</sup>	14,5	0,380	8,5	3,15	22,0
Au <sup>197</sup>	13,8	0,475	4,7	3,04	22,6
Bi <sup>209</sup>	13,2	0,455	5,9	2,89	23,2

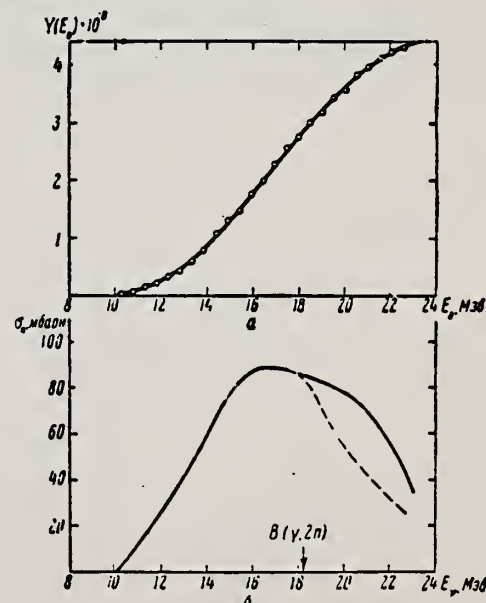


Рис. 4.

a — Выход фотонейтронов для As; б —  $\sigma_n(E_\gamma)$  и  $\sigma_n(\gamma)$  для As

ELEM. SYM.	A	Z
As	75	33

METHOD					REF. NO.	
Betatron; neutron threshold; ion chamber					60 Ge 3	NVB
REACTION	RESULT	EXCITATION ENERGY	SOURCE		DETECTOR	
			TYPE	RANGE	TYPE	RANGE
G,N	N $\alpha$ X	THR	C	THR	BF <sub>3</sub> -I	4 PI

THRESHOLD

TABLE I. Summary and comparison of neutron separation energies inferred from present threshold measurements with values predicted from mass data and reaction energies. All energies are expressed in the center-of-mass system in Mev.

Reaction	No. runs	Present results	Other results	Method	Reference
As <sup>76</sup> ( $\gamma, n$ )As <sup>75</sup>	4	10.259 $\pm$ 0.031	10.11 $\pm$ 0.16	mass data Q( $\beta^+$ )	m o
			10.14 $\pm$ 0.13	mass data Q( $\beta^-$ )	m o
			10.24 $\pm$ 0.08	threshold	f

- \* Henry E. Duckworth, *Mass Spectroscopy* (Cambridge University Press, New York, 1958), p. 177.
- \* L. J. Lidoisky, *Revs. Modern Phys.* 29, 773 (1957).
- \* R. W. King, *Revs. Modern Phys.* 26, 327 (1954).



METHOD						REF. NO.	
betatron; fast neutron yield; angular distribution; Al and Si threshold detectors; ion chamber						61 Ba 2	NVB
REACTION	RESULT	EXCITATION ENERGY	SOURCE		DETECTOR		ANGLE
			TYPE	RANGE	TYPE	RANGE *	
G, XN	ABY	THR-22	C	22	THR-I	3-+	DST
G, XN	ABY	THR-22	C	22	THR-I	5-+	DST

In Tables 2 and 4:

\* "3-+" is the detector range of Aluminum and "5-+" of Silicon.

$\bar{\sigma}$  = average cross section of detector weighted with neutron spectrum

$\bar{\phi}$  = neutrons/100 roentgen/mole

$$W(\theta) = a_0 \sum_{n=1}^{\infty} [1 + A_n P_n(\cos \theta)]$$

TABLE II  
Normalized yields for aluminum detectors

Element	Al( $\pi, \gamma$ ) reaction				Al( $\pi, p$ ) reactions						
	30°	90°	150°	$a_0$	30°	60°	90°	$a_2$	$a_4$	$a_6$	$(\bar{\sigma}\phi)^{\circ} \times 10^6$
Bismuth	399	567 ± 130	620	541 ± 83	3632	5139 ± 290	3168	4368 ± 185	0.06 ± 0.06	-0.35 ± 0.1	17.76
	478	423 ± 130	641	484 ± 85	2562	5353 ± 290	2955	4144 ± 185	-0.05 ± 0.06	-0.53 ± 0.1	16.87
Lead	426	312 ± 120	725	429 ± 77	3123	5754 ± 260	3154	4591 ± 106	-0.004 ± 0.05	-0.51 ± 0.07	18.63
Tantalum	378	367 ± 100	683	441 ± 122	2757	3024 ± 425	2088	2757 ± 275	0.14 ± 0.14	-0.19 ± 0.17	11.22
Lanthanum	208	222 ± 110	330	243 ± 70	2139	3371 ± 250	1891	2768 ± 160	0.05 ± 0.07	-0.43 ± 0.10	11.27
Arsenic	77	100 ± 50	108	97 ± 32	788	937 ± 115	764	865 ± 74	0.02 ± 0.11	-0.16 ± 0.14	3.52
Copper	13	65 ± 30	70	55 ± 20	710	748 ± 70	569	700 ± 45	0.11 ± 0.08	-0.14 ± 0.11	2.85

$(\bar{\sigma}\phi) = 4.07 \times 10^{-6}$  millibarn-neutron.

TABLE IV

I Element	II $a_0$	III $a_1$	IV $a_2$	V $(\bar{\sigma}\phi) \times 10^6$	VI $\phi_{\text{fast}}(22 \text{ Mev}) \times 10^6$	VII $\phi_{\text{fast}}/\phi_{\text{total}}$
Vanadium	245 (1 ± 0.06)	0.01 ± 0.08	-0.00 ± 0.10	6.05	0.21	0.12
Chromium	164 (1 ± 0.03)	0.04 ± 0.04	-0.05 ± 0.05	4.05	0.17	0.10
Manganese	308 (1 ± 0.02)	0.07 ± 0.02	-0.09 ± 0.04	7.61	0.25	0.12
Iron	200 (1 ± 0.03)	0.05 ± 0.04	-0.17 ± 0.05	4.94	0.18	0.11
Cobalt	390 (1 ± 0.02)	0.08 ± 0.03	-0.22 ± 0.04	9.63	0.26	0.15
Nickel	145 (1 ± 0.05)	0.07 ± 0.07	-0.23 ± 0.09	3.58	0.12	0.12
Copper	347 (1 ± 0.02)	0.05 ± 0.03	-0.29 ± 0.04	8.57	0.30	0.12
Zinc	482 (1 ± 0.03)	0.11 ± 0.04	-0.24 ± 0.05	11.91	0.33	0.15
Cadmium	638 (1 ± 0.05)	0.13 ± 0.06	-0.14 ± 0.08	15.76		
Strontium	409 (1 ± 0.05)	0.10 ± 0.06	-0.17 ± 0.08	10.10		
Yttrium	290 (1 ± 0.10)	0.08 ± 0.12	-0.12 ± 0.15	7.16		
Silver	590 (1 ± 0.04)	0.10 ± 0.06	-0.22 ± 0.08	14.57	0.87	0.07
Cadmium	905 (1 ± 0.02)	0.02 ± 0.02	-0.26 ± 0.03	22.35		
Iodine	1133 (1 ± 0.03)	0.04 ± 0.04	-0.29 ± 0.05	27.99	1.42	0.08
Barium	1048 (1 ± 0.04)	0.10 ± 0.06	-0.38 ± 0.08	25.80		
Lanthanum	1595 (1 ± 0.02)	0.02 ± 0.03	-0.42 ± 0.04	39.40	1.04	0.15
Cerium	1316 (1 ± 0.05)	0.05 ± 0.06	-0.39 ± 0.08	32.50		
Dysprosium	1652 (1 ± 0.08)	0.04 ± 0.10	-0.34 ± 0.13	40.80		
Tantalum	1558 (1 ± 0.02)	0.04 ± 0.03	-0.23 ± 0.04	38.48	2.50	0.06
Tungsten	1365 (1 ± 0.02)	0.07 ± 0.03	-0.24 ± 0.04	33.71		
Mercury	1345 (1 ± 0.02)	0.04 ± 0.03	-0.31 ± 0.04	33.22		
Lead	2274 (1 ± 0.01)	0.02 ± 0.02	-0.42 ± 0.03	56.17	2.72	0.08
Bismuth	2162 (1 ± 0.02)	0.05 ± 0.03	-0.45 ± 0.04	53.40	3.36	0.06
Thorium	3031 (1 ± 0.04)	0.06 ± 0.05	-0.32 ± 0.07	74.87		
Uranium	4630 (1 ± 0.02)	0.05 ± 0.03	-0.17 ± 0.04	114.36		

$(\bar{\sigma}\phi) = 2.47 \times 10^{-6}$  millibarn-neutron. Errors are standard errors due to counting statistics only.



Elem. Sym.	A	Z
As	75	33

Method 22 MeV betatron;  $\text{Si}^{28}(\text{n,p})\text{Al}^{28}$  threshold detector.

Ref. No.	
61 Ta 1	JHH

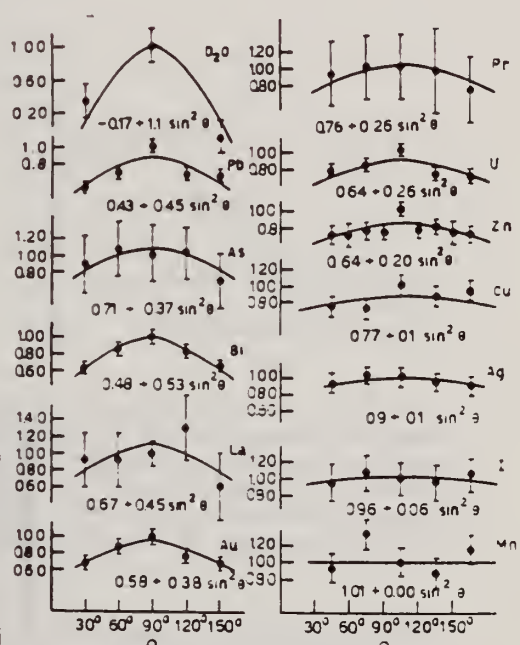
Reaction	E or $\Delta E$	$E_0$	$\Gamma$	$\int \sigma dE$	$J\pi$	Notes
$\text{As}^{75}(\gamma, \text{n})$	Bremss. 22					<p><math>E_n &gt; 6 \text{ MeV.}</math></p> <p><math>W(\theta_n) = A + B \sin^2 \theta</math> where <math>B/A = 0.52 \pm 0.21</math></p> 

Figure 4: Angular distributions of fast photoneutron as observed with the  $\text{Si}^{28}(\text{n,p})\text{Al}^{28}$  detector. Data normalized at  $90^\circ$  in each case.

METHOD

Radioactive source; total absorption

REF. NO.

62 Me 2

NVB

REACTION	RESULT	EXCITATION ENERGY	SOURCE		DETECTOR		ANGLE
			TYPE	RANGE	TYPE	RANGE	
G,G	LFT	1	D	1	NAI-D		0
		(265 keV)		(265 keV)			

LIFETIME

Mean life:

$$\tau = (1.57 \pm 0.10) 10^{-11} \text{ sec.}$$

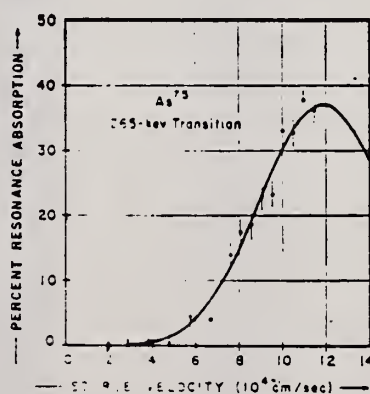


Fig. 3. Comparison of experimental points with calculated curve for  $F = 4.07 \times 10^{-5} \text{ eV}$ .

Table I. Experimental results of the transmission experiments carried out with the  $16.05 \text{ g/cm}^2$  arsenic absorber. The absorptions expected for  $F_0 = 1.07 \times 10^{-5} \text{ eV}$  are tabulated for comparison purposes. In the last column, the widths calculated from the observed absorptions are listed.

Source velocity ( $10^8 \text{ cm/sec}$ )	Absorption in %		Width $\Gamma_0$ from experimental absorption ( $10^{-5} \text{ eV}$ )
	Experiment	Calculated for $F = 4.07 \times 10^{-5} \text{ eV}$	
1.89	$0.9 \pm 2.0$	0.07	$1.55 \pm 120$
2.84	$0.7 \pm 1.4$	0.24	$12 \pm 65$
3.79	$0.9 \pm 2.0$	0.7	$5.4 \pm 12$
4.74	$0.4 \pm 1.4$	1.7	$3.0 \pm 3.4$
5.69	$4.4 \pm 2.1$	3.7	$4.8 \pm 2.4$
6.65	$11.1 \pm 1.6$	7.4	$2.1 \pm 0.9$
7.60	$14.1 \pm 1.9$	12.6	$4.2 \pm 0.8$
8.58	$17.4 \pm 2.1$	20.0	$4.8 \pm 0.7$
9.56	$18.6 \pm 2.1$	29.6	$3.8 \pm 0.6$
10.04	$23.0 \pm 2.1$	33.4	$4.0 \pm 0.4$
10.53	$23.3 \pm 2.1$	37.2	$3.8 \pm 0.4$
11.01	$33.0 \pm 1.9$	50.5	$4.8 \pm 0.3$
11.49	$32.7 \pm 1.9$	53.4	$4.0 \pm 0.3$
11.97	$37.8 \pm 1.9$	55.6	$4.4 \pm 0.3$
12.46	$36.2 \pm 1.9$	56.8	$4.0 \pm 0.3$
12.94		57.3	
13.41		56.5	
13.87		52.4	

Ref. M. Sugawara, S. Mori, A. Ono, A. Hotta, M. Kimura  
J. Phys. Soc. Japan 18, 17 (1963)

Elem. Sym.	A	Z
As	75	33

Method 25 MeV betatron; photon scattering; NaI spectrometer; NBS chamber

Ref. No.	
63 Su 1	NVB

Reaction	E or $\Delta E$	$E_0$	$\Gamma$	$\int \sigma dE$	$J\pi$	Notes
$As^{75}(\gamma, \gamma)$	Bremss. 4-14					<p>Detector at <math>120^\circ</math>.</p> <p><math>\sigma_{\max} = 0.6 \text{ mb}</math></p> <p>[Corrects results in J. Phys. Soc. Japan <u>16</u>, 1657 (1961)]</p> <div data-bbox="990 1087 1389 1351" data-label="Figure"> </div> <p>(d)</p>

Fig. 2. The elastic scattering cross sections for Mg, Fe, Zn, As, Cd, Sb and Bi. The indicated spread in energy is the width of the sum-up channels, and the vertical lines are the statistical errors including background counts. The arrows represent the positions of the threshold energies of  $(\gamma, p)$  or  $(\gamma, n)$  reaction taken from Ref. 16. The open squares at 7 Mev are Reibel and Mann's data<sup>9</sup>. In Fig. 2(c), the cross section values, which are analyzed by displacing the sum-up channels by five channels to lower energy side than the positions generally used, are indicated by the closed triangles.

- |  |   |
|--|---|
| 9) K. Reibel and A. K. Mann: Phys. Rev. <b>118</b> (1960) 701. | 1857.   |
| 10) J. S. Pruitt and S. R. Domen: NBS Monograph 48 (1962).     | 15) J. A. Stratton: <i>Electromagnetic Theory</i> (McGraw-Hill Book Co., New York, 1941). |
| 11) E. G. Fuller and E. Hayward: J. Research                   | 16) <i>Nuclear Data Sheets</i> , National Academy of Sciences (N. R. C.).                 |

427400

Synchrotron;  $C^{12}(\gamma, n)$  monitor

[Page 1 of 2]

REF. NO.

64 Co 2

JOC

REACTION	RESULT	EXCITATION ENERGY	SOURCE		DETECTOR		ANGLE
			TYPE	RANGE	TYPE	RANGE	
G, XN	ABY	THR - 80	C	80	BF3-I		4 PI

Table 1

Element	Yield (36) eV cm <sup>2</sup> mol MeV	60 NZ/A (mb MeV)	$\Sigma$ 0	$\Sigma$ 0	$\Sigma$ / $\Sigma$ 0 / 0	$E_m$ (MeV)	$\sigma_m$ (mb)
$^{24}\text{Cr}$	$83 \times 10^{-5}$	777	1.21	2.1	0.58	18.5	97
$^{25}\text{Mn}$	$108 \times 10^{-5}$	813	1.52	2.33	0.65	18.5	114
$^{26}\text{Fe}$	$68 \times 10^{-5}$	832	0.58	1.46	0.80	17.5	75
$^{27}\text{Co}$	$89 \times 10^{-5}$	878	1.06	1.32	0.59	17.5	92
$^{28}\text{Ni}$	$44 \times 10^{-5}$	879	0.55	1.07	0.51	18.5	56
$^{29}\text{Cu}$	$95 \times 10^{-5}$	947	1.06	1.99	0.53	17.5	98
$^{30}\text{Zn}$	$38 \times 10^{-5}$	975	0.94	1.68	0.56	17.5	86
$^{31}\text{Ga}$	$130 \times 10^{-5}$	1034	1.29	2.13	0.59	17.5	151
$^{32}\text{Ge}$	$139 \times 10^{-5}$	1034	1.35	2.29	0.59	17.5	168
$^{33}\text{As}$	$137 \times 10^{-5}$	1109	1.22	2.18	0.56	17.5	127

$$\frac{\int_0^{30} \sigma(\gamma, xn) dE}{\Sigma = 0} = \frac{30}{60 \text{ NZ/A}}$$

Table 2

Element	maximum yield ( $\times 10^{-3}$ )	$\sigma_{-1}(\gamma, n)$	$\sigma_{-1}(\gamma, n)$ $\times \left[ \frac{3}{4\pi^2} \frac{hc}{c^2} \left( \frac{A-1}{NZ} \right) A^{-2/3} \right]$
$^{12}\text{C}$	4.0	3.54	2.13
$^{16}\text{O}$	5.2	4.95	1.92
$^{23}\text{Na}$	12.6	11.60	2.49
$^{27}\text{Al}$	10.0	8.81	1.73
$^{29}\text{Si}$	13.9	13.92	2.30
$^{31}\text{P}$	11.6	9.96	1.55
$^{35}\text{S}$	19.3	17.56	2.92
$^{39}\text{K}$	9.5	8.55	1.67
$^{41}\text{K}$	19.3	17.90	1.61
$^{45}\text{Ca}$	12.1	11.68	1.92
$^{51}\text{Cr}$	86	61.6	3.56
$^{55}\text{Mn}$	113	76.1	3.56
$^{59}\text{Fe}$	71	50.5	2.55
$^{63}\text{Co}$	94	63.5	2.94
$^{65}\text{Ni}$	46	34.2	1.59
$^{67}\text{Cu}$	102	72.6	2.96
$^{70}\text{Zn}$	93	65.7	2.65
$^{71}\text{Ga}$	140	93.6	3.31
$^{73}\text{Ge}$	150	101.5	3.36
$^{75}\text{As}$	151	99.3	3.12

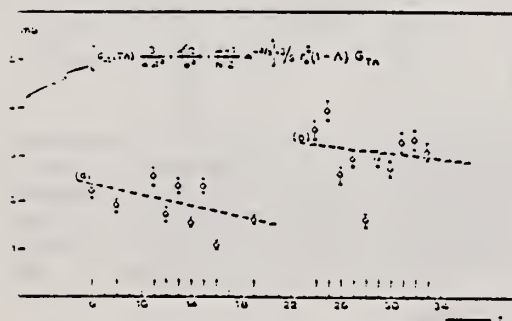


Fig. 2. Bremsstrahlung-weighted cross sections,  $\sigma_{-1}(\gamma, n)$ , conventionally normalized, versus  $Z$ .

REF.

S. Costa, F. Ferroni, S. Ferroni and C. Molino  
 Phys. Letters 11, 324 (1964)

ELEM. STM.

A

As

75

33

METHOD

Synchrotron;  $C^{12}(\gamma, n)$  monitor

[Page 2 of 2]

REF. NO.

64 Co 2

JOC

REACTION	RESULT	EXCITATION ENERGY	SOURCE		DETECTOR		ANGLE
			TYPE	RANGE	TYPE	RANGE	

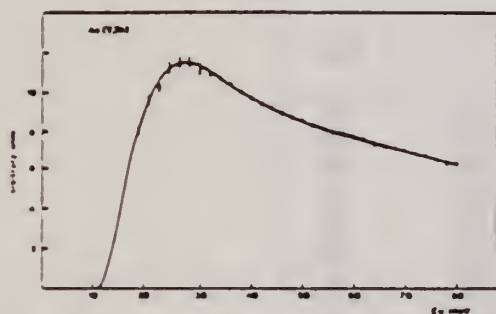


Fig. 1. A typical yield curve ( $As(\gamma, Tn)$ ).



REF.

S. Costa, F. Ferrero, S. Ferroni and R. Malvano  
Proc. Paris Conference 1034 (1964)

ELEM. SYM.	A	Z
AS	75	33

METHOD

100 MeV synchrotron

REF. NO.

64 Co 3

JDM

REACTION	RESULT	EXCITATION ENERGY	SOURCE		DETECTOR		ANGLE
			TYPE	RANGE	TYPE	RANGE	
G <sub>1</sub> N	AB $\bar{I}$	THR-80	C	10-80	BF3-I		4PI

TABLE

ELEMENT	Yield (36 MeV) $\left(\frac{n \cdot cm^2}{mol \cdot MeV}\right)$ $\times 10^5$	$\Sigma_0^{30}$	$\Sigma_0^{80}$	$\Sigma_0^{30}/\Sigma_0^{80}$	$\sigma_{-1}$ (mb)
<sup>24</sup> Cr .....	83	1.21	2.1	0.58	62
<sup>25</sup> Mn .....	108	1.52	2.33	0.65	76
<sup>26</sup> Fe .....	68	0.88	1.46	0.60	50
<sup>27</sup> Co .....	89	1.08	1.82	0.59	64
<sup>28</sup> Ni .....	44	0.55	1.07	0.51	34
<sup>29</sup> Cu .....	95	1.06	1.99	0.53	72
<sup>30</sup> Zn .....	88	0.94	1.68	0.56	66
<sup>31</sup> Ga .....	130	1.29	2.18	0.59	94
<sup>32</sup> Ge .....	139	1.35	2.29	0.59	101
<sup>33</sup> As .....	137	1.22	2.18	0.56	100

$\Sigma_0 = \frac{A}{60 NZ} \int_0^b \sigma(E) dE$  is the integrated cross section measured in units of the classical dipole  $60 NZ/A$  mb. MeV.

REF.

Yu. K. Shubnyĭ, D. K. Kaipov, and R.B. Begzhanov  
 J. Exptl. Theoret. Phys. (USSR) 47, 16 (1964)  
 Soviet Phys. JETP 20, 11 (1965)

ELEM. SYM. A Z

As

75

33

## METHOD

Resonance scattering; high temperature source

REF. NO.

64 Sh 5

JOC

REACTION	RESULT	EXCITATION ENERGY	SOURCE		DETECTOR		ANGLE
			TYPE	RANGE	TYPE	RANGE	
G,G	LFT	1	D	1	NAI-D		122

$$\tau_Y(M1) = (1.7 \pm 0.3) \times 10^{-11} \text{ sec for } 0.265 \text{ MeV level.}$$

REF.

D.S. Fielder, J. Le Tourneux, K. Min, and W. D. Whitehead  
 Phys. Rev. Letters 15, 33 (1965)

ELEM. SYM.

A

Z

As

75

33

METHOD

REF. NO.

65 F1 1

JOC

REACTION	RESULT	EXCITATION ENERGY	SOURCE		DETECTOR		ANGLE
			TYPE	RANGE	TYPE	RANGE	
G,XN	ABX	10 - 25	C	10-25	BF3 - I		4 PI

$$\int_{10}^{23} \sigma(xn) = 744 \pm 56 \text{ MeV-mb}$$

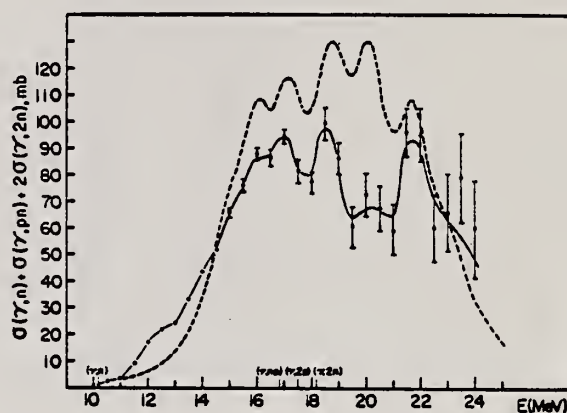


FIG. 1. Solid line: photoneutron production cross section of  $\text{As}^{75}$ ; dashed line: total photoabsorption cross section.

See: Phys. Rev. Letters 15, 530 (1965)  
 for Danos et al. fit.

U. Amaldi, Jr., G. Campos Venuti, G. Cortellessa, E. De Sanctis,  
S. Frullani, R. Lombard, P. Salvadori  
Lincei-Rend.Sc.fis.mat. e nat. 41, 494 (1966)

As

75

33

METHOD

REF. NO.

66 Am 2

hmg

REACTION	RESULT	EXCITATION ENERGY	SOURCE		DETECTOR		ANGLE
			TYPE	RANGE	TYPE	RANGE	
E, E/P	SPC	105-365	D	560-880	MAG-D	475	62

ANGLE OF E/ is 51

TABLE I.

	A	B	C
$E_M$ (MeV) . . . . .	$27 \pm 8$	$58 \pm 14$	$111 \pm 12$
$\sigma$ (MeV) . . . . .	$28 \pm 12$	$32 \pm 25$	$52 \pm 20$

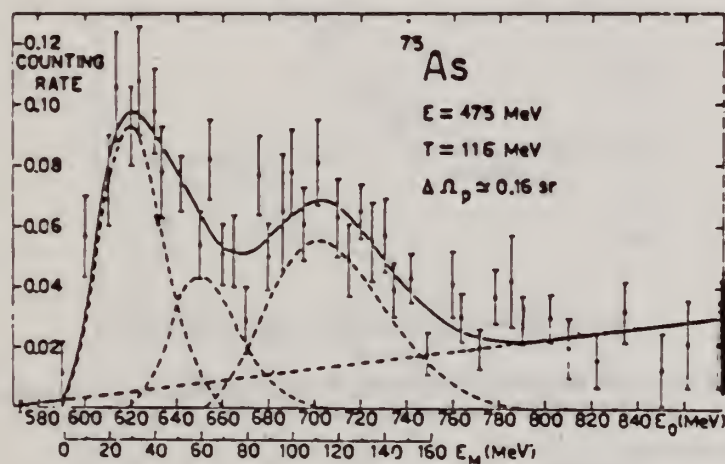


Fig. 1.

REACTION	RESULT	EXCITATION ENERGY	SOURCE		DETECTOR		ANGLE
			TYPE	RANGE	TYPE	RANGE	
G,N	ABX	11	D	11	BF3-I		4PI

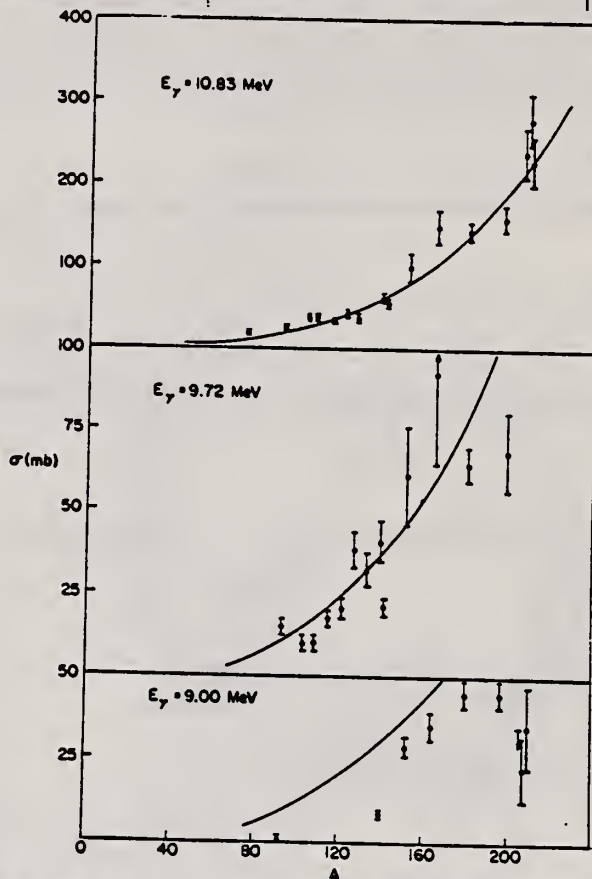


TABLE 1 Photoneutron cross sections (mb) Fig. 1. Cross section (in mb) versus mass number of the target for gamma-ray energies of 9.00, 9.72 and 10.83 MeV. The solid lines are plots of eq. (1) in the text.

Target	7.72 MeV	9.00 MeV	9.72 MeV	10.83 MeV
<sup>60</sup> Co				9.0 ± 0.8
<sup>75</sup> As				20.4 ± 1.7
<sup>93</sup> Nb		0.53 ± 0.10	14.6 ± 2.2	25.8 ± 2.1
<sup>103</sup> Rh			10.6 ± 1.7	38.8 ± 3.1
<sup>107</sup> Ag			10.0 ± 1.5	37.6 ± 2.9
<sup>109</sup> Ag			17.1 ± 2.6	33.3 ± 2.7
<sup>116</sup> In			20.7 ± 3.1	42.5 ± 3.6
<sup>121</sup> Sb			38.7 ± 5.8	38.8 ± 3.1
<sup>122</sup> Sb			31.7 ± 4.8	52.5 ± 3.8
<sup>127</sup> I			40.8 ± 6.5	63.0 ± 5.0
<sup>133</sup> Cs			21.5 ± 3.2	58.3 ± 4.1
<sup>138</sup> La		8.61 ± 0.86	61.3 ± 14.7	102 ± 18
<sup>141</sup> Pr		28.9 ± 3.2	92.2 ± 27.6	150 ± 20
<sup>151</sup> Eu			65.0 ± 5.5	146 ± 12
<sup>152</sup> Eu			68.4 ± 13.5	160 ± 15
<sup>180</sup> Ho	4.14 ± 0.36	35.6 ± 4.3		238 ± 29
<sup>181</sup> Ta		45.4 ± 3.7		280 ± 31
<sup>187</sup> Au		44.5 ± 3.6		226 ± 27
<sup>209</sup> Pb		<34.3		
<sup>209</sup> Pb		22.6 ± 11.3		
<sup>209</sup> Bi		36.1 ± 12.0		



REF.

H. Langhoff and M. Schumacher  
Phys. Rev. 155, 1246 (1967)

ELEM. STM.

A

L

As

75

33

METHOD

Resonance Fluorescence

REF. NO.

67 La 1

JDM

REACTION	RESULT	EXCITATION ENERGY	SOURCE		DETECTOR		ANGLE
			TYPE	RANGE	TYPE	RANGE	
G,G	LFT	1	D	1	NAI-D		DST

$$d\sigma/d\Omega = \sigma_0 [1 + A_2 P_2(\cos\theta)].$$

TABLE I. Results of the present investigation.

$E_\gamma$ (keV)	Spin	$A_2$	$\delta_{E1}/M_1$	$(g_2/g_1)\Gamma_2/\Gamma$ (eV)	$\Gamma_2/\Gamma$	$\tau_{level}$ (sec)
265	$\frac{1}{2}$	$0.14 \pm 0.05$	$-0.01 \pm 0.04$	$(3.62 \pm 0.20) \times 10^{-4}$	0.97	$(1.71 \pm 0.10) \times 10^{-10}$
280	$\frac{1}{2}$	$0.92 \pm 0.12$	$-0.42 \pm 0.08$	$(2.40 \pm 0.18) \times 10^{-4}$	0.99	$(4.02 \pm 0.30) \times 10^{-10}$

REF. W. J. Alston III, H. H. Wilson and E. C. Booth  
Nucl. Phys. A116, 281 (1968)

ELEM. SYM.	A	Z
As	75	33
REF. NO.		
68 Al 1		egf

METHOD						REF. NO.	
						68 Al 1	egf
REACTION	RESULT	EXCITATION ENERGY	SOURCE		DETECTOR		ANGLE
			TYPE	RANGE	TYPE	RANGE	
G,G	LFT	0 - 1	C	4	SCD-D	0-3	130
		(1.35)					

Angle greater than 90° for all measurements.

SELF-ABSORPTION

TABLE I  
Direct and absorption measurements of resonance fluorescence

Nucleus	$E_r$ (MeV)	$J_r$	$\Gamma_0/\Gamma$	$gW\Gamma_0\Gamma_0/\Gamma$ (meV)	Error (%)	This work $\Gamma_0$ (meV)	Other work $\Gamma_0$
<sup>55</sup> Mn	0.000	$\frac{1}{2}^-$					
	1.527	$(\frac{1}{2}^-)$	0.9	5.2 abs a)	25 40	8-12 8.0	
	1.884	?	0.82 b)	41 abs a)	25 10	50/gW 55/g	
	2.197	?	(0.8) c)	17 abs	25 20	21/gW 17/g	
	2.252	?	(0.9) c)	17 abs	25 20	19/gW 13/g	
	2.365	?	?	3.5	36	(2-6) $\Gamma/\Gamma_0$	
	2.564	?	(1.0)	50 abs a)	25 20	50/gW 61/g	
	2.751	?	?	6.7	42	6.7( $\Gamma/\Gamma_0$ )/gW	
	0.000	$\frac{7}{2}^-$					
	1.187	$(\frac{7}{2}^-)$	(1.0)	6.8 abs	25 25 a)	7.5 12	0.33(E2) <sup>d)</sup>
<sup>63</sup> Co		$(\frac{7}{2}^-)$	(1.0)	6.8 abs	25 25 a)	(5.4-6.5) 9.6	0.27(E2)
	0.000	$\frac{3}{2}^-$					
	1.414	$\frac{1}{2}^-$	?	1.6	30	(1.1-1.7) $\Gamma/\Gamma_0$	
<sup>67</sup> Ga	1.551	$\frac{3}{2}^-$	?	1.7	37	(1.7-2.5) $\Gamma/\Gamma_0$	0.1(E2) c)
	0.000	$\frac{3}{2}^-$					
<sup>75</sup> As	0.872	$(\frac{3}{2}^-)$	0.95	1.1	35	0.8/W	
	1.107	$(\frac{3}{2}^-)$	0.95	8.0	20	8.4/W	
	0.000	$\frac{1}{2}^-$					
<sup>89</sup> Y	0.86	?	?	1.7	20	1.7 $\Gamma/gW\Gamma_0$	
	1.07	?	?	2.6	30	2.6 $\Gamma/gW\Gamma_0$	
	1.35	?	?	3.6	20	3.6 $\Gamma/gW\Gamma_0$	
	0.000	$\frac{1}{2}^-$					
<sup>91</sup> Y	1.51	$\frac{3}{2}^-$	(1.0)	52 a) abs a)	30 15	28 22	0.37(E2) <sup>f)</sup>

a) Measured with NaI.

b) Ref. <sup>24)</sup>.

c) Measured with a Ge(Li) detector to  $\pm 10\%$ .

d) Ref. <sup>13)</sup>. e) Ref. <sup>14)</sup>. f) Ref. <sup>23)</sup>.

<sup>13</sup> D.G. Alkhazov, K.I. Erokhina and I.K. Lemberg, Izv. Akad.Nauk.SSSR(ser.fiz.) 28 (1964) 1667.

<sup>14</sup> B.G. Harvey, J.R. Meriwether and A.Bussiere, Nucl. Phys. 70 (1965) 305.

<sup>23</sup> G.A. Peterson and J.Alster, Phys. Rev. 166 (1968) 136.

<sup>24</sup> N. Nath, M.A. Rothman, D.M. Van Patter and C.E. Mandeville, Nucl. Phys. 13 (1959) 74.

REACTION	RESULT	EXCITATION ENERGY	SOURCE		DETECTOR		ANGLE
			TYPE	RANGE	TYPE	RANGE	
G <sub>1</sub> N	ABX	THR-30	D	10-30	BF3-I		4PI
G <sub>2</sub> N	ABX	THR-30	D	18-30	BF3-I		4PI

TABLE VI. Integrated cross sections.

Nucleus	$\sigma_{\text{tot}}[(\gamma, n) + (\gamma, pn)]$ (MeV-b) <sup>a</sup>	$\sigma_{\text{tot}}(\gamma, 2n)$ (MeV-b) <sup>a</sup>	$\frac{\sigma_{\text{tot}}(\gamma, 2n)}{\sigma_{\text{tot}}(\gamma, \text{total})}$ <sup>b</sup>	$\frac{1}{2}\pi\sigma_m\Gamma$ (MeV-b) <sup>c</sup>	$0.06(NZ/A)$ (MeV-b)
As <sup>75</sup>	0.69	0.22	0.24	1.13	1.11
Ag <sup>107</sup>	1.09	0.26	0.19	1.56	1.58
Cs <sup>133</sup>	1.48	0.50	0.25 <sup>d</sup>	2.27	1.94

<sup>a</sup> All measured integrated cross-section values are given for an energy region from threshold to 29.5 MeV.

<sup>b</sup> The word "total" in this table refers to the total photoneutron cross section  $\sigma[(\gamma, n) + (\gamma, pn) + (\gamma, 2n) + (\gamma, 3n)]$ , and excludes the  $(\gamma, \gamma)$  and  $(\gamma, p)$  cross sections.

<sup>c</sup> For As<sup>75</sup> and Ag<sup>107</sup>, the quantity tabulated is  $\frac{1}{2}\pi(\sigma_m(1)\Gamma(1) + \sigma_m(2)\Gamma(2))$ .

<sup>d</sup> This value includes the contribution of  $\sigma_{\text{tot}}(\gamma, 3n)$ , which equals 0.01 MeV-b from threshold to 29.5 MeV.

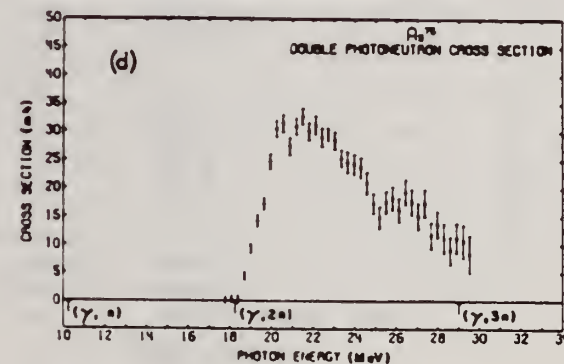
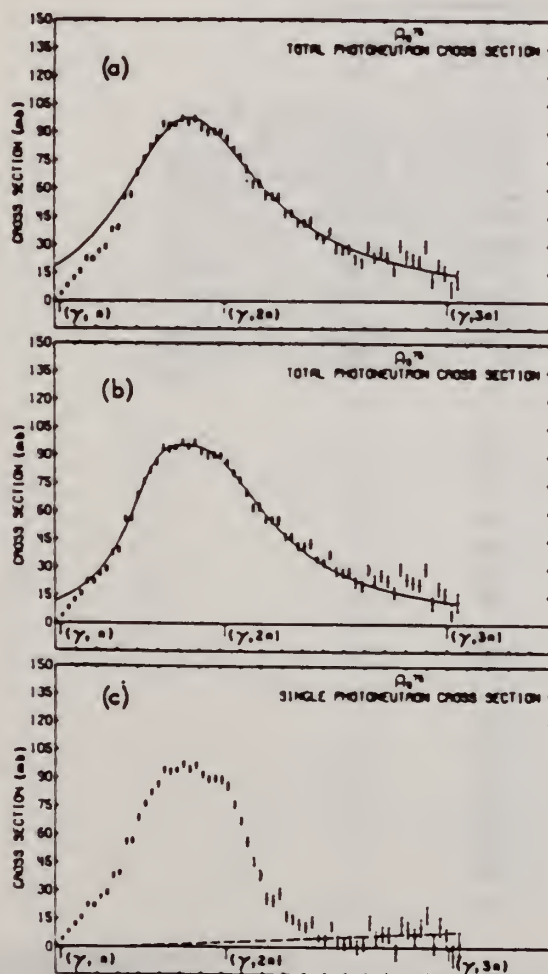


FIG. 5. Photoneutron cross sections for As<sup>75</sup>. (a) Total photoneutron cross section  $\sigma[(\gamma, n) + (\gamma, pn) + (\gamma, 2n)]$ . The solid line is a single-component Lorentz-curve fit to the giant-resonance data (13.6 to 21.3 MeV). (b) Total photoneutron cross section, repeated. The solid line is a two-component Lorentz-curve fit to the giant-resonance data. (c) Single photoneutron cross section  $\sigma[(\gamma, n) + (\gamma, pn)]$ . The dashed line represents the maximum systematic error owing to the uncertainty in the normalization of the positron bremsstrahlung subtraction. (d) Double photoneutron cross section  $\sigma(\gamma, 2n)$ .



ELEM. SYM.	A	Z
As	75	33
REF. NO.		
69 Mo 3		hmg

METHOD		REF. NO.			
		69 Mo 3		hmg	
REACTION	RESULT	EXCITATION ENERGY	SOURCE		ANGLE
			TYPE	RANGE	
G, G	ABX	8	D	8	DST

Elastic and inelastic nuclear resonant scattering of monochromatic photons from  $^{75}\text{As}$  have been studied using a 47-cc Ge(Li) detector. The  $\gamma$  source was provided by thermal-neutron capture in iron. The energy of the resonance level in  $^{75}\text{As}$  was found to be 7.646 MeV. Assuming the high-energy lines to be primary transitions deexciting the resonance level, 25 energy levels were found from the ground state up to 2.6 MeV, seven of which may be identified with recently reported levels. By measuring the angular distribution of the scattered radiation, the spin of the scattering level was determined to be  $\frac{1}{2}$  and the spins of 14 low-lying levels were thus found to be either  $\frac{1}{2}$  or  $\frac{3}{2}$ . The total radiative width of the resonance level was determined and was found to be  $\Gamma = 0.36 \pm 0.10$  eV and  $\Gamma_0/\Gamma = 0.11$ . The  $^{75}\text{As}$  levels are compared with the predictions of the Coriolis coupling model.

J-PI, G-WIDTH, 7.646

TABLE I.  $\gamma$  energies and level energies in  $^{75}\text{As}$  from  $(\gamma, \gamma')$  reaction. The level energies are obtained by assuming that the  $\gamma$  lines are emitted in primary transitions. The branching ratios of the decay of the 7.646-MeV level are given. Line energies are accurate to  $\pm 4$  keV. Branching ratios of the strong intensity lines are accurate to  $\pm 8\%$ . The existence of  $\gamma$  lines and levels in parentheses is uncertain.

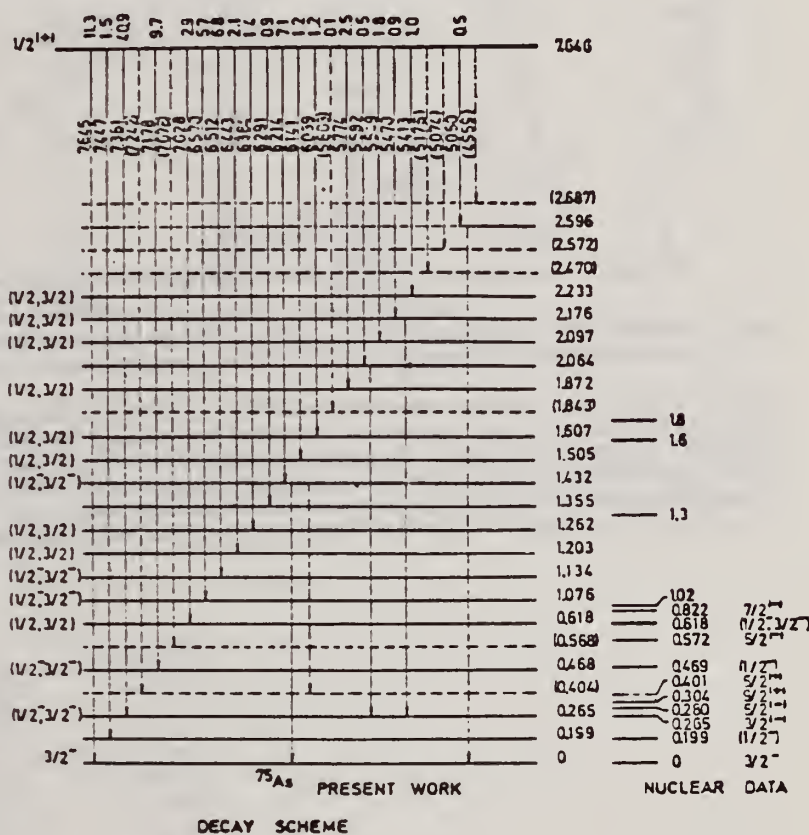
$\gamma$ energy (MeV)	Branching ratio (%)	Level energies (MeV)	
		Present work	Ref. 5
7.646	11.3	0	0
7.447	1.5	0.199	0.199
7.381	40.9	0.265	0.265
...	...	...	0.280
...	...	...	0.304
(7.242)	...	(0.404)	0.401
7.178	9.7	0.468	0.469
(7.078)	...	(0.568)	0.572
7.028	2.9	0.618	0.618
...	...	...	0.822
...	...	...	1.021
6.570	5.7	1.076	...
6.512	6.8	1.134	...
6.443	2.1	1.203	...
6.384	1.4	1.262	...
...	...	...	1.3
6.291	0.9	1.355	...
6.214	7.1	1.432	...
6.141	1.2	1.505	...
6.039	1.2	1.607	1.6
...	...	...	1.8
(5.803)	0.1	(1.843)	...
5.774	2.5	1.872	...
5.582	0.5	2.064	...
5.549	1.8	2.097	...
5.470	0.9	2.176	...
5.413	1.0	2.233	...
(5.176)	...	(2.470)	...
(5.074)	...	(2.572)	...
5.050	0.5	2.596	...
(4.959)	...	(2.687)	...
2.596	...	...	...
1.911	...	...	...
1.799	...	...	...
1.432	...	...	...
1.028	...	...	...

[over]

TABLE II. Partial radiation widths  $\Gamma_\gamma$  and  $E1$  and  $M1$  radiation strengths of intense transitions from the 7.646-MeV resonance state; the most probable spins and parities are also given where values in parentheses indicate uncertain determinations. The level spacing  $D$  was taken to be 750 eV.

Transition energy (MeV)	Level energy (MeV)	Spin and parity	$\Gamma_\gamma \times 10^3$ (eV)	$k_{E1} \times 10^9$ (MeV) $^{-1}$	$k_{M1} \times 10^9$ (MeV) $^{-1}$
7.646	0	$\frac{1}{2}^-$	41	6.8	121
7.381	0.265	$(\frac{1}{2}^-, \frac{1}{2}^-)$	147	27.5	488
7.173	0.463	$(\frac{1}{2}^-, \frac{1}{2}^-)$	35	7.1	126
7.028	0.618	$(\frac{1}{2}^-, \frac{1}{2}^-)$	10	2.3	40
6.870	1.076	$(\frac{1}{2}^-, \frac{1}{2}^-)$	21	5.4	97
6.812	1.134	$(\frac{1}{2}^-, \frac{1}{2}^-)$	25	6.6	118
6.443	1.203	$(\frac{1}{2}^-, \frac{1}{2}^-)$	8	2.1	38
6.384	1.262	$(\frac{1}{2}^-, \frac{1}{2}^-)$	5	1.5	26
6.214	1.432	$(\frac{1}{2}^-, \frac{1}{2}^-)$	26	8.0	142
6.141	1.505	$(\frac{1}{2}^-, \frac{1}{2}^-)$	4	1.4	25
6.039	1.607	$(\frac{1}{2}^-, \frac{1}{2}^-)$	4	1.5	26
5.774	1.872	$(\frac{1}{2}^-, \frac{1}{2}^-)$	9	3.5	62
5.549	2.097	$(\frac{1}{2}^-, \frac{1}{2}^-)$	7	2.8	51
5.470	2.176	$(\frac{1}{2}^-, \frac{1}{2}^-)$	3	1.5	26
5.413	2.233	$(\frac{1}{2}^-, \frac{1}{2}^-)$	4	1.7	30
	7.646	$\frac{1}{2}^-(\gamma)$			

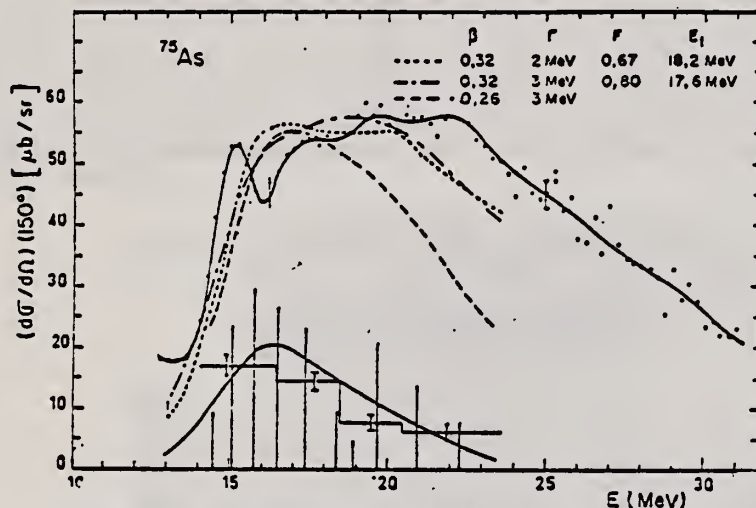
FIG. 4. Decay scheme of 7.646-MeV level of  $^{75}\text{As}$  showing level energies and corresponding branching ratios as constructed by assuming that all high-energy  $\gamma$  lines in the scattered spectrum are emitted in primary transitions; broken lines indicate uncertain transitions and hence uncertain levels. Most probable spin and parities for some levels, assigned in the present work, are given where assignments in parentheses are uncertain. For comparison, the energy-level diagram as reported in Ref. 5 is also shown.





ELEM. SYM.	A	Z
As	75	33
REF. NO.		
70 Ar 1		egf

REACTION	RESULT	EXCITATION ENERGY	SOURCE		DETECTOR		ANGLE
			TYPE	RANGE	TYPE	RANGE	
G,G	ABX	12-30	C	32	NAI	12-30	DST



GETS G,G/ TO 2+

Fig. 7. Differential total scattering cross section at 150° for  $^{75}\text{As}$ . See caption for fig. 4. In particular is shown the influence of parameter  $\beta$  on the shape of the scattering cross section.

Fig. 4. Differential total scattering cross section at 150° for natural Ti. The full curve through experimental points is only a guide for the eyes. The vertical bars represent the relative strength of dipole levels calculated by the D.C.M. with parameters of table 1. Theoretical elastic plus inelastic scattering is computed from these levels with a common width  $\Gamma$  (dashed curve). Experimental inelastic scattering (histogram) and theoretical inelastic scattering to the first  $2^+$  (full curve) are shown in the lower part of the figure. Open circles give the cross section after background subtraction.

TABLE 4  
Integrated inelastic scattering cross section

Nucleus	Limits of integration (in MeV)	Experimental <sup>a)</sup> $\int \sigma_i(E) dE$ (MeV · $\mu\text{b}$ )	$2^+$	Theoretical <sup>a)</sup> $2^+$ (MeV · $\mu\text{b}$ )	Total
Ti( $^{48}\text{Ti}$ )	16 - 24	$250 \pm 50$	425	109	534
$^{51}\text{V}$ ( $^{52}\text{Cr}$ )	16.4 - 24.9	$492 \pm 50$	509	116	579
Cr	16.4 - 23.4	$431 \pm 60$	509	116	579
$^{75}\text{As}$ ( $^{76}\text{Se}$ )	14.1 - 23.6	$1254 \pm 120$	1373	414	1787
Se( $^{80}\text{Se}$ )	14.1 - 24.6	$1035 \pm 100$	1066	353	1419
$^{89}\text{Y}$					364
Cd( $^{112}\text{Cd}$ )	13.6 - 23.3	$3264 \pm 240$	1894	370	2264
In( $^{114}\text{Cd}$ )	13.6 - 23.6	$2840 \pm 220$	2173	388	2561
Sn( $^{116}\text{Sn}$ )	14.2 - 24.2	$2363 \pm 220$			643

<sup>a)</sup> We assume an angular distribution of the form  $1 + \frac{1}{3} \cos^2 \theta$ .

ELEM. SYM.	A	Z
As	75	33
REF. NO.		hmg
70 Mo 2		

REACTION	RESULT	EXCITATION ENERGY	SOURCE		DETECTOR		ANGLE
			TYPE	RANGE	TYPE	RANGE	
G,G	ABX	8	D	8	SCD-D		DST
		(7.646)		(7.646)			

8 = 7.646, LFT

TABLE III. Summary of the results of spins, parities, and total widths of resonance levels excited by  $\gamma$  rays obtained from neutron capture in iron. Parities in parentheses are uncertain.

Isotope	Energy (MeV)	$\delta =  E_r - E_g $ (eV)	$J^\pi_r$	$J^\pi_g$	Transition	$\Gamma_0/\Gamma_\gamma$ ( $\pm 8\%$ )	$\Gamma_\gamma$ ( $10^{-3}$ eV)
$^{56}\text{Cr}$	8.338	$18 \pm 1$	$0^+$	1	...	0.90	$750 \pm 200$
$^{62}\text{Ni}$	7.646	$14 \pm 1$	$0^+$	$1^-$	E1	0.64	$480 \pm 50$
$^{74}\text{Ge}$	6.013	$4.5 \pm 0.5$	$0^+$	$1^-$	E1	0.19	$120 \pm 15$
$^{75}\text{As}$	7.646	$7.4 \pm 0.3$	$3/2^-$	$1/2^+ (?)$	...	0.11	$360 \pm 100$
$^{109}\text{Ag}$	7.632	$9 \pm 1$	$1/2^-$	$3/2$	...	0.7	$2 \pm 1$
$^{112}\text{Cd}$	7.632	$4.8 \pm 0.4$	$0^+$	$1^-$	E1	0.55	$86 \pm 15$
$^{133}\text{La}$	6.013	$8.2 \pm 0.6$	$7/2^+$	$7/2^-$	E1	0.50	$51^{+14}_{-4}$
$^{141}\text{Pr}$	7.632	$11.4^{+3.3}_{-1.3}$	$5/2^+$	$5/2^+$	M1	0.46	$72^{+14}_{-4}$
$^{205}\text{Tl}$	7.646	$9.3 \pm 0.3$	$1/2^+$	$1/2^+ (?)$	...	0.58	$980 \pm 90$
$^{208}\text{Pb}$	7.279	$7.1 \pm 0.3$	$0^+$	$1^+$	M1	1.00	$780 \pm 60$

TABLE IV. Effective elastic scattering cross section  $\langle \sigma_r \rangle = \sigma_0^2 (\Gamma_0/\Gamma_\gamma) \psi(x_0, t_0)$ , where  $\delta$ ,  $J$ ,  $\Gamma_0$ ,  $\Gamma_\gamma$  were taken from Table III. The temperature of the scatterer was 300°K, while that of the iron  $\gamma$  source was 640°K.

Target	Resonance energy (MeV)	$\langle \sigma_r \rangle$ (mb)
$^{56}\text{Cr}$	8.333	905
$^{62}\text{Ni}$	7.646	569
$^{74}\text{Ge}$	6.013	61
$^{75}\text{As}$	7.646	4.4
$^{109}\text{Ag}$	7.632	3.5
$^{112}\text{Cd}$	7.632	193
$^{133}\text{La}$	6.018	39
$^{141}\text{Pr}$	7.632	20
$^{205}\text{Tl}$	7.646	574
$^{208}\text{Pb}$	7.279	5560

METHOD

REF. NO.

71 Ku 2

egf

REACTION	RESULT	EXCITATION ENERGY	SOURCE		DETECTOR		ANGLE
			TYPE	RANGE	TYPE	RANGE	
G, SPL	ABY	THR-999	C	900	ACT- I		4PI

$\sigma_q(A, Z) = K \exp [PA - R(A - SZ + TZ^2)^2]$ , cross section per equivalent quantum.

999 = 1.5 GEV

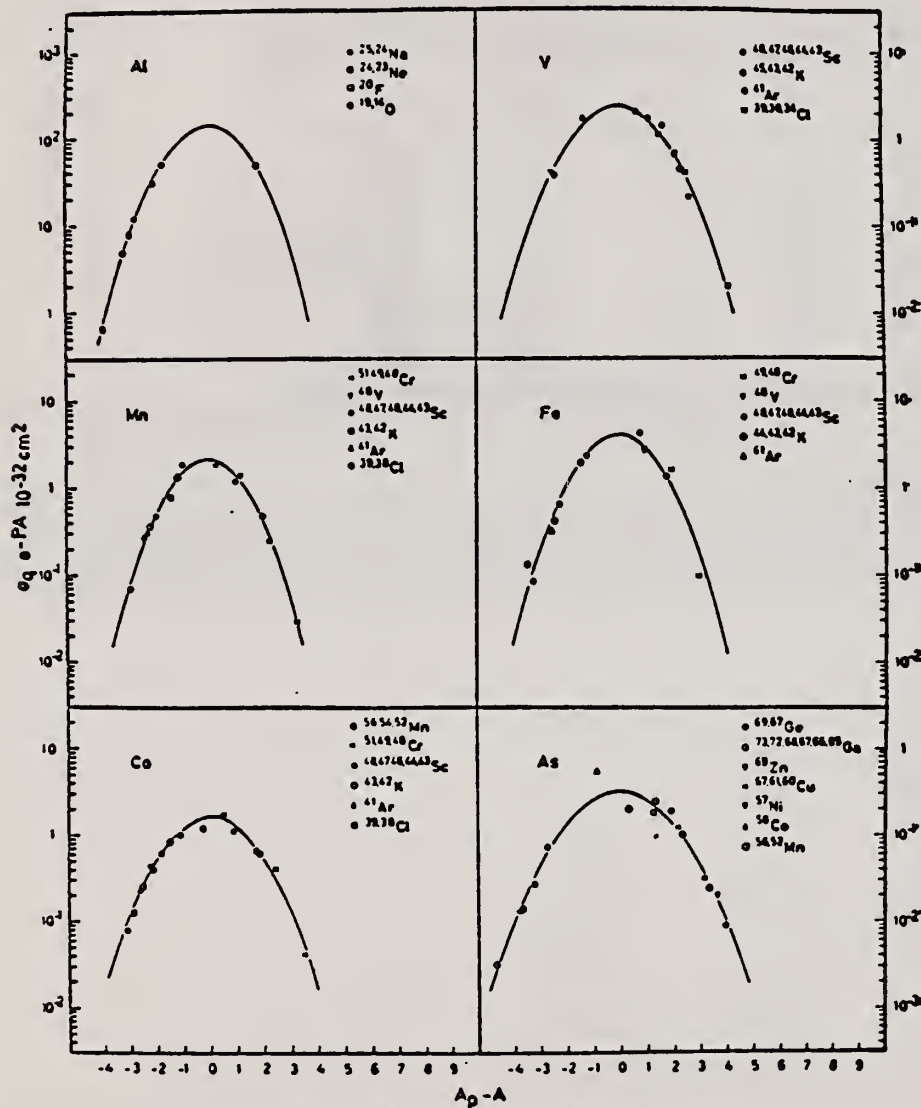


Fig. 4. Yield distributions from various targets with bremsstrahlung of 1.5 GeV.

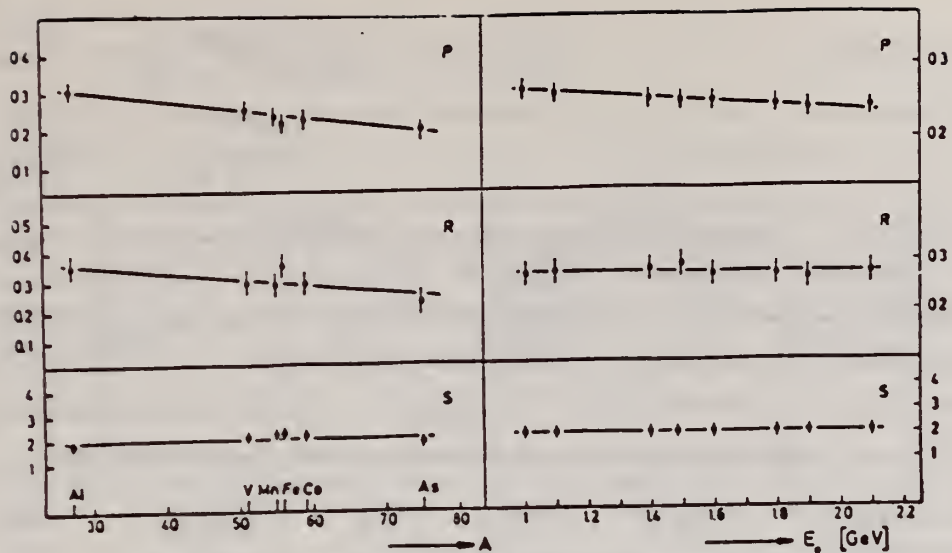


Fig. 6. Behaviour of the parameters  $P$ ,  $R$  and  $S$  as functions of  $A$  and  $E_0$ .

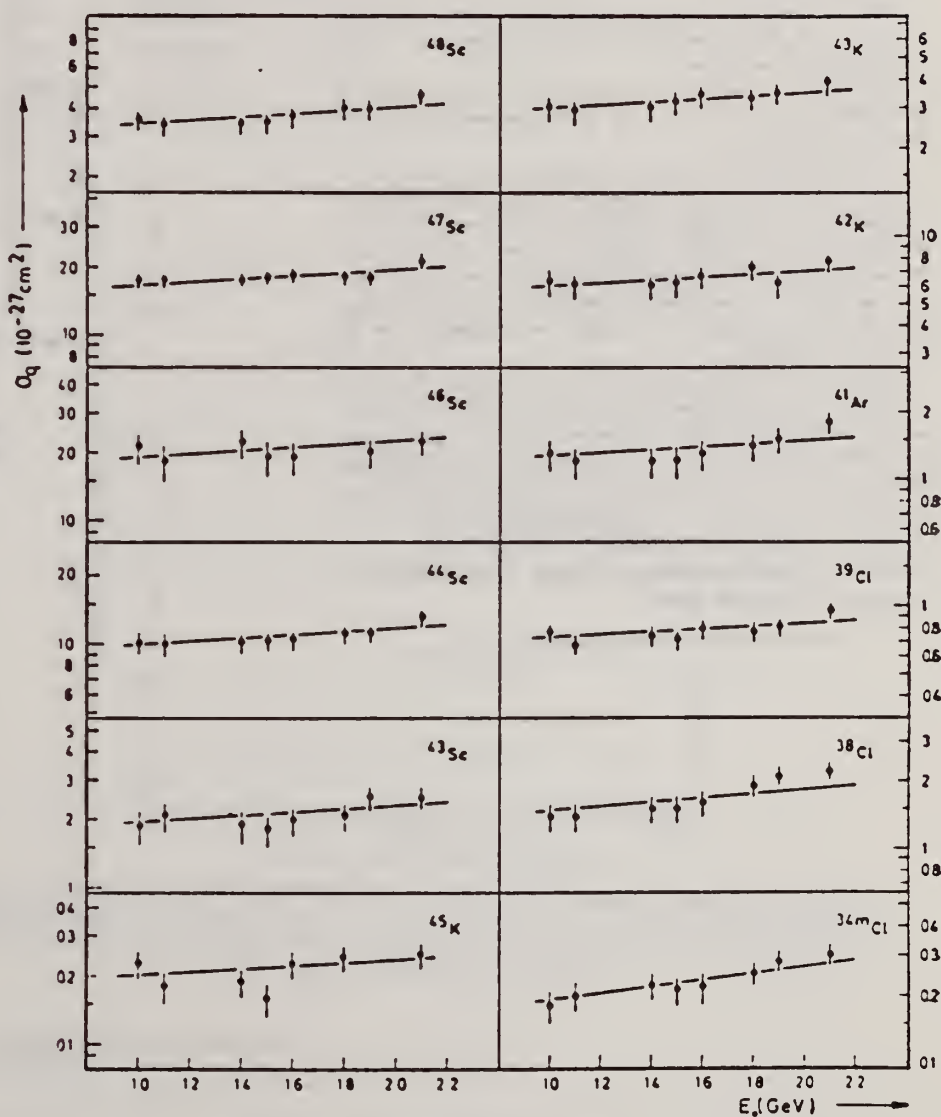


Fig. 5. Yields of spallation products using vanadium targets.



REACTION	RESULT	EXCITATION ENERGY	SOURCE		DETECTOR		ANGLE
			TYPE	RANGE	TYPE	RANGE	
G,N	ABY	10-68	C	10-68	ACT-I		4PI

Nippon Kagaku Zasshi, 92, 164~168(1971)

The Yields of Radioactivities Induced by ( $\gamma, n$ ) Reactions  
with Bremsstrahlung up to 68 MeV

by Tatsuya SAITO

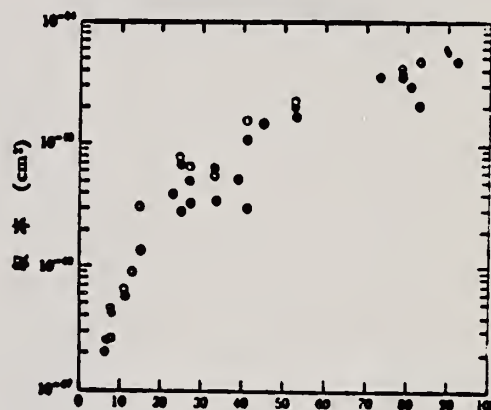
The ( $\gamma, n$ ) yields of 12 target nuclides have been measured at 10, 13, 16, 30, 45 and 68 MeV bremsstrahlung by observing the induced activities.

The energy dependence of the yields has been investigated extensively in the same way as in the previous work at 20 MeV bremsstrahlung.

In the case of heavy nuclides, the yields rise greatly as a function of maximum bombarding energy up to 20 MeV, and rise gradually from 20 MeV up to 68 MeV. However, in the case of light nuclides, the yields rise greatly up to 30 MeV, because the neutron separation energies of light ones are larger than those of heavy ones, and the bremsstrahlung spectrum covers the giant resonance and so the yields rise gradually from 30 MeV up to 68 MeV.

The yields have approximately been estimated from the parameter of the giant resonance, that is the peak cross section and the half width, in order to compare with the experimental data. As a result, the experimental data of light nuclides and heavy ones are nearly in agreement with the estimated data of Nathans et al., Johns et al. and Montalbetti et al., but those of medium weight ones are relatively lower values.

Department of Chemistry, Faculty of Science, Tohoku University,  
Katahira-cho, Sendai-shi, Japan



原子番号

●: 実験値, ⊕: Johns ら,  
⊙: Nathans ら, ○: Montalbetti ら

図 4 ( $\gamma, n$ ) 反応の収率の比較



METHOD

REF. NO.

75 Er 2

egf

REACTION	RESULT	EXCITATION ENERGY	SOURCE		DETECTOR		ANGLE
			TYPE	RANGE	TYPE	RANGE	
G, SC44	ABY	THR-800	C	250-800	ACT-I		4PI

TABLE 2

Comparison between experimental and calculated cross sections and isomeric ratios

Target	$\sigma_{exp}$ (mb)	$\sigma_{MC}$ (mb)	$\sigma_{sg}$ (mb)	$\sigma(m)/\sigma(g)_{exp}$	$\sigma(m)/\sigma(g)_{calc}$	ISOMER RATIO
	250-800 MeV	400 MeV	250-800 MeV	250-800 MeV	400 MeV	
<sup>44</sup> Sc	$\approx 0.5$	$0.58 \pm 0.05$		$\approx 0$	0.05	
<sup>51</sup> V	$\approx 0.5$	$0.48 \pm 0.05$	0.47	0.7	0.72	
<sup>55</sup> Mn	$0.40 \pm 0.14$	$0.59 \pm 0.05$	0.28	$1.08 \pm 0.04$	1.04	
Fe	$0.40 \pm 0.14$		0.26	$1.00 \pm 0.05$		
<sup>59</sup> Co	$0.26 \pm 0.10$	$0.34 \pm 0.04$	0.18	$1.26 \pm 0.06$	1.12	
<sup>73</sup> As		$0.65 \pm 0.07^*)$	0.044	$1.9 \pm 0.3$	$1.15^*)$	

\*) 325 MeV.

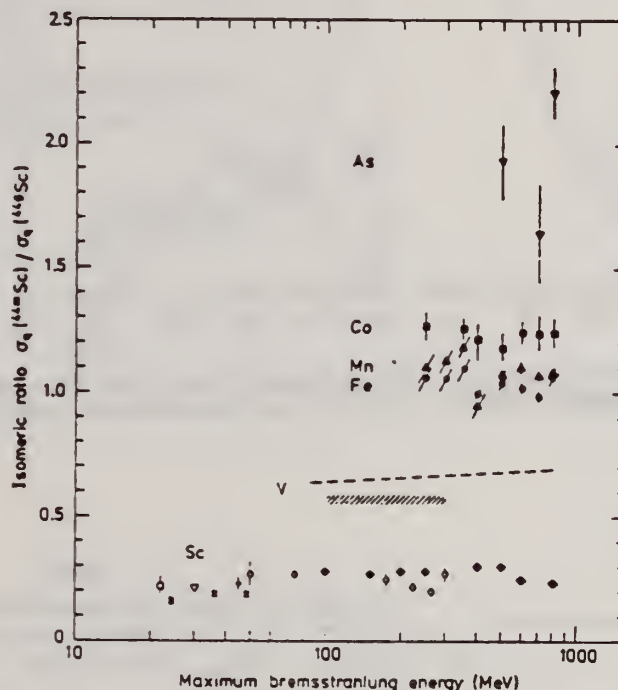


Fig. 6. Isomeric ratio  $\sigma_g(^{44m}\text{Sc}) / \sigma_g(^{44g}\text{Sc})$  versus bremsstrahlung end-point energy for the different targets. Sc target:  $\diamond$  - this work,  $\square$  - ref. <sup>15</sup>,  $\times$  - ref. <sup>16</sup>,  $\nabla$  - ref. <sup>17</sup>,  $+$  - ref. <sup>18</sup>,  $\circ$  - ref. <sup>19</sup>; V target: dashed curve - ref. <sup>20</sup>, dashed area - ref. <sup>21</sup>; Fe target:  $\bullet$  - this work; Mn target:  $\blacktriangle$  - this work; Co target:  $\blacksquare$  - this work; As target:  $\blacktriangledown$  - this work.

- 15) S. A. Steinberg, B. Sc. thesis, Univ. of Illinois, 1963, unpublished (value taken from ref. <sup>17</sup>)
- 16) J. R. Tatarczuk and H. A. Medicus, Phys. Rev. 143 (1966) 815
- 17) T. Kato and Y. Oka, Talanta 19 (1972) 515
- 18) R. Völpe, Nucl. Phys. A182 (1972) 411
- 19) W. B. Walters and J. P. Hummel, Phys. Rev. 150 (1966) 367
- 20) B. Bülow, Lund, private communication (preliminary results)
- 21) R. A. Meyer, thesis, Univ. of Illinois, 1963, unpublished

ELEM. SYM.	A	Z
As	75	33
REF. NO.		egf
76 Ca 1		

REACTION	RESULT	EXCITATION ENERGY	SOURCE		DETECTOR		ANGLE
			TYPE	RANGE	TYPE	RANGE	
G,N	ABX	10- 26	D	10- 26	MOD-I		4PI
G,2N	ABX	18- 26	D	10- 26	MOD-I		4PI

987+

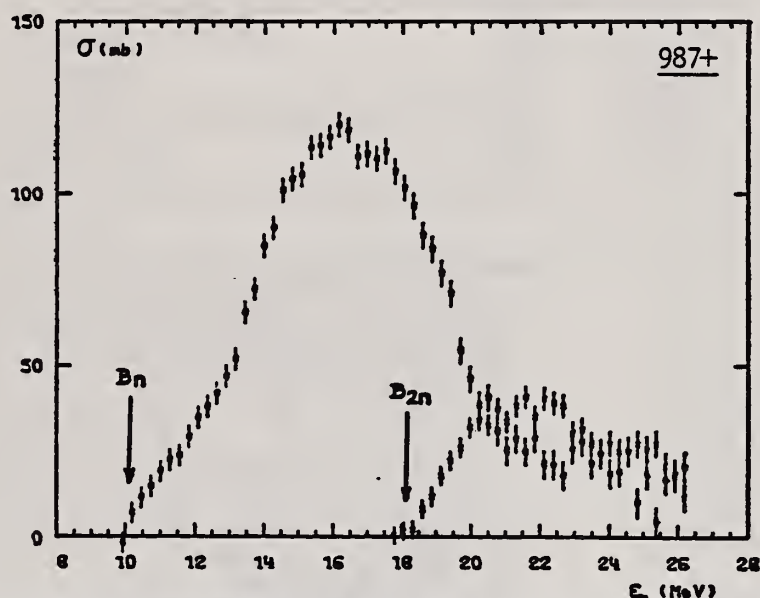


Fig. 7. Partial photoneutron cross sections  $[\sigma(\gamma, n) + \sigma(\gamma, pn)]$  and  $\sigma(\gamma, 2n)$  for  $^{75}\text{As}$ . Arrows  $B_n$  and  $B_{2n}$  indicate theoretical threshold values for  $(\gamma, n)$  and  $(\gamma, 2n)$  reactions respectively.

TABLE 3  
Integrated photoneutron cross sections and comparison with sum rules

Nucleus	$^{64}\text{Zn}$	$^{69}\text{Ga}$ $^{71}\text{Ga}$	$^{70}\text{Ge}$	$^{73}\text{Ge}$	$^{74}\text{Ge}$	$^{76}\text{Ge}$	$^{75}\text{As}$	$^{76}\text{Se}$	$^{78}\text{Se}$	$^{80}\text{Se}$	$^{82}\text{Se}$
$E_M$ (MeV)	29	26.5	26.5	26.5	26.5	26.5	26.5	26.5	26.5	26.5	26.5
$\sigma_{0n}$ (MeV · b)	0.75	0.91	0.78	0.94	1.02	1.12	1.09	1.01	1.06	1.11	1.13
$\frac{\sigma_{0n} A}{0.06 NZ}$	0.78	0.87	0.75	0.88	0.94	1	0.98	0.90	0.92	0.94	0.95
$B_n - B_p$ (MeV)	4.2	$\begin{Bmatrix} 3.7 \\ 1.4 \end{Bmatrix}$	3	1	-0.8	-2.6	3.3	1.7	0.1	-1.5	-3
$\sigma_{-1n}$ (mb)	38	52	44	54	59	64	63	58	62	65	67
$\sigma_{-1n} A^{-1/2}$ (mb)	0.15	0.18	0.15	0.18	0.19	0.20	0.20	0.18	0.19	0.19	0.19
$\sigma_{-2n}$ (mb · MeV $^{-1}$ )	2.0	3.1	2.5	3.2	3.6	3.9	3.7	3.4	3.8	3.9	4.2
$\sigma_{-2n} A^{-1/2}$ ( $\mu\text{b} \cdot \text{MeV}^{-1}$ )	1.9	2.6	2.1	2.6	2.8	2.9	2.8	2.5	2.7	2.6	2.7

FORM N (REV. 7. USCOM) The notation used is defined in the text. The average experimental errors  $\Delta\sigma_{0n}/\sigma_{0n}$ ,  $\Delta\sigma_{-1n}/\sigma_{-1n}$  and  $\Delta\sigma_{-2n}/\sigma_{-2n}$  are approximately 8%. 88

REF. Y. Cauchois, H. Ben Abdelaziz, R. Khérouf, C. Schloesing-Möller  
J. Phys. G7, 1539 (1981)

ELEM. SYM.	A	Z
As	75	33
REF. NO.		hg
81 Ca 2		

METHOD

REACTION	RESULT	EXCITATION ENERGY	SOURCE		DETECTOR		ANGLE
			TYPE	RANGE	TYPE	RANGE	
G,G	LFT	0 - 2	C	0 - 2	SCD-D		
		(.572 - 1.370)					

# 7 LEVELS, .57-1.37MEV

**Abstract.** Lifetimes of 49 excited states below 1.65 MeV have been measured in <sup>24</sup>Mg, <sup>27</sup>Al, <sup>48</sup>Ti, <sup>58</sup>Ni, <sup>59</sup>Co, <sup>61,62</sup>Ni, <sup>63,65</sup>Cu, <sup>64,66,68</sup>Zn, <sup>75</sup>As, <sup>103</sup>Rh, <sup>113,115</sup>In, <sup>116,118,120</sup>Sn and <sup>121,123</sup>Sb by means of nuclear resonance fluorescence experiments. The levels are excited by bremsstrahlung x-ray photons. The self-absorption technique applied to suitable cases provides nuclear absorption cross sections, widths and lifetimes from which the x-ray spectral distributions are also obtained. Scattering experiments are performed for all other cases in order to obtain widths and lifetimes from these x-ray photon curves. The Compton effect in the sample is taken into account. Self-absorption provides  $g\Gamma_0$  from which  $\Gamma$  is deduced using adopted  $J^\pi$  and  $\Gamma_0/\Gamma$  values; scattering provides  $u = g(\Gamma_0^2/\Gamma)W(\theta)$  from which  $\Gamma$  is also deduced with  $J$ ,  $\Gamma_0/\Gamma$  and mixing ratios taken from the literature. Thanks to simultaneous determination of the x-ray spectra all the lifetimes as given by our programs with their statistical errors form an unusually coherent set of values.

NUCLEAR REACTIONS ( $\gamma, \gamma$ ), bremsstrahlung excitation; natural isotopes: <sup>24</sup>Mg, <sup>27</sup>Al, <sup>48</sup>Ti, <sup>58</sup>Ni, <sup>59</sup>Co, <sup>61,62</sup>Ni, <sup>63,65</sup>Cu, <sup>64,66,68</sup>Zn, <sup>75</sup>As, <sup>103</sup>Rh, <sup>113,115</sup>In, <sup>116,118,120</sup>Sn and <sup>121,123</sup>Sb;  $E \approx 0.5-1.65$  MeV; measured  $g\Gamma_0$  or  $g(\Gamma_0^2/\Gamma)W(\theta)$ ; deduced  $T_{1/2}$ .

(OVER)



Tableau 3. Résultats des mesures des niveaux étudiés par diffusion.

Table 3. Results obtained using the diffusion method.

Isotope	Energie (keV)	$J^\pi$	$J_0^\pi$	$\Gamma_0/\Gamma$	$\delta$	$u = g(\Gamma_0^2/\Gamma)W(\theta)$ (meV)	$\tau$ (ps) ce travail	$\tau_{ref}$ (ps)	Références†
<sup>24</sup> Mg	1368.59(4)	2 <sup>+</sup>	0 <sup>+</sup>	1	E2	1.08(13)	1.76(21)	1.98(4)	Endt et van der Leun (1978)
<sup>27</sup> Al	1014.45(3)	$\frac{1}{2}^+$	$\frac{1}{2}^+$	0.971	+0.351(12)	0.186(13)	2.20(16)	2.12(8)	Endt et van der Leun (1978)
<sup>48</sup> Ti	983.512(3)	2 <sup>+</sup>	0 <sup>+</sup>	1	E2	0.282(23)	6.74(55)	6.1(13)	Been (1978)
<sup>58</sup> Ni	1454.45(15)	2 <sup>+</sup>	0 <sup>+</sup>	1	E2	2.11(26)	0.90(11)	0.92(3)	Kocher et Auble (1976)
<sup>59</sup> Co	1099.224(25)	$\frac{1}{2}^-$	$\frac{1}{2}^-$	1	(E2)	0.069(8)	4.79(55)	3.17(58)	Kim (1976)
<sup>59</sup> Co	1458.8(3)	$\frac{1}{2}^-$	$\frac{1}{2}^-$	0.91	(E2)	0.68(8)	1.17(14)	1.52(16)	Kim (1976)
<sup>59</sup> Co	1480.9(3)	$\frac{1}{2}^-$	$\frac{1}{2}^-$	0.8	<0.35 <sup>a</sup>	1.23(15)	0.254(31)	0.31(3)	Kim (1976)
<sup>61</sup> Ni	1185.7(6)	$\frac{1}{2}^-$	$\frac{1}{2}^-$	0.77(8) <sup>i</sup>	0.14	1.88(49)	0.21(5)	0.16(3)	Andreev et al (1974)
<sup>62</sup> Ni	1172.91(9)	2 <sup>+</sup>	0 <sup>+</sup>	1	E2	0.88(17)	2.15(42)	2.09(3)	Halbert (1979a)
<sup>63</sup> Cu	1327.00(7)	$\frac{1}{2}^-$	$\frac{1}{2}^-$	0.84	(E2)	1.04(14)	0.84(11)	0.88(4)	Auble (1979b)
<sup>63</sup> Cu	1412.05(4)	$\frac{1}{2}^-$	$\frac{1}{2}^-$	0.72	+0.61(-0.8)	0.260(38)	1.90(28)	1.61(3)	Auble (1979b)
<sup>66</sup> Zn	991.54(7)	2 <sup>+</sup>	0 <sup>+</sup>	1	E2	0.640(54)	2.97(25)	2.60(13)	Halbert (1979b)
<sup>65</sup> Cu	1481.83(5)	$\frac{1}{2}^-$	$\frac{1}{2}^-$	0.85	(E2)	1.13(19)	0.79(13)	0.49(5)	Auble (1975a)
<sup>66</sup> Zn	1039.37(6)	2 <sup>+</sup>	0 <sup>+</sup>	1	E2	0.70(6)	2.71(23)	2.25(15)	Auble (1975b)
<sup>68</sup> Zn	1077.38(5)	2 <sup>+</sup>	0 <sup>+</sup>	1	E2	0.70(6)	2.71(23)	2.34(23)	Lewis (1975)
<sup>75</sup> As	572.5(10)	$\frac{1}{2}^-$	$\frac{1}{2}^-$	1 <sup>d</sup>	0.39 <sup>b</sup>	0.236(26)	4.14(46)	3.5(9)	Horen et Lewis (1975)
<sup>75</sup> As	823.0(10)	$\frac{1}{2}^-$	$\frac{1}{2}^-$	0.86 <sup>d</sup>	(E2)	0.214(22)	4.27(43)	3.5(3)	Robinson et al (1967)
<sup>75</sup> As	865.5(10)	$\frac{1}{2}^-$	$\frac{1}{2}^-$	0.83 <sup>d</sup>	— <sup>c</sup>	0.78(6)	0.863(68)	0.60(12)	Celliers et al (1977)
<sup>75</sup> As	1076.0(10)	$\frac{1}{2}^-$	$\frac{1}{2}^-$	0.94 <sup>d</sup>	0.38 <sup>d</sup>	1.97(13)	0.287(19)	0.32(7)	Celliers et al (1977)
<sup>75</sup> As	1128.5(10)	$\frac{1}{2}^-$	$\frac{1}{2}^-$	1	E1 <sup>d</sup>	0.224(24)	1.47(16)	—	
<sup>75</sup> As	1349.0(10)	$\frac{1}{2}^-$	$\frac{1}{2}^-$	0.67 <sup>d</sup>	0.20 <sup>d</sup>	1.61(29)	0.180(32)	0.12(3)	Wilson (1970)
<sup>75</sup> As	1370.0(10)	$\frac{1}{2}^-$	$\frac{1}{2}^-$	0.47 <sup>d</sup>	0.47 <sup>d</sup>	0.64(13)	0.218(44)	—	
<sup>103</sup> Rh	803.1(2)	$\frac{1}{2}^-$	$\frac{1}{2}^-$	0.70	M1	1.85(16)	0.174(15)	—	Harmatz (1979)
<sup>103</sup> Rh	1277.0(2)	$\frac{1}{2}^-$	$\frac{1}{2}^-$	0.75	-0.62(30) <sup>e</sup>	0.81(9)	0.87(10)	1.3(9)	Harmatz (1979)
<sup>113</sup> In	1177(1)	$\frac{1}{2}^-$	$\frac{1}{2}^-$	1	+0.5(2)	9.1(8)	0.086(8)	0.10(6)	Tuttle et al (1976)
<sup>113</sup> In	1510(1)	$\frac{1}{2}^-$	$\frac{1}{2}^-$	0.935	-0.5(-0.1)	6.4(9)	0.071(10)	0.11(-0.3)	Tuttle et al (1976)
<sup>113</sup> In	1077.7(10)	$\frac{1}{2}^-$	$\frac{1}{2}^-$	0.81 <sup>j</sup>	(E2)	0.159(24)	1.61(24)	1.23(7)	Tuttle et al (1976)
<sup>113</sup> In	1290.59(3)	$\frac{1}{2}^-$	$\frac{1}{2}^-$	0.98 <sup>j</sup>	(E2)	1.31(11)	0.66(6)	0.55(4)	Tuttle et al (1976)
<sup>113</sup> In	1448.78(3)	$\frac{1}{2}^-$	$\frac{1}{2}^-$	0.86	-8 <sup>f</sup>	0.90(11)	0.50(6)	0.52(20)	Tuttle et al (1976)
<sup>113</sup> In	1486.1(1)	$\frac{1}{2}^-$	$\frac{1}{2}^-$	0.787	-0.8 <sup>f</sup>	0.63(9)	0.63(9)	0.4(3)	Tuttle et al (1976)
<sup>113</sup> In	1497.2(4)	$\frac{1}{2}^-$	$\frac{1}{2}^-$	<1	(E2)	1.33(16)	<0.30(4)	—	
<sup>113</sup> In	1607.8(15)	$\frac{1}{2}^-$	$\frac{1}{2}^-$	≤1	(E2)	1.54(24)	≤0.26(4)	—	
<sup>116</sup> Sn	1293.54(2)	2 <sup>+</sup>	0 <sup>+</sup>	1	E2	3.58(37)	0.53(6)	0.522(14)	Carlson et al (1975)
<sup>118</sup> Sn	1229.64(4)	2 <sup>+</sup>	0 <sup>+</sup>	1	E2	2.75(28)	0.69(7)	0.67(2)	Carlson et al (1976)
<sup>120</sup> Sn	1171.6(2)	2 <sup>+</sup>	0 <sup>+</sup>	1	E2	1.83(16)	1.04(9)	0.91(2)	Kocher (1976)
<sup>121</sup> Sb	1023.5(10)	$\frac{1}{2}^-$	$\frac{1}{2}^-$	1	0.57  <sup>g</sup>	3.69(34)	0.228(21)	0.20(7) <sup>h</sup>	Tamura et al (1979)
<sup>121</sup> Sb	1105.5(10)	$\frac{1}{2}^-$	$\frac{1}{2}^-$	0.4	—	0.47(4)	0.42(4)	—	
<sup>121</sup> Sb	1142.5(10)	$\frac{1}{2}^-$	$\frac{1}{2}^-$	0.6	(E2)	0.85(8)	0.449(40)	0.41(8) <sup>h</sup>	Booth et al (1973)
<sup>121</sup> Sb	1384.0(10)	$\frac{1}{2}^-$	$\frac{1}{2}^-$	1	0.45  <sup>g</sup>	4.7(5)	0.092(10)	0.088(14) <sup>h</sup>	Booth et al (1973)
<sup>123</sup> Sb	1029.5(10)	$\frac{1}{2}^-$	$\frac{1}{2}^-$	1	0.57  <sup>g</sup>	2.96(27)	0.272(25)	0.26(4) <sup>h</sup>	Booth et al (1973)
<sup>123</sup> Sb	1086.5(10)	$\frac{1}{2}^-$	$\frac{1}{2}^-$	1	δ  > 1.26 <sup>g</sup>	1.06(9)	0.67(6)	0.72(15) <sup>h</sup>	Booth et al (1973)

† Références pour les colonnes 3, 4, 5, 6 et 9 de chaque ligne, sauf indication appelée au bas de ce tableau. Pour les autres données se reporter au texte.

Remarque. Pour calculer  $\delta^2$  quand nous ne disposons que de  $B(E2)$ , pour un mélange  $(E2) + (M1)$ , nous déduisons  $g\Gamma_0(E2) \propto B(E2)E_2^3$ ; en admettant  $W(\theta) = 1$  et connaissant  $\Gamma_0/\Gamma$ , notre détermination de  $u$  donne une première approximation de  $g\Gamma_0$  d'où une valeur de  $\delta^2 = (g\Gamma_0(E2))/(g\Gamma_0 - g\Gamma_0(E2))$  qui permet d'améliorer  $W(\theta)$  et  $g\Gamma_0$  de proche en proche.

<sup>a</sup> Swann (1971); <sup>b</sup> Robinson et al (1967); <sup>c</sup>  $W(\theta) = 0.99$  calculé d'après la formule de Celliers et al (1977); <sup>d</sup> Abbondanno et al (1978); <sup>e</sup> Sayer et al (1972); <sup>f</sup> Tuttle et al (1976); <sup>g</sup> d'après  $B(E2)$  de Barnes et al (1966); <sup>h</sup> calculé d'après Booth et al (1973); <sup>i</sup> Williams et al (1975); <sup>j</sup> Dietrich et al (1970).

## SELENIUM

 $Z=34$ 

Selenium was identified as an element in 1817 by J. J. Berzelius a professor of chemistry in Stockholm, Sweden. While looking for a method of producing sulfuric acid, he observed a sediment with an offensive odor — an indicator of the scarce element tellurium discovered thirty-five years earlier. Further analysis showed it to be a new element with chemical properties similar to tellurium. Because these elements were so closely related, Berzelius named the new substance selenium, from the Greek word *selene*, meaning the moon since tellurium was named from the Latin word *tellus*, meaning the earth.





METHOD Linac; isomer yield; activity

REF. NO. 63 Ka 2  
 NVB

REACTION	RESULT	EXCITATION ENERGY	SOURCE		DETECTOR		ANGLE
			TYPE	RANGE	TYPE	RANGE	
G,G/	RLY	1	C5		ACT-I		4PI
		(0.16)					

Table II. The isomers observed

Isomer	Observed value		Referenced value <sup>(1)(13)</sup>	
	Half-life	Energy (MeV)	Half-life	Energy (MeV)
Se-77m	17.5 sec	0.160	17.5 sec	0.161
Br-79m	4.80 sec	0.209	4.8 sec	0.208
Sr-87m	2.3 hr	0.390	2.8 hr	0.338
Y-89m	15.0 sec	0.920	14 sec	0.915
Rh-103m	53 min	*	57 min	0.040
Ag-107m	42 sec	0.95	44 sec	0.094
Ag-109m			40 sec	0.088
Cd-111m	47 min	0.150, 0.255	49 min	0.150, 0.247
In-115m	4.5 hr	0.335	4.5 hr	0.335
Sn-117m	17 day	0.160	14 day	0.159, 0.161
Ba-137m	2.6 min	0.660	2.6 min	0.662
Er-167m	2.10 sec	0.209	2.5 sec	0.208
Hf-179m	18.5 sec	0.157, 0.215	19 sec	0.161, 0.217
W-183m	5.4 sec	0.200, 0.170, 0.115	5.5 sec	0.1025, 0.2315 others
Ir-191m	4.90 sec	0.129, <0.07	4.9 sec	0.042-0.129
Pt-195m	4.5 day	0.065**	4.1 day	0.031-0.130
Au-197m	7.0 sec	0.10, 0.27, 0.40	7.2 sec	0.130, 0.270, 0.407
Hg-199m	43 min	0.160, 0.370	42 min	0.158, 0.368

\* This isomer was measured with a G-M flow counter.

\*\* This value corresponds to Pt-K X-ray energy.

Table III. Induced activation rate

Element	Beam energy (MeV)	Counting rate ( $\times 10000$ cpm)	Sample form
Se	5	1300	metallic pellet
Br	4	1600	NaBr grain
Sr	6	0.3	SrCO <sub>3</sub> powder
Y	5	90	metallic grain
Rh	5	0.2*	RhCl <sub>3</sub> grain
Ag	5	180	metallic plate
Cd	6	0.5	CdCl <sub>2</sub> grain
In	6	3	metallic plate
Sn	6	0.0005	metallic plate
Ba	5	0.6	BaS powder
Er	4	4900	Er <sub>2</sub> O <sub>3</sub> powder
Hf	5	1600	metallic plate
W	5	120	metallic powder
Ir	5	2100	metallic powder
Pt	5	0.3	metallic plate
Au	4	4300	metallic plate
Hg	6	0.09	metallic liquid

\* The value measured with a G-M flow counter

REF.	A. Veres Acta Phys. Acad. Sci. Hung. 16, 261-73 (1963)		ELEM. STM.	Se	34
METHOD			REF. NO.		
Radioactive source			63 Ve 2		NVB

REACTION	RESULT	EXCITATION ENERGY	SOURCE		DETECTOR		ANGLE
			TYPE	RANGE	TYPE	RANGE	
G <sub>1</sub> G <sub>2</sub> /	ABX	0-1	D	0-1	NAI-D		

ISOMERS

Таблица 11  
Измеренные значения после облучения, сравниваемые с другими литературными данными

Элемент	Активность облучения после первого измерения (имп/мин.)	Активн. экстрп. в конце оолуч. (имп/мин.)	Лутературные данные		Данные измерений		$\sigma_{\text{м}}$ (10 <sup>-28</sup> см <sup>2</sup> )	$\Gamma_{\text{ум}}$ (10 <sup>-28</sup> эв)
			$T_{1/2}$	$E$ (кэв)	$T_{1/2}$	$E$ (кэв)		
Se-77m	3842±96	5400	17,5 сек.	160	18,1±1 сек.	160±10	9,5	1,75
Sr-87m	191±5	200	2,8 ч.	390	2,9±0,1 ч.	365±25	0,85	0,2
Y-89m	96±20	170	16 сек.	910	16,7±5 сек.		0,08	0,02
Rh-103m	28±5	31	57 мин.	40	58±2 мин.	20,5±0,5	0,08	0,01
Ag-107m	220±14	250	44 сек.	93	43,8±0,6 сек.	91±10	0,8	0,2
Ag-109m			39 сек.	88				
Hf-179m	80±18	155	19 сек.	160; 215	19±2 сек.		1	0,2
Ir-191m	90±20	250	4,9 сек.	42; 130	5±2 сек.		5,6	1
Pt-195m	90±9	100	3,5 д.	31; 100; 130;	3,5±0,2 д.	32±3 67,5±5 96±5 130±10	0,2	0,04
Au-197m	240±16	520	7,2 сек.	130; 277; 407	7,2±1 сек.	68;130; 280±20 390±20	0,07	0,01
Hg-199m	9,6±3,2		42 мин.	160; 370			0,005	0,001

Acta Phys. Hung. Tom. XVI. Fasc. 3.

ELEM. SYM.	A	Z
Se		34
METHOD		REF. NO.
Nuclear Resonance Scattering using N,G reactions.		66 Be 3
		JDM

REACTION	RESULT	EXCITATION ENERGY	SOURCE		DETECTOR		ANGLE
			TYPE	RANGE	TYPE	RANGE	
G,G	RLX	5 - 10	D	5 - 10	NAI-D	5 - 10	135

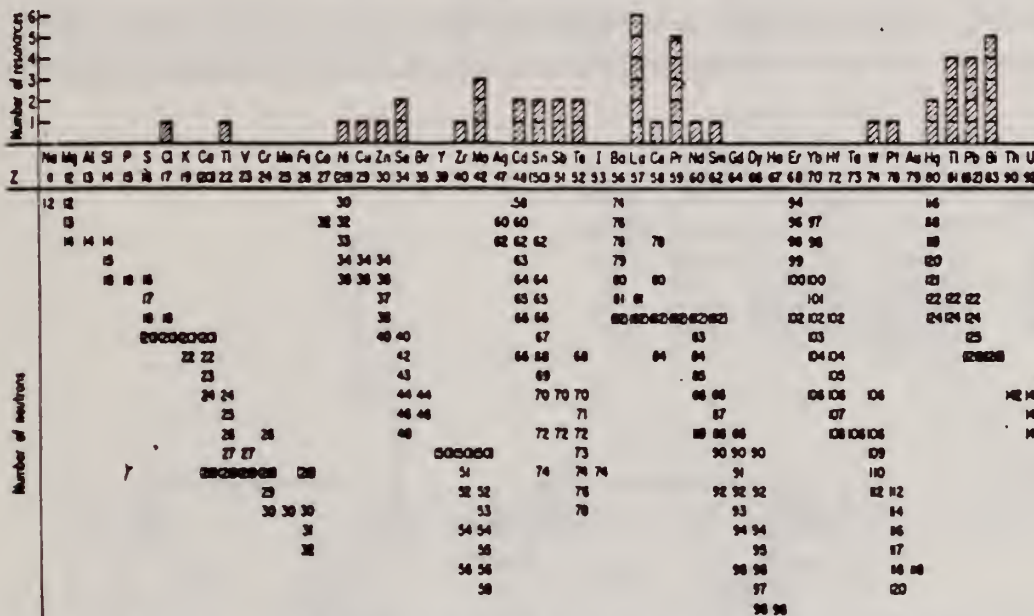


FIG. 3. Histogram of distribution of observed resonances among the different targets. The atomic number is given directly beneath the chemical symbol followed by the neutron numbers of the naturally occurring isotopes. Magic numbers are shown in brackets.

TABLE III. List of effective cross sections.

Scatterer	Energy (MeV)	Gamma source	$\delta$ (mb)	Scatterer	Energy (MeV)	Gamma source	$\delta$ (mb)
Sm <sup>146</sup>	8.907	Ni	100	Sn	7.01	Cu	110
Pr <sup>144</sup>	8.881	Cr	9	Nd	6.867	Co	30
La	8.532	Ni	6	Pr <sup>144</sup>	6.867	Co	3
Te	8.532	Ni	3 <sup>a</sup>	Te	6.7	Ni	...
Cu	8.499	Cr	24	La	6.54	Ag	12
Zr	8.496	Se	3050	Cd	6.474	Co	110
Se	8.119	Ni	13	Mo	6.44	Hg	25 <sup>a</sup>
Se	7.817	Ni	50	La	6.413	Ti	72
Se	7.76	K	90	Mo	6.413	Ti	10
Sb	7.67	V	...	Ti	6.413	Ti	25
Cd	7.64	Fe	40 <sup>b</sup>	W	6.3	Ti	...
Ni	7.64	Fe	7 <sup>c</sup>	Sb	6.31	Hg	6 <sup>a</sup>
Pr <sup>144</sup>	7.64	Fe	12 <sup>a</sup>	Ti	6.31	Hg	2 <sup>a</sup>
Ti	7.64	Fe	370 <sup>a</sup>	Sn	6.27	Ag	75
La	7.634	Cu	7	Pb <sup>208</sup>	6.15	Gd	...
Mo	7.634	Cu	11	Te	5.8	Ni	...
Bi <sup>209</sup>	7.634	Cu	4	La	6.12	Cl	35
Te	7.528	Ni	66 <sup>d</sup>	Pr <sup>144</sup>	6.12	Cl	110
Bi <sup>209</sup>	7.416	Se	100	Pt	5.99	Hg	40 <sup>a</sup>
Bi <sup>209</sup>	7.300	As	80 <sup>e</sup>	Tl	5.99	Hg	5 <sup>a</sup>
Pb <sup>208</sup>	7.285	Fe	4100	Pb <sup>208</sup>	5.9	Sr	...
Cl	7.285	Fe	34	Ce	5.646	Co	17
Pr <sup>144</sup>	7.185	Se	80	Bi <sup>209</sup>	5.646	Co	55
Ti	7.16	Cu	120	Pb <sup>208</sup>	5.53	Ag	70
La	7.15	Mn	50	Hg	5.44	Hg	75 <sup>a</sup>
Bi <sup>209</sup>	7.149	Ti	2000	Hg	4.903	Co	385

<sup>a</sup> High-energy component of a complex spectrum.  
<sup>b</sup> A broad scattered spectrum with no observable peak structure.  
<sup>c</sup> There are actually two lines of energies 7.647 and 7.633 MeV having equal intensities in the iron capture gamma spectrum. The cross section has therefore been corrected, although there is no possibility at present of deciding which line is responsible for each resonance.  
<sup>d</sup> Is probably an independent level in the complex spectrum of Ni  $\gamma$  rays on Te.  
<sup>e</sup> Rough estimate.  
<sup>f</sup> May be inelastic component from 7.528 level in Te.  
<sup>g</sup> The relative line intensities in this case are due to Grosse and co-workers.  
<sup>h</sup> No line is known for the source at this energy.  
<sup>i</sup> Difficult to resolve among the many source lines present at this energy.



REF.

R. Wendling and R. Kosiek  
Z. für Physik 192, 502 (1966)

ELEM. SYM.

A

Z

Se

34

METHOD

REF. NO.

66 We 2

EGF

REACTION	RESULT	EXCITATION ENERGY	SOURCE		DETECTOR		ANGLE
			TYPE	RANGE	TYPE	RANGE	
G,A	ABX	6-33	C	33 (32.5)	SCD-D	4-16	90

Tabelle

Element	Dicke (mg/cm <sup>2</sup> )	Gesamt- auflösung (keV)	Gesamtzahl gemessener α-Teilchen	Ausbeute ( $\mu\text{b}/\text{MeV} \cdot \text{ster}$ )	Ausbeute $10^4 N_{\alpha}$ Mol <sup>-1</sup> r	$E_{\alpha \text{ max (exp)}}$ (MeV)	$E_{\alpha \text{ min}}$ (MeV)
Al	2,35	770	14600	$1,3 \pm 0,2$	$3,5 \pm 0,6$	( $\approx 3,5$ )	3,5
Ar	200 Torr	480	5200	$3,0 \pm 0,5$	$8,3 \pm 1,3$	5,2	3,5
Se	3,72	790	12200	$0,28 \pm 0,04$	$0,76 \pm 0,12$	9,2	4,5
Ag	3,12	670	3150	$0,12 \pm 0,02$	$0,33 \pm 0,05$	11,8	6,5

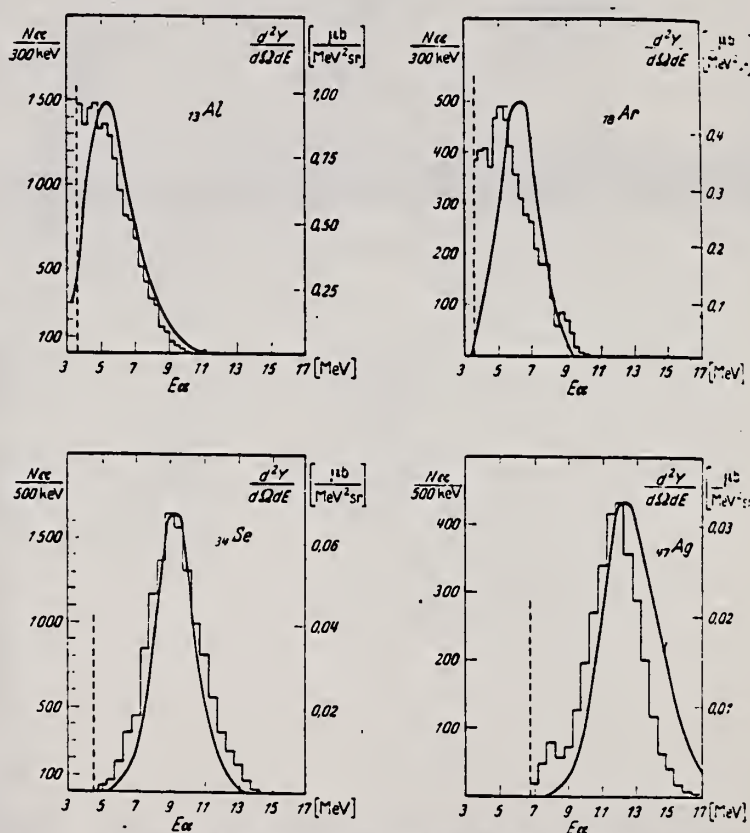


Fig. 1. a Histogramm: Gemessene Energieverteilung und differentielle Ausbeute der Photo- $\alpha$ -Teilchen.  
b Kurve: Berechnetes Spektrum. Nähere Angaben im Text



REF.			S. Costa, F. Ferrero, C. Manfredotti, L. Pasqualini, G. Piragino, and H. Arenhovel Nuovo Cimento <u>51B</u> , 199 (1967)			ELEM. SYM.	A	Z
						Se		34
METHOD						REF. NO.		
						67 Co 2		EGF
REACTION	RESULT	EXCITATION ENERGY	SOURCE		DETECTOR		ANGLE	
			TYPE	RANGE	TYPE	RANGE		
G,XN	ABX	THR- 24	C	11-24	BF3-I		4PI	

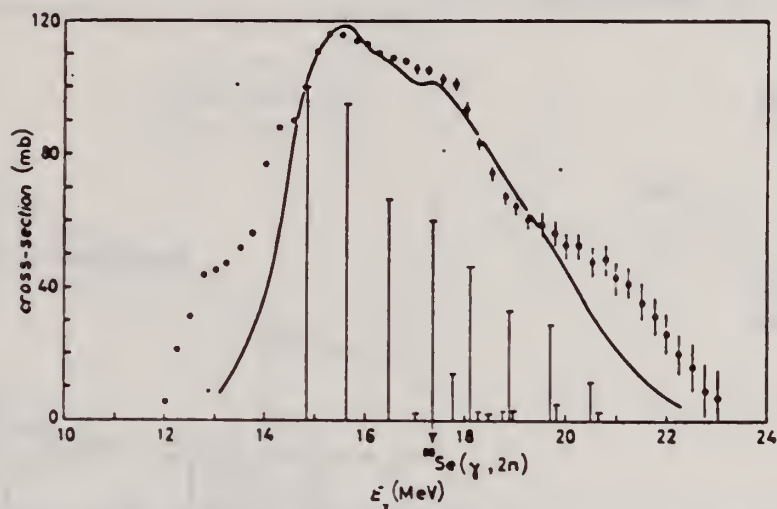
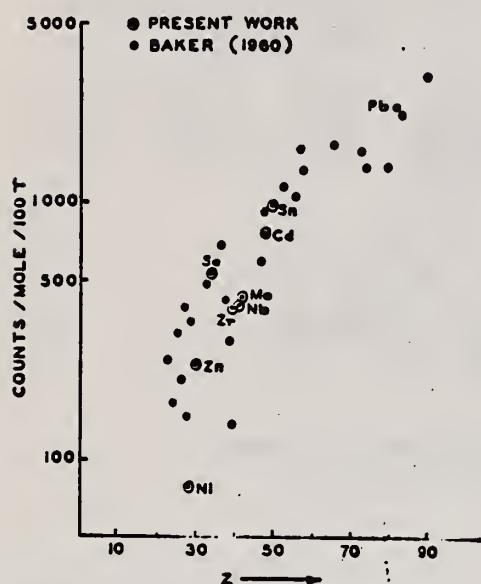


Fig. 1. - Corrected  $(\gamma, 2n)$  cross-section for Se. The dipole strengths, calculated for  $^{76}\text{Se}$ , are indicated by the vertical bars.

METHOD		REF. NO.		EGF	
		67 Hu 2			
REACTION	RESULT	EXCITATION ENERGY	SOURCE		ANGLE
			TYPE	RANGE	
G,N	ABY	THR-22	C	22	DST

YIELD AT  $E_0 = 22$  MeV  
 $^{28}\text{Si}(n,p)$  ACTIVATION BY PHOTONEUTRONS

FIG. 3. The yields of fast photoneutrons from various elements as measured in the present work and by Baker. The present results have been normalized to Baker's measurements for lead.



ANISOTROPY COEFFICIENT  $-a_2$

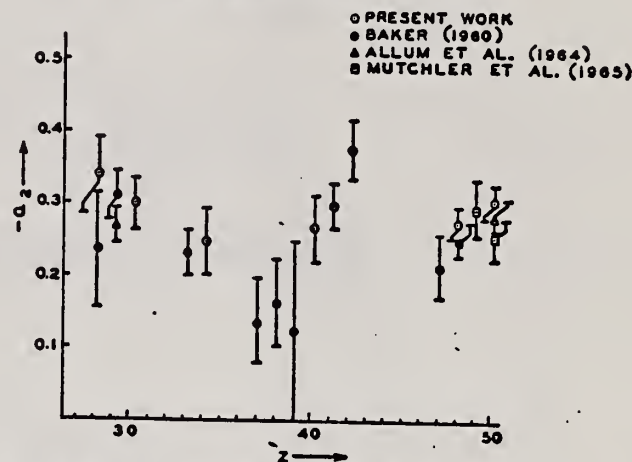


FIG. 2. The anisotropy coefficients  $a_2$  in the formula  $W(\theta) = a_0(1 + a_1P_1 + a_2P_2)$ , obtained in the present work, and those obtained by other workers in the same part of the Periodic Table.

TABLE I

Element	$a_0^*$	$a_1$	$a_2$
Nickel	77 (1.0±0.05)	0.14±0.04	-0.34±0.06
Zinc	236 (1.0±0.04)	0.06±0.03	-0.30±0.04
Selenium	525 (1.0±0.05)	0.10±0.04	-0.25±0.05
Zirconium	380 (1.0±0.05)	0.03±0.04	-0.27±0.05
Niobium	392 (1.0±0.03)	0.04±0.02	-0.30±0.03
Molybdenum	410 (1.0±0.03)	0.05±0.03	-0.41±0.04
Cadmium	755 (1.0±0.02)	0.05±0.01	-0.28±0.02
Tin	955 (1.0±0.02)	0.08±0.02	-0.30±0.02
Lead	2274 (1.0±0.02)	0.06±0.02	-0.48±0.02

\*For comparison purposes the experimental value of  $a_0$  for Pb has been normalized to coincide with that obtained by Baker and McNeill (1961) and is the yield per mole per 100 roentgen. All other values of  $a_0$  have also been quoted with the same normalization.

METHOD

REF. NO.	
70 Ar 1	egf

REACTION	RESULT	EXCITATION ENERGY	SOURCE		DETECTOR		ANGLE
			TYPE	RANGE	TYPE	RANGE	
G,G	ABX	12-30	C	32	NAI	12-30	DST

GETS G,G/ TO 2+

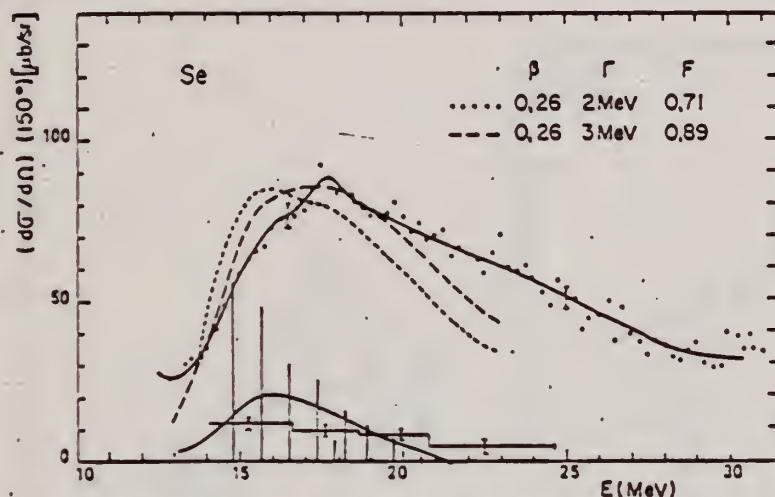


Fig. 8. Differential total scattering cross section at 150° for natural Se. See caption for fig. 4.

Fig. 4. Differential total scattering cross section at 150° for natural Ti. The full curve through experimental points is only a guide for the eyes. The vertical bars represent the relative strength of dipole levels calculated by the D.C.M. with parameters of table 1. Theoretical elastic plus inelastic scattering is computed from these levels with a common width  $\Gamma$  (dashed curve). Experimental inelastic scattering (histogram) and theoretical inelastic scattering to the first  $2^+$  (full curve) are shown in the lower part of the figure. Open circles give the cross section after background subtraction.

TABLE 4  
Integrated inelastic scattering cross section

Nucleus	Limits of integration (in MeV)	Experimental <sup>a)</sup> $\int \sigma_i(E) dE$ (MeV $\cdot$ $\mu$ b)	$2^+$	Theoretical <sup>a)</sup> $2^+$ (MeV $\cdot$ $\mu$ b)	Total
Ti( <sup>48</sup> Ti)	16 - 24	250 $\pm$ 50	425	109	534
<sup>51</sup> V( <sup>52</sup> Cr)	16.4 - 24.9	492 $\pm$ 50	509	116	579
Cr	16.4 - 23.4	431 $\pm$ 60	509	116	579
<sup>73</sup> As( <sup>76</sup> Se)	14.1 - 23.6	1254 $\pm$ 120	1373	414	1787
Se( <sup>80</sup> Se)	14.1 - 24.6	1035 $\pm$ 100	1066	333	1419
<sup>88</sup> Y					364
Cd( <sup>112</sup> Cd)	13.6 - 23.3	3264 $\pm$ 240	1894	370	2264
In( <sup>115</sup> Cd)	13.6 - 23.6	2840 $\pm$ 220	2173	338	2561
Sn( <sup>110</sup> Sn)	14.2 - 24.2	2363 $\pm$ 220			643

<sup>a)</sup> We assume an angular distribution of the form  $1 - \frac{1}{3} \cos^2 \theta$ .

METHOD

REF. NO.

71 Co 2

egf

REACTION	RESULT	EXCITATION ENERGY	SOURCE		DETECTOR		ANGLE
			TYPE	RANGE	TYPE	RANGE	
G,XN	ABI	36-64	C	10-64	BF3-I		4PI

\*31 FAST N YIELD

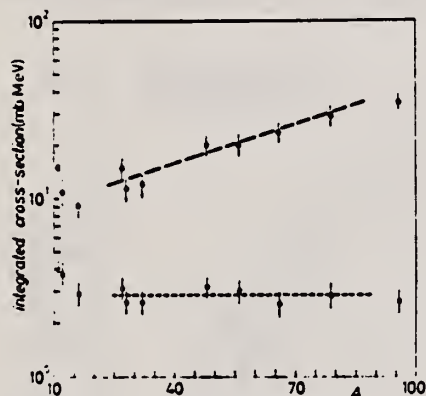


Fig. 2.

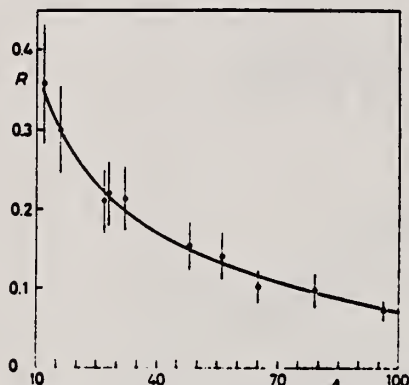


Fig. 3.

Fig. 2. - Experimental photoneutron cross-sections integrated over photon energy between 36 and 64 MeV and divided by  $NZ/A$  are plotted as a function of the mass number. Black dots are total cross-sections not corrected for neutron multiplicity; open circles represent fast neutron cross-sections (see text). The dashed lines are drawn only to guide the eye.

Fig. 3. - The ratio between fast and total photoneutron integrated cross-sections as a function of the mass number  $A$ . The solid line represents a fit of the ratios calculated for some nuclei by taking into account the theoretical neutron energy spectra given by GABRIEL and ALAMILLER (\*) and the efficiencies of our detector (see Fig. 1).



REACTION	RESULT	EXCITATION ENERGY	SOURCE		DETECTOR		ANGLE
			TYPE	RANGE	TYPE	RANGE	
G,N	NOX	THR- 27	C	10- 27	BF3-I		4PI

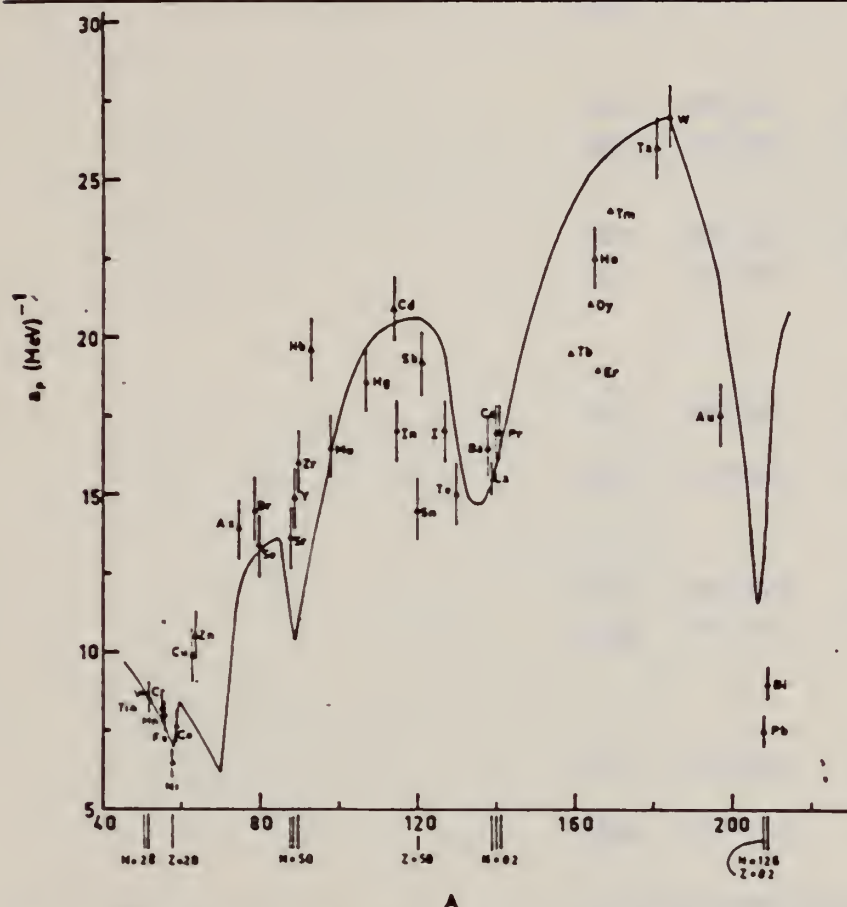


Fig. 12. Experimental values of the level density parameter  $a_p$  (Fermi gas formula plus pairing correction) versus atomic number  $A$ . The continuous curve is a least-squares fit to the data of a theoretical calculation from Newton<sup>15</sup>).

- 1 H. Baba and S. Baba, Japan Atomic Energy Research Institute report JAERI-1183 (1969).
- 2 H. Baba, Nucl. Phys. **A159**, 625 (1970).
- 15 T.D. Newton, Can. J. Phys. **34**, 804 (1956).

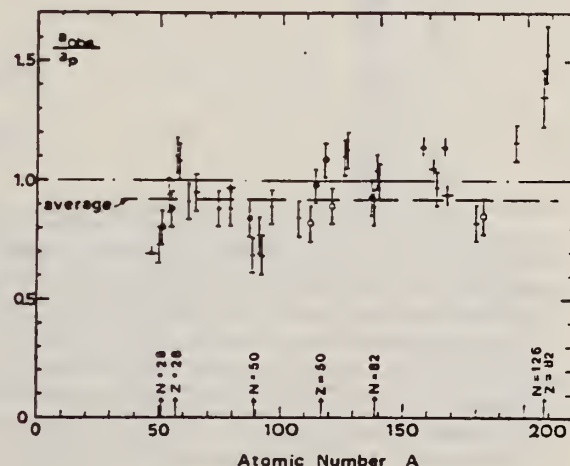


Fig. 15. Ratio  $a_{nu}/a_p$  versus atomic number  $A$ . Here  $a_{nu}$  is the level density parameter taken from the neutron resonance work of refs. 1, 2, and  $a_p$  is the level density parameter derived from the present  $(\gamma, n)$  work. Filled circles represent points where nuclei in the neutron resonance and in the  $(\gamma, n)$  experiment were the same. Open circles represent points where the respective nuclei were approximately matched. Triangles represent points which are based on measurement of neutron mean energies at two bremsstrahlung energies only.

(over)



TABLE 3

Comparison of experimental and theoretical data on nuclear level densities with Fermi gas formulae, and comparison of nuclear level density parameters from  $(\gamma, n)$  and n-resonance absorption experiments

Target	N (residual nucleus) <sup>a)</sup>		Goodness of fit <sup>b)</sup>		$\bar{E}_n(24)$ (MeV) <sup>c)</sup>	T (MeV) <sup>d)</sup>	$a_p$ (MeV <sup>-1</sup> ) <sup>e)</sup>	$a_{obs}$ (MeV <sup>-1</sup> ) <sup>f)</sup>	$a_{obs}/a_p$
			no p.c.	with p.c.					
Ti <sup>g)</sup>	23	8%			1.93		8.1- <sup>47</sup> Ti	6.41- <sup>47</sup> Ti	0.79
	24	8%							
	25	73%							
	26	5%							
	27	5%							
V <sup>g)</sup>	27	100%			1.96		8.7- <sup>50</sup> V	6.35- <sup>51</sup> V	0.73
Cr	25	4%	P	G	1.89		8.6- <sup>51</sup> Cr	6.9 - <sup>51</sup> Cr	<u>0.80</u>
	27	84%							
	28	10%							
	29	2%							
Mn	29	100%	V.P.	G	2.1		8.2- <sup>54</sup> Mn	7.82- <sup>56</sup> Mn	0.94
Fe	27	6%	F	G	1.96		8.0- <sup>55</sup> Fe	7.06- <sup>55</sup> Fe	<u>0.88</u>
	29	92%							
	30	2%							
Co	31	100%	P	F	2.12		7.7- <sup>58</sup> Co	8.35- <sup>60</sup> Co	1.08
Ni (Z = 28)	29	68%	V.P.	P	2.04	1.4	6.5- <sup>57,7</sup> Ni	7.19- <sup>59</sup> Ni	1.10
	31	26%							
	32	1%							
	33	4%							
	35	1%							
Cu	33	69%	V.P.	P	1.78	1.0	9.8- <sup>62</sup> Cu	8.90- <sup>64</sup> Cu	0.91
	35	31%							
Zn	33	49%	F	F	1.61		10.5- <sup>64,6</sup> Zn	10.0- <sup>65</sup> Zn	0.95
	35	28%							
	36	4%							
	37	19%							
As	41	100%	V.P.	F	1.44		14.5- <sup>74</sup> As	12.81- <sup>76</sup> As	0.88
Se <sup>g)</sup>	41	9%			1.39		13.3- <sup>78</sup> Se	12.8 - <sup>78</sup> Se	<u>0.97</u>
	42	8%							
	43	24%							
	45	50%							
	47	9%							
Br	43	45%	V.P.	V.P.	1.41		14.5- <sup>79</sup> Br	12.69- <sup>80</sup> Br	0.88
	45	49%							
Sr	47	10%	F	G	1.31		13.6- <sup>87</sup> Sr	11.4 - <sup>87</sup> Sr	<u>0.84</u>
	48	7%							
	49	83%							

<sup>a)</sup> Neutron numbers and abundances of respective residual nuclei in  $(\gamma, n)$  experiments.

<sup>b)</sup> These give an assessment of the goodness of fit of a calculated  $\bar{E}_n$  versus  $E_0$  curve to the observed data, using the Fermi gas level density formula both without and with pairing corrections.

<sup>c)</sup> Bremsstrahlung photoneutron mean energies  $\bar{E}_n$  for peak bremsstrahlung energy  $E_0 = 24$  MeV.

<sup>d)</sup> Nuclear temperature from fit with constant-temperature formula.

<sup>e)</sup> Level density parameter  $a_p$  derived from the present  $(\gamma, n)$  experiment, using a Fermi gas formula plus pairing correction, and corresponding residual nucleus (the atomic weight shown is the weighted average of atomic weights of the respective isotopes present).

<sup>f)</sup> As column 7, but using data on n-resonance absorption from refs. 1, 2).

<sup>g)</sup> Measurements of  $\bar{E}_n(E_0)$  for these nuclei were made only for  $E_0 = 21, 23$  and 24 MeV.

SE  
A=74

SE  
A=74

SE  
A=74



REF. F.Z. Khien N.K. Zui, N.T. An  
Yad. Fiz. 35, 257 (1982)  
Sov. J. Nucl. Phys. 35, 145 (1982)

ELEM. SYM.	A	Z
Se	74	34
REF. NO. 82 Kh 2		egf

METHOD						REF. NO.	egf
						82 Kh 2	
REACTION	RESULT	EXCITATION ENERGY	SOURCE		DETECTOR		ANGLE
			TYPE	RANGE	TYPE	RANGE	
G,N	NOX	12-14	C	14	ACT-I		4PI

# ISOMERIC RATIO

The method is developed for calculation of the isomeric ratio for the case of low excitation energy of the residual nucleus, and the isomeric ratio is measured in the  $(n, 2n)$  and  $(\gamma, n)$  reactions in the neutron-deficient nuclei  $^{110}\text{Mo}$ ,  $^{90}\text{Zr}$ ,  $^{88}\text{Sr}$ , and  $^{74}\text{Se}$ . The good agreement between the experimental and theoretical results on the  $(\gamma, n)$  reaction has confirmed the reliability of the characteristics of the residual nuclei, the transmission coefficients of the emitted neutrons, etc., used in the calculations. From study of the  $(n, 2n)$  reaction we have obtained values of the parameters of the spin dependence of the level density of the nucleus in the excitation-energy region  $\sim 14$  MeV.

PACS numbers: 25.20. + y, 25.40.Gr, 27.50. + e, 27.60. + j

TABLE III. Isomeric ratio in the  $(\gamma, n)$  reaction.

Target nucleus	$\alpha_{\text{exp}}$	$\alpha_{\text{theor}}$	Published data <sup>1)</sup>
$^{110}\text{Mo}$	$1.54 \pm 0.15$	1.36	$1.52 \pm 0.15$ (70) [2] $1.03 \pm 0.21$ [10] $0.85 \pm 0.07$ (30) [15]
$^{90}\text{Zr}$	$1.52 \pm 0.04$	1.19	$0.50 \pm 0.15$ (30) [15]
$^{88}\text{Sr}$	$0.70 \pm 0.07$	0.56	$0.68 \pm 0.14$ (30) [15]
$^{74}\text{Se}$	$7.5 \pm 1.0$	$10.5^{+1.1}_{-1.1}$	

<sup>1)</sup>In parentheses we have given the values of the bremsstrahlung maximum energy.

<sup>2)</sup>In the calculations we used the  $^{74}\text{Se}$  level scheme of Ref. 2.

$I_1 = 7/2^+$  and  $I_2 = 1/2^+$ .

<sup>3)</sup>In the calculations we used the level scheme of  $^{74}\text{Se}$  in Ref. 3.

$I_1 = 9/2^+$  and  $I_2 = 3/2^+$ .





SE  
A=76

SE  
A=76

SE  
A=76



N. N. Delyagin  
J. Exptl. Theoret. Phys. (USSR) 38, 1111 (1960)  
Soviet Phys. JETP 11, 303 (1960)

Se

76

34

METHOD

REF. NO.

60 De 2

EGF

REACTION	RESULT	EXCITATION ENERGY	SOURCE		DETECTOR		ANGLE
			TYPE	RANGE	TYPE	RANGE	
G,G	LFT	.56	D	.56			

Cascade transition used to supply recoil energy.

No data given on detector

LFT  $(1.3 \pm 0.2) \times 10^{-11}$  sec

REF. J. R. Pruett  
Phys. Rev. 129, 2583 (1963).

ELEM. SYM.	A	Z
Se	76	34

METHOD Radioactive source; photon scattering; NaI spectrometer						REF. NO. 63 Pr 2		NVB	
REACTION	RESULT	EXCITATION ENERGY	SOURCE		DETECTOR		ANGLE		
			TYPE	RANGE	TYPE	RANGE			
G,G	LFT	1	D	1	NAI-D				
		(0.559 MeV)	(0.559 MeV)						

Lifetime:

$$\tau_{0.559} = (1.55^{+0.13}_{-0.19}) 10^{-11} \text{ sec.}$$

$$\tau_{1.216} > 3 \times 10^{-12} \text{ sec.}$$

REF.

A.M. Goryachev, G.N. Zalesnyi, and B.A. Tulupov  
 Izv. Akad. Nauk SSSR. Ser. Fiz. 39, 134 (1975)  
 Bull. Acad. Sci. USSR Phys. Ser. 39, 116 (1975)

ELEM. SYM.

A

Z

Se

76

34

METHOD

REF. NO.

75 Go 1

hmg

REACTION	RESULT	EXCITATION ENERGY	SOURCE		DETECTOR		ANGLE
			TYPE	RANGE	TYPE	RANGE	
G,XN	ABX	11- 25	C	9- 25	BF3-I		4PI

$\sigma(G,SN)$ . Statistical theory used to obtain SN cross section from XN cross section.

Table 2

Nuclide	$\beta_0$	$E_2$ , MeV	$E_1$ , MeV	Nuclide	$\beta_0$	$E_2$ , MeV	$E_1$ , MeV
$^{61}\text{Zn}$	0.25	0.99	18	$^{76}\text{Ge}$	0.25	0.562	18
$^{66}\text{Zn}$	0.23	1.04	18	$^{78}\text{Ge}$	0.33	0.559	18
$^{68}\text{Zn}$	0.2	1.08	18	$^{80}\text{Ge}$	0.3	0.618	18
$^{70}\text{Ge}$	0.23	1.04	18	$^{82}\text{Ge}$	0.25	0.654	18
$^{72}\text{Ge}$	0.25	0.835	18	$^{84}\text{Ge}$	0.2	0.633	18
$^{74}\text{Ge}$	0.3	0.6	18				

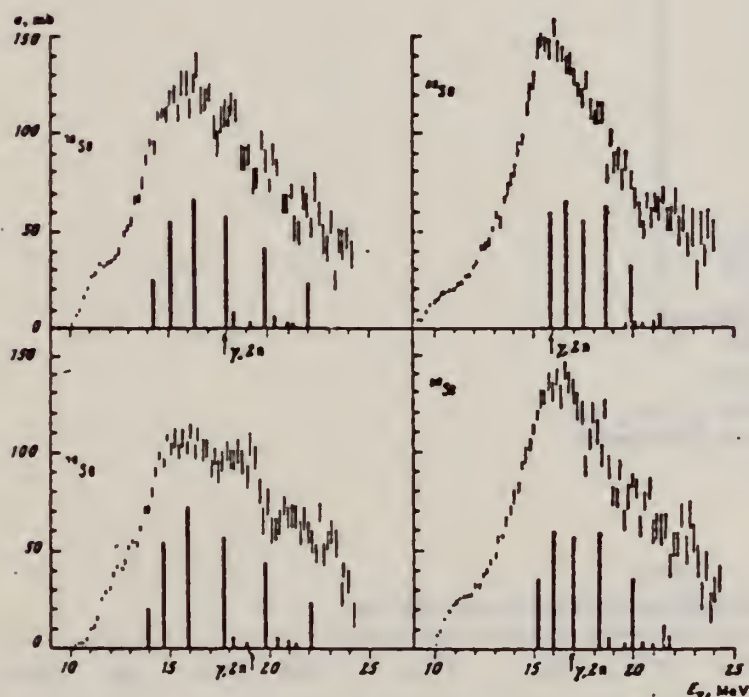


Fig. 3. The same as in Fig. 1, but for  $^{76,78,80,82}\text{Se}$ .

Cross sections of photoneutron reactions.  
 The dipole photoabsorption forces are taken  
 from [6,7] (the solid black columns).

<sup>6</sup>M.G.Huber et al., Phys.Rev.155,1073(67)

<sup>7</sup>M.G.Huber et al., Phys.Rev.192,223(66).

Table 3

Nuclide	$\sigma$ , mb	Nuclide	$\sigma$ , mb	Nuclide	$\sigma$ , mb
$^{61}\text{Zn}$	$397 \pm 19$	$^{76}\text{Ge}$	$760 \pm 37$	$^{76}\text{Se}$	$1021 \pm 52$
$^{66}\text{Zn}$	$579 \pm 27$	$^{78}\text{Ge}$	$872 \pm 41$	$^{78}\text{Se}$	$1029 \pm 50$
$^{68}\text{Zn}$	$718 \pm 35$	$^{80}\text{Ge}$	$911 \pm 43$	$^{80}\text{Se}$	$1067 \pm 53$
$^{70}\text{Ge}$	$733 \pm 37$	$^{82}\text{Ge}$	$930 \pm 50$		

\*Mean - square errors



REF.

P. Carlos, H. Beil, R. Bergere, J. Fagot, A. Lepretre,  
A. Veyssiere, G. V. Solodukhov  
Nucl. Phys. A258, 365 (1976)

ELEM. SYM.	A	Z
Se	76	34

METHOD

REF. NO.

76 Ca 1

egf

REACTION	RESULT	EXCITATION ENERGY	SOURCE		DETECTOR		ANGLE
			TYPE	RANGE	TYPE	RANGE	
G,N	ABX	10- 26	D	10- 26	MOD-I		4PI
G,2N	ABX	17- 26	D	10- 26	MOD-I		4PI

990+

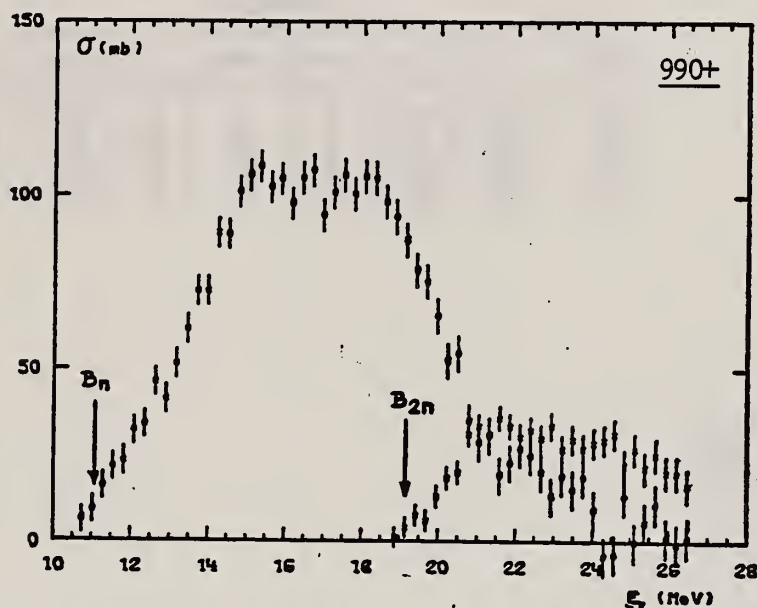


Fig. 8. Partial photoneutron cross section [ $\sigma(\gamma, n) + \sigma(\gamma, pn)$ ] and  $\sigma(\gamma, 2n)$  for  $^{76}\text{Se}$ . Arrows  $B_n$  and  $B_{2n}$  indicate theoretical threshold values for  $(\gamma, n)$  and  $(\gamma, 2n)$  reactions respectively. Data were not corrected for impurities.

TABLE 3

Integrated photoneutron cross sections and comparison with sum rules

Nucleus	$^{64}\text{Zn}$	$\begin{Bmatrix} ^{68}\text{Ga} \\ ^{71}\text{Ga} \end{Bmatrix}$	$^{70}\text{Ge}$	$^{72}\text{Ge}$	$^{74}\text{Ge}$	$^{76}\text{Ge}$	$^{73}\text{As}$	$^{76}\text{Se}$	$^{78}\text{Se}$	$^{80}\text{Se}$	$^{82}\text{Se}$
$E_M$ (MeV)	29	26.5	26.5	26.5	26.5	26.5	26.5	26.5	26.5	26.5	26.5
$\sigma_{0n}$ (MeV · b)	0.75	0.91	0.78	0.94	1.02	1.12	1.09	1.01	1.06	1.11	1.13
$\frac{\sigma_{0n} A}{0.06 N Z}$	0.78	0.87	0.75	0.88	0.94	1	0.98	0.90	0.92	0.94	0.95
$B_n - B_p$ (MeV)	4.2	$\begin{Bmatrix} 3.7 \\ 1.4 \end{Bmatrix}$	3	1	-0.8	-2.6	3.3	1.7	0.1	-1.5	-3
$\sigma_{-1n}$ (mb)	38	52	44	54	59	64	63	58	62	65	67
$\sigma_{-1n} A^{-1/2}$ (mb)	0.15	0.18	0.15	0.18	0.19	0.20	0.20	0.18	0.19	0.19	0.19
$\sigma_{-2n}$ (mb · MeV $^{-1}$ )	2.0	3.1	2.5	3.2	3.6	3.9	3.7	3.4	3.8	3.9	4.2
$\sigma_{-2n} A^{-1/2}$ (mb · MeV $^{-1}$ )	1.9	2.6	2.1	2.6	2.8	2.9	2.8	2.5	2.7	2.6	2.7

FORM N35-4  
(REV. 7-14-6)  
USCOMM-NB:

The notation used is defined in the text. The average experimental errors  $\Delta\sigma_{0n}/\sigma_{0n}$ ,  $\Delta\sigma_{-1n}/\sigma_{-1n}$  and  $\Delta\sigma_{-2n}/\sigma_{-2n}$  are approximately 8%.

SE  
A=77

SE  
A=77

SE  
A=77



REACTION	RESULT	EXCITATION ENERGY	SOURCE		DETECTOR		ANGLE
			TYPE	RANGE	TYPE	RANGE	
G,P	ABY	THR-20	C	20	ACT-I		4PI

TABLE I. SUMMARY OF DATA ON ( $\gamma$ , p) REACTIONS WITH 20 MeV BREMSSTRAHLUNG

Nuclide		$S_p$ (MeV)	Observed $\gamma$ -ray			Yield determined	
Parent (Natural abundance, %)	Residual (Half-life)		Energy (MeV)	Branching ratio (%)	Type of multipole transition	$\mu\text{Ci/mg}^a$	Yield/mol-R
$^{24}\text{Mg}$ (10.11)	$^{24}\text{Na}$ (15 hr)	12.06	1.37	100	E2	$1.48 \times 10^{-1}$	$1.7 \times 10^3$
$^{28}\text{Si}$ (4.71)	$^{28}\text{Al}$ (2.27 min)	12.33	1.78	100	E2	1.91	$2.8 \times 10^3$
$^{28}\text{Si}$ (3.12)	$^{28}\text{Al}$ (6.56 min)	13.59	1.28	93.8	E2 + M1	$6.51 \times 10^{-1}$	$1.5 \times 10^3$
$^{40}\text{Ca}$ (2.06)	$^{40}\text{K}$ (22.4 hr)	12.17	0.374	85	E2 + M1	$7.86 \times 10^{-1}$	$1.3 \times 10^3$
$^{48}\text{Ti}$ (7.32)	$^{48}\text{Sc}$ (84.1 d)	10.47	0.887	100	E2	$7.11 \times 10^{-1}$	$3.1 \times 10^3$
$^{48}\text{Ti}$ (73.99)	$^{48}\text{Sc}$ (3.4 d)	11.44	0.160	100	E2 + M1	$6.83 \times 10^{-1}$	$1.2 \times 10^3$
$^{48}\text{Ti}$ (5.46)	$^{48}\text{Sc}$ (1.8 d)	11.35	1.31	100	E2	$4.40 \times 10^{-1}$	$5.8 \times 10^3$
$^{52}\text{Cr}$ (9.55)	$^{52}\text{V}$ (3.8 min)	11.15	1.43	100	E2	$5.01 \times 10^{-1}$	$6.6 \times 10^3$
$^{56}\text{Fe}$ (2.17)	$^{56}\text{Mn}$ (2.58 hr)	10.57	1.81	23.5	E2 + M1	$8.10 \times 10^{-1}$	$2.1 \times 10^3$
$^{70}\text{Ge}$ (36.74)	$^{70}\text{Ga}$ (4.8 hr)	10.92	0.295	97	(E2)	$3.70 \times 10^{-1}$	$1.3 \times 10^3$
$^{78}\text{Se}$ (7.58)	$^{78}\text{As}$ (26.5 hr)	9.61	0.559	41	E2	$1.48 \times 10^{-1}$	$1.3 \times 10^3$
$^{84}\text{Sr}$ (7.02)	$^{84}\text{Rb}$ (19 d)	9.41	1.08	9	E2	$5.15 \times 10^{-1}$	$9.9 \times 10^3$
$^{110}\text{Cd}$ (12.26)	$^{110}\text{Ag}$ (3.2 hr)	9.74	1.39	35	E2	$1.91 \times 10^{-1}$	$2.1 \times 10^3$
$^{117}\text{Sn}$ (7.57)	$^{117}\text{In}$ (54 min)	9.58	1.27	84	E2	$9.80 \times 10^{-1}$	$6.9 \times 10^3$
$^{137}\text{Ba}$ (11.32)	$^{137}\text{Cs}$ (13 d)	8.67	0.830	100	E2	$1.68 \times 10^{-1}$	$2.2 \times 10^3$
$^{198}\text{Hg}$ (16.84)	$^{198}\text{Au}$ (2.7 d)	7.27	0.412	100	E2	$8.43 \times 10^{-1}$	$2.2 \times 10^3$

a) The value corrected at the end of 1 hr irradiation ( $9.4 \times 10^4$  R/min).

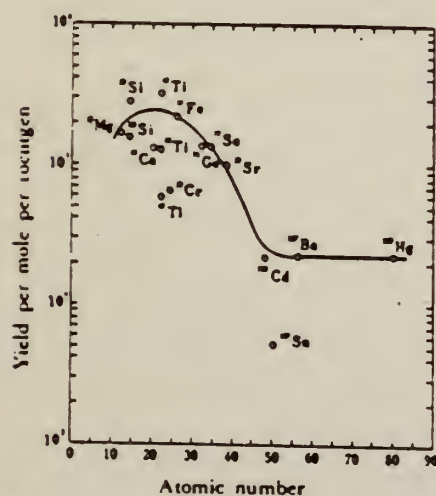


Fig. 2. The yield curve for the ( $\gamma$ , p) reaction with 20 MeV bremsstrahlung.

METHOD

REF. NO.

69 Bo 3

egf

REACTION	RESULT	EXCITATION ENERGY	SOURCE		DETECTOR		ANGLE
			TYPE	RANGE	TYPE	RANGE	
G, G	ABX	0-2	C	0-2	ACT-I		4PI

8 LEVELS

TABLEAU I

Energie des niveaux excités, sections efficaces intégrées et  $u = g\Gamma_e \Gamma_a / \Gamma$  pour le  $^{77}\text{Se}$

$E(\text{keV})$	$\sigma (\mu\text{b} \cdot \text{MeV})$	$u(\text{eV})$
$250 \pm 10$	$8 \begin{smallmatrix} +7 \\ -2.5 \end{smallmatrix} \times 10^{-4}$	$1.3 \begin{smallmatrix} +1 \\ -0.4 \end{smallmatrix} \times 10^{-8}$
$440 \pm 10$	$1.8 \begin{smallmatrix} +1.2 \\ -0.4 \end{smallmatrix} \times 10^{-3}$	$9.1 \begin{smallmatrix} +5 \\ -2 \end{smallmatrix} \times 10^{-8}$
$520 \pm 10$	$5.7 \begin{smallmatrix} +5 \\ -1.5 \end{smallmatrix} \times 10^{-3}$	$4.1 \begin{smallmatrix} +3.5 \\ -1 \end{smallmatrix} \times 10^{-8}$
$825 \pm 10$	$4.6 \begin{smallmatrix} +4 \\ -1 \end{smallmatrix} \times 10^{-3}$	$8.0 \begin{smallmatrix} +7 \\ -2 \end{smallmatrix} \times 10^{-7}$
$932 \pm 10$	$3.5 \begin{smallmatrix} +3 \\ -1 \end{smallmatrix} \times 10^{-2}$	$7.8 \begin{smallmatrix} +6.5 \\ -2 \end{smallmatrix} \times 10^{-6}$
$1000 \pm 10$	$3.2 \begin{smallmatrix} +3 \\ -1 \end{smallmatrix} \times 10^{-2}$	$8.4 \begin{smallmatrix} +8 \\ -2.5 \end{smallmatrix} \times 10^{-6}$
$1190 \pm 10$	$0.18 \begin{smallmatrix} +0.12 \\ -0.04 \end{smallmatrix}$	$6.7 \begin{smallmatrix} +4.5 \\ -1.5 \end{smallmatrix} \times 10^{-5}$
$1600 \pm 10$	$0.52 \begin{smallmatrix} +0.4 \\ -0.1 \end{smallmatrix}$	$3.5 \begin{smallmatrix} +2.5 \\ -0.5 \end{smallmatrix} \times 10^{-5}$

Indirect Activation of 17.38s 162.0 keV level by .5-2.0 MeV bremsstrahlung.



SE  
A=78

SE  
A=78

SE  
A=78



REF. Y. Oka, T. Kato and A. Yamadera  
Bull. Chem. Soc. Japan 41, 1606 (1968)

ELEM. SYM.	A	Z
Se	78	34

METHOD	REF. NO.	
	68 Ok 2	egf

REACTION	RESULT	EXCITATION ENERGY	SOURCE		DETECTOR		ANGLE
			TYPE	RANGE	TYPE	RANGE	
G,N	ABY	THR-20	C	20	ACT- I		4PI

ISOMERIC YIELD

TABLE 1. THE PARTICULARS OF THE ( $\gamma,n$ ) REACTION PRODUCTS AND THE DATA OBTAINED WITH 20 MeV BREMSSTRAHLUNG

Nuclide		Half-life of product (sec)	Gamma-ray determined			Limit of detection ( $\mu$ g)	Yield ( $\text{mol}^{-1}\cdot\text{R}^{-1}$ )
Parent (Natural abundance, %)	Residual		Energy (MeV)	Branching ratio (%)	Photopeak activity (cpm/mg) <sup>a)</sup>		
<sup>24</sup> Mg(78.60)	<sup>23</sup> Mg	9.9	0.511	200	$2.04 \times 10^6$	0.49	$8.1 \times 10^6$
<sup>76</sup> Ge(7.67)	<sup>75m</sup> Ge	48	0.139	100	$6.37 \times 10^5$	1.6	$1.1 \times 10^6$
<sup>78</sup> Se(23.52)	<sup>77m</sup> Se	17	0.162	100	$1.82 \times 10^6$	0.55	$1.2 \times 10^6$
<sup>92</sup> Mo(15.86)	<sup>91m</sup> Mo	65	0.650	57	$2.22 \times 10^6$	4.5	$2.7 \times 10^6$
<sup>140</sup> Ce(88.48)	<sup>139m</sup> Ce	58	0.745	100	$1.06 \times 10^6$	0.95	$1.3 \times 10^6$
<sup>142</sup> Nd(27.13)	<sup>141m</sup> Nd	64	0.760	100	$3.19 \times 10^6$	3.1	$1.4 \times 10^6$
<sup>158</sup> Tb(100)	<sup>157m</sup> Tb	11	0.111	100	$2.56 \times 10^6$	3.8	$2.2 \times 10^6$

a) The value corrected at the end of one-minute irradiation with the dose rate of  $10^7$  R/min; Counting geometry is 20% with a 3"dia.  $\times$  3"NaI(Tl) detector.

Values given are for  $\sigma_0$  (24.2 MeV).

REF.

A.M. Goryachev, G.N. Zalesnyi, and B.A. Tulupov  
 Izv. Akad. Nauk SSSR. Ser. Fiz. 39, 134 (1975)  
 Bull. Acad. Sci. USSR Phys. Ser. 39, 116 (1975)

ELEM. SYM.	A	Z
Se	78	34

METHOD

REF. NO.

75 Go 1

hmg

REACTION	RESULT	EXCITATION ENERGY	SOURCE		DETECTOR		ANGLE
			TYPE	RANGE	TYPE	RANGE	
G, XN	ABX	10 - 25	C	9 - 25	BF3-I		4PI

$\sigma(G, SN)$ . Statistical theory used to obtain SN cross section from XN cross section.

Table 2

Nuclide	$\beta$	$E_2$ , MeV	$E_1$ , MeV	Nuclide	$\beta$	$E_2$ , MeV	$E_1$ , MeV
$^{64}\text{Zn}$	0.25	0.99	18	$^{76}\text{Ge}$	0.25	0.562	18
$^{66}\text{Zn}$	0.23	1.04	18	$^{78}\text{Se}$	0.33	0.559	18
$^{68}\text{Zn}$	0.2	1.08	18	$^{80}\text{Se}$	0.3	0.616	18
$^{70}\text{Ge}$	0.23	1.04	18	$^{82}\text{Se}$	0.25	0.654	18
$^{72}\text{Ge}$	0.25	0.835	18	$^{84}\text{Se}$	0.2	0.555	18
$^{74}\text{Ge}$	0.3	0.6	18				

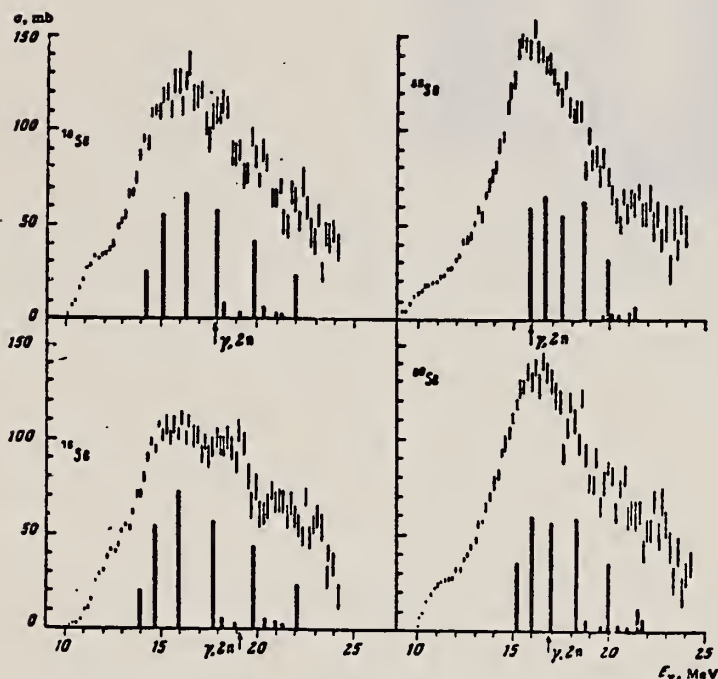


Fig. 3. The same as in Fig. 1, but for  $^{76,78,80,82}\text{Se}$ .

Cross sections of photoneutron reactions.  
 The dipole photoabsorption forces are taken from [6,7] (the solid black columns).

<sup>6</sup>M.G.Huber et al., Phys.Rev.155,1073(67)  
<sup>7</sup>M.G.Huber et al., Phys.Rev.192,223(66).

Values given are for  $\sigma_0$  (24.2 MeV).

Table 3

Nuclide	$\sigma$ , mb	Nuclide	$\sigma$ , mb	Nuclide	$\sigma$ , mb
$^{64}\text{Zn}$	$397 \pm 19$	$^{76}\text{Ge}$	$760 \pm 37$	$^{78}\text{Se}$	$1021 \pm 52$
$^{66}\text{Zn}$	$579 \pm 27$	$^{78}\text{Se}$	$872 \pm 41$	$^{80}\text{Se}$	$1029 \pm 50$
$^{68}\text{Zn}$	$718 \pm 35$	$^{80}\text{Se}$	$911 \pm 43$	$^{82}\text{Se}$	$1167 \pm 53$
$^{70}\text{Ge}$	$733 \pm 37$	$^{82}\text{Se}$	$930 \pm 50$		

\* Mean - square errors

ELEM. SYM.	A	Z
Se	78	34
REF. NO.		egf
76 Ca 1		

REACTION	RESULT	EXCITATION ENERGY	SOURCE		DETECTOR		ANGLE
			TYPE	RANGE	TYPE	RANGE	
$G, N$	ABX	10- 26	D	10- 26	MOD-I		4PI
$G, 2N$	ABX	18- 26	D	10- 26	MOD-I		4PI

993+

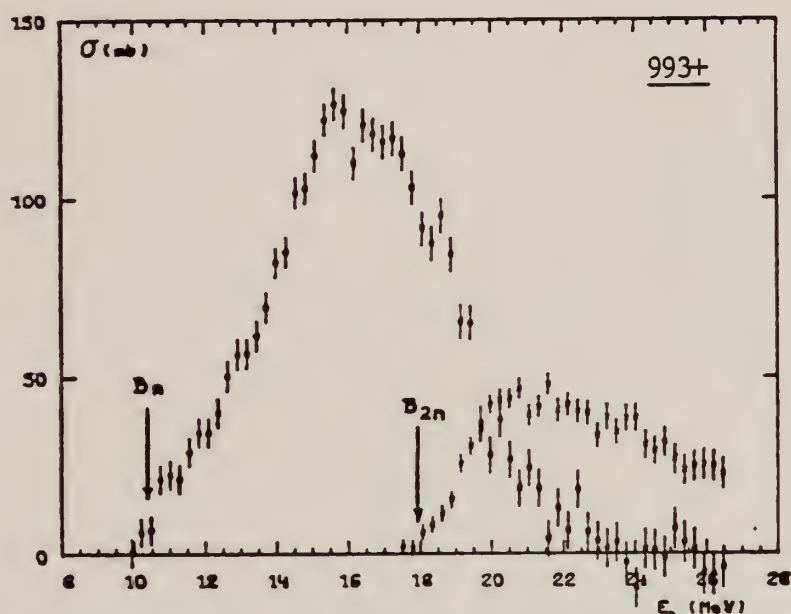


Fig. 9. Partial photoneutron cross sections [ $\sigma(\gamma, n) + \sigma(\gamma, pn)$ ] and  $\sigma(\gamma, 2n)$  for  $^{76}\text{Se}$ . Arrows  $B_n$  and  $B_{2n}$  indicate theoretical threshold values for  $(\gamma, n)$  and  $(\gamma, 2n)$  reactions respectively.

TABLE 3  
Integrated photoneutron cross sections and comparison with sum rules

Nucleus	$^{64}\text{Zn}$	$\begin{Bmatrix} ^{66}\text{Ga} \\ ^{71}\text{Ga} \end{Bmatrix}$	$^{70}\text{Ge}$	$^{72}\text{Ge}$	$^{74}\text{Ge}$	$^{76}\text{Ge}$	$^{75}\text{As}$	$^{76}\text{Se}$	$^{78}\text{Se}$	$^{80}\text{Se}$	$^{82}\text{Se}$
$E_x$ (MeV)	29	26.5	26.5	26.5	26.5	26.5	26.5	26.5	26.5	26.5	26.5
$\sigma_{00}$ (MeV · b)	0.75	0.91	0.78	0.94	1.02	1.12	1.09	1.01	1.06	1.11	1.13
$\frac{\sigma_{00}A}{0.06NZ}$	0.78	0.87	0.75	0.88	0.94	1	0.98	0.90	0.92	0.94	0.95
$B_n - B_p$ (MeV)	4.2	$\begin{Bmatrix} 3.7 \\ 1.4 \end{Bmatrix}$	3	1	-0.8	-2.6	3.3	1.7	0.1	-1.5	-3
$\sigma_{-10}$ (mb)	38	52	44	54	59	64	63	58	62	65	67
$\sigma_{-10}A^{-1}$ (mb)	0.15	0.18	0.15	0.18	0.19	0.20	0.20	0.18	0.19	0.19	0.19
$\sigma_{-20}$ (mb · MeV $^{-1}$ )	2.0	3.1	2.5	3.2	3.6	3.9	3.7	3.4	3.8	3.9	4.2
$\sigma_{-20}A^{-1}$ (mb · MeV $^{-1}$ )	1.9	2.6	2.1	2.6	2.8	2.9	2.8	2.5	2.7	2.6	2.7

FORM N35  
(REV. 7-14)  
USCOMM-N

The notation used is defined in the text. The average experimental errors  $\Delta\sigma_{00}/\sigma_{00}$ ,  $\Delta\sigma_{-10}/\sigma_{-10}$  and  $\Delta\sigma_{-20}/\sigma_{-20}$  are approximately 8%.





SE  
A=80

SE  
A=80

SE  
A=80



REF.

A. Hofmann, P. Stoll  
 Helv. Phys. Acta 31, 591 (1958)

ELEM. SYM.	A	Z
Se	80	34

METHOD

REF. NO.

58 Ho 1

egf

REACTION	RESULT	EXCITATION ENERGY	SOURCE		DETECTOR		ANGLE
			TYPE	RANGE	TYPE	RANGE	
G,NP	ABI	20- 32	C	32	ACT-I		4PI

( $\gamma$ ,np) yields include ( $\gamma$ ,d).

Tabelle I

Reaktion	Q-Wert MeV	I.W.Q. $\bar{\sigma}$ MeV barn	$\sigma_{\max}$ mb	$E_{\max}$ MeV	$\Gamma$ MeV
Ca <sup>40</sup> ( $\gamma$ , pn) K <sup>39</sup>	-24,3	0,005	2,4	30 $\pm$ 1	2,1
Zn <sup>64</sup> ( $\gamma$ , pn) Cu <sup>63</sup>	-18,36	0,03			
Zn <sup>66</sup> ( $\gamma$ , pn) Cu <sup>64</sup>	-18,65	0,031	7,2	28 $\pm$ 1	4
Zn <sup>68</sup> ( $\gamma$ , p) Cu <sup>67</sup>	-10,01	0,19	11,4	22,7 $\pm$ 1	6
Sc <sup>45</sup> ( $\gamma$ , pn) As <sup>75</sup>	-20,43	0,02			
Zn <sup>64</sup> ( $\gamma$ , 2n) Zn <sup>62</sup>	-20,82	0,08			
Mo <sup>98</sup> ( $\gamma$ , pn) Nb <sup>96</sup>	-19,5	0,02			
Sb <sup>123</sup> ( $\gamma$ , pn) Sn <sup>121</sup>	-18,2	0,0006			

Se

80

34

METHOD

REF. NO.

73 Sz 17

hmg

REACTION	RESULT	EXCITATION ENERGY	SOURCE		DETECTOR		ANGLE
			TYPE	RANGE	TYPE	RANGE	
G,G	LFT	8	D	8	SCD-D		DST
		(7.819)		(7.819)			

8=7.819 MEVTABLE I. Reduced partial radiation widths of the 7818.9-keV resonance level in <sup>83</sup>Se.

Energy of transitions (keV)	Energy of final state (keV)	Relative intensity (%)	Reduced widths (eV MeV <sup>-1</sup> × 10 <sup>3</sup> )		Most likely character
			<i>h</i> (E1)	<i>h</i> (M1)	
7818.9	0	100 ± 0.5	6 ± 1	117 ± 22	E1
6369.4	1449.5 ± 0.3	8.4 ± 0.2	1.0 ± 0.2	13 ± 4	E1 or M1
6339.4	1479.5 ± 0.1	9.4 ± 0.2	1.1 ± 0.2	21 ± 4	E1 or M1
5944.7	1874.2 ± 0.8	1.1 ± 0.2	0.2	3 ± 1	E1 or M1
5858.4	1960.5 ± 0.2	27.3 ± 0.3	4 ± 1	78 ± 14	E1
5507.2	2311.8 ± 0.7	4.2 ± 0.5	0.8 ± 0.2	14 ± 3	E1 or M1
5304.4	2514.5 ± 0.3	6.4 ± 0.3	1.3 ± 0.2	24 ± 5	E1 or M1
5191.6	2627.3 ± 0.4	1.0 ± 0.3	0.3 ± 0.1	4 ± 2	E1 or M1
5004.3	2814.6 ± 0.5	3.5 ± 0.3	0.8 ± 0.2	16 ± 3	E1 or M1
4991.4	2827.5 ± 0.2	12.4 ± 0.4	3 ± 1	56 ± 10	E1
4692.4	3126.5 ± 0.2	12.5 ± 0.3	4 ± 1	68 ± 13	E1
4619.1	3199.8 ± 0.3	5.5 ± 0.3	1.6 ± 0.3	30 ± 6	E1 or M1
4570.1	3248.8 ± 0.5	7.3 ± 0.3	2.2 ± 0.4	43 ± 8	E1
4502	3317 ± 1	2.2 ± 0.4	0.7 ± 0.2	14 ± 3	E1 or M1
4468.2	3350.7 ± 0.2	9.2 ± 0.4	3 ± 1	58 ± 11	E1
4427.1	3391.9 ± 0.3	8.5 ± 0.3	3 ± 1	55 ± 10	E1
4376.8	3442.1 ± 0.3	5.2 ± 0.4	1.9 ± 0.3	35 ± 7	E1 or M1
4212.0	3606.9 ± 0.4	3.7 ± 0.3	1.5 ± 0.3	28 ± 6	E1 or M1
4199.1	3619.8 ± 0.5	2.8 ± 0.3	1.1 ± 0.2	21 ± 5	E1 or M1
4163	3656 ± 1	1.3 ± 0.3	0.5 ± 0.1	10 ± 3	E1 or M1
3949.1	3869.8 ± 0.5	3.0 ± 0.4	1.5 ± 0.3	27 ± 6	E1 or M1
3866.9	3952.0 ± 0.4	3.0 ± 0.5	1.6 ± 0.4	30 ± 7	E1 or M1
3756.1	4062.8 ± 0.4	4.3 ± 0.4	3 ± 1	50 ± 10	E1

(over)



TABLE II. Experimental  $A_{22}$  coefficients compared with theory, assuming pure dipole.

Energy of transition (keV)	Energy of final state (keV)	Transitions in $^{80}\text{Se}$ Theoretical $A_{22}$ coefficients for various assumed spin sequences		
		0-1-0	0-1-1	0-1-2
		0.500	-0.250	0.050
7818.9	0	+0.500		
6369.4	1449.5			+0.15±0.13
6339.4	1479.5	+0.58±0.06		
5944.7	1874.2	+0.62±0.58		+0.62±0.58
5858.4	1960.5			+0.06±0.03
5507.2	2311.8			-0.03±0.17
5304.4	2514.5			+0.17±0.09
5004.3	2814.6	+0.37±0.37		+0.37±0.37 <sup>a</sup>
4991.4	2827.5			+0.13±0.07
4692.4	3126.5			+0.14±0.08
4619.1	3199.8			+0.21±0.10
4570.1	3248.8			+0.01±0.09
4502	3317	+1.2 ±0.7		
4468.2	3350.7		-0.25±0.08	
4427.1	3391.8			+0.11±0.07
4376.8	3442.1	+0.40±0.18		
4212.0	3606.9			+0.19±0.19
4190.1	3619.8	+0.46±0.23		
3949.1	3869.8		-0.25±0.30	-0.25±0.30
3866.9	3952.0		-0.30±0.38	-0.30±0.38
3756.1	4062.8	+0.39±0.24		

<sup>a</sup> Only spin assignment of 2 is valid for the final state, since the transition to the ground state was observed (see Fig. 1)

REF.

A.M. Goryachev, G.N. Zalesnyi, and B.A. Tulupov  
 Izv. Akad. Nauk SSSR. Ser. Fiz. 39, 134 (1975)  
 Bull. Acad. Sci. USSR Phys. Ser. 39, 116 (1975)

ELEM. SYM.

A

Z

Se

80

34

METHOD

REF. NO.

75 Go 1

hmg

REACTION	RESULT	EXCITATION ENERGY	SOURCE		DETECTOR		ANGLE
			TYPE	RANGE	TYPE	RANGE	
G, XN	ABX	9- 25	C	9- 25	BF3-I		4PI

$\sigma(G, SN)$ . Statistical theory used to obtain SN cross section from XN cross section.

Table 2

Nuclide	$\beta_0$	$E_2$ , MeV	$E_1$ , MeV	Nuclide	$\beta_0$	$E_2$ , MeV	$E_1$ , MeV
$^{64}\text{Zn}$	0.25	0.99	18	$^{76}\text{Ge}$	0.25	0.562	18
$^{66}\text{Zn}$	0.23	1.03	18	$^{78}\text{Se}$	0.33	0.559	18
$^{68}\text{Zn}$	0.2	1.08	18	$^{80}\text{Se}$	0.3	0.616	18
$^{70}\text{Zn}$	0.23	1.04	18	$^{82}\text{Se}$	0.25	0.654	18
$^{72}\text{Ge}$	0.25	0.835	18	$^{84}\text{Se}$	0.2	0.653	18
$^{74}\text{Ge}$	0.3	0.6	18				

<sup>6</sup>M.G. Huber et al., Phys. Rev. 155, 1073 (67)  
<sup>7</sup>M.G. Huber et al., Phys. Rev. 192, 223 (66).

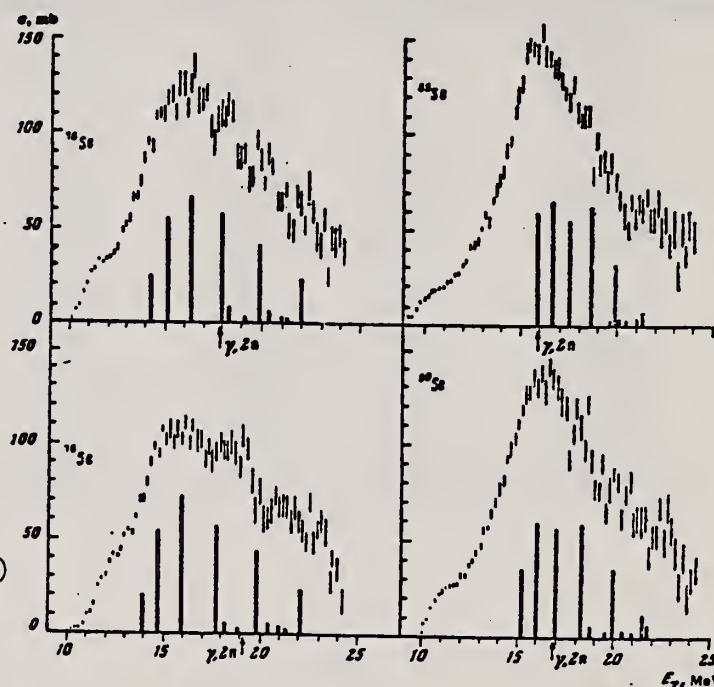
Fig. 3. The same as in Fig. 1, but for  $^{76,78,80,82}\text{Se}$ .

Table 3

Nuclide	$\sigma$ , mb	Nuclide	$\sigma$ , mb	Nuclide	$\sigma$ , mb
$^{64}\text{Zn}$	$397 \pm 19^*$	$^{72}\text{Ge}$	$760 \pm 37$	$^{76}\text{Se}$	$1021 \pm 52$
$^{66}\text{Zn}$	$579 \pm 27$	$^{74}\text{Ge}$	$872 \pm 41$	$^{78}\text{Se}$	$1029 \pm 50$
$^{68}\text{Zn}$	$718 \pm 35$	$^{76}\text{Ge}$	$911 \pm 43$	$^{80}\text{Se}$	$1067 \pm 53$
$^{70}\text{Zn}$	$731 \pm 37$	$^{78}\text{Se}$	$930 \pm 50$		

\*Mean - square errors

Cross sections of photoneutron reactions.  
 The dipole photoabsorption forces are taken from [6,7] (the solid black columns).

Values given are for  $\sigma_0$  (24.2 MeV).

REF.

P. Carlos, H. Beil, R. Bergere, J. Fagot, A. Lepretre,  
A. Veyssiere, G. V. Solodukhov  
Nucl. Phys. A258, 365 (1976)

ELEM. SYM.

A

Z

Se

80

34

METHOD

REF. NO.

76 Ca 1

egf

REACTION	RESULT	EXCITATION ENERGY	SOURCE		DETECTOR		ANGLE
			TYPE	RANGE	TYPE	RANGE	
$G, N$	ABX	10- 28	D	10- 28	MOD-I		4PI
$G, 2N$	ABX	16- 28	D	10- 28	MOD-I		4PI

996+

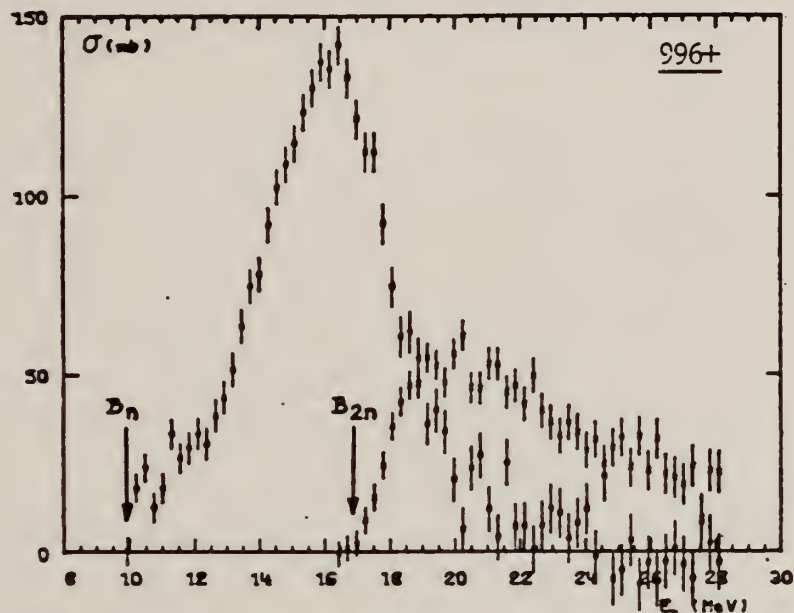


Fig. 10. Partial photoneutron cross section [ $\sigma(\gamma, n) + \sigma(\gamma, pn)$ ] and  $\sigma(\gamma, 2n)$  for  $^{80}\text{Se}$ . Arrows  $B_n$  and  $B_{2n}$  indicate theoretical threshold values for  $(\gamma, n)$  and  $(\gamma, 2n)$  reactions respectively.

TABLE 3

Integrated photoneutron cross sections and comparison with sum rules

Nucleus	$^{44}\text{Zn}$	$^{60}\text{Ga}$ $^{71}\text{Ga}$	$^{70}\text{Ge}$	$^{72}\text{Ge}$	$^{74}\text{Ge}$	$^{76}\text{Ge}$	$^{78}\text{As}$	$^{76}\text{Se}$	$^{78}\text{Se}$	$^{80}\text{Se}$	$^{82}\text{Se}$
$E_M$ (MeV)	29	26.5	26.5	26.5	26.5	26.5	26.5	26.5	26.5	26.5	26.5
$\sigma_{00}$ (MeV · b)	0.75	0.91	0.78	0.94	1.02	1.12	1.09	1.01	1.06	1.11	1.13
$\frac{\sigma_{00} A}{0.06 NZ}$	0.78	0.87	0.75	0.88	0.94	1	0.98	0.90	0.92	0.94	0.95
$B_n - B_p$ (MeV)	4.2	$\begin{Bmatrix} 3.7 \\ 1.4 \end{Bmatrix}$	3	1	-0.8	-2.6	3.3	1.7	0.1	-1.5	-3
$\sigma_{-10}$ (mb)	38	52	44	54	59	64	63	58	62	65	67
$\sigma_{-10} A^{-1/2}$ (mb)	0.15	0.18	0.15	0.18	0.19	0.20	0.20	0.18	0.19	0.19	0.19
$\sigma_{-20}$ (mb · MeV $^{-1}$ )	2.0	3.1	2.5	3.2	3.6	3.9	3.7	3.4	3.8	3.9	4.2
$\sigma_{-20} A^{-1/2}$ (mb · MeV $^{-1}$ )	1.9	2.6	2.1	2.6	2.8	2.9	2.8	2.5	2.7	2.6	2.7

FORM N35-1  
(REV. 7-16-61)  
USCOMM-N2

The notation used is defined in the text. The average experimental errors  $\Delta\sigma_{00}/\sigma_{00}$ ,  $\Delta\sigma_{-10}/\sigma_{-10}$  and  $\Delta\sigma_{-20}/\sigma_{-20}$  are approximately 3%. 129



SE  
A=82

SE  
A=82

SE  
A=82





ELEM. SÍM.	Z	A
Se	82	34

METHOD  
Betatron

REF. NO.  
56 S1 2 NVB

REACTION	RESULT	EXCITATION ENERGY	SOURCE		DETECTOR		ANGLE
			TYPE	RANGE	TYPE	RANGE	
G,N	ABX	9-22	C	9-22	ACT-I		4PI

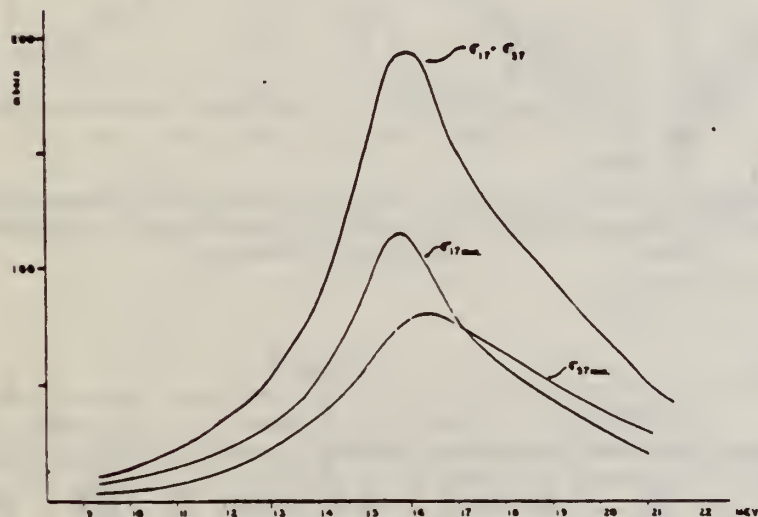


Fig. 5

TABELA I

REAÇÃO	$\sigma_{\text{max}}$ (barns)	$\Gamma$ (largura) (Mev)	$\int \sigma dE$ Experimental	$\int \sigma dE$ teórico	
				$x = 0$	$x = 0,55$
$\text{Se}^{82}(\gamma, n) \text{Se}^{81}$ e $\text{Se}^{81}$	0,19	4,6	0,87 Mev-barn	1,23 Mev-barn	1,77 Mev-barn

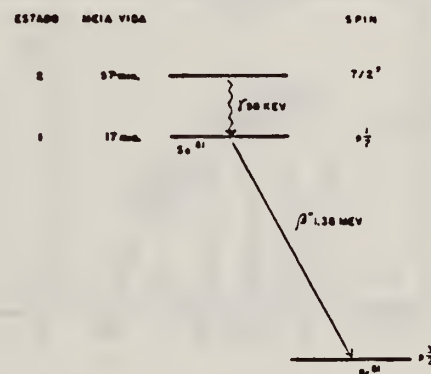


Fig. 1

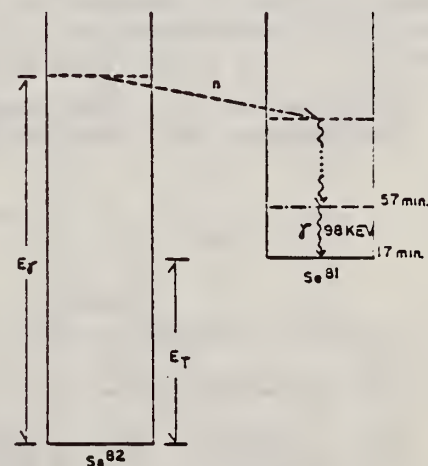


Fig. 2

REF. A.M. Goryachev, G.N. Zalesnyi, and B.A. Tulupov  
Izv. Akad. Nauk SSSR. Ser. Fiz. 39, 134 (1975)  
Bull. Acad. Sci. USSR Phys. Ser. 39, 116 (1975)

ELEM. SYM.	A	Z
Se	82	34

METHOD			REF. NO.		
			75 Go 1		hmg
REACTION	RESULT	EXCITATION ENERGY	SOURCE		ANGLE
			TYPE	RANGE	
G, XN	ABX	9- 25	C	9- 25	4PI

$\sigma(G,SN)$ . Statistical theory used to obtain SN cross section from XN cross section.

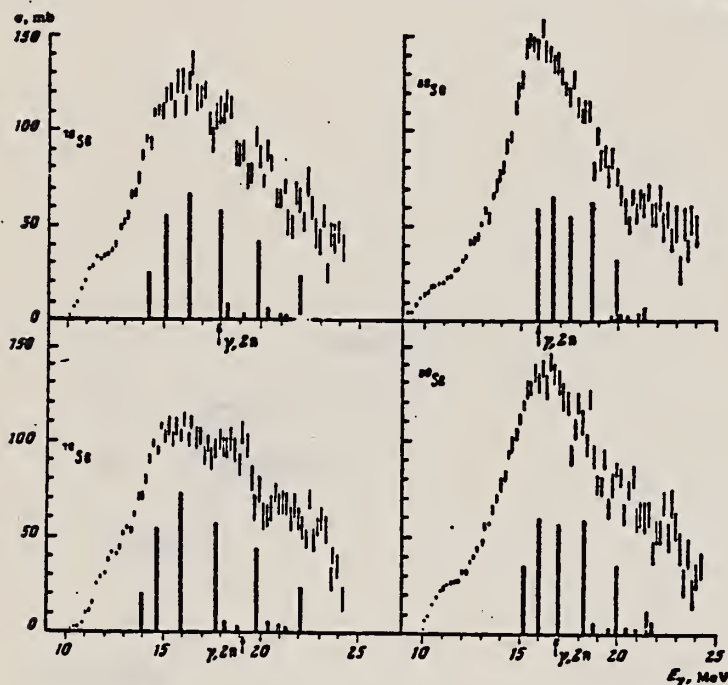


Fig. 3. The same as in Fig. 1, but for  $^{76,78,80,82}\text{Se}$ .

Cross sections of photoneutron reactions.  
The dipole photoabsorption forces are taken from [6,7] (the solid black columns).

<sup>6</sup>M.G.Huber et al., Phys.Rev.155,1073(67)  
<sup>7</sup>M.G.Huber et al., Phys.Rev.192,223(66).

Table 2

Nuclide	$\beta_0$	$E_2$ , MeV	$E_1$ , MeV	Nuclide	$\beta_0$	$E_2$ , MeV	$E_1$ , MeV
$^{64}\text{Zn}$	0.25	0.99	18	$^{76}\text{Se}$	0.25	0.562	18
$^{66}\text{Zn}$	0.23	1.01	18	$^{78}\text{Se}$	0.33	0.539	18
$^{68}\text{Zn}$	0.2	1.08	18	$^{80}\text{Se}$	0.3	0.616	18
$^{70}\text{Zn}$	0.23	1.04	18	$^{82}\text{Se}$	0.25	0.654	18
$^{72}\text{Ge}$	0.25	0.835	18				
$^{74}\text{Ge}$	0.3	0.6	18				

Table 3

Nuclide	$\sigma$ , mb	Nuclide	$\sigma$ , mb	Nuclide	$\sigma$ , mb
$^{64}\text{Zn}$	$397 \pm 19$	$^{76}\text{Se}$	$769 \pm 37$	$^{76}\text{Se}$	$1021 \pm 32$
$^{66}\text{Zn}$	$379 \pm 27$	$^{78}\text{Se}$	$872 \pm 41$	$^{80}\text{Se}$	$1029 \pm 30$
$^{68}\text{Zn}$	$718 \pm 37$	$^{80}\text{Se}$	$911 \pm 43$	$^{82}\text{Se}$	$1067 \pm 33$
$^{70}\text{Ge}$	$733 \pm 37$	$^{82}\text{Se}$	$930 \pm 50$		

\*Mean - square errors

FORM NBS-418  
(REV. 7-14-64)  
USCOMM-OC 26010-P64

Values given are for  $\sigma_0$  (24.2 MeV).

ELEM. SYM.	A	Z
Se	82	34
REF. NO.		
76 Ca 1		egf

REACTION	RESULT	EXCITATION ENERGY	SOURCE		DETECTOR		ANGLE
			TYPE	RANGE	TYPE	RANGE	
G,N	ABX	9- 26	D	9- 26	MOD-I		4PI
G,2N	ABX	16- 26	D	9- 26	MOD-I		4PI

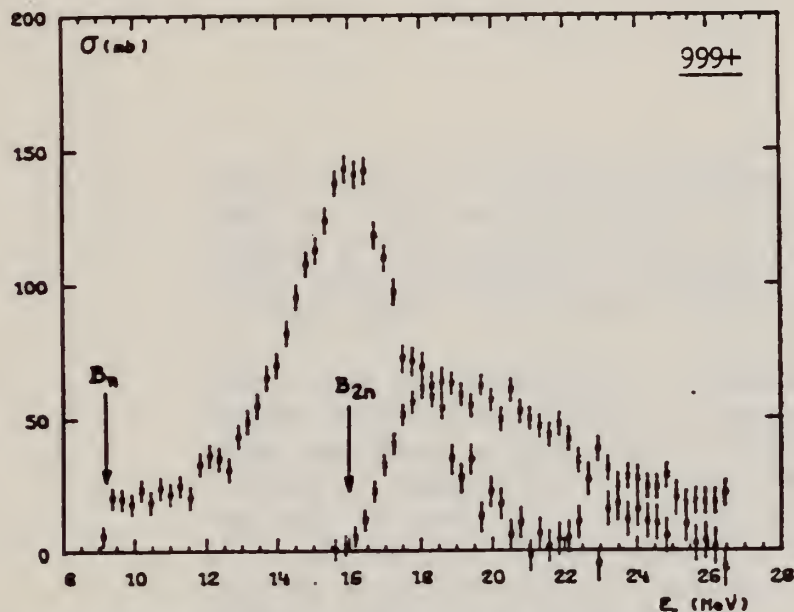


Fig. 11. Partial photoneutron cross sections  $[\sigma(\gamma, n) + \sigma(\gamma, pn)]$  and  $\sigma(\gamma, 2n)$  for  $^{82}\text{Se}$ . Arrows  $B_n$  and  $B_{2n}$  indicate theoretical threshold values for  $(\gamma, n)$  and  $(\gamma, 2n)$  reactions respectively. Data were not corrected for impurities.

TABLE 3  
Integrated photoneutron cross sections and comparison with sum rules

Nucleus	$^{64}\text{Zn}$	$\begin{Bmatrix} ^{69}\text{Ga} \\ ^{71}\text{Ga} \end{Bmatrix}$	$^{70}\text{Ge}$	$^{72}\text{Ge}$	$^{74}\text{Ge}$	$^{76}\text{Ge}$	$^{78}\text{As}$	$^{76}\text{Se}$	$^{78}\text{Se}$	$^{80}\text{Se}$	$^{82}\text{Se}$
$E_{\text{th}}$ (MeV)	29	26.5	26.5	26.5	26.5	26.5	26.5	26.5	26.5	26.5	26.5
$\sigma_{00}$ (MeV · b)	0.75	0.91	0.78	0.94	1.02	1.12	1.09	1.01	1.06	1.11	1.13
$\frac{\sigma_{00} A}{0.06 NZ}$	0.78	0.87	0.75	0.88	0.94	1	0.98	0.90	0.92	0.94	0.95
$B_n - B_p$ (MeV)	4.2	$\begin{Bmatrix} 3.7 \\ 1.4 \end{Bmatrix}$	3	1	-0.8	-2.6	3.3	1.7	0.1	-1.5	-3
$\sigma_{-10}$ (mb)	38	52	44	54	59	64	63	58	62	65	67
$\sigma_{-10} A^{-1}$ (mb)	0.15	0.18	0.15	0.18	0.19	0.20	0.20	0.18	0.19	0.19	0.19
$\sigma_{-20}$ (mb · MeV $^{-1}$ )	2.0	3.1	2.5	3.2	3.6	3.9	3.7	3.4	3.8	3.9	4.2
$\sigma_{-20} A^{-1}$ (mb · MeV $^{-1}$ )	1.9	2.6	2.1	2.6	2.8	2.9	2.8	2.5	2.7	2.6	2.7





D.P.

## BROMINE

Z=35

Tyrian purple (an organic compound of bromine) was used as a rich and costly dye centuries before the element bromine was discovered. It was prepared from a white juice secreted by the Mediterranean mollusk that was mentioned in the Bible (Ezek. 27:7,16).

Credit for the discovery of bromine is given to Antoine-Jérôme Balard (1802-1876), a Frenchman and an obscure young assistant at the chemistry department of the College of Montpellier. At the time of his discovery he was only 23 years old. In 1824, while studying the flora of a salt marsh, Balard noticed a deposit of sodium sulfate which had crystallized out in a pan containing mother liquid from common salt. In an attempt to find a use for these waste liquors he made a series of observations which led to the discovery of bromine. He suggested the name "muride" for the new element to the French Academy of Science. They, in turn, proposed the name "brome" from the Greek word *bromos* meaning stench, to indicate its strong irritating odor.

D.P.

D.P.



METHOD

Linac; isomer yield; activity

REF. NO.

63 Ka 2

NVB

REACTION	RESULT	EXCITATION ENERGY	SOURCE		DETECTOR		ANGLE
			TYPE	RANGE	TYPE	RANGE	
G,G/	RLY	1	C4		ACT-I		4PI
		(0.21)					

Table II. The isomers observed

Isomer	Observed value		Referenced value <sup>(1)(13)</sup>	
	Half-life	Energy (MeV)	Half-life	Energy (MeV)
Se-77m	17.5 sec	0.160	17.5 sec	0.161
Br-79m	4.80 sec	0.209	4.8 sec	0.208
Sr-87m	2.3 hr	0.390	2.8 hr	0.388
Y-89m	15.0 sec	0.920	14 sec	0.915
Rh-103m	58 min	*	57 min	0.040
Ag-107m	42 sec	0.95	44 sec	0.094
Ag-109m			40 sec	0.088
Cd-111m	47 min	0.150,0.255	49 min	0.150,0.247
In-115m	4.5 hr	0.335	4.5 hr	0.335
Sn-117m	17 day	0.160	14 day	0.159,0.161
Ba-137m	2.6 min	0.660	2.6 min	0.662
Er-167m	2.10 sec	0.209	2.5 sec	0.208
Hf-179m	18.5 sec	0.157,0.215	19 sec	0.161,0.217
W-183m	5.4 sec	0.200,0.170,0.115	5.5 sec	0.1025,0.2915 others
Ir-191m	4.90 sec	0.129, <0.07	4.9 sec	0.042-0.129
Pt-195m	4.5 day	0.065**	4.1 day	0.031-0.130
Au-197m	7.0 sec	0.10,0.27,0.40	7.2 sec	0.130,0.270,0.407
Hg-199m	43 min	0.160,0.370	42 min	0.158,0.368

\* This isomer was measured with a G-M flow counter.

\*\* This value corresponds to Pt-K X-ray energy.

Table III. Induced activation rate

Element	Beam energy (MeV)	Counting rate ( $\times 10000$ cpm)	Sample form
Se	5	1300	metallic plate
Br	4	1600	NaBr grain
Sr	6	0.3	SrCO <sub>3</sub> powder
Y	5	90	metallic grain
Rh	5	(0.2)*	RhCl <sub>3</sub> grain
Ag	5	180	metallic plate
Cd	6	0.5	CdCl <sub>2</sub> grain
In	6	8	metallic plate
Sn	6	0.0005	metallic plate
Ba	5	0.6	BaS powder
Er	4	4900	Er <sub>2</sub> O <sub>3</sub> powder
Hf	5	1600	metallic plate
W	5	120	metallic powder
Ir	5	2100	metallic powder
Pt	5	0.3	metallic plate
Au	4	4200	metallic plate
Hg	6	0.09	metallic liquid

\* The value measured with a G-M flow counter.

REF.

J. W. Jury, J. S. Hewitt, and K. G. McNeill  
 Can. J. Phys. 46, 1823 (1968)

ELEM. SYM.	A	Z
Br		35
METHOD		REF. NO.
		68 Ju 1
		EGF

REACTION	RESULT	EXCITATION ENERGY	SOURCE		DETECTOR		ANGLE
			TYPE	RANGE	TYPE	RANGE	
G,N	NOX	THR - 27	C	27	THR	5-	DST

$$W(\theta) = a_0 + a_1 P_1 + a_2 P_2$$

TABLE I

Target element	Z	Energy	$a_0^*$	$a_1/a_0$	$a_2/a_0$
Vanadium	23	32	$640 \pm 50$	$0.11 \pm 0.10$	$-0.09 \pm 0.11$
Chromium	24	22	$365 \pm 39$	$0.02 \pm 0.08$	$0.00 \pm 0.10$
Manganese	25	22	$450 \pm 33$	$0.07 \pm 0.05$	$-0.11 \pm 0.06$
Bromine	35	27	$874 \pm 54$	$0.05 \pm 0.06$	$-0.15 \pm 0.08$
Molybdenum	42	22	$610 \pm 60$	$0.09 \pm 0.05$	$-0.35 \pm 0.06$
Ruthenium	44	27	$1100 \pm 25$	$0.12 \pm 0.02$	$-0.29 \pm 0.03$
Rhodium	45	27	$1270 \pm 47$	$0.06 \pm 0.03$	$-0.14 \pm 0.03$
Palladium	46	27	$1350 \pm 29$	$0.26 \pm 0.02$	$-0.12 \pm 0.02$
Antimony	51	27	$2140 \pm 62$	$0.04 \pm 0.08$	$-0.25 \pm 0.11$
Lanthanum	57	27	$1940 \pm 70$	$0.12 \pm 0.10$	$-0.52 \pm 0.14$
Praseodymium	59	30	$1800 \pm 58$	$0.20 \pm 0.08$	$-0.40 \pm 0.09$
Platinum	78	27	$2600 \pm 52$	$0.17 \pm 0.02$	$-0.15 \pm 0.03$
Lead	82	22	$2274 \pm 59$	$0.08 \pm 0.08$	$-0.46 \pm 0.09$

\*The yield per mole per 100 r was normalized to a yield of 2274 for the lead sample at the same energy.

REF. R.F. Barrett, J.R. Birkelund, B.J.,Thomas, K.S. Lam, and H.H. Thies Nucl. Phys. <u>A210</u> , 355 (1973)			ELEM. SYM. A		Z		
			Br		35		
METHOD			REF. NO.				
			73 Ba 20				
			egf				
REACTION	RESULT	EXCITATION ENERGY	SOURCE		DETECTOR		ANGLE
			TYPE	RANGE	TYPE	RANGE	
G,N	NOX	THR- 27	C	10- 27	BF3-I		4PI

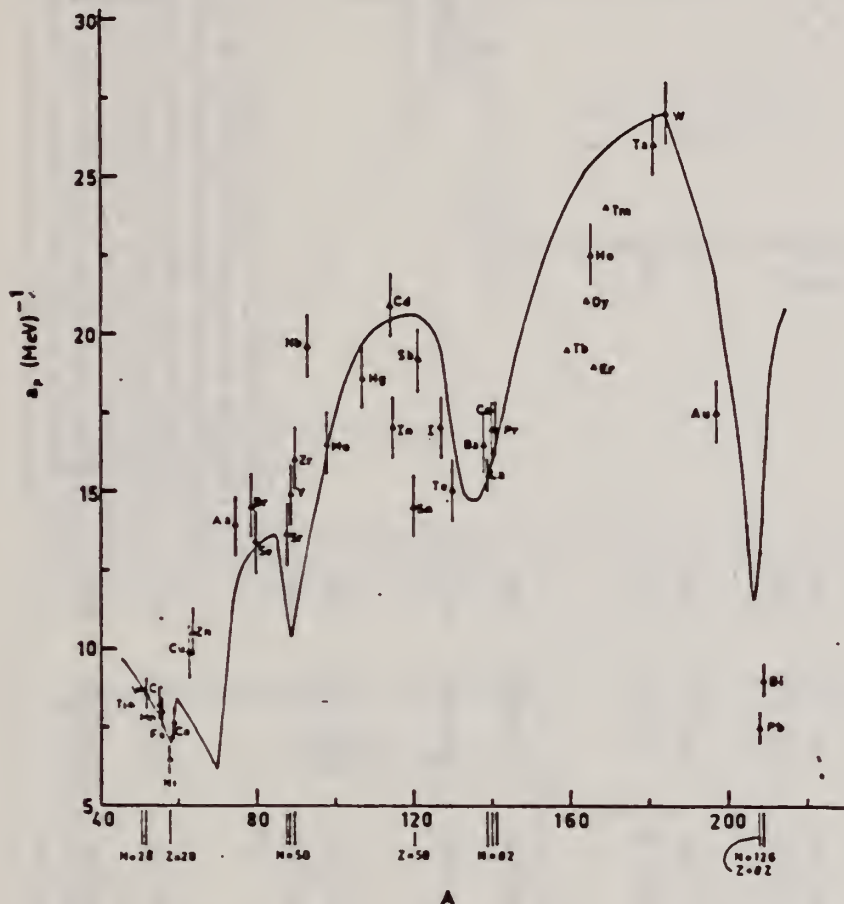


Fig. 12. Experimental values of the level density parameter  $a_p$  (Fermi gas formula plus pairing correction) versus atomic number  $A$ . The continuous curve is a least-squares fit to the data of a theoretical calculation from Newton <sup>15</sup>).

- 1 H. Baba and S. Baba, Japan Atomic Energy Research Institute report JAERI-1183 (1969).
- 2 H. Baba, Nucl. Phys. A159, 625 (1970).
- 15 T.D. Newton, Can. J. Phys. 34, 804 (1956).

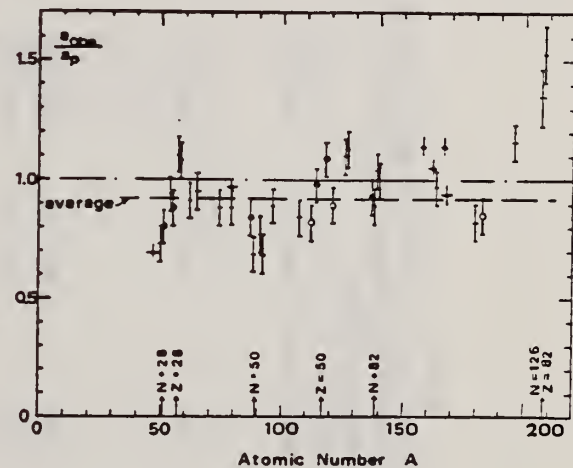


Fig. 15. Ratio  $a_{obs}/a_p$  versus atomic number  $A$ . Here  $a_{obs}$  is the level density parameter taken from the neutron resonance work of refs. <sup>1,2</sup>, and  $a_p$  is the level density parameter derived from the present  $(\gamma, n)$  work. Filled circles represent points where nuclei in the neutron resonance and in the  $(\gamma, n)$  experiment were the same. Open circles represent points where the respective nuclei were approximately matched. Triangles represent points which are based on measurement of neutron mean energies at two bremsstrahlung energies only.

(over)



TABLE 3

Comparison of experimental and theoretical data on nuclear level densities with Fermi gas formulae, and comparison of nuclear level density parameters from  $(\gamma, n)$  and  $n$ -resonance absorption experiments

Target	N (residual nucleus) <sup>a)</sup>	Goodness of fit <sup>b)</sup>	$E_n(24)$ (MeV) <sup>c)</sup>	T (MeV) <sup>d)</sup>	$a_p$ (MeV <sup>-1</sup> ) <sup>e)</sup>	$a_{nR}$ (MeV <sup>-1</sup> ) <sup>f)</sup>	$a_{nR}/a_p$
Ti <sup>g)</sup>	23 8%		1.93	8.1- <sup>47</sup> Ti	6.41- <sup>47</sup> Ti	0.79	
	24 8%						
	25 73%						
	26 5%						
	27 5%						
V <sup>h)</sup>	27 100%		1.96	8.7- <sup>50</sup> V	6.35- <sup>51</sup> V	0.73	
Cr	25 4%	P	1.89	8.6- <sup>51</sup> Cr	6.9- <sup>51</sup> Cr	<u>0.80</u>	
	27 84%						
	28 10%						
	29 2%						
Mn	29 100%	V.P.	2.1	8.2- <sup>54</sup> Mn	7.82- <sup>50</sup> Mn	0.94	
Fe	27 6%	F	1.96	8.0- <sup>53</sup> Fe	7.06- <sup>53</sup> Fe	<u>0.88</u>	
	29 92%						
	30 2%						
Co	31 100%	P	2.12	7.7- <sup>50</sup> Co	8.35- <sup>60</sup> Co	1.08	
Ni (Z = 28)	29 68%	V.P.	2.04	6.5- <sup>57</sup> Ni	7.19- <sup>59</sup> Ni	1.10	
	31 26%						
	32 1%						
	33 4%						
	35 1%						
Cu	33 69%	V.P.	1.78	9.8- <sup>63</sup> Cu	8.90- <sup>64</sup> Cu	0.91	
	35 31%						
Zn	33 49%	F	1.61	10.5- <sup>64</sup> Zn	10.0- <sup>65</sup> Zn	0.95	
	35 28%						
	36 4%						
	37 19%						
As	41 100%	V.P.	1.44	14.5- <sup>74</sup> As	12.81- <sup>76</sup> As	0.88	
Se <sup>h)</sup>	41 9%		1.39	13.3- <sup>76</sup> Se	12.8- <sup>78</sup> Se	<u>0.97</u>	
	42 8%						
	43 24%						
	45 50%						
	47 9%						
Br	43 43%	V.P.	1.41	14.5- <sup>79</sup> Br	12.69- <sup>80</sup> Br	0.88	
	45 49%						
Sr	47 10%	F	1.31	13.6- <sup>87</sup> Sr	11.4- <sup>87</sup> Sr	<u>0.84</u>	
	48 7%						
	49 83%						

- <sup>a)</sup> Neutron numbers and abundances of respective residual nuclei in  $(\gamma, n)$  experiments.  
<sup>b)</sup> These give an assessment of the goodness of fit of a calculated  $\bar{E}_n$  versus  $E_0$  curve to the observed data, using the Fermi gas level density formula both without and with pairing corrections.  
<sup>c)</sup> Bremsstrahlung photon neutron mean energies  $\bar{E}_n$  for peak bremsstrahlung energy  $E_0 = 24$  MeV.  
<sup>d)</sup> Nuclear temperature from fit with constant-temperature formula.  
<sup>e)</sup> Level density parameter  $a_p$  derived from the present  $(\gamma, n)$  experiment, using a Fermi gas formula plus pairing correction, and corresponding residual nucleus (the atomic weight shown is the weighted average of atomic weights of the respective isotopes present).  
<sup>f)</sup> As column 7, but using data on  $n$ -resonance absorption from refs. 1, 2).  
<sup>g)</sup> Measurements of  $\bar{E}_n$  ( $E_0$ ) for these nuclei were made only for  $E_0 = 21, 23$  and  $24$  MeV.

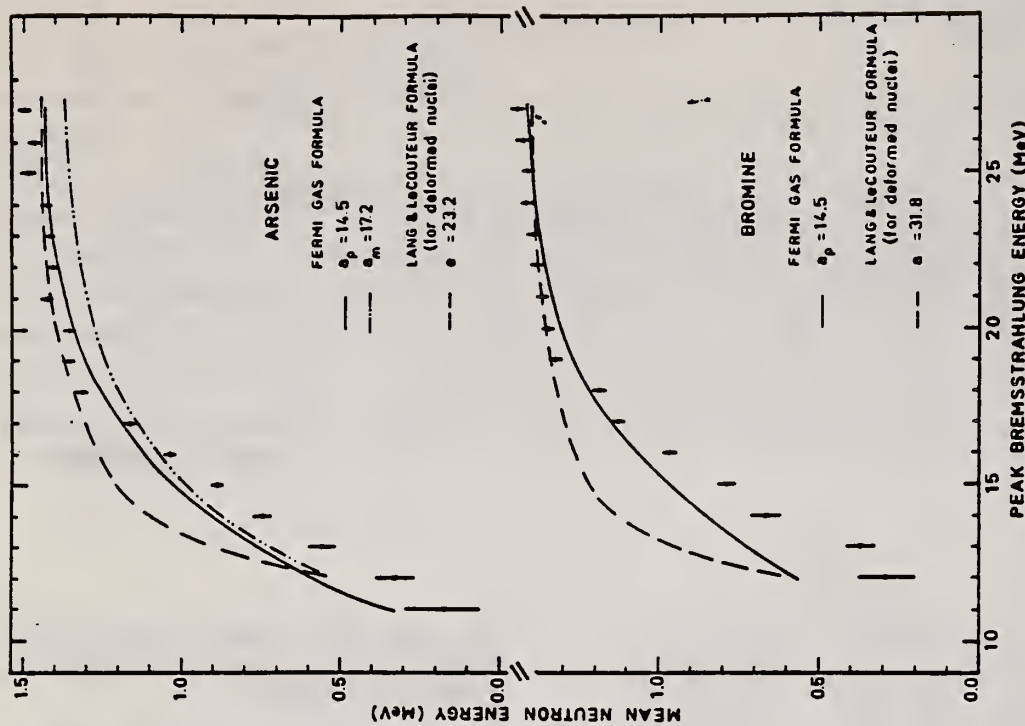


Fig. 7. Same as fig. 5, for arsenic and bromine.

REACTION	REAGENT	EXCITATION ENERGY	SOURCE		DETECTOR		ANGLE
			TYPE	RANGE	TYPE	RANGE	
G,NA24	ABY	THR-999	C	400-999	ACT-I		4PI

999=1 GEV

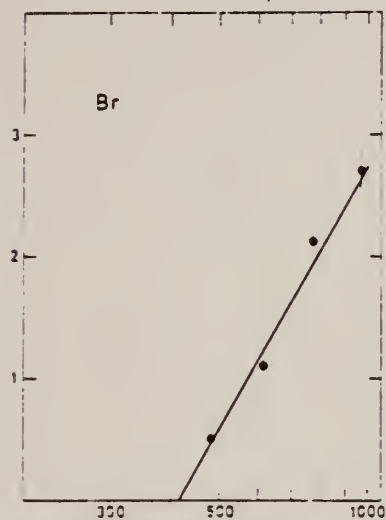


Fig. 1b Bremsstrahlung energy (MeV)

Fig. 1a-j. The measured yield as a function of bremsstrahlung and point energy. The error bars give the statistical errors in the numbers of  $\gamma$ -quanta detected. The solid lines are fitted to the yield points with the least-squares method. The yield from Cu (Fig. 1a) is measured in [1] and has been recalculated using the monitor curve of [5].

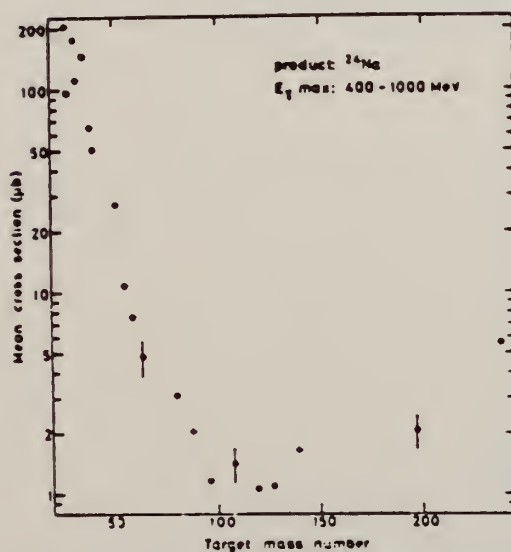


Fig. 2. The mean cross section in the energy range 400 to 1000 MeV calculated from the yields of Figure 1 in this work and of Figures 1 and 2 in [1]. The energy is given by  $E_{\gamma}$  in some points.

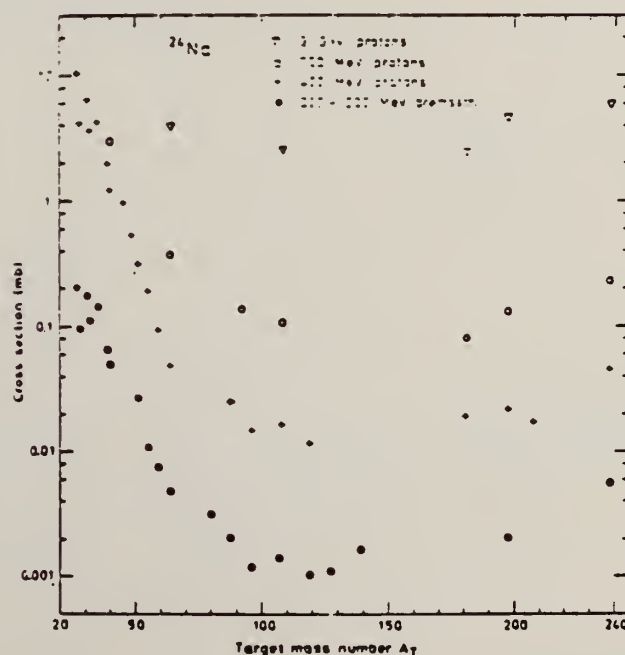


Fig. 4. Mean cross sections of the present work and of [1] (●) compared with the cross sections in proton irradiations: + 400 MeV from [4], ○ 700 MeV from [16] and an extrapolated value from [17], ▽ 3 GeV from [18].



Dr  
A=79

Dr  
A=79

Dr  
A=79





REF.

H. Langhoff, L. Frevert, W. Schott and A. Flammersfeld  
Nucl. Phys. 79, 145 (1966)

ELEM. SYM.

A

Z

Br

79

35

METHOD

REF. NO.

Resonance Fluorescence

[Page 1 of 2]

66 La 1

JDM

REACTION	RESULT	EXCITATION ENERGY	SOURCE		DETECTOR		ANGLE
			TYPE	RANGE	TYPE	RANGE	
G <sub>1</sub> G	LFT	0 - 1	D	0 - 1	NAI-D	0 - 1	123

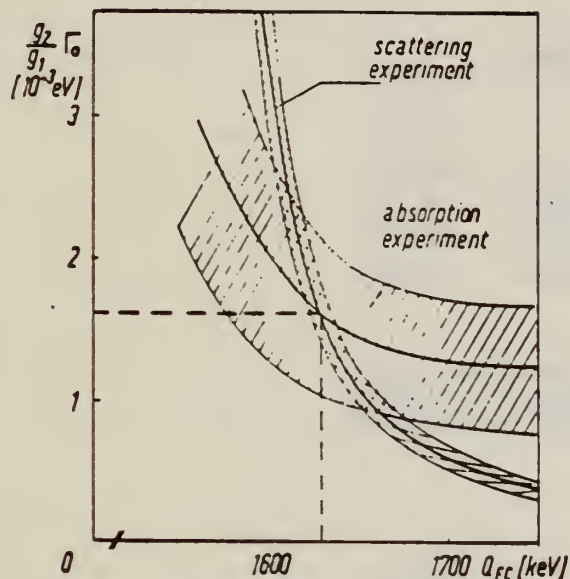


Fig. 5.  $g_2/g_1$  for the 834 keV transition determined by the scattering and by the absorption experiments is plotted as a function of the transition energy  $Q_{ec}$ .

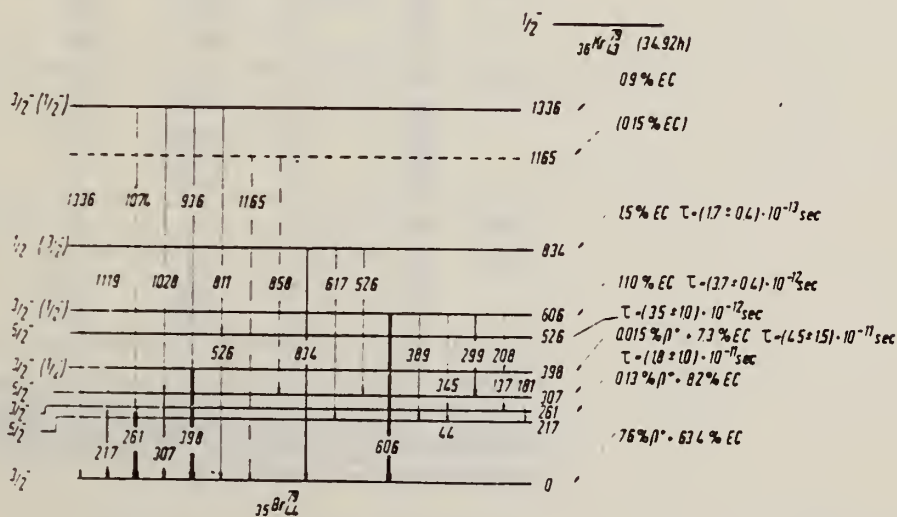


Fig. 7. Decay scheme of  $^{78}\text{Kr}$  supplemented by the results of the present investigation.

H. Langhoff, L. Frevert, W. Schött and A. Flammersfeld  
Nucl. Phys. 79, 145 (1966)

Br

79

35

## METHOD

REF. NO.

Resonance Fluorescence

[Page 2 of 2]

66 La 1

JDM

REACTION	RESULT	EXCITATION ENERGY	SOURCE		DETECTOR		ANGLE
			TYPE	RANGE	TYPE	RANGE	

TABLE I

Results of resonance scattering and absorption experiments

$E_\gamma$ (keV)	$\sigma_{sc}$ (mb)	$\frac{g_1 \Gamma_0^2}{g_0 \Gamma}$ (meV)	$\frac{\Gamma_0}{\Gamma}$	$\epsilon$	$\frac{g_1}{g_0} \Gamma_0$ (meV)
834	$70 \pm 10$	$1.25 \pm 0.28$	0.80	$(18.1 \pm 6.7) \%$	$1.6 \pm 0.6$
606	$60 \pm 4$	$(0.95 \pm 0.07) \cdot 10^{-1}$	0.73	$(6.0 \pm 1.7) \%$	$0.15 \pm 0.04$
526 a	$330 \pm 90$	$(2.8 \pm 0.7) \cdot 10^{-1}$	1.00	$(20.7 \pm 8.8) \%$	$0.28 \pm 0.12$
b	$115 \pm 30$	$(1.0 \pm 0.3) \cdot 10^{-1}$			
398	$23 \pm 4$	$(1.23 \pm 0.22) \cdot 10^{-2}$	0.92		
307	$240 \pm 110$	$(5.4 \pm 2.5) \cdot 10^{-2}$	0.99		

The average cross sections for scattering  $\sigma_{sc}$  yield the values for  $g_1 \Gamma_0^2 / g_0 \Gamma$  given in column 3.  $\epsilon$  represents the self absorption in the NaBr absorber and allows the calculation of  $g_1 \Gamma_0 / g_0 \Gamma$ .  $\Gamma_0 / \Gamma$  have been obtained from the measurements described in sect. 3.

TABLE 4

 $\gamma$ -transition probabilities in  $^{79}\text{Br}$ 

$E_{\text{level}}$ (keV)	$E_\gamma$ (keV)	Spins	$\frac{\Gamma_i}{\Gamma}$	$T_{M1+E2}$ [ $10^{10} \text{ sec}^{-1}$ ]	$T_{E2}$ [ $10^{10} \text{ sec}^{-1}$ ]	$ \delta $	$\frac{T_{M1}}{T_{E2}}$	$\frac{T_{E2}}{T_{E2}}$
834	834	$(\frac{1}{2}) \rightarrow \frac{3}{2}$	0.80	485			2	
	617	$\frac{1}{2} \rightarrow \frac{1}{2}$	0.04	20				(90)
	526	$\frac{1}{2} \rightarrow \frac{1}{2}$	0.16	100				(1000)
606	606	$\frac{1}{2} \rightarrow \frac{1}{2}$	0.73	20	2.1	0.32	21	10
	389	$\frac{1}{2} \rightarrow \frac{1}{2}$	0.12	3.2			35	
	345	$\frac{1}{2} \rightarrow \frac{1}{2}$	0.00072	0.2			400	
	299	$\frac{1}{2} \rightarrow \frac{1}{2}$	0.077	2.1			25	
	208	$\frac{1}{2} \rightarrow \frac{1}{2}$	0.040	1.1			15	
526	526	$\frac{1}{2} \rightarrow \frac{1}{2}$	1.00	28	3.1	0.33	10	30
398	398	$\frac{1}{2} \rightarrow \frac{1}{2}$	0.92	2.0	0.05	0.16	61	2
	181	$\frac{1}{2} \rightarrow \frac{1}{2}$	0.008	0.018			610	
	137	$\frac{1}{2} \rightarrow \frac{1}{2}$	0.065	0.14			34	
307	307	$\frac{1}{2} \rightarrow \frac{1}{2}$	0.99	5.6	0.05	0.10	10	7

$T_{M1+E2}$  represents the partial transition probability determined in the resonance fluorescence investigation. The  $E2$  transition probabilities  $T_{E2}$  obtained from Coulomb excitation experiments yield together with  $T_{M1+E2}$  the mixing ratios  $|\delta|$ . The results are compared with predictions of the single-particle model in column 8 and 9.

BR  
A=81

BR  
A=81

BR  
A=81



REF.

J. Schmouker, P. Erdos, P. Jordan and P. Stoll  
 J. Phys. Radium 16, 169 (1955)

ELEM. SYM.	A	Z
Br	81	35

METHOD

REF. NO.	EGF
55 Sc 2	

REACTION	RESULT	EXCITATION ENERGY	SOURCE		DETECTOR		ANGLE
			TYPE	RANGE	TYPE	RANGE	
G,A	ABY	THR - 32	C	32	ACT-I		4PI

Betatron run at 31.5 MeV. Yields measured relative to  $^{65}\text{Cu}(\gamma, n)^{64}\text{Cu} = 1.4$  barn-MeV

$^{63}\text{Cu}(\gamma, n)^{62}\text{Cu} = 0.7$  barn-MeV

$\sigma$   $^{31}\text{Br}(\gamma, \alpha)^{77}\text{As} = 1.8 \pm 0.8$  MeV-mb



Ref. P. Erdos, P. Scherrer, P. Stoll  
Helva. Phys. Acta 30, 639 (1957)

Elem. Sym.	A	Z
Br	81	35

Method Betatron;  $\alpha$  yield; radioactivity;  $\text{Cu}^{65}(\gamma, n)$  reaction

Ref. No.	
57 Er 1	EGF

Reaction	E or $\Delta E$	$E_0$	$\Gamma$	$\int \sigma dE$	$J\pi$	Notes
$\text{Br}^{81}(\gamma, \alpha)$	Bremss. 32			$1.3 \pm 0.5$ MeV-mb		Based on yield measurement.

Method Iowa State 70 MeV synchrotron; neutron counter

Ref. No.	EGF
57 Ki 1	

Reaction	E or $\Delta E$	$E_0$	$\Gamma$	$\int \sigma dE$	$J\pi$	Notes
$\text{Br}^{81}(\gamma, n)$	Bremss. 15-70					Measured relative yield of ground state to 4.4 hour $\text{Br}^{80}$ : (17 min.) gs J = 2 (4.4 hr.) J = 5

TABLE I. Relative yields of  $\text{Br}^{80}$  and  $\text{Br}^{80m}$  from the photoneutron reaction in  $\text{Br}^{81}$ .

Experi- ment	Maximum bremsstrahlung energy	$C_1^a$	$C_2^a$	$t_{1/2}$ isomeric state (hr)	$t_{1/2}$ ground state (min)	$R_2/R_1$
1	15.7 $\pm$ 1	4046 $\pm$ 16	88190 $\pm$ 2000	4.39 $\pm$ 0.03	16.26 $\pm$ 0.86	3.46 $\pm$ 0.82
2	25 $\pm$ 5	100 $\pm$ 4	3927 $\pm$ 183	4.38 $\pm$ 0.02	17.60 $\pm$ 0.03	2.48 $\pm$ 0.12
3	25 $\pm$ 5	124 $\pm$ 11	4286 $\pm$ 18	4.36 $\pm$ 0.12	16.65 $\pm$ 0.81	2.38 $\pm$ 0.21
4	27.4 $\pm$ 1	257 $\pm$ 2	4206 $\pm$ 501	4.38 $\pm$ 0.03	17.40 $\pm$ 0.80	2.31 $\pm$ 0.31
5	68.0 $\pm$ 1	1687 $\pm$ 18	41046 $\pm$ 944	4.37 $\pm$ 0.05	16.79 $\pm$ 0.37	2.50 $\pm$ 0.08
6	70 $\pm$ 1	1000 $\pm$ 10	29170 $\pm$ 605	4.39 $\pm$ 0.05	17.56 $\pm$ 0.10	2.51 $\pm$ 0.17
7	70 $\pm$ 1	305 $\pm$ 6	9885 $\pm$ 300	4.36 $\pm$ 0.07	16.72 $\pm$ 0.17	2.36 $\pm$ 0.07

<sup>a</sup> Contribution No. 490. Work performed in the Ames Laboratory of the U. S. Atomic Energy Commission.

<sup>1</sup> Katz, Pease, and Moody, Can. J. Phys. 30, 476 (1952).

<sup>1a</sup> Chien and Willard, J. Am. Chem. Soc. 77, 3441 (1955).

<sup>3</sup> Katz, Baker, and Montalbetti, Can. J. Phys. 31, 250 (1953).

<sup>4</sup> J. Goldemberg and L. Katz, Phys. Rev. 90, 308 (1953).

<sup>5</sup> K. Strauch, Phys. Rev. 81, 973 (1951).

<sup>6</sup> Koch, McElhinney, and Cunningham, Phys. Rev. 81, 318 (1951).

<sup>7</sup> J. L. Lawson and M. L. Perlman, Phys. Rev. 74, 1190 (1948).

METHOD					REF. NO.	
Betatron; neutron threshold; ion chamber					60 Ge 3	NVB
REACTION	RESULT	EXCITATION ENERGY	SOURCE		DETECTOR	
			TYPE	RANGE	TYPE	RANGE
G, N	NØX	THR	C	THR	BF3-I	4 PI

THRESHOLD

TABLE I. Summary and comparison of neutron separation energies inferred from present threshold measurements with values predicted from mass data and reaction energies. All energies are expressed in the center-of-mass system in Mev.

Reaction	No. runs	Present results	Other results	Method	Reference
$\text{Br}^{81}(\gamma, n)\text{Br}^{80}$	1	$10.130 \pm 0.035$	$10.03 \pm 0.13$	mass data	m
				$Q(\beta^-)$	n
			$10.03 \pm 0.13$	mass data	m
				$Q(\beta^+)$	o

- Henry E. Duckworth, *Mass Spectroscopy* (Cambridge University Press, New York, 1958), p. ....
- L. J. Lidoisky, *Revs. Modern Phys.* 29, 773 (1957).
- R. W. King, *Revs. Modern Phys.* 26, 327 (1954).

Elem. Sym.	A	Z
Br	81	35
Ref. No.		
62 Ca 1		JHH

Method 30 MeV electron synchrotron; activation; NaI

Reaction	E or $\Delta E$	$E_0$	$\Gamma$	$\int \sigma dE$	$J\pi$	Notes
Br <sup>81</sup> ( $\gamma, n$ )	Bremss. 30					<sup>10</sup> L. Katz <u>et al.</u> , Can. J. Phys. <u>30</u> (1952) 476. <sup>11</sup> L. Katz <u>et al.</u> , Can. J. Phys. <u>31</u> (1953) 250. <sup>12</sup> E. Silva <u>et al.</u> , An Acad. Brasil Ciẽnce <u>28</u> (1956) 275. <sup>23</sup> J. Goldemberg <u>et al.</u> , Phys. Rev. <u>90</u> (1953) 308.

TABLE I  
Isomeric ratios from ( $\gamma, n$ ) reactions

Target nucleus		$J_0$		Residual nucleus						Isomer ratio $Y_1/(Y_1+Y_2)$	$\sigma$
				Ground state		Metastable state		Intermediate state			
				Spin	Half-life	Spin	Half-life		Spin		
Co <sup>59</sup>	$\frac{1}{2}^-$	Co <sup>58</sup>	$2^+$	71.3 d		$5^+$	9.2 h			$0.44 \pm 0.02$	$3.2 \pm 0.2$
Ge <sup>74</sup>	$0^+$	Ge <sup>73</sup>	$\frac{1}{2}^-$	82 min		$\frac{1}{2}^+$	49 s			$0.48 \pm 0.07$	$2.8 \pm 0.5$
Br <sup>81</sup>	$\frac{3}{2}^-$	Br <sup>80</sup>	$1^+$	18 min		$5^-$	4.4 h		$2^-$	$0.32 \pm 0.02$	$6.5 \pm 1.0$
Sr <sup>86</sup>	$0^+$	Sr <sup>85</sup>	$\frac{1}{2}^+$	64 d		$\frac{1}{2}^-$	70 min		$\frac{1}{2}^+$	$0.36 \pm 0.07$	$2.2 \pm 0.4$
Zr <sup>90</sup>	$0^+$	Zr <sup>89</sup>	$\frac{3}{2}^+$	79 h		$\frac{1}{2}^-$	4.4 min			$0.33 \pm 0.10$	$2.8 \pm 0.7$
Mo <sup>93</sup>	$0$	Mo <sup>91</sup>	$\frac{1}{2}^+$	15.7 min		$\frac{1}{2}^-$	66 s			$0.46 \pm 0.04$	$6.1 \pm 1.1$
Ag <sup>107</sup>	$\frac{1}{2}^-$	Ag <sup>106</sup>	$1^+$	24 min		$6$	8.3 d			$0.04 \pm 0.02$	$2.0 \pm 0.3$
In <sup>113</sup>	$\frac{3}{2}^+$	In <sup>112</sup>	$1^+$	14.5 min		$4^+$	20.7 min		$7^-$	$0.8 \pm 0.1$	$3.1 \pm 0.7$
Cd <sup>116</sup>	$0^+$	Cd <sup>115</sup>	$\frac{1}{2}^-$	53 h		$\frac{1}{2}^-$	43 d			$\leq 0.2$	$\leq 3$
Ce <sup>140</sup>	$0^+$	Ce <sup>139</sup>	$\frac{1}{2}^+$	140 d		$\frac{1}{2}^-$	55 s			$0.03 \pm 0.01$	$2.5 \pm 0.2$
Hg <sup>198</sup>	$0^+$	Hg <sup>197</sup>	$\frac{1}{2}^-$	65 h		$\frac{1}{2}^+$	24 h		$\frac{1}{2}^-$ $\frac{1}{2}^-$	$0.05 \pm 0.01$	$3.4 \pm 0.5$

Ref.	Previous work									
Br <sup>81</sup> <sup>10)</sup>	$\frac{1}{2}^-$	Br <sup>80</sup>	$1^+$	18 min		$5^-$	4.4 h	$2^-$	0.33	6.5
Se <sup>82</sup> <sup>12)</sup>	$0^+$	Se <sup>81</sup>	$\frac{1}{2}^-$	18 min		$\frac{1}{2}^-$	57 min		0.5	3.0
Zr <sup>90</sup> <sup>11)</sup>	$0^+$	Zr <sup>89</sup>	$\frac{3}{2}^+$	79 h		$\frac{1}{2}^-$	4.3 min		$0.44 \pm 0.06$	$4.5 \pm 1$
In <sup>113</sup> <sup>22)</sup>	$\frac{3}{2}^+$	In <sup>112</sup>	$1^+$	72 s		$5^-$	50 d	8	0.55	5.0

( $T_{1/2} = 2.5$  s)

The yields  $Y_1$  and  $Y_2$  are for ( $\gamma, n$ ) reactions ending in the isomeric- or ground-state. The yield  $Y_1$  is for the higher-spin state.

REF.

Y. Oka, T. Kato, K. Nomura, T. Saito and H. T. Tsai  
Bull. Chem. Soc. Japan 41, 2660 (1968)

ELEM. SYM.

A

Z

Br

81

35

METHOD

REF. NO.

68 Ok 1

egf

REACTION	RESULT	EXCITATION ENERGY	SOURCE		DETECTOR		ANGLE
			TYPE	RANGE	TYPE	RANGE	
G,A	ABY	THR-20	C	20	ACT-I		4PI

TABLE 1. SUMMARY OF DATA ON  $(\gamma, \alpha)$  REACTIONS WITH 20 MeV BREMSSTRAHLUNG

Nuclide		$E_{th}$ (-Q, MeV)	Observed gamma-ray			Results obtained	
Parent (Natural abundance, %)	Product (Half-life)		Energy (MeV)	Branching ratio (%)	Type of multipole transition	$\mu\text{Ci/mg}^a$	Yield (mol <sup>-1</sup> ·R <sup>-1</sup> )
<sup>51</sup> V (99.75)	<sup>47</sup> Sc (3.4 d)	10.27	0.160	100	M1 + E2	$1.99 \times 10^{-3}$	$2.8 \times 10^3$
<sup>63</sup> Cu (30.9)	<sup>51</sup> Co (99 min)	6.75	0.068	99	M1 + E2	$7.23 \times 10^{-3}$	$9.7 \times 10^3$
<sup>71</sup> Ga (39.6)	<sup>67</sup> Cu (61 hr)	5.15	0.184	41	M1	$2.70 \times 10^{-3}$	$9.6 \times 10^3$
<sup>72</sup> Ge (7.67)	<sup>68</sup> Zn (14 hr)	5.89	0.435	100	M4	$1.11 \times 10^{-3}$	$5.0 \times 10^3$
<sup>81</sup> Br (49.48)	<sup>77</sup> As (39 hr)	6.46	0.246	2.81	M1 + E2	$1.97 \times 10^{-4}$	$4.3 \times 10^2$
<sup>108</sup> Ag (48.65)	<sup>106</sup> Rh (36 hr)	3.28	0.319 + 0.306	24.8	M1 + E2	$8.29 \times 10^{-4}$	$3.7 \times 10^1$
<sup>113</sup> In (95.77)	<sup>111</sup> Ag (7.6 d)	3.78	0.340	6	M1 + E2	$5.70 \times 10^{-5}$	$4.3 \times 10^1$

a) The value corrected at the end of 1 hr irradiation ( $9.4 \times 10^6$  R/min).

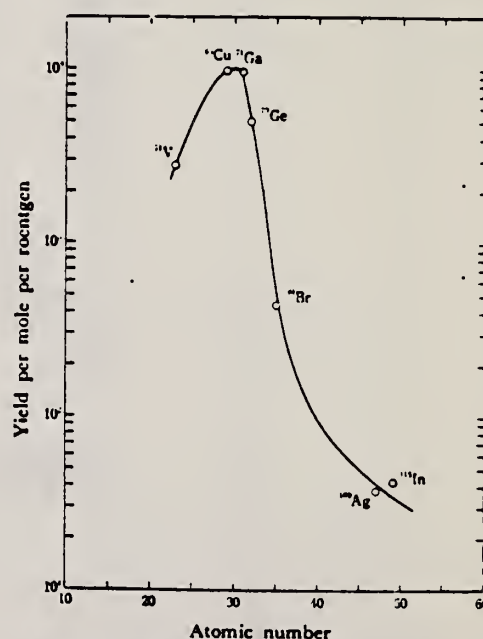


Fig. 1. The yield curve for  $(\gamma, \alpha)$  reaction with 20 MeV bremsstrahlung.



## KRYPTON

Z=36

Krypton was discovered by William Ramsey and his assistant Morris Travers in 1898. They had tried in vain to find an inert gas, with an atomic weight between that of argon and helium, by heating rare minerals. Their next attempt was to diffuse argon and hopefully fractionate it into gases of different densities. They had been given a liter of liquid air which they used, not for liquefying their precious fifteen liters of argon but for obtaining sufficient skill in gas manipulation. Fortunately they were careful to save the residue of the liquid air for they found 25 cm<sup>3</sup> of an inert gas. This was placed in a Plücker tube and connected to an induction coil. Ramsey and Travers observed a bright yellow line with a green tint which did not coincide with any of the known lines. They named the new gas "krypton" meaning "hidden" in Greek.



REF. J. Goldemberg, Y. Torizuka, W. C. Barber, J. D. Walecka  
Nuclear Phys. 43, 242 (1963)

ELEM. SYM.	A	Z
Kr		36
REF. NO.		JHH
63 Go 4		

METHOD  
Linac; electron scattering; magnetic spectrometer

REACTION	RESULT	EXCITATION ENERGY	SOURCE		DETECTOR		ANGLE
			TYPE	RANGE	TYPE	RANGE	
E, E/	ABX	15-21	D	41	MAG-D	17-42	180

METHOD

REF. NO.

69 Ho 1

egf

REACTION	RESULT	EXCITATION ENERGY	SOURCE		DETECTOR		ANGLE
			TYPE	RANGE	TYPE	RANGE	
G,XP	ABY	THR- 33	C	24-33	SCI-D	3-14	90

Tabelle 1. Daten zu den einzelnen Reaktionen. Die Werte für den integrierten Wirkungsquerschnitt wurden unter der Annahme ausschließlicher Grundzustandsübergänge berechnet. Für  $^{23}\text{Na}$  und  $^{39}\text{K}$  als Ausnahme s. Text

Tar- get	Anreiche- rungsgrad %	( $\gamma$ , p)- Schwelle MeV	Druck oder Dicke	End- energie MeV	Zahl gemess. Protonen	Ausbeute $\mu\text{b}/\text{MeV sr}$	$\int_{32,5}^{\infty} \sigma(E) dE$ MeVmb	Figur
$^{18}\text{O}$	99	16,0	230 Torr	32,5	36074	$58 \pm 7$	$38 \pm 6$	1, 2
$^{20}\text{Ne}$	90,9	12,8	450 Torr	28,0	3175	$7,4 \pm 1$	—	—
			610 Torr	32,5	6293	$14,9 \pm 2$	$61 \pm 11$	5, 6
$^{22}\text{Ne}$	99,9	15,3	240 Torr	24,0	1960	$2,3 \pm 0,4$	—	4, 5
				28,0	4790	$3,6 \pm 0,6$	—	4, 5
				32,5	5210	$6,7 \pm 0,9$	$45 \pm 8$	4, 5
$^{23}\text{Na}$	100	8,8	65 $\mu$	24,0	14182	$6,3 \pm 1,0$	—	7
			60 $\mu$	32,5	11152	$12,8 \pm 2,0$	$117 \pm 30$	7
$^{36}\text{Ar}$	99	8,5	250 Torr	32,5	45173	$57 \pm 6$	$270 \pm 40$	8, 10
$^{40}\text{Ar}$	99,6	12,5	230 Torr	32,5	29559	$14,2 \pm 15$	$104 \pm 15$	9, 11
$^{39}\text{K}$	93,1	6,4	80 $\mu$	24,0	24230	$17,4 \pm 2,8$	—	12
			90 $\mu$	32,5	24941	$41,9 \pm 6,7$	$405 \pm 100$	12
$^{84}\text{Kr}$	99	10,7	170 Torr	32,5	35515	$12,7 \pm 2,0$	$80 \pm 20$	14
Kr	natürl.	10	170 Torr	32,5	13570	$12,5 \pm 2,0$	$75 \pm 20$	13
Xe	natürl.	9	150 Torr	32,5	7553	$7,6 \pm 0,9$	$40 \pm 7$	15

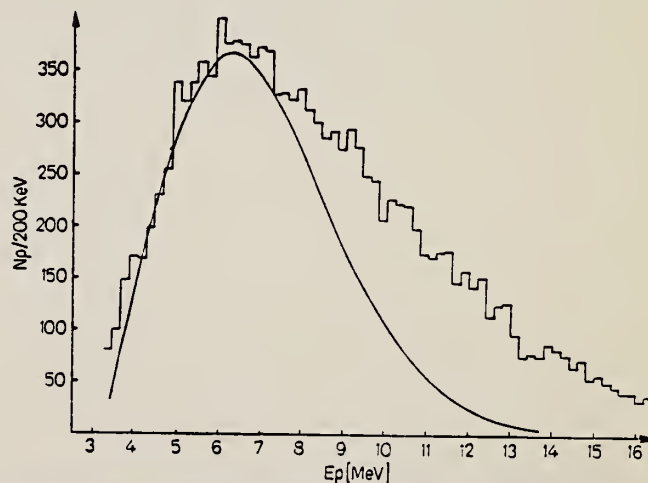


Fig. 13. Energieverteilung der Photoprotonen aus Kr für  $E_0 = 32,5$  MeV.  
Kurve: Berechnetes Verdampfungsspektrum

1/2  
A=82

1/2  
A=82

1/2  
A=82





G. B. Beard  
Phys. Rev. 145, B862 (1966)

ELEM. SYM.	A	Z
Kr	82	36

## METHOD

Resonance fluorescence; gaseous HBr source

## REF. NO.

66 Be 2

JDM

REACTION	RESULT	EXCITATION ENERGY	SOURCE		DETECTOR		ANGLE
			TYPE	RANGE	TYPE	RANGE	
G,G	LFT	1(.77 - 1.47)	C	1	NaI-D	0-2	113

Used recoil energy from  $\beta$ -decay to give Doppler broadened spectrum.

Measured  $\int \sigma_{ss} dE$ .

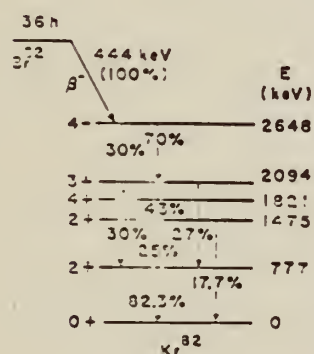


FIG. 1. Decay scheme of  $Br^{82}$ , showing only the major transitions and their percentages based on the summary (Ref. 2) of the results of recent measurements of relative gamma-ray intensities. The percentages of the gamma rays shown are adjusted to agree with the results of the decays of the  $2648 keV$  transition.

TABLE II. Summary of properties of the first ( $2^+$ ) excited states of even-even Kr isotopes. The values for the relative  $B(E2)$  are taken from Ref. 1. Column 6 gives the ratio of the observed transition probabilities to the Weisskopf estimate (Ref. 10) for  $E2$  transitions.

Isotope	$E(2^+)$ (keV)	Relative $B(E2)^\dagger$	Absolute $B(E2)^\dagger$ ( $e^2 \times 10^{-48} \text{ cm}^4$ )	$\tau$ (sec)	$B(E2)$ $B(E2)_W$
$^{78}Kr$	450	0.51	0.59	$3.8 \times 10^{-11}$	54
$^{80}Kr$	620	0.34	0.39	$1.13 \times 10^{-11}$	36
$^{82}Kr$	777	0.18	0.21	$6.9 \times 10^{-12}$	19
$^{84}Kr$	880	0.15	0.17	$4.7 \times 10^{-12}$	16



KR  
A=81

KR  
A=84

KR  
A=81





METHOD

REF. NO.

69 Ho 1

egf

REACTION	RESULT	EXCITATION ENERGY	SOURCE		DETECTOR		ANGLE
			TYPE	RANGE	TYPE	RANGE	
G,XP	ABY	THR- 33	C	24-33	SCI-D	3-14	90

Tabelle 1. Daten zu den einzelnen Reaktionen. Die Werte für den integrierten Wirkungsquerschnitt wurden unter der Annahme ausschließlicher Grundzustandsübergänge berechnet. Für  $^{23}\text{Na}$  und  $^{39}\text{K}$  als Ausnahme s. Text

Tar- get	Anreiche- rungsgrad %	( $\gamma, p$ )- Schwelle MeV	Druck oder Dicke	End- energie MeV	Zahl gemess. Protonen	Ausbeute $\mu\text{b/MeV sr}$	$\frac{32.5}{\sigma(E)} \frac{dE}{E}$ MeVmb	Figur
$^{18}\text{O}$	99	16,0	230 Torr	32,5	36074	$58 \pm 7$	$38 \pm 6$	1, 2
$^{20}\text{Ne}$	90,9	12,8	450 Torr	28,0	3175	$7,4 \pm 1$	—	—
			610 Torr	32,5	6293	$14,9 \pm 2$	$61 \pm 11$	5, 6
$^{22}\text{Ne}$	99,9	15,3	240 Torr	24,0	1960	$2,3 \pm 0,4$	—	4, 5
				28,0	4790	$3,6 \pm 0,6$	—	4, 5
				32,5	5210	$6,7 \pm 0,9$	$45 \pm 8$	4, 5
$^{23}\text{Na}$	100	3,8	65 $\mu$	24,0	14182	$6,3 \pm 1,0$	—	7
			60 $\mu$	32,5	11152	$12,8 \pm 2,0$	$117 \pm 30$	7
$^{36}\text{Ar}$	99	3,5	250 Torr	32,5	45173	$57 \pm 6$	$270 \pm 40$	8, 10
$^{40}\text{Ar}$	99,6	12,5	230 Torr	32,5	29559	$14,2 \pm 15$	$104 \pm 15$	9, 11
$^{39}\text{K}$	93,1	6,4	80 $\mu$	24,0	24230	$17,4 \pm 2,8$	—	12
			90 $\mu$	32,5	24941	$41,9 \pm 6,7$	$405 \pm 100$	12
$^{84}\text{Kr}$	99	10,7	170 Torr	32,5	35515	$12,7 \pm 2,0$	$80 \pm 20$	14
Kr	natürl.	10	170 Torr	32,5	13570	$12,5 \pm 2,0$	$75 \pm 20$	13
Xe	natürl.	9	150 Torr	32,5	7553	$7,6 \pm 0,9$	$40 \pm 7$	15

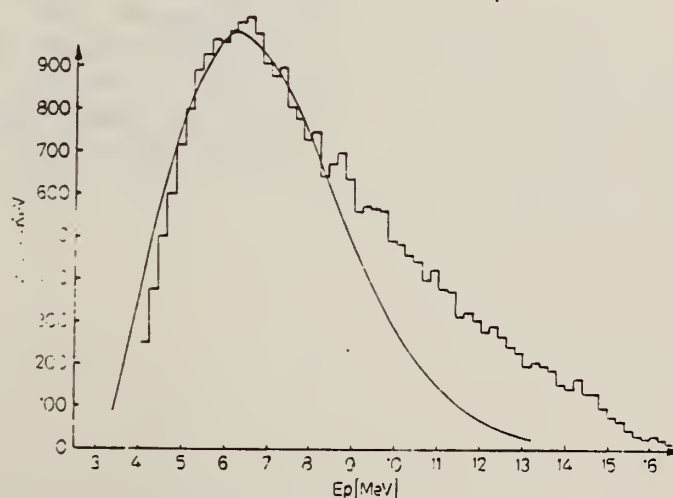


Fig. 14. Energieverteilung der Photoprotonen aus  $^{84}\text{Kr}$  für  $E_0 = 32,5$  MeV.  
Kurve: Berechnetes Verdampfungsspektrum



## RUBIDIUM

$Z=37$

Rubidium was discovered by Gustav Kirchhoff and Robert Bunsen who announced their discovery to the Berlin Academy of Sciences on February 23, 1861. The achievement was made possible by the spectroscope that the two investigators had developed.

Kirchhoff's mind was more speculative than Bunsen's and he was thoroughly familiar with the researches of Josef Fraunhofer. Kirchhoff showed Bunsen that, instead of looking through colored glass to distinguish between similarly colored flames, he should use a prism to separate the light into its constituent rays or lines. This was the basic idea of the spectroscope which they used to examine the mineral lepidolite from Saxony. They observed two remarkable red lines just beyond the brilliant Fraunhofer lines at the extreme red end of the solar spectrum. The new lines were attributed to an unknown substance which they called rubidium from the Latin *rubidus* meaning dark red.



METHOD

REF. NO.

71 Le 1

egf

REACTION	RESULT	EXCITATION ENERGY	SOURCE		DETECTOR		ANGLE
			TYPE	RANGE	TYPE	RANGE	
G,N 375	ABX	11-24	D	11-24	MOD-I		4PI
G,2N 376+	ABX	17-24	D	11-24	MOD-I		4PI

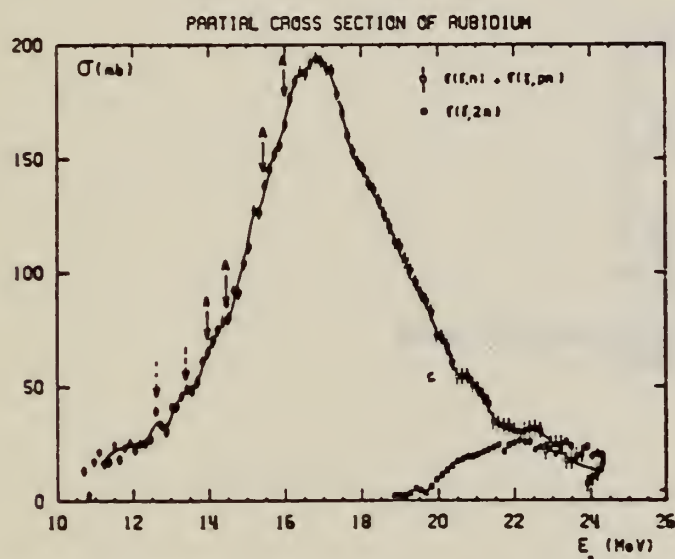


Fig. 1. Partial photoneutron cross sections  $\sigma(y, n)$  and  $\sigma(y, 2n)$  of Rb.

TABLE 1

Lorentz line parameters corresponding to fits shown in fig. 6.

	Rb	Sr	<sup>89</sup> Y	<sup>90</sup> Zr	<sup>93</sup> Nb
$\sigma_1$ (mb)	192 ± 10	207 ± 10	225 ± 10	211 ± 10	202 ± 10
$\Gamma_1$ (MeV)	4.1 ± 0.15	4.2 ± 0.1	4.1 ± 0.1	4.0 ± 0.1	4.7 ± 0.2
$E_1$ (MeV)	16.75 ± 0.05	16.7 ± 0.05	16.7 ± 0.05	16.65 ± 0.05	16.5 ± 0.05

TABLE 3

Integrated cross sections (the notation used is defined in the text)

	Rb	Sr	<sup>89</sup> Y	<sup>90</sup> Zr	<sup>93</sup> Nb
$\sigma_0$ (MeV · b)	1.14 ± 0.06	1.42 ± 0.07	1.36 ± 0.07	1.26 ± 0.07	1.33 ± 0.07
$\frac{\sigma_0}{0.06 NZ A^{-1}}$	0.915 ± 0.05	1.09 ± 0.05	1.04 ± 0.05	0.95 ± 0.05	0.97 ± 0.05
$\sigma_{-1}$ (mb)	67 ± 4	80 ± 5	77 ± 5	71 ± 5	79 ± 5
$\sigma_{-2}$ (mb · MeV <sup>-1</sup> )	4 ± 0.2	4.6 ± 0.2	4.4 ± 0.2	4 ± 0.2	4.8 ± 0.2
$E_M$ (MeV)	24	27	27	26	24

(over)

U.S. DEPARTMENT OF COMMERCE  
NATIONAL BUREAU OF STANDARDS



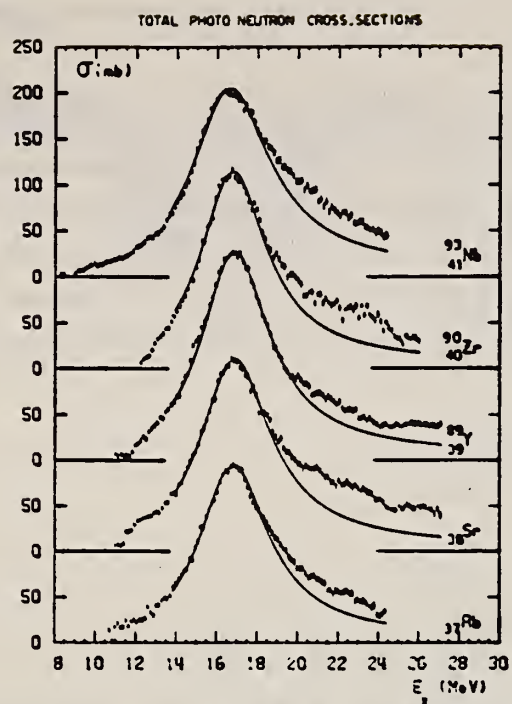


Fig. 6. Total photoneutron cross sections  $\sigma_T$  of Rb, Sr,  $^{89}\text{Y}$ ,  $^{90}\text{Zr}$  and  $^{93}\text{Nb}$  and best one Lorentz line fit corresponding to parameters given in table I.

PB  
A=85

PB  
A=85

PB  
A=85



Method 22 MeV Betatron

Ref. No.	EH
58 To 1	

Reaction	E or $\Delta E$	$E_0$	$\Gamma$	$\int \sigma dE$	$J\pi$	Notes
$\text{Rb}^{85}(\gamma, n)$	Bremss 22					$E_{th} = 10.50 \pm 0.08$ , based on counting isomers.

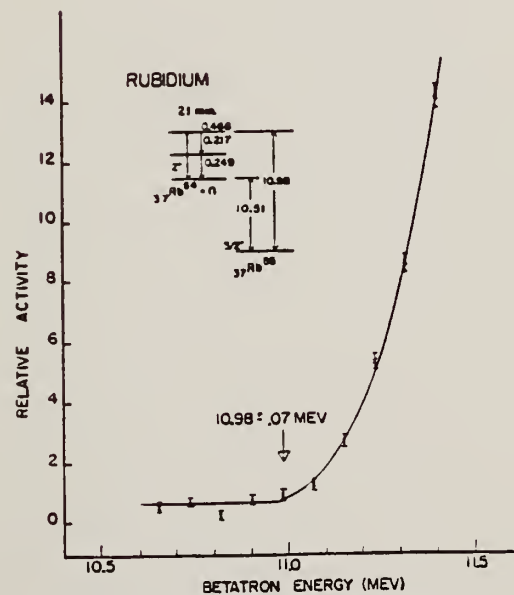


FIG. 6. Relative activity of the 21-minute isomeric state of  $\text{Rb}^{84}$  as a function of betatron energy.

Rb

85

37

METHOD

Betatron; neutron threshold; ion chamber

REF. NO.

60 Ge 3

NVB

REACTION	RESULT	EXCITATION ENERGY	SOURCE		DETECTOR		ANGLE
			TYPE	RANGE	TYPE	RANGE	
G,N	NØX	THR	C	THR	BF3-I		4 PI

THRESHOLD

TABLE I. Summary and comparison of neutron separation energies inferred from present threshold measurements with values predicted from mass data and reaction energies. All energies are expressed in the center-of-mass system in Mev.

Reaction	No. runs	Present results	Other results	Method	Reference
$Rb^{85}(\gamma,n)Rb^{84}$	1	$10.65 \pm 0.08$	$10.26 \pm 0.16$	mass data	m
				$Q(\beta^+)$	n
			$10.13 \pm 0.25$	mass data	m
				$Q(\beta^-)$	n

\* Henry E. Duckworth, *Mass Spectroscopy* (Cambridge University Press, New York, 1958), p. 177.  
\* L. J. Lidofsky, *Revs. Modern Phys.* 29, 773 (1957).



METHOD

REF. NO.

69 Kn 1

egf

REACTION	RESULT	EXCITATION ENERGY	SOURCE		DETECTOR		ANGLE
			TYPE	RANGE	TYPE	RANGE	
G,N	RLY	10-45	C	45	ACT-I		4PI

ISOMERE YIELD

### 5. Ergebnisse

Die Rechnungen für beide Reaktionen wurden mit Spin-cut-off-Parametern  $\sigma = 3.5$  und  $\sigma = 4$  durchgeführt und mit den gemessenen Isomerenverhältnissen verglichen. Durch Interpolation wurden Werte von  $\sigma$  ermittelt, für die die berechneten Isomerenverhältnisse mit den gemessenen Werten  $R_{is}$  übereinstimmen.

Es ergaben sich folgende Resultate:

Reaktion	$R_{is}$	$\sigma$
(n, 2n)	$1.07 \pm 0.05$	$3.96 \pm 0.06$
( $\gamma$ , n)	$0.37 \pm 0.01$	$3.78 \pm 0.03$
		korr. $4.04 \pm 0.03$

Herrn A. Heß danken wir für seine Hilfe bei der Bestrahlung am n-Generator, dem Bundesministerium für wiss. Forschung für die Bereitstellung von Sachmitteln.



B  
A=67

B  
A=87

B  
A=87







Ref. R. Tobin, J. McElhinney, L. Cohen  
Phys. Rev. 110, 1388 (1958)

Elem. Sym.	A	Z
Rb	87	37
Ref. No.		
58 To 1		EH

Method 22 MeV Betatron; neutron counters

Reaction	E or $\Delta E$	$E_0$	$\Gamma$	$\int \sigma dE$	$J\pi$	Notes
$\text{Rb}^{87}(\gamma, n)$	Bremss 22					$E_{th} = 9.89 \pm 0.05$

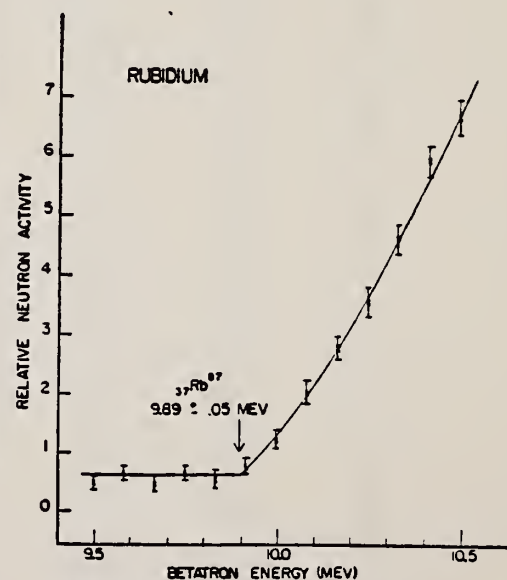


FIG. 5. Photoneutron yield from rubidium as a function of betatron energy.

REF. K. N. Geller, J. Halpern, and E. G. Muirhead  
Phys. Rev. 118, 1302-12 (1960)

ELEM. S. M.	A	
Rb	87	37
REF. NO.		
60 Ge 3		NVB

METHOD  
Betatron; neutron threshold; ion chamber

REACTION	RESULT	EXCITATION ENERGY	SOURCE		DETECTOR		ANGLE
			TYPE	RANGE	TYPE	RANGE	
G, N	NØX	THR	C	THR	BF3-I		4 PI

THRESHOLD

TABLE I. Summary and comparison of neutron separation energies inferred from present threshold measurements with values predicted from mass data and reaction energies. All energies are expressed in the center-of-mass system in Mev.

Reaction	No. runs	Present results	Other results	Method	Reference
Rb <sup>87</sup> ( $\gamma, n$ )Rb <sup>86</sup>	1	9.99 $\pm$ 0.07	9.91 $\pm$ 0.20	mass data	m
			9.89 $\pm$ 0.05	Q( $\beta^-$ ) threshold	n k

- <sup>2</sup> See reference 1.  
<sup>1</sup> See reference 3.  
<sup>3</sup> Henry E. Duckworth, *Mass Spectroscopy* (Cambridge University Press, New York, 1958), p. 177.  
<sup>4</sup> L. J. Lidofsky, *Revs. Modern Phys.* 29, 773 (1957).



## STRONTIUM

Z=38

Strontium was first detected in 1790 by Dr. Adair Crawford (1748-1795) of Edinburgh. He had obtained a new mineral that was found in the lead mine at Strontian, Argyleshire; most mineralogists considered the material to be an aerated barium carbonate. Crawford published a paper that showed that the salt (strontium chloride) obtained by dissolving the new mineral in hydrochloric acid differs in several respects from barium chloride. He further concluded that "the Scotch mineral is a new species of earth which has not hitherto been sufficiently examined."





METHOD

Betatron; fast neutron yield, angular distribution; Si threshold detector; ion chamber

REF. NO.

61 Ba 2 NVB

REACTION	RESULT	EXCITATION ENERGY	SOURCE		DETECTOR		ANGLE
			TYPE	RANGE	TYPE	RANGE	
G, XN	ABY	THR-22	C	22	THR-I	5-+	0-90

In Table 4:

$\bar{\sigma}$  = average cross section of detector  
weighted with neutron spectrum

$\bar{\phi}$  = neutrons/100 roentgen/mole

$$W(\theta) = a_0 \sum_{n=1}^{\infty} [1 + A_n P_n(\cos \theta)]$$

TABLE IV

I Element	II $a_0$	III $a_1$	IV $a_2$	V $(\bar{\sigma}\bar{\phi}) \times 10^{10}$	VI $\Phi_{\text{total}} (22 \text{ Mev}) \times 10^9$	VII $\Phi_{\text{fast}}/\Phi_{\text{total}}$
Vanadium	245 (1±0.06)	0.01±0.08	-0.00±0.10	6.05	0.21	0.12
Chromium	164 (1±0.03)	0.04±0.04	-0.05±0.05	4.05	0.17	0.10
Manganese	308 (1±0.02)	0.07±0.02	-0.09±0.04	7.61	0.25	0.12
Iron	200 (1±0.03)	0.05±0.04	-0.17±0.05	4.94	0.18	0.11
Cobalt	390 (1±0.02)	0.08±0.03	-0.22±0.04	9.63	0.26	0.15
Nickel	145 (1±0.05)	0.07±0.07	-0.23±0.09	3.58	0.12	0.12
Copper	347 (1±0.02)	0.05±0.03	-0.29±0.04	8.57	0.30	0.12
Arsenic	482 (1±0.03)	0.11±0.04	-0.24±0.05	11.91	0.33	0.15
Rubidium	638 (1±0.03)	0.13±0.06	-0.14±0.08	15.76		
Strontium	409 (1±0.03)	0.10±0.06	-0.17±0.08	10.10		
Yttrium	290 (1±0.10)	0.08±0.12	-0.12±0.15	7.16		
Silver	590 (1±0.04)	0.10±0.06	-0.22±0.08	14.57	0.87	0.07
Cadmium	905 (1±0.02)	0.02±0.02	-0.26±0.03	22.35		
Iodine	1133 (1±0.03)	0.04±0.04	-0.29±0.05	27.99	1.42	0.08
Barium	1048 (1±0.04)	0.10±0.06	-0.38±0.08	25.89		
Lanthanum	1595 (1±0.02)	0.02±0.03	-0.42±0.04	39.40	1.04	0.15
Cerium	1316 (1±0.05)	0.05±0.06	-0.39±0.08	32.50		
Dysprosium	1652 (1±0.03)	0.01±0.10	-0.34±0.13	40.80		
Tantalum	1558 (1±0.02)	0.01±0.03	-0.22±0.04	38.48	2.50	0.06
Tungsten	1365 (1±0.02)	-0.07±0.03	-0.24±0.04	33.71		
Mercury	1345 (1±0.02)	0.04±0.03	-0.31±0.04	33.22		
Lead	2274 (1±0.01)	0.02±0.02	-0.42±0.03	56.17	2.72	0.08
Bismuth	2162 (1±0.02)	0.05±0.03	-0.45±0.04	53.40	3.36	0.06
Thorium	3031 (1±0.04)	0.06±0.05	-0.32±0.07	74.87		
Uranium	4630 (1±0.02)	0.05±0.03	-0.17±0.04	114.38		

$(\bar{\sigma}\bar{\phi}) = 2.47 \times 10^9$  cc millibara-neutrons. Errors are standard errors due to counting statistics only.

METHOD

Linac; isomer yield; activity

REF. NO.

63 Ka 2

NVB

REACTION	RESULT	EXCITATION ENERGY	SOURCE		DETECTOR		ANGLE
			TYPE	RANGE	TYPE	RANGE	
G,G/	RLY	1	C6		ACT-I		4PI
		(0.39)					

Table II. The isomers observed

Isomer	Observed value		Referenced value <sup>(1)(13)</sup>	
	Half-life	Energy (MeV)	Half-life	Energy (MeV)
Se-77m	17.5 sec	0.160	17.5 sec	0.161
Br-79m	4.80 sec	0.209	4.8 sec	0.208
Sr-87m	2.3 hr	0.390	2.3 hr	0.338
Y-89m	15.0 sec	0.920	14 sec	0.915
Rh-103m	58 min	*	57 min	0.040
Ag-107m	42 sec	0.95	44 sec	0.094
Ag-109m			40 sec	0.088
Cd-111m	47 min	0.150,0.255	49 min	0.150,0.247
In-115m	4.5 hr	0.335	4.5 hr	0.335
Sn-117m	17 day	0.160	14 day	0.159,0.161
Ba-137m	2.6 min	0.660	2.6 min	0.662
Er-167m	2.10 sec	0.209	2.5 sec	0.208
Hf-179m	18.5 sec	0.157,0.215	19 sec	0.161,0.217
W-183m	5.4 sec	0.200,0.170,0.115	5.5 sec	0.1025,0.2915 others
Ir-191m	4.90 sec	0.129, <0.07	4.9 sec	0.042-0.129
Pt-195m	4.5 day	0.065**	4.1 day	0.031-0.130
Au-197m	7.0 sec	0.10,0.27,0.40	7.2 sec	0.130,0.270,0.407
Hg-199m	43 min	0.160,0.370	42 min	0.158,0.368

\* This isomer was measured with a G-M flow counter.

\*\* This value corresponds to Pt-K X-ray energy.

Table III. Induced activation rate

Element	Beam energy (MeV)	Counting rate ( $\times 10000$ cpm)	Sample form
Se	5	1300	metallic pellet
Br	4	1600	NaBr grain
Sr	6	0.3	SrCO <sub>3</sub> powder
Y	5	90	metallic grain
Rh	5	(0.2)*	RhCl <sub>3</sub> grain
Ag	5	180	metallic plate
Cd	6	0.5	CdCl <sub>2</sub> grain
In	6	8	metallic plate
Sn	6	0.0005	metallic plate
Ba	5	0.6	BaS powder
Er	4	4900	Er <sub>2</sub> O <sub>3</sub> powder
Hf	5	1600	metallic plate
W	5	120	metallic powder
Ir	5	2100	metallic powder
Pt	5	0.3	metallic plate
Au	4	4300	metallic plate
Hg	6	0.09	metallic liquid

\* The value measured with a G-M flow counter.

## METHOD

Radioactive source

REF. NO.

63 Ve 2

NVB

REACTION	RESULT	EXCITATION ENERGY	SOURCE		DETECTOR		ANGLE
			TYPE	RANGE	TYPE	RANGE	
G,G/	ABX	0-1	D	0-1	NAI-D		

ISOMERS

Таблица II

Измеренные значения после облучения, сравниваемые с другими литературными данными

Элемент	Активность облучения после первого измерения (имп/мин.)	Активн. экстрп. в конце облуч. (имп/мин.)	Литературные данные		Данные измерения		$\sigma_{\text{от}}$ ( $10^{-28}$ см <sup>2</sup> )	$\Gamma_{\text{ит}}$ ( $10^{-28}$ см <sup>2</sup> )
			$T_{1/2}$	E (кэв)	$T_{1/2}$	E (кэв)		
Se-77m	3842 ± 96	5400	17,5 сек.	160	18,1 ± 1 сек.	160 ± 10	9,5	1,75
Sr-87m	191 ± 5	200	2,8 ч.	390	2,9 ± 0,1 ч.	365 ± 25	0,85	0,2
Y-89m	96 ± 20	170	16 сек.	910	16,7 ± 5 сек.		0,08	0,02
Rh-103m	28 ± 5	31	57 мин.	40	58 ± 2 мин.	20,5 ± 0,5	0,08	0,01
Ag-107m	220 ± 14	250	44 сек.	93	43,8 ± 0,6 сек.	91 ± 10	0,8	0,2
Ag-109m			39 сек.	88				
Hf-179m	80 ± 18	155	19 сек.	160; 215	19 ± 2 сек.		1	0,2
Ir-191m	90 ± 20	250	4,9 сек.	42; 130	5 ± 2 сек.		5,6	1
Pt-195m	90 ± 9	100	3,5 д.	31; 100; 130;	3,5 ± 0,2 д.	32 ± 3 67,5 ± 5 96 ± 5 130 ± 10	0,2	0,04
Au-197m	240 ± 16	520	7,2 сек.	130; 277; 407	7,2 ± 1 сек.	68:130; 280 ± 20 390 ± 20	0,07	0,01
Hg-199m	9,6 ± 3,2		42 мин.	160; 370			0,005	0,001

Acta Phys. Hung. Tom. XVI. Fasc. 3.

REF. R. S. Hicks and B. M. Spicer  
Nucl. Phys. A159, 265 (1970)

ELEM. SYM.	A	Z
Sr		38
REF. NO.		
70 Hi 1		egf

METHOD			SOURCE		DETECTOR		ANGLE
REACTION	RESULT	EXCITATION ENERGY	TYPE	RANGE	TYPE	RANGE	
G,XN	ABX	10-27	C	10-27	BF3-I		4PI

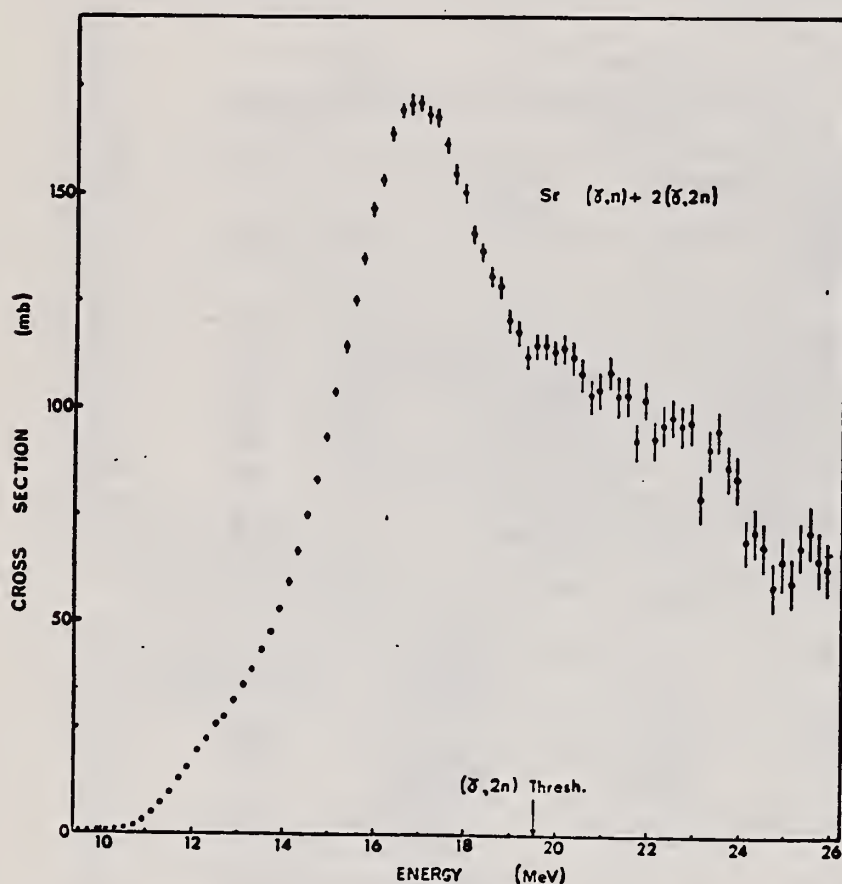


Fig. 1. The  $[Sr(\gamma, n) - 2Sr(\gamma, 2n)]$  cross section obtained by analysis of the yield curve using three interfering second difference calculations. The resolution applied is 1.08 MeV.

[over]



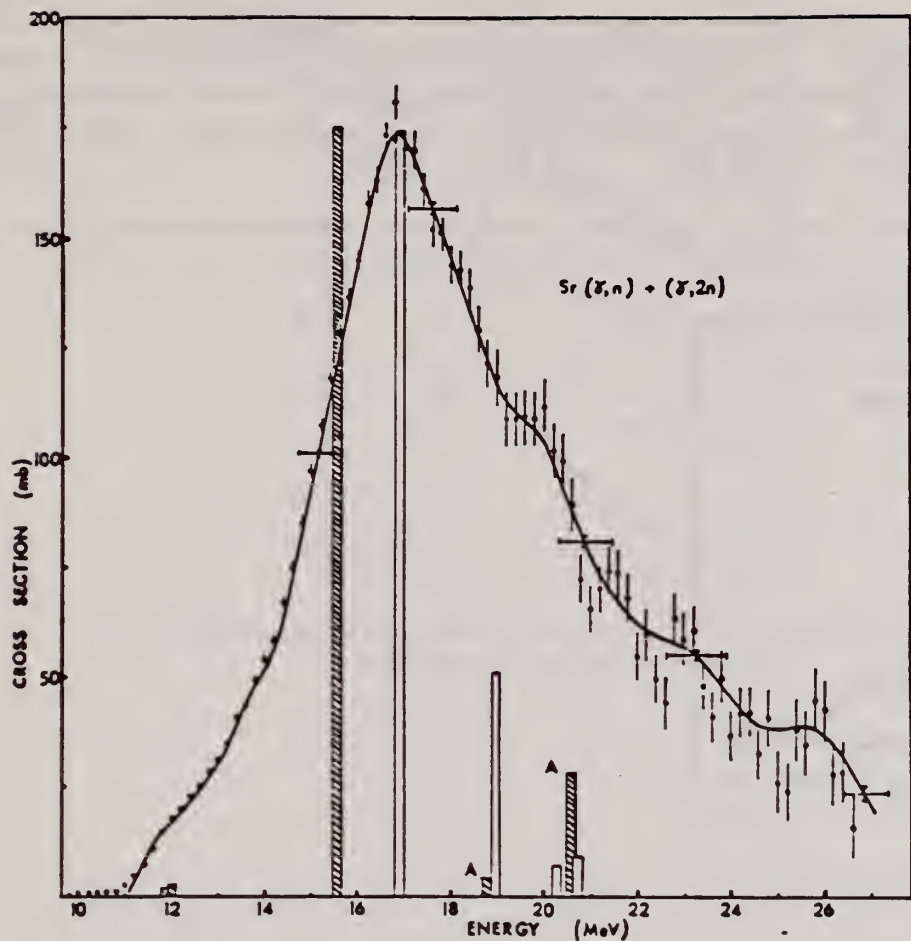


Fig. 2. The  $[Sr(\gamma, n) + Sr(\gamma, 2n)]$  cross section and calculated dipole spectra. The points portray the result obtained by 0.72 MeV second difference analysis and the continuous curve is obtained by Cook least-structure analysis, for which the resolution, implicit within the method, is indicated by the horizontal bars. Plain vertical bars represent the predictions of the dynamic collective model, whilst the hatched bars show the results of the particle-hole calculation of ref. <sup>1</sup>). Analogue  $T_{\gamma}$  states arising from the latter calculation are designated A.

1) B. Goulard, T.A. Hughes, S. Fallieros,  
Phys. Rev. 176 (1968) 1345.



ELEM. SYM.	A	Z
Sr		38
REF. NO.	71 Le 1	
	egf	

REACTION	RESULT	EXCITATION ENERGY	SOURCE		DETECTOR		ANGLE
			TYPE	RANGE	TYPE	RANGE	
G, N <u>378</u>	ABX	11-27	D	11-27	MOD-I		4PI
G, 2N <u>379+</u>	ABX	19-27	D	11-27	MOD-I		4PI

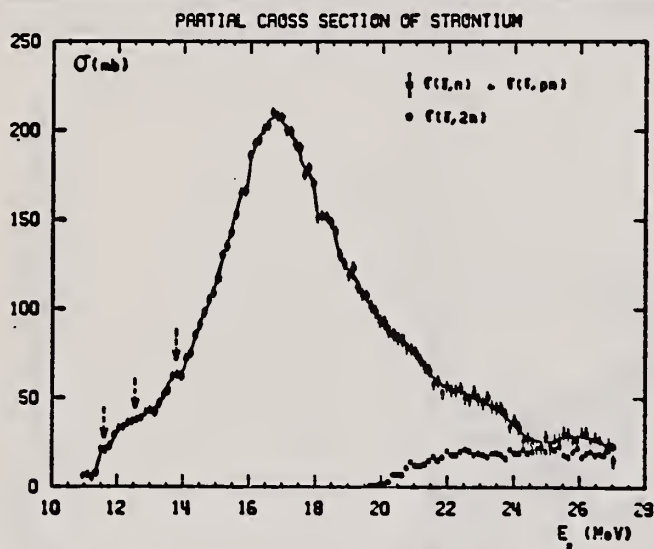


Fig. 2. Partial photoneutron cross sections  $\sigma(\gamma, n)$  and  $\sigma(\gamma, 2n)$  of Sr.

TABLE 1  
Lorentz line parameters corresponding to fits shown in fig. 6.

	Rb	Sr	<sup>89</sup> Y	<sup>90</sup> Zr	<sup>93</sup> Nb
$\sigma_1$ (mb)	192 ± 10	207 ± 10	225 ± 10	211 ± 10	202 ± 10
$\Gamma_1$ (MeV)	4.1 ± 0.15	4.2 ± 0.1	4.1 ± 0.1	4.0 ± 0.1	4.7 ± 0.2
$E_1$ (MeV)	16.75 ± 0.05	16.7 ± 0.05	16.7 ± 0.05	16.65 ± 0.05	16.5 ± 0.05

TABLE 3  
Integrated cross sections (the notation used is defined in the text)

	Rb	Sr	<sup>89</sup> Y	<sup>90</sup> Zr	<sup>93</sup> Nb
$\sigma_0$ (MeV · b)	1.14 ± 0.06	1.42 ± 0.07	1.36 ± 0.07	1.26 ± 0.07	1.33 ± 0.07
$\frac{\sigma_0}{0.06 NZ A^{-1}}$	0.915 ± 0.05	1.09 ± 0.05	1.04 ± 0.05	0.95 ± 0.05	0.97 ± 0.05
$\sigma_{-1}$ (mb)	67 ± 4	80 ± 5	77 ± 5	71 ± 5	70 ± 5
$\sigma_{-2}$ (mb · MeV <sup>-1</sup> )	4 ± 0.2	4.6 ± 0.2	4.4 ± 0.2	4 ± 0.2	4.3 ± 0.2
$E_M$ (MeV)	24	27	27	26	24

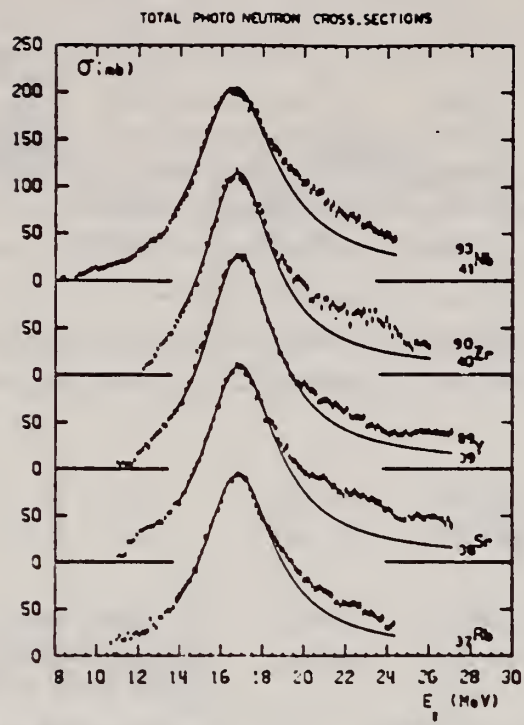


Fig. 6. Total photoneutron cross sections  $\sigma_T$  of Rb, Sr,  $^{89}\text{Y}$ ,  $^{90}\text{Zr}$  and  $^{93}\text{Nb}$  and best one Lorentz line fit corresponding to parameters given in table I.

REACTION	RESULT	EXCITATION ENERGY	SOURCE		DETECTOR		ANGLE
			TYPE	RANGE	TYPE	RANGE	
G,N	NOX	THR- 27	C	10- 27	BF3-I		4PI

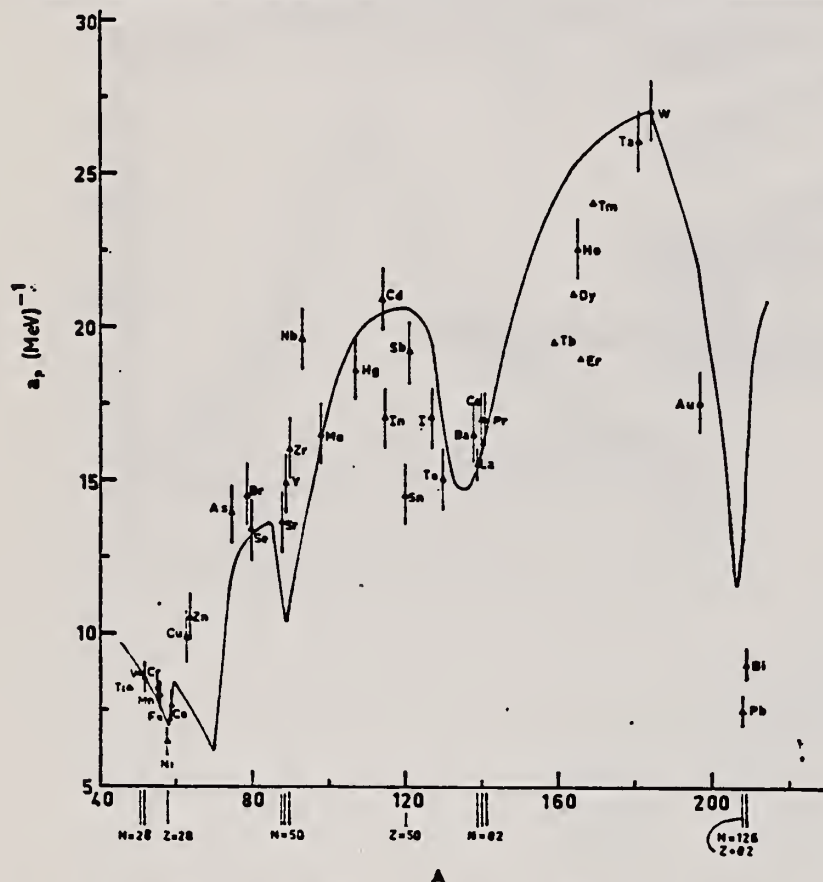


Fig. 12. Experimental values of the level density parameter  $a_p$  (Fermi gas formula plus pairing correction) versus atomic number  $A$ . The continuous curve is a least-squares fit to the data of a theoretical calculation from Newton <sup>15</sup>.

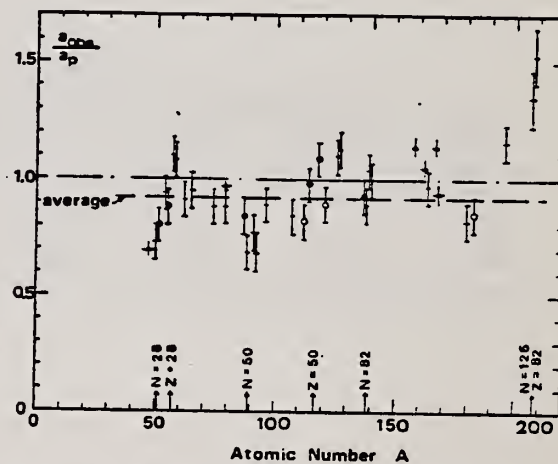


Fig. 15. Ratio  $a_{obs}/a_p$  versus atomic number  $A$ . Here  $a_{obs}$  is the level density parameter taken from the neutron resonance work of refs. <sup>1,2</sup>, and  $a_p$  is the level density parameter derived from the present  $(\gamma, n)$  work. Filled circles represent points where nuclei in the neutron resonance and in the  $(\gamma, n)$  experiment were the same. Open circles represent points where the respective nuclei were approximately matched. Triangles represent points which are based on measurement of neutron mean energies at two bremsstrahlung energies only.

(over)

TABLE 3

Comparison of experimental and theoretical data on nuclear level densities with Fermi gas formulae, and comparison of nuclear level density parameters from  $(\gamma, n)$  and n-resonance absorption experiments

Target	N (residual nucleus) <sup>a)</sup>		Goodness of fit <sup>b)</sup>		$\bar{E}_n(24)$ (MeV) <sup>c)</sup>	T (MeV) <sup>d)</sup>	$a_p$ (MeV <sup>-1</sup> ) <sup>e)</sup>	$a_{\text{obs}}$ (MeV <sup>-1</sup> ) <sup>f)</sup>	$a_{\text{obs}}/a_p$
			no p.c.	with p.c.					
Ti <sup>g)</sup>	23	8%			1.93		8.1- <sup>47</sup> Ti	6.41- <sup>47</sup> Ti	0.79
	24	8%							
	25	73%							
	26	5%							
	27	5%							
V <sup>g)</sup>	27	100%			1.96		8.7- <sup>50</sup> V	6.35- <sup>51</sup> V	0.73
Cr	25	4%	P	G	1.89		8.6- <sup>51</sup> Cr	6.9 - <sup>51</sup> Cr	<u>0.80</u>
	27	84%							
	28	10%							
	29	2%							
Mn	29	100%	V.P.	G	2.1		8.2- <sup>54</sup> Mn	7.82- <sup>56</sup> Mn	0.94
Fe	27	6%	F	G	1.96		8.0- <sup>55</sup> Fe	7.06- <sup>55</sup> Fe	<u>0.88</u>
	29	92%							
	30	2%							
Co	31	100%	P	F	2.12		7.7- <sup>58</sup> Co	8.35- <sup>60</sup> Co	1.08
Ni (Z = 28)	29	68%	V.P.	P	2.04	1.4	6.5- <sup>57,7</sup> Ni	7.19- <sup>59</sup> Ni	1.10
	31	26%							
	32	1%							
	33	4%							
	35	1%							
Cu	33	69%	V.P.	P	1.78	1.0	9.8- <sup>63</sup> Cu	8.90- <sup>64</sup> Cu	0.91
	35	31%							
Zn	33	49%	F	F	1.61		10.5- <sup>64,4</sup> Zn	10.0- <sup>65</sup> Zn	0.95
	35	28%							
	36	4%							
	37	19%							
As	41	100%	V.P.	F	1.44		14.5- <sup>74</sup> As	12.81- <sup>76</sup> As	0.88
Se <sup>g)</sup>	41	9%			1.39		13.3- <sup>78</sup> Se	12.8 - <sup>78</sup> Se	<u>0.97</u>
	42	8%							
	43	24%							
	45	50%							
	47	9%							
Br	43	45%	V.P.	V.P.	1.41		14.5- <sup>79</sup> Br	12.69- <sup>80</sup> Br	0.88
	45	49%							
Sr	47	10%	F	G	1.31		13.6- <sup>87</sup> Sr	11.4 - <sup>87</sup> Sr	<u>0.84</u>
	48	7%							
	49	83%							

<sup>a)</sup> Neutron numbers and abundances of respective residual nuclei in  $(\gamma, n)$  experiments.

<sup>b)</sup> These give an assessment of the goodness of fit of a calculated  $\bar{E}_n$  versus  $E_0$  curve to the observed data, using the Fermi gas level density formula both without and with pairing corrections.

<sup>c)</sup> Bremsstrahlung photoneutron mean energies  $\bar{E}_n$  for peak bremsstrahlung energy  $E_0 = 24$  MeV.

<sup>d)</sup> Nuclear temperature from fit with constant-temperature formula.

<sup>e)</sup> Level density parameter  $a_p$  derived from the present  $(\gamma, n)$  experiment, using a Fermi gas formula plus pairing correction, and corresponding residual nucleus (the atomic weight shown is the weighted average of atomic weights of the respective isotopes present).

<sup>f)</sup> As column 7, but using data on n-resonance absorption from refs. 1, 2).

<sup>g)</sup> Measurements of  $\bar{E}_n(E_0)$  for these nuclei were made only for  $E_0 = 21, 23$  and  $24$  MeV.



REACTION	PRODUCT	EXCITATION ENERGY	SOURCE		DETECTOR		ANGLE
			TYPE	RANGE	TYPE	RANGE	
G,NA24	ABY	THR-999	C	400-999	ACT-I		4PI

999=1 GEV

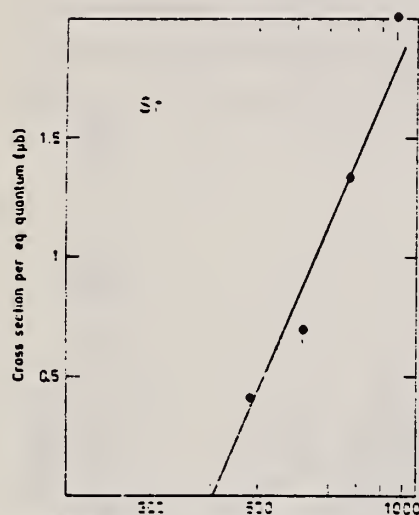


Fig. 1a-j. Bremsstrahlung energy (MeV)

Fig. 1a-j. The measured yield as a function of bremsstrahlung end point energy. The error bars give the statistical errors in the numbers of  $\gamma$ -quanta detected. The solid lines are fitted to the yield points with the least-squares method. The yield from Cu (Fig. 1a) is measured in [1] and has been recalculated using the monitor curve of [5].

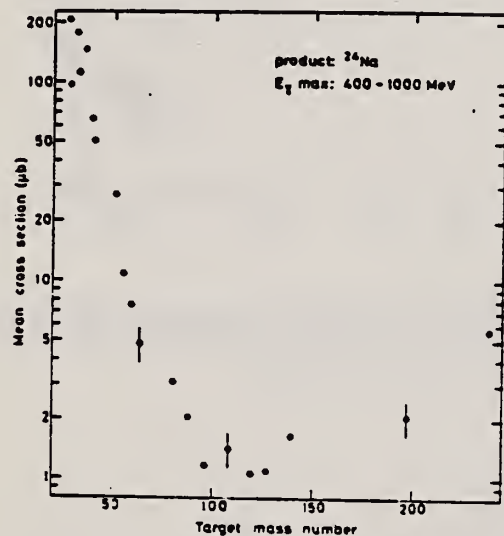


Fig. 2. The mean cross section in the energy range 400 to 1000 MeV calculated from the yields of Figure 1 in this work and of Figures 1 to 4 in [1]. The error is given by bars in some points

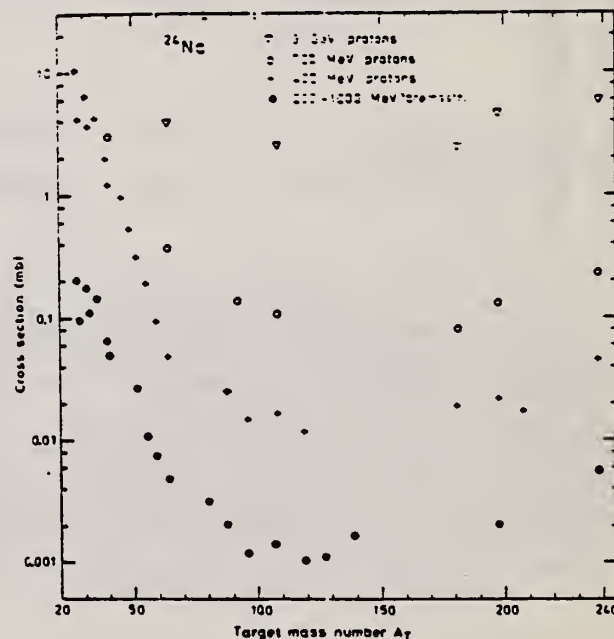


Fig. 4. Mean cross sections of the present work and of [1] (●) compared with the cross sections in proton irradiations: + 400 MeV from [4], ○ 700 MeV from [16] and an extrapolated value from [17], ▽ 3 GeV from [18]



S<sub>R</sub>  
A=86

S<sub>R</sub>  
A=86

S<sub>R</sub>  
A=86



Elem. Sym.	A	Z
Sr	86	38
Ref. No.		EGF
56 Ye 2		

Method 24 MeV Betatron; 250r Victoreen in 3.75 Lucite; neutron detector

Reaction	E or ΔE	E <sub>0</sub>	Γ	∫σdE	Jπ
Sr <sup>86</sup> (γ,xn)	Bremss. 24	15.9	5.0MeV	∫ <sub>0</sub> <sup>23</sup> = 0.92 MeV-b	

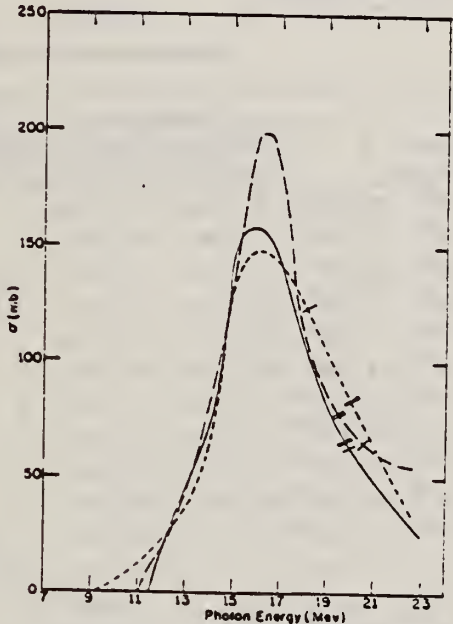


FIG. 2. Cross sections for the (γ,n) reactions in strontium isotopes. Full curve Sr<sup>86</sup>, short dashes Sr<sup>87</sup>, long dashes Sr<sup>88</sup>. The single and double slash marks on each curve represent the locations of the (γ,pn) and (γ,2n) thresholds, respectively. The units of the ordinate are 10<sup>-27</sup> cm<sup>2</sup>.

TABLE III. Parameters of giant-resonance cross-section curves for (γ,n) reactions in nuclei near 50 neutrons. Nuclides <sup>42</sup>As<sup>78</sup>, <sup>44</sup>Nb<sup>83</sup>, and <sup>46</sup>Rh<sup>103</sup> from reference 4, <sup>48</sup>Zr<sup>92</sup> and <sup>50</sup>Zr<sup>94</sup> from reference 5 recomputed in present work. Neutron number is shown in column 2, location of peak cross-section value in column 3, peak cross-section value in column 4, half-height width of curve in column 5, and area under curve from threshold to 23 Mev in column 6.

Nuclide	N	E <sub>m</sub> (MeV)	σ <sub>m</sub> (millibarns)	Γ (MeV)	∫ <sub>th</sub> <sup>23</sup> σdE (MeV-barns)
<sup>42</sup> As <sup>78</sup>	42	17.5	90.3	9.0	0.80
<sup>44</sup> Nb <sup>83</sup>	48	15.9	160	5.0	0.92
<sup>46</sup> Rh <sup>103</sup>	49	15.8	146	5.3	1.00
<sup>48</sup> Zr <sup>92</sup>	50	16.3	201	4.0	1.05
<sup>50</sup> Zr <sup>94</sup>	50	16.3	191	3.8	0.87
<sup>51</sup> Nb <sup>93</sup>	50	15.8	199	4.3	0.98
<sup>52</sup> Zr <sup>92</sup>	51	16.5	200	5.0	1.22
<sup>52</sup> Zr <sup>94</sup>	52	16.9	193	5.5	1.24
<sup>52</sup> Nb <sup>93</sup>	52	17.0	195	6.8	1.46
<sup>58</sup> Rh <sup>103</sup>	58	16.5	205	8.9	1.94

Method 30 MeV electron synchrotron; activation; NaI

Ref. No.	JHH
62 Ca 1	

Reaction	E or ΔE	E <sub>0</sub>	Γ	ΣσdE	Jπ	Notes
Sr <sup>86</sup> (γ,n)	Bremss. 30					

TABLE 1  
Isomeric Ratios from (γ,n) reactions

Target Nucleus	J <sub>0</sub>	Residual Nucleus				Isomer ratio Y <sub>1</sub> /(Y <sub>1</sub> + Y <sub>2</sub> )	σ	
		Ground state		Metastable state				
		Spin	Half-life	Spin	Half-life			
Co <sup>59</sup>	7/2 <sup>-</sup>	Co <sup>58</sup>	2 <sup>+</sup>	71.3d	5 <sup>+</sup>	9.2h	0.44 ± 0.02	3.2 ± 0.2
Co <sup>76</sup>	0 <sup>+</sup>	Co <sup>75</sup>	1/2 <sup>-</sup>	82m	7/2 <sup>+</sup>	49s	0.48 ± 0.07	2.8 ± 0.5
Hf <sup>91</sup>	3/2 <sup>-</sup>	Hf <sup>90</sup>	1 <sup>+</sup>	18m	5 <sup>-</sup>	4.4h	0.32 ± 0.02	6.5 ± 1.0
Hf <sup>96</sup>	0 <sup>+</sup>	Hf <sup>95</sup>	9/2 <sup>+</sup>	64d	1/2 <sup>-</sup>	70m	0.36 ± 0.07	2.2 ± 0.4
Zr <sup>90</sup>	0 <sup>+</sup>	Zr <sup>89</sup>	9/2 <sup>+</sup>	79h	1/2 <sup>-</sup>	4.4m	0.33 ± 0.10	2.8 ± 0.7
Mo <sup>92</sup>	0	Mo <sup>91</sup>	9/2 <sup>+</sup>	15.7m	1/2 <sup>-</sup>	66s	0.46 ± 0.04	6 <sup>+4</sup> <sub>-2</sub>
Ag <sup>107</sup>	1/2 <sup>-</sup>	Ag <sup>106</sup>	1 <sup>+</sup>	24m	6	8.3d	0.04 ± 0.02	2.0 ± 0.3
In <sup>113</sup>	9/2 <sup>+</sup>	In <sup>112</sup>	1 <sup>+</sup>	14.5m	4 <sup>+</sup>	20.7m	0.8 ± 0.1	3.1 ± 0.7
Gd <sup>116</sup>	0 <sup>+</sup>	Gd <sup>115</sup>	1/2 <sup>+</sup>	53h	11/2 <sup>-</sup>	43d	≤ 0.2	≤ 3
Ce <sup>140</sup>	0 <sup>+</sup>	Ce <sup>139</sup>	3/2 <sup>+</sup>	140d	11/2 <sup>-</sup>	55s	0.08 ± 0.01	2.5 ± 0.2
Hg <sup>198</sup>	0 <sup>+</sup>	Hg <sup>197</sup>	1/2 <sup>-</sup>	65h	13/2 <sup>+</sup>	24h	0.05 ± 0.01	3.4 ± 0.5
Previous work								
Br <sup>81(10)</sup>	3/2 <sup>-</sup>	Br <sup>80</sup>	1 <sup>+</sup>	18m	5 <sup>-</sup>	4.6h	0.33	6.5
Se <sup>82(12)</sup>	0 <sup>+</sup>	Se <sup>81</sup>	1/2 <sup>-</sup>	18m	7/2 <sup>+</sup>	57m	0.5	3.0
Zr <sup>90(11)</sup>	0 <sup>+</sup>	Zr <sup>89</sup>	9/2 <sup>+</sup>	79h	1/2 <sup>-</sup>	4.3m	0.44 ± 0.06	4.5 ± 1
In <sup>115(23)</sup>	9/2 <sup>+</sup>	In <sup>114</sup>	1 <sup>-</sup>	72s	5 <sup>+</sup>	50d	0.85	5.0
(T <sub>1/2</sub> = 2.5s)								

# REFERENCES

- 1) J. R. Huizenga and R. Vandenbosch, Phys. Rev. 120 (1960) 1305
- 2) T. Ericson, Advances in Physics, 2 (1960) 425
- 3) D. L. Allan, Nuclear Physics 24 (1961) 274
- 4) C. T. Hibdon, Phys. Rev. 114 (1959) 179
- 5) C. T. Hibdon, Phys. Rev. 122 (1961) 1235
- 6) T. Ericson, Nuclear Physics 11 (1959) 481
- 7) J. H. Carver and G. A. Jones, Nuclear Physics 12 (1960) 184
- 8) A. C. Douglas and N. Macdonald, Nuclear Physics 11 (1959) 382
- 9) T. Ericson and V. M. Scrutinski, Nuclear Physics 2 (1958) 284
- 10) L. Katz, L. Pease and H. Moody, Can. J. Phys. 30 (1952) 476
- 11) L. Katz, R. G. Baker and R. Montalbetti, Can. J. Phys. 31 (1953) 250
- 12) E. Silva and J. Goldenberg, An. Acad. Brasil Cienc. 28 (1956) 275
- 13) J. H. Carver and D. C. Peaslee, Phys. Rev. 120 (1960) 2155
- 14) J. M. Blatt and V. F. Weisskopf, "Theoretical Nuclear Physics" New York: Wiley (1952)
- 15) S. H. Vegors, L. L. Marsden and R. L. Heath, U.S. Atomic Energy Commission Report IDO-16370 (1958)
- 16) Nuclear Data Sheets, National Research Council, Washington (1960, up to and including Set 5)
- 17) R. Vandenbosch and J. R. Huizenga, Phys. Rev. 120 (1960) 1313
- 18) E. Weigold and R. Glover, Nuclear Physics (in press)
- 19) K. J. Le Couteur and D. W. Lang, Nuclear Physics 11 (1959) 32
- 20) T. D. Newton, Can. J. Phys. 34 (1956) 804
- 21) D. W. Lang, Nuclear Physics 26 (1961) 434
- 22) M. E. Rose, "Internal Conversion Coefficients", Amsterdam: North Holland Publishing Co. (1958)
- 23) J. Goldenberg and L. Katz, Phys. Rev. 90 (1953) 308

REF. F.Z. Khien, N.K. Zui, N.T. An  
Yad. Fiz. 35, 257 (1982)  
Sov. J. Nucl. Phys. 35, 145 (1982)

ELEM. SYM.	A	Z
Sr	86	38

METHOD	REF. NO.	
	82 Kh 2	egf

REACTION	RESULT	EXCITATION ENERGY	SOURCE		DETECTOR		ANGLE
			TYPE	RANGE	TYPE	RANGE	
G, N	NOX	12-14	C	14	ACT-I		4PI

# ISOMERIC RATIO

The method is developed for calculation of the isomeric ratio for the case of low excitation energy of the residual nucleus, and the isomeric ratio is measured in the  $(n, 2n)$  and  $(\gamma, n)$  reactions in the neutron-deficient nuclei  $^{92}\text{Mo}$ ,  $^{90}\text{Zr}$ ,  $^{88}\text{Sr}$ , and  $^{76}\text{Se}$ . The good agreement between the experimental and theoretical results on the  $(\gamma, n)$  reaction has confirmed the reliability of the characteristics of the residual nuclei, the transmission coefficients of the emitted neutrons, etc., used in the calculations. From study of the  $(n, 2n)$  reaction we have obtained values of the parameters of the spin dependence of the level density of the nucleus in the excitation-energy region  $\sim 14$  MeV.

PACS numbers: 25.20. + y, 25.40.Gr, 27.50. + e, 27.60. + j

TABLE III. Isomeric ratio in the  $(\gamma, n)$  reaction.

Target nucleus	$R_{\text{exp}}$	$R_{\text{theor}}$	Published data <sup>1)</sup>
$^{92}\text{Mo}$	$1.54 \pm 0.15$	1.36	$1.82 \pm 0.15$ (70) [9] $1.03 \pm 0.21$ [10] $0.85 \pm 0.07$ (30) [15]
$^{90}\text{Zr}$	$1.52 \pm 0.04$	1.19	$0.50 \pm 0.15$ (30) [15]
$^{88}\text{Sr}$	$0.70 \pm 0.07$	0.96	$0.68 \pm 0.14$ (30) [15]
$^{76}\text{Se}$	$7.5 \pm 1.0$	$10.5^{+1.0}_{-0.8}$	

<sup>1)</sup>In parentheses we have given the values of the bremsstrahlung maximum energy.

<sup>2)</sup>In the calculations we used the  $^{76}\text{Se}$  level scheme of Ref. 2,  $I_{\pi} = 7/2^+$  and  $I_{\sigma} = 1/2^+$ .

<sup>3)</sup>In the calculations we used the level scheme of  $^{76}\text{Se}$  in Ref. 3,  $I_{\pi} = 9/2^+$  and  $I_{\sigma} = 3/2^+$ .





SR  
A=87

SR  
A=87

SR  
A=87



Elem. Sym.	A	Z
Sr	87	38
Ref. No. 56 Ye 2		EGF

Method 24 MeV Betatron; 250 r Victoreen in 3.75 cm Lucite; neutron detector

Reaction	E or $\Delta E$	$E_0$	$\Gamma$	$\int \sigma dE$	$J\pi$	Notes
$\text{Sr}^{87}(\gamma, xn)$	Bremss. 24	15.8	5.3 MeV	$\int_0^{23} = 1.00 \text{ MeV-b}$		

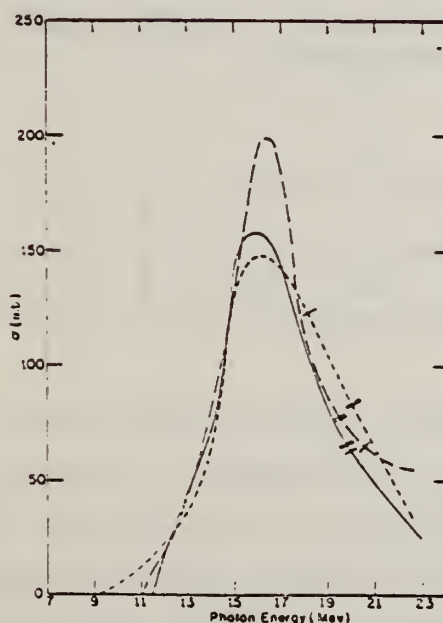


FIG. 2. Cross sections for the  $(\gamma, n)$  reactions in strontium isotopes. Full curve  $\text{Sr}^{86}$ , short dashes  $\text{Sr}^{87}$ , long dashes  $\text{Sr}^{88}$ . The single and double slash marks on each curve represent the locations of the  $(\gamma, pn)$  and  $(\gamma, 2n)$  thresholds, respectively. The units of the ordinate are  $10^{-27} \text{ cm}^2$ .

TABLE III. Parameters of giant-resonance cross-section curves for  $(\gamma, n)$  reactions in nuclei near 50 neutrons. Nuclides  $^{75}\text{As}$ ,  $^{121}\text{Sb}$ , and  $^{135}\text{Rh}$  from reference 4,  $^{90}\text{Zr}$  and  $^{92}\text{Zr}$  from reference 5 recomputed in present work. Neutron number is shown in column 2, location of peak cross-section value in column 3, peak cross-section value in column 4, half-height width of curve in column 5, and area under curve from threshold to 23 MeV in column 6.

Nuclide	N	$E_m$ (MeV)	$\sigma_m$ (millibarns)	$\Gamma$ (MeV)	$\int_{\text{th}}^{23} \sigma dE$ (MeV-barns)
$^{75}\text{As}$	42	17.3	90.3	9.0	0.80
$^{121}\text{Sb}$	48	15.9	160	5.0	0.92
$^{135}\text{Rh}$	49	15.8	146	5.3	1.00
$^{90}\text{Zr}$	50	16.3	201	4.0	1.05
$^{92}\text{Zr}$	50	16.3	191	3.8	0.87
$^{90}\text{Zr}$	50	15.8	199	4.3	0.98
$^{92}\text{Zr}$	51	16.5	200	5.0	1.22
$^{92}\text{Zr}$	52	16.9	193	5.5	1.24
$^{135}\text{Rh}$	52	17.0	195	6.8	1.46
$^{135}\text{Rh}$	58	16.5	205	8.9	1.94

REF. Y. Oka, T. Kato, K. Nomura, T. Saito, Hui-Tuh Tsai  
Bull. Chem. Soc. Japan 41, 380 (1968)

ELEM. SYM.	A	Z
Sr	87	38

METHOD

REF. NO.	
68 Ok 3	egf

REACTION	RESULT	EXCITATION ENERGY	SOURCE		DETECTOR		ANGLE
			TYPE	RANGE	TYPE	RANGE	
G,P	ABY	THR-20	C	20	ACT-I		4PI

TABLE I. SUMMARY OF DATA ON ( $\gamma, p$ ) REACTIONS WITH 20 MeV BREMSSTRAHLUNG

Nuclide			Observed $\gamma$ -ray				Yield determined	
Parent (Natural abundance, %)	Residual (Half-life)	$S_p$ (MeV)	Energy (MeV)	Branching ratio (%)	Type of multipole transition		$\mu\text{Ci/mg}^a$	Yield/mol-R
$^{23}\text{Mg}$ (10.11)	$^{24}\text{Na}$ (15 hr)	12.06	1.37	100	E2		$1.48 \times 10^{-1}$	$1.7 \times 10^3$
$^{28}\text{Si}$ (4.71)	$^{29}\text{Al}$ (2.27 min)	12.33	1.78	100	E2		1.91	$2.8 \times 10^3$
$^{30}\text{Si}$ (3.12)	$^{30}\text{Al}$ (6.56 min)	13.59	1.28	93.8	E2+M1		$6.51 \times 10^{-1}$	$1.5 \times 10^3$
$^{40}\text{Ca}$ (2.06)	$^{41}\text{K}$ (22.4 hr)	12.17	0.374	85	E2+M1		$7.86 \times 10^{-3}$	$1.3 \times 10^3$
$^{47}\text{Ti}$ (7.32)	$^{48}\text{Sc}$ (84.1 d)	10.47	0.887	100	E2		$7.11 \times 10^{-4}$	$3.1 \times 10^3$
$^{48}\text{Ti}$ (73.99)	$^{48}\text{Sc}$ (3.4 d)	11.44	0.160	100	E2+M1		$6.83 \times 10^{-3}$	$1.2 \times 10^3$
$^{49}\text{Ti}$ (5.46)	$^{49}\text{Sc}$ (1.8 d)	11.35	1.31	100	E2		$4.40 \times 10^{-3}$	$5.8 \times 10^4$
$^{52}\text{Cr}$ (9.55)	$^{52}\text{V}$ (3.8 min)	11.15	1.43	100	E2		$5.01 \times 10^{-1}$	$6.6 \times 10^4$
$^{57}\text{Fe}$ (2.17)	$^{56}\text{Mn}$ (2.58 hr)	10.57	1.81	23.5	E2+M1		$8.10 \times 10^{-3}$	$2.1 \times 10^3$
$^{74}\text{Ge}$ (36.74)	$^{73}\text{Ga}$ (4.8 hr)	10.92	0.295	97	(E2)		$3.70 \times 10^{-1}$	$1.3 \times 10^3$
$^{77}\text{Se}$ (7.58)	$^{76}\text{As}$ (26.5 hr)	9.61	0.559	41	E2		$1.48 \times 10^{-3}$	$1.3 \times 10^3$
$^{87}\text{Sr}$ (7.02)	$^{86}\text{Rb}$ (19 d)	9.41	1.08	9	E2		$5.15 \times 10^{-4}$	$9.9 \times 10^4$
$^{110}\text{Cd}$ (12.26)	$^{112}\text{Ag}$ (3.2 hr)	9.74	1.39	35	E2		$1.91 \times 10^{-2}$	$2.1 \times 10^4$
$^{117}\text{Sn}$ (7.57)	$^{118}\text{In}$ (54 min)	9.58	1.27	84	E2		$9.80 \times 10^{-3}$	$6.9 \times 10^3$
$^{181}\text{Ba}$ (11.32)	$^{180}\text{Cs}$ (13 d)	8.67	0.830	100	E2		$1.68 \times 10^{-4}$	$2.2 \times 10^4$
$^{199}\text{Hg}$ (16.84)	$^{199}\text{Au}$ (2.7 d)	7.27	0.412	100	E2		$8.43 \times 10^{-4}$	$2.2 \times 10^4$

a) The value corrected at the end of 1 hr irradiation ( $9.4 \times 10^4$  R/min).

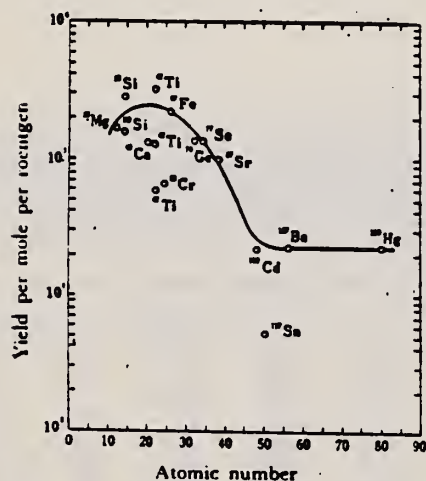


Fig. 2. The yield curve for the ( $\gamma, p$ ) reaction with 20 MeV bremsstrahlung.



Sr

87

38

METHOD

REF. NO.

73 W1 6

hmg

REACTION	RESULT	EXCITATION ENERGY	SOURCE		DETECTOR		ANGLE
			TYPE	RANGE	TYPE	RANGE	
G,N	ABX	8- 11	C	9- 12	TOF-D		130

NO PEAK OBSERVED

Table I

Reaction	Thres- hold (MeV)	Energy Range of Experiment (MeV)	Observed Peaks		
			Peak Energy (MeV)	$\frac{d\sigma}{d\Omega}$ at peak (mb/ster.)	$4\pi \int \left(\frac{d\sigma}{d\Omega}\right)_{130^\circ} dE_\gamma$ peak
$^{87}\text{Sr}(\gamma, n_0)$	8.44	9.4-11.1			(MeV-mb)
$^{87}\text{Sr}(\gamma, n_1)$	9.52	10.5-11.1			
$^{91}\text{Zr}(\gamma, n_0)$	7.19	7.8-10.3	9.1	1.2	20
$^{97}\text{Nb}(\gamma, n_0)$	6.82	7.8-9.2	8.1	0.3	3
$^{113}\text{Cd}(\gamma, n_0)$	6.54	7.4-9.3	7.7	0.9	7
$^{117}\text{Sn}(\gamma, n_0)$	6.94	7.6-8.8	7.8	2.5	20
$^{119}\text{Sn}(\gamma, n_0)$	6.48	7.1-9.0	7.8	1.6	18

The  $^{87}\text{Sr}$  cross sections display no peaking. The ground state  $(\gamma, n_0)$  cross section is small and by 11 MeV is overwhelmed by the  $(\gamma, n_1)$  cross section to the first excited state of  $^{86}\text{Sr}$ . At 11 MeV the  $(\gamma, n_1)$  cross section is roughly 0.8 millibarns per steradian, and is order-of-magnitude larger than the  $(\gamma, n_0)$  cross section, and comparable to the extrapolated giant resonance cross section. This general behavior is not unexpected since  $^{87}\text{Sr}$  has  $J^\pi = 9/2^+$  so that for dipole absorption the emitted ground state neutrons must have  $\geq 3$ .

REF. Yoshihisa Watanabe, Takeshi Mukoyama  
Nucl. Sci. Eng. 80, 92 (1982)

ELEM. SYM.	A	Z
Sr	87	38

METHOD

REF. NO.	
82 Wa4	egf

REACTION	RESULT	EXCITATION ENERGY	SOURCE		DETECTOR		ANGLE
			TYPE	RANGE	TYPE	RANGE	
G,G/	ABY	1	C	1.3*	ACT-I		4PI

1=1.23 MEV, \*CO-60

A photoexcitation process by gamma rays from a  $^{60}\text{Co}$  source has been studied for the nuclei of  $^{87}\text{Sr}$ ,  $^{111}\text{Cd}$ ,  $^{115}\text{In}$ , and  $^{176}\text{Lu}$ . The induced isomeric activity was measured with a Ge(Li) detector. The flux of photons scattered into the target has been estimated with the Monte Carlo method using the single-scattering approximation. From the observed induced activities and the calculated photon flux, the integral cross sections for isomer production by photoexcitation were obtained and compared with other experimental data.

TABLE II

Integral Cross Sections for the Isomer Production by Photoexcitation ( $\times 10^{-25} \text{ cm}^2 \cdot \text{eV}$ )

	$^{87}\text{Sr}$	$^{111}\text{Cd}$	$^{115}\text{In}$	$^{176}\text{Lu}$	Photon Source	Reference
Chertok and Booth		$0.6 \pm 0.2$	$0.71 \pm 0.23$		Bremsstrahlung	5
Booth and Brownson	$0.85^{+0.4}_{-0.3}$		$1.15 \pm 0.4$		Bremsstrahlung	6
Boivin et al.		$0.8^{+0.4}_{-0.05}$	$3^{+4}_{-2}$		Bremsstrahlung	7
Lakosi et al.		$1.02 \pm 0.26$	$1.05 \pm 0.27$		$^{60}\text{Co}$	11
Yoshihara	$3.0 \pm 0.8^a$	$1.5 \pm 0.3$	$2.3 \pm 0.4$	$69 \pm 12^a$ $140 \pm 30^a$	$^{60}\text{Co}$	3
Veres	0.5 to 0.62	0.8 to 1.5	0.9 to 5		$^{60}\text{Co}$	23
Present work	$4.2 \pm 0.6^b$	$1.1 \pm 0.2$	$3.5 \pm 0.2$	$39 \pm 27^b$	$^{60}\text{Co}$	
	$5.6 \pm 0.8^c$			$48 \pm 34^c$		

<sup>a</sup>Obtained as the relative value to  $^{115}\text{In}$ .

<sup>b</sup>Provided that the partial level width  $g\Gamma_0 = 1 \times 10^{-3} \text{ eV}$ .

<sup>c</sup>Provided that the partial level width  $g\Gamma_0 = 1 \times 10^{-4} \text{ eV}$ .

SR  
A=88

SR  
A=88

SR  
A=88



METHOD					REF. NO.		
					56 He 3	hmg	
REACTION	RESULT	EXCITATION ENERGY	SOURCE		DETECTOR		ANGLE
			TYPE	RANGE	TYPE	RANGE	
E, E/	FMP	1-7	D	187	MAG-D		DST

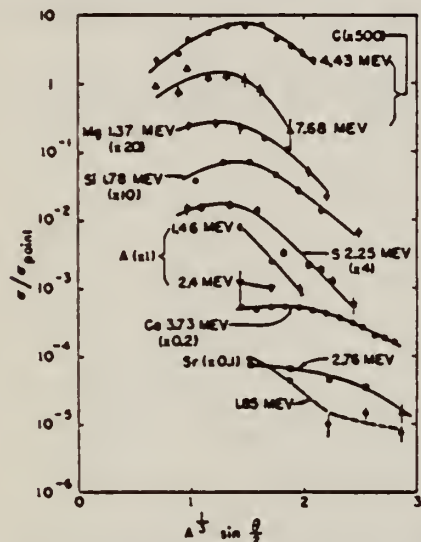


FIG. 3. Inelastic angular distributions (observed cross section divided by Feshbach point-charge cross sections). The results of Hahn *et al.* (reference 8) for Ca and of Fregeau and Hofstadter (reference 11) are included for comparison.

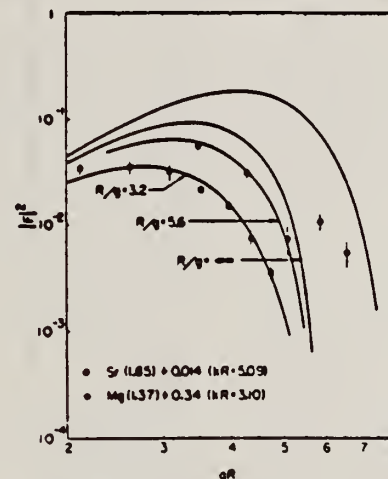


FIG. 6. Comparison of typical experimental and calculated squared inelastic form factors. Both the Sr (1.85 Mev) and Mg (1.37 Mev) are known to be  $2+$  levels. The calculated curves are for a "smeared  $\delta$ -function" transition charge density (see Sec. V) with values of  $R/g$  taken from the elastic results. The abscissae for the experimental data are scaled by values of  $R$  taken from the elastic results [Table III (a)]. Shown for comparison (upper curve) is a squared form factor calculated from a quadrupole transition charge density whose radial dependence is constant for  $r < R$ , zero for  $r > R$ . This would give a poorer fit to the data than the  $\delta$ -function distribution, indicating that the quadrupole vibrational mode is approximated better by a transverse wave in an incompressible nuclear fluid than by some sort of a compressional body wave.

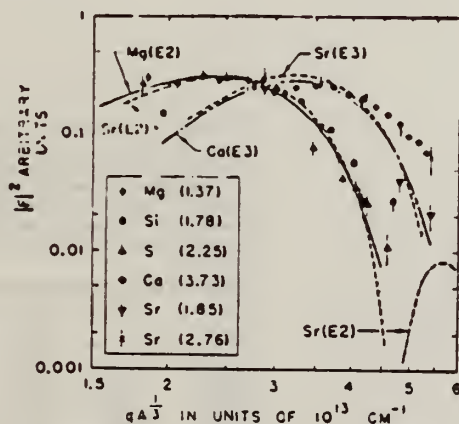


FIG. 7. Inelastic "universal curves." A composite plot of inelastic data from Mg, Si, S, Ca, and Sr against  $q\lambda$ . The various form factors are arbitrarily normalized to minimize the spread of points. The point from sulfur and the point from silicon which seem to deviate from the "universal curve" are assumed to contain undetected experimental errors. The curves labeled Mg(E2), Sr(E2), Ca(E3), and Sr(E3) are calculated for electric-quadrupole and octupole transitions using the "smeared  $\delta$ -function" transition charge densities of Sec. V, and are arbitrarily normalized.



Method  
24 MeV Betatron; 250 r Victoreen in 3.75 cm Lucite; neutron detector

Ref. No.	
56 Ye 2	EGF

Reaction	E or $\Delta E$	$E_0$	$\Gamma$	$\int \sigma dE$	$J\pi$	Notes
$\text{Sr}^{88}(\gamma, xn)$	Bremss. 24	16.3	4.0 MeV	$\int_0^{23} = 1.05 \text{ MeV-b}$		

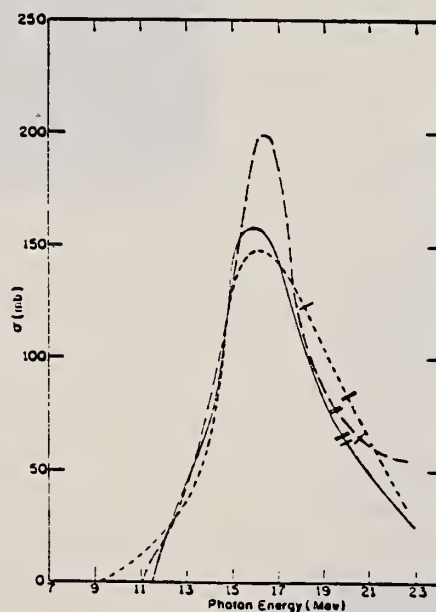


FIG. 2. Cross sections for the  $(\gamma, n)$  reactions in strontium isotopes. Full curve  $\text{Sr}^{88}$ , short dashes  $\text{Sr}^{87}$ , long dashes  $\text{Sr}^{86}$ . The single and double slash marks on each curve represent the locations of the  $(\gamma, pn)$  and  $(\gamma, 2n)$  thresholds, respectively. The units of the ordinate are  $10^{-27} \text{ cm}^2$ .

TABLE III. Parameters of giant-resonance cross-section curves for  $(\gamma, n)$  reactions in nuclei near 50 neutrons. Nuclides  $^{88}\text{Sr}$ ,  $^{87}\text{Sr}$ , and  $^{86}\text{Sr}$  from reference 4,  $^{90}\text{Zr}$  and  $^{91}\text{Zr}$  from reference 5 recomputed in present work. Neutron number is shown in column 2, location of peak cross-section value in column 3, peak cross-section value in column 4, half-height width of curve in column 5, and area under curve from threshold to 23 MeV in column 6.

Nuclide	N	$E_m$ (MeV)	$\sigma_m$ (millibarns)	$\Gamma$ (MeV)	$\int_{th}^{23} \sigma dE$ (MeV-barns)
$^{88}\text{Sr}$	42	17.3	90.3	9.0	0.80
$^{87}\text{Sr}$	48	15.9	160	5.0	0.92
$^{86}\text{Sr}$	49	15.8	146	5.3	1.00
$^{90}\text{Zr}$	50	16.3	291	4.0	1.05
$^{91}\text{Zr}$	50	16.3	191	3.8	0.87
$^{90}\text{Zr}$	50	15.8	199	4.3	0.98
$^{91}\text{Zr}$	51	16.5	200	5.0	1.22
$^{92}\text{Zr}$	52	16.9	193	5.5	1.24
$^{93}\text{Nb}$	52	17.0	195	6.8	1.46
$^{103}\text{Rh}$	58	16.5	205	8.9	1.94

REF.

R.B. Begzhanov and A. A. Islamov  
 J. Exptl. Theoret. Phys. (USSR) 47, 768 (1964)  
 Soviet Phys. JETP 20, 513 (1965)

ELEM. SYM.

A

Z

Sr

88

38

METHOD

REF. NO.

Resonance scattering, self-absorption

64 Be 7

JOC

REACTION	RESULT	EXCITATION ENERGY	SOURCE		DETECTOR		ANGLE
			TYPE	RANGE	TYPE	RANGE	
G,G	LFT	2	D	2	D		
		(1.85)		(1.85)			

$$\Gamma_Y = (6.0 \pm 1.2) \times 10^{-3} \text{ eV or}$$

$$\tau_Y = (1.10 \pm 0.22) \times 10^{-13} \text{ sec, for the 1.85 MeV level.}$$

REACTION	RESULT	EXCITATION ENERGY	SOURCE		DETECTOR		ANGLE
			TYPE	RANGE	TYPE	RANGE	
E, E/	RLX	1-7	D	65,70	MAG-D	58-70	DST

B(EL); SEP ISOTPS

TABLE I. Experimentally determined values of the reduced nuclear radiative transition probabilities  $B(EL)$  for the excitation of a nucleus to a level at energy  $E^*$  above its ground state by a transition of electric character and multipolarity  $L$ , in units of  $e^2 F^{2L}$ , where  $1 F = 10^{-13}$  cm. The last column gives  $B(EL)$  in single-particle Weisskopf units according to Eq. (4).

$E^*$	$L$	$B(E0 \rightarrow L)$ ( $e^2 F^{2L}$ )	$G$ (W.u.)
<b>Sr<sup>88</sup></b>			
1.84	2	990 ± 50	8.5
2.74	3	80 600 ± 3000	25.0
4.0	2	190 ± 40	1.6
6.5	(2)	130 ± 30	1.1
	(3)	13 000 ± 3000	4.0
<b>Y<sup>88</sup></b>			
1.50	2	120 ± 50	1.0
1.73	2	140 ± 40	1.2
2.21	3	33 700 ± 3000	10.2
2.52	3	37 800 ± 3000	11.4
2.86	3	32 300 ± 3000	9.8

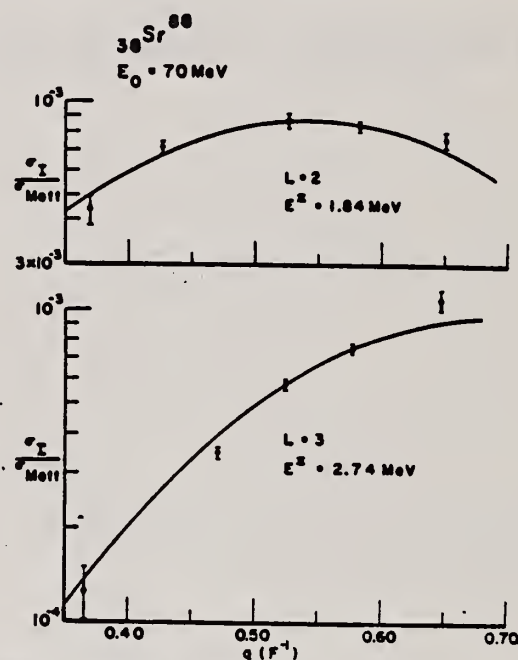


FIG. 5. Distorted-wave inelastic cross section in units of the Mott cross section versus momentum transferred to the  $\text{Sr}^{88}$  nucleus for the electric quadrupole excitation at 1.84 MeV and for the electric octupole excitation at 2.74 MeV. An incompressible and irrotational hydrodynamical model was assumed.

METHOD

REF. NO.

69 Ha 1

egf

REACTION	RESULT	EXCITATION ENERGY	SOURCE		DETECTOR		ANGLE
			TYPE	RANGE	TYPE	RANGE	
P,G	RLX	15-22	D	4-12	NAI-D	10-22	90

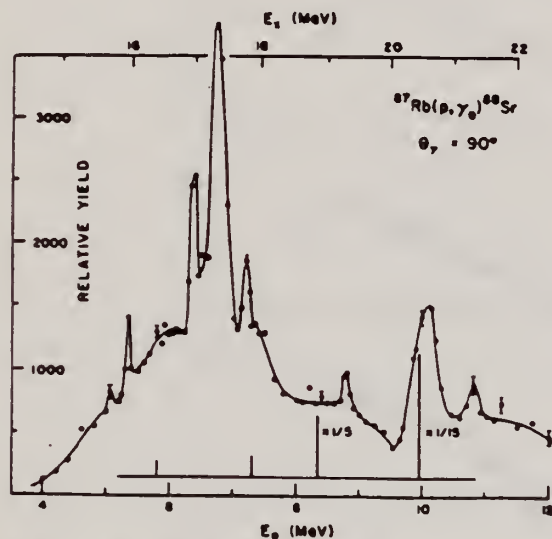


Fig. 3. Yield curve of  $^{87}\text{Rb}(p, \gamma_0)^{88}\text{Sr}$  at  $90^\circ$ . The predicted resonances [1] are shown as vertical lines whose heights are proportional to  $\Gamma_{\gamma_0}$ . The two highest lines have been suppressed by factors of 5 and 15, as indicated.

K. Shoda, M. Sugawara, T. Saito, and H. Miyase  
Phys. Rev. Letters 23, 800 (1969)

REF. NO.	69 Sh 5	hmg
SR	88	38

REACTION	RESULT	EXCITATION ENERGY	SOURCE		DETECTOR		ANGLE
			TYPE	RANGE	TYPE	RANGE	
E,P	ABX	14-25	D	16-30	MAG-D		

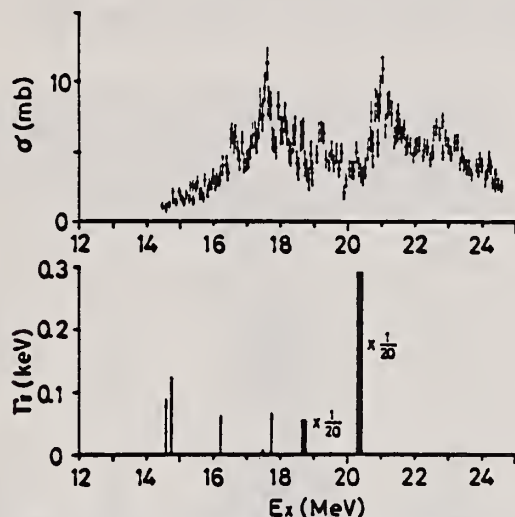


FIG. 1. Cross section of  $^{88}\text{Sr}(\gamma, p_0)$ . The vertical lines show the theoretical radiative widths of LAs from Ref. 5.

Assumption is made that photoproton emission leaves the residual nucleus in the ground state.

<sup>5</sup>B. Goulard, T. A. Hughes, and S. Fallieros, Phys. Rev. 176, 1345 (1968).



REF. K. Shoda, M. Sugawara, T. Saito & H. Miyase  
 PICNS-69 Proceedings of the Conference on Nuclear Isospin.  
 Asilomar-Pacific Grove, California, 1969 (Academic Press,  
 New York & London 1969) p.125.

ELEM. SYM.	A	Z
Sr	88	38
REF. NO.		
69 Sh 6		egf

METHOD			SOURCE		DETECTOR		ANGLE
REACTION	RESULT	EXCITATION ENERGY	TYPE	RANGE	TYPE	RANGE	
E,P	SPC	14-30	D	30	MAG-D		UKN

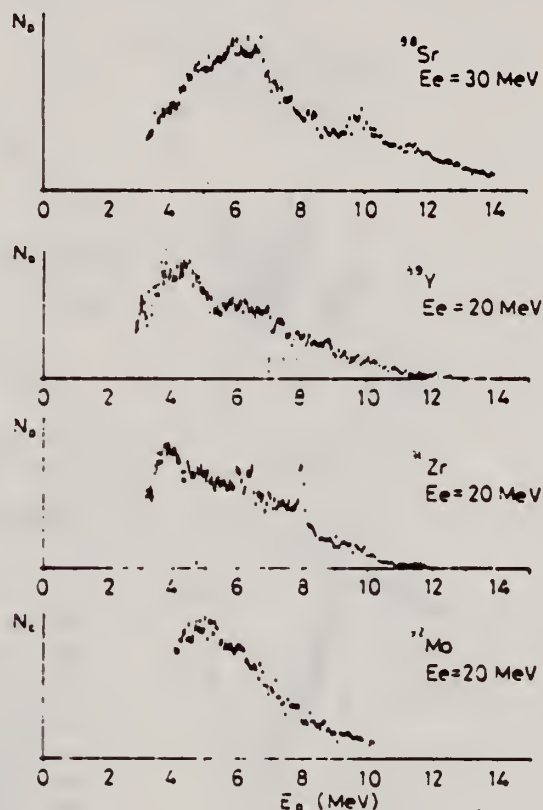


Fig. 1. Energy distributions of photoprotons. Vertical broken lines and solid lines indicate the position of  $p_0$  corresponding to the ground IAS and electric dipole IAS (2-4) respectively.

REF. I. Blomqvist, G. Nydahl and B. Forkman  
Nucl. Phys. A162, 193 (1971)

ELEM. SYM.	A	Z
Sr	88	38

METHOD	REF. NO.	
	71 B1 1	egf

REACTION	RESULT	EXCITATION ENERGY	SOURCE		DETECTOR		ANGLE
			TYPE	RANGE	TYPE	RANGE	
G,PI+	ABY	150-700	C	150-700	ACT-I		4PI

SEE 68 NY 1

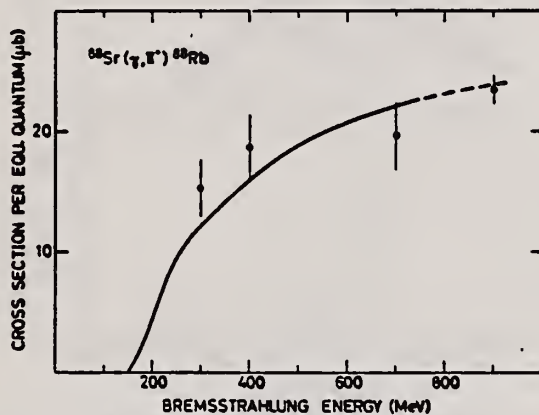


Fig. 4. Absolute yield for  $^{88}\text{Sr}(\gamma, \pi^+)^{88}\text{Rb}$ .

K. Shoda, M. Sugawara, T. Saito, H. Miyase, A. Suzuki, S. Oikawa,  
and J. Uegaki  
PICNS-72, 321 Sendai

Sr

88

38

METHOD

REF. NO.

72 Sh 10

hvm

REACTION	RESULT	EXCITATION ENERGY	SOURCE		DETECTOR		ANGLE
			TYPE	RANGE	TYPE	RANGE	
E,P	SPC	17	C	16- 18	MAG-D		UKN
		(17.2)					

## I A STATES

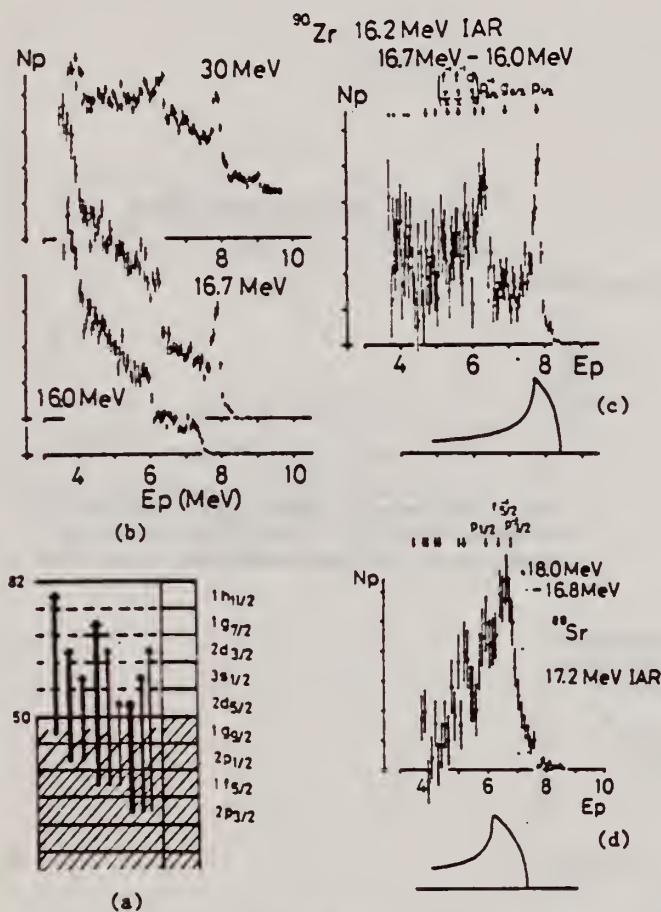


Fig. 7 (a): Shell model diagram of  $^{90}\text{Zr}$  and  $^{88}\text{Sr}$ .

(b): Energy distributions of  $^{90}\text{Zr}(e,e'p)$ .

(c): Energy distributions obtained from difference method. Residual states for 16.2 MeV IAR are shown by arrows.

(d): Energy distributions obtained from difference method for  $^{88}\text{Sr}$ . Residual states for 17.2 MeV IAR are shown by arrows.

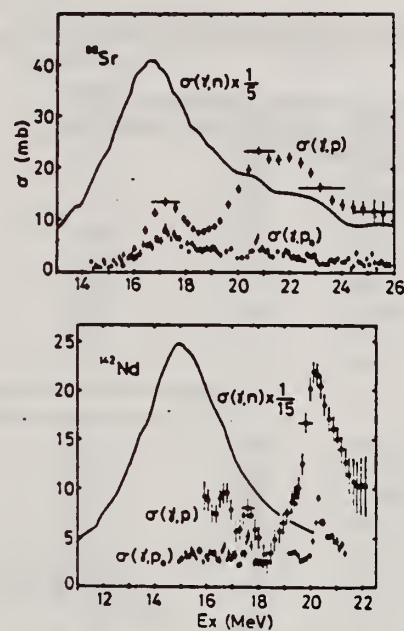


Fig. 11 The  $(\gamma,p)$  cross sections of  $^{88}\text{Sr}$  and  $^{142}\text{Nd}$ . The  $(\gamma,p_0)$  and  $(\gamma,n)$  cross sections are also shown.

REACTION	RESULT	EXCITATION ENERGY	SOURCE		DETECTOR		ANGLE
			TYPE	RANGE	TYPE	RANGE	
G,G	ABX	8- 12	D	8- 12	NAI-D		131

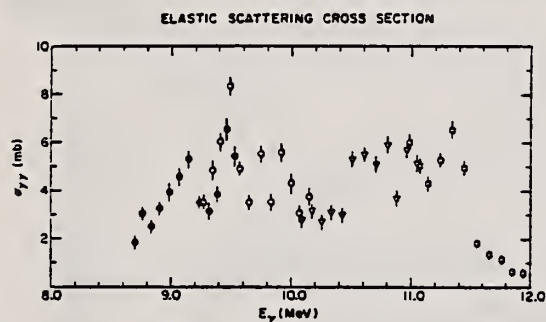


FIG. 1. The elastic scattering cross section of monochromatic photons on  $^{88}\text{Sr}$ . The different symbols represent four sets of experimental data.

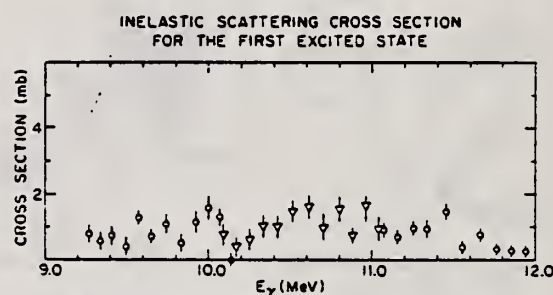


FIG. 2. The inelastic scattering cross section for the first excited state of  $^{88}\text{Sr}$ . The different symbols represent three sets of our experimental data.

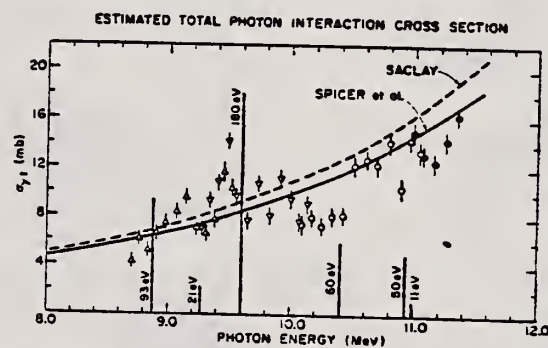


FIG. 3. The total photon-interaction cross section estimated from four sets of elastic scattering data. The dashed curve is an extrapolation of the  $(\gamma, n)$  cross section of  $^{88}\text{Sr}$  measured by Lepetre *et al.* (Ref. 2). The solid curve is an extrapolation of the  $^{88}\text{Sr}(\gamma, n)$  cross section of Spicer *et al.* (Ref. 1). Both of these curves were drawn with the assumption that the giant dipole resonance can be represented by a Lorentz resonance function. The levels predicted by Goulard, Hughes, and Fallieros (Ref. 4) are shown by vertical bars with values of the predicted ground-state radiative widths in eV.



REF.

S. P. Fivozinsky, S. Penner, J.W. Lightbody, Jr., and D. Blum  
Phys. Rev. C9, 1533 (1974)

ELEM. SYM.	A	Z
Sr	88	38

METHOD

REF. NO.

74 F1 1

hmg

REACTION	RESULT	EXCITATION ENERGY	SOURCE		DETECTOR		ANGLE
			TYPE	RANGE	TYPE	RANGE	
E, E/	FMF	1, 3	C	45-121	MAG-D		DST
		(1.84, 2.74)					

LEVELS 1.84, 2.74 MEV

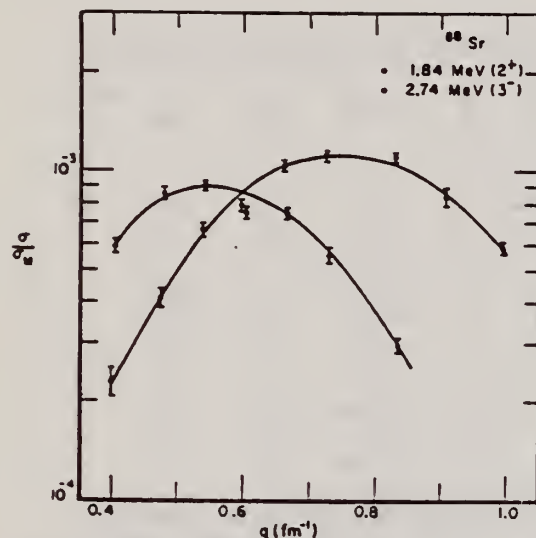


FIG. 5. Tassie-model fits to  $^{88}\text{Sr}$   $2^+$  and  $3^-$  form factors.

Elastic scattering data for  $^{88}\text{Sr}$  and  $^{89}\text{Y}$ .

TABLE III. Electron scattering form factors for  $^{88}\text{Sr}$ .

Level	Incident energy (MeV)	Lab scattering angle (deg)	$q$ ( $\text{fm}^{-1}$ )	$ F ^2$	Standard deviation (%)
Ground state $0^+$	120.85	110.5	1.005	$0.6695 \times 10^{-2}$	1.2
	100.87	128.2	0.919	$0.8558 \times 10^{-2}$	1.6
	101.17	110.5	0.842	$0.6633 \times 10^{-2}$	1.2
	80.86	128.2	0.737	$0.1004 \times 10^{-1}$	1.7
	80.95	110.5	0.674	$0.1984 \times 10^{-1}$	0.7
	67.07	128.2	0.611	$0.4660 \times 10^{-1}$	0.6
	60.48	128.3	0.551	$0.9065 \times 10^{-1}$	0.7
	53.46	128.3	0.487	0.1790	0.6
1.84 MeV $2^+$	45.42	128.3	0.414	0.3351	0.5
	120.85	110.5	...	...	...
	100.87	128.2	...	...	...
	101.17	110.5	0.834	$0.2953 \times 10^{-3}$	4.7
	80.86	128.2	0.728	$0.5591 \times 10^{-3}$	5.8
	80.95	110.5	0.666	$0.7535 \times 10^{-3}$	3.6
	67.07	128.2	0.603	$0.7610 \times 10^{-3}$	4.1
	60.48	128.3	0.543	$0.9175 \times 10^{-3}$	3.1
2.74 MeV $3^-$	53.46	128.3	0.479	$0.8745 \times 10^{-3}$	4.1
	45.42	128.3	0.406	$0.6099 \times 10^{-3}$	4.6
	120.85	110.5	0.994	$0.5636 \times 10^{-3}$	4.1
	100.87	128.2	0.906	$0.8164 \times 10^{-3}$	5.9
	101.17	110.5	0.830	$0.1086 \times 10^{-2}$	2.2
	80.86	128.2	0.724	$0.1139 \times 10^{-2}$	3.2
	80.95	110.5	0.662	$0.1048 \times 10^{-2}$	2.9
	67.07	128.2	0.499	$0.7969 \times 10^{-3}$	3.8
	60.48	128.3	0.539	$0.6788 \times 10^{-3}$	4.7
	53.46	128.3	0.475	$0.4209 \times 10^{-3}$	5.9
	45.42	128.3	0.401	$0.2373 \times 10^{-3}$	9.1

(over)



TABLE V. Reduced transition probabilities  $[B(EL)\dagger]$ .

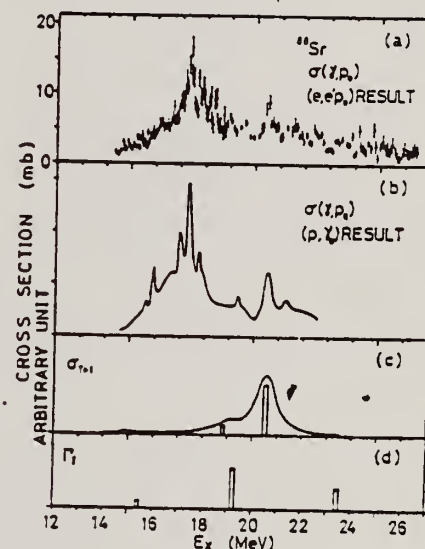
Nucleus	Level	$B(EL)\dagger$ (Tassie model)		Prediction of mixed model	
		$(e^2 \text{ fm}^{2L})$	Weisskopf units	$B(EL)\dagger$ for $^{89}\text{Y}$ $3^-$ transitions	Weisskopf units
$^{88}\text{Sr}$	$2^+, 1.84 \text{ MeV}$	$822.4 \pm 23.8$	$7.0 \pm 0.2$		
	$3^-, 2.74 \text{ MeV}$	$62\,034 \pm 4015$	$19.3 \pm 1.2$		
$^{89}\text{Y}$	$\frac{1}{2}^-, L=2$ 1.51 MeV	$130.7 \pm 17.57$	$1.1 \pm 0.1$		
	$\frac{3}{2}^-, L=2$ 1.74 MeV	$196.8 \pm 13.89$	$1.7 \pm 0.1$		
	$\frac{5}{2}^+, L=3$ 2.21 MeV	$25\,777 \pm 2251$	$7.8 \pm 0.7$	24 836	7.5
	$\frac{7}{2}^+, L=3$ 2.52 MeV	$36\,603 \pm 2818$	$11.1 \pm 0.9$	25 764	7.8
	$(\frac{5}{2}^+, \frac{1}{2}^+), L=3$ 2.86 MeV	$50\,536 \pm 5000$	$15.3 \pm 1.5$	30 160	9.2
	$(\frac{3}{2}^-, \frac{1}{2}^-), L=2$ 3.1 MeV	$144.6 \pm 11.66$	$1.2 \pm 0.1$		

REACTION	RESULT	EXCITATION ENERGY	SOURCE		DETECTOR		ANGLE
			TYPE	RANGE	TYPE	RANGE	
E, p	ABX	14- 26	D	14- 30	MAG-D		DST

TABLE 5

The radiative width of the narrow EI IAR obtained from the proton group in the proton spectra

Nucleus	$E_x$ (MeV)	$E_p$ (MeV)	$E_{x1}(J^\pi)$ (MeV)	$\Gamma_\gamma \frac{\Gamma_{p1}}{\Gamma}$ (eV)	$\Gamma_\gamma^{(2)}$ (eV)	$2(T+1) \frac{\Gamma_\gamma^{(2)}}{\Gamma_w}$	$2(T+1) \frac{\Gamma_\gamma^{(2)}}{\Gamma_{i.p.}}$	(p, $\gamma_0$ ) data $\Gamma_\gamma$ (eV)
$^{90}\text{Zr}$	14.5	6.0	0 ( $\frac{1}{2}^-$ )	26	26 <sup>b)</sup>	0.076		> 30 <sup>b)</sup>
	16.3	7.9	0 ( $\frac{1}{2}^-$ )	74	74 <sup>b)</sup>			
	16.3	6.3	1.51 ( $\frac{3}{2}^-$ )	52	126 <sup>c)</sup>	0.26		> 60 <sup>b)</sup>
$^{88}\text{Y}$	13.0 <sup>d)</sup>	5.9	0 ( $0^+$ )	13	13 <sup>b)</sup>		0.13 <sup>f)</sup>	13 $\pm$ 3 <sup>b)</sup>
	14.5 <sup>e)</sup>	7.3	0 ( $0^+$ )	16	16 <sup>b)</sup>		0.14 <sup>f)</sup>	11 $\pm$ 2 <sup>b)</sup>
	15.9 <sup>e)</sup>	8.7	0 ( $0^+$ )	42	42 <sup>b)</sup>		0.68 <sup>f)</sup>	40 $\pm$ 8 <sup>b)</sup>
$^{88}\text{Sr}$	17.1	6.5	0 ( $\frac{1}{2}^-$ )	9.5				
	17.1	5.6	0.85 ( $\frac{1}{2}^-$ )	4.9	14 <sup>e)</sup>	0.029		
	17.3	6.7	0 ( $\frac{1}{2}^-$ )	30				
	17.3	5.9	0.85 ( $\frac{1}{2}^-$ )	18	48 <sup>e)</sup>	0.094		

The available data with the (p,  $\gamma_0$ ) experiment are shown in the last column.<sup>a)</sup> The errors may be  $\approx 30\%$  (for  $^{90}\text{Zr}$ ,  $^{88}\text{Sr}$ ) and  $\approx 50\%$  (for  $^{88}\text{Y}$ ) including the uncertainty of the process to separate the proton group.<sup>b)</sup>  $\Gamma_{p0}/\Gamma = 1$  was assumed.<sup>c)</sup>  $(\Gamma_{p0} + \Gamma_{p1})/\Gamma = 1$  was assumed.<sup>d)</sup>  $J^\pi = \frac{1}{2}^+$  was assigned as shown in table 3.<sup>e)</sup>  $J^\pi = \frac{1}{2}^+$  was assigned as shown in table 3.<sup>f)</sup> Correction was made for the spectroscopic factors on the ground state and the excited state with the data of the (He<sup>3</sup>, d) and (d, p) reactions respectively.<sup>g)</sup> Ref. <sup>27</sup>).<sup>h)</sup> Ref. <sup>6</sup>).Fig. 13. Comparison of photoproton cross sections of  $^{88}\text{Sr}$ . (a) Present result. (b) Ref. <sup>5</sup>). (c), (d) Theoretical estimates, refs. <sup>11</sup>, <sup>15</sup>) respectively.

- <sup>5</sup> M. Hasinoff et al., Phys. Lett. 30B (1969) 337.
- <sup>6</sup> P. Paul, Proc. nuclear structure studies using electron scattering and photoreaction, ed. K. Shoda and H. Ui (Research report of Lab. Nucl. Sci. Tohoku Univ., vol. 5, 1972) p. 343.
- <sup>11</sup> B. Goulard et al., Phys. Rev. 176 (1968) 1345.
- <sup>15</sup> J.D. Vergados et al., Phys. Lett. 35B (1971) 93.
- <sup>27</sup> J.L. Black et al., Nucl. Phys. A92 (1967) 365.

(over)

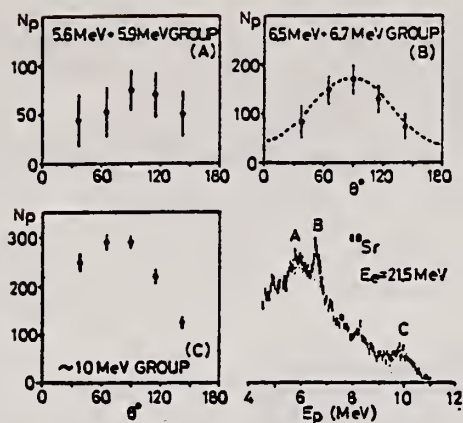


Fig. 16. Angular distributions of proton groups indicated by hatching in the proton spectrum which is summed over various angles. The result for group B is compared with that of the  $E_p = 7.9$  MeV group of  $^{90}\text{Zr}$  (dashed line).

REF. F. R. Metzger  
Phys. Rev. C11, 2085 (1975)

ELEM. SYM.	A	Z
Sr	88	38

METHOD

REF. NO.	
75 Me 5	hmg

REACTION	RESULT	EXCITATION ENERGY	SOURCE		DETECTOR		ANGLE
			TYPE	RANGE	TYPE	RANGE	
G,G	LFT	4	C	4	SCD-D		DST
		(4.744)		(4.944)			

$$\Gamma_0^2 / \Gamma = 95 \pm 20 \text{ meV}$$

$$4 = 4.744 \text{ MEV}$$

TABLE L. Comparison of the angular distribution results with theoretical predictions.

		$\frac{N_{\pi}(98^\circ)}{N_{\pi}(127^\circ)}$
EXPERIMENT	3487 1*	0.70 ± 0.05
	4743	0.75 ± 0.20
THEORY	Spin 1 (0-1-0)	0.75
	Spin 2 (0-2-0)	2.08

ELEM. SYM.	A	Z
Sr	88	38
REF. NO.		egf
75 Sh 4		

METHOD					REF. NO.		egf
					75 Sh 4		
REACTION	RESULT	EXCITATION ENERGY	SOURCE		DETECTOR		ANGLE
			TYPE	RANGE	TYPE	RANGE	
E.P	ABX	16- 26	D	14- 25	MAG-D		90
El virtual photon spectrum used to obtain ( $\gamma$ ,p) cross sections.							

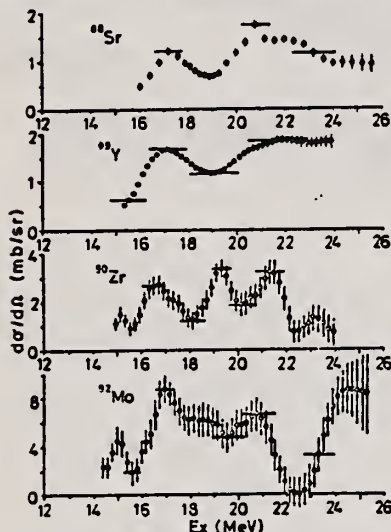


Fig. 3. Differential ( $\gamma$ , p) cross sections at  $\theta = 90^\circ$  analysed from (e, e'p) cross sections by the least structure method.

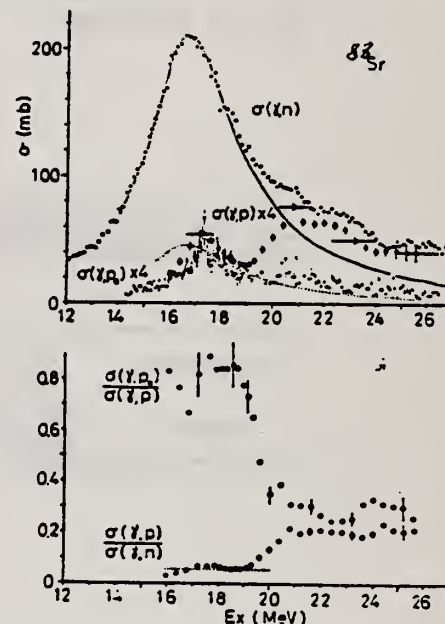


Fig. 5. Upper figure: open circles,  $\sigma(\gamma, p)$ ; closed circles,  $\sigma(\gamma, n)$  [ref. <sup>18</sup>]; closed points,  $\sigma(\gamma, p_0)$  [ref. <sup>18</sup>]; solid line, Lorentz line fit to the  $T_{<}$  region of  $\sigma(\gamma, n)$  [ref. <sup>18</sup>]; dotted line, Lorentz line fit to the  $T_{<}$  region of  $\sigma(\gamma, p)$  with  $\Gamma_1$  and  $E_n$  equal to those of  $\sigma(\gamma, n)$ . Lower figure: ratio between cross sections. Dotted line: constant for  $\sigma(\gamma, p)/\sigma(\gamma, n)$  determined around  $T_{<}$  GDR.

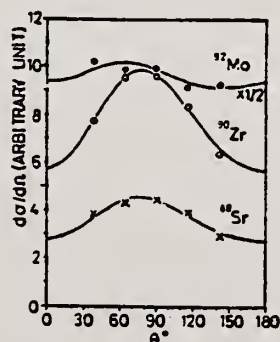


Fig. 4. Angular distributions of protons from the (e, e'p) reaction. The bombarding energies are 21.5, 22 and 20 MeV for  $^{88}\text{Sr}$ ,  $^{90}\text{Zr}$  and  $^{92}\text{Mo}$  respectively. The best fit curves obtained with eq. (7) are also shown.

15

K. Shoda et al., Nucl. Phys. A221 (1974) 125

18

A. Lepretre et al., Nucl. Phys. A175 (1971) 609

(over)



TABLE 2

The parameters of the angular distributions determined by the least-squares fits with  
 $d\sigma/d\Omega = A[1 + B\sin^2\theta(1 - p\cos\theta)]$

	<sup>88</sup> Sr	<sup>90</sup> Zr	<sup>92</sup> Mo
$E_0$ (MeV)	21.5	22	20
$A^*)$	1	2.04	6.67
$B$	0.59	0.69	0.057
$p$	0.59	0.47	2.3

\*) Relative value.

REF. F.R. Metzger  
Phys. Rev. C 15, 2253 (1977)

ELEM. SYM.	A	Z
Sr	88	38
REF. NO.		
77 Me 5		hmg

METHOD					
REACTION	RESULT	EXCITATION ENERGY	SOURCE		ANGLE
			TYPE	RANGE	
G,G	LFT	1	C	2-3	DST
				(2-2.31)	

[NUCLEAR REACTIONS  $^{88}\text{Sr}(\gamma, \gamma)$ , bremsstrahlung  $2.0 \leq E_\gamma \leq 2.31$  MeV; measured  $\sigma(96^\circ)$  and  $\sigma(126^\circ)$ , deduced  $\Gamma(1.836)$ . Natural target.]

$\Gamma = 1.836$  MeV

TABLE II. Summary of experimental values for the width of the 1.836-MeV  $2^+$  level in  $^{88}\text{Sr}$ .

Method	Ref.	1.836 (meV)
$(\gamma, \gamma)$ , $^{85}\text{Rb}$ source	6	$4.2 \pm 1.0$
Coulomb excitation	7	$6.7 \pm 3.0$
Coulomb excitation	9	$3.8 \pm 0.5$
$(e, e')$	5	$4.7 \pm 0.3$
$(e, e')$	8	$3.33 \pm 0.17$
$(e, e')$	10	$2.76 \pm 0.08$
$(\gamma, \gamma)$ , bremsstrahlung	This paper	$2.94 \pm 0.15$

REF. G. Isoyama, T. Ishimatsu, E. Tanaka, K. Kageyama, N. Kumagai  
Nuc1. Phys. A342, 124 (1980)

ELEM. SYM.	A	Z
Sr	88	38

METHOD

REF. NO.  
80 Is 1  
hg

REACTION	RESULT	EXCITATION ENERGY	SOURCE		DETECTOR		ANGLE
			TYPE	RANGE	TYPE	RANGE	
G,G	LFT	6-8	C	14	SCD-D		DST

Abstract: The resonant scattering of bremsstrahlung  $\gamma$ -rays by a  $\text{SrCO}_3$  target has been studied for  $\gamma$ -ray energies of 5-11 MeV. Six  $\gamma$ -transitions of energies between 6-8 MeV, which indicate six resonant states in  $^{88}\text{Sr}$ , were observed. The relative intensities of the resonantly scattered  $\gamma$ -rays at 125 and 150° were found to be compatible only with the assignment of spin 1 to the six states. Radiative widths of the resonant states were deduced. The possibility that these states are components of the giant M1 resonance in  $^{88}\text{Sr}$  is discussed.

### BML, SIX SPIN 1 STATES

E

NUCLEAR REACTIONS  $^{88}\text{Sr}(\gamma, \gamma)$ ,  $E = 14$  MeV bremsstrahlung; measured  $E_\gamma$ ,  $I_\gamma(\theta)$ .  
 $^{88}\text{Sr}$  deduced levels,  $J$ ,  $\Gamma_\gamma$ . Natural targets.

TABLE 2  
Summary of the experimental results

Level energy (MeV)	R	J	$\Gamma^a$ (eV)	$B(M1; 1^+ \rightarrow 0^+)^b$ ( $\mu_N^2$ )	$\Gamma_0^c$ (eV)
6.215	$1.45 \pm 0.29$	1	$1.81 \pm 0.22$	0.65	$3.0 \pm 0.4$
6.335	$1.37 \pm 0.20$	1	$2.83 \pm 0.29$	0.96	$4.5 \pm 0.6$
7.091	$1.39 \pm 0.19$	1	$4.14 \pm 0.45$	1.00	
7.537	$1.18 \pm 0.42$	1	$1.31 \pm 0.27$	0.26	
7.841	$1.50 \pm 0.41$	1	$2.53 \pm 0.45$	0.45	
8.047	$1.34 \pm 0.47$	1	$3.76 \pm 0.77$	0.62	

<sup>a</sup>) Deduced on the assumption of 100% ground-state decay.

<sup>b</sup>) Deduced on the assumption of positive parity.

<sup>c</sup>) Ref. <sup>a</sup>).

REF. K. Wienhard, C. Bläsing, K. Ackermann, K. Bangert, U.E.P. Berg,  
K. Kobras, W. Naatz, D. Rück, R.K.M. Schneider, R. Stock  
Z. Phys. A302, 185 (1981)

ELEM. SYM.	A	Z
Sr	88	38
REF. NO.		
81 Wi 1		hg

METHOD			SOURCE		DETECTOR		ANGLE
REACTION	RESULT	EXCITATION ENERGY	TYPE	RANGE	TYPE	RANGE	
\$ G,G	NOX	6-8	C	UKN	SCD-D		90

Abstract. The unknown parities of five strong dipole states between 6 and 8 MeV in  $^{88}\text{Sr}$  are shown to be negative.

# POL INCOMING PHOTONS

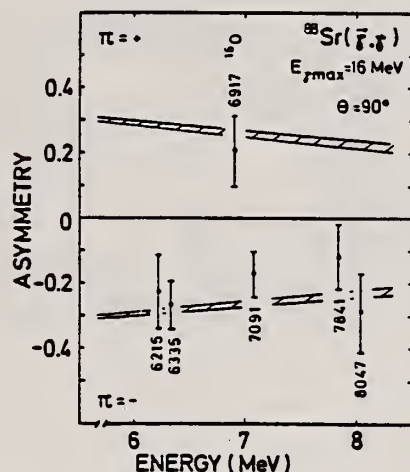


Fig. 1. Observed asymmetries for five ground state dipole transitions in  $^{88}\text{Sr}$  and for the  $2^+$  transition at 6917 keV in  $^{16}\text{O}$ . The energies for the  $^{88}\text{Sr}$  states were taken from /2/. The hatched band represents the expected asymmetry for states with positive parity (upper part) and negative parity (lower part)

SR  
A=29

SR  
A=89

SR  
A=89





REF. A. Likar, A. Lindholm, L. Nilsson, I. Bergqvist and  
B. Palsson  
Nucl. Phys. A298, 217 (1978)

ELEM. SYM.	A	Z
Sr	89	38

METHOD

REF. NO.

78 Li 2

rs

REACTION	RESULT	EXCITATION ENERGY	SOURCE		DETECTOR		ANGLE
			TYPE	RANGE	TYPE	RANGE	
N,G	RLX	13- 17	D	7- 11	NAI-D		DST

**Abstract:** Gamma-ray spectra from neutron capture in natural samples of strontium and yttrium have been recorded at various angles with respect to the direction of the incident neutron flux. Angular yields have been observed at six neutron energies in the range 7 to 11 MeV using time-of-flight techniques to improve the signal-to-background ratio. The  $\gamma$ -radiation was detected by a large NaI(Tl) crystal placed in a heavy radiation shield. Certain combinations of Legendre polynomial coefficients were extracted for transitions to low-lying single-particle states ( $2d_{5/2}$  and  $3s_{1/2}$ ) in the final nuclei. The energy dependence of the angular distribution coefficients indicates interference between the electric dipole amplitude and amplitudes of opposite parity. The results are compared with theoretical calculations based on the direct-semidirect model.

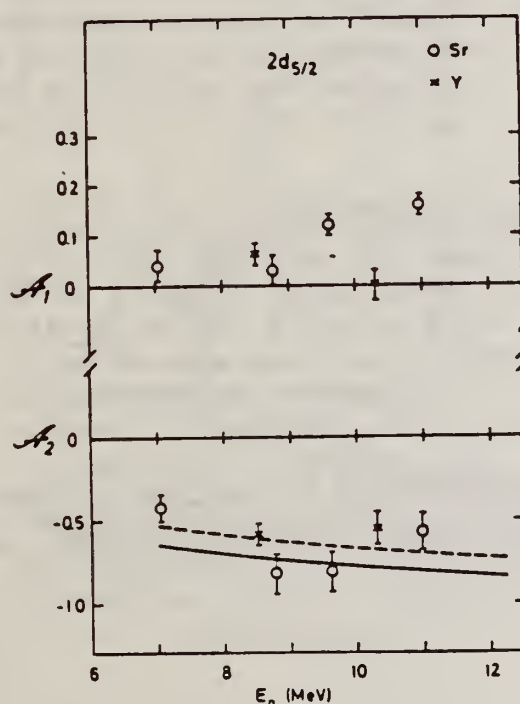


Fig. 2. Angular distribution coefficients  $A_1$  and  $A_2$  versus neutron energy for the reactions  $^{89}\text{Sr}(n, \gamma_0)^{90}\text{Sr}$  (open circles) and  $^{89}\text{Y}(n, \gamma_0 + \gamma_1)^{90}\text{Y}$  (crosses). The curves for the  $A_2$  coefficient represent the results of theoretical calculations for E1 transitions to the  $2d_{5/2}$  state in  $^{89}\text{Sr}$  from the direct (solid line) and DSD (dashed line) capture models.

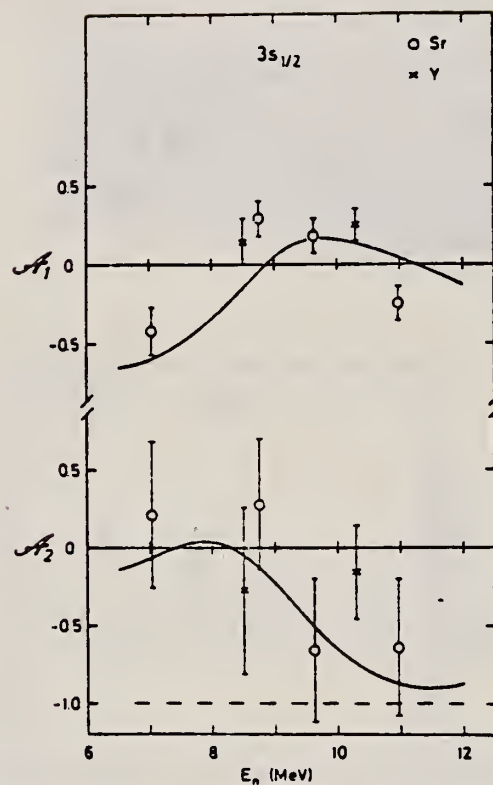


Fig. 3. Angular distribution coefficients  $A_1$  and  $A_2$  versus neutron energy for  $\gamma$ -rays to the  $3s_{1/2}$  states from the reactions  $^{88}\text{Sr}(n, \gamma)^{88}\text{Sr}$  (open circles) and  $^{89}\text{Y}(n, \gamma)^{89}\text{Y}$  (crosses). The theoretical result for DSD model calculations are shown as dashed curve for pure E1 transitions and as solid curves assuming E1 and E2 transitions associated with collective excitation of the GDR and the isoscalar GQR.

YTTRIUM  
Z=39

*"The rare earths perplex us in our researches, baffle us in our speculations, and haunt us in our very dreams. They stretch like an unknown sea before us, mocking, mystifying, and murmuring strange revelations and possibilities."(1)*

Yttrium was discovered in 1794 by the Scandinavian chemist Johan Gadolin (1760-1852) and was named after the small town of Ytterby, Sweden where the ore was found. It always occurs with the other rare earth elements and is very similiar to them in both chemical and metalurgical respects. In 1848 Carl Gustav Mosander (1797-1858) showed that yttria from which all the ceria, lanthana, and didymia had been removed contains at least three other rare earths. These are: a colorless oxide, for which he kept the name yttria; a yellow earth erbia, and a rose colored ore, terbia. These were all seperated by fractional precipitation with ammonium hydroxide.

Y  
A=89

(1) Quotation from Sir William Crookes.

Y  
A=89





Elem. Sym.	A	Z
Y	89	39
Ref. No.		
56 Ye 2		
EGF		

Method 24 MeV betatron; 250 r Victoreen in 3.75 cm Lucite; neutron detector

Reaction	E or ΔE	E <sub>0</sub>	Γ	∫σdE	Jπ	Notes
Y <sup>89</sup> (γ,xn)	Bremss 24	16.3	3.8 MeV	$\int_0^{23} = 0.87 \text{ MeV-b}$		

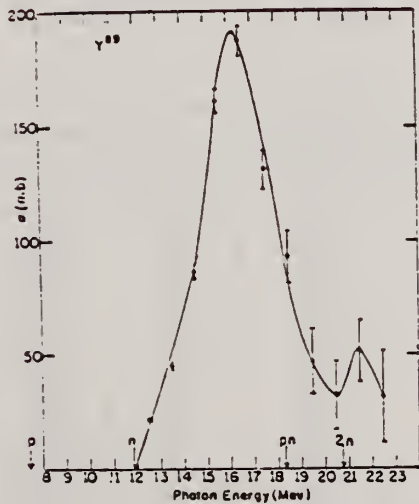


FIG. 1. Cross section for the (γ,n) reaction in Y<sup>89</sup>, calculated from the yield data, at an intermediate stage of the smoothing process (see text). The vertical lines through the calculated points show the rms uncertainty in the cross-section values, produced by the statistical uncertainty of the recorded counts of the raw yield data. Other sources of errors, and the partial smoothing already done have been ignored in calculating these uncertainties. The arrows along the abscissa indicate the thresholds for emission of the particles indicated by the labels therewith. The units of the ordinate are 10<sup>-27</sup> cm<sup>2</sup>.

TABLE III. Parameters of giant-resonance cross-section curves for (γ,n) reactions in nuclei near 50 neutrons. Nuclides <sup>42</sup>As<sup>75</sup>, <sup>44</sup>Ni<sup>72</sup>, and <sup>45</sup>Rh<sup>103</sup> from reference 4, <sup>46</sup>Zr<sup>92</sup> and <sup>48</sup>Zr<sup>94</sup> from reference 5 recomputed in present work. Neutron number is shown in column 2, location of peak cross-section value in column 3, peak cross-section value in column 4, half-height width of curve in column 5, and area under curve from threshold to 23 Mev in column 6.

Nuclide	N	E <sub>m</sub> (Mev)	σ <sub>m</sub> (millibarns)	Γ (Mev)	∫ <sub>0</sub> <sup>23</sup> σdE (Mev-barns)
<sup>42</sup> As <sup>75</sup>	42	17.3	90.3	9.0	0.80
<sup>44</sup> Ni <sup>72</sup>	43	15.9	160	5.0	0.92
<sup>45</sup> Rh <sup>103</sup>	49	15.8	146	5.3	1.00
<sup>46</sup> Zr <sup>92</sup>	50	16.3	201	4.0	1.05
<sup>48</sup> Zr <sup>94</sup>	50	16.3	191	3.8	0.87
<sup>49</sup> Ti <sup>90</sup>	50	15.8	199	4.3	0.98
<sup>50</sup> Cr <sup>92</sup>	51	16.5	200	5.0	1.22
<sup>51</sup> Cr <sup>94</sup>	52	16.9	193	5.5	1.24
<sup>52</sup> Nb <sup>93</sup>	52	17.0	195	6.8	1.46
<sup>53</sup> Rh <sup>105</sup>	58	16.5	205	8.9	1.94

G. Chidley, L. Katz, S. Kowalski  
 Can. J. Phys. 36, 407 (1958)

ELEM. SYM.	A	Z
Y	89	39

Betatron					REF. NO.	
					58 Ch 2	NVB
REACTION	RESULT	EXCITATION ENERGY	SOURCE		DETECTOR	
			TYPE	RANGE	TYPE	RANGE
G,N	RLY	THR	C	THR	BF3-I	4PI

See 58 Ka 1 for cross sections;

TABLE I

THRESHOLD

MEASURED PHOTONEUTRON THRESHOLDS

Reaction	Measured Q value, Mev.	Other Q values, Mev.	Method	Reference
$Y^{88}(\gamma, n)Y^{87}$	$11.82 \pm 0.05$			
		$11.76 \pm 0.15$	Mass data	Duckworth (unpublished)
			Q* value	Way <i>et al.</i> (1955)
		$11.80 \pm 0.33$	Mass data	Wapstra (1955)

NVB

U.S. DEPARTMENT OF COMMERCE  
NATIONAL BUREAU OF STANDARDS

Method      Betatron; photon difference analysis

Ref. No. 58 Si 1

EH

Reaction	E or $\Delta E$	$E_0$	$\Gamma$	$\int \sigma dE$	$J\pi$	Notes
$(\gamma, \gamma')$	4-22	10.5 16				

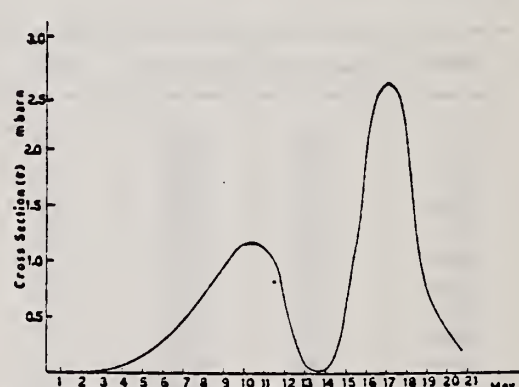


FIG. 2. Cross section as a function of energy for formation of the isomeric state of  $Y^{40}$ .

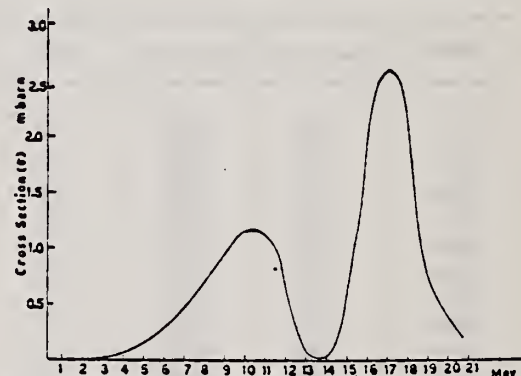


FIG. 2. Cross section as a function of energy for formation of the isomeric state of  $Y^{80}$ .



METHOD

Betatron; neutron threshold; ion chamber

REF. NO.

60 Ge 3

NVB

REACTION	RESULT	EXCITATION ENERGY	SOURCE		DETECTOR		ANGLE
			TYPE	RANGE	TYPE	RANGE	
G,N	NØX	THR	C	THR	BF3-I		4 PI

THRESHOLD

TABLE I. Summary and comparison of neutron separation energies inferred from present threshold measurements with values predicted from mass data and reaction energies. All energies are expressed in the center-of-mass system in Mev.

Reaction	No. runs	Present results	Other results	Method	Reference
$Y^{90}(\gamma,n)Y^{89}$	3	$\leq 11.59 \pm 0.08$	$11.53 \pm 0.40$ $11.82 \pm 0.05$	mass data $Q(\beta^+)$ threshold	m n f

\* Henry E. Duckworth, *Mass Spectroscopy* (Cambridge University Press, New York, 1958), p. 177.  
\* L. J. Lidofsky, *Revs. Modern Phys.* 29, 773 (1957).

TABLE II. Comparison of measured threshold energies with neutron binding energies predicted by mass data for transitions with  $\Delta I \geq 7/2$ . All energies in Mev.

Reaction	$\Delta I^a$	Observed threshold	Mass data $Q$ value	$E_{th} - Q$	Excited state energy
$Cr^{52}(\gamma,n)Cr^{51}$	7/2	$12.18 \pm 0.14$	$12.053 \pm 0.004^b$	$0.13 \pm 0.14$	...
$Y^{90}(\gamma,n)Y^{89}$	7/2	$11.59 \pm 0.08$	$11.53 \pm 0.40^c$	$0.06 \pm 0.41$	$0.387^d$
$In^{115}(\gamma,n)In^{114}$	7/2	$9.22 \pm 0.03$	$9.35 \pm 0.43^e$	$-0.13 \pm 0.43$	$0.191^a$
$Ce^{140}(\gamma,n)Ce^{139}$	(7/2) <sup>e</sup>	$7.24 \pm 0.07$	$6.97 \pm 0.07^f$	$0.27 \pm 0.10$	...
$Nd^{144}(\gamma,n)Nd^{143}$	7/2	$6.38 \pm 0.16$	$5.97 \pm 0.19^f$	$0.41 \pm 0.25$	$0.690^a$
$Sm^{147}(\gamma,n)Sm^{146}$	7/2	$6.45 \pm 0.16$	$5.87 \pm 0.28^f$	$0.58 \pm 0.33$	$0.562^a$
$Er^{167}(\gamma,n)Er^{166}$	7/2	$6.65 \pm 0.08$	$6.45 \pm 0.06^g$	$0.20 \pm 0.10$	$0.081^a$
$Hf^{177}(\gamma,n)Hf^{176}$	7/2	$6.69 \pm 0.03$	$6.28 \pm 0.06^g$	$0.64 \pm 0.07$	$0.088^a$
$Hf^{178}(\gamma,n)Hf^{177}$	9/2	$6.31 \pm 0.07$	$6.17 \pm 0.06^g$	$0.14 \pm 0.09$	$0.093^a$
$Hf^{179}(\gamma,n)Hf^{178}$	9/2	$7.85 \pm 0.11$	$7.32 \pm 0.06^g$	$0.53 \pm 0.13$	$0.375^a$

<sup>a</sup> D. Strominger, J. M. Hollander, and G. T. Seaborg, *Revs. Modern Phys.* 30, 585 (1958).

<sup>b</sup> C. F. Giese and J. L. Benson, *Phys. Rev.* 110, 712 (1958).

<sup>c</sup> Henry E. Duckworth, *Mass Spectroscopy* (Cambridge University Press, New York, 1958), p. 177.

<sup>d</sup> D. E. G. Peck, Atomic Energy of Canada Limited Report Tr. AECL-457 (unpublished).

<sup>e</sup> The discrepancy in the case of  $Ce^{140}$  predicts a ground-state spin for  $Ce^{140}$  of 0, since the spin of  $Ce^{141}$  is known to be 7/2.

<sup>f</sup> W. H. Johnson, Jr., and A. O. Nier, *Phys. Rev.* 103, 1014 (1957).

<sup>g</sup> W. H. Johnson, Jr., and V. B. Bhanot, *Phys. Rev.* 107, 6 (1957).



METHOD					REF. NO.		
Betatron; fast neutron yield, angular distribution; Si threshold detector; ion chamber					61 Ba 2		
					NVB		
REACTION	RESULT	EXCITATION ENERGY	SOURCE		DETECTOR		ANGLE
			TYPE	RANGE	TYPE	RANGE	
G,XN	ABY	THR-22	C	22	THR-I	5-+	DST

In Table 4:

$\bar{\sigma}$  = average cross section of detector weighted with neutron spectrum

$\bar{n}$  = neutrons/100 roentgen/mole

$$W(\theta) = a_0 \sum_{n=1}^{\infty} [1 + A_n P_n(\cos \theta)]$$

TABLE IV

I Element	II $a_0$	III $a_1$	IV $a_2$	V $(\bar{\sigma}\bar{n}) \times 10^{10}$	VI $\Phi_{total}(22 \text{ Mev}) \times 10^9$	VII $\Phi_{fast}/\Phi_{total}$
Vanadium	245 (1±0.05)	0.01±0.08	-0.90±0.10	9.05	0.21	0.12
Chromium	164 (1±0.03)	0.04±0.04	-0.05±0.05	4.03	0.17	0.16
Manganese	308 (1±0.02)	0.07±0.03	-0.09±0.04	7.61	0.25	0.12
Iron	200 (1±0.03)	0.05±0.04	-0.17±0.05	4.94	0.18	0.11
Cobalt	390 (1±0.02)	0.08±0.03	-0.22±0.04	9.63	0.26	0.15
Nickel	145 (1±0.05)	0.07±0.07	-0.23±0.09	3.58	0.12	0.12
Copper	347 (1±0.02)	0.08±0.03	-0.29±0.04	8.57	0.30	0.12
Arsenic	482 (1±0.03)	0.11±0.04	-0.24±0.05	11.91	0.33	0.15
Rubidium	638 (1±0.05)	0.12±0.06	-0.14±0.08	15.76		
Strontium	409 (1±0.05)	0.10±0.06	-0.17±0.08	10.10		
Yttrium	290 (1±0.10)	0.08±0.12	-0.12±0.15	7.16		
Silver	590 (1±0.04)	0.10±0.06	-0.22±0.08	14.57	0.57	0.07
Cadmium	905 (1±0.02)	0.02±0.02	-0.26±0.03	22.35		
Iodine	1133 (1±0.03)	0.04±0.04	-0.29±0.05	27.99	1.42	0.08
Barium	1048 (1±0.04)	0.10±0.06	-0.38±0.08	25.89		
Lanthanum	1595 (1±0.02)	0.02±0.03	-0.32±0.04	39.40	1.04	0.15
Cerium	1216 (1±0.05)	0.05±0.06	-0.39±0.08	32.50		
Dysprosium	7052 (1±0.03)	0.04±0.10	-0.34±0.13	40.80		
Terbium	1558 (1±0.02)	0.04±0.03	-0.22±0.04	38.48	2.50	0.06
Dysprosium	1365 (1±0.02)	0.07±0.03	-0.24±0.04	33.71		
Mercury	1345 (1±0.02)	0.04±0.03	-0.31±0.04	33.22		
Lead	2274 (1±0.01)	0.02±0.02	-0.42±0.03	56.17	2.72	0.03
Bismuth	2162 (1±0.02)	0.05±0.03	-0.45±0.04	53.40	3.36	0.06
Thorium	3031 (1±0.04)	0.00±0.05	-0.32±0.07	74.87		
Uranium	4630 (1±0.02)	0.05±0.03	-0.17±0.04	114.36		

\* $(\bar{\sigma}\bar{n}) = 2.47 \times 10^9$  cc millibarns-neutron. Errors are standard errors due to counting statistics only.

Method 55 MeV betatron; synchrotron; Si<sup>28</sup>(n,p)Al<sup>28</sup> activity; Cu<sup>63</sup>(γ,n)Cu<sup>62</sup> monitor.

Ref. No.	EGF
62 Re 1	

Reaction	E or ΔE	E <sub>0</sub>	Γ	∫σdE	Jπ	Notes
Y <sup>89</sup> (γ,n)	Bremss. 55					Figure 11: Dotted curve is of form $a_0 + a_1 \cos \theta + a_2 \cos^2 \theta + a_2 \cos^2 \theta - a_1 \cos^2 \theta$ ; solid curve is of form $a_0 + a_1 \cos \theta + a_2 \cos^2 \theta$ ; errors on points are statistical errors in counting only.

TABLE 2

Parameters of the fit (1) for the expressions  $a_0 + a_1 \cos \theta + a_2 \cos^2 \theta$ ,  $a + b \sin^2 \theta + c \cos \theta$  and  $A_0 + A_1 P_1 + A_2 P_2$

	Bi(1)	Bi(2)	Pr	Au	Y	Ho	La
$a_0$	1.00 ± 0.02	1.00 ± 0.02	1.00 ± 0.02	1.00 ± 0.02	1.00 ± 0.03	1.00 ± 0.02	1.00 ± 0.01
$a_1$	0.15 ± 0.03	0.18 ± 0.04	0.17 ± 0.04	0.14 ± 0.03	0.17 ± 0.06	0.12 ± 0.03	0.14 ± 0.03
$-a_2$	0.47 ± 0.08	0.40 ± 0.08	0.41 ± 0.09	0.21 ± 0.07	0.15 ± 0.11	0.34 ± 0.06	0.39 ± 0.06
$A_1^*)$	0.18 ± 0.04	0.21 ± 0.05	0.20 ± 0.05	0.15 ± 0.04	0.18 ± 0.06	0.14 ± 0.04	0.10 ± 0.03
$-A_2^*)$	0.37 ± 0.05	0.31 ± 0.06	0.32 ± 0.07	0.15 ± 0.05	0.11 ± 0.08	0.26 ± 0.05	0.30 ± 0.04
$a$	0.53 ± 0.06	0.60 ± 0.08	0.59 ± 0.09	0.79 ± 0.07	0.85 ± 0.11	0.66 ± 0.06	0.61 ± 0.06
$b$	0.47 ± 0.06	0.40 ± 0.08	0.41 ± 0.09	0.21 ± 0.07	0.15 ± 0.11	0.34 ± 0.06	0.39 ± 0.06
$c$	0.15 ± 0.03	0.18 ± 0.04	0.17 ± 0.04	0.14 ± 0.03	0.17 ± 0.06	0.12 ± 0.03	0.14 ± 0.03

\*) Renormalized so that  $A_0 = 1$

TABLE 4

Parameters of the fit (3) for the expressions  $a_0 + a_1 \cos \theta + a_2 \cos^2 \theta - a_3 \cos^3 \theta$ ,  $1 - A_1 P_1 - A_2 P_2 - A_3 P_3$

	Bi(1)	Bi(2)	Pr	Au	Y	Ho	La
$a_0$	1.01 ± 0.02	1.00 ± 0.02	1.01 ± 0.03	0.98 ± 0.02	1.00 ± 0.03	1.00 ± 0.02	1.01 ± 0.02
$a_1$	0.19 ± 0.05	0.17 ± 0.07	0.21 ± 0.07	0.07 ± 0.06	0.16 ± 0.09	0.12 ± 0.05	0.17 ± 0.05
$-a_2$	0.56 ± 0.11	0.37 ± 0.15	0.50 ± 0.16	0.05 ± 0.12	0.13 ± 0.20	0.33 ± 0.12	0.47 ± 0.11
$a_3$	-0.17 ± 0.18	0.05 ± 0.24	-0.17 ± 0.25	0.31 ± 0.19	0.05 ± 0.32	0.03 ± 0.19	-0.17 ± 0.17
$A_1^*)$	0.11 ± 0.15	0.23 ± 0.18	0.13 ± 0.20	0.27 ± 0.13	0.20 ± 0.22	0.15 ± 0.14	0.09 ± 0.13
$-A_2^*)$	0.45 ± 0.09	0.28 ± 0.11	0.39 ± 0.12	0.03 ± 0.08	0.09 ± 0.14	0.24 ± 0.09	0.37 ± 0.09
$A_3^*)$	-0.08 ± 0.09	0.02 ± 0.11	-0.08 ± 0.12	0.13 ± 0.08	0.02 ± 0.13	0.01 ± 0.08	-0.08 ± 0.08

\*) Renormalized so that  $A_0 = 1$

Method Betatron; neutron yield;  $4\pi$  neutron

Ref. No.	JHH
63 Ge 1	

Reaction	E or $\Delta E$	$E_0$	$\Gamma$	$\int \sigma dE$	$J\pi$	Notes
$Y^{89}(\gamma, n)$	Bremss. ~11~12					$E_{(\gamma, n)th}$ to ground state of $Y^{88} = 11.54 \pm 0.04$ MeV

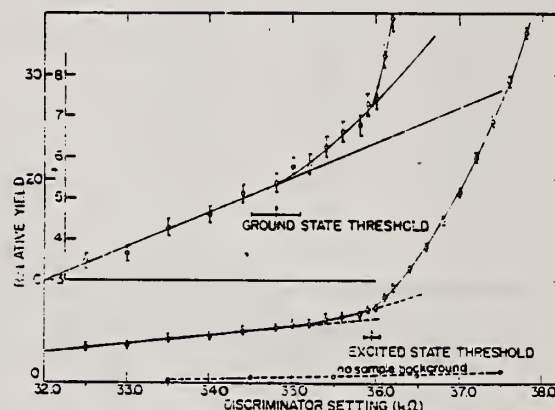


Fig. 1. The  $Y^{89}(\gamma, n)$  yield curve in the vicinity of threshold.

TABLE I  
Summary of experimental threshold observation for  $Y^{89}(\gamma, n)$

Threshold observed	Threshold energy (MeV)
Ground state	$11.55 \pm 0.10$
Excited state	$11.947 \pm 0.039$
Ground state (computed) <sup>a</sup>	$11.554 \pm 0.039$
Ground state, corrected for extrapolation error <sup>b</sup>	$11.539 \pm 0.039$

- a) Ground state threshold obtained by combining energy of excited state (393 keV) with observed excited state threshold.  
b) An extrapolation error of 15 keV exists in the  $(\gamma, n)$  threshold determination when the energy calibration is based on a resonance observation (see text).



METHOD

Linac; isomer yield; activity

REF. NO.

63 Ka 2

NVB

REACTION	RESULT	EXCITATION ENERGY	SOURCE		DETECTOR		ANGLE
			TYPE	RANGE	TYPE	RANGE	
G,G/	RLY	1	C5		ACT-I		4PI
		(0.92)					

Table II. The isomers observed

Isomer	Observed value		Referenced value <sup>(1)(2)(3)</sup>	
	Half-life	Energy (MeV)	Half-life	Energy (MeV)
Se-77m	17.5 sec	0.160	17.5 sec	0.161
Br-79m	4.80 sec	0.209	4.8 sec	0.208
Sr-87m	2.3 hr	0.390	2.8 hr	0.338
Y-89m	15.0 sec	0.920	14 sec	0.915
Rh-103m	58 min	*	57 min	0.040
Ag-107m	42 sec	0.95	44 sec	0.094
Ag-109m			40 sec	0.088
Cd-111m	47 min	0.150,0.255	49 min	0.150,0.247
In-115m	4.5 hr	0.335	4.5 hr	0.335
Sn-117m	17 day	0.160	14 day	0.159,0.161
Ba-137m	2.6 min	0.660	2.6 min	0.662
Er-167m	2:10 sec	0.209	2.5 sec	0.208
Hf-179m	18.5 sec	0.157,0.215	19 sec	0.161,0.217
W-183m	5.4 sec	0.200,0.170,0.115	5.5 sec	0.1025,0.2915 others
Ir-191m	4.90 sac	0.129, <0.07	4.9 sec	0.042-0.129
Pt-195m	4.5 day	0.065**	4.1 day	0.031-0.130
Au-197m	7.0 sec	0.10,0.27,0.40	7.2 sec	0.130,0.270,0.407
Hg-199m	43 min	0.160,0.370	42 min	0.158,0.368

\* This isomer was measured with a G-M flow counter.

\*\* This value corresponds to Pt-K X-ray energy.

Table III. Induced activation rate

Element	Beam energy (MeV)	Counting rate ( $\times 10000$ cpm)	Sample form
Se	5	1300	metallic pellet
Br	4	1600	NaBr grain
Sr	6	0.3	SrCO <sub>3</sub> powder
Y	5	90	metallic grain
Rh	5	(0.2)*	RhCl <sub>3</sub> grain
Ag	5	180	metallic plate
Cd	6	0.5	CdCl <sub>2</sub> grain
In	6	8	metallic plate
Sn	6	0.0005	metallic plate
Ba	5	0.6	BaS powder
Er	4	4900	Er <sub>2</sub> O <sub>3</sub> powder
Hf	5	1600	metallic plate
W	5	120	metallic powder
Ir	5	2100	metallic powder
Pt	5	0.3	metallic plate
Au	4	4300	metallic plate
Hg	6	0.09	metallic liquid

\* The value measured with a G-M flow counter.

REF.			ELEM. SYM.			A	Z
A. Veres Acta Phys. Acad. Sci.Hung. <u>16</u> , 261-73 (1963)			Y			89	39
METHOD			REF. NO.				
Radioactive source			63 Ve 2			NVB	
REACTION	RESULT	EXCITATION ENERGY	SOURCE		DETECTOR		ANGLE
			TYPE	RANGE	TYPE	RANGE	
G,G/	ABX	0-1	D	0-1	NAI-D		

ISOMERS

Таблица II  
Измеренные значения после облучения, сравниваемые с другими литературными данными

Элемент	Активность облучения после первого измерения (имп/мин.)	Активн. экстрп. в конце облуч. (имп/мин.)	Литературные данные		Данные измерений		отн (10 <sup>-12</sup> см <sup>2</sup> )	Г <sub>уп</sub> (10 <sup>-12</sup> см <sup>2</sup> )
			T <sub>1/2</sub>	E (кэв)	T <sub>1/2</sub>	E (кэв)		
Se-77m	3842±96	5400	17,5 сек.	160	18,1±1 сек.	160±10	9,5	1,75
Sr-87m	191±5	200	2,8 ч.	390	2,9±0,1 ч.	365±25	0,85	0,2
Y-89m	96±20	170	16 сек.	910	16,7±5 сек.		0,08	0,02
Rh-103m	28±5	31	57 мин.	40	58±2 мин.	20,5±0,5	0,08	0,01
Ag-107m	220±14	250	44 сек.	93	43,8±0,6 сек.	91±10	0,8	0,2
Ag-109m			39 сек.	88				
Hf-179m	80±18	155	19 сек.	160; 215	19±2 сек.		1	0,2
Ir-191m	90±20	250	4,9 сек.	42; 130	5±2 сек.		5,6	1
Pt-195m	90±9	100	3,5 д.	31; 100; 130;	3,5±0,2 д.	32±3 67,5±5 96±5 130±10	0,2	0,04
Au-197m	240±16	520	7,2 сек.	130; 277; 407	7,2±1 сек.	68:130: 280±20 390±20	0,07	0,01
Hg-199m	9,6±3,2		42 мин.	160; 370			0,005	0,001

Acta Phys. Hung. Tom. XVI. Fasc. 3.



REF. S. C. Fultz, R. L. Bramblett, B. L. Berman, J. T. Caldwell,  
and M. A. Kelly  
Proc. Gatlinburg Conference 397 (1966)

ELEM. SYM.	A	Z
Y	89	39

METHOD

REF. NO.

66 Fu 2

hmg

REACTION	RESULT	EXCITATION ENERGY	SOURCE		DETECTOR		ANGLE
			TYPE	RANGE	TYPE	RANGE	
G,XN	ABI	THR-28	D	THR-28	BF3-I		4PI
G,2N	ABI	THR-28	D	THR-28	BF3-I		4PI

TABLE I

Integrated Cross Sections for Zirconium and Yttrium

Isotope	$E_{max}$ $a = \int \sigma_{tot} dE$ (MeV - barns)	$E_{max}$ $b = \int \sigma_{2n} dE$ (MeV - barns)	b/a	$E_{max}$ (MeV)
<sup>90</sup> Zr	0.980	0.108	0.110	28
<sup>91</sup> Zr	1.078	0.202	0.187	30
<sup>92</sup> Zr	1.096	0.447	0.408	28
<sup>94</sup> Zr	1.041	0.577	0.554	30
<sup>89</sup> Y	0.991	0.095	0.096	28

REF.

REF.

W. B. Walters and J. P. Hummel  
Phys. Rev. 150, 867 (1966)

ELEM. SYM.	A	Z
Y	89	39

METHOD

Betatron

REF. NO.

66 Wa 1

JDM

REACTION	RESULT	EXCITATION ENERGY	SOURCE		DETECTOR		ANGLE
			TYPE	RANGE	TYPE	RANGE	
G, 2N	RLY	THR-280	C	150, 280	ACT-I		4PI

Measured isomeric yield ratios.

TABLE IV. Summary of the results for the photoproduction of the  $Y^{87}$  isomers (spins  $\frac{1}{2}$  and  $\frac{3}{2}$ ).

Target isotope and spin	Bremsstrahlung energy (MeV)	Fraction of yield to high-spin isomer
$Y^{88}$ ( $I = \frac{1}{2}$ )	150	$0.42 \pm 0.03$
	280	$0.42 \pm 0.03$
$Nb^{93}$ ( $I = \frac{3}{2}$ )	150	$0.71 \pm 0.13$
	280	$0.69 \pm 0.13$

REF. B.L. Berman, J.T. Caldwell, R.R. Harvey, M.A. Kelly, R.L. Bramblett,  
and S.C. Fultz  
Phys. Rev. 162, 1098 (1967)

ELEM. SYM.	A	Z
Y	89	39
REF. NO.		hmg
67 Be 2		

METHOD

REACTION	RESULT	EXCITATION ENERGY	SOURCE		DETECTOR		ANGLE
			TYPE	RANGE	TYPE	RANGE	
G,N 1	ABX	THR-28	D	THR-28	BF3-I		4PI
G,2N 2+	ABX	THR-28	D	THR-28	BF3-I		4PI

TABLE IV. Integrated cross sections.

Nucleus	$\sigma_{\text{int}}[(\gamma,n) + (\gamma,pn)]$ (MeV-b) <sup>a</sup>	$-\sigma_{\text{int}}(\gamma,2n)$ (MeV-b) <sup>a</sup>	$E_{\gamma\text{max}}$ (MeV)	$\frac{\sigma_{\text{int}}(\gamma,2n)}{\sigma_{\text{int}}(\gamma, \text{total})^b}$	$(\frac{1}{2}\pi)\sigma_m\Gamma$ (MeV-b)	$0.06NZ/A$ (MeV-b)
Y <sup>89</sup>	0.94	0.10	28	0.10	1.14	1.31
Zr <sup>90</sup>	0.96	0.10	28	0.09	1.16	1.33
Zr <sup>91</sup>	0.88	0.20	30	0.19	1.22	1.35
Zr <sup>92</sup>	0.65	0.45	28	0.41	1.23	1.36
Zr <sup>94</sup>	0.43	0.58	30	0.56 <sup>c</sup>	1.32	1.38

<sup>a</sup> All measured integrated cross-section values are given for an energy region from threshold to  $E_{\gamma\text{max}}$ . For the Zr<sup>91</sup> and Zr<sup>92</sup> cases, it was necessary to extrapolate the low-energy part of the total photoneutron cross section down to threshold; the error introduced in this process, however, is less than 0.5%.  
<sup>b</sup> The word "total" in this table refers to the total photoneutron cross section  $\sigma[(\gamma,n) + (\gamma,pn) + (\gamma,2n) + (\gamma,3n)]$ , and excludes the  $(\gamma,\gamma)$  and  $(\gamma,p)$  cross sections.  
<sup>c</sup> This value includes the contribution of  $\sigma_{\text{int}}(\gamma,3n)$ , which equals 0.03 MeV-b from threshold to 30 MeV.

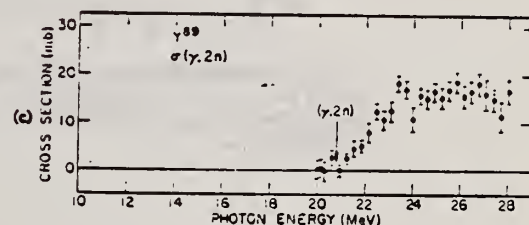
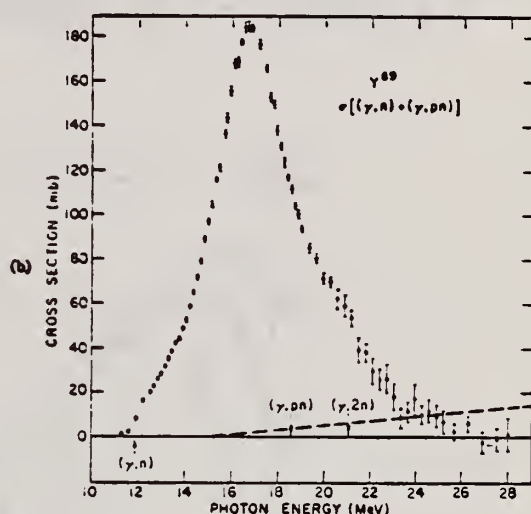
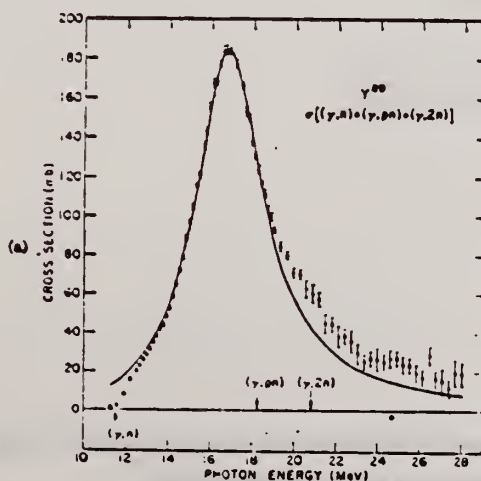


FIG. 8 (a) Total photoneutron cross section  $\sigma[(\gamma,n) + (\gamma,pn) + (\gamma,2n)]$  for Y<sup>89</sup>. The solid curve is a Lorentz-line fit to the giant-resonance data (14 to 19 MeV). The thresholds (arrows), except when otherwise noted, are from Ref. 10. In this case, the  $(\gamma,2n)$  threshold is taken from the data. (b) Single photoneutron cross section  $\sigma[(\gamma,n) + (\gamma,pn)]$  for Y<sup>89</sup>. The dashed line represents the maximum possible systematic error owing to the uncertainty in the normalization constant for the bremsstrahlung subtraction (see text). (c) The  $(\gamma,2n)$  cross section for Y<sup>89</sup>. The threshold determination of  $20.8 \pm 0.1$  MeV determines the mass of Y<sup>87</sup> (see text). The threshold value is taken from the data. The cross-section scale has been doubled for clarity.

REF. N. G. Shevchenko, N. G. Afanas'ev, G. A. Savitskii, V. M. Khvastunov,  
V. D. Kovalev, A. S. Omelaenko, and I. S. Gul'karov  
J. Nucl. Phys. (USSR) 5, 948 (1967)  
Sov. J. Nucl. Phys. 5, 676 (1967)

ELEM. SYM.	A	Z
Y	89	39
REF. NO.		HMG
67 Sh 1		HMG

METHOD					REF. NO.	HMG	
					67 Sh 1		
REACTION	RESULT	EXCITATION ENERGY	SOURCE		DETECTOR		ANGLE
			TYPE	RANGE	TYPE	RANGE	
E,E/	FMF	2-3	D	225	MAG-D	DST	
		(2.2)					

G-WIDTH, J-PI

Table II

Absolute differential cross section for inelastic scattering of electrons with energy  $225 \pm 1$  MeV by  $Y^{89}$  with excitation of levels at  $2.5 \pm 0.2$  MeV

$\theta$ , deg	Cross section, $cm^2/sr$	$\theta$ , deg	Cross section, $cm^2/sr$	$\theta$ , deg	Cross section, $cm^2/sr$
35	$(3.15 \pm 0.33) \cdot 10^{-29}$	50	$(2.44 \pm 0.09) \cdot 10^{-30}$	80	$(3.34 \pm 0.21) \cdot 10^{-32}$
35	$(3.77 \pm 0.28) \cdot 10^{-29}$	50	$(2.28 \pm 0.23) \cdot 10^{-30}$	82	$(3.40 \pm 0.23) \cdot 10^{-32}$
40	$(1.26 \pm 0.06) \cdot 10^{-29}$	52	$(2.45 \pm 0.14) \cdot 10^{-30}$	84	$(2.97 \pm 0.22) \cdot 10^{-32}$
44	$(7.72 \pm 0.31) \cdot 10^{-30}$	55	$(9.13 \pm 0.28) \cdot 10^{-31}$	86	$(2.42 \pm 0.18) \cdot 10^{-32}$
46	$(5.05 \pm 0.18) \cdot 10^{-30}$	60	$(4.48 \pm 0.55) \cdot 10^{-31}$	88	$(1.94 \pm 0.15) \cdot 10^{-32}$
48	$(4.74 \pm 0.18) \cdot 10^{-30}$	65	$(2.12 \pm 0.19) \cdot 10^{-31}$	90	$(1.68 \pm 0.15) \cdot 10^{-32}$
48	$(2.59 \pm 0.12) \cdot 10^{-30}$	78	$(4.32 \pm 0.32) \cdot 10^{-32}$	95	$(1.46 \pm 0.18) \cdot 10^{-32}$

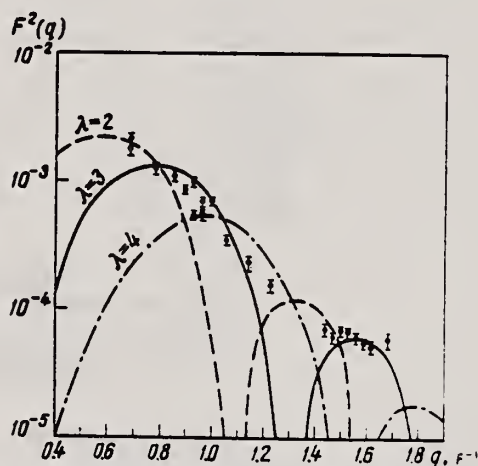


Fig. 4. Squared form factor as a function of momentum transfer for the  $2.5 \pm 0.2$  MeV inelastic peak of  $Y^{89}$ . The curves are calculated in the Born approximation for different values of transition multipolarity  $\lambda$ .



REF. H. Taneichi and K. Shoda  
J. Phys. Soc. Japan 22, 664 (1967)

ELEM. SYM.	A	Z
Y	89	39

METHOD

REF. NO.	
67 Ta 2	egf

REACTION	RESULT	EXCITATION ENERGY	SOURCE		DETECTOR		ANGLE
			TYPE	RANGE	TYPE	RANGE	
G, XP	SPC	THR-24	C	17,24	EMU-D	2-16	4PI

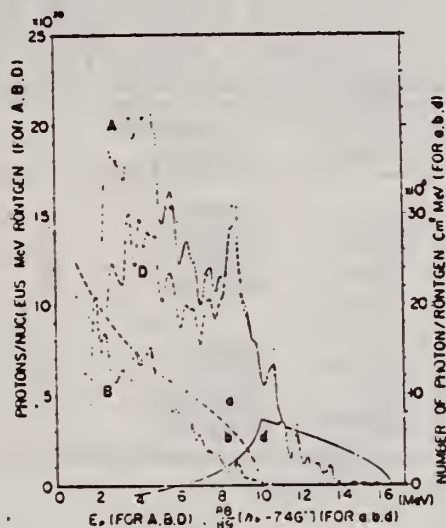


Fig. 1. Energy distributions of photoprotons. Plots and curves A and B—The observed results for 24.0 and 17.5 MeV of the bremsstrahlung maximum energy respectively. Curve a and b—The corresponding spectra of the bremsstrahlung. Curve D and d—The difference between A and B and between a and b.  $\uparrow 7.46$  is the threshold energy of  $Y^*(7, p)$  in MeV.



ELEM. SYM.	A	Z
Y	89	39
REF. NO.		
68 A1 1		egf

METHOD			SOURCE		DETECTOR		ANGLE
REACTION	RESULT	EXCITATION ENERGY	TYPE	RANGE	TYPE	RANGE	
G <sub>2</sub> G	LFT	0-2	C	4	SCD-D	0-3	130
		(1.51)					

Angle greater than 90° for all measurements.

SELF-ABSORPTION

TABLE I  
Direct and absorption measurements of resonance fluorescence

Nucleus	$E_r$ (MeV)	$J_r$	$\Gamma_0/\Gamma$	$gW\Gamma_0\Gamma_0/\Gamma$ (meV)	Error (%)	This work $\Gamma_0$ (meV)	Other work $\Gamma_0$
<sup>55</sup> Mn	0.000	$\frac{1}{2}^-$					
	1.527	$(\frac{3}{2}^-)$	0.9	5.2	25	8-12	
				abs <sup>a)</sup>	40	8.0	
	1.884	?	0.82 <sup>b)</sup>	41	25	50/gW	
				abs <sup>a)</sup>	10	55/g	
	2.197	?	(0.8) <sup>c)</sup>	17	25	21/gW	
				abs	20	17/g	
	2.252	?	(0.9) <sup>c)</sup>	17	25	19/gW	
				abs	20	13/g	
	2.365	?	?	3.5	36	(2-6) $\Gamma/\Gamma_0$	
<sup>59</sup> Co	2.564	?	(1.0)	50	25	50/gW	
				abs <sup>a)</sup>	20	61/g	
	2.751	?	?	6.7	42	6.7( $\Gamma/\Gamma_0$ )/gW	
	0.000	$\frac{3}{2}^-$					
	1.187	$(\frac{1}{2}^-)$	(1.0)	6.8	25	7.5	0.33(E2) <sup>d)</sup>
				abs	25 <sup>a)</sup>	12	
		$(\frac{3}{2}^-)$	(1.0)	6.8	25	(5.4-6.5)	0.27(E2)
				abs	25 <sup>a)</sup>	9.6	
	0.000	$\frac{1}{2}^-$					
	1.414	$\frac{1}{2}^-$	?	1.6	30	(1.1-1.7) $\Gamma/\Gamma_0$	
<sup>67</sup> Ga	1.551	$\frac{1}{2}^-$	?	1.7	37	(1.7-2.5) $\Gamma/\Gamma_0$	0.1(E2) <sup>e)</sup>
	0.000	$\frac{1}{2}^-$					
	0.872	$(\frac{1}{2}^-)$	0.95	1.1	35	0.8/W	
	1.107	$(\frac{1}{2}^-)$	0.95	8.0	20	8.4/W	
	0.000	$\frac{1}{2}^-$					
	0.86	?	?	1.7	20	1.7 $\Gamma/gW\Gamma_0$	
	1.07	?	?	2.6	30	2.6 $\Gamma/gW\Gamma_0$	
	1.35	?	?	3.6	20	3.6 $\Gamma/gW\Gamma_0$	
	0.000	$\frac{1}{2}^-$					
	1.51	$\frac{1}{2}^-$	(1.0)	52 <sup>a)</sup>	30	28	0.37(E2) <sup>f)</sup>
<sup>88</sup> Y				abs <sup>a)</sup>	15	22	

<sup>a)</sup> Measured with NaI.

<sup>b)</sup> Ref. <sup>20)</sup>.

<sup>c)</sup> Measured with a Ge(Li) detector to  $\pm 10\%$ .

<sup>d)</sup> Ref. <sup>13)</sup>.

<sup>e)</sup> Ref. <sup>14)</sup>.

<sup>f)</sup> Ref. <sup>15)</sup>.

- <sup>13</sup> D.G. Alkhazov, K.I. Erokhina and I.K. Lemberg, Izv.Akad.Nauk.SSSR(ser.fiz.) 28 (1964) 1667.  
<sup>14</sup> B.G. Harvey, J.R. Meriwether and A.Bussiére, Nucl. Phys. 70 (1965) 305.  
<sup>23</sup> G.A. Peterson and J. Alster, Phys. Rev. 166 (1968) 136.  
<sup>24</sup> N. Nath, M.A. Rothman, D.M. Van Patter and C.E. Mandeville, Nucl. Phys. 13 (1959) 74.

REF. G. A. Peterson and J. Alster Phys. Rev. <u>166</u> , 1136 (1968)				ELEM. SYM.	A	Z	
				Y	89	39	
METHOD				REF. NO.			
				68 Pe 1		HMG	
REACTION	RESULT	EXCITATION ENERGY	SOURCE		DETECTOR		ANGLE
			TYPE	RANGE	TYPE	RANGE	
E, E/	RLX	1-3	D	65,70	MAG-D	60-70	DST

TABLE I. Experimentally determined values of the reduced nuclear radiative transition probabilities  $B(EL)$  for the excitation of a nucleus to a level at energy  $E^\circ$  above its ground state by a transition of electric character and multipolarity  $L$ , in units of  $e^2 F^{2L}$ , where  $1 F = 10^{-13}$  cm. The last column gives  $B(EL)$  in single-particle Weisskopf units according to Eq. (4).

$E^\circ$	$L$	$B(E0 \rightarrow L)$ ( $e^2 F^{2L}$ )	$G$ (W.u.)
$Sr^{90}$			
1.84	2	$990 \pm 50$	8.5
2.74	3	$80\,600 \pm 3000$	25.0
4.0	2	$190 \pm 40$	1.6
6.5	(2)	$130 \pm 30$	1.1
	(3)	$13\,000 \pm 3000$	4.0
$Y^{90}$			
1.50	2	$120 \pm 50$	1.0
1.73	2	$140 \pm 40$	1.2
2.21	3	$33\,700 \pm 3000$	10.2
2.52	3	$37\,800 \pm 3000$	11.4
2.86	3	$32\,300 \pm 3000$	9.8

SEP ISOTPS

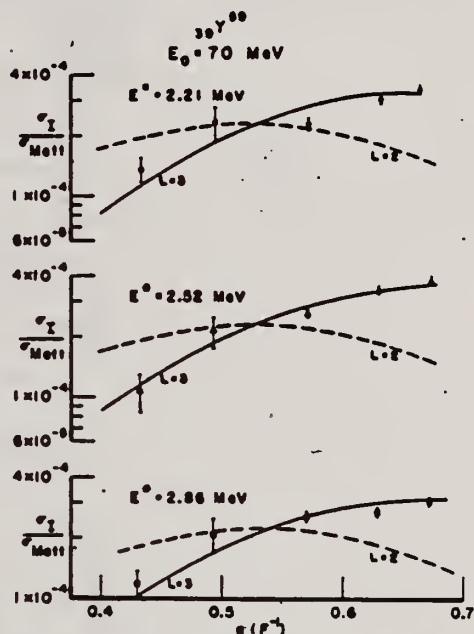


FIG. 6. Distorted-wave inelastic cross section in units of the Mott cross section versus momentum transferred to the  $Y^{90}$  nucleus for electric octupole (solid lines) excitations at 2.21, 2.52, and 2.86 MeV. An incompressible and irrotational hydrodynamical model was assumed. For comparison, curves are shown for electric quadrupole excitations.

REF. S. M. Shafroth and G. J. F. Legge  
Nucl. Phys. A107, 181 (1968)

ELEM. SYM.	A	Z
Y	89	39

METHOD

[Page 1 of 2]

REF. NO.

68 Sh 1

EGF

REACTION	RESULT	EXCITATION ENERGY	SOURCE		DETECTOR		ANGLE
			TYPE	RANGE	TYPE	RANGE	
P,G	ABX	13-15	D	5-9	NAI-D	0-15	DST

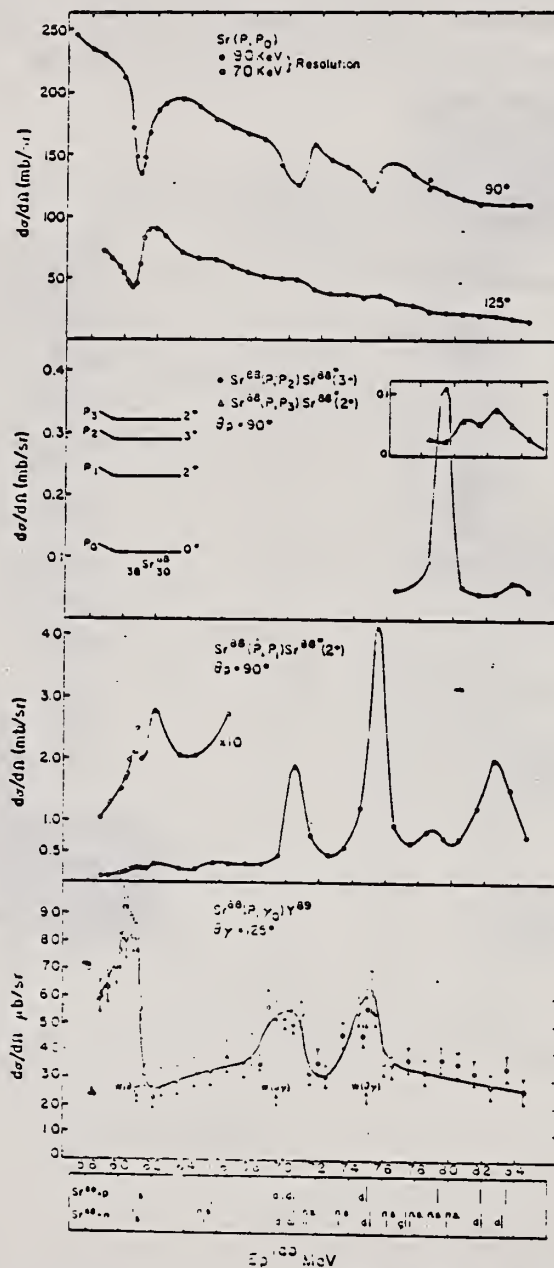


Fig. 3. Excitation curves for several exit channels taken simultaneously. Upper two curves elastic proton scattering from Sr at 90° and 125°. Inset at far right excitation curve for the reaction  $^{88}\text{Sr}(p, p_2)$  at 90°. Curve labeled  $p_3$  excitation curve for the  $^{88}\text{Sr}(p, p_3)$  reaction at 90°. Note the striking resonance at 7.92 MeV. Curves labeled  $p_1$  excitation curve for the  $^{88}\text{Sr}(p, p_1)$  reaction at 90°. Bottom curve excitation curve for the  $^{88}\text{Sr}(p, \gamma_2)$  reaction at 25°. Underlying box upper set of levels: resonance energies (lab) in  $^{88}\text{Sr}+p$  reaction. The energy scale was set to agree with that of ref. 14). Lower set of levels from ref. 9) arbitrarily matched at 7.0 MeV and with energy intervals stretched by 89/88 to convert to "equivalent" lab energy. Levels shown with half the usual length are non-stripping levels.

REF. S. M. Shafroth and G. J. F. Legge  
Nucl. Phys. A107, 181 (1968)

ELEM. SYM.	A	Z
Y	89	39

METHOD

[Page 2 of 2]

REF. NO.

68 Sh 1

EGF

REACTION	RESULT	EXCITATION ENERGY	SOURCE		DETECTOR		ANGLE
			TYPE	RANGE	TYPE	RANGE	

TABLE 1

Radiative widths of analogue resonances in <sup>89</sup>Y (present work)

Resonance energy $E_p$ lab (MeV)	Single-particle component of resonance	$J^\pi$	$(2J+1)\Gamma_p\Gamma_{70}/\Gamma$ (eV)
6.10	$s_{\frac{1}{2}}$	$\frac{1}{2}^+$	$14 \pm 5$
7.00 <sup>a)</sup>	$(d_{\frac{3}{2}})$	$(\frac{3}{2}^+)$	$(13 \pm 5) d)$
7.07 <sup>a)</sup>	$d_{\frac{3}{2}}$	$\frac{3}{2}^+ b)$	
7.51	$d_{\frac{5}{2}}$	$\frac{5}{2}^+ c)$	$17 \pm 5$

<sup>a)</sup> Ref. <sup>2)</sup>.

<sup>b)</sup> Ref. <sup>7)</sup>.

<sup>c)</sup> Present work.

<sup>d)</sup> Unresolved (assuming a single  $\frac{1}{2}^+$  level).

TABLE 1a

Partial widths of analogue resonances in <sup>89</sup>Y

Parent level in <sup>88</sup> Sr	$E_p$ lab resonance	$l_f$	$(2T_0+1)\Gamma_p^2/\theta_n^2$	$\Gamma$ (keV)	$\Gamma_p$ (keV)	$\Gamma_{70}$ (eV)	$\Gamma_{s.p.} c)$ (keV)	$(2T_0+1)\Gamma_{70}/\Gamma_{s.p.}$
1.031	6.10	$s_{\frac{1}{2}}$	0.96 <sup>a)</sup>	70 <sup>a)</sup>	45 <sup>a)</sup>	$11 \pm 4$	1.66	0.08
1.931	7.00	$d_{(\frac{3}{2})}$	0.30 <sup>a)</sup>	50 <sup>a)</sup>	11 <sup>a)</sup>	$7 \pm 3$	3.32	0.03
2.000	7.07	$d_{\frac{3}{2}}$	0.60 <sup>a)</sup>	50 <sup>a)</sup>	23 <sup>a)</sup>			
2.455	7.51	$d_{\frac{5}{2}}$	0.3 <sup>b)</sup>	60 <sup>b)</sup>	13 <sup>b)</sup>	$14 \pm 5$	3.36	0.05

<sup>a)</sup> Ref. <sup>2)</sup>.

<sup>b)</sup> Ref. <sup>16)</sup>.

<sup>c)</sup> Calculated using shell-model wave functions. See text.

TABLE 2

Gamma-ray angular distribution results

lab $E_p$ (MeV)	$l_f$	$W(\theta)$
6.10	$s_{\frac{1}{2}}$	$1 - (0.1 \pm 0.1) P_2(\cos^2 \theta)$
7.51	$d_{\frac{5}{2}}$	$1 - (0.53 \pm 0.12) P_2(\cos^2 \theta)$



ELEM. SYM.	A	Z
Y	89	39
REF. NO.	69 Be 4	egf

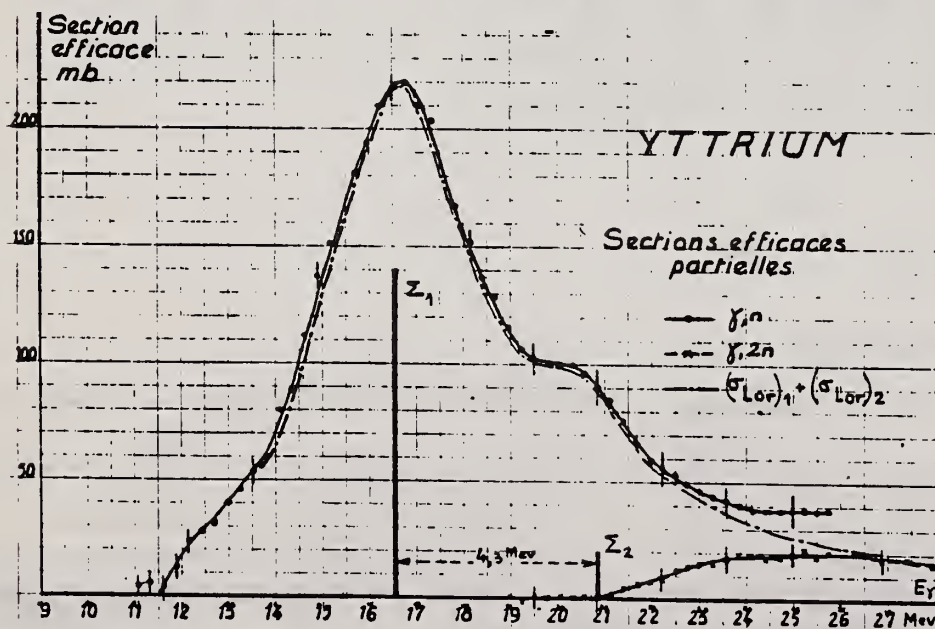
METHOD						REF. NO.	
						69 Be 4	egf
REACTION	RESULT	EXCITATION ENERGY	SOURCE		DETECTOR		ANGLE
			TYPE	RANGE	TYPE	RANGE	
G,N 188	ABX	11-25	D	11-26	MOD-I		4PI
G,2N 189	ABX	21-27	D	19-28	MOD-I		4PI

# RECHERCHE D'ETATS QUASI-LIES ANALOGUES 2p-2h dans la RESONANCE GEANTE de $Y^{89}$

R. BERGERE, P. CARLOS, A. VEYSSIERE, H. BEIL - CEN/Saclay - FRANCE - (91)

Nous avons étudié avec des  $\gamma$  monochromatiques les réactions  $Y^{89}(\gamma,n)$  et  $Y^{89}(\gamma,2n)$ . Les résultats  $\sigma_{\gamma,n}$  et à fortiori  $\sigma_{\gamma,n} + \sigma_{\gamma,2n}$  montrent sans ambiguïté le dédoublement de la résonance géante déjà signalé par R.L. Berman dans cette même région de masse (Phys. Rev. 169, 1967, 1098). On peut représenter entre 13 Mev et 22 Mev la section efficace photoneutronique totale  $\sigma_{\gamma,n}$  par une somme de deux raies de Lorentz ayant respectivement les paramètres:  $E_1 = 16,57$  Mev;  $\Gamma_1 = 4,25$  Mev;  $\sigma_1 = 215$  mbarns;  $E_2 = 20,87$  Mev;  $\Gamma_2 = 2,87$  Mev;  $\sigma_2 = 45$  mbarns. Les sections efficaces intégrées sous chacune de ces deux raies sont respectivement  $\int \sigma_1 = 1,435$  Mev barns et  $\int \sigma_2 = 0,203$  Mev barns et sont donc dans le rapport  $\frac{\int \sigma_1}{\int \sigma_2} = 0,14$ . Un essai de détermination de la section efficace nucléaire totale  $\sigma_{\gamma,n} + \sigma_{\gamma,2n}$  a été fait par une mesure de transmission de  $\gamma$  monochromatiques à travers  $Y^{89}$ . Les incertitudes sur les données actuelles de l'absorption électronique des  $\gamma$  (rapport UCRL 50 400 et NBS 583) permettent simplement de conclure que de 16 à 21 Mev on a  $\sigma_{\gamma,p} \approx 15 \pm 30$  mbarns.

Ce dédoublement est à rapprocher de la prédiction de S. Fallieros sur le dédoublement isobarique des états dipolaires (Phys. Lett. 19, 1965, 398) caractérisé par  $\Delta E \approx 0 \frac{T_1}{T_2} \approx 5$  Mev pour  $Y^{89}$  ( $U$  = énergie de symétrie et  $T = \frac{11}{2}$ ) en bon accord avec notre valeur expérimentale 4,3 Mev. Fallieros prévoit un rapport des intensités dipolaires des transitions  $\frac{T_2}{T_1} = \frac{1}{T_1} \approx 0,48$ . Cette valeur n'est pas incompatible avec nos mesures si on suppose que  $\sigma_{\gamma,p} \approx 0,25 \sigma_{\gamma,n}(\tau_p)$ . Goulard et al (Can. Journ. Phys. 45, 1967, 3221 et 46, 1968, 2771 - Phys. Rev. 176, 1968, 1345) tenant compte de tous les états 1p-1h concluent à un dédoublement  $\Delta E$  trop faible et à un rapport d'intensité  $\frac{T_2}{T_1} \approx 0,11$  ce qui est insuffisant même en ne tenant compte que de la valeur  $\sigma_{\gamma,n}(\tau_p)$ . Il est probable que la considération du couplage d'états du continu aux états quasi-liés 2p-2h permettrait de mieux préciser les caractéristiques de ce dédoublement (V. Gillet et al - Nucl. Phys. A 97, 1967, 631). Notons enfin que notre valeur expérimentale  $\sigma_{\gamma,n}(\tau_p)$  plus grande que  $\sigma_{\gamma,p}$  pourrait provenir, comme indiqué par Gellie (Aust. J. Phys. 1968, 765) d'une désexcitation de  $Y^{89}(\tau_p)$  par émission d'un neutron vers les états  $T_{p,6}$  de  $Y^{88}$  dès que cette voie est ouverte.





ELEM. SYM.	A	Z
Y	89	39
REF. NO.		egf
69 Ri 1		

METHOD						REF. NO.	
						69 Ri 1	egf
REACTION	RESULT	EXCITATION ENERGY	SOURCE		DETECTOR		ANGLE
			TYPE	RANGE	TYPE	RANGE	
P,G	ABX	12	D	5	SCD_D	9-12	90
			(4.97-5.15)				

5=4.97-5.15 MEV

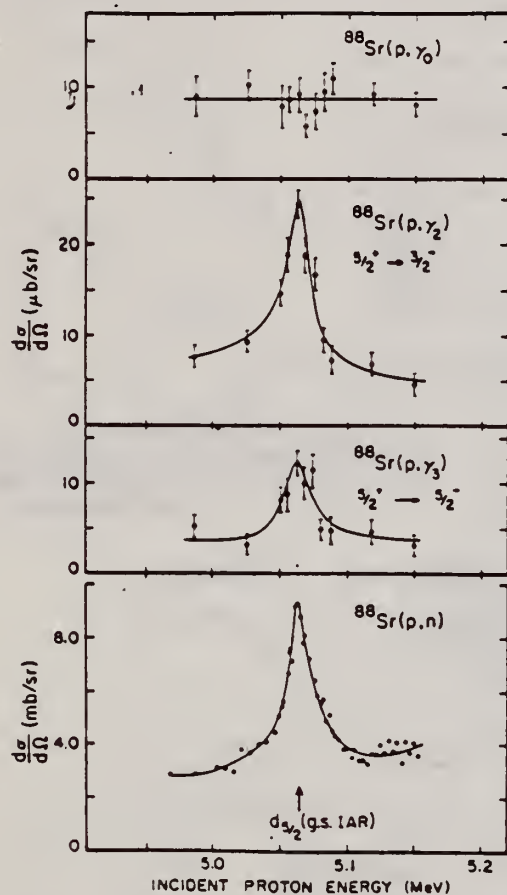


Fig. 2. The excitation functions for the indicated reactions in a proton energy range covering the  $d_{3/2}^+$  ground-state isobaric analogue resonance.

Table 1  
Results for the  $^{88}\text{Sr}(p, \gamma)^{89}\text{Y}$  reaction.

		$\gamma_0$	$\gamma_2$	$\gamma_3$
$\frac{d\sigma}{d\Omega}(90^\circ)(\mu\text{b/sr})$	off resonance	8.7	6	4
	on resonance	8.7	25	12
$\Gamma_\gamma^{\text{exp}}$	(eV)	-	$7 \pm 2$	$4 \pm 3$
$\Gamma_\gamma^{\text{SD}}$	(eV)	-	1840	27
$\Gamma_\gamma^{\text{TH}}$	(eV)	-	49	0.9
$\sigma_n/\sigma_\gamma$		-	360	560

METHOD

[Page 1 of 2]

REACTION	RESULT	EXCITATION ENERGY	SOURCE		DETECTOR		ANGLE
			TYPE	RANGE	TYPE	RANGE	
G,P	ABX	7-24	C	17-24	EMU-D	2-16	DST
				(17.5)			

Table II. Anisotropic factor  $B/A$  and asymmetry factor  $p$  of angular distributions determined by least-square fits with  $A+B(1+p \cos \theta) \sin^2 \theta$ .

$^{88}\text{Y}$						
$E_p(\text{MeV})$	$(E_{\text{max}}=17.5 \text{ MeV})$		$(E_{\text{max}}=19.0 \text{ MeV})$		$(E_{\text{max}}=24.0 \text{ MeV})$	
	$B/A$	$p$	$B/A$	$p$	$B/A$	$p$
3.5-5.1	$0.3 \pm 0.2$	$0.6 \pm 0.7$	$1.1 \pm 0.4$	$0.3 \pm 0.3$	$0.5 \pm 0.2$	$-0.4 \pm 0.5$
5.1-7.2	$1.1 \pm 0.4$	$0.0 \pm 0.3$	$2.2 \pm 0.4$	$0.1 \pm 0.1$	$0.9 \pm 0.3$	$0.2 \pm 0.2$
7.2-10.0	$\infty^a$	$0.2 \pm 0.2$	$3.2 \pm 2.0$	$-0.2 \pm 0.2$	$1.6 \pm 0.6$	$0.0 \pm 0.2$
10.0-					$4.5 \pm 3.0$	$-0.2 \pm 0.2$

a) The notation  $\infty$  indicates that the distribution is almost  $(1+p \cos \theta) \sin^2 \theta$ . It is used when the result has stronger maximum than that of  $1+10(1+p \cos \theta) \sin^2 \theta$ .

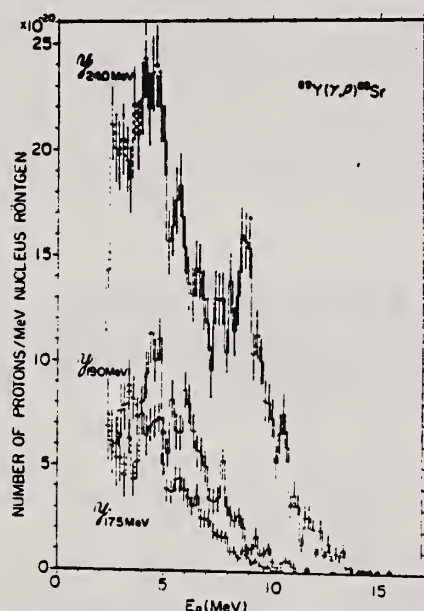


Fig. 1. Energy distributions of photoprotons from  $^{88}\text{Y}$  irradiated with the bremsstrahlung at maximum energies of 24.0, 19.0 and 17.5 MeV.

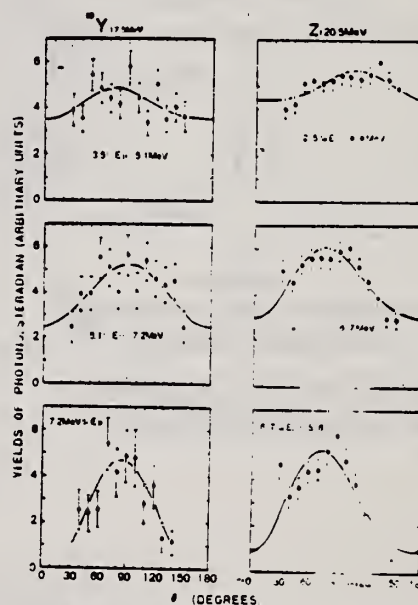


Fig. 3. Examples of angular distributions of photoprotons from  $^{88}\text{Y}$  and Zr.

REF.

K. Shoda and H. Taneichi  
J. Phys. Soc. Japan 26, 217 (1969)

ELEM. SYM.	A	Z
Y	89	39

METHOD

[Page 2 of 2]

REF. NO.

69 Sh 4

hmg

REACTION	RESULT	EXCITATION ENERGY	SOURCE		DETECTOR		ANGLE
			TYPE	RANGE	TYPE	RANGE	

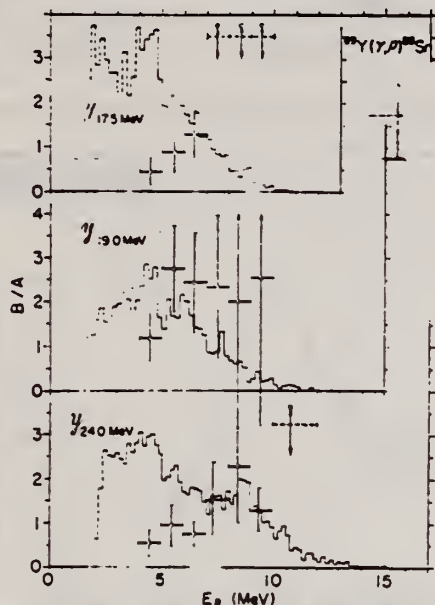


Fig. 4. Energy dependence of the anisotropic factor  $B/A$  of the angular distributions for photoprotons from  $^{89}\text{Y}$ . A sign - indicates that  $B/A$  is too large to plot the figure.

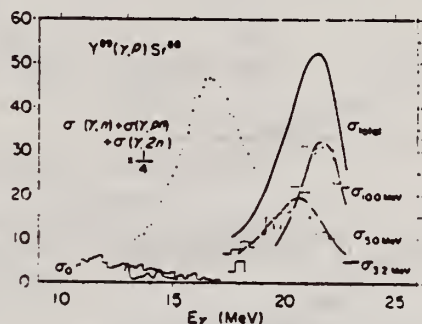


Fig. 10. Cross sections for strong photoproton transitions on  $^{89}\text{Y}$ . The neutron emission cross section<sup>10)</sup> and the result of the  $^{89}\text{Sr}(p, \gamma)^{89}\text{Y}$  reaction<sup>11)</sup> are also shown.

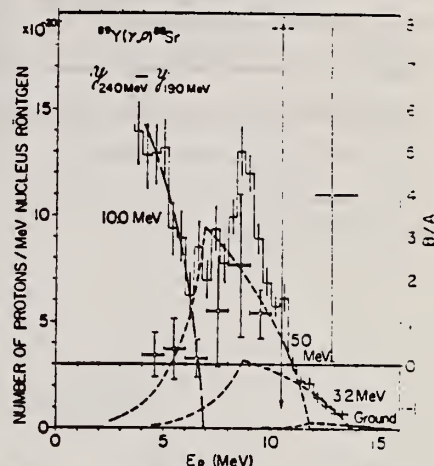


Fig. 6. The energy distribution and the anisotropic factor  $B/A$  for photoprotons from  $^{89}\text{Y}$  obtained by subtraction of  $\mathcal{Y}_{19.0\text{MeV}}$  from  $\mathcal{Y}_{24.0\text{MeV}}$ . The broken curves show transition groups to the selected residual states.

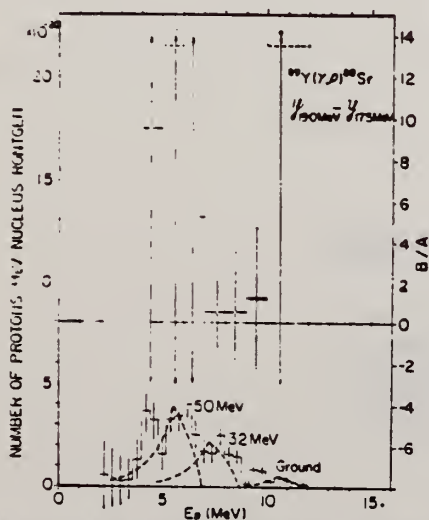


Fig. 7. The energy distribution and the anisotropic factor  $B/A$  for photoprotons from  $^{89}\text{Y}$  obtained by subtraction of  $\mathcal{Y}_{17.5\text{MeV}}$  from  $\mathcal{Y}_{19.0\text{MeV}}$ . See also the caption for Fig. 6.

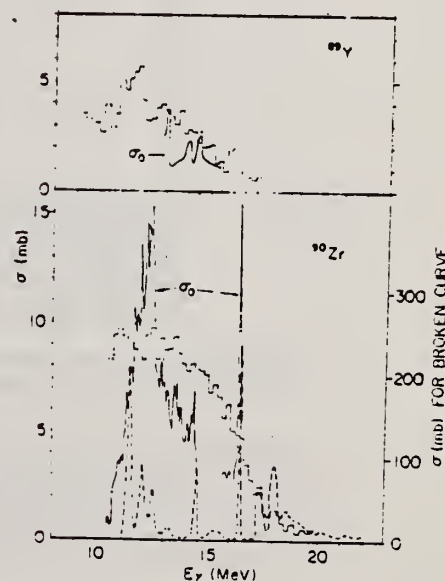


Fig. 9. The  $(\gamma, p)$  cross sections of  $^{89}\text{Y}$  and  $^{89}\text{Zr}$  in the photon energy region lower than 20 MeV. The  $(\gamma, p)$  cross sections deduced from the inverse reaction cross sections are shown by solid lines indicated by  $\sigma_n$ . Theoretical  $^{89}\text{Zr}(\gamma, p)^{89}\text{Y}$  cross section<sup>12)</sup> is shown by broken line.

REF.

K. Shoda, M. Sugawara, T. Saito & H. Miyase  
 PICNS-69 Proceedings of the Conference on Nuclear Isospin.  
 Asilomar-Pacific Grove, California 1969 (Academic Press,  
 New York & London 1969) p.125.

ELEM. SYM.

A

Z

Y

89

39

METHOD

REF. NO.

69 Sh 6

egf

REACTION	RESULT	EXCITATION ENERGY	SOURCE		DETECTOR		ANGLE
			TYPE	RANGE	TYPE	RANGE	
E,P	SPC	10-26	D	20	MAG-D		UKN

UKN= UNKNOWN

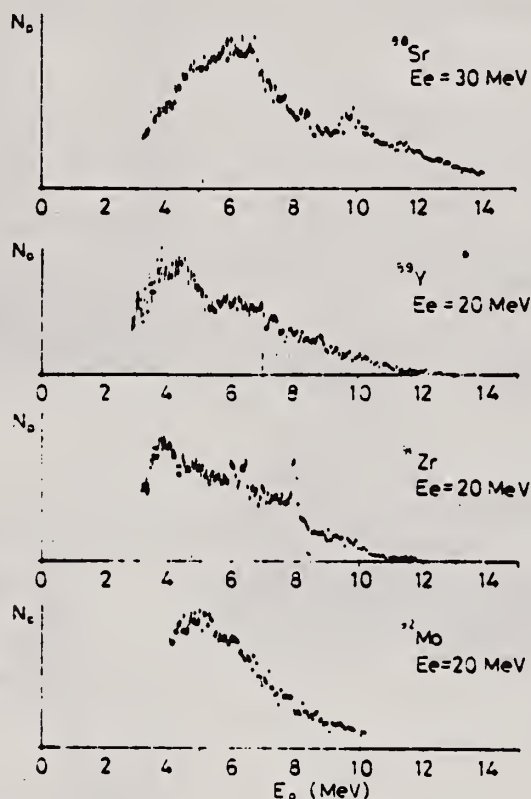


Fig. 1. Energy distributions of photoprotons. Vertical broken lines and solid lines indicate the position of  $p_0$  corresponding to the ground IAS and electric dipole IAS ( $2-1$ ) respectively.



REF. H. Arenhovel, J. M. Maison  
Nucl. Phys. A147, 305 (1970)

ELEM. SYM.	A	Z
Y	89	39

METHOD	REF. NO.
	70 Ar 1
	egf

REACTION	RESULT	EXCITATION ENERGY	SOURCE		DETECTOR		ANGLE
			TYPE	RANGE	TYPE	RANGE	
G <sub>1</sub> G	ABX	12-30	C	32	NAI	12-30	DST

GETS G<sub>1</sub>G/ TO 2+

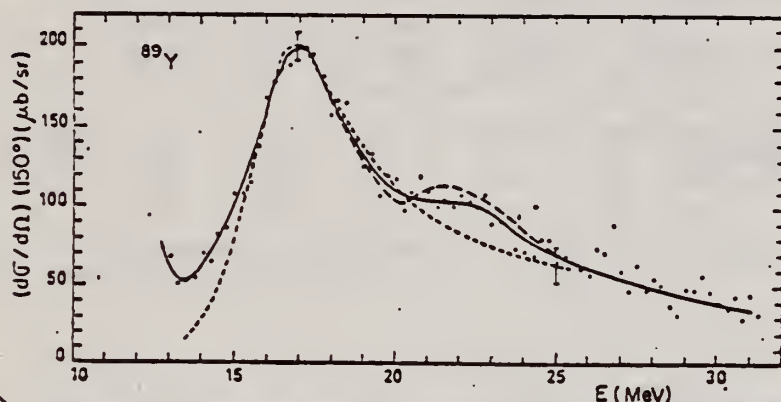


Fig. 9. Differential total scattering cross section at 150° for <sup>89</sup>Y. The dashed curves are the scattering cross section calculated with one Lorentz line at  $E_1 = 16.4$  MeV and with two Lorentz lines at  $E_1 = 16.4$  MeV and  $E_1 = 21.5$  MeV.

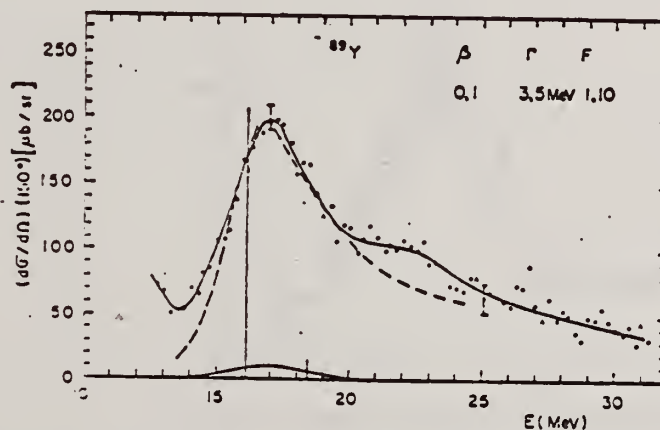


Fig. 10. Differential total scattering cross section at 150° for <sup>89</sup>Y and theoretical scattering cross section (dashed curve) given by the D.C.M. calculations. See caption for fig. 4. Here  $E_1$  is given by table 3.

Fig. 4. Differential total scattering cross section at 150° for natural Ti. The full curve through experimental points is only a guide for the eyes. The vertical bars represent the relative strength of dipole levels calculated by the D.C.M. with parameters of table 1. Theoretical elastic plus inelastic scattering is computed from these levels with a common width  $\Gamma$  (dashed curve). Experimental inelastic scattering (histogram) and theoretical inelastic scattering to the first 2<sup>+</sup> (full curve) are shown in the lower part of the figure. Open circles give the cross section after background subtraction.



TABLE 4  
Integrated inelastic scattering cross section

Nucleus	Limits of integration (in MeV)	Experimental <sup>a)</sup> $\int \sigma_i(E) dE$ (MeV $\cdot \mu b$ )	$2\pi$	Theoretical <sup>a)</sup> $2\pi'$ (MeV $\cdot \mu b$ )	Total
Ti( <sup>48</sup> Ti)	16 - 24	$250 \pm 50$	425	109	534
<sup>51</sup> V( <sup>52</sup> Cr)	16.4 - 24.9	$492 \pm 50$	509	116	579
Cr	16.4 - 23.4	$431 \pm 60$	509	116	579
<sup>73</sup> As( <sup>76</sup> Se)	14.1 - 23.6	$1254 \pm 120$	1373	414	1787
Se( <sup>80</sup> Se)	14.1 - 24.6	$1035 \pm 100$	1066	353	1419
<sup>89</sup> Y					364
Cd( <sup>112</sup> Cd)	13.6 - 23.3	$3264 \pm 240$	1894	370	2264
In( <sup>114</sup> Cd)	13.6 - 23.6	$2840 \pm 220$	2173	388	2561
Sn( <sup>110</sup> Sn)	14.2 - 24.2	$2363 \pm 220$			643

<sup>a)</sup> We assume an angular distribution of the form  $1 + \frac{1}{13} \cos^2 \theta$ .

REF. B. S. Ishkhanov, I. M. Kapitonov, E. V. Lazutin, I. M. Piskarev,  
and O. P. Shevchenko  
Izv. Akad. Nauk Fiz. 34, 2232 (1970)  
Bull. Acad. Sci. USSR Phys. 34, 1991 (1970)

ELEM. SYM.	A	Z
Y	89	39
REF. NO.		
70 Is 8		hmg

METHOD

REACTION	RESULT	EXCITATION ENERGY	SOURCE		DETECTOR		ANGLE
			TYPE	RANGE	TYPE	RANGE	
G, XN	ABX	11- 29	C	11- 29	BF3-I		4PI

Reaction	Position of peak MeV	Cross section at peak mb	Width of peak MeV	Integral cross section mb-MeV	Integration limit MeV	Reference
$\sigma(\gamma, Tn)$	16.0	270	3.7	1.57	29	The present work
$\sigma(\gamma, Tn)$	16.6	184	3.7	1.14	28	Ref. 5
$\sigma_n$	16.0	270	3.7	1.36	29	The present work
$\sigma_n$	16.6	184	3.7	1.04	28	Ref. 5

5. B.L.Berman, J.T.Caldwell, R.R.Harvey, M.A.Kelly, R.L.Bramblett & S.C.Fultz, Phys. Rev. 162, 1098 (1967).

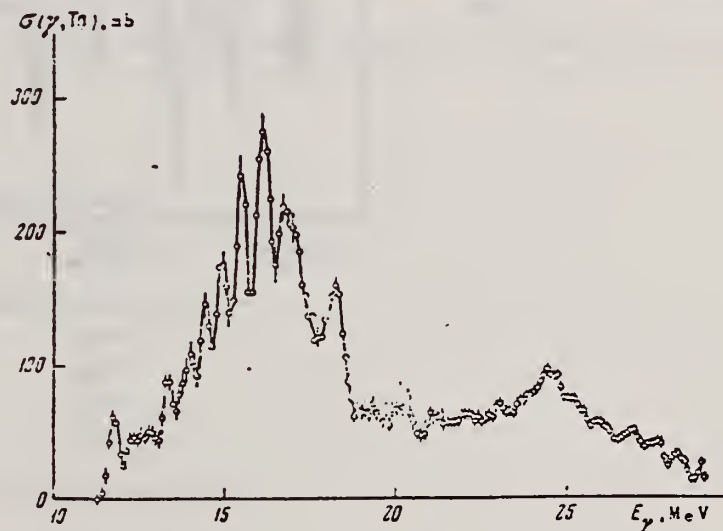


Fig.1. Cross section for the  $^{89}\text{Y}(\gamma, Tn)$  reaction.

REF. W. B. Walters, J. R. Van Hise, W. L. Switzer, J. P. Hummel  
Nucl. Phys. A157, 73 (1970)

ELEM. SYM.	A	Z
Y	89	39

METHOD

REF. NO.	
70 Wa 3	egf

REACTION	RESULT	EXCITATION ENERGY	SOURCE		DETECTOR		ANGLE
			TYPE	RANGE	TYPE	RANGE	
G,2N	RLY	THR-305	C	150-305	ACT-I		4PI
G,pn	RLY	THR-305	C	150-305	ACT-I		4PI

TABLE 1  
Summary of measured yield ratios

Target	Bremsstrahlung energy (MeV)	Measured yield ratio
natural Cr	150	$^{48}\text{Cr}/^{48}\text{V} = 0.043 \pm 0.002$
	250	$0.047 \pm 0.009$
	305	$0.042 \pm 0.002$
enriched $^{52}\text{Cr}$	250	$0.025 \pm 0.005$
natural Fe	250	$^{52}\text{Fe}/^{52}\text{Mn} = 0.037 \pm 0.003$
enriched $^{56}\text{Fe}$	250	$0.024 \pm 0.005$
		$^{52}\text{Mn}/(^{52}\text{Mn} + ^{55}\text{Mn}) = 0.47 \pm 0.02$
natural Y	150	$^{87}\text{Y}/^{87}\text{Sr} = 12.9 \pm 1.6$
natural Mo	150	$^{90}\text{Mo}/^{90}\text{Nb} = 0.41 \pm 0.05$
	280	$0.49 \pm 0.05$

TABLE 2  
Summary of experimental and theoretical ratios of ( $\gamma$ , 2n) to ( $\gamma$ , pn) yields

Target isotope	Bremsstrahlung energy (MeV)	Experimental ( $\gamma$ , 2n)/( $\gamma$ , pn) yield ratio	Calculated ( $\gamma$ , 2n)/( $\gamma$ , pn) yield ratio
$^{50}\text{Cr}$	250	$0.095 \pm 0.025$	0.14
$^{54}\text{Fe}$	250	$0.10 \pm 0.03$	0.07
$^{89}\text{Y}$	150	$7.4 \pm 1.0$	6.7
$^{92}\text{Mo}$	150	$0.41 \pm 0.05$	0.15
	280	$0.49 \pm 0.05$	0.16

REF.

B.I. Goryachev, B.S. Ishkhanov, and V.G. Shevchenko  
 Proceedings of the Second Symposium on the Problems  
 of Nuclear Physics, Novosibirsk, USSR, June 1970  
 (Kolybasov, V.M., Ed., Izdatel'stvo Nauka, Moscow 1971),  
 pp. 362-78

ELEM. SYM.	A	Z
Y	89	39

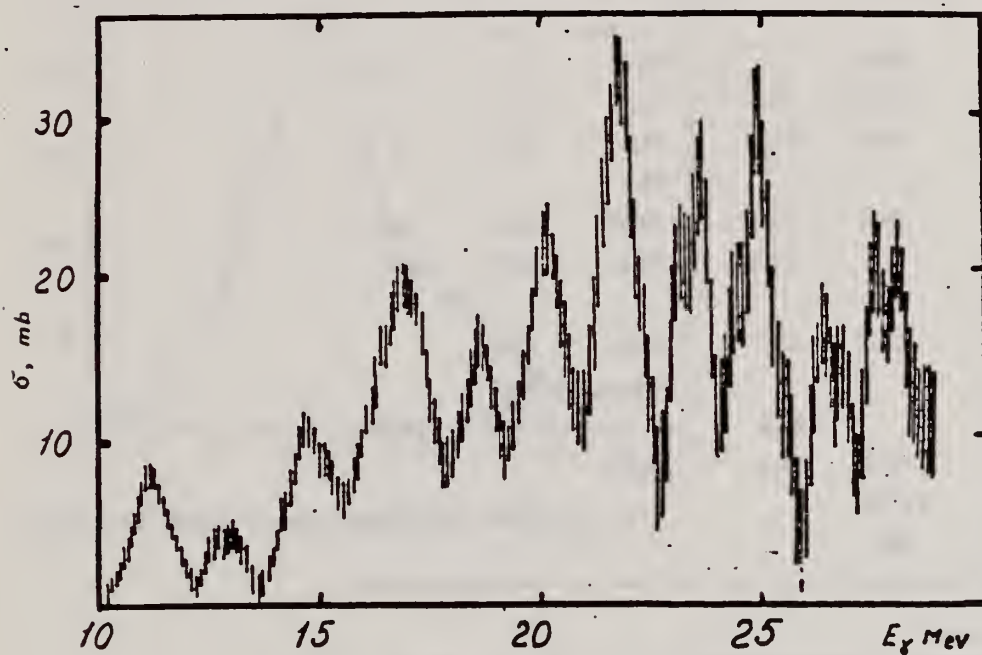
METHOD

REF. NO.

71 Go 3

egf

REACTION	RESULT	EXCITATION ENERGY	SOURCE		DETECTOR		ANGLE
			TYPE	RANGE	TYPE	RANGE	
G,P	ABX	10- 29	C	10- 29	UKN		4PI



Фиг. 8. Сечение реакции  $Y^{89}(n, \gamma)$ .

(over)

Т а б л и ц а 3

$Cr^{52} E_m$ МэВ	$Ni^{58} E_m$ МэВ	$Ni^{60} E_m$ МэВ	$Y^{89} E_m$ МэВ	$Nb^{93} E_m$ МэВ	$Ag^{107} E_m$ МэВ	$Cd^{110} E_m$ МэВ
			11,2	12,0	11,3	
			12,7		12,7	
	13,9				13,9	14,2
			14,7	14,5	14,6	
	15,1					
16,0		16,4		16,2		16,5
	16,8	(17,0)	16,8	17,0	17,0	
18,7	18,4	18,6	18,6	18,4	18,4	18,7
	19,1			19,3		
20,4		20,4	20,1	(19,7)	20,3	20,8
	21,1		21,8	21,5	21,7	22,4
22,2	(22,1)					
22,9	23,4	23,3	23,7	23,3	23,7	
23,8					24,2	
24,8	25,2		25,0			25,0
26,2	26,5	25,8	26,4	26,5		
	28,2	(27,5)			27,0	27,0
	29,7	29,4				



METHOD

REF. NO.

71 Le 1

egf

REACTION	RESULT	EXCITATION ENERGY	SOURCE		DETECTOR		ANGLE
			TYPE	RANGE	TYPE	RANGE	
G, N <b>381</b>	ABX	11-27	D	11-27	MOD-I		4PI
G, 2N <b>382+</b>	ABX	21-27	D	11-27	MOD-I		4PI

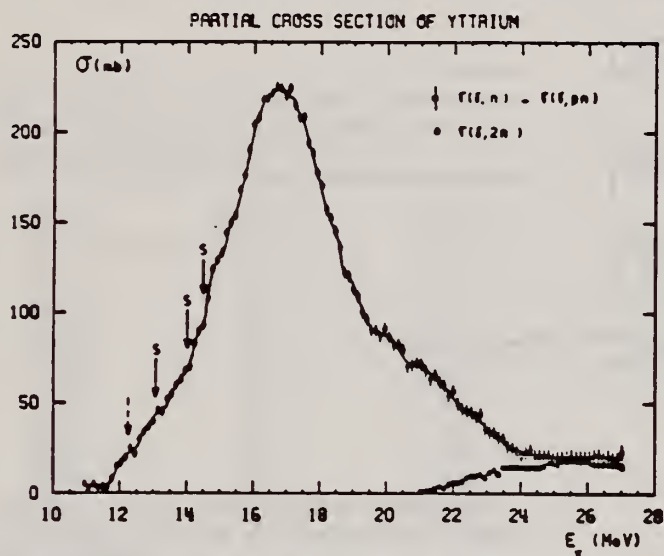


Fig. 3. Partial photoneutron cross sections  $\sigma(\gamma, n)$  and  $\sigma(\gamma, 2n)$  of  $^{89}\text{Y}$ .

TABLE 1

Lorentz line parameters corresponding to fits shown in fig. 6.

	Rb	Sr	$^{89}\text{Y}$	$^{90}\text{Zr}$	$^{93}\text{Nb}$
$\sigma_0$ (mb)	$192 \pm 10$	$207 \pm 10$	$225 \pm 10$	$211 \pm 10$	$202 \pm 10$
$\Gamma_1$ (MeV)	$4.1 \pm 0.15$	$4.2 \pm 0.1$	$4.1 \pm 0.1$	$4.0 \pm 0.1$	$4.7 \pm 0.2$
$E_1$ (MeV)	$16.75 \pm 0.05$	$16.7 \pm 0.05$	$16.7 \pm 0.05$	$16.65 \pm 0.05$	$16.5 \pm 0.05$

TABLE 3

Integrated cross sections (the notation used is defined in the text)

	Rb	Sr	$^{89}\text{Y}$	$^{90}\text{Zr}$	$^{93}\text{Nb}$
$\sigma_0$ (MeV · b)	$1.14 \pm 0.06$	$1.42 \pm 0.07$	$1.36 \pm 0.07$	$1.26 \pm 0.07$	$1.33 \pm 0.07$
$\frac{\sigma_0}{0.06 NZ A^{-1}}$	$0.915 \pm 0.05$	$1.09 \pm 0.05$	$1.04 \pm 0.05$	$0.95 \pm 0.05$	$0.97 \pm 0.05$
$\sigma_{-1}$ (mb)	$67 \pm 4$	$80 \pm 5$	$77 \pm 5$	$71 \pm 5$	$79 \pm 5$
$\sigma_{-2}$ (mb · MeV $^{-1}$ )	$4 \pm 0.2$	$4.6 \pm 0.2$	$4.4 \pm 0.2$	$4 \pm 0.2$	$4.8 \pm 0.2$
$E_M$ (MeV)	24	27	27	26	24

(over)

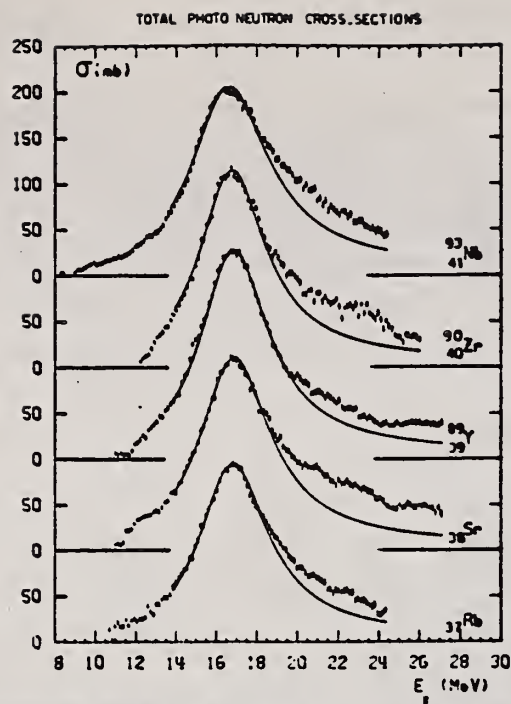


Fig. 6. Total photoneutron cross sections  $\sigma_T$  of Rb, Sr,  $^{89}\text{Y}$ ,  $^{90}\text{Zr}$  and  $^{93}\text{Nb}$  and best one Lorentz line fit corresponding to parameters given in table I.

REF.

E. J. Moniz, I. Sick, R. R. Whitney, J. R. Ficenec, R. G. Kephart  
and W. P. Trower  
Phys. Rev. Letters 26, 445 (1971)

ELEM. SYM.

A

Z

Y

89

39

METHOD

REF. NO.

71 Mo 3

hmg

REACTION	RESULT	EXCITATION ENERGY	SOURCE		DETECTOR		ANGLE
			TYPE	RANGE	TYPE	RANGE	
E, E/	ABX	0-240	D	500	MAG-D		60

Table I. Nuclear Fermi momentum  $k_F$  and average nucleon interaction energy  $\bar{\epsilon}$  determined by least-squares fit of theory to quasielastic peak.

Nucleus	$k_F$ (MeV/c) <sup>a</sup>	$\bar{\epsilon}$ (MeV) <sup>b</sup>
${}^6_3\text{Li}$	169	17
${}^{12}_6\text{C}$	221	25
${}^{24}_{12}\text{Mg}$	235	32
${}^{40}_{20}\text{Ca}$	251	28
${}^{58.7}_{28}\text{Ni}$	260	36
${}^{89}_{39}\text{Y}$	254	39
${}^{118.7}_{50}\text{Sn}$	260	42
${}^{181}_{73}\text{Tl}$	265	42
${}^{208}_{82}\text{Pb}$	265	44

<sup>a</sup>The fitting uncertainty in these numbers is approximately  $\pm 5$  MeV/c.

<sup>b</sup>The fitting uncertainty in these numbers is approximately  $\pm 3$  MeV. Simple estimates for  $\bar{\epsilon}$  give numbers in reasonable agreement with those in the table.

Tatsuya Saito  
Nippon Kagaku Zasshi 92, 164 (1971)

Y 89 39

METHOD

REF. NO.

71 Sa 1

egf

REACTION	RESULT	EXCITATION ENERGY	SOURCE		DETECTOR		ANGLE
			TYPE	RANGE	TYPE	RANGE	
G,N	ABY	11-68	C	10-68	ACT-I		4PI

Nippon Kagaku Zasshi. 92. 164~168(1971)

The Yields of Radioactivities Induced by ( $\gamma, n$ ) Reactions with Bremsstrahlung up to 68 MeV

by Tatsuya SAITO

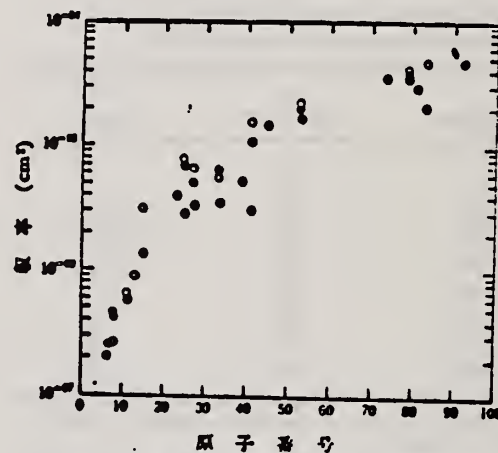
The ( $\gamma, n$ ) yields of 12 target nuclides have been measured at 10, 13, 16, 30, 45 and 68 MeV bremsstrahlung by observing the induced activities.

The energy dependence of the yields has been investigated extensively in the same way as in the previous work at 20 MeV bremsstrahlung.

In the case of heavy nuclides, the yields rise greatly as a function of maximum bombarding energy up to 20 MeV, and rise gradually from 20 MeV up to 68 MeV. However, in the case of light nuclides, the yields rise greatly up to 30 MeV, because the neutron separation energies of light ones are larger than those of heavy ones, and the bremsstrahlung spectrum covers the giant resonance and so the yields rise gradually from 30 MeV up to 68 MeV.

The yields have approximately been estimated from the parameter of the giant resonance, that is the peak cross section and the half width, in order to compare with the experimental data. As a result, the experimental data of light nuclides and heavy ones are nearly in agreement with the estimated data of Nathans et al., Jolins et al. and Montalbetti et al., but those of medium weight ones are relatively lower values.

Department of Chemistry, Faculty of Science, Tohoku University; Katahira-cho, Sendai-shi, Japan



●: 実験値, ⊕: Johns ら,  
①: Nathans ら, ○: Montalbetti ら  
図 4 ( $\gamma, n$ ) 反応の収率の比較



REF.

C.J. Umbarger, D.A. Close, W.L. Sievers, and R.C. Bearse  
Phys. Rev. C3, 199 (1971)

ELEM. SYM.

A

Z

Y

89

39

METHOD

REF. NO.

71 Um 1

hmg

REACTION	RESULT	EXCITATION ENERGY	SOURCE		DETECTOR		ANGLE
			TYPE	RANGE	TYPE	RANGE	
P,G	ABX	10-11	D	2-3	NAI-D		0
				(2.3-3.0)			

The  $^{88}\text{Sr}(\rho, \gamma)^{88}\text{Y}$  and  $^{88}\text{Y}(\rho, \gamma)^{88}\text{Zr}$  reactions have been investigated in the energy range  $E_p = 2.3$  to  $3.0$  MeV. Excitation functions for the transition to the ground state, with a total resolution of  $2$  keV, were determined for each reaction over this energy region. Using thick targets and both a single Ge(Li) detector and a Ge(Li) detector incorporated into a pair spectrometer, total summed spectra for the  $700$ -keV region were obtained. The average total cross section of  $^{88}\text{Sr}(\rho, \gamma)^{88}\text{Y}$  and  $^{88}\text{Y}(\rho, \gamma)^{88}\text{Zr}$  was  $12 \pm 5 \mu\text{b}$  and  $17 \pm 7 \mu\text{b}$ , respectively. These total summed spectra, which represent the total  $\gamma$ -ray yield in this region, have been examined for a possible dependence of the intensity on the  $J^\pi$  of the final state. The data suggest such a  $J$ -dependence hypothesis, but detailed theoretical analysis of the  $^{88}\text{Sr}(\rho, \gamma)^{88}\text{Y}$  reaction does not completely agree with experiment. A spectrum from a Ge(Li) detector in coincidence with a NaI(Tl) detector was accumulated for the  $^{88}\text{Sr}(\rho, \gamma)^{88}\text{Y}$  reaction. The decay scheme of the states of  $^{88}\text{Y}$  up to an excitation energy of  $3.621$  MeV was determined and the implications about spins and parities are consistent with accepted assignments.

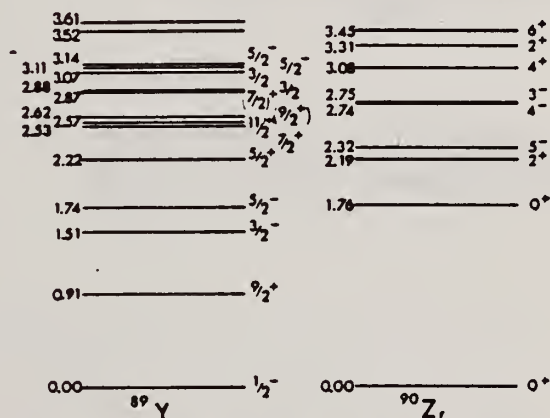


FIG. 1. Presently accepted level schemes for  $^{88}\text{Y}$  and  $^{88}\text{Zr}$  taken from the data of Van Patter (Ref. 8) and Ball (Ref. 9), respectively.

<sup>8</sup>D. M. Van Patter, Bull. Am. Phys. Soc. 15, 573 (1970).

<sup>9</sup>J. B. Ball, Bull. Am. Phys. Soc. 15, 574 (1970).

[over]



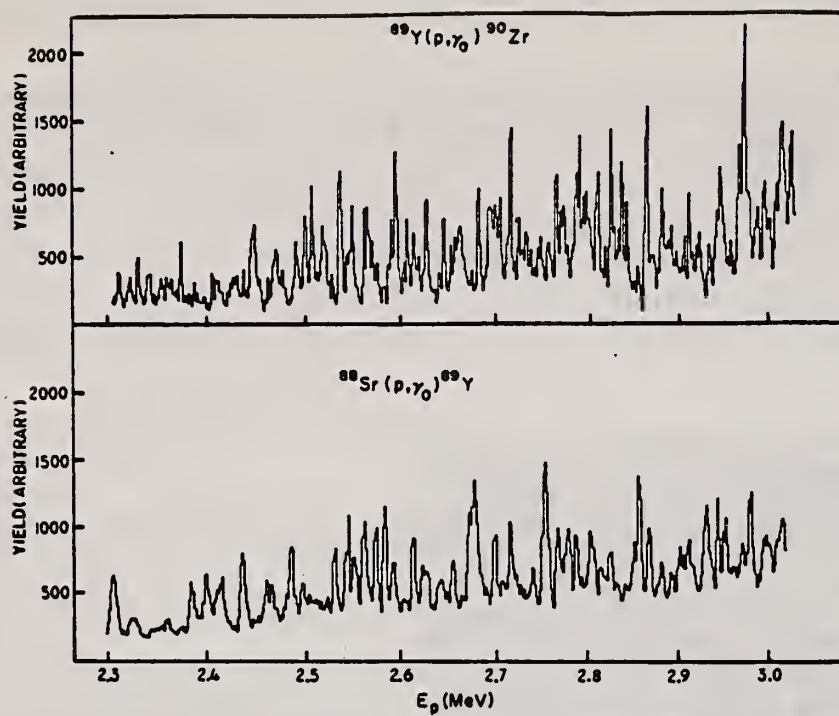


FIG. 2. Excitation functions for  $^{88}\text{Sr}(p,\gamma)^{88}\text{Y}$  and  $^{88}\text{Y}(p,\gamma)^{90}\text{Zr}$  over the energy region  $E_p = 2.3$  to  $3.0$  MeV.

METHOD

REF. NO.

72 Pa 4

hvm

REACTION	RESULT	EXCITATION ENERGY	SOURCE		DETECTOR		ANGLE
			TYPE	RANGE	TYPE	RANGE	
P,G	LFT	13- 15	D	5- 9	NAI-D		DST

Table III. E1 transition strengths from the  $2d_{5/2}$ ,  $3s_{1/2}$  and  $2d_{3/2}$  IAR in  $Y^{87,89}$  and  $Nb^{91}$ .

	Transition	$E_p$ (MeV)	$\Gamma_Y$ (ex) (eV)	$S(d,p)$	$S(He^3,d)$	$\Gamma_Y$ (ex)/ $\Gamma_Y$ (th)
$Y^{87}$	$5/2^+ \rightarrow 5/2^-$	4.80	$7 \pm 2$	0.46	0.19	$28^*$
	$5/2^+ \rightarrow 3/2^-$	"	$13 \pm 3$	"	0.14	$1.5^*$
	$5/2^+ \rightarrow 5/2^-$	"	$7 \pm 2$	"	0.19	$28^*$
$Y^{89}$	$5/2^+ \rightarrow 3/2^-$	5.08	$8 \pm 2$	0.8	0.11	$0.6^*$
	$5/2^+ \rightarrow 5/2^-$	"	$3.5 \pm 1$	"	0.09	$17^*$
	$1/2^+ \rightarrow 1/2^-$	6.08	$18 \pm 3$	"	0.9	0.18
$Nb^{91}$	$3/2^+ \rightarrow 1/2^-$	7.51	$11 \pm 2$	0.34	"	0.10
	$1/2^+ \rightarrow 1/2^-$	8.86	$40 \pm 8$	0.11	"	0.65
	$3/2^+ \rightarrow 1/2^-$	6.82	$26 \pm 6$	0.63	0.36	$0.52^*$

\* Below effective neutron threshold

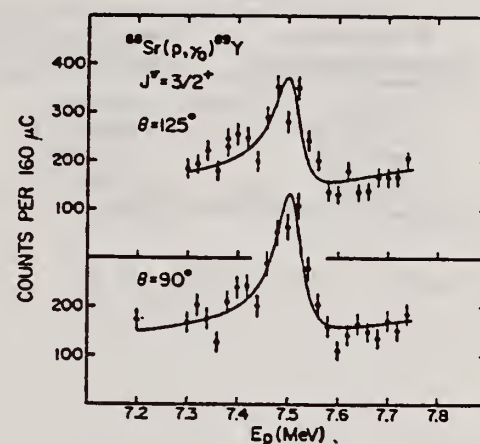


Fig.7. Observation of the transition to the ground state ( $2p_{1/2}$ ) of  $Y^{89}$  near a  $2d_{3/2}$  IAR. The solid curves are theoretical fits (see text).

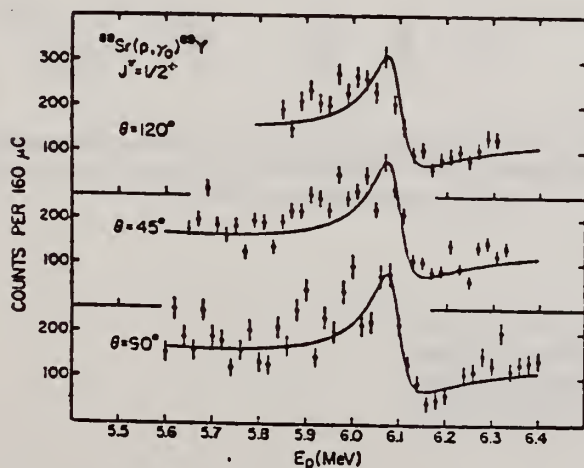


Fig. 6. Excitation functions of the ground-state transition in  $Y^{89}$  near the  $3s_{1/2}$  IAR observed in radiative proton capture. The solid curves are theoretical fits described in the text.

REF. J.W. Watson, H.A. Medicus, and R.E. Turner  
Phys. Rev. C6, 497 (1972)  
See Erratum: Phys. Rev. C7, 1273 (1973)

ELEM. SYM.	A	Z
Y	89	39
REF. NO.		
72 Wa 3		egf

METHOD					REF. NO.	
					72 Wa 3	
REACTION	RESULT	EXCITATION ENERGY	SOURCE		DETECTOR	
			TYPE	RANGE	TYPE	RANGE
G, 2N	NOX	20- 50	D	23- 50	ACT-I	4PI

# ISOMERS

TABLE I. Experimental isomer ratios:  
 $Y^{89}(\gamma, 2n)Y^{87m}, Y^{87}$ .

Bremsstrahlung end-point energy (MeV)	Measured isomer ratio Metastable state/total
23.0 ± 1.5	0.2 ± 0.02
25.6 ± 1.5	0.26 ± 0.025
28.6 ± 1.6	0.30 ± 0.03
50.0 ± 2.3	0.35 ± 0.03

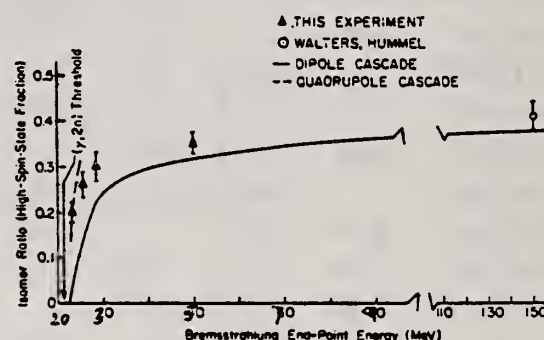


FIG. 4. Isomer ratio in  $Y^{87}$  from the reaction  $Y^{89}(\gamma, 2n)Y^{87}$  vs end-point energy of thin-target bremsstrahlung.

Isomer Ratios from Low Primary Excitation of Residual Nuclei. J. W. Watson, H. A. Medicus, and R. E. Turner [Phys. Rev. C 6, 497 (1972)]. In Figs. 3 and 4 the abscissas are incorrectly labeled. In Fig. 3 all energy values should be increased by 2 MeV, and in Fig. 4 they should be increased by 10 MeV in the range up to 90 MeV. Furthermore, on p. 505, right column, second line from top, Refs. 11 and 22 should read Refs. 12 and 23.

## METHOD

REF. NO.

73 Ba 20

egf

REACTION	RESULT	EXCITATION ENERGY	SOURCE		DETECTOR		ANGLE
			TYPE	RANGE	TYPE	RANGE	
G,N	NOX	THR- 27	C	10- 27	BF3-I		4PI

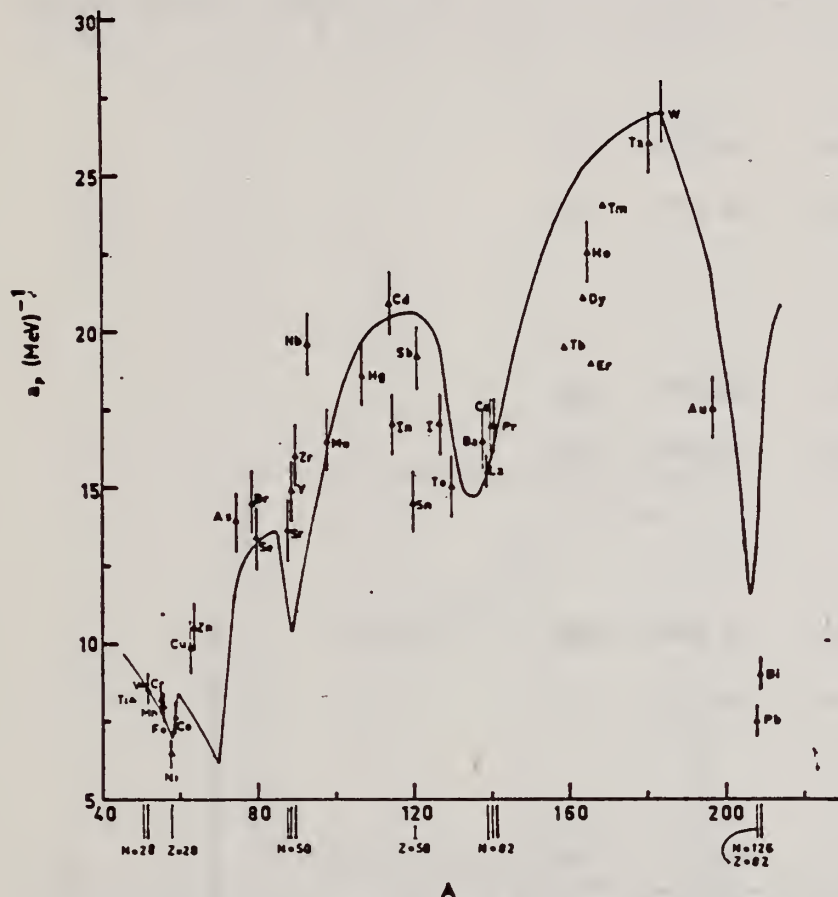


Fig. 12. Experimental values of the level density parameter  $a_p$  (Fermi gas formula plus pairing correction) versus atomic number  $A$ . The continuous curve is a least-squares fit to the data of a theoretical calculation from Newton <sup>15</sup>.

1  
H. Baba and S. Baba, Japan Atomic Energy Research Institute report JAERI-1183 (1969).

2  
H. Baba, Nucl. Phys. A159, 625 (1970).

15  
T.D. Newton, Can. J. Phys. 34, 804 (1956).

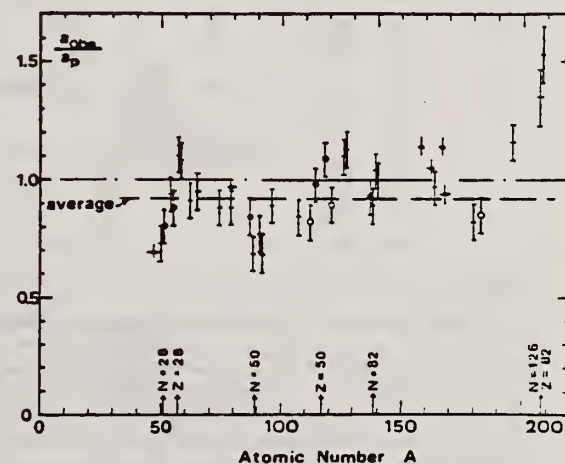


Fig. 15. Ratio  $a_{obs}/a_p$  versus atomic number  $A$ . Here  $a_{obs}$  is the level density parameter taken from the neutron resonance work of refs. <sup>1,2</sup>, and  $a_p$  is the level density parameter derived from the present  $(\gamma, n)$  work. Filled circles represent points where nuclei in the neutron resonance and in the  $(\gamma, n)$  experiment were the same. Open circles represent points where the respective nuclei were approximately matched. Triangles represent points which are based on measurement of neutron mean energies at two bremsstrahlung energies only.

(over)



TABLE 3 (continued)

Target	N (residual nucleus) <sup>a)</sup>	Goodness of fit <sup>b)</sup>		$\bar{E}_n(24)$ (MeV) <sup>c)</sup>	T (MeV) <sup>d)</sup>	$a_p$ (MeV <sup>-1</sup> ) <sup>e)</sup>	$a_{obs}$ (MeV <sup>-1</sup> ) <sup>f)</sup>	$a_{obs}/a_p$
		no p.c.	with p.c.					
Y	49 100%	G	G	1.30		14.9- <sup>88</sup> Y	10.17- <sup>90</sup> Y	0.68
Zr	49 52%	F	F	1.28		16.0- <sup>90</sup> Zr	12.2 - <sup>91</sup> Zr	0.77
	50 11%							
	51 17%							
	53 17%							
	55 3%							
Nb	51 100%	F	F	1.28		19.6- <sup>92</sup> Nb	13.15- <sup>94</sup> Nb	0.68
Mo	49 16%	G	G	1.27		16.5- <sup>93</sup> Mo	14.7 - <sup>97</sup> Mo	0.89
	51 9%							
	52 16%							
	53 17%							
	54 10%							
	55 24%							
	57 8%							
Ag	59 51%	V.P.	F	1.27	0.55	18.6- <sup>107</sup> Ag	15.61- <sup>108</sup> Ag	0.84
	61 49%							
Cd	57 1%	V.P.	F	1.24	0.54	20.9- <sup>111,4</sup> Cd	17.0 - <sup>112</sup> Cd	0.82
	61 12%							
	62 13%							
	63 24%							
	64 12%							
	65 29%							
	67 8%							
In	63 4%	V.P.	F	1.26	0.57	17.0- <sup>114</sup> In	16.66- <sup>114</sup> In	<u>0.98</u>
	65 96%							
Sn (Z = 50)	65 14%	V.P.	V.P.	1.38	0.73	14.5- <sup>118</sup> Sn	15.9 - <sup>118</sup> Sn	<u>1.09</u>
	66 8%							
	67 24%							
	68 9%							
	69 33%							
	71 5%							
	73 6%							
Sb	69 57%	V.P.	P	1.2	0.68	19.2- <sup>121</sup> Sb	17.0 - <sup>121</sup> Sb	<u>0.89</u>
	71 43%							
Te	69 2%	V.P.	F	1.36	0.83	15.0- <sup>127</sup> Te	17.0 - <sup>127</sup> Te	1.13
	71 5%							
	72 7%							
	73 19%							
	75 32%							
	77 34%							
I	73 100%	F	G	1.23	0.70	17.0- <sup>126</sup> I	17.02- <sup>126</sup> I	1.00

<sup>a)</sup> Neutron numbers and abundances of respective residual nuclei in ( $\gamma$ , n) experiments.

<sup>b)</sup> These give an assessment of the goodness of fit of a calculated  $\bar{E}_n$  versus  $E_0$  curve to the observed data, using the Fermi gas level density formula both without and with pairing corrections.

<sup>c)</sup> Bremsstrahlung photoneutron mean energies  $\bar{E}_n$  for peak bremsstrahlung energy  $E_0 = 24$  MeV.

<sup>d)</sup> Nuclear temperature from fit with constant-temperature formula.

<sup>e)</sup> Level density parameter  $a_p$  derived from the present ( $\gamma$ , n) experiment, using a Fermi gas formula plus pairing correction, and corresponding residual nucleus (the atomic weight shown is the weighted average of atomic weights of the respective isotopes present).

<sup>f)</sup> As column 7, but using data on n-resonance absorption from refs. <sup>1,2</sup>).

<sup>g)</sup> Measurements of  $\bar{E}_n(E_0)$  for these nuclei were made only for  $E_0 = 21, 23$  and 24 MeV.



REF.

K. Lindgren, G. G. Jonsson and B. Forkman  
PICNS-73, Vol.II, p.991 (1973) Asilomar

ELEM. SYM.

A

Z

Y

89

39

METHOD

REF. NO.

73 L1 3

egf

REACTION	RESULT	EXCITATION ENERGY	SOURCE		DETECTOR		ANGLE
			TYPE	RANGE	TYPE	RANGE	
G,G/	ABX	0-800	C	100-800	ACT-I		4PI

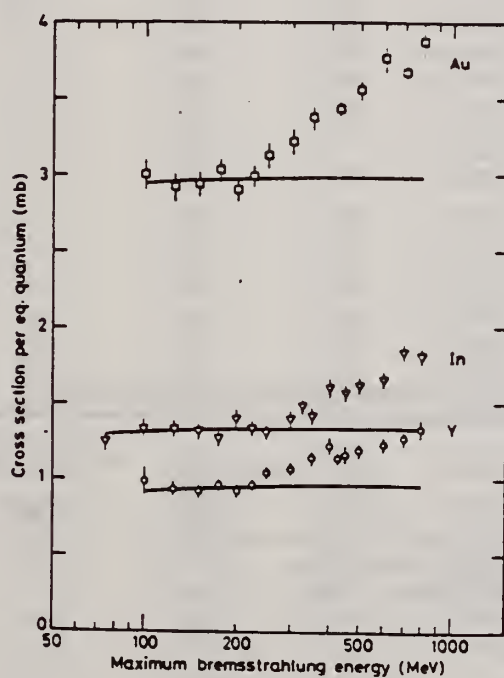


Fig. 1

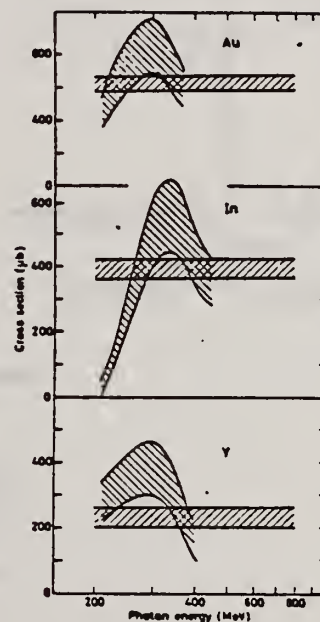


Fig. 2

REF.

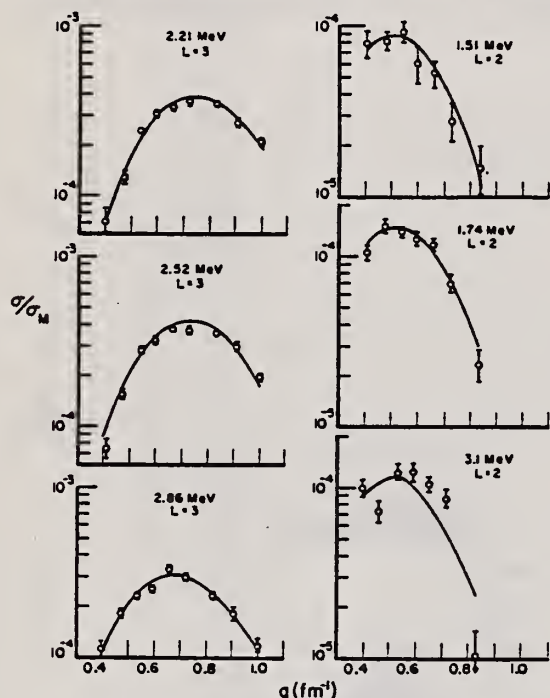
S. P. Fivozinsky, S. Penner, J.W. Lightbody, Jr., and D. Blum  
Phys. Rev. C9, 1533 (1974)

ELEM. SYM.	A	Z
Y	89	39
REF. NO.		
74F1 1		hmg

METHOD

REACTION	RESULT	EXCITATION ENERGY	SOURCE		DETECTOR		ANGLE
			TYPE	RANGE	TYPE	RANGE	
E, E/	FMF	1- 4	C	45-121	MAG-D		DST

6 LEVELS

Elastic scattering data for  $^{88}\text{Sr}$  and  $^{89}\text{Y}$ .FIG. 6. Tassie-model fits to  $^{89}\text{Y}$  form factors.TABLE V. Reduced transition probabilities  $[B(EL)]^\dagger$ .

Nucleus	Level	$B(EL)^\dagger$ (Tassie model)		Prediction of mixed model	
		$(e^2 \text{ fm}^{2L})$	Weisskopf units	$B(EL)^\dagger$ for $^{89}\text{Y}$ $3^-$ transitions $(e^2 \text{ fm}^6)$	Weisskopf units
$^{88}\text{Sr}$	$2^+, 1.84 \text{ MeV}$	$822.4 \pm 23.8$	$7.0 \pm 0.2$		
	$3^-, 2.74 \text{ MeV}$	$62\,034 \pm 4015$	$19.3 \pm 1.2$		
$^{89}\text{Y}$	$\frac{1}{2}^-, L=2, 1.51 \text{ MeV}$	$130.7 \pm 17.57$	$1.1 \pm 0.1$		
	$\frac{3}{2}^-, L=2, 1.74 \text{ MeV}$	$196.8 \pm 13.89$	$1.7 \pm 0.1$		
	$\frac{5}{2}^-, L=3, 2.21 \text{ MeV}$	$25\,777 \pm 2251$	$7.8 \pm 0.7$	$24\,836$	$7.5$
	$\frac{7}{2}^-, L=3, 2.52 \text{ MeV}$	$36\,603 \pm 2818$	$11.1 \pm 0.9$	$25\,764$	$7.8$
	$(\frac{5}{2}^-, \frac{1}{2}^+), L=3, 2.86 \text{ MeV}$	$50\,536 \pm 5000$	$15.3 \pm 1.5$	$30\,160$	$9.2$
	$(\frac{3}{2}^-, \frac{3}{2}^+), L=2, 3.1 \text{ MeV}$	$144.6 \pm 11.66$	$1.2 \pm 0.1$		

[over]

TABLE IV. Electron scattering form factors for  $^{89}\text{Y}$ .

Level	Incident energy (MeV)	Lab scattering angle (deg)	$q$ ( $\text{fm}^{-1}$ )	$ F ^2$	Standard deviation (%)
Ground state $\frac{1}{2}^+$	120.85	110.5	1.005	$0.6027 \times 10^{-2}$	0.9
	100.87	128.2	0.919	$0.8147 \times 10^{-2}$	1.0
	101.17	110.5	0.842	$0.6544 \times 10^{-2}$	0.8
	80.86	128.2	0.737	$0.9522 \times 10^{-2}$	1.1
	80.95	110.5	0.674	$0.1802 \times 10^{-1}$	0.4
	67.07	128.2	0.611	$0.3496 \times 10^{-1}$	0.5
	60.48	128.3	0.551	$0.8321 \times 10^{-1}$	0.5
	53.46	128.3	0.487	0.1641	0.4
	45.42	128.3	0.414	0.3258	0.3
1.51 MeV					
$L=2$ $\frac{3}{2}^-$	120.85	110.5	...	...	...
	100.87	128.2	...	...	...
	101.17	110.5	0.836	$0.1463 \times 10^{-4}$	37.5
	80.86	128.2	0.730	$0.2769 \times 10^{-4}$	39.0
	80.95	110.5	0.667	$0.5404 \times 10^{-4}$	18.6
	67.07	128.2	0.604	$0.6197 \times 10^{-4}$	24.1
	60.48	128.3	0.544	$0.9577 \times 10^{-4}$	13.5
	53.46	128.3	0.480	$0.8497 \times 10^{-4}$	12.4
	45.42	128.3	0.407	$0.8282 \times 10^{-4}$	17.4
1.74 MeV					
$L=2$ $\frac{3}{2}^-$	120.85	110.5	...	...	...
	100.87	128.2	...	...	...
	101.17	110.5	0.835	$0.2266 \times 10^{-4}$	20.8
	80.86	128.2	0.729	$0.6865 \times 10^{-4}$	18.3
	80.95	110.5	0.666	$0.1193 \times 10^{-3}$	8.5
	67.07	128.2	0.603	$0.1301 \times 10^{-3}$	10.5
	60.48	128.3	0.543	$0.1427 \times 10^{-3}$	7.2
	53.46	128.3	0.479	$0.1548 \times 10^{-3}$	8.0
	45.42	128.3	0.406	$0.1105 \times 10^{-3}$	11.6
2.21 MeV					
$L=3$ $\frac{5}{2}^+$	120.85	110.5	0.996	$0.1969 \times 10^{-3}$	4.5
	100.87	128.2	0.909	$0.2645 \times 10^{-3}$	7.8
	101.17	110.5	0.833	$0.3397 \times 10^{-3}$	2.9
	80.86	128.2	0.727	$0.3584 \times 10^{-3}$	5.1
	80.95	110.5	0.664	$0.3334 \times 10^{-3}$	3.4
	67.07	128.2	0.601	$0.3048 \times 10^{-3}$	5.7
	60.48	128.3	0.541	$0.2478 \times 10^{-3}$	5.0
	53.46	128.3	0.477	$0.1328 \times 10^{-3}$	6.5
	45.42	128.3	0.404	$0.7320 \times 10^{-4}$	15.5
2.52 MeV					
$L=3$ $\frac{5}{2}^+$	120.85	110.5	0.995	$0.1883 \times 10^{-3}$	4.8
	100.87	128.2	0.907	$0.2926 \times 10^{-3}$	7.3
	101.17	110.5	0.831	$0.3498 \times 10^{-3}$	2.8
	80.86	128.2	0.725	$0.3711 \times 10^{-3}$	4.5
	80.95	110.5	0.663	$0.3793 \times 10^{-3}$	3.0
	67.07	128.2	0.600	$0.3286 \times 10^{-3}$	5.1
	60.48	128.3	0.540	$0.2918 \times 10^{-3}$	2.9
	53.46	128.3	0.476	$0.1593 \times 10^{-3}$	7.2
	45.42	128.3	0.402	$0.7639 \times 10^{-4}$	12.9
2.86 MeV					
$L=3$ $(\frac{5}{2}^+, \frac{7}{2}^+)$	120.85	110.5	0.994	$0.1158 \times 10^{-3}$	7.7
	100.87	128.2	0.906	$0.1772 \times 10^{-3}$	9.6
	101.17	110.5	0.830	$0.2310 \times 10^{-3}$	4.1
	80.86	128.2	0.724	$0.2997 \times 10^{-3}$	5.4
	80.95	110.5	0.662	$0.3339 \times 10^{-3}$	3.6
	67.07	128.2	0.598	$0.2550 \times 10^{-3}$	5.0
	60.48	128.3	0.538	$0.2357 \times 10^{-3}$	4.5
	53.46	128.3	0.474	$0.1861 \times 10^{-3}$	5.2
	45.42	128.3	0.401	$0.1158 \times 10^{-3}$	8.9
3.1 MeV					
$L=2$ $(\frac{3}{2}^-, \frac{5}{2}^-)$	120.85	110.5	...	...	...
	100.87	128.2	...	...	...
	101.17	110.5	0.829	$0.1007 \times 10^{-4}$	38.1
	80.86	128.2	0.722	$0.8593 \times 10^{-4}$	12.8
	80.95	110.5	0.661	$0.1056 \times 10^{-3}$	9.0
	67.07	128.2	0.597	$0.1260 \times 10^{-3}$	11.2
	60.48	128.3	0.537	$0.1256 \times 10^{-3}$	8.9
	53.46	128.3	0.473	$0.6261 \times 10^{-4}$	15.2
	45.42	128.3	0.400	$0.1038 \times 10^{-3}$	11.1



REACTION	RESULT	EXCITATION ENERGY	SOURCE		DETECTOR		ANGLE
			TYPE	RANGE	TYPE	RANGE	
E, p	ABX	10- 24	D	10- 30	MAG-D		90

(u, c'p)

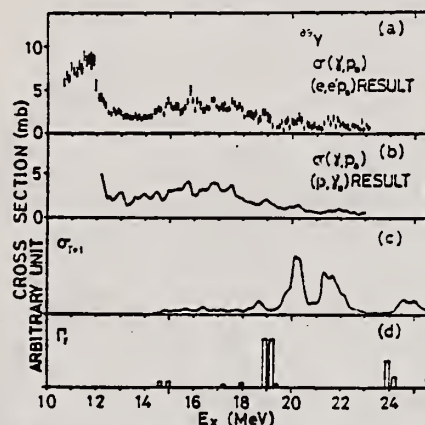


Fig. 12. Comparison of photoproton cross sections of  $^{89}\text{Y}$ . (a) Present result. (b) Ref. 7). (c), (d) Theoretical estimates, refs. 13, 16) respectively.

TABLE 5

The radiative width of the narrow E1 IAR obtained from the proton group in the proton spectra

Nucleus	$E_x$ (MeV)	$E_p$ (MeV)	$E_{R1}(J^\pi)$ (MeV)	$\Gamma_\gamma \frac{\Gamma_{p1}^*}{\Gamma}$ (eV)	$\Gamma_\gamma^*$ (eV)	$2(T+1) \frac{\Gamma_\gamma^*}{\Gamma_w}$	$2(T+1) \frac{\Gamma_\gamma^*}{\Gamma_{n.p.}}$	(p, $\gamma_0$ ) data $\Gamma_\gamma$ (eV)
$^{90}\text{Zr}$	14.5	6.0	$0^-(\frac{1}{2}^-)$	26	26 <sup>b)</sup>	0.076		$> 30^a)$
	16.3	7.9	$0^-(\frac{1}{2}^-)$	74	126 <sup>c)</sup>	0.26		$> 60^a)$
	16.3	6.3	$1.51(\frac{3}{2}^-)$	52				
$^{89}\text{Y}$	13.0 <sup>d)</sup>	5.9	$0(0^+)$	13	13 <sup>b)</sup>		0.13 <sup>f)</sup>	$18 \pm 3^b)$
	14.5 <sup>e)</sup>	7.3	$0(0^+)$	16	16 <sup>b)</sup>		0.14 <sup>f)</sup>	$11 \pm 2^b)$
	15.9 <sup>e)</sup>	8.7	$0(0^+)$	42	42 <sup>b)</sup>		0.68 <sup>f)</sup>	$40 \pm 8^b)$
$^{88}\text{Sr}$	17.1	6.5	$0(\frac{3}{2}^-)$	9.5	14 <sup>c)</sup>	0.029		
	17.1	5.6	$0.85((\frac{1}{2}^-))$	4.9				
	17.3	6.7	$0(\frac{3}{2}^-)$	30	48 <sup>c)</sup>	0.094		
	17.3	5.9	$0.85((\frac{1}{2}^-))$	18				

The available data with the (p,  $\gamma_0$ ) experiment are shown in the last column.

<sup>a)</sup> The errors may be  $\approx 30\%$  (for  $^{90}\text{Zr}$ ,  $^{88}\text{Sr}$ ) and  $\approx 50\%$  (for  $^{89}\text{Y}$ ) including the uncertainty of the process to separate the proton group.

<sup>b)</sup>  $\Gamma_{p0}/\Gamma = 1$  was assumed.

<sup>c)</sup>  $(\Gamma_{p0} + \Gamma_{p2})/\Gamma = 1$  was assumed.

<sup>d)</sup>  $J^\pi = \frac{1}{2}^+$  was assigned as shown in table 3.

<sup>e)</sup>  $J^\pi = \frac{3}{2}^+$  was assigned as shown in table 3.

<sup>f)</sup> Correction was made for the spectroscopic factors on the ground state and the excited state with the data of the ( $\text{He}^3$ , d) and (d, p) reactions respectively.

<sup>g)</sup> Ref. 27).

<sup>h)</sup> Ref. 6).

(over)

- <sup>6</sup>P. Paul, Proc. nuclear structure studies using electron scattering and photoreaction, ed. K. Shoda and H. Ui (Research report of Lab. Nucl. Sci. Tohoku Univ. 5, 1972) p.343.
- <sup>7</sup>P. Paul, Proc. Int. Conf. on photonuclear reactions and applications, ed. B.L. Berman (Lawrence Livermore Laboratory Univ. of California, 1973)p.407.
- <sup>13</sup>T.A. Hughes et al., Phys. Rev. C3 (1971) 1950.
- <sup>16</sup>J.D. Vergados et al., Nucl. Phys. A168 (1971) 225.
- <sup>27</sup>J.L. Black et al., Nucl. Phys. A92 (1967) 365.



R.R. Whitney, I. Sick, J.R. Ficanec, R.D. Kephart, and  
 REF. W.P. Trower  
 Phys. Rev. C9, 2230 (1974)

ELEM. SYM.	A	Z
Y	89	39
REF. NO.		74 Wh 3
		hmg

METHOD			SOURCE		DETECTOR		ANGLE
REACTION	RESULT	EXCITATION ENERGY	TYPE	RANGE	TYPE	RANGE	
E, E/	ABX	0-300	D	500	MAG-D		60

See further analysis of this data in reference 79Z11

# QUASIELASTIC SCAT

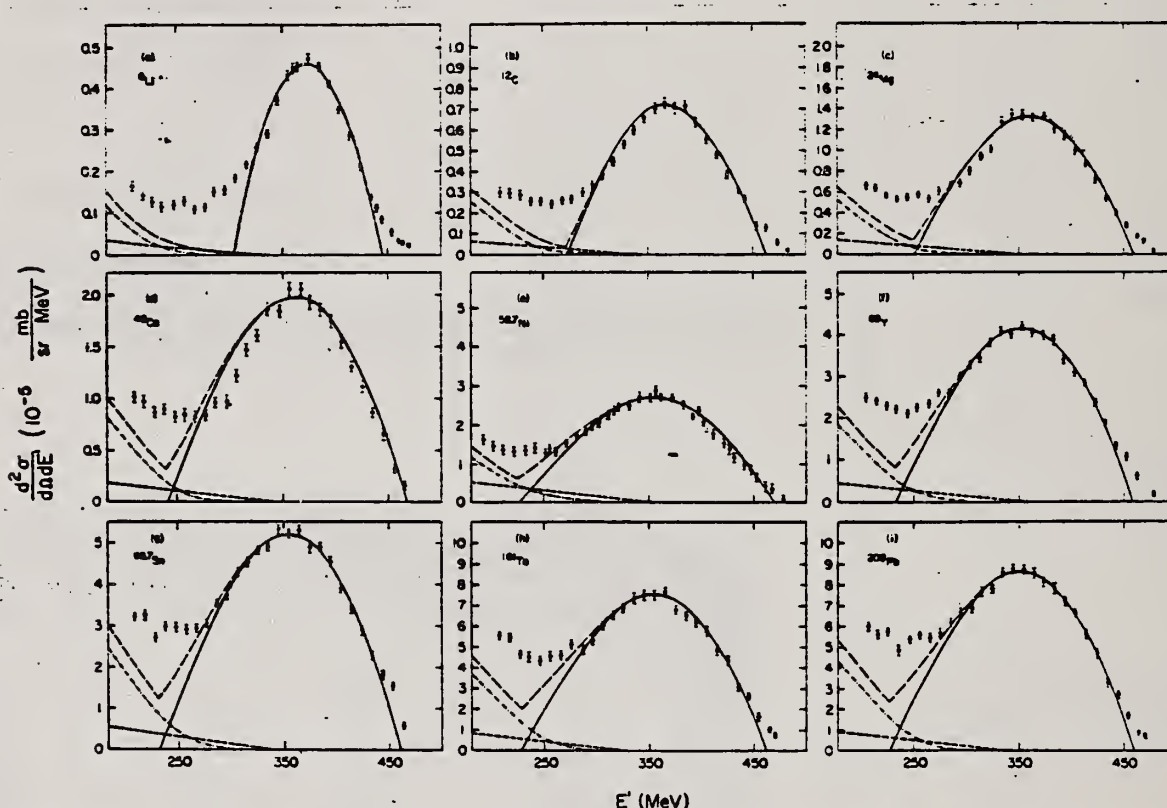


FIG. 1. The measured quasielastic peaks; the errors on the data points do not include an over-all 3% normalization uncertainty. The solid curve is a fit by the Fermi-gas model which yielded  $k_F$  (in MeV/c) and  $\bar{\epsilon}$  (in MeV) as follows: (a)  ${}^6\text{Li}$  (169, 17); (b)  ${}^{12}\text{C}$  (221, 25); (c)  ${}^{24}\text{Mg}$  (235, 32); (d)  ${}^{40}\text{Ca}$  (249, 33); (e)  ${}^{58}\text{Ni}$  (260, 36); (f)  ${}^{89}\text{Y}$  (254, 39); (g)  ${}^{118.7}\text{Sm}$  (260, 42); (h)  ${}^{181}\text{Ta}$  (265, 42); (i)  ${}^{208}\text{Pb}$  (265, 44). The fitting uncertainty in  $k_F$  is  $\pm 5$  MeV/c and in  $\bar{\epsilon}$  it is  $\pm 3$  MeV. The small-amplitude dashed curve is the s-wave  $\pi$ -production contribution, the dot-dashed curve is the isobar excitation, and the large-amplitude dashed curve is the total result.

(over)

TABLE I. Proton-normalized and radiative-corrected cross sections  $d^2\sigma/d\Omega dE' = (N \pm \Delta N) \times 10^{-34}$  in mb/er MeV, for  $E = 500$  MeV and  $\theta = 60^\circ$ .

$E'$ (MeV)	$^6\text{Li}$			$^{12}\text{C}$			$^{24}\text{Mg}$			$^{40}\text{Ca}$			$^{58}\text{Ni}$			$^{89}\text{Y}$			$^{133}\text{Ba}$			$^{159}\text{Tb}$			$^{208}\text{Pb}$		
	N	$\Delta N$	n	N	$\Delta N$	n	N	$\Delta N$	n	N	$\Delta N$	n	N	$\Delta N$	n	N	$\Delta N$	n	N	$\Delta N$	n	N	$\Delta N$	n	N	$\Delta N$	n
480.0	...	...	...	1.79	0.19	7	3.83	0.32	7	...	...	...	1.22	0.17	6	1.71	0.19	6	...	...	...	...	...	...	...	...	...
474.0	...	...	...	1.02	0.13	7	...	...	...	...	...	...	...	...	...	...	...	...	...	...	...	...	...	...	...	...	...
470.0	1.72	0.18	7	5.75	0.52	7	1.55	0.15	6	...	...	...	3.90	0.29	6	5.65	0.41	6	...	...	...	...	...	...	...	...	...
464.0	2.49	0.29	7	1.38	0.11	6	1.91	0.17	6	2.72	0.15	6	4.48	0.33	6	5.68	0.37	6	6.32	0.71	6	1.16	0.06	5	9.82	0.79	6
460.0	2.96	0.30	7	1.20	0.09	6	2.58	0.19	6	...	...	...	...	...	...	...	...	...	...	...	...	1.54	0.10	5	1.81	0.10	5
454.1	5.02	0.47	7	9.21	0.71	7	2.96	0.20	6	4.20	0.17	6	7.00	0.41	6	1.07	0.05	5	1.85	0.09	5	1.70	0.11	5	2.31	0.11	5
450.0	...	...	...	...	...	...	...	...	...	...	...	...	6.92	0.47	6	1.03	0.05	5	1.63	0.09	5	...	...	...	...	...	...
444.3	8.68	0.58	7	1.20	0.07	6	4.11	0.25	6	6.87	0.27	6	1.02	0.05	5	1.33	0.05	5	...	...	...	2.77	0.14	5	2.74	0.12	5
440.0	1.11	0.06	6	2.59	0.13	6	5.23	0.26	6	...	...	...	...	...	...	...	...	...	...	...	...	3.43	0.16	5	3.24	0.13	5
434.2	1.32	0.06	6	2.99	0.14	6	5.50	0.26	6	8.74	0.35	6	...	...	...	...	...	...	...	...	...	3.14	0.15	5	3.34	0.14	5
430.0	...	...	...	...	...	...	...	...	...	...	...	...	1.19	0.05	5	1.90	0.07	5	2.27	0.09	5	...	...	...	...	...	...
424.3	2.12	0.08	6	3.75	0.15	6	7.31	0.29	6	1.12	0.04	5	1.54	0.08	5	2.31	0.09	5	2.66	0.12	5	...	...	...	...	...	...
414.4	2.88	0.12	6	4.75	0.19	6	8.78	0.35	6	1.32	0.05	5	1.76	0.10	5	2.88	0.11	5	3.40	0.14	5	4.43	0.18	5	4.74	0.19	5
404.5	3.51	0.14	6	5.46	0.22	6	1.02	0.04	5	1.56	0.06	5	2.09	0.08	5	3.39	0.12	5	3.90	0.17	5	4.98	0.20	5	5.64	0.23	5
400.0	...	...	...	6.25	0.25	6	1.09	0.04	5	...	...	...	2.35	0.09	5	3.34	0.13	5	4.29	0.17	5	5.89	0.24	5	6.57	0.26	5
394.7	4.16	0.17	6	6.32	0.26	6	1.15	0.05	5	1.75	0.07	5	2.22	0.09	5	3.41	0.14	5	4.56	0.18	5	6.29	0.25	5	7.25	0.29	5
385.7	4.55	0.18	6	7.09	0.28	6	1.21	0.05	5	1.86	0.07	5	2.51	0.10	5	3.91	0.16	5	4.88	0.19	5	6.36	0.26	5	7.88	0.32	5
374.9	4.76	0.19	6	6.97	0.28	6	1.33	0.05	5	1.94	0.08	5	2.72	0.11	5	4.02	0.16	5	4.88	0.19	5	6.67	0.26	5	8.19	0.33	5
365.0	4.56	0.18	6	7.28	0.29	6	1.32	0.05	5	2.08	0.08	5	2.69	0.10	5	4.04	0.16	5	5.34	0.21	5	7.77	0.31	5	6.61	0.34	5
360.0	4.50	0.18	6	6.61	0.28	6	1.32	0.05	5	...	...	...	2.88	0.11	5	4.11	0.16	5	5.69	0.23	5	7.92	0.33	5	6.42	0.34	5
355.2	4.35	0.17	6	6.97	0.28	6	1.36	0.05	5	2.08	0.08	5	2.69	0.11	5	4.23	0.17	5	5.22	0.21	5	7.51	0.30	5	...	...	...
345.3	3.68	0.15	6	6.54	0.20	6	1.35	0.05	5	1.85	0.07	5	2.72	0.11	5	4.02	0.16	5	5.37	0.21	5	7.59	0.30	5	8.63	0.35	5
335.4	2.90	0.12	6	5.91	0.24	6	1.29	0.05	5	1.87	0.08	5	2.46	0.10	5	4.08	0.16	5	4.92	0.19	5	7.44	0.29	5	8.66	0.35	5
325.5	2.59	0.10	6	5.23	0.21	6	1.05	0.04	5	1.61	0.07	5	2.46	0.11	5	3.78	0.15	5	4.63	0.19	5	6.93	0.26	5	7.61	0.31	5
320.0	...	...	...	...	...	...	...	...	...	...	...	...	2.35	0.09	5	3.34	0.14	5	4.53	0.18	5	...	...	...	...	...	...
315.7	2.16	0.10	6	4.43	0.18	6	9.41	0.38	6	1.47	0.06	5	2.26	0.09	5	3.43	0.14	5	4.34	0.17	5	6.61	0.26	5	7.76	0.31	5
305.8	1.84	0.09	6	3.79	0.15	6	8.61	0.32	6	1.23	0.05	5	2.03	0.06	5	3.27	0.13	5	4.32	0.17	5	6.11	0.24	5	6.92	0.28	5
300.0	...	...	...	...	...	...	...	...	...	...	...	...	1.97	0.08	5	3.11	0.12	5	4.03	0.16	5	...	...	...	...	...	...
295.9	1.55	0.09	6	3.38	0.14	6	6.77	0.29	6	9.97	0.40	6	1.80	0.07	5	3.02	0.12	5	3.74	0.15	5	5.38	0.22	5	6.73	0.27	5
285.9	1.50	0.09	6	2.96	0.14	6	6.64	0.31	6	9.73	0.39	6	1.72	0.07	5	2.60	0.13	5	3.55	0.15	5	4.92	0.23	5	6.30	0.29	5
276.2	1.14	0.08	6	2.64	0.13	6	6.03	0.32	6	8.35	0.41	6	1.50	0.07	5	2.64	0.13	5	3.10	0.15	5	5.22	0.24	5	5.73	0.30	5
266.3	1.08	0.08	0	2.61	0.14	6	5.32	0.33	6	8.57	0.43	6	1.31	0.08	5	2.37	0.14	5	2.72	0.16	5	4.62	0.26	5	5.51	0.31	5
260.0	...	...	...	...	...	...	...	...	...	...	...	...	1.39	0.08	5	1.95	0.13	5	2.94	0.18	5	...	...	...	...	...	...
256.4	1.28	0.09	6	2.43	0.15	6	5.71	0.35	6	8.33	0.45	6	1.27	0.06	5	2.27	0.14	5	2.67	0.16	5	4.57	0.26	5	5.63	0.33	5
246.6	1.20	0.09	6	2.55	0.16	6	5.47	0.36	6	8.56	0.48	6	1.30	0.09	5	2.14	0.14	5	2.95	0.19	5	4.33	0.26	5	5.40	0.35	5
236.7	1.15	0.10	6	2.54	0.16	6	5.18	0.38	6	8.71	0.51	6	1.31	0.09	5	2.24	0.15	5	3.02	0.20	5	4.35	0.30	5	4.90	0.34	5
226.8	1.27	0.11	6	2.86	0.19	6	5.62	0.42	6	8.72	0.51	6	1.29	0.10	5	2.29	0.16	5	2.73	0.20	5	4.57	0.30	5	5.88	0.37	5
210.9	1.43	0.14	6	2.94	0.21	6	6.35	0.49	6	9.61	0.56	6	1.34	0.10	5	2.38	0.17	5	3.26	0.22	5	5.42	0.36	5	5.76	0.36	5
207.0	1.60	0.16	6	2.94	0.21	6	6.59	0.52	6	1.02	0.06	5	1.43	0.11	5	2.51	0.18	5	3.24	0.22	5	5.56	0.37	5	6.11	0.40	5
197.2	1.78	0.17	6	3.42	0.24	6	7.01	0.59	6	...	...	...	1.59	0.12	5	2.77	0.20	5	3.43	0.24	5	5.67	0.38	5	5.99	0.41	5

REF. K. Shoda, H. Miyase, M. Sugawara, T. Saito, S. Oikawa,  
A. Suzuki, J. Uegaki  
Nucl. Phys. A239, 397 (1975)

ELEM. SYM.	A	Z
Y	89	39
REF. NO.		
75 Sh 4		egf

METHOD

REACTION	RESULT	EXCITATION ENERGY	SOURCE		DETECTOR		ANGLE
			TYPE	RANGE	TYPE	RANGE	
E, P	ABX	15- 24	D	14- 25	MAG-D		90

E1 virtual photon spectrum used to obtain ( $\gamma$ , p) cross sections.

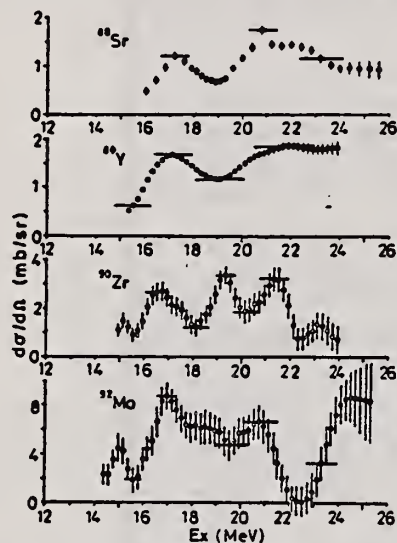


Fig. 3. Differential ( $\gamma$ , p) cross sections at  $\theta = 90^\circ$  analysed from (e, e'p) cross sections by the least-structure method.

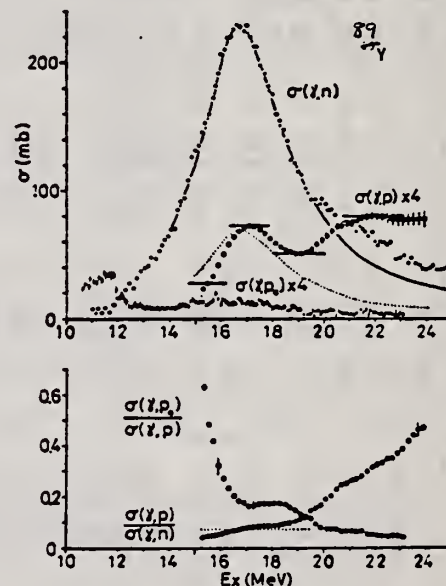


Fig. 6. The caption is the same as in fig. 5.

Fig. 5. Upper figure: open circles,  $\sigma(\gamma, p)$ ; closed circles,  $\sigma(\gamma, n)$  [ref. <sup>18</sup>]; closed points,  $\sigma(\gamma, p_0)$  [ref. <sup>15</sup>]; solid line, Lorentz line fit to the  $T_{<}$  region of  $\sigma(\gamma, n)$  [ref. <sup>18</sup>]; dotted line, Lorentz line fit to the  $T_{<}$  region of  $\sigma(\gamma, p)$  with  $T_i$  and  $E_k$  equal to those of  $\sigma(\gamma, n)$ . Lower figure: ratio between cross sections. Dotted line: constant for  $\sigma(\gamma, p)/\sigma(\gamma, n)$  determined around  $T_{<}$  GDR.

15 K. Shoda et al., Nucl.  
Phys. A221 (1974) 125  
18 A. Lepretre et al., Nucl.  
Phys. A175 (1971) 609



REF. H. Bartsch, K. Huber, U. Kneissl, H. Krieger  
Nucl. Phys. A256, 243 (1976)

ELEM. SYM.	A	Z
Y	89	39

METHOD

REF. NO.	
76 Ba 1	egf

REACTION	RESULT	EXCITATION ENERGY	SOURCE		DETECTOR		ANGLE
			TYPE	RANGE	TYPE	RANGE	
G,N	RLY	THR-UKN	C	UKN	SCD-D		4PI

ISOMER RATIO

TABLE I  
Experimental and theoretical results

Process	Target-spin	$E_{\gamma}$ (keV)	$T_{1/2}$	Spin high	Spin low	$R_{exp} = \frac{\sigma_{high}}{\sigma_{low}}$	SCOP (A)
$^{181}\text{Ta}(\gamma, 3n)$	$\frac{1}{2}^+$	93	2.2 h 9.31 min 8.15 h	$7^-$	$1^+$	$0.51 \pm 0.09$	$3.6 \pm 0.2$
$^{142}\text{Nd}(\gamma, n)$	$0^+$	755 1100-1300, 145	63 s 2.5 h	$\frac{1}{2}^-$	$\frac{3}{2}^+$	$0.055 \pm 0.006$ $0.19 \pm 0.01^*)$	$2.20 \pm 0.06$
$^{92}\text{Mo}(\gamma, n)$	$0^+$	652.9 1208, 1508, 1581, 1637	66 s 15.49 min	$\frac{1}{2}^+$	$\frac{1}{2}^-$	$1.03 \pm 0.21$ $0.85 \pm 0.07^*)$ $1.92 \pm 0.15^*)$	$5.03 \pm 0.75$ $4 \pm \frac{1}{2}$
$^{100}\text{Mo}(\gamma, n)$	$0^+$	97.3 140.5	16.8 $\mu\text{s}$ 66.02 h	$\frac{1}{2}^+$	$\frac{1}{2}^+$	$0.85 \pm 0.24$	$1.72 \pm 0.25$
$^{100}\text{Pd}(\gamma, n)$	$0^+$	214.5 115	22 s 850 ns	$\frac{1}{2}^-$	$\frac{1}{2}^+$	$0.5 \pm 0.2$	$3.4 \pm 0.5$
$^{110}\text{Pd}(\gamma, n)$	$0^+$	188 113 87.7	4.7 min 390 ns 13.47 h	$\frac{1}{2}^-$ $\frac{1}{2}^-$ $\frac{1}{2}^+$	$\frac{1}{2}^+$ $\frac{1}{2}^+$ $\frac{1}{2}^+$	$0.11 \pm 0.02$ $0.41 \pm 0.09$ $3.2 \pm 0.7$	$3.14 \pm 0.15$ $3.0 \pm 0.25$ $3.3 \pm 0.4$
$^{89}\text{Y}(\gamma, n)$	$\frac{1}{2}^-$	231.7 442.3 392.5	14.2 ms 300 $\mu\text{s}$	$8^+$	$1^+$	$0.056 \pm 0.008$	

<sup>a)</sup> Ref. <sup>14)</sup>. <sup>b)</sup> Ref. <sup>15)</sup>.

<sup>14</sup> P.E. Haustein et al., J. Inorg. Nucl. Chem. 33, 289 (1971)

<sup>15</sup> J. H. Carver et al., Nucl. Phys. 37, 449 (1962)

ELEM. SYM.	A	Z
Y	89	39
REF. NO.	77 Pi 1	
	hmg	

METHOD			REF. NO.		
REACTION	RESULT	EXCITATION ENERGY	SOURCE TYPE	DETECTOR RANGE	ANGLE
E <sub>0</sub> E/	ABX	2- 55	C	93	MAG-D
				(92.5)	

NUCLEAR REACTIONS  $^{89}\text{Y}(e,e')$ ,  $E_0=92.5\text{ MeV}$ . Measured  $d^2\sigma/d\Omega dE_{e'}$ , bound and continuum states. Deduced multipolarity  $\lambda$ , reduced matrix element  $B(E\lambda)$ , radiative width  $\Gamma^0_\gamma$ , sum rule exhaustion, single particle strength, and total width of the continuum and clustered states.

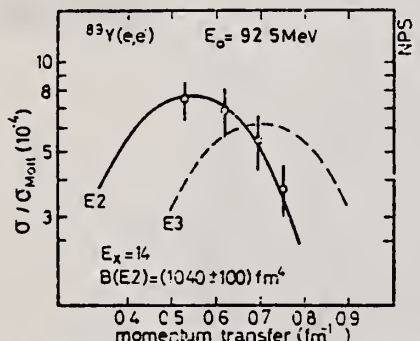


FIG. 8. Relative DWBA cross section, calculated using the Goldhaber-Teller model, as fitted to the experimental cross sections for the resonance at 14 MeV with a width of  $\Gamma=4.5\text{ MeV}$ . The comparison rules out any assignment other than E2.

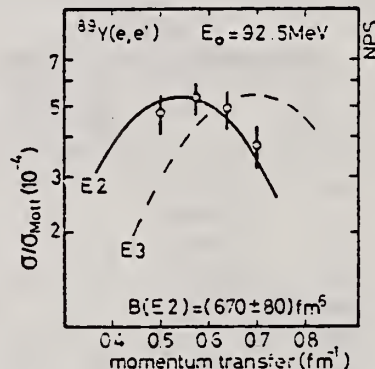


FIG. 9. Relative DWBA cross section using the Goldhaber-Teller model as compared with the resonance at 28 MeV assuming a width of  $\Gamma=9\text{ MeV}$ . The comparison shows that the cross section in this region is predominantly E2 with the possibility of some E3 contribution.

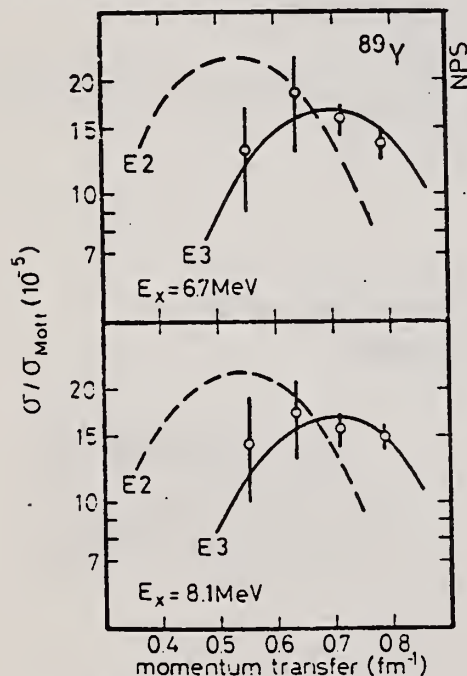


FIG. 10. Relative DWBA cross section using the Goldhaber-Teller model as compared with the cluster of states concentrated around 7 and 9 MeV. The comparison favors an E3 assignment for these states. The large error at the lower momentum transfer is due to the subtraction of the ghost peak.

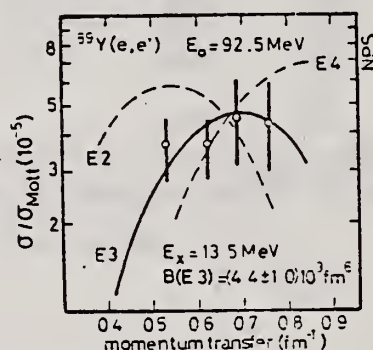


FIG. 11. Relative DWBA cross section calculated with the Goldhaber-Teller model for the structure at 13.5 MeV with a width of 1.2 MeV. Comparison with experiment favors an E3 assignment. M2 assignment would be possible, too, but was not considered seriously possible, due to the great M2 strength necessary to explain the data.

[over]



TABLE I. Comparison of some results for the  $E1$  (GDR) resonance in  $N=50$  nuclei.

Ref.	$E_0$ (MeV)	$\Gamma$ (MeV)	$R$ (%) <sup>a</sup>	Method	Nucleus
22	16.79	$3.95 \pm 0.06$	$87 \pm 6$	( $\gamma, n$ )	<sup>83</sup> Y
23	16.74	$4.1 \pm 0.1$	$111 \pm 5$	( $\gamma, n$ )	<sup>83</sup> Y
5	16.65	4.0	$107 \pm 32$	( $e, e'$ )	<sup>90</sup> Zr
9	... <sup>b</sup>	4.0	$113 \pm 25$	( $e, e'$ )	<sup>90</sup> Zr
This work	16.6	$3.9 \pm 0.2$	$104 \pm 10$	( $e, e'$ )	<sup>83</sup> Y

$$^a R = E_0 B(E1) / \text{EWSR}(E1, \Delta T=1) \times 100.$$

<sup>b</sup>The authors used the ( $\gamma, n$ ) value.

<sup>22</sup>S. Fukuda and Y. Torizuka, Phys. Rev. Lett. **29**, 1109 (1972).

<sup>23</sup>S. Fukuda and Y. Torizuka, Phys. Lett. **62B**, 146 (1976).

<sup>5</sup>B. L. Berman, J. T. Caldwell, R. R. Harvey, M. A. Kelly, R. L. Bramblett, and S. C. Fultz, Phys. Rev. **162**, 1099 (1967).

<sup>9</sup>A. Leprêtre, H. Beil, R. Bergère, P. Carlos, A. Veyssié, and M. Sugawara, Nucl. Phys. **A175**, 609 (1971).

TABLE II. Compilation of some results for the  $E2$  ( $\Delta T=0$ ) resonance in  $N=50$  nuclei.

Ref.	$E_0$ (MeV)	$\Gamma$ (MeV)	$R$ (%) <sup>a</sup>	Method	Nucleus
5	14	$4.8 \pm 0.6$	$56 \pm 17$	( $e, e'$ )	<sup>90</sup> Zr
6	$14.5 \pm 0.3$	$4.0 \pm 0.2$	$54 \pm 15$	( $\alpha, \alpha'$ )	<sup>90</sup> Zr
8	14 <sup>b</sup>	4.5 <sup>b</sup>	84	( $e, e'$ )	<sup>90</sup> Zr
40	$13.8 \pm 0.2$	3.2	$24 \pm 5$	( $p, p'$ )	<sup>83</sup> Y
This work	$14.0 \pm 0.2$	$4.5 \pm 0.4$	$56 \pm 6$ <sup>c</sup>	( $e, e'$ )	<sup>83</sup> Y

$$^a R = E_0 B(E2) / \text{EWSR}(\Delta T=0, E2) \times 100.$$

<sup>b</sup>Values were taken from Ref. 41.

<sup>c</sup>The rms radius  $R=4.27$  fm of Ref. 13 was used for calculating the sum rule yielding an EWSR ( $E2, \Delta T=0$ ) of 25 800 MeV fm<sup>4</sup>.

<sup>5</sup>S. Fukuda and Y. Torizuka, Phys. Rev. Lett. **29**, 1109 (1972).

<sup>6</sup>D. H. Youngblood, J. M. Moss, C. M. Rozsa, J. D. Bronson, A. D. Bacher, and D. R. Brown, Phys. Rev. **C 13**, 994 (1976).

<sup>40</sup>S. Fukuda and Y. Torizuka, Phys. Lett. **62B**, 146 (1976).

<sup>40</sup>N. Marty, M. Morlet, A. Willis, Y. Comparat, and R. Frascaria, Nucl. Phys. **A238**, 93 (1975).

TABLE III. Compilation of results for the  $E2$  ( $\Delta T=1$ ) resonance in some  $N=50$  nuclei.

Ref.	$E_0$ (MeV)	$\Gamma$ (MeV)	$R$ (%) <sup>a</sup>	Method	Nucleus
5	27	...	23	( $e, e'$ )	<sup>90</sup> Zr
8	26	7	73	( $e, e'$ )	<sup>90</sup> Zr
43	...	...	$\approx 40$ <sup>b</sup>	( $p, \gamma$ )	<sup>90</sup> Zr
This work	$28.0 \pm 0.5$	10	$82 \pm 10$	( $e, e'$ )	<sup>83</sup> Y
		8	$57 \pm 6$		
		7	$48 \pm 5$		

<sup>a</sup> $R = E_0 B(E2) / \text{EWSR}(\Delta T=1, E2) \times 100$ . The  $\Delta T=1$  sum rule is connected with that of Table II by a factor of  $N/Z$ .

<sup>b</sup>The value for the sum rule percentage depends on the coupling used for the model.

<sup>5</sup>S. Fukuda and Y. Torizuka, Phys. Rev. Lett. **29**, 1109 (1972).

<sup>8</sup>S. Fukuda and Y. Torizuka, Phys. Lett. **62B**, 146 (1976).

<sup>43</sup>F. S. Dietrich, D. W. Heikkinen, K. A. Snover, and K. Ebisawa, Phys. Rev. Lett. **39**, 156 (1977).

TABLE VI. Compilation of all the results from this experiment.

$E_x$ (MeV)	$E_x$ ( $A^{-1/3}$ MeV)	$\Gamma$ (MeV) <sup>a</sup>	$B$ (fm <sup>2</sup> )	$R$ (%) <sup>b</sup>	$\Gamma_1^2$ (eV)	spu	$\lambda$	$\Delta T$
2.6	...	$1.0 \pm 0.2$	$(1.12 \pm 0.15) \times 10^5$	$15 \pm 3$	$5.3 \times 10^{-6}$	34	3	0
4.0	...	$1.0 \pm 0.2$	$700 \pm 140$	$11 \pm 3$	$1.2 \times 10^{-1}$	6	2	0
6.75	30	$1.0 \pm 0.2$	$(16.5 \pm 3.0) \times 10^3$	$6 \pm 1$	$6.2 \times 10^{-4}$	5	3	0
8.05	36	$1.2 \pm 0.2$	$(16.5 \pm 2.5) \times 10^3$	$7 \pm 1$	$2.1 \times 10^{-3}$	5	3	0
13.5	60	$1.2 \pm 0.2$	$(4.4 \pm 1.0) \times 10^3$	$2.5 \pm 0.6$	$2.1 \times 10^{-2}$	1.4	3	1
14.0	63	$4.5 \pm 0.4$	$1040 \pm 100$	$56 \pm 6$	$9.0 \times 10^1$	8.8	2	0
16.6	74	$3.9 \pm 0.2$	$20.5 \pm 2.0$	$104 \pm 10$	$3.3 \times 10^4$	5.3	1	1
28.0	125	$\Gamma = 7$	$565 \pm 65$	$48 \pm 5$	$1.57 \times 10^3$	4.8		
		$\Gamma = 8$	$670 \pm 80$	$57 \pm 6$	$1.86 \times 10^3$	5.6	2	1
		$\Gamma = 10$	$960 \pm 130$	$82 \pm 10$	$2.67 \times 10^3$	8.1		

<sup>a</sup>The width may be either the width of the enveloping curve of unresolved discrete states or the width of a coherent resonant state.

$$^b R = E_x B(E\lambda) / \text{EWSR}(E\lambda, \Delta T) \times 100.$$

ELEM. SYM.	A	Z
Y	89	39

METHOD	REF. NO.
	78 Ma 10

	hg
--	----

REACTION	RESULT	EXCITATION ENERGY	SOURCE		DETECTOR		ANGLE
			TYPE	RANGE	TYPE	RANGE	
G,N	ABY	12-68	C	30-68	ACT		4PI

Analysis is made of reactions interfering with photon activation analysis procedures.

The activation yield curves have been presented for a number of photonuclear reactions in the energy range from 30 to 68 MeV, in order to evaluate quantitatively the interferences due to competing reactions in multielement photon activation analysis. The general features of the yields as functions of both target mass number and excitation energy were elucidated from the data obtained, discussion being given on the results in terms of the reaction mechanism.

Simultaneous neutron activation due to appreciable neutron production from the converter and surrounding materials has also been studied, and, finally, the magnitudes of interferences in real multielement analysis were given in the form of their energy dependences.

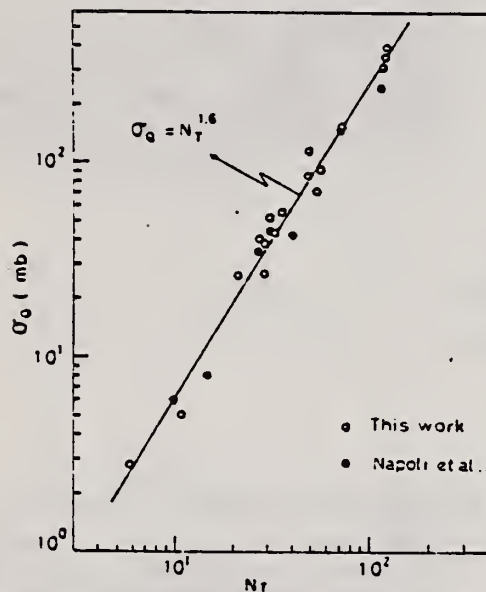


Fig. 2. Yield per equivalent quanta versus target neutron number.

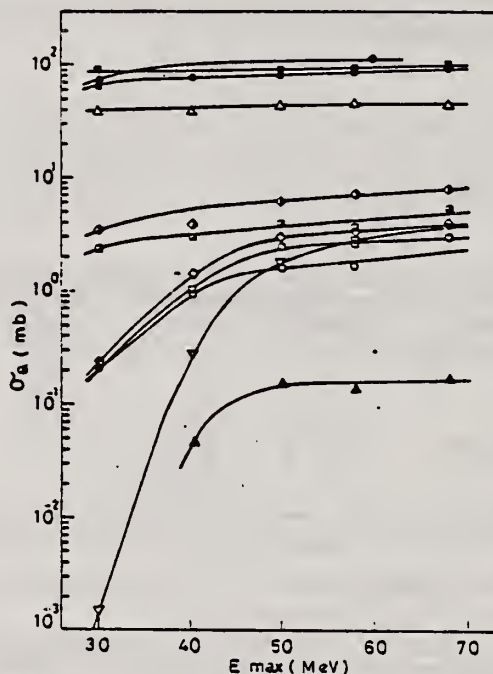


Fig. 7. Activation yield curves for the reactions on Y, Zr, Nb and Mo.  
 ◆  $^{89}\text{Y}(\gamma, n)^{88}\text{Y}$ , ●  $^{90}\text{Zr}(\gamma, n)^{89}\text{Zr}$ , ○  $^{90}\text{Zr}(\gamma, pn)^{88}\text{Y}$ ,  
 △  $^{93}\text{Nb}(\gamma, n)^{92\text{m}}\text{Nb}$ , ▲  $^{93}\text{Nb}(\gamma, xn)^{88}\text{Y}$ , ▣  $^{100}\text{Mo}(\gamma, n)^{99}\text{Mo}$ ,  
 ◇  $^{97}\text{Mo}(\gamma, p)^{96}\text{Nb}$ , ▤  $^{96}\text{Mo}(\gamma, p)^{95\text{m}}\text{Nb}$ , ◊  $^{94}\text{Mo}(\gamma, pn)^{92\text{m}}\text{Nb}$ ,  
 □  $^{92}\text{Mo}(\gamma, 2n)^{90}\text{Mo}$ , ▽  $^{94}\text{Mo}(\gamma, xn)^{89}\text{Zr}$ .

(over)

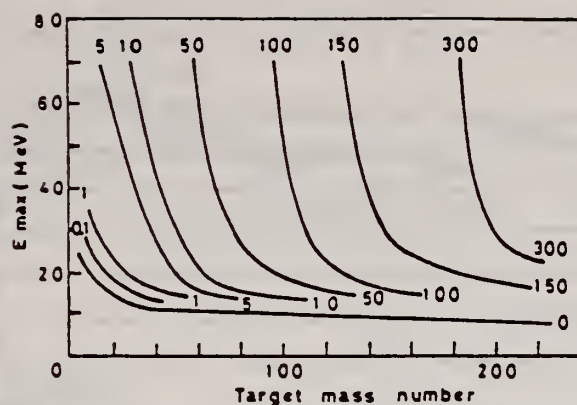


Fig. 9. Yields of the  $(\gamma, n)$  reactions as a function of bremsstrahlung maximum energy and target mass number. The numerical values in the figure are yields per equivalent quanta in mb.



REF.	H.R. Weller, N.R. Roberson & S.R. Cotanch Phys. Rev. C18, 65 (1978)	ELEM. SYM.	A	Z
		Y	89	39
METHOD		REF. NO.	78 We 4	hmg

REACTION	RESULT	EXCITATION ENERGY	SOURCE		DETECTOR		ANGLE
			TYPE	RANGE	TYPE	RANGE	
\$ P,G	RLX	14-24	D	6-16	UKN-D		DST

Analysis of data in reference 5.

POLARIZED PROTONS

Measurements of cross sections and analyzing powers are examined for polarized proton capture on  $^{14}\text{C}$ ,  $^{30}\text{Si}$ ,  $^{54}\text{Fe}$ ,  $^{56}\text{Fe}$ ,  $^{59}\text{Co}$ , and  $^{88}\text{Sr}$  at energies which cover the giant dipole resonance region. These data are used to extract the relative amplitudes and phases of the contributing  $E1$   $T$ -matrix elements. A typical result exhibits two solutions. Calculations using the direct (or a direct-semidirect) capture model appear to provide a means for choosing the physical solution.

[NUCLEAR REACTIONS:  $^{14}\text{C}(\bar{p}, \gamma_0)$ ,  $^{30}\text{Si}(\bar{p}, \gamma_0)$ ,  $^{54}\text{Fe}(\bar{p}, \gamma_0)$ ,  $^{56}\text{Fe}(\bar{p}, \gamma_0)$ ,  $^{59}\text{Co}(\bar{p}, \gamma_0)$ ,  $^{88}\text{Sr}(\bar{p}, \gamma_0)$ ; measured  $\sigma(\theta)$  and  $A(\theta)$  over energy region of the giant dipole resonance. Deduced  $T$ -matrix amplitudes and phases. Compare results to direct-semidirect model calculations.]

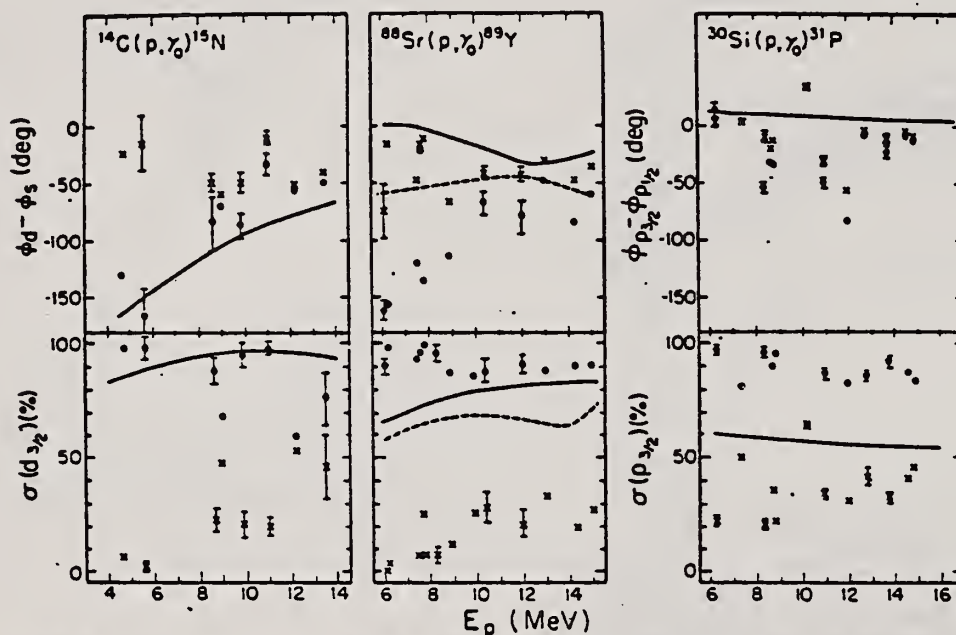


FIG. 1. The two solutions (dots and x's) resulting from a pure  $E1$  analysis of the data are shown along with the results of the calculation for target nuclei of  $^{14}\text{C}$ ,  $^{88}\text{Sr}$ , and  $^{30}\text{Si}$ . The remaining cross section in the case of  $^{14}\text{C}$  and  $^{88}\text{Sr}$  is due to the  $s_{1/2}$  matrix element. In the case of  $^{30}\text{Si}$  it arises from the  $p_{1/2}$  matrix element. The error bars represent typical statistical errors associated with the data points. The amplitudes are presented in terms of the percentage of the total cross section for which they are responsible. The curves represent DSD calculations as described in the text. The dashed curves in the case of  $^{88}\text{Sr}$  were obtained using the optical model parameters of Ref. 16 while the solid lines were obtained from the parameters of Ref. 18.

[over]

- <sup>2</sup>H. R. Weller, R. A. Blue, N. R. Roberson, D. G. Rickel, S. Maripuu, C. P. Cameron, R. D. Ledford, and D. R. Tilley, Phys. Rev. C 13, 922 (1976). (Note: an error exists in the sign of the phase in this paper. The quantity  $\phi_s - \phi_d$  should be  $\phi_d - \phi_s$  wherever it appears.)
- <sup>3</sup>C. P. Cameron, N. R. Roberson, D. G. Rickel, R. D. Ledford, H. R. Weller, R. A. Blue, and D. R. Tilley, Phys. Rev. C 14, 553 (1976).
- <sup>4</sup>C. P. Cameron, Ph.D. thesis, Duke University, 1976 (unpublished).
- <sup>5</sup>R. D. Ledford, Ph.D. thesis, Duke University, 1976 (unpublished).
- <sup>6</sup>J. D. Turner, C. P. Cameron, N. R. Roberson, H. R. Weller, and D. R. Tilley, Phys. Rev. C 17, 1853 (1978).



ELEM. SYM.	A	Z
Y	89	39
REF. NO.		
80 Va 1		hg

METHOD					REF. NO.	
					80 Va 1	
REACTION	RESULT	EXCITATION ENERGY	SOURCE		DETECTOR	
			TYPE	RANGE	TYPE	RANGE
G,P0	ABX	13-25	C	13-25	SCD-D	DST
G,P1	ABX	15-25	C	13-25	SCD-D	DST

Absolute  $(\gamma, p_0)$  and  $(\gamma, p_1)$  differential cross sections for  $^{89}\text{Y}$  were measured at seven angles in the energy interval between 13 and 24.6 MeV, from which the angular distribution coefficients were deduced by fitting a sum of Legendre polynomials. In these cross sections we observe a number of isolated resonances which can be identified as the isobaric analogs of known  $1/2^+$  and  $3/2^+$  excited states in the  $^{89}\text{Sr}$  parent nucleus. The appearance of a maximum around 21 MeV excitation energy in both total cross sections may indicate the existence of the  $T_1$  coherent dipole state. From the angular distribution coefficients in the  $(\gamma, p_0)$  channel, an upper and lower limit for the  $E2$  photon absorption were estimated as being equal to 22% and 6%, respectively, of the total  $E2$  energy-weighted sum rule.

NUCLEAR REACTIONS  $^{89}\text{Y}(\gamma, p_0)$ ,  $(\gamma, p_1)$ ,  $E=13.0-24.6$  MeV,  $\theta=37-143^\circ$ ; measured  $\sigma(E; \theta)$  absolutely. Deduced  $\sigma(E; p_0)$ ,  $\sigma(E; p_1)$ ;  $E1$ ,  $E2$  strengths, isobaric analog states, isospin splitting. Natural target.

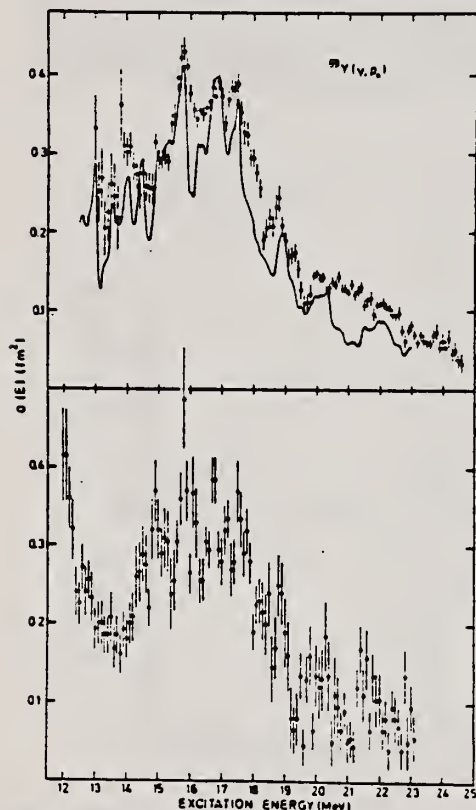


FIG. 5. The points with error bars in the upper half of the figure show our experimentally determined total  $^{89}\text{Y}(\gamma, p_0)$  cross section, while the full line represents the results deduced from the  $^{89}\text{Sr}(\gamma, \gamma_0)$  data of Paul *et al.* (Ref. 8); the bottom half of the figure shows the  $(\gamma, p_0)$  cross section resulting from the  $(c, e'p)$  experiment of Shoda *et al.* (Ref. 9).

Only statistical shown, systematic uncertainty is of the order of 5%.

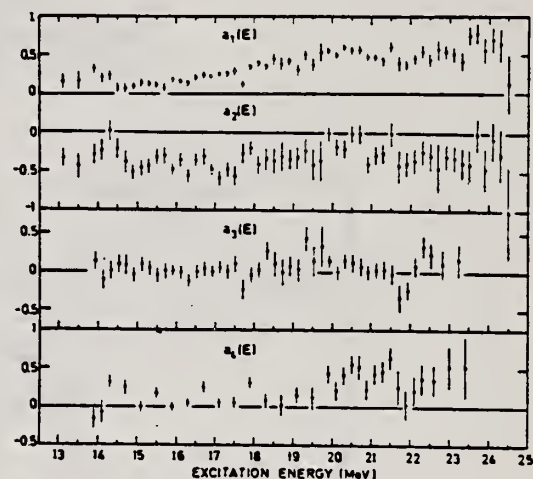


FIG. 6. The angular distribution coefficients  $a_l(E)$ ,  $l=1, \dots, 4$ , as a function of excitation energy for the  $^{89}\text{Y}(\gamma, p_0)$  reaction.

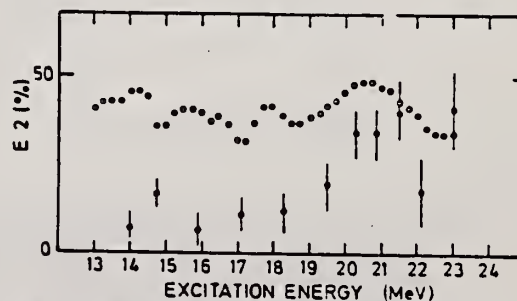


FIG. 7. Upper (open circles) and lower (dotted points) limits of the  $E2$  contribution to the  $^{89}\text{Y}(\gamma, p_0)$  photoabsorption.

(OVER)

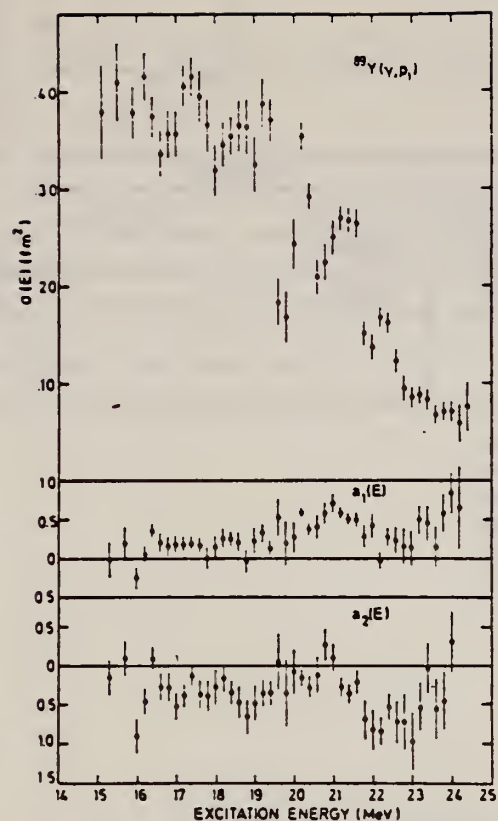


FIG. 8. The upper half of the figure shows the total  $\sigma(Y, p_1)$  cross section, while in the lower half the angular distribution coefficients  $a_1(E)$  and  $a_2(E)$  are represented.

REF. E. Van Camp, R. Van de Vyver, E. Kerkhove, D. Ryckbosch, H. Ferdinande,  
P. Van Otten, P. Berkvens  
Phys. Rev. C24, 2499 (1981)

ELEM. SYM.	A	Z
Y	89	39
REF. NO.		hg
81 Va 1		

METHOD

REACTION	RESULT	EXCITATION ENERGY	SOURCE		DETECTOR		ANGLE
			TYPE	RANGE	TYPE	RANGE	
G, p0	ABX	7-25	C	14-25	SCD-D		DST
G, PL	ABX	7-25	C	14-25	SCD-D		DST

The  $^{89}\text{Y}(\gamma, p)^{88}\text{Sr}$  reaction was studied at various bremsstrahlung end point energies in the giant dipole resonance region. Using an artificially constructed pseudomonoenergetic photon spectrum, it was possible to determine the absolute cross sections for various photoproton reaction channels. From the direct decay cross sections the proton escape width  $\Gamma_p'$  of the  $T_{-}$  giant dipole resonance was derived; its value amounts to 0.30–0.35 MeV. The nondirect contribution equals about 25% of the total energy-integrated photoproton cross section.

[NUCLEAR REACTIONS  $^{89}\text{Y}(\gamma, p)$ ,  $E = 14\text{--}24$  MeV; measured  $\sigma(E)$  absolutely. Deduced  $\Gamma_p'$ . Natural target.]

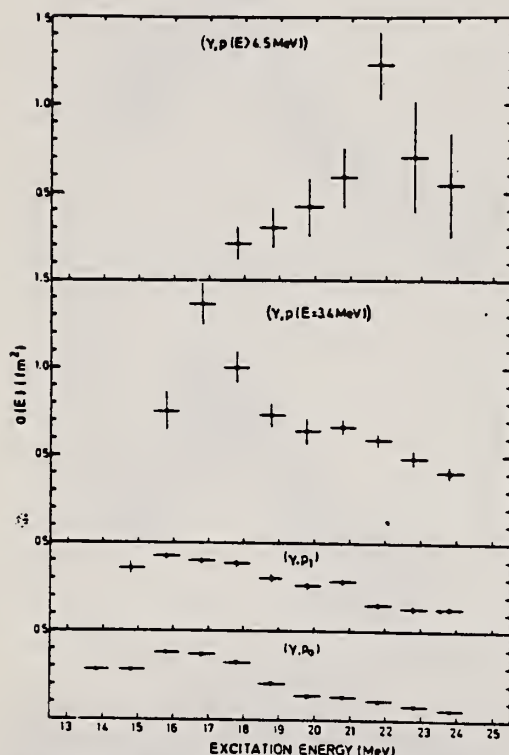


FIG. 6. The absolute  $^{89}\text{Y}(\gamma, p)$  cross sections for the various proton channels which could be identified.

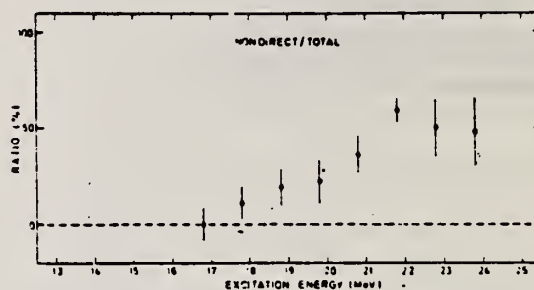


FIG. 7. The ratio of the nondirect to the total cross section for the  $^{89}\text{Y}(\gamma, p)$  reaction, as a function of excitation energy.

TABLE II. Integrated cross sections for the various photoproton channels observed in the  $^{89}\text{Y}(\gamma, p)$  reactions.

Channel	Integration limits $E_1$ (MeV)– $E_2$ (MeV)	$\int_{E_1}^{E_2} \sigma(E) dE$ (MeV fm <sup>2</sup> )	$\frac{\int \sigma(p_i, E) dE}{\int \sigma(p, E) dE} \times 100$
$(\gamma, p_0)$	13.8–24.6	$2.45 \pm 0.02$	15.6
$(\gamma, p_1)$	15.1–24.4	$2.77 \pm 0.03$	17.7
$[\gamma, p(E = 3.4 \text{ MeV})]$	15.8–23.8	$6.59 \pm 0.18$	42.1
$[\gamma, p(E > 4.5 \text{ MeV})]$	17.8–23.8	$3.86 \pm 0.57$	24.6
$(\gamma, p)_{\text{total}}$	13.8–24.6	$15.67 \pm 0.60$	100.0

Y  
A=90

Y  
A=90

Y  
A=90





REF.

L. Nilsson, A. Lindholm, I. Bergqvist, B. Palsson, and  
J. Eriksson  
PICNS-73, Vol.II, p.949 (1973) Asilomar

ELEM. SYM.	A	Z
Y	90	39
REF. NO.		
73 N1 2		egf

METHOD

REACTION	RESULT	EXCITATION ENERGY	SOURCE		DETECTOR		ANGLE
			TYPE	RANGE	TYPE	RANGE	
N,G	RLY	14- 16	D	6- 9	NAI-D		-

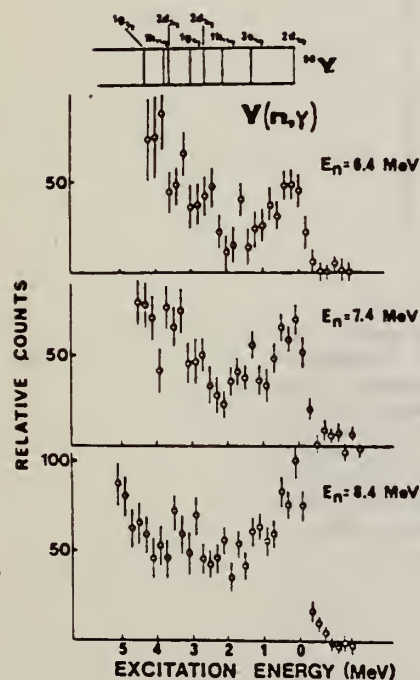


Fig 1. Gamma-ray spectra from  $^{89}\text{Y}(n,\gamma)^{90}\text{Y}$  at various neutron energies plotted versus residual excitation energy. The spectra are normalized to the same neutron flux. The single-particle structure of  $^{90}\text{Y}$  is given on top of the figure.

REF. I. Bergqvist, B. Palsson, L. Nilsson, A. Lindholm, D.M. Drake,  
E. Arthur, D.K. McDaniels and P. Varghese  
Nucl. Phys. A295, 256 (1978)

ELEM. SYM.	A	Z
Y	90	39
REF. NO.		
78 Be 1		rs

METHOD

REACTION	RESULT	EXCITATION ENERGY	SOURCE		DETECTOR		ANGLE
			TYPE	RANGE	TYPE	RANGE	
N.G	ABX	13- 23	D	6- 16	NAI-D		90

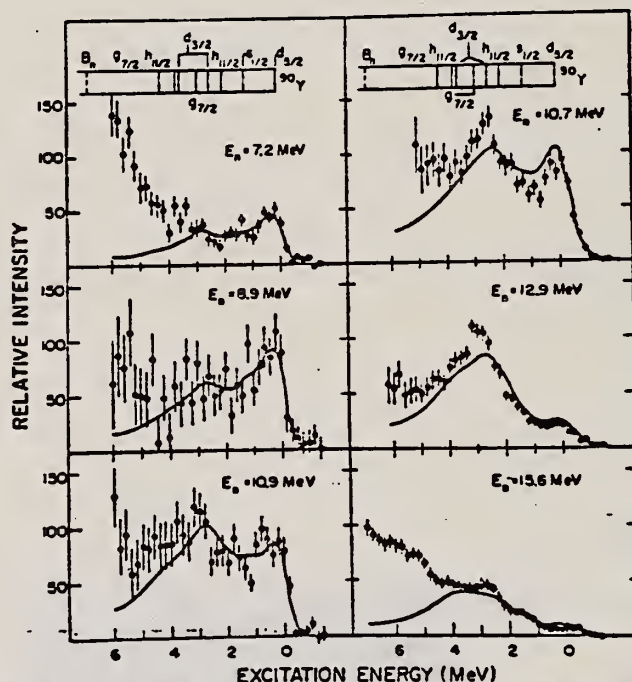


Fig. 1. Comparison of the measured spectra from the reaction  $^{89}\text{Y}(n, \gamma)^{90}\text{Y}$  and those predicted from the direct-semidirect (DSD) capture theory at neutron energies from 7.2 to 15.6 MeV. The theoretical spectra were computed using the DSD cross section predictions with a complex interaction for  $\gamma$ -ray transitions to the single-particle states of  $^{90}\text{Y}$  shown on top of the figure. The cross sections were multiplied by the NaI(Tl) detector response function and corrected for  $\gamma$ -ray attenuation and detector efficiency. The observed and theoretical spectra were normalized to each other in the region corresponding to excitation energies below 3.2 MeV. The GDR parameters used are given in the text while the interaction parameters chosen were  $v_1 = 75$  MeV, and  $w_1 = 110$  MeV. The data at neutron energies of 7.2, 8.9 and 10.9 MeV were taken with the TLU system while the higher energy data were taken at LASL.

over

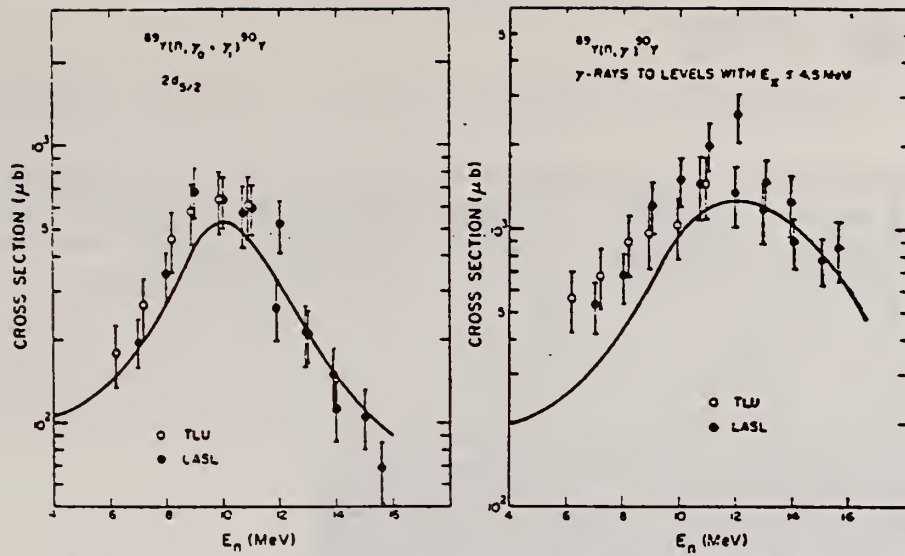


Fig. 3. Experimental  $(n, \gamma)$  cross sections for  $\gamma$ -ray transitions to the two  $2d_{3/2}$  states at 0 and 203 keV in  $^{89}\text{Y}$  and the integrated cross section for  $\gamma$ -rays to levels below  $E_x = 4.5$  MeV. The differential cross sections at 90 were multiplied by  $4\pi$ . The results from the TLU experiment are indicated by open circles and the LASL data are shown by solid circles. The solid lines represent the cross section predicted from the DSD theory using a complex coupling function for the particle-vibration interaction.

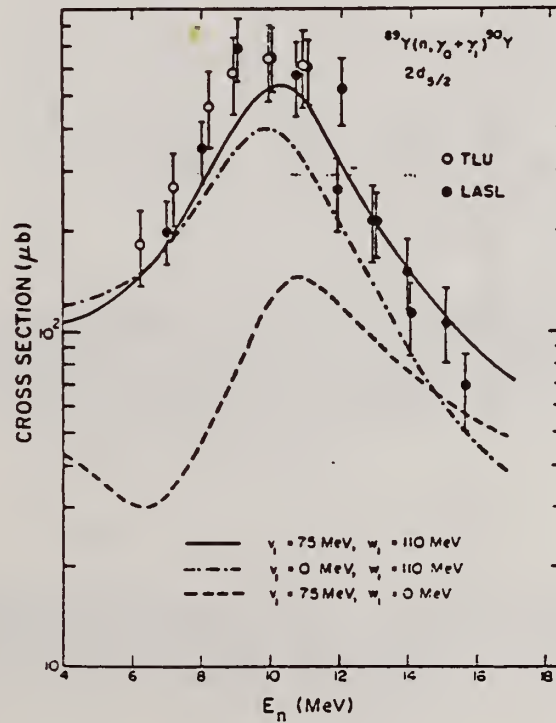


Fig. 5. Detailed comparison of the experimental  $(n, \gamma)$  cross sections for  $\gamma$ -ray transitions to the ground-state doublet of  $^{90}\text{Y}$ . The data are compared to the predictions of the DSD model using various particle-vibration interaction functions.

REF. A. Likar, A. Lindholm, L. Nilsson, I. Bergqvist and  
B. Palsson  
Nucl. Phys. A298, 217 (1978)

ELEM. SYM.	A	Z
Y	90	39

METHOD	REF. NO.	
	78 Li 2	rs

REACTION	RESULT	EXCITATION ENERGY	SOURCE		DETECTOR		ANGLE
			TYPE	RANGE	TYPE	RANGE	
N,G	RLX	14- 18	D	7- 11	NAI-D		DST

**Abstract:** Gamma-ray spectra from neutron capture in natural samples of strontium and yttrium have been recorded at various angles with respect to the direction of the incident neutron flux. Angular yields have been observed at six neutron energies in the range 7 to 11 MeV using time-of-flight techniques to improve the signal-to-background ratio. The  $\gamma$ -radiation was detected by a large NaI(Tl) crystal placed in a heavy radiation shield. Certain combinations of Legendre polynomial coefficients were extracted for transitions to low-lying single-particle states ( $2d_{5/2}$  and  $3s_{1/2}$ ) in the final nuclei. The energy dependence of the angular distribution coefficients indicates interference between the electric dipole amplitude and amplitudes of opposite parity. The results are compared with theoretical calculations based on the direct-semidirect model.

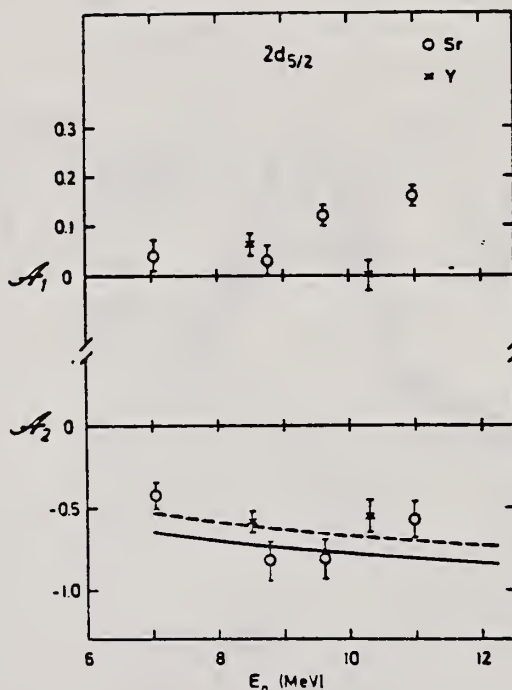


Fig. 2. Angular distribution coefficients  $A_1$  and  $A_2$  versus neutron energy for the reactions  $^{88}\text{Sr}(n, \gamma_0)^{88}\text{Sr}$  (open circles) and  $^{89}\text{Y}(n, \gamma_0 + \gamma_1)^{89}\text{Y}$  (crosses). The curves for the  $A_2$  coefficient represent the results of theoretical calculations for E1 transitions to the  $2d_{5/2}$  state in  $^{88}\text{Sr}$  from the direct (solid line) and DSD (dashed line) capture models.

over

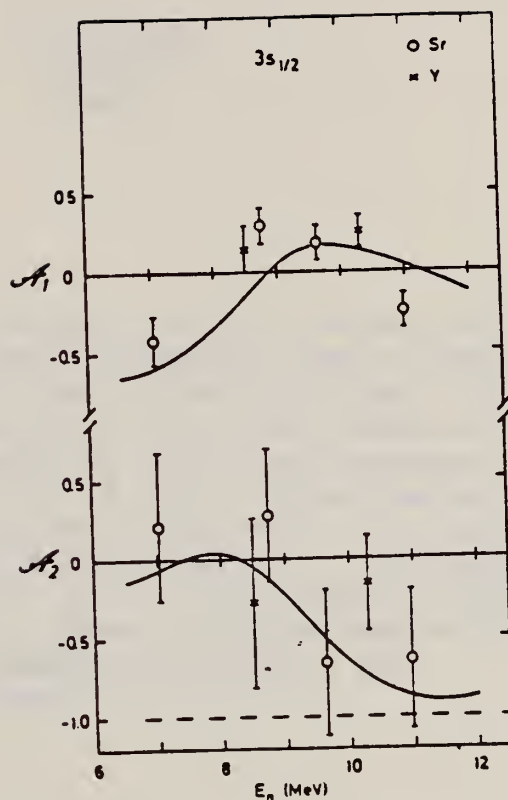


Fig. 3. Angular distribution coefficients  $A_1$  and  $A_2$  versus neutron energy for  $\gamma$ -rays to the  $3s_{1/2}$  states from the reactions  $^{88}\text{Sr}(n, \gamma)^{88}\text{Sr}$  (open circles) and  $^{90}\text{Y}(n, \gamma)^{90}\text{Y}$  (crosses). The theoretical result for DSD model calculations are shown as dashed curve for pure E1 transitions and as solid curves assuming E1 and E2 transitions associated with collective excitation of the GDR and the isoscalar GQR.





## ZIRCONIUM

Z=40

Although zircon was frequently used by the ancients for intagli and although hyacinth and jargon (semiprecious stones) were known in the middle ages, the presence in these minerals of an unknown metal was not suspected until near the end of the eighteenth century. The earth zirconia was overlooked because of its great similarity to alumin, and it took the analytical skill of Klaproth to detect it. He worked with zirconium silicate in the form of semiprecious gemstones from Ceylon. These zircon gems derive their name from the Arabic *zargun* (gold color), and Klaproth named the element zirconium.

Zr

Zr

*[Faint, illegible text, possibly bleed-through from the reverse side of the page]*

Ref. **E. Reibel; A.K. Mann**  
**Phys. Rev. 118, 701 (1960)**

Elem. Sym.	A	Z
Zr		40

Method  **$\gamma$ 's from  $F^{19}(\gamma, \gamma)$  reaction; protons from Van de Graaff; Na I.**

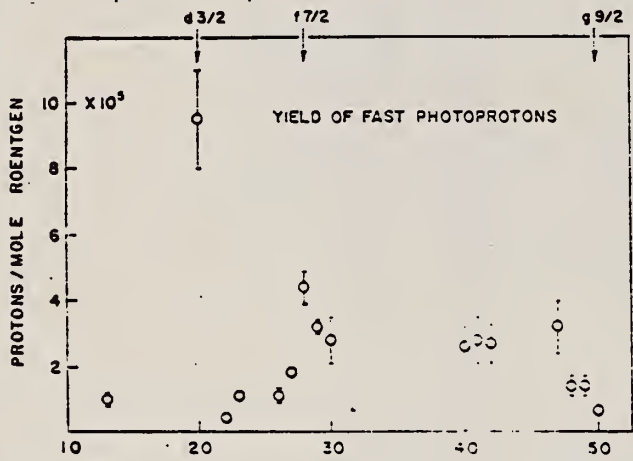
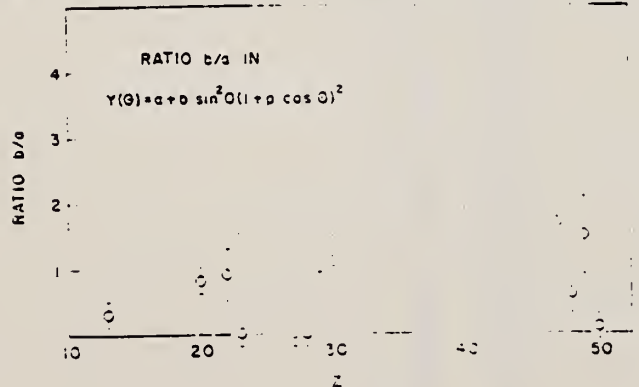
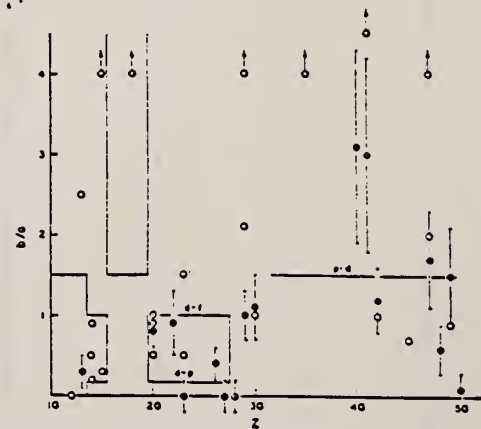
Ref. No.	JHH
60 Re 1	

Reaction	E or $\Delta E$	$E_0$	$\Gamma$	$\int \sigma dE$	$J\pi$	Notes
<b><math>(\gamma, \gamma)</math></b>	<b><math>E_\gamma \sim 7</math></b>					<b><math>\langle \sigma \rangle (E_\gamma = 2.05 \text{ MeV}) = 1.0 \pm 0.1 \text{ mb}</math></b>

Ref. O.M.M. Mitchell, K.G. McNeill  
Can. J. Phys. 41, 871 (1963)

Elem. Sym.	A	Z
Zr		40
Ref. No.		
63 Mi 5		NVB

Method Betatron; proton yield; angular distribution; scintillator;  
ion chamber.

Reaction	E or $\Delta E$	$E_0$	$\Gamma$	$\int \sigma dE$	$J\pi$	Notes
Zr( $\gamma, xp$ )	Bremss. 22					<p>Angular distribution:  <math>Y(\theta) = a + b \sin^2 \theta (1 + p \cos \theta)^2</math>            where <math>a = 24 \pm 8</math>; <math>b = 74 \pm 14</math>;  <math>p = 0.2 \pm 0.1</math> and <math>b/a = 3.1 \pm 1.2</math>.</p> <p>Yield (<math>E_p &gt; 8</math> MeV):  <math>(2.6 \pm 0.6) \cdot 10^5</math> protons/mole-r.</p> <p>Yield (<math>3.7 &lt; E_p &lt; 14</math>): <math>(29 \pm 3) \cdot 10^5</math></p>
						
						
						
<p>Fig. 2. The yields of fast photoprotons (<math>E_p &gt; 8</math> MeV) of various elements when irradiated with 22 Mev bremsstrahlung. The energies 15.1 to 37.2 Mev (about 8 Mev for protons). The errors noted are statistical.</p> <p>Fig. 3. The anisotropy coefficient <math>b/a</math> for fast photoprotons (<math>E_p &gt; 8</math> MeV). The errors noted are statistical.</p> <p>Fig. 4. The values of the fast photoproton anisotropy coefficient <math>b/a</math> found by the present authors (●) and other workers (○) in the region of the periodic table <math>10 &lt; Z &lt; 50</math>. Arrows indicate missing points. The references to the results of other workers are given in Table II. The denunciations are explained in the text.</p>						



REF.

I.I. Dushkov, B.S. Ishkhanov, I.M. Kapitonov, B.A. Yur'ev, V.G. Shevchenko

Phys. Letters 10, 310 (1964)

ELEM. SYM. A Z

Zr

40

METHOD

Betatron

[Page 1 of 2]

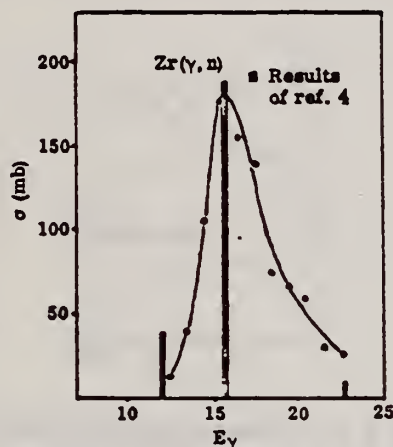
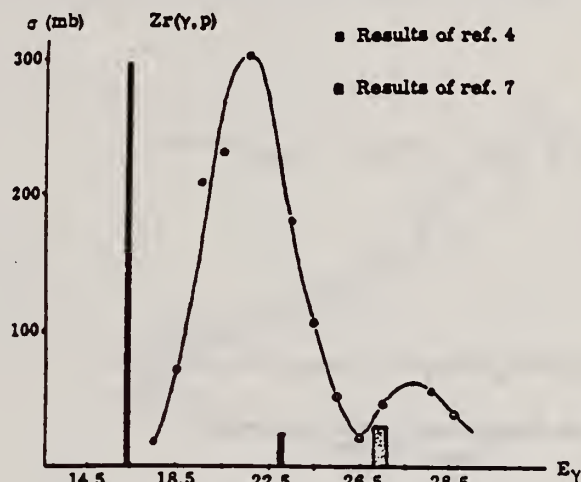
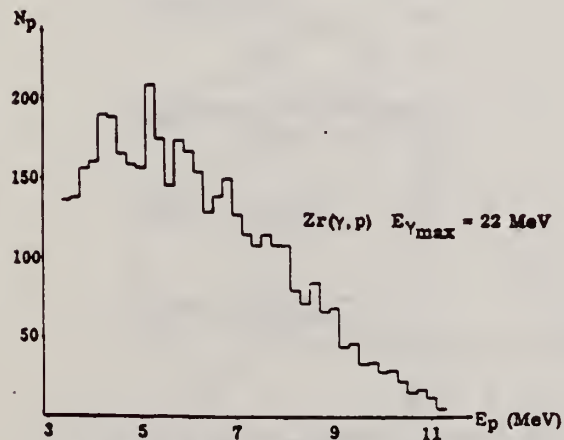
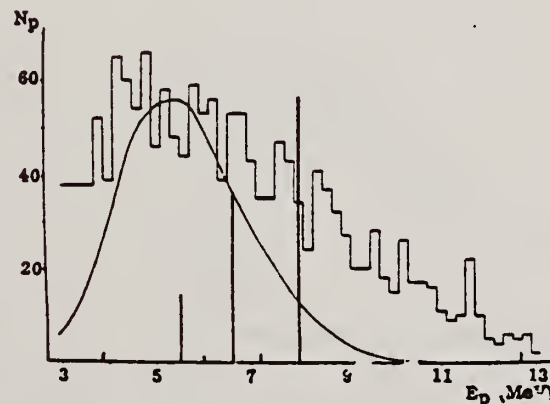
REF. NO.

64 Du 1

JOC

REACTION	RESULT	EXCITATION ENERGY	SOURCE		DETECTOR		ANGLE
			TYPE	RANGE	TYPE	RANGE	
G,P	ABX	THR-34	C	22-34	MAG-D	2-16	DST

ABX

Fig. 1. Comparison of theoretical and experimental data for the  $(\gamma, n)$  reaction.Fig. 2. Comparison of theoretical and experimental data for the  $(\gamma, p)$  reaction.Fig. 3a. Energy distribution of photoprotons at  $E_{\gamma \max} = 22$  MeV.Fig. 3b. Energy distribution of photoprotons at  $E_{\gamma \max} = 25$  MeV.

REF.						ELEM. SYM.		A		Z	
I.I. Dushkov, B.S. Ishkhanov, I.M. Kapitonov, B.A. Yur'ev, Phyŝ. Letters <u>10</u> , 310 (1964)						Zr				40	
METHOD						REF. NO.					
Betatron						[Page 2 of 2]		64 Du 1		JOC	
REACTION	RESULT	EXCITATION ENERGY	SOURCE		DETECTOR				ANGLE		
			TYPE	RANGE	TYPE	RANGE					

[Page 2 of 2]

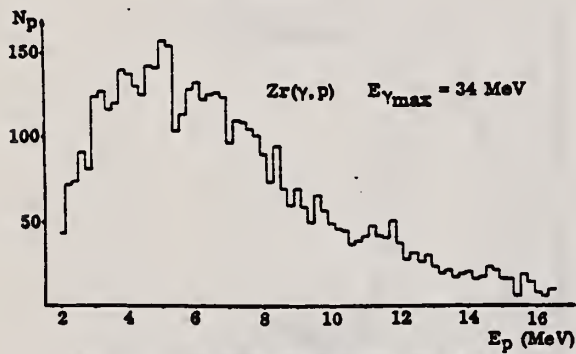


Fig. 3c. Energy distribution of photoprotons at  $E_{\gamma\max} = 34$  MeV.

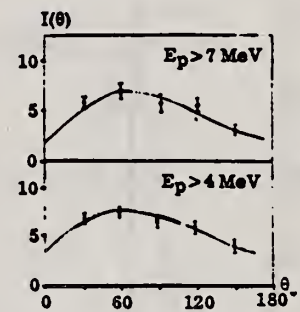


Fig. 4. Angular distributions of photoprotons at  $E_{\gamma\max} = 25$  MeV.

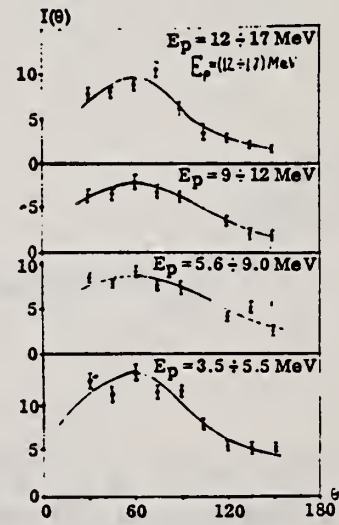


Fig. 5. Angular distributions of photoproton at  $E_{\gamma\max} = 34$  MeV.

REF. I. I. Dushkov, B. S. Ishkhanov, I. M. Kapitonov, V. G. Shevchenko,  
and B. A. Yur'ev  
Izv. Akad. Nauk Fiz. 29, 213 (1965)  
Bull. Acad. Sci. USSR- Phys. 29, 213 (1965)

ELEM. SYM.	A	Z
Zr		40
REF. NO.		EGF
65 Du 1		

METHOD

[Page 1 of 2]

REACTION	RESULT	EXCITATION ENERGY	SOURCE		DETECTOR		ANGLE
			TYPE	RANGE	TYPE	RANGE	
G,P	ABX	18-26	D	17-24	EMU-D	3-13	DST

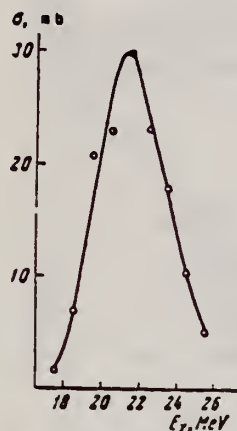


Fig. 1. Variation of the  $Zr(\gamma, p)$  reaction cross section with  $E_\gamma$ .

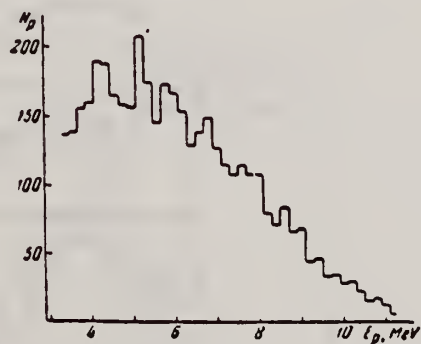


Fig. 2

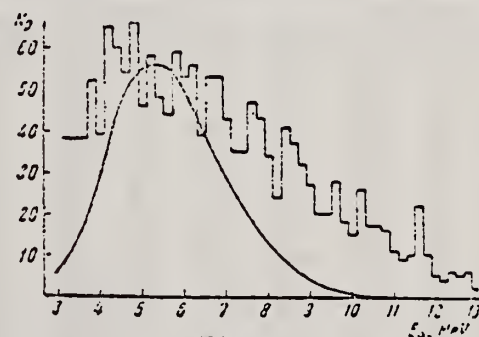


Fig. 3

Fig. 2. Spectrum of photoprotons from zirconium with irradiation of the target by  $\gamma$  rays with  $E_\gamma \text{ max} = 22 \text{ MeV}$ .

Fig. 3. Spectrum of photoprotons from zirconium with  $E_\gamma \text{ max} = 25 \text{ MeV}$ . The smooth curve represents the spectrum calculated on the basis of the statistical model.

REF. I. I. Dushkov, B. S. Ishkhanov, I. M. Kapitonov, V. G. Shevchenko,  
and B. A. Yur'ev  
Izv. Akad. Nauk fiz. 29, 213 (1965)  
Bull. Acad. Sci. USSR-Phys. 29, 213 (1965)

ELEM. SYM.	A	Z
Zr		40
REF. NO.		EGF
65 Du 1		

METHOD

[Page 2 of 2]

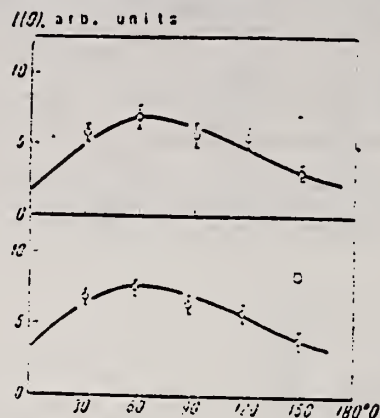


Fig. 5

Fig. 4. Spectrum of photoprotons from zirconium with  $E_{\gamma \text{ max}} = 34$  MeV.

Fig. 5. Angular distributions of different groups of protons (Zr target irradiated with  $E_{\gamma \text{ max}} = 25$  MeV bremsstrahlung): a -  $E_p > 7$  MeV, b -  $E_p > 4$  MeV.

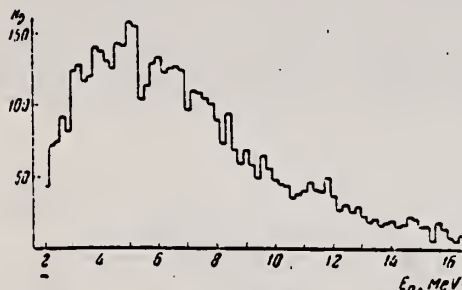


Fig. 4

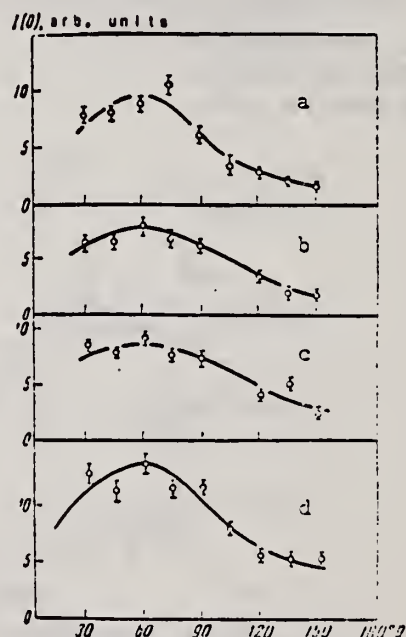


Fig. 6. Angular distributions of different proton groups (target irradiated with  $E_{\gamma \text{ max}} = 34$  MeV bremsstrahlung): a -  $E_p = 12-17$  MeV, b -  $E_p = 9-12$  MeV, c -  $E_p = 5.6-9.0$  MeV, d -  $E_p = 3.5-5.5$  MeV.



ELEM. SYM.	A	Z
Zr		40
REF. NO.		
66 Be 3		
JDM		

METHOD

Nuclear Resonance Scattering using N,G reactions.

REACTION	RESULT	EXCITATION ENERGY	SOURCE		DETECTOR		ANGLE
			TYPE	RANGE	TYPE	RANGE	
G,G	RLX	5 - 10	D	5 - 10	NAI-D	5 - 10	135

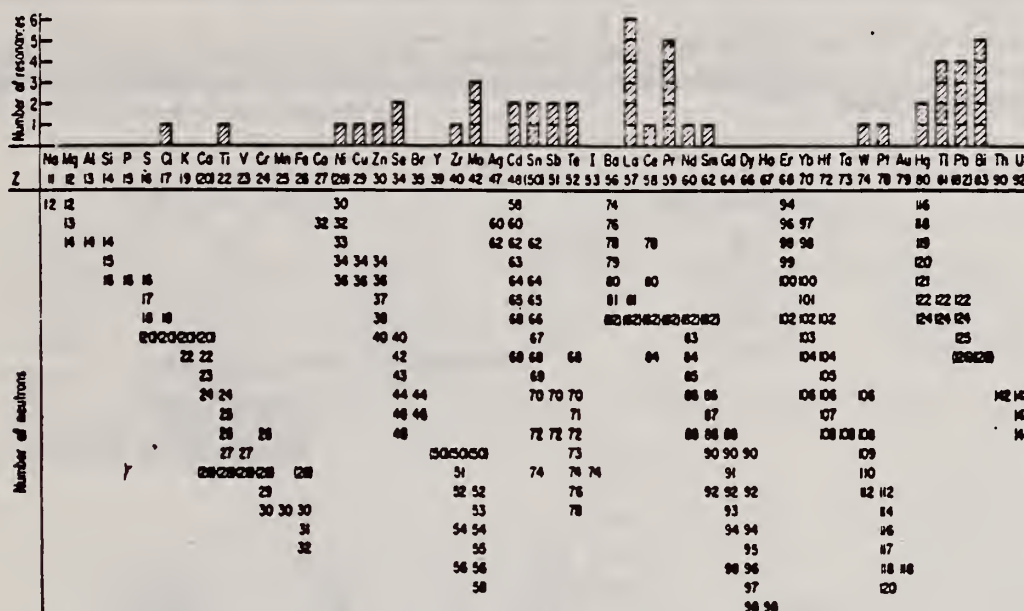


Fig. 3. Histogram of distribution of observed resonances among the different targets. The atomic number is given directly beneath the chemical symbol followed by the neutron numbers of the naturally occurring isotopes. Magic numbers are shown in brackets.

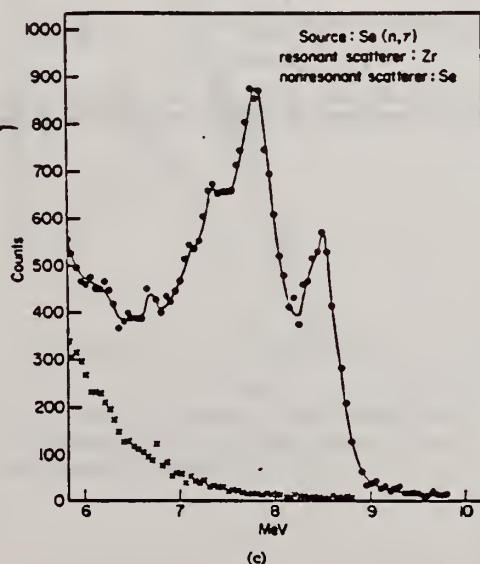


Fig. 1.(c)Complex scattered spectrum from Zr excited by Se capture gamma rays (with Se background).

TABLE III. List of effective cross sections.

Scatterer	Energy (MeV)	Gamma source	σ (mb)	Scatterer	Energy (MeV)	Gamma source	σ (mb)
Sm <sup>146</sup>	8.997	Ni	100	Sn	7.01	Cu	110
Pri <sup>146</sup>	8.881	Cr	9	Nd	6.867	Co	30
La	8.532	Ni	6	Pri <sup>146</sup>	6.867	Co	3
Te	8.532	Ni	3*	La	6.7	Ni	...
Cu	8.499	Cr	24	La	6.54	Ag	12
Zr	8.496	Se	3050	Cd	6.474	Co	110
Zn	8.119	Ni	13	Mo	6.44	Hg	25*
Se	7.817	Ni	50	La	6.413	Ti	72
Se	7.76	K	90	Mo	6.413	Ti	10
Sb	7.67	V	...	Ti	6.413	Ti	25
Cd	7.64	Fe	40*	W	~6.3	Ti	...
Ni	7.64	Fe	7*	Sb	6.31	Hg	6*
Pri <sup>146</sup>	7.64	Fe	12*	Ti	6.31	Hg	2*
La	7.64	Fe	370*	Sn	6.27	Ag	75
Mo	7.634	Cu	11	Pb <sup>208</sup>	6.15	Gd	...
Hg <sup>200</sup>	7.634	Cu	4	La	5.8	Ni	...
Te	7.528	Ni	66*	La	6.12	Cl	35
Bi <sup>209</sup>	7.416	Se	100	Pri <sup>146</sup>	6.12	Cl	110
Bi <sup>209</sup>	7.300	As	80*	Pt	5.99	Hg	40*
Pb <sup>208</sup>	7.285	Fe	4100	Tl	5.99	Hg	5*
Cl	7.285	Fe	34	Pb <sup>208</sup>	5.9	Sr	...
Pri <sup>146</sup>	7.185	Se	80	Ce	5.646	Co	17
Ti	7.16	Cu	120	Bi <sup>209</sup>	5.646	Co	55
La	7.15	Mn	50	Pb <sup>208</sup>	5.53	Ag	70
Bi <sup>209</sup>	7.149	Ti	2000	Hg	5.44	Hg	75*
				Hg	4.903	Co	385

- \* High-energy component of a complex spectrum.
- \* A broad scattered spectrum with no observable peak structure.
- \* There are actually two lines of energies 7.647 and 7.633 MeV having equal intensities in the iron capture gamma spectrum. The cross section has therefore been corrected, although there is no possibility at present of deciding which line is responsible for each resonance.
- \* is probably an independent level in the complex spectrum of Ni γ rays on Te.
- \* Rough estimate.
- \* May be inelastic component from 7.528 level in Te.
- \* The relative line intensities in this case are due to Groshev and co-workers.
- \* No line is known for the source at this energy.
- \* Difficult to resolve among the many source lines present at this energy.



REF. S. M. Hussain and K. G. McNeill  
Can. J. Phys. 45, 2851 (1967)

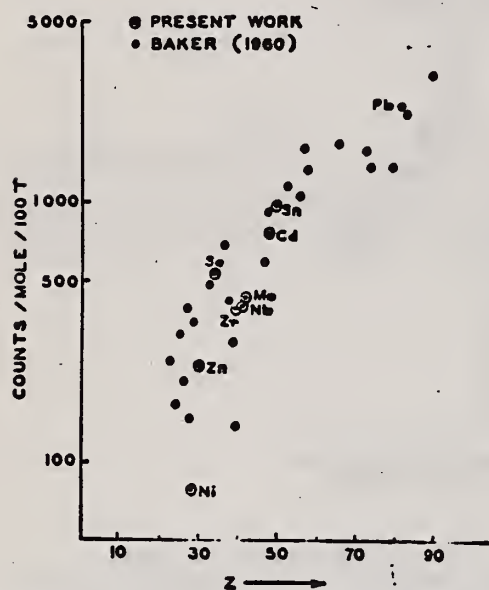
ELEM. SYM.	A	Z
Zr		40

METHOD	REF. NO.	
	67 Hu 2	EGF

REACTION	RESULT	EXCITATION ENERGY	SOURCE		DETECTOR		ANGLE
			TYPE	RANGE	TYPE	RANGE	
G,N	ABY	THR-22	C	22	THR	4-	DST

YIELD AT  $E_0 = 22$  MeV  
 $^{28}\text{Si}(n,p)$  ACTIVATION BY PHOTONEUTRONS

FIG. 3. The yields of fast photoneutrons from various elements as measured in the present work and by Baker. The present results have been normalized to Baker's measurements for lead.



ANISOTROPY COEFFICIENT  $-Q_2$

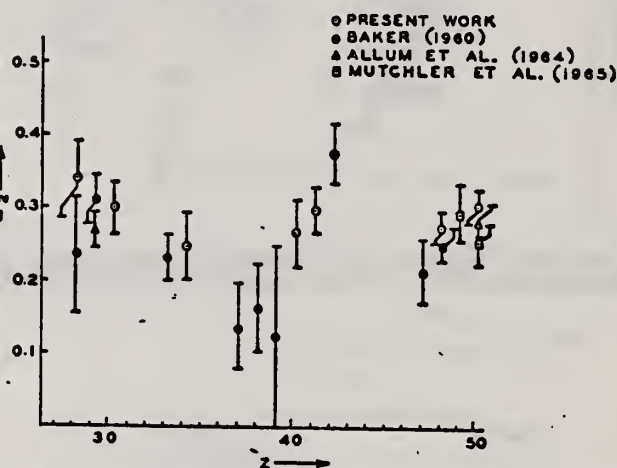


FIG. 2. The anisotropy coefficients  $a_1$ , in the formula  $W(\theta) = a_0(1 + a_1P_1 + a_2P_2)$ , obtained in the present work, and those obtained by other workers in the same part of the Periodic Table.

TABLE I

Element	$a_0^*$	$a_1$	$a_2$
Nickel	77 (1.0±0.05)	0.14±0.04	-0.34±0.06
Zinc	236 (1.0±0.04)	0.06±0.03	-0.30±0.04
Selenium	525 (1.0±0.05)	0.10±0.04	-0.25±0.05
Zirconium	380 (1.0±0.05)	0.03±0.04	-0.27±0.05
Niobium	392 (1.0±0.03)	0.01±0.02	-0.30±0.03
Molybdenum	410 (1.0±0.03)	0.05±0.03	-0.41±0.04
Cadmium	755 (1.0±0.02)	0.05±0.01	-0.28±0.02
Tin	955 (1.0±0.02)	0.08±0.02	-0.30±0.02
Lead	2274 (1.0±0.02)	0.06±0.02	-0.48±0.02

\*For comparison purposes the experimental value of  $a_0$  for Pb has been normalized to coincide with that obtained by Baker and McNeill (1961) and is the yield per mole per 100 roentgen. All other values of  $a_0$  have also been quoted with the same normalization.

METHOD

REF. NO.

[Page 1 of 2]

69 Sh 4

hmg

REACTION	RESULT	EXCITATION ENERGY	SOURCE		DETECTOR		ANGLE
			TYPE	RANGE	TYPE	RANGE	
G,P	ABX	8-24	C	20,24 (20.5)	EMU-D	2-14	DST

Table II. Anisotropic factor  $B/A$  and asymmetry factor  $p$  of angular distributions determined by least-square fits with  $A+B(1+p \cos \theta) \sin^2 \theta$ .

Zr					
$(E_{\gamma \max} = 20.5 \text{ MeV})$			$(E_{\gamma \max} = 24.0 \text{ MeV})$		
$E_p(\text{MeV})$	$B/A$	$p$	$E_p(\text{MeV})$	$B/A$	$p$
2.5-4.4	$6.26 \pm 0.09$	$-0.9 \pm 0.4$	3.5-7.3	$-0.1 \pm 0.1$	$-2.4 \pm 2.6$
4.4-6.7	$1.0 \pm 0.2$	$0.6 \pm 0.2$	7.3-11.5	$0.7 \pm 0.4$	$1.0 \pm 0.7$
6.7-8.6	$4.3 \pm 3.4$	$0.7 \pm 0.3$	11.5 $\leq$	$1.3 \pm 1.9$	$1.2 \pm 1.6$
8.6 $\leq$	$7.1 \pm 9.5$	$1.3 \pm 0.4$			

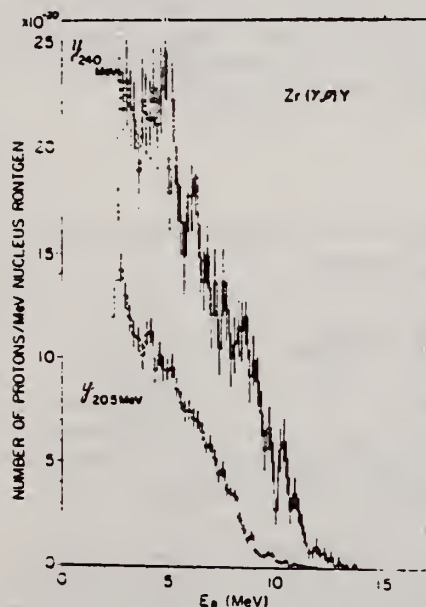


Fig. 2. Energy distributions of photoprotons from Zr irradiated with the bremsstrahlung at maximum energy of 24.0 and 20.5 MeV.

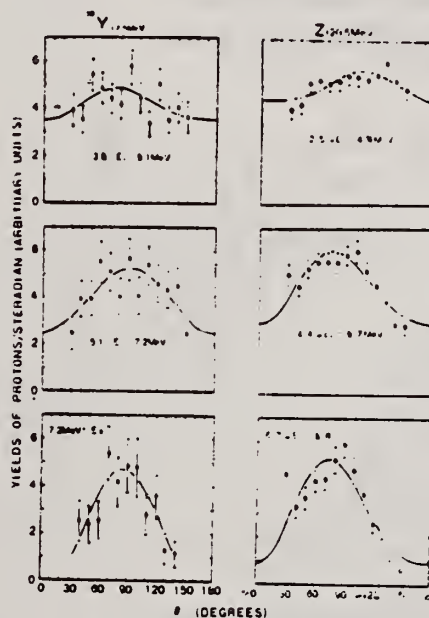


Fig. 3. Examples of angular distributions of photoprotons from  $^{88}\text{Y}$  and Zr.

REACTION	RESULT	EXCITATION ENERGY	SOURCE		DETECTOR		ANGLE
			TYPE	RANGE	TYPE	RANGE	

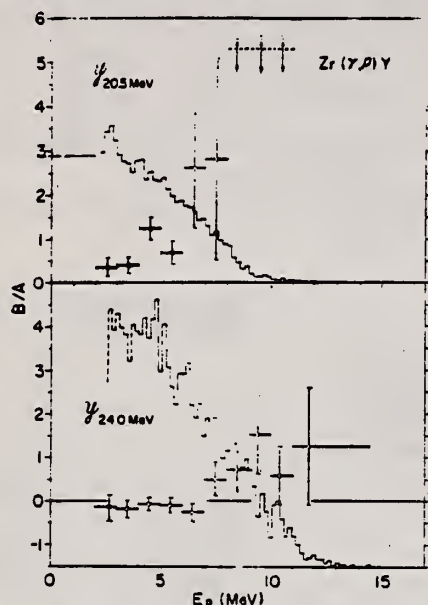


Fig. 5. Energy dependence of the anisotropic factor  $B/A$  of the angular distributions for photoprotons from Zr. See also the caption for Fig. 4.

A sign -- indicates that  $B/A$  is too large to plot the figure.

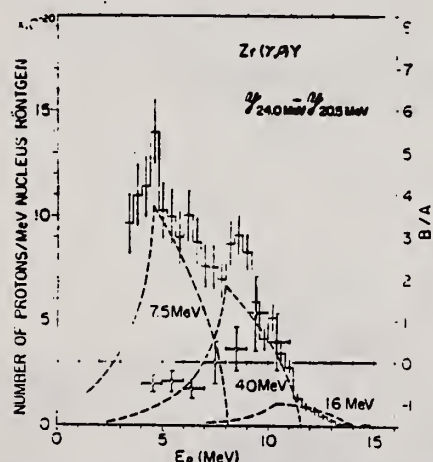


Fig. 8. The energy distribution and the anisotropic factor  $B/A$  for photoprotons from Zr obtained by subtraction of  $\gamma_{20.5\text{ MeV}}$  from  $\gamma_{26.0\text{ MeV}}$ . See also the caption for Fig. 6.

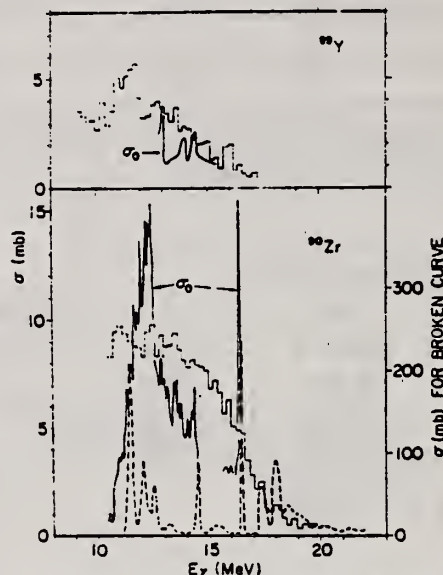


Fig. 9. The  $(\gamma, p)$  cross sections of  $^{90}\text{Y}$  and Zr in the photon energy region lower than 20 MeV. The  $(\gamma, p_0)$  cross sections deduced from the inverse reaction cross sections are shown by solid lines indicated by  $\sigma_0$ . Theoretical  $^{90}\text{Zr}(\gamma, p_0)^{90}\text{Y}$  cross section<sup>10</sup> is shown by broken line.

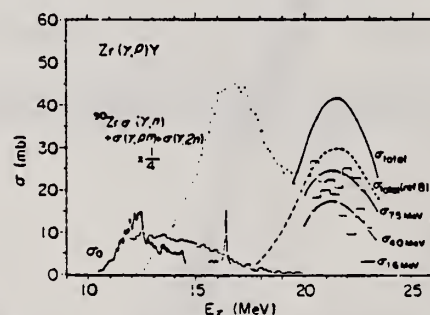


Fig. 11. Cross sections for strong photoproton transitions on Zr. Photoproton cross section obtained from the yield curve,<sup>11</sup> neutron emission cross section<sup>10</sup> and the results of the  $^{90}\text{Y}(p, \gamma_0)^{90}\text{Zr}$  reaction<sup>4, 5, 11, 12</sup> are also shown.



METHOD

REF. NO.

70 Ax 1

hmg

REACTION	RESULT	EXCITATION ENERGY	SOURCE		DETECTOR		ANGLE
			TYPE	RANGE	TYPE	RANGE	
G,G	ABX	8-13	D	8-13	NAI-D		22

Total photon interaction cross section inferred.

<sup>13</sup>B.L. Berman, J.T. Caldwell, R.R. Harvey, M.A. Kelly, R.L. Bramblett, and S.C. Fultz, Phys. Rev. 162, 1098 (1967).

<sup>19</sup>E. Obst, F. Rauch, and E. Rossle, Phys. Letters 21, 50 (1966).

<sup>20</sup>E. Obst, F. Rauch, and H. G. Wahsweiler, Nucl. Phys. A103, 17 (1967).

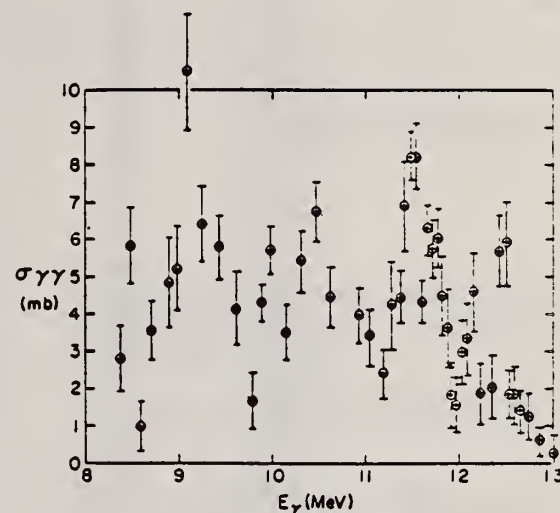


FIG. 1. The photon elastic-scattering cross section of Zr. The values assume that only <sup>90</sup>Zr contributes above 8.68 MeV. Numerical values are given in Table II.

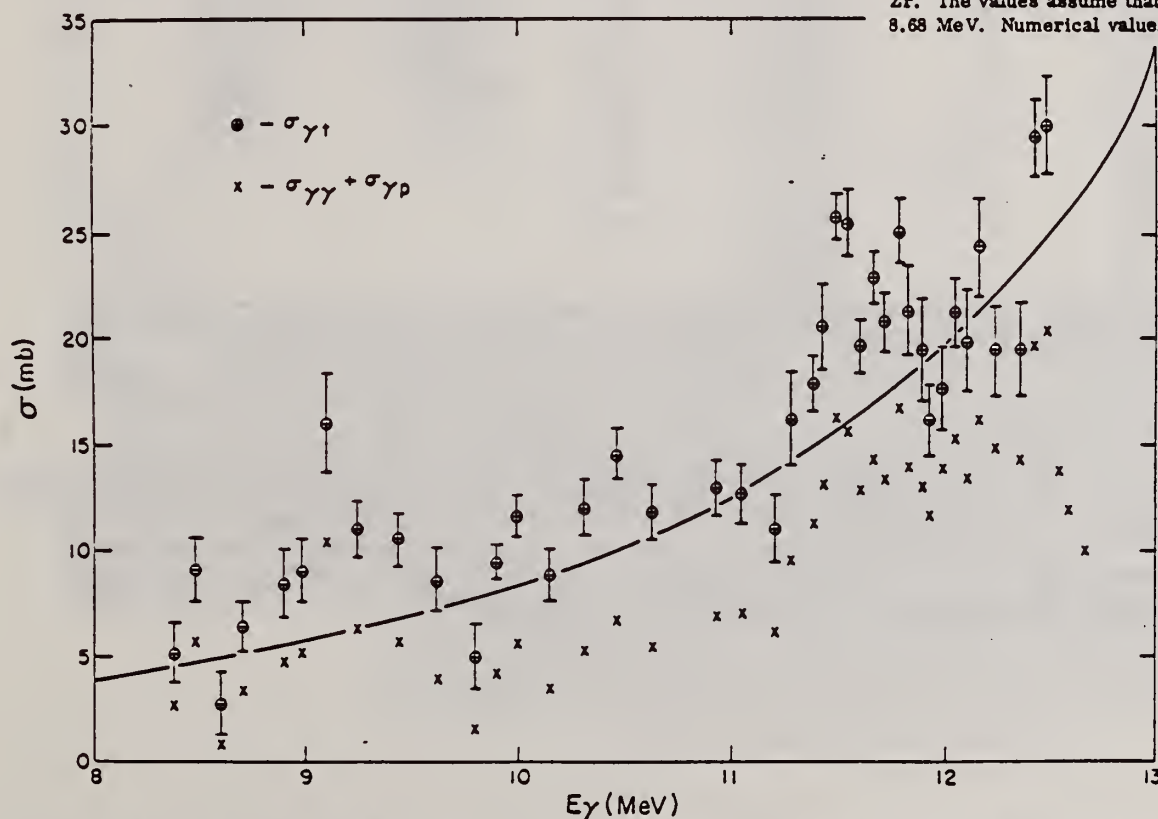


FIG. 4. The photon interaction cross section of <sup>90</sup>Zr. It was assumed that the elastic photon scattering above 8.68 MeV was due to <sup>90</sup>Zr. The inferred cross sections are shown by the circled crosses with experimental errors corresponding to the statistical uncertainty in only the elastic-scattering cross section. Below 10.62 MeV, the measured photon scattering cross section is shown by the diagonal crosses; at and above the 10.62 MeV the diagonal crosses represent the sum of the elastic scattering and photoproton cross sections inferred from the data in Refs. 19 and 20. The line is the low-energy extrapolation of the Lorentz line which matches the photoneutron cross section of <sup>90</sup>Zr in the giant resonance region according to Ref. 19.

TABLE II. Photon cross sections for  $^{90}\text{Zr}$ . See Sec. III for an explanation of the headings and entries in this table.

$E_\gamma$ (MeV)	$\Delta E_\gamma$ (keV)	$\sigma_{\gamma\gamma}^a$ (mb)	$\sigma_{\gamma p_0}^b$ (mb)	$\sigma_{\gamma s}^a$ (mb)	Single-particle units per MeV
8.38	60	$2.79 \pm 0.90$		$5.2 \pm 1.4$	0.047
8.49	60	$5.84 \pm 1.03$		$9.2 \pm 1.5$	0.082
8.60	60	$1.00 \pm 0.69$		$2.8 \pm 1.5$	0.024
8.70	110	$3.55 \pm 0.80$		$6.5 \pm 1.2$	0.055
8.89	60	$4.84 \pm 1.22$		$8.5 \pm 1.6$	0.068
8.98	60	$5.21 \pm 1.15$		$9.1 \pm 1.5$	0.072
9.09	60	$10.51 \pm 1.61$		$15.8 \pm 2.3$	0.125
9.24	60	$6.38 \pm 0.95$		$11.1 \pm 1.3$	0.083
9.43	120	$5.78 \pm 0.87$		$10.6 \pm 1.2$	0.076
9.61	60	$4.14 \pm 0.99$		$8.7 \pm 1.5$	0.061
9.79	60	$1.68 \pm 0.76$		$5.0 \pm 1.5$	0.033
9.88	70	$4.31 \pm 0.49$		$9.5 \pm 0.8$	0.063
9.98	70	$5.70 \pm 0.63$		$11.7 \pm 1.0$	0.075
10.14	110	$3.48 \pm 0.74$		$8.9 \pm 1.3$	0.055
10.31	70	$5.40 \pm 0.85$		$12.1 \pm 1.3$	0.073
10.46	80	$6.75 \pm 0.08$		$14.6 \pm 1.2$	0.085
10.62	120	$4.45 \pm 0.78$	1.1	$11.9 \pm 1.3$	0.056
10.92	70	$3.95 \pm 0.73$	3.1	$13.0 \pm 1.3$	0.069
11.04	70	$3.39 \pm 0.76$	3.7	$12.7 \pm 1.4$	0.067
11.20	70	$2.41 \pm 0.66$	3.8	$11.1 \pm 1.6$	0.057
11.28	70	$4.28 \pm 1.15$	5.3	$16.3 \pm 2.2$	0.082
11.38	70	$4.48 \pm 0.73$	6.8	$17.9 \pm 1.3$	0.088
11.42	70	$6.88 \pm 1.19$	6.3	$20.6 \pm 2.0$	0.100
11.49	70	$8.20 \pm 0.66$	8.0	$25.7 \pm 1.1$	0.124
11.54	70	$8.20 \pm 0.88$	7.5	$25.4 \pm 1.6$	0.122
11.60	70	$4.33 \pm 0.57$	8.6	$19.6 \pm 1.2$	0.095
11.66	70	$6.28 \pm 0.67$	8.1	$22.9 \pm 1.2$	0.109
11.71	70	$5.75 \pm 0.80$	7.7	$21.8 \pm 1.4$	0.101
11.78	70	$6.05 \pm 0.80$	10.7	$25.0 \pm 1.5$	0.116
11.82	70	$4.50 \pm 1.04$	9.6	$21.3 \pm 2.1$	0.098
11.88	70	$3.63 \pm 1.08$	9.5	$19.5 \pm 2.4$	0.089
11.92	70	$1.85 \pm 0.87$	9.9	$16.2 \pm 1.7$	0.073
11.98	70	$1.55 \pm 0.74$	12.4	$17.7 \pm 2.0$	0.079
12.04	70	$2.99 \pm 0.87$	12.3	$21.2 \pm 1.6$	0.093
12.09	70	$3.33 \pm 0.97$	10.2	$19.9 \pm 2.4$	0.088
12.16	70	$4.60 \pm 1.08$	11.6	$24.3 \pm 2.3$	0.105
12.23	70	$1.88 \pm 0.81$	13.0	$19.4 \pm 2.1$	0.083
12.35	70	$2.05 \pm 0.84$	12.3	$19.5 \pm 2.2$	0.082
12.42	70	$5.71 \pm 0.94$	14.0	$29.4 \pm 1.8$	0.122
12.47	70	$5.91 \pm 1.14$	14.4	$30.0 \pm 2.3$	0.124
12.54	80	$1.85 \pm 0.64$	12.0		
12.58	80	$1.85 \pm 0.81$	10.2		
12.66	80	$1.38 \pm 0.57$	8.6		
12.74	80	$1.28 \pm 0.64$			
12.86	80	$0.60 \pm 0.40$			
13.01	80	$0.27 \pm 0.50$			

<sup>a</sup> Assuming that  $^{90}\text{Zr}$  and  $^{92}\text{Zr}$  have equal cross sections below 8.68 MeV and that only  $^{90}\text{Zr}$  contributes above 8.68 MeV. The listed errors include only the effects of the statistical uncertainty in the number of scattered  $\gamma$  rays.

<sup>b</sup> The photoproton cross sections were calculated from the graphs of the  $p, \gamma_0$  reaction in Refs. 19 and 20. An isotropic angular distribution was assumed. The cross section in Ref. 20 was used to obtain an absolute scale for the data of Ref. 19 near 12-MeV excitation. In accordance with a private communication from Rauch, it was assumed that the detector used in Ref. 19 decreased in efficiency with increasing energy by 5% per MeV. Above 11.95 MeV, the photoproton cross sections are averages of the precise, very good resolution data of Ref. 20 over 100-keV intervals; the relative cross sections in this energy region should have negligible error. The reliability of the relative cross sections at lower energy appears to be of the order of or less than 10%. For example, there are local maxima at about 11.36, 11.45, and 11.63 MeV which are about 10% and which appeared in both the 0 and 90° data of Ref. 19; on the other hand, the 0 and 90° data differ from each other by about 10% in the energy range covered. The absolute cross section was estimated to have an uncertainty of 20% in Ref. 20. However, near 12.4 MeV, the absolute cross section of Ref. 21 (which is also estimated as being correct to within 20%) is about 1.5 times the value given in Ref. 20.



METHOD

REF. NO.

73 Ba 20

egf

REACTION	RESULT	EXCITATION ENERGY	SOURCE		DETECTOR		ANGLE
			TYPE	RANGE	TYPE	RANGE	
G,N	NOX	THR- 27	C	10- 27	BF3-I		4PI

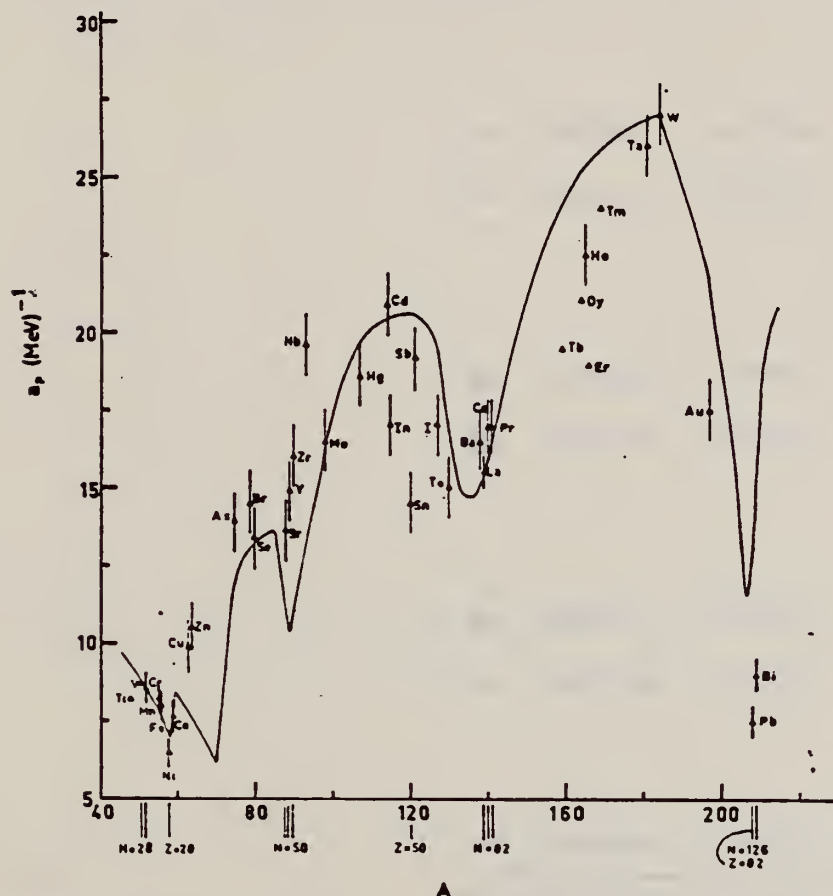


Fig. 12. Experimental values of the level density parameter  $a_p$  (Fermi gas formula plus pairing correction) versus atomic number  $A$ . The continuous curve is a least-squares fit to the data of a theoretical calculation from Newton <sup>15</sup>.

- 1 H. Baba and S. Baba, Japan Atomic Energy Research Institute report JAERI-1183 (1969).
- 2 H. Baba, Nucl. Phys. A159, 625 (1970).
- 15 T.D. Newton, Can. J. Phys. 34, 804 (1956).

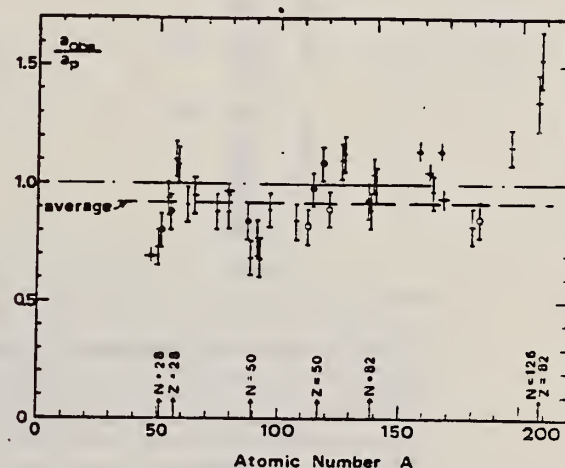


Fig. 15. Ratio  $a_{obs}/a_p$  versus atomic number  $A$ . Here  $a_{obs}$  is the level density parameter taken from the neutron resonance work of refs. <sup>1,2</sup>, and  $a_p$  is the level density parameter derived from the present  $(\gamma, n)$  work. Filled circles represent points where nuclei in the neutron resonance and in the  $(\gamma, n)$  experiment were the same. Open circles represent points where the respective nuclei were approximately matched. Triangles represent points which are based on measurement of neutron mean energies at two bremsstrahlung energies only.

(over)

TABLE 3 (continued)

Target	$N$ (residual nucleus) <sup>a)</sup>	Goodness of fit <sup>b)</sup>		$\bar{E}_n(24)$ (MeV) <sup>c)</sup>	$T$ (MeV) <sup>d)</sup>	$a_p$ (MeV <sup>-1</sup> ) <sup>e)</sup>	$a_{obs}$ (MeV <sup>-1</sup> ) <sup>f)</sup>	$a_{obs}/a_p$
Y	49 100%	G	G	1.30		14.9- <sup>88</sup> Y	10.17- <sup>90</sup> Y	0.68
Zr	49 52%	F	F	1.28		16.0- <sup>90</sup> Zr	12.2 - <sup>91</sup> Zr	0.77
	50 11%							
	51 17%							
	53 17%							
	55 3%							
Nb	51 100%	F	F	1.28		19.6- <sup>92</sup> Nb	13.15- <sup>94</sup> Nb	0.68
Mo	49 16%	G	G	1.27		16.5- <sup>93</sup> Mo	14.7 - <sup>97</sup> Mo	0.89
	51 9%							
	52 16%							
	53 17%							
	54 10%							
	55 24%							
	57 8%							
Ag	59 51%	V.P.	F	1.27	0.55	18.6- <sup>107</sup> Ag	15.61- <sup>108</sup> Ag	0.84
	61 49%							
Cd	57 1%	V.P.	F	1.24	0.54	20.9- <sup>111.4</sup> Cd	17.0 - <sup>112</sup> Cd	0.82
	61 12%							
	62 13%							
	63 24%							
	64 12%							
	65 29%							
	67 8%							
In	63 4%	V.P.	F	1.26	0.57	17.0- <sup>114</sup> In	16.66- <sup>114</sup> In	0.98
	65 96%							
Sn (Z = 50)	65 14%	V.P.	V.P.	1.38	0.73	14.5- <sup>118</sup> Sn	15.9 - <sup>118</sup> Sn	1.09
	66 8%							
	67 24%							
	68 9%							
	69 33%							
	71 5%							
	73 6%							
Sb	69 57%	V.P.	P	1.2	0.68	19.2- <sup>121</sup> Sb	17.0 - <sup>121</sup> Sb	0.89
	71 43%							
Te	69 2%	V.P.	F	1.36	0.83	15.0- <sup>127</sup> Te	17.0 - <sup>127</sup> Te	1.13
	71 5%							
	72 7%							
	73 19%							
	75 32%							
	77 34%							
I	73 100%	F	G	1.23	0.70	17.0- <sup>124</sup> I	17.02- <sup>124</sup> I	1.00

<sup>a)</sup> Neutron numbers and abundances of respective residual nuclei in ( $\gamma$ , n) experiments.

<sup>b)</sup> These give an assessment of the goodness of fit of a calculated  $\bar{E}_n$  versus  $E_0$  curve to the observed data, using the Fermi gas level density formula both without and with pairing corrections.

<sup>c)</sup> Bremsstrahlung photoneutron mean energies  $\bar{E}_n$  for peak bremsstrahlung energy  $E_0 = 24$  MeV.

<sup>d)</sup> Nuclear temperature from fit with constant-temperature formula.

<sup>e)</sup> Level density parameter  $a_p$  derived from the present ( $\gamma$ , n) experiment, using a Fermi gas formula plus pairing correction, and corresponding residual nucleus (the atomic weight shown is the weighted average of atomic weights of the respective isotopes present).

<sup>f)</sup> As column 7, but using data on n-resonance absorption from refs. 1, 2).

<sup>g)</sup> Measurements of  $\bar{E}_n(E_0)$  for these nuclei were made only for  $E_0 = 21, 23$  and 24 MeV.

Zr  
A=89

Zr  
A=89

Zr  
A=89



REF. S. Costa, F. Ferrero, S. Ferroni, L. Pasquallini and E. Silva - also  
Istituto Nazionale di Fisica Nucleare - Sezione di Torino  
Nuclear Phys. 72, 158 (1965)

ELEM. SYM.	A	Z
Zr	89	40

METHOD	REF. NO.	
	65 Co 1	EGF

REACTION	RESULT	EXCITATION ENERGY	SOURCE		DETECTOR		ANGLE
			TYPE	RANGE	TYPE	RANGE	
G,N	ABX	THR - 70	C	12 - 70	ACT-I		4PI

Measured isomer production ratio.  
Spin cut off < 1.5

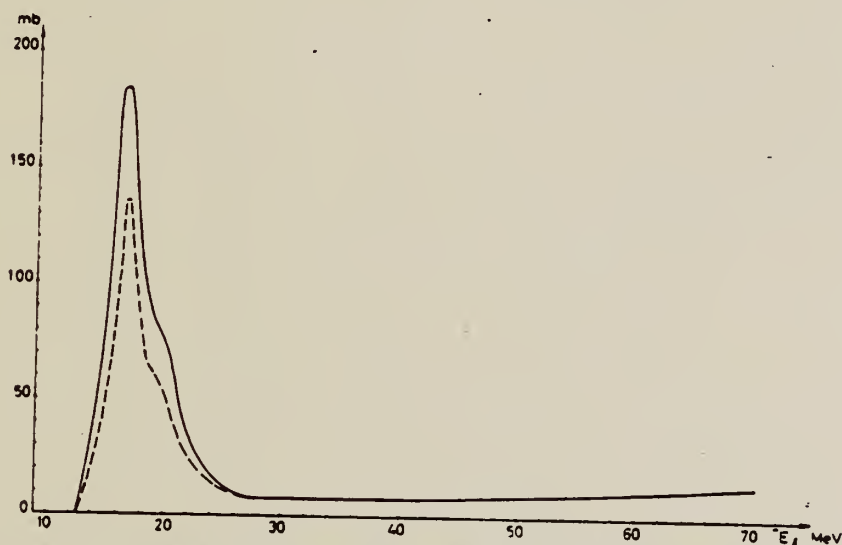


Fig. 2. ( $\gamma$ , n) reaction in  $^{90}\text{Zr}$ , total (solid line) and  $\frac{1}{2}^-$  state (dashed line) cross sections.

TABLE I  
Spins and half-lives of isomeric states

Target nucleus	Spin of isomeric states	Half-life	Modes of decay (used for detection)	Detection method
$^{40}\text{K}$	$0^+$	0.95 sec	$\beta^+$ (100 %)	$\gamma$ - $\gamma$ fast-slow coincidence (resolving time 0.2 and 2 $\mu\text{sec}$ )
$J = \frac{1}{2}$	$3^+$	7.7 min	$\beta^+$ (> 99 %)	$\gamma$ - $\gamma$ coincidence
$^{90}\text{Zr}$	$\frac{1}{2}^-$	4.3 min	$\gamma$ (93 %) $\beta^+$ (1.7 %)	Nal (well type) spectrometer centered on the 0.588 MeV $\gamma$ ray line $\gamma$ - $\gamma$ coincidence
$J = 0$	$\frac{1}{2}^+$	79 h	$\beta^+$ (30 %)	$\gamma$ - $\gamma$ coincidence
$^{99}\text{Mo}$	$\frac{1}{2}^-$	66 sec	$\gamma$ (57 %) $\beta^+$ (38 %)	Nal (well type) spectrometer centered on the 0.658 MeV $\gamma$ ray line $\gamma$ - $\gamma$ coincidence
$J = 0$	$\frac{1}{2}^+$	16 min	$\beta^+$ (94 %)	$\gamma$ - $\gamma$ coincidence





$Z_R$   
 $A=90$

$Z_R$   
 $A=90$

$Z_R$   
 $A=90$



Elem. Sym.	A	Z
Zr	90	40
Ref. No.		
56 Ax 1		EGF

Method Betatron; Victoreen ionization in 8 cm Lucite; radioactivity

Reaction	E or $\Delta E$	$E_0$	$\Gamma$	$\int \sigma dE$	$J\pi$	Notes
( $\gamma, n$ )	Bremss. 11.8-22.5					<p>79 hour (ground state) <math>E_{th}=11.78\pm0.09</math> MeV.</p> <p>4.4 min (m.s.), <math>E_{th}=12.37\pm0.09</math> MeV.</p> <p>Figure 7: Work based on separation of 913 keV <math>\gamma</math> (79 hour) from 588 keV (4.4 min). Rise in "c" above 18.5 MeV probably comes from <math>Zr^{91}(\gamma, 2n)Zr^{89}</math> ground state.</p> <p> <math>Zr^{90}</math> - 51.5%  <math>Zr^{91}</math> - 11.2%  <math>Zr^{92}</math> - 17.1%  <math>Zr^{94}</math> - 17.4%  <math>Zr^{96}</math> - 2.8% </p>

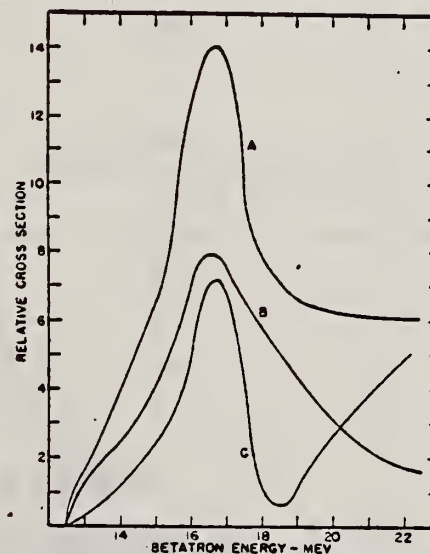


FIG. 7. Relative cross sections. Curve A is the cross section for the formation of the 79-hour activity, Curve B the formation cross section of the 4.4-minute activity, and Curve C the direct production cross section of the 79-hour activity.

Ref. P.F. Yergin, B.P. Fabricand  
Phys. Rev. 104, 1334 (1956)

Elem. Sym.	A	Z
Zr	90	40

Method	Ref. No.
24 MeV betatron; 250r Victoreen in 3.75 cm Lucite; neutron detector	56 Ye 2
	EGF

Reaction	E or ΔE	E <sub>0</sub>	Γ	∫σdE	Jπ	Notes
Zr <sup>90</sup> (γ,xn)	Bremss. 24	15.8	4.3 MeV	∫ <sub>0</sub> <sup>23</sup> = 0.98 MeV-b		

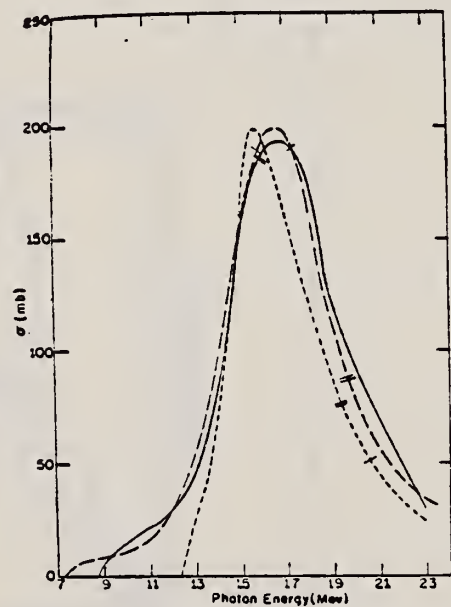


FIG. 5. Cross sections for the (γ,n) reactions in zirconium isotopes. Short dashes Zr<sup>20</sup>, long dashes Zr<sup>21</sup>, full curve Zr<sup>22</sup>. The previously published Zr<sup>20</sup> and Zr<sup>21</sup> results have been recomputed, taking into account the present Zr<sup>22</sup> measurements. The single and double slash marks on each curve represent the locations of the (γ,pn) and (γ,2n) thresholds respectively. The units of the ordinate are 10<sup>-27</sup> cm<sup>2</sup>.

TABLE III. Parameters of giant-resonance cross-section curves for (γ,n) reactions in nuclei near 50 neutrons. Nuclides <sup>42</sup>As<sup>75</sup>, <sup>44</sup>Nb<sup>93</sup>, and <sup>45</sup>Rh<sup>103</sup> from reference 4, <sup>40</sup>Zr<sup>90</sup> and <sup>40</sup>Zr<sup>91</sup> from reference 5 recomputed in present work. Neutron number is shown in column 2, location of peak cross-section value in column 3, peak cross-section value in column 4, half-height width of curve in column 5, and area under curve from threshold to 23 MeV in column 6.

Nuclide	N	E <sub>m</sub> (MeV)	σ <sub>m</sub> (millibarns)	Γ (MeV)	∫ <sub>thr</sub> <sup>23</sup> σdE (MeV-barns)
<sup>42</sup> As <sup>75</sup>	42	17.3	90.3	9.0	0.80
<sup>44</sup> Nb <sup>93</sup>	48	15.9	160	5.0	0.92
<sup>45</sup> Rh <sup>103</sup>	49	15.8	146	5.3	1.00
<sup>40</sup> Zr <sup>90</sup>	50	16.3	201	4.0	1.05
<sup>40</sup> Zr <sup>91</sup>	50	16.3	191	3.8	0.87
<sup>40</sup> Zr <sup>90</sup>	50	15.8	199	4.3	0.98
<sup>40</sup> Zr <sup>91</sup>	51	16.5	200	5.0	1.22
<sup>40</sup> Zr <sup>92</sup>	52	16.9	193	5.5	1.24
<sup>41</sup> Nb <sup>93</sup>	52	17.0	195	6.8	1.46
<sup>45</sup> Rh <sup>103</sup>	58	16.5	205	8.9	1.94



Method Betatron; neutron yield; radioactivity; r- chamber

Ref. No.	
59 Mu 2	NVB

Reaction	E or $\Delta E$	$E_0$	$\Gamma$	$\int \sigma dE$	$J\pi$	Notes
$Zr^{90}(\gamma, n)$	Bremss. 12-25	16.8	2.9 MeV			

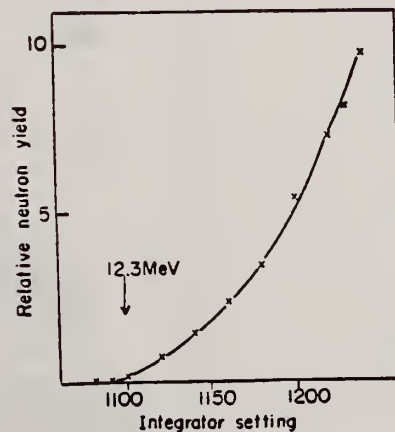


Fig. 3-1. Activation curve near threshold for  $Zr^{90}(\gamma, n)Zr^{89m}$ .

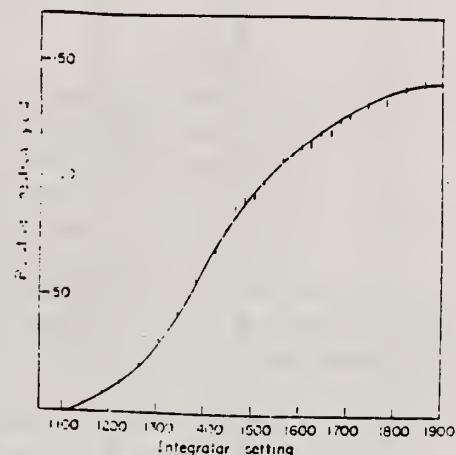


Fig. 4-1. Activation curve for  $Zr^{90}(\gamma, n)Zr^{89m}$ .

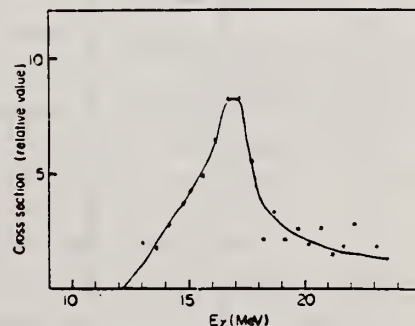


Fig. 5-1. Cross section curve for  $Zr^{90}(\gamma, n)Zr^{89m}$ .

Elem. Sym.	A	Z
Zr	90	40
Ref. No. 59 Na 1		
EGF		

Method  $\text{BF}_3$  counters; 24 MeV Bremss.; Betatron

Reaction	E or $\Delta E$	$E_0$	$\Gamma$	$\int \sigma dE$	$J\pi$	Notes
$(\gamma, xn)$	5.0-24	16.0	4.1	0.89 MeV-mb		<p><math>E_{th} = 12.2 \text{ MeV}; \sigma_{max} = 18.5 \text{ mb.}</math></p> <p>No Corrections.</p> <p>[NOTE: <u>Figure 3</u>: Ref 8: Katz, Baker, Montalbetti, Can j. Phys. <u>31</u>, 250 (1953).]</p>

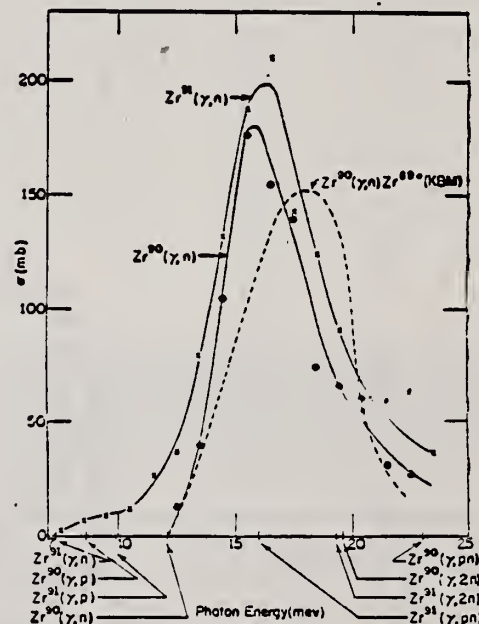


FIG. 3.  $(\gamma, n)$  cross sections for  $\text{Zr}^{90}$  and  $\text{Zr}^{91}$ . The ordinate scale is in millibarns ( $10^{-27} \text{ cm}^2$ ). The points shown are those calculated from the yield data. The solid curves are drawn to fit the points. The dashed curve is the cross section reported (see reference 8) for the production of the isomeric state of  $\text{Zr}^{99}$  by photon bombardment of natural Zr. The locations of the thresholds for various reactions in the two isotopes are indicated by the arrows.

Method 30 MeV electron synchrotron; activation; NaI

Ref. No.	JHH
62 Ca 1	

Reaction	E or ΔE	E <sub>0</sub>	Γ	∫σdE	Jπ	Notes
Zr <sup>90</sup> (γ,n)	Bremss. 30					

TABLE 1  
Isomeric Ratios from (γ,n) reactions

Target Nucleus	J <sub>0</sub>	Residual Nucleus				Isomer ratio		
		Ground state		Metastable state		Y <sub>1</sub> /(Y <sub>1</sub> + Y <sub>2</sub> )	Y <sub>1</sub>	
		Spin	Half-life	Spin	Half-life			
Co <sup>59</sup>	7/2 <sup>+</sup>	Co <sup>58</sup>	2 <sup>+</sup>	71.3d	5 <sup>+</sup>	3.2h	0.24 ± 0.02	3.2 ± 0.1
Ce <sup>76</sup>	0 <sup>+</sup>	Ce <sup>75</sup>	1/2 <sup>+</sup>	82m	7/2 <sup>+</sup>	49m	0.38 ± 0.07	2.8 ± 0.1
Zr <sup>81</sup>	3/2 <sup>+</sup>	Zr <sup>80</sup>	1 <sup>+</sup>	10m	5 <sup>+</sup>	4.3h	0.32 ± 0.02	6.5 ± 1.0
Zr <sup>86</sup>	0 <sup>+</sup>	Zr <sup>85</sup>	9/2 <sup>+</sup>	64d	1/2 <sup>+</sup>	70m	0.36 ± 0.07	2.2 ± 0.1
Zr <sup>90</sup>	0 <sup>+</sup>	Zr <sup>89</sup>	9/2 <sup>+</sup>	79h	1/2 <sup>+</sup>	4.4m	0.33 ± 0.10	2.8 ± 0.7
Mo <sup>92</sup>	0	Mo <sup>91</sup>	9/2 <sup>+</sup>	15.7m	1/2 <sup>+</sup>	56m	0.46 ± 0.04	6 ± 2
Ag <sup>107</sup>	1/2 <sup>+</sup>	Ag <sup>106</sup>	1 <sup>+</sup>	24m	6	3.3d	0.22 ± 0.02	2.0 ± 0.3
In <sup>113</sup>	9/2 <sup>+</sup>	In <sup>112</sup>	1 <sup>+</sup>	14.5m	3 <sup>+</sup>	20.7m	0.8 ± 0.1	3.1 ± 0.7
Cd <sup>116</sup>	0 <sup>+</sup>	Cd <sup>115</sup>	1/2 <sup>+</sup>	53h	11/2 <sup>+</sup>	43d	≤ 0.2	≤ 3
Ce <sup>140</sup>	0 <sup>+</sup>	Ce <sup>139</sup>	3/2 <sup>+</sup>	140d	11/2 <sup>+</sup>	35d	0.38 ± 0.01	2.5 ± 0.2
Hg <sup>198</sup>	0 <sup>+</sup>	Hg <sup>197</sup>	1/2 <sup>+</sup>	65h	5/2 <sup>+</sup>	24m	0.05 ± 0.01	5.4 ± 0.5
						3/2 <sup>+</sup> 5/2 <sup>+</sup>		
Previous work								
Zr <sup>81(10)</sup>	3/2 <sup>+</sup>	Zr <sup>80</sup>	1 <sup>+</sup>	10m	5 <sup>+</sup>	4.3h	0.33	6.5
Zr <sup>82(12)</sup>	0 <sup>+</sup>	Zr <sup>81</sup>	1/2 <sup>+</sup>	10m	7/2 <sup>+</sup>	57m	0.3	3.0
Zr <sup>80(11)</sup>	0 <sup>+</sup>	Zr <sup>89</sup>	9/2 <sup>+</sup>	79h	1/2 <sup>+</sup>	4.3h	0.44 ± 0.06	4.5 ± 1
In <sup>115(23)</sup>	9/2 <sup>+</sup>	In <sup>114</sup>	1 <sup>+</sup>	72m	5 <sup>+</sup>	50d	0.85	5.0
							(Y <sub>1</sub> = 2.5%)	

Previous work

Zr <sup>81(10)</sup>	3/2 <sup>+</sup>	Zr <sup>80</sup>	1 <sup>+</sup>	10m	5 <sup>+</sup>	4.3h	0.33	6.5
Se <sup>82(12)</sup>	0 <sup>+</sup>	Se <sup>81</sup>	1/2 <sup>+</sup>	10m	7/2 <sup>+</sup>	57m	0.5	3.0
Zr <sup>90(11)</sup>	0 <sup>+</sup>	Zr <sup>89</sup>	9/2 <sup>+</sup>	79h	1/2 <sup>+</sup>	4.3m	0.44 ± 0.06	4.5 ± 1
In <sup>115(23)</sup>	9/2 <sup>+</sup>	In <sup>114</sup>	1 <sup>+</sup>	72s	5 <sup>+</sup>	50d	0.85	3.0

The yields, Y<sub>1</sub> and Y<sub>2</sub>, are for (γ,n) reactions ending in the isomeric - or ground - state. The yield Y<sub>1</sub> is for the higher-spin state.

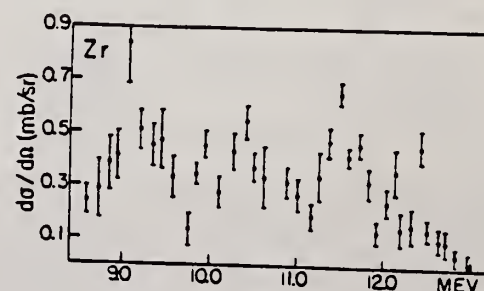
# REFERENCES

- 1) J. R. Huizenga and R. Vandenbosch, Phys. Rev. 120 (1960) 1305
- 2) T. Ericson, Advances in Physics, 2 (1960) 425
- 3) D. L. Allan, Nuclear Physics 24 (1961) 274
- 4) C. T. Hibdon, Phys. Rev. 114 (1959) 179
- 5) C. T. Hibdon, Phys. Rev. 122 (1961) 1235
- 6) T. Ericson, Nuclear Physics 11 (1959) 481
- 7) J. H. Carver and G. A. Jones, Nuclear Physics 19 (1960) 184
- 8) A. C. Douglas and N. MacDonald, Nuclear Physics 13 (1959) 382
- 9) T. Ericson and V. M. Scuturski, Nuclear Physics 2 (1958) 284
- 10) L. Katz, L. Pease and H. Moody, Can. J. Phys. 30 (1952) 476
- 11) L. Katz, R. G. Baker and R. Montalbetti, Can. J. Phys. 31 (1953) 250
- 12) E. Silva and J. Goldenberg, An. Acad. Brasil Cienc. 28 (1956) 275
- 13) J. H. Carver and D. C. Peaslee, Phys. Rev. 122 (1960) 2155
- 14) J. M. Blatt and V. F. Weisskopf, "Theoretical Nuclear Physics" New York: Wiley (1952)
- 15) S. E. Vogors, L. L. Marsden and R. L. Heath, U.S. Atomic Energy Commission Report IDO-16370 (1958)
- 16) Nuclear Data Sheets, National Research Council, Washington (1960, up to and including Set 5)
- 17) R. Vandenbosch and J. R. Huizenga, Phys. Rev. 120 (1960) 1313
- 18) E. Weigold and R. Glover, Nuclear Physics (in press)
- 19) K. J. Le Couteur and D. W. Lang, Nuclear Physics 13 (1959) 32
- 20) T. D. Newton, Can. J. Phys. 34 (1956) 904
- 21) D. W. Lang, Nuclear Physics 26 (1961) 434
- 22) M. E. Rose, "Internal Conversion Coefficients", Amsterdam: North Holland Publishing Co. (1958)
- 23) J. Goldenberg and L. Katz, Phys. Rev. 90 (1953) 308

Elem. Sym.	A	Z
Zr	90	40

Method Betatron; bremsstrahlung monochromator; photon scattering;  
NaI spectrometerRef. No.  
63Ax1

Reaction	E or $\Delta E$	$E_0$	$\Gamma$	$\int \sigma dE$	$J\pi$	Notes
$Zr^{90}(\gamma, \gamma)$		9.1 10.4 11.5	( 500 KeV)			<p>Quasi-elastic scattering - poor resolution of photon detector did not separate high-energy inelastic scattering from elastic scattering.</p> <p>Fig.: <math>135^\circ</math>-quasi elastic cross section.</p> <p>Optical model considered.</p> <p>Natural target - assumes all scattering from <math>Zr^{90}</math>.</p>





REF.	J. L. Black and N. W. Tanner Phys. Letters <u>11</u> , 135 (1964)		ELEM. SYM.	A	Z	
			Zr	90	40	
METHOD	Tandem; $Y^{89}(p,\gamma_0)Zr^{90}$		REF. NO.			
			64 B1 2		JOC	
REACTION	RESULT	EXCITATION ENERGY	SOURCE		ANGLE	
			TYPE	RANGE		
DETECTOR						
TYPE	RANGE	TYPE	RANGE			
P,G	RLX	13-17	D	5-9	NAI-D	DST
			(5.5 - 8.5)			

ANALOGUE T =

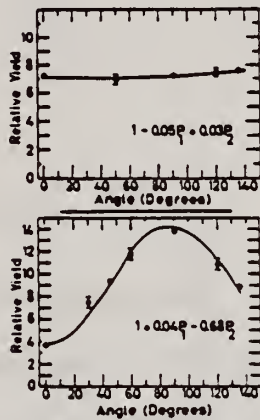


Fig. 2. Angular distributions of  $Y^{89}(p,\gamma)Zr^{90}$ . Upper: Measured at the peak of the 6.15 MeV resonance. Lower: Measured at the peak of the 8.04 MeV resonance. The full curves are plots of the Legendre polynomial fits given on the figure.

$E_p = 6.15 \text{ MeV} \quad W(\theta) = 1 - (0.05 \pm .03) P_1(\cos \theta)$

$E_p = 8.04 \text{ MeV} \quad W(\theta) = 1 + (0.04 \pm 0.04) P_1(\cos \theta) - (0.68 \pm .04) P_2(\cos \theta)$

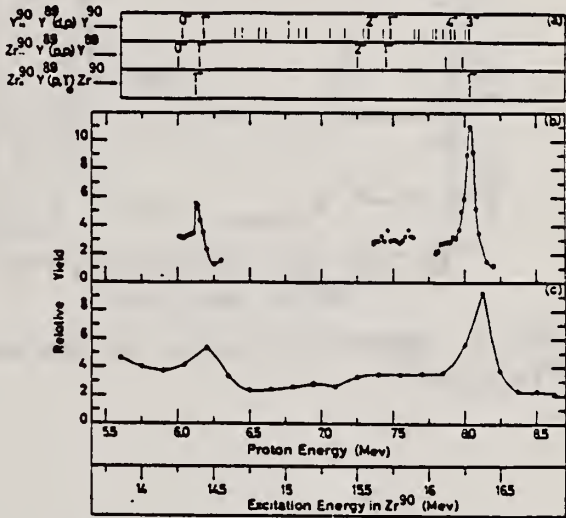


Fig. 1a. Upper: Energy levels of  $Y^{90}$  from  $Y^{89}(d,p)Y^{90}$ . The energy scale has been adjusted so that the ground state corresponds to the 4.82 MeV bombarding energy resonance seen in  $Y^{89}(p,n)Zr^{89}$ . Middle: Sharp resonances observed in  $Y^{89}(p,p)Y^{89}$  and  $Y^{89}(p,n)Zr^{89}$ . Lower: Sharp resonances observed in  $Y^{89}(p,\gamma)Zr^{90}$ . The energy scale for the three sections is the same as the energy scale for the main diagram. 1b. Excitation function measured at  $90^\circ$  for the  $Y^{89}(p,\gamma)Zr^{90}$  reaction. Resolution 20 keV. 1c. Excitation function measured at  $90^\circ$  with 150 keV resolution.



REF. J. Black, M. M. Islam, G. A. Jones, G. C. Morrison and R. B. Taylor  
Conference on Isobaric Spin (1966)

ELEM. SYM.	A	Z
Zr	90	40

METHOD

REF. NO.

66 B1 1

JOC

REACTION	RESULT	EXCITATION ENERGY	SOURCE		DETECTOR		ANGLE
			TYPE	RANGE	TYPE	RANGE	
P,G	RLY	14-17	D	5-9	NAI-D		DST

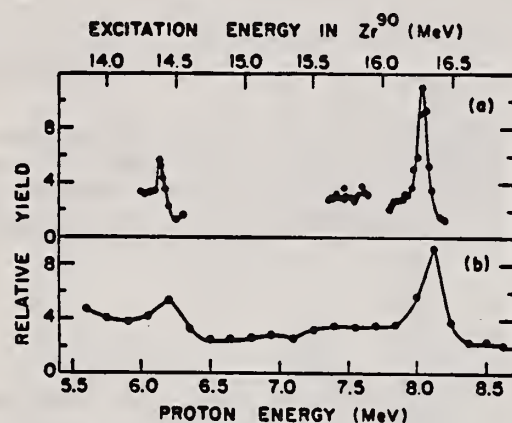


Fig. 1. Excitation function for the reaction  $Y^{89}(p, \gamma)Zr^{90}$ .

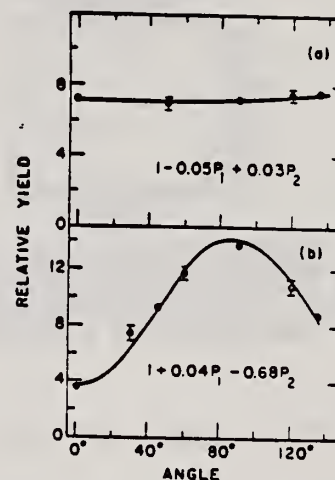


Fig. 2. Upper: Angular distribution of resonance at 6.15 MeV in  $Y^{89}(p, \gamma)$ ; Lower: Angular distribution of resonance at 8.04 MeV in  $Y^{89}(p, \gamma)$ .

$$W(\theta) = 1 - (0.05 \pm 0.03)P_1 + (0.03 \pm 0.04)P_2 \text{ for the } 6.15 \text{ MeV resonance and}$$

$$W(\theta) = 1 + (0.04 \pm 0.04)P_1 - (0.68 \pm 0.04)P_2 \text{ for the } 8.04 \text{ MeV resonance.}$$

REF. S. C. Fultz, R. L. Bramblett, B. L. Berman, J. T. Caldwell  
and M. A. Kelly  
Proc. Gatlinburg Conference 397 (1966)

ELEM. SYM.	A	Z
Zr	90	40

METHOD	REF. NO.	
	66 Fu 2	hmg

REACTION	RESULT	EXCITATION ENERGY	SOURCE		DETECTOR		ANGLE
			TYPE	RANGE	TYPE	RANGE	
G,XN	ABI	THR-28	D	THR-28	BF3-I		4PI
G,2N	ABI	THR-28	D	THR-28	BF3-I		4PI

TABLE 1

Integrated Cross Sections for Zirconium and Yttrium

Isotope	$E_{max}$ $a = \int \sigma_{int} dE$ (MeV - barns)	$E_{max}$ $b = \int \sigma_{7,28} dE$ (MeV - barns)	b/a	$E_{max}$ (MeV)
<sup>90</sup> Zr	0.980	0.108	0.110	28
<sup>91</sup> Zr	1.078	0.202	0.187	30
<sup>92</sup> Zr	1.096	0.447	0.408	28
<sup>94</sup> Zr	1.041	0.577	0.554	30
<sup>89</sup> Y	0.991	0.095	0.096	28

REF.			ELEM. SYM.			A			Z		
E. Obst, F. Rauch and E. Rossle Phys. Letters <u>21</u> , 50 (1966)			Zr			90			40		
METHOD			REF. NO.			66 Ob 1			EGF		
REACTION	RESULT	EXCITATION ENERGY	SOURCE		DETECTOR		ANGLE				
			TYPE	RANGE	TYPE	RANGE					
P,G	RLX	11 - 14	D	2 - 6	NAI-D	0 - 14	0,90				

$E_0$  3.5-6.5

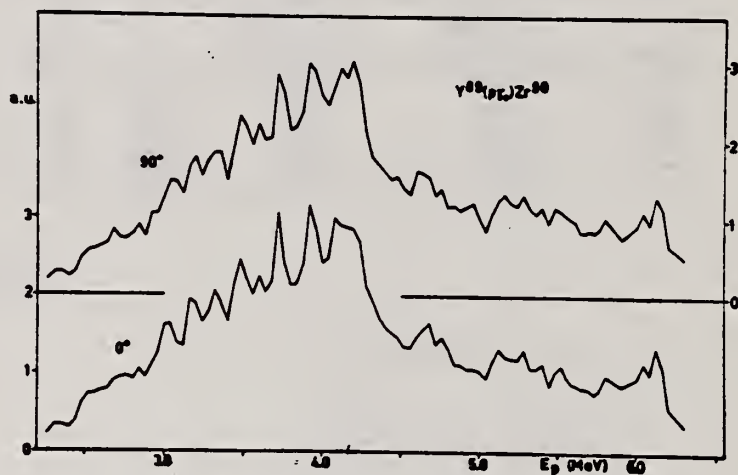


Fig. 1. Excitation curves of the reaction  $^{89}\text{Y}(p,\gamma)^{90}\text{Zr}$  at  $0^\circ$  and  $90^\circ$  in relative units.

REF. P. Axel, D. M. Drake, S. Whetstone and S. S. Hanna  
Phys. Rev. Letters 19, 1343 (1967)

ELEM. SYM.	A	Z
Zr	90	40

METHOD

REF. NO.

67 Ax 1

EGF

REACTION	RESULT	EXCITATION ENERGY	SOURCE		DETECTOR		ANGLE
			TYPE	RANGE	TYPE	RANGE	
P,G	ABX	14-25	D	5-17	NAI-D	10-24	90

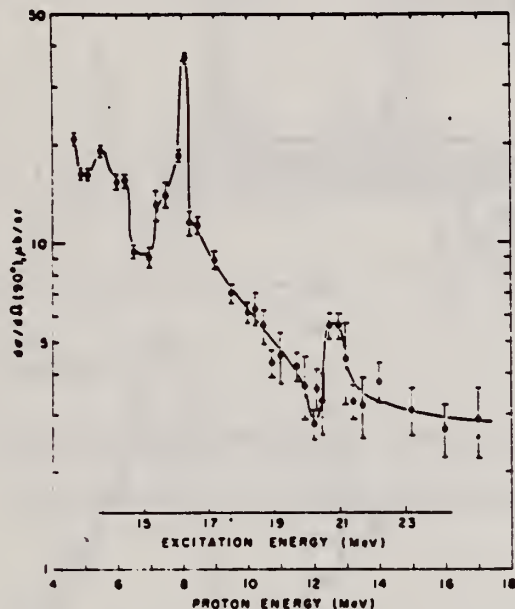


FIG. 1. Differential cross section of process  $^{88}\text{Y}(p, \gamma)^{90}\text{Zr}$  at  $90^\circ$ . The errors shown are statistical. Because of some uncertainty in the gamma-detector efficiency, absolute values are good probably to within 35%.

ELEM. SYM.	A	Z
Zr	90	40
REF. NO.	67 Be 2	
	hmg	

METHOD

REACTION	RESULT	EXCITATION ENERGY	SOURCE		DETECTOR		ANGLE
			TYPE	RANGE	TYPE	RANGE	
G,N <u>6+</u>	ABX	THR-28	D	THR-28	BF3-I		4PI
G,2N <u>5</u>	ABX	THR-28	D	THR-28	BF3-I		4PI

TABLE IV. Integrated cross sections.

Nucleus	$\sigma_{\text{int}}[(\gamma,n) + (\gamma,pn)]$ (MeV-b) <sup>a</sup>	$\sigma_{\text{int}}(\gamma,2n)$ (MeV-b) <sup>a</sup>	$E_{\gamma\text{max}}$ (MeV)	$\frac{\sigma_{\text{int}}(\gamma,2n)}{\sigma_{\text{int}}(\gamma, \text{total})^b}$	$(\frac{1}{2}\pi)\sigma_{\text{int}}\Gamma$ (MeV-b)	$0.06NZ/A$ (MeV-b)
$\text{Y}^{90}$	0.94	0.10	28	0.10	1.14	1.31
$\text{Zr}^{90}$	0.96	0.10	28	0.09	1.16	1.33
$\text{Zr}^{91}$	0.88	0.20	30	0.19	1.22	1.35
$\text{Zr}^{92}$	0.65	0.45	28	0.41	1.23	1.36
$\text{Zr}^{94}$	0.43	0.58	30	0.56 <sup>c</sup>	1.32	1.38

<sup>a</sup> All measured integrated cross-section values are given for an energy region from threshold to  $E_{\gamma\text{max}}$ . For the  $\text{Zr}^{90}$  and  $\text{Zr}^{91}$  cases, it was necessary to extrapolate the low-energy part of the total photoneutron cross section down to threshold; the error introduced in this process, however, is less than 0.5%.

<sup>b</sup> The word "total" in this table refers to the total photoneutron cross section  $\sigma[(\gamma,n) + (\gamma,pn) + (\gamma,2n) + (\gamma,3n)]$ , and excludes the  $(\gamma,\gamma)$  and  $(\gamma,p)$  cross sections.

<sup>c</sup> This value includes the contribution of  $\sigma_{\text{int}}(\gamma,3n)$ , which equals 0.03 MeV-b from threshold to 30 MeV.

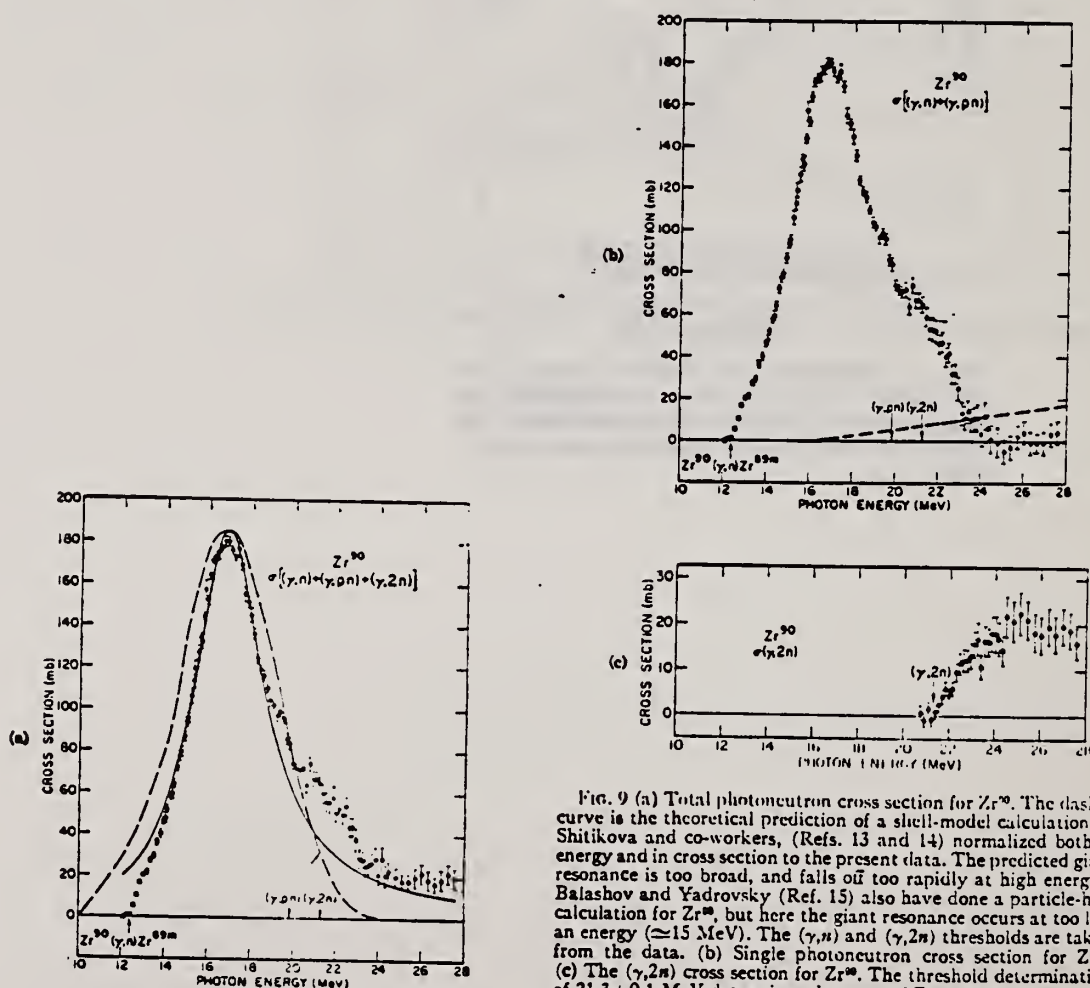


Fig. 9 (a) Total photoneutron cross section for  $\text{Zr}^{90}$ . The dashed curve is the theoretical prediction of a shell-model calculation by Shitikova and co-workers, (Refs. 13 and 14) normalized both in energy and in cross section to the present data. The predicted giant resonance is too broad, and falls off too rapidly at high energies. Balashov and Yarovskiy (Ref. 15) also have done a particle-hole calculation for  $\text{Zr}^{90}$ , but here the giant resonance occurs at too low an energy ( $\approx 15$  MeV). The  $(\gamma,n)$  and  $(\gamma,2n)$  thresholds are taken from the data. (b) Single photoneutron cross section for  $\text{Zr}^{90}$ . (c) The  $(\gamma,2n)$  cross section for  $\text{Zr}^{90}$ . The threshold determination of  $21.3 \pm 0.1$  MeV determines the mass of  $\text{Zr}^{92}$  (see text).



ELEM. SYM.	A	Z
Zr	90	40
REF. NO.		
67 Ob 1		EGF

METHOD			SOURCE		DETECTOR		ANGLE
REACTION	RESULT	EXCITATION ENERGY	TYPE	RANGE	TYPE	RANGE	
P,G	ABX	12-13	D	4-5	NAI-D	9-13	0

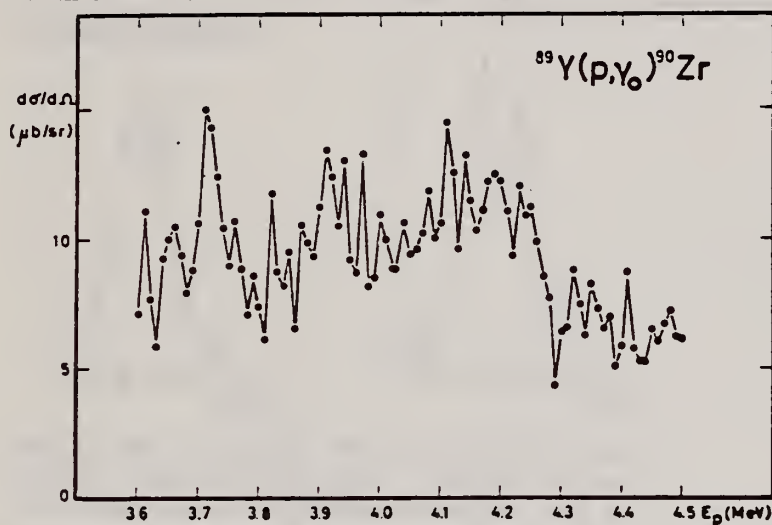


Fig. 4. Excitation curve of the transition  $\gamma_0$  measured in steps of 10 keV.

TABLE I  
Cross-section values

	$\frac{\sigma_i}{\sigma_0}$	$\frac{B_i(E1)}{B_0(E1)}$
$\gamma_0$	1	1
$\gamma_1$	$0.3 \pm 0.1$	$0.45 \pm 0.15$
$\gamma_2$	$1.0 \pm 0.2$	$1.75 \pm 0.35$

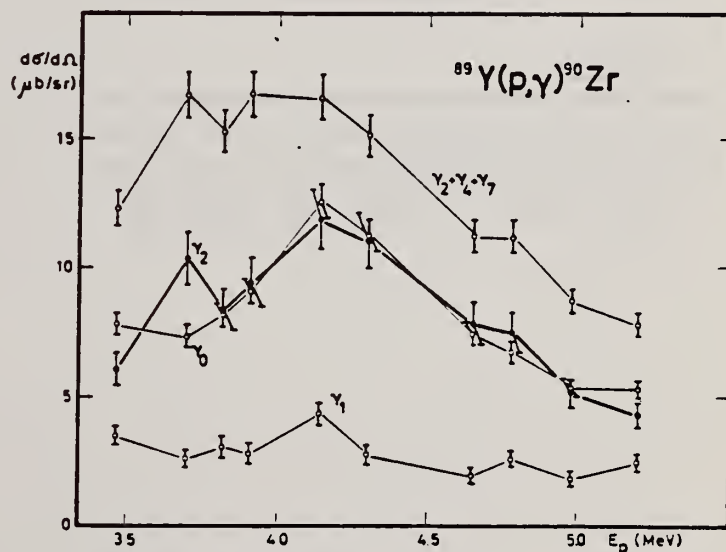


Fig. 5. Excitation curves of the transitions  $\gamma_0$ ,  $\gamma_1$ ,  $\gamma_2$ , and  $\gamma_2 + \gamma_4 + \gamma_7$ .

ELEM. SYM.	A	Z
Zr	90	40
REF. NO.		
68 Sh 4		egf

METHOD

REACTION	RESULT	EXCITATION ENERGY	SOURCE		DETECTOR		ANGLE
			TYPE	RANGE	TYPE	RANGE	
E,P	SPC	11-20	D	20	MAG-D	3-12	90

ANALOGUE STATES

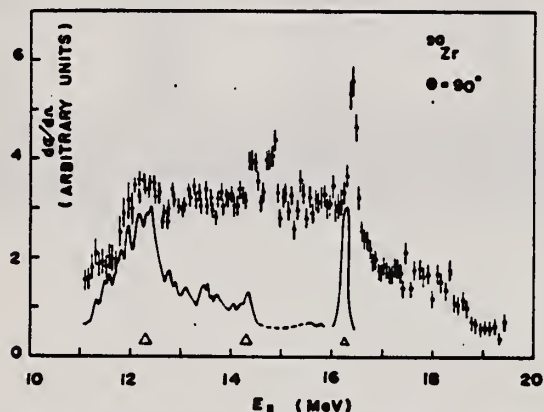


Fig. 1. Photoproton cross section for  $^{90}\text{Zr}$  calculated from the energy distribution of the  $E_p = 20.0$  MeV bombardment. The scale was constructed under the assumption that observed protons correspond to ground-state transitions. The triangles show the energy resolution. The solid curve is the  $(\gamma, p)$  cross section calculated from the  $(p, \gamma)$  data.

REF. G. P. Antropov, I. E. Mitrofanov, A. I. Prokof'ev and V. S. Russkikh  
Izv. Akad. Nauk Fiz. 33, 700 (1969)  
Bull. Acad. Sci. USSR-Phys. 33, 645 (1969)

ELEM. SYM.	A	Z
Zr	90	40

METHOD	REF. NO.
	69 An 7
	egf

REACTION	RESULT	EXCITATION ENERGY	SOURCE		DETECTOR		ANGLE
			TYPE	RANGE	TYPE	RANGE	
G,XN	ABX	12-23	C	12-23	BF3-I		4PI

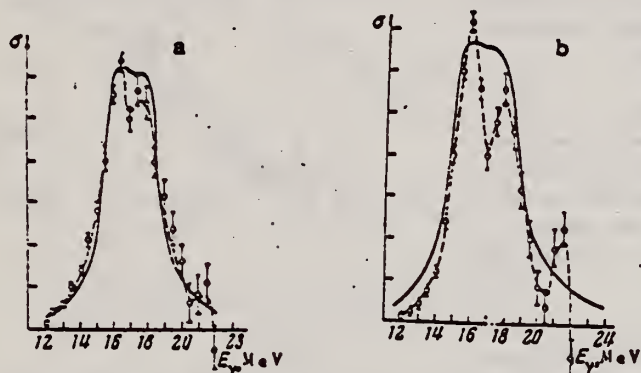


Fig.1. Cross section for the  $(\gamma, n)$  reaction in  $^{90}\text{Zr}$  (a) and  $^{91}\text{Zr}$  (b). The points and the dashed curve are experimental; the full curve is the sum of two Lorentz curves.

Table 1

Nucleus	$0.05 NZ/A$	$\frac{22.5 \text{ MeV}}{\int \sigma(E) dE}$	$\Gamma_{\text{exp}}, \text{ MeV}$	$\sigma_{\text{th}} = 0.00225 A^{1/2}$
$^{90}\text{Zr}$	1.33	1.27	4.0	0.91
$^{91}\text{Zr}$	1.35	1.42	4.2	1.02

Table 2

Nucleus	$\sigma_0$	$\sigma_1$	$\Gamma_0, \text{ MeV}$	$\Gamma_1, \text{ MeV}$	$E_0, \text{ MeV}$	$E_1, \text{ MeV}$
$^{90}\text{Zr}$	175	120	2.3	1.7	16.5	17.7
$^{91}\text{Zr}$	200	135	2.75	2	16.0	18

## METHOD

REF. NO.

69 Bo 2

egf

REACTION	RESULT	EXCITATION ENERGY	SOURCE		DETECTOR		ANGLE
			TYPE	RANGE	TYPE	RANGE	
E, E/	FME	2-4	D	58	MAG-D	50-58	DST
		(2.18, 2.74, 3.84)					

INELASTIC ELECTRON SCATTERING FROM  $^{90}\text{Zr}$ 

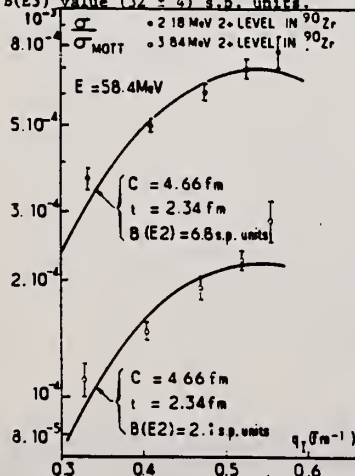
2.18 - 3.84 MEV

C.K. Bockelman, T.H. Curtiss, R.A. Eisenstein and D.W. Madsen, Electron Accelerator Laboratory, Yale University, New Haven, Connecticut, U.S.A. and J.B. Bellicard and P. Leconte, Service de Physique Nucléaire à Haute Energie, Centre d'Etudes Nucléaires de Saclay, France.

We have studied the collective states of zirconium-90 with the 70 MeV Lineac of the Yale University. At low energy such measurements determine by a unique way the reduced transition probabilities. For  $^{90}\text{Zr}$  these  $B(\text{EL})$  values may be compared with those given by the R.P.A. description of vibration for even isotones (Gillet et al., Phys. Letters 27B (1968) 483). We have carried out measurements on an enriched target of  $^{90}\text{Zr}$  using 58 MeV electrons. The momentum transfer varied from 0.3 to 0.6 fm. The total energy resolution was 120 keV. The prominent peaks at 2.18, 2.74 and 3.84 MeV are known to be  $2^+$ ,  $3^-$  and  $2^+$  respectively.

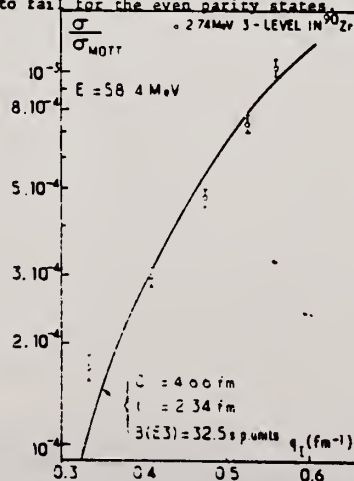
At high  $Z$ , we must use a distorted wave calculation to analyse our inelastic data, we have chosen the GEROW code (D.S. Onley, Phys. Rev. 134B (1964) 945). This code assumes an hydrodynamical model for the nucleus. For an EL transition, the transition charge density  $\rho_L \approx r^{L-1} \delta(r)$  contains the derivative of the static charge density described by the Fermi model. At low energy absolute Zr elastic static measurements have given us the value of the r.m.s. radius of  $\rho(r)$ . Starting from this r.m.s. value  $\langle r^2 \rangle^{1/2} = (4.12 \pm 0.05) \text{ fm}$ , we may choose the values  $c = 4.66 \text{ fm}$  and  $t = 2.34 \text{ fm}$  to compute the inelastic cross-sections.

Figure 2 is a plot of  $\sigma/\sigma_{\text{Mott}}$  vs  $q_L$  for  $2^+$  levels at 2.18 and 3.84 MeV. The solid curves are a theoretical calculation using the GEROW code with the indicated parameters. These states are not very collective as may be shown from their  $B(\text{E}2)$  values. Figure 3 shows the fit for the  $3^-$  state at 2.74 MeV. The collective character of this level is emphasized by the  $B(\text{E}3)$  value ( $32 \pm 4$ ) s.p. units.



$J^\pi$	E (MeV)	$B(\text{EL})$ s.p. units		
		2 Q.P.	2 Q.P. + core	Experiment
$2^+$	2.18	1.35	1.71	$6.8 \pm 1$
$3^-$	2.74	4.35	16.9	$32 \pm 4$

The comparison with the R.P.A. description given by Gillet is shown on the table. For the  $3^-$  state the inclusion of the particle hole core polarization has increased the  $B(\text{EL})$  by an order of magnitude. This helps to account for the experiment although there is still a discrepancy by a factor two which may not be serious because the  $B(\text{EL})$  depend strongly on the detail shape of the transition charge density. However, for the  $2^+$ , the discrepancy is much more important. Thus it is seen that the particle hole core excitation model may account for the odd parity state collectivity; however it seems to fail for the even parity states.





REF. M. Hasinoff, G. A. Fisher, H. M. Kuan and S. S. Hanna Phys. Letters <u>30B</u> , 337 (1969)			ELEM. SYM. Zr		90	40
METHOD			REF. NO. 69 Ha 1		egf	
REACTION	RESULT	EXCITATION ENERGY	SOURCE		DETECTOR	
			TYPE	RANGE	TYPE	RANGE
P,G	RLX	16-22	D	7-14	NAI-D	10-22

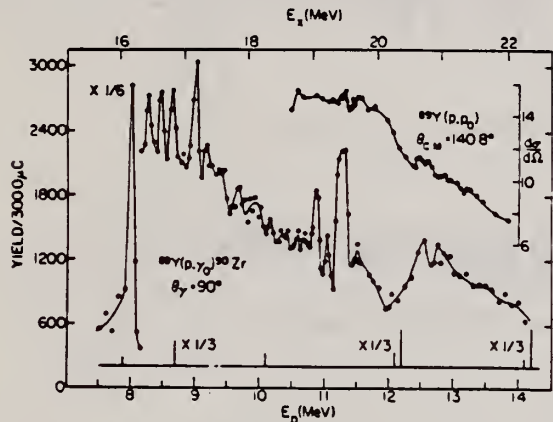


Fig. 1. Yield curves of  $^{89}\text{Y}(p,\gamma)^{90}\text{Zr}$  at  $90^\circ$  and  $^{89}\text{Y}(p,p_0)^{89}\text{Y}$  at  $140.8^\circ$ . The predicted resonances [2] are shown as vertical lines whose heights are proportional to  $\Gamma_{\gamma_0}$ . The 2nd, 4th, 5th, 6th, and 7th lines have been suppressed by a factor of 3.

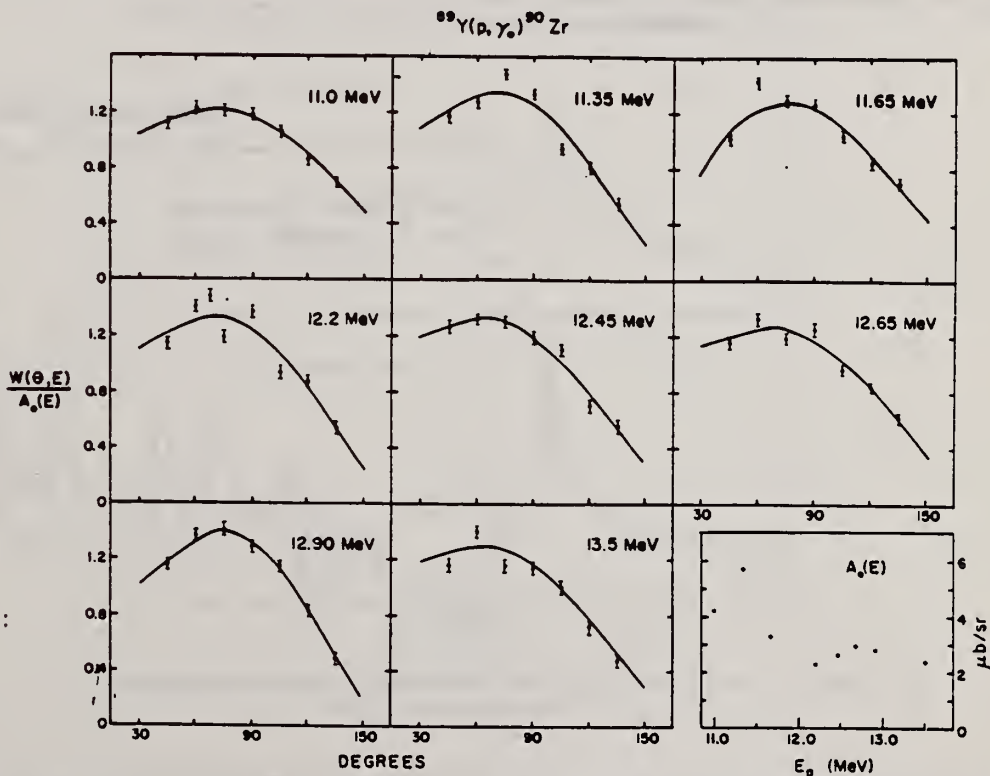


Fig. 2. Angular distributions in  $^{89}\text{Y}(p,\gamma)^{90}\text{Zr}$  at several energies on and off the resonances of fig. 1. The listed energies are values of  $E_p$ .



METHOD

REF. NO.

Page 1 of 3 69 Ma 4

egf

REACTION	RESULT	EXCITATION ENERGY	SOURCE		DETECTOR		ANGLE
			TYPE	RANGE	TYPE	RANGE	
P,G	ABX	10-27	D	2-19	NAI-D	10-27	DST

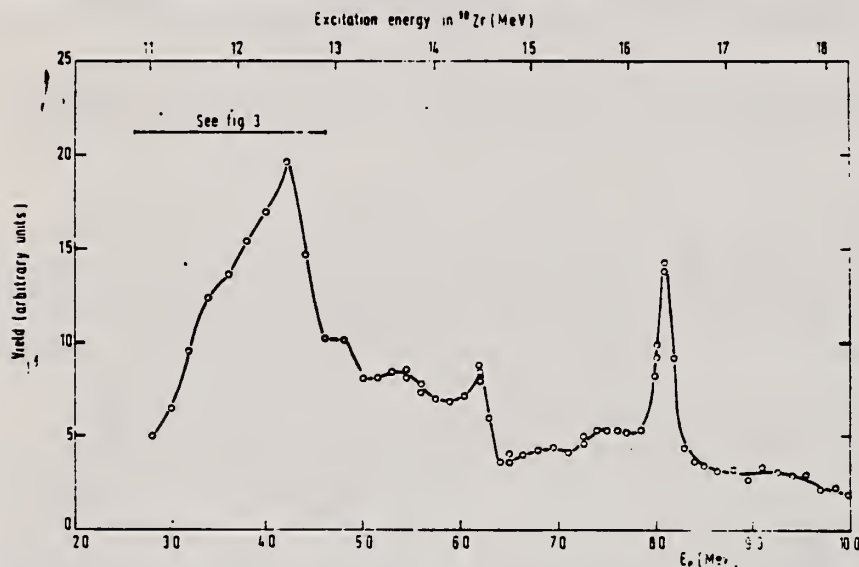


Fig. 2. The excitation function for the reaction  $^{88}\text{Y}(p, \gamma)^{88}\text{Zr}$  measured at  $\theta = 90^\circ$  with an energy resolution of 150 to 200 keV.

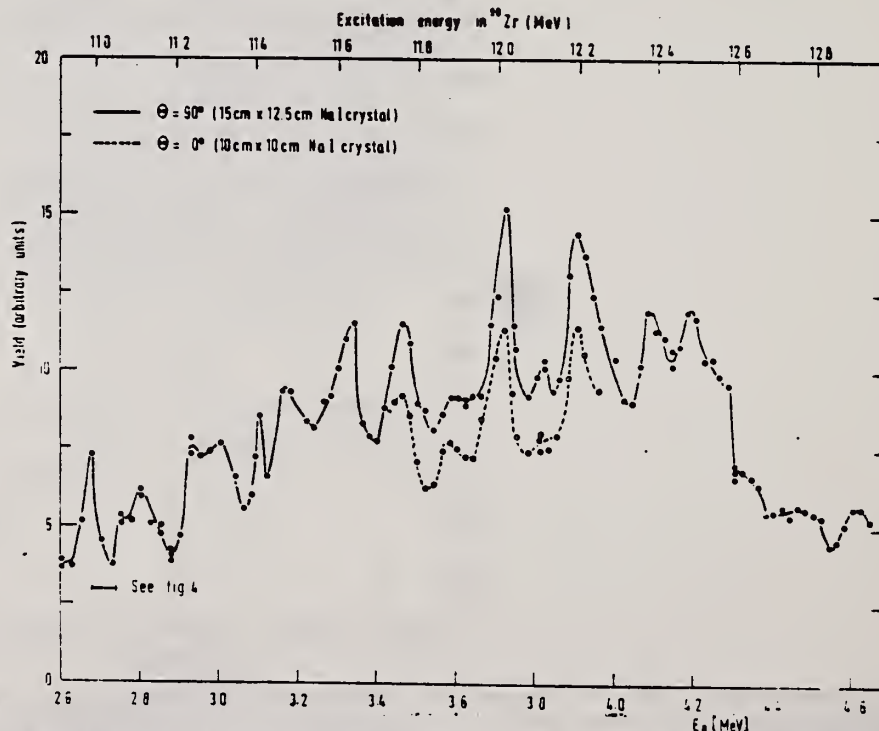


Fig. 3. The excitation functions for the reaction  $^{88}\text{Y}(p, \gamma)^{88}\text{Zr}$  measured at  $\theta = 90^\circ$  and  $\theta = 0^\circ$  with an energy resolution of 25 keV. The curves are not normalized to one another.

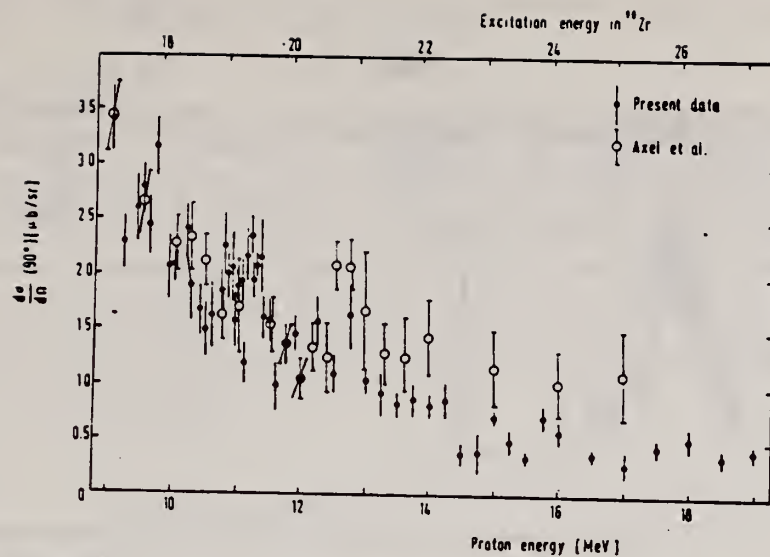
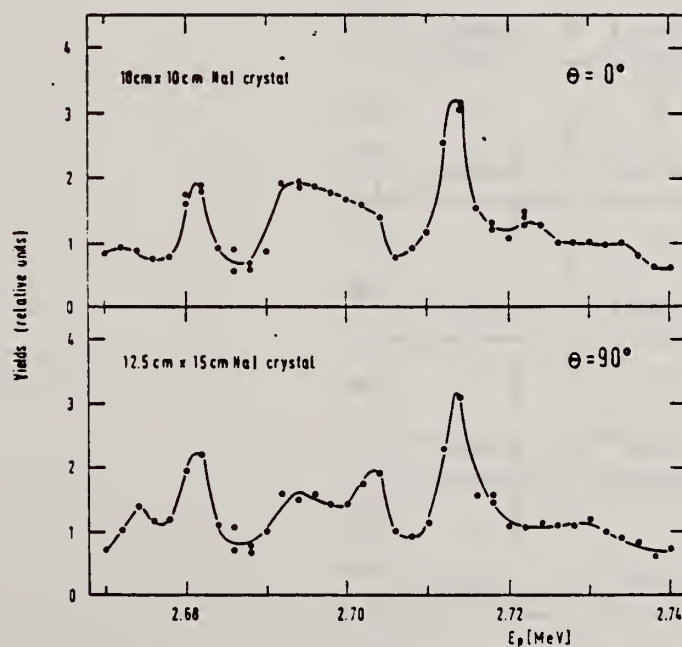


Fig. 6. The excitation function for the reaction  $^{88}\text{Y}(p, \gamma)^{88}\text{Zr}$  measured at  $\theta = 90^\circ$  with the 24 cm  $\times$  30 cm NaI(Tl) crystal. Points measured by Axel *et al.*<sup>9)</sup> have been included but scaled by a factor 5.3/14.

<sup>9</sup>P. Axel, D. M. Drake, S. Whetstone and S. S. Hanna, Phys. Rev. Lett. **19** (1967) 1343



The excitation functions for the reaction  $^{88}\text{Y}(p, \gamma)^{88}\text{Zr}$  measured at  $\theta = 0^\circ$  and  $\theta = 90^\circ$  with an energy resolution of 2 keV.

METHOD

Page 3 of 3

REACTION	RESULT	EX. E

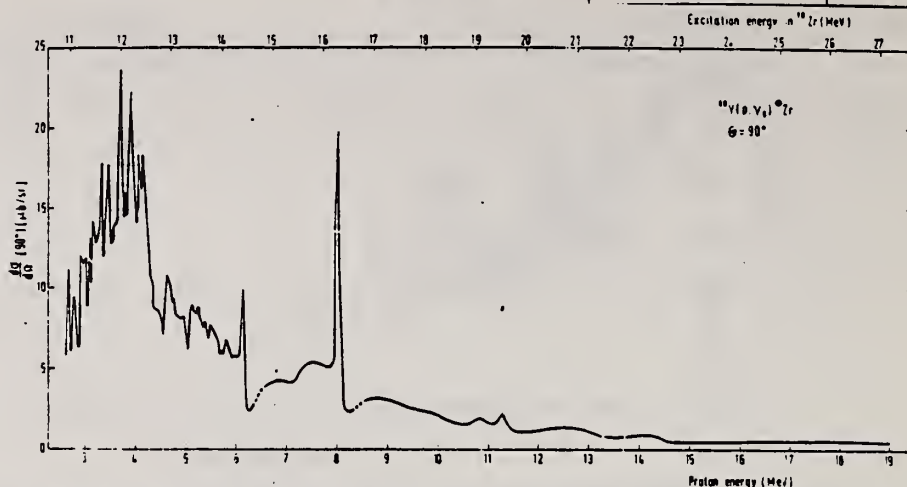


Fig. 9. Combined lower and higher energy excitation functions at  $\theta = 90^\circ$  with inclusion of some data from refs. <sup>6, 10</sup>. The cross section is normalized to the values given in the text. For the energy regions  $E_p = 6.5-7.8$  MeV and  $E_p = 8.6-9$  MeV, the data from the 150 keV excitation function (fig. 2) were used.

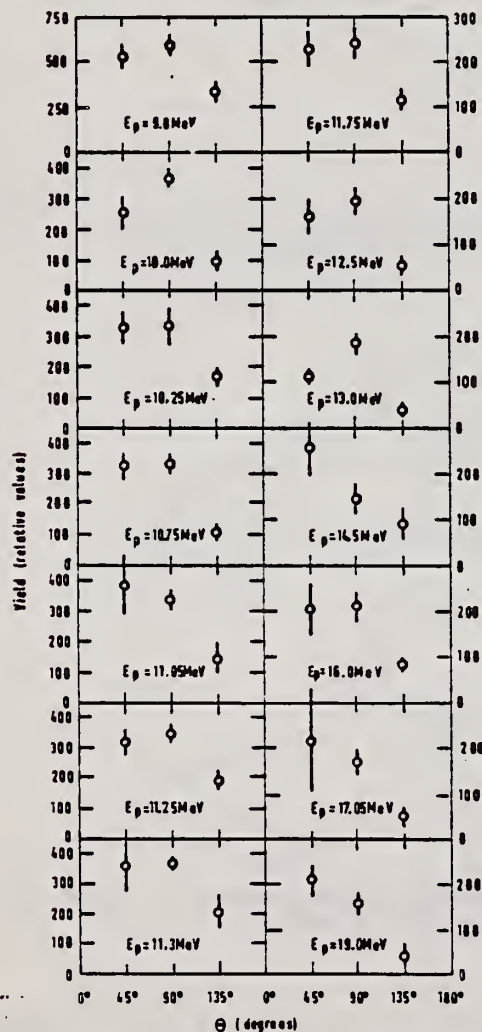


Fig. 7. Three point "angular distributions" for the energy region  $E_p = 9-19$  MeV.

<sup>6</sup>J. L. Black and N. W. Tanner, Phys. Lett. 11 (1964) 135  
<sup>10</sup>E. Obst, F. Rauch and E. Rössle, Phys. Lett. 21 (1966) 50;  
E. Obst, F. Rauch and H. G. Wahsweiler, Nucl. Phys. A103 (1967) 17

REF.

S. Ramchandran and J. A. McIntyre  
Phys. Rev. 179, 1153 (1969)

Zr

90

40

METHOD

REF. NO.

69 Ra 1

hmg

REACTION	RESULT	EXCITATION ENERGY	SOURCE		DETECTOR		ANGLE
			TYPE	RANGE	TYPE	RANGE	
G,G	LFT	9	D	9	NAI		DST

9 = 8.496 MEV

$$W(\theta) \sim [1 + a P_2(\cos\theta)]$$

over

Table II. Experiment compared to theory assuming a pure dipole transition.

$\alpha \pm \Delta\alpha$ (Experimental)											
$^{90}\text{Zr}$	Cd	Sn	Hg	$^{207}\text{Tl}$	$^{208}\text{Pb}$	$^{209}\text{Bi}$ (7.416 MeV)	$^{209}\text{Bi}$ (7.149 MeV)	$A^{1/2}(J_i, J_f, L=1)$ (Theoretical)	$J_i$	$J_f$	
$0.489 \pm 0.027$	$0.488 \pm 0.034$	$0.490 \pm 0.095$	$0.48 \pm 0.11$		$0.485 \pm 0.026$			0.500	0	1	
	$0.488 \pm 0.034$	$0.490 \pm 0.095$	$0.48 \pm 0.11$	$0.0017 \pm 0.0110$				0.000	1/2	1/2	
	$0.488 \pm 0.034$	$0.490 \pm 0.095$	$0.48 \pm 0.11$	$0.0017 \pm 0.0110$				0.250	1/2	3/2	
			$0.48 \pm 0.11$					0.000	3/2	1/2	
			$0.48 \pm 0.11$					0.160	3/2	3/2	
			$0.48 \pm 0.11$					0.140	3/2	5/2	
						$0.195 \pm 0.033$	$0.184 \pm 0.074$	0.024	9/2	7/2	
						$0.195 \pm 0.033$	$0.184 \pm 0.074$	0.194	9/2	9/2	
						$0.195 \pm 0.033$	$0.184 \pm 0.074$	0.083	9/2	11/2	

Table V. Summary of energy-level parameters.

Element	$^{90}\text{Zr}$	Cd	Sn	Hg	$^{207}\text{Tl}$	$^{208}\text{Pb}$	$^{209}\text{Bi}$	$^{209}\text{Bi}$
Level energy (MeV)	8.496 <sup>a</sup>	6.485 <sup>b</sup>	6.988 <sup>c</sup>	4.906 <sup>b</sup>	7.647 <sup>d</sup>	7.277 <sup>e</sup>	7.416 <sup>f</sup>	7.149 <sup>g</sup>
$\gamma$ ray source	Sc 0 $\rightarrow$ 1	Co 0 $\rightarrow$ 1	Cu 0 $\rightarrow$ 1	Co 0 $\rightarrow$ 1	Fe 1/2 $\rightarrow$ 1/2	Fe 0 $\rightarrow$ 1	Sc 9/2 $\rightarrow$ 7/2	Ti 9/2 $\rightarrow$ 7/2
$J_i \rightarrow J_f$		(1/2 $\rightarrow$ 3/2)	(1/2 $\rightarrow$ 3/2)	3/2 $\rightarrow$ 5/2	(1/2 $\rightarrow$ 3/2)		9/2 $\rightarrow$ 11/2	9/2 $\rightarrow$ 11/2
				(3/2 $\rightarrow$ 3/2)				
$\Gamma_0/\Gamma$	$0.8 \pm 0.2$				$0.85 \pm 0.17^i$	$0.95_{-0.17}^{+0.08}$	$0.6 \pm 0.2$	
$\Gamma_0$ (eV)	$1.68 \pm 0.02$				$1.0^j$	$0.68 \pm 0.03$	$0.14 \pm 0.09$	
$\sigma$ (eV)	$5.60 \pm 0.15$				$11.5 \pm 0.2^k$	$8.00 \pm 0.14$	$3.4 \pm 1.6$	

<sup>a</sup> L. V. Groshov, V. N. Lutsenko, A. M. Demidov, and V. I. Polekov, *Atlas of Gamma Spectra from Radiative Capture of Thermal Neutrons* (Pergamon Press, Inc., New York, 1959).

<sup>b</sup> E. B. Shera and D. W. Halemeister, *Phys. Rev.* **150**, 894 (1966).

<sup>c</sup> H. H. Bolotin (private communication from L. M. Bollinger).

<sup>d</sup> R. Moroh and G. Ben-Yaacov, *Nuclear Research Center—Neger Report*, NRCN-180, 1967, (unpublished).

<sup>e</sup> L. V. Groshov, A. M. Demidov, G. A. Korienikov, and V. N. Lutsenko, *Nucl. Phys.* **58**, 465 (1964);

<sup>f</sup> G. T. Ewan and A. J. Tavendale, *Nucl. Instr. Methods* **26**, 183 (1964).

<sup>g</sup> See Ref. 24a.



METHOD

REF. NO.

69 Sh 5

hmg

REACTION	RESULT	EXCITATION ENERGY	SOURCE		DETECTOR		ANGLE
			TYPE	RANGE	TYPE	RANGE	
E,p	ABX	12-23	D	16-24	MAG-D		

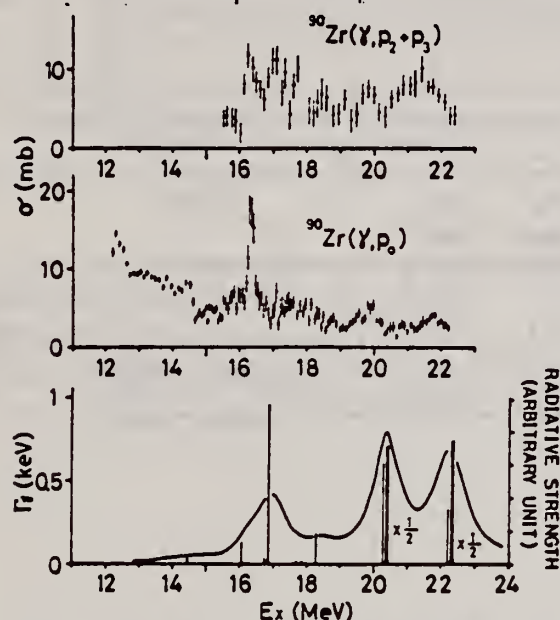


FIG. 2.  $(\gamma, p_0)$  and  $(\gamma, p_2 + p_3)$  cross sections of  $^{90}\text{Zr}$ . The vertical lines show the theoretical radiative widths of the IAS from Ref. 6. The smooth curve is an averaging of them (see Ref. 6).

Assumption is made that photoproton emission leaves the residual nucleus in the ground state.

<sup>6</sup>T. A. Hughes and S. Fallieros, private communication.

REF.	K. Shoda, M. Sugawara, T. Saito & H. Miyase PICNS-69 Proceedings of the Conference on Nuclear Isospin. Asilomar-Pacific Grove, California 1969 (Academic Press, New York & London 1969) p.125.				ELEM. SYM.	A	Z
					Zr	90	40
METHOD					REF. NO.		
					69 Sh 6		egf
REACTION	RESULT	EXCITATION ENERGY	SOURCE		DETECTOR		ANGLE
			TYPE	RANGE	TYPE	RANGE	
E,P	ABX	12-22	D	16-23	MAG-D		DST

Table 1. Angular distributions of strong proton groups on  $^{90}\text{Zr}$ .

$E_p$ (MeV)	$E_R$ (MeV)	$E_{ex}$ (MeV)	$W(\theta)$
6.0	0	14.4	$1 + (0.1 \pm 0.1)P_1 - (0.2 \pm 0.2)P_2$
6.4	1.5	16.3	$1 + (0.1 \pm 0.1)P_1 - (1.2 \pm 0.2)P_2$
7.9	0	16.3	$1 + (0.02 \pm 0.06)P_1 - (0.6 \pm 0.1)P_2$

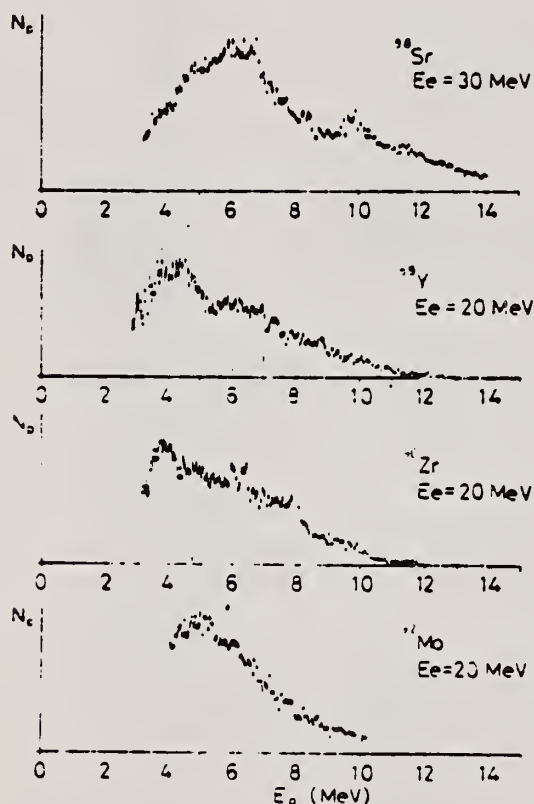


Fig. 1. Energy distributions of photoprotons. Vertical broken lines and solid lines indicate the position of  $p_0$  corresponding to the ground IAS and electric dipole IAS (2-4) respectively.

(over)

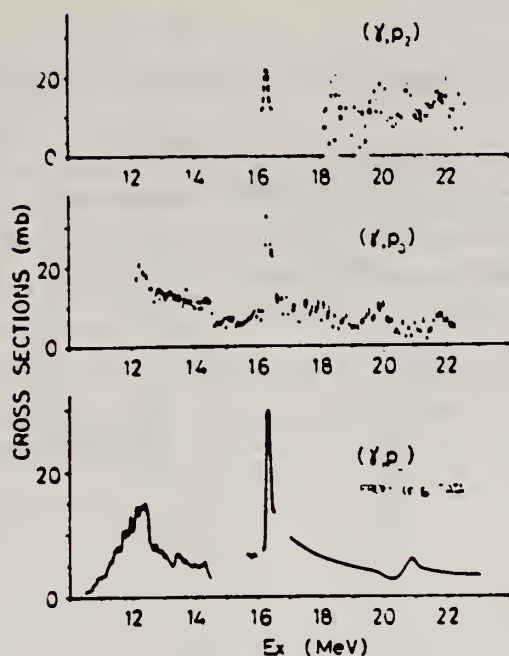


Fig. 2. Cross sections for  $(\gamma, p_0)$ ,  $(\gamma, p_2)$  of  $^{90}\text{Zr}$ . Those of  $(\gamma, p_0)$  obtained from  $^{89}\text{Y}(p, \gamma_0)^{90}\text{Zr}$  experiment (3,5,6) are also shown.

Table 2. The radiative width of main IAS. The result is compared with the single particle unit (W.u.).

Nucleus	$E_p$ (MeV)	$E_{ex}$ (MeV)	$\Gamma_{p0}/\Gamma$	$\Gamma_{\gamma_0}$ (eV)	$2(T+1)\Gamma_{\gamma_0}$ (W.u.)
$^{90}\text{Zr}$	7.0	14.0	23/50(a)	60	0.2
	7.5	14.4	18/60(a)	90	0.3
	6.0	14.4	1 (b)	30	0.09
$^{90}\text{Zr}$	6.4	16.3	1/1.4(c)	180	0.4

(a) E. R. Cosman, J. M. Joyce and S. M. Shafroth, Nucl. Phys. A108 519 (1968).

(b) Assumption.

(c) From present data.

(\*) The possibility of such method of determination of  $\Gamma_{\gamma_0}$  is also suggested by G. M. Temmer (10).

<sup>3</sup> J.L. Black et al., Phys. Lett. 11, 135 (1964).

<sup>5</sup> E. Obst et al., Phys. Lett. 21, 50 (1966).

<sup>6</sup> P. Axel et al., Phys. Rev. Lett. 19, 1343 (1967).

<sup>10</sup> G.M. Temmer, Fundamentals in Nuclear Theory, International Atomic Energy Agency, Vienna p.237 ('67).

Zr	90	40
REF. NO.		
70 Be 2		egf

METHOD

REACTION	RESULT	EXCITATION ENERGY	SOURCE		DETECTOR		ANGLE
			TYPE	RANGE	TYPE	RANGE	
$E, E/$	ABX	0-4	D	42-61	MAG-D	38-61	DST

2.18, 2.74, 3.84

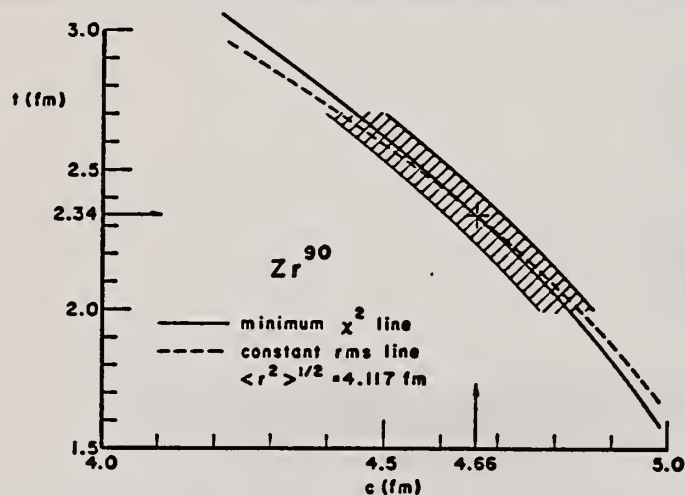


Fig. 2. Values of half-density radius  $c$  and skin thickness  $t$  consistent with the experimental results lie within the cross-hatched area. The solid line locates the best fit (minimum  $\chi^2$ ), and the dashed line corresponds to a fixed rms radius of 4.12 fm.

TABLE 3  
Inelastic scattering results

	$B(EL\uparrow)$ ( $e^2 \cdot fm^{2L}$ )	$B(EL\uparrow)$ (s.p.u.)	$\Gamma_0^*$ (eV)	$R_{tr}^2$ ( $fm^2$ )	$\chi^2/N$
2.18 MeV, $2^+$					
hydrodynamical model	$830 \pm 19$	6.9	$6.60 \cdot 10^{-3}$	32.5	9.7/6
single-particle model	$1000 \pm 23$	8.3	$8.0 \cdot 10^{-3}$	34.4	9.7/6
2.74 MeV $3^-$					
hydrodynamical model	$(1.08 \pm 0.03) \cdot 10^5$	32	$6.71 \cdot 10^{-6}$	37.7	23/5
3.84 MeV, $2^+$					
hydrodynamical model	$244 \pm 9$	2.0	$3.29 \cdot 10^{-2}$	32.5	15/5

TABLE 4  
Electromagnetic strengths in  $^{90}Zr$  (s.p.u.)

$E_{\alpha}$ (MeV)	$J^\pi$	Present experiment	Coulomb excitation <sup>18)</sup>	$(\alpha, \alpha')^{13)}$	$(p, p')^{14)}$	Theory <sup>25)</sup>
2.18	$2^+$	$6.9 \pm 1.4$	$3.5 \pm 1.3$	$5.7 \pm 1.7$	3.6	1.7
2.74	$3^-$	$32 \pm 6.4$		$20.0 \pm 1.6$	19	17
3.84	$2^+$	$2.0 \pm 0.4$		$1.5 \pm 0.5$	2.3	

[over]



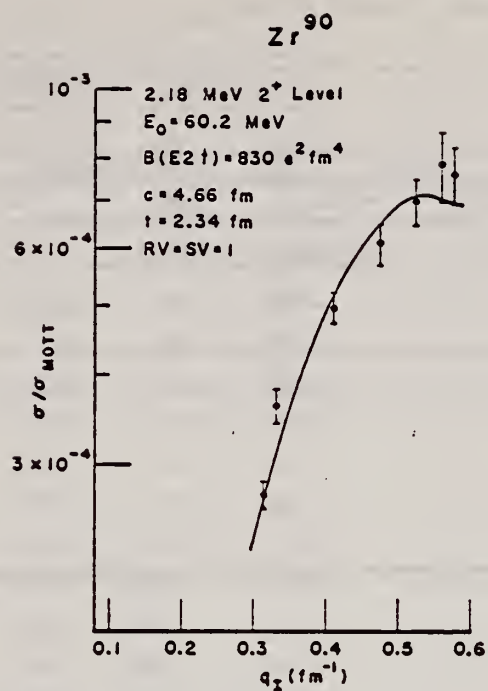


Fig. 3. Inelastic scattering cross sections for excitation of 2.18 MeV level plotted versus momentum transfer. The solid line is the theoretical fit.

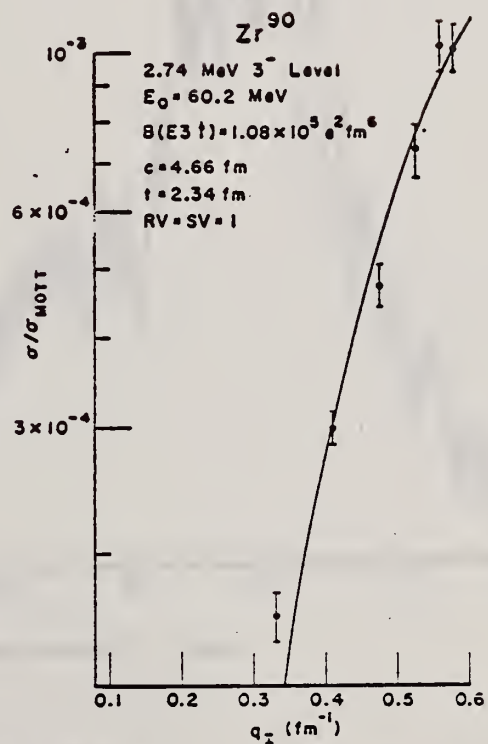


Fig. 4. Inelastic scattering cross sections for excitation of the 2.74 MeV level plotted versus momentum transfer. The solid line is the theoretical fit.



REF.

B.I. Goryachev, B.S. Ishkhanov, and V.G. Shevchenko  
 Proceedings of the Second Symposium on the Problems  
 of Nuclear Physics, Novosibirsk, USSR, June 1970  
 (Kolybasov, V.M., Ed., Izdatel'stvo Nauka, Moscow 1971),  
 pp. 362-78

ELEM. SYM.

A

Z

Zr

90

40

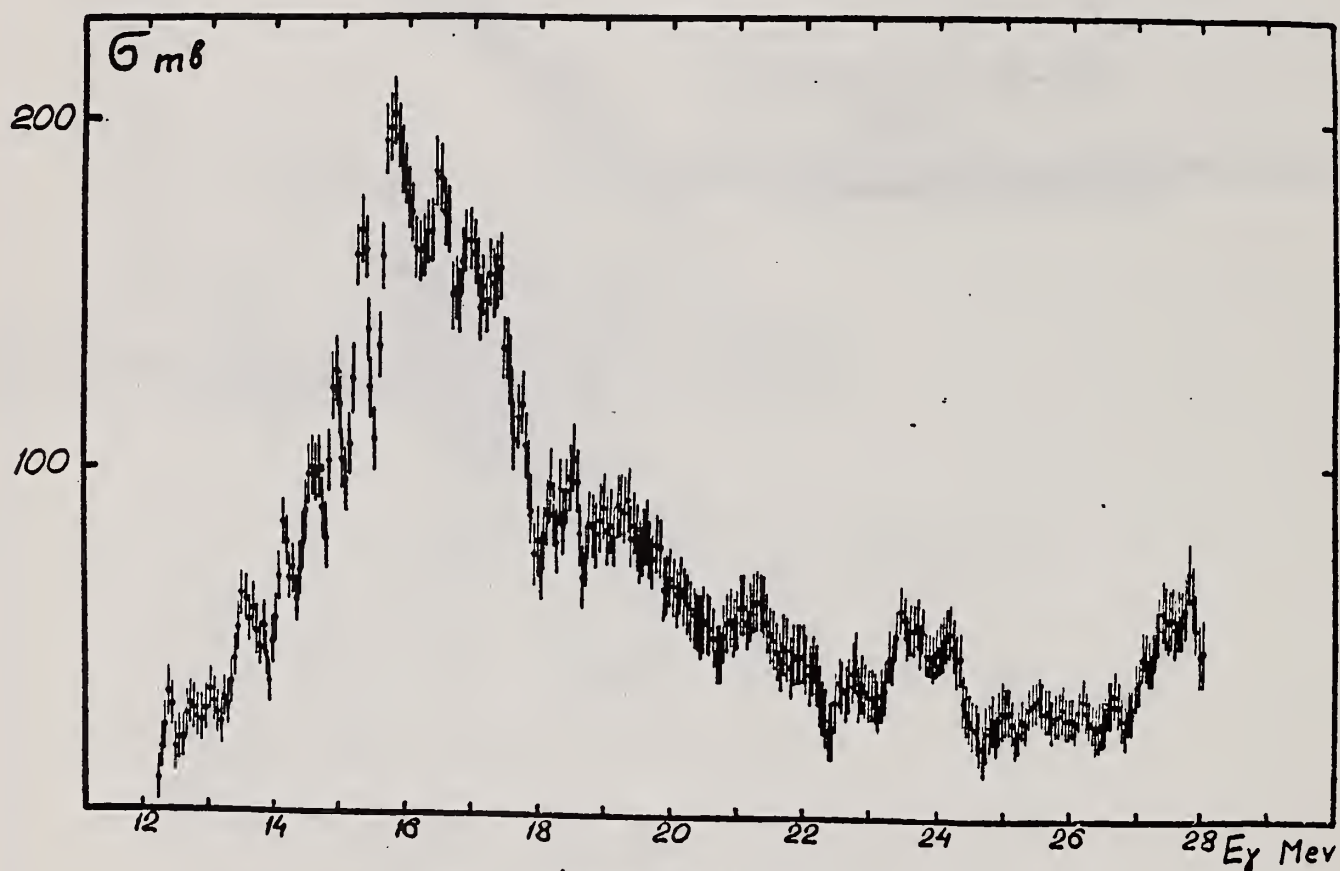
METHOD

REF. NO.

71 Go 3

egf

REACTION	RESULT	EXCITATION ENERGY	SOURCE		DETECTOR		ANGLE
			TYPE	RANGE	TYPE	RANGE	
G,XN	ABX	12- 28	C	12- 28	MOD-I		4PI



Фиг. 4. Сечение реакции  $Zr^{90}(\gamma, n)$

(over)

Т а б л и ц а 2

$Zr^{90}$	$Pb^{208}$		
$E_m(\text{МэВ})$	$E_m(\text{МэВ})$	$P_m^{int}(\text{МэВ} \cdot \text{мбн})$	$\sigma_m^{int}(\%)$
	7,65	19,5	0,58
	8,08	12,63	0,38
	8,38	18,58	0,47
	8,78	18,61	0,53
	9,03	33,4	0,98
	9,40	34,2	0,98
	9,81	71,1	2,04
	10,29	72,2	2,07
	10,62	83,8	1,83
	10,93	78,6	2,20
	11,24	145,0	4,15
	11,76	247	7,10
12,4	12,3	285	7,61
12,6	12,84	331	9,5
13,1	13,25	344	9,87
13,7	13,78	214	6,14
14,2	14,08	316	9,08
14,6	14,68	245	7,03
14,9	15,13	210	6,02
15,3	15,73	88	2,52
15,8	16,40	114	3,28
16,5	17,13	98	2,81
16,9	17,95	150	4,30
17,3	18,78	78	2,24
18,6	19,52	88	2,52
19,3	20,83	135	3,87
21,3			
22,0			
22,8			
23,5			
24,2			
(25,5)			
27,8			

B.S. Ishkhanov, I.M. Kapitonov, I.M. Piskarev, O.P. Shevchenko  
 Yad. Fiz. 14, 27 (1971)  
 Sov. J. Nucl. Phys. 14, 16 (1972)

Zr

90

40

METHOD

REF. NO.

71 Is 2

hmg

REACTION	RESULT	EXCITATION ENERGY	SOURCE		DETECTOR		ANGLE
			TYPE	RANGE	TYPE	RANGE	
G,XN	ABX	12-28	C	12-28	BF3-I		4PI

Reaction	Location of resonance peak $E_{\gamma}$ , MeV	Cross section at the peak $\sigma_m$ , mb	Resonance width $\Gamma_m$ , MeV	Integrated cross section $E_{\gamma}$ max for $E_{\gamma}$ max mb-MeV	$E_{\gamma}$ max, MeV	Source of data
$Zr^{90}(\gamma, Tn)$	16.8	180	4.5	1170	28	[1]
	16.0	185	4.1	950	24	[1]
	16.0	200	3.7	950	28	Present work
$Zr^{90}(\gamma, n)$	16.8	180	4.5	960	28	[1]
	16.0	190	2.7	1480	25	[1]
	16.0	200	3.7	930	28	Present work
$Zr^{90}(\gamma, 2n)$				110	28	[1]
				100	28	Present work

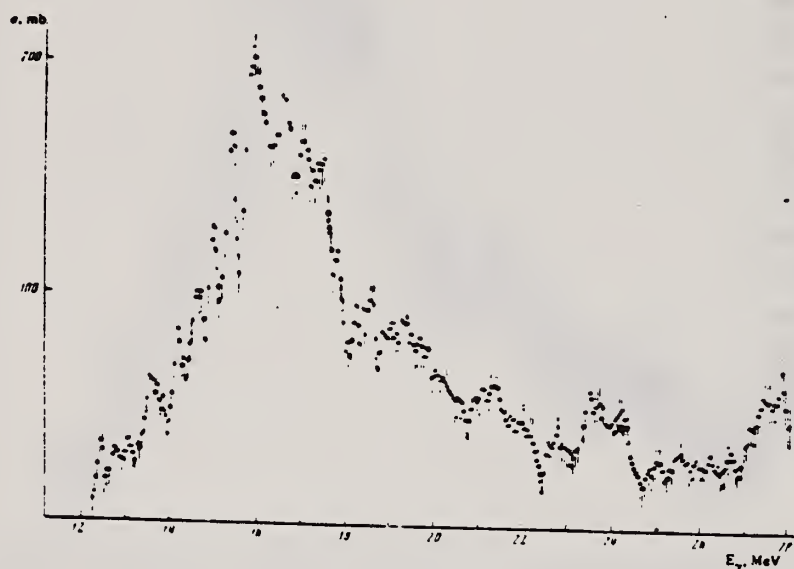


FIG. 1. Cross section for the reaction  $Zr^{90}(\gamma, Tn)$ .

REACTION	RESULT	EXCITATION ENERGY	SOURCE		DETECTOR		ANGLE
			TYPE	RANGE	TYPE	RANGE	
G,N	ABX	12-26	D	12-26	MOD-I		4PI
G,2N	ABX	21-26	D	12-26	MOD-I		4PI

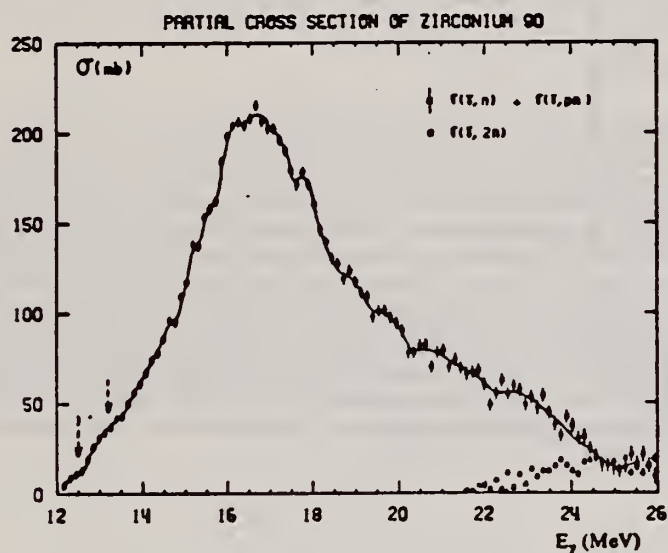


Fig. 4. Partial photoneutron cross sections  $\sigma(\gamma, n)$  and  $\sigma(\gamma, 2n)$  of  $^{90}\text{Zr}$ .

TABLE I

Lorentz line parameters corresponding to fits shown in fig. 6.

	Rb	Sr	$^{89}\text{Y}$	$^{90}\text{Zr}$	$^{93}\text{Nb}$
$\sigma_1$ (mb)	$192 \pm 10$	$207 \pm 10$	$225 \pm 10$	$211 \pm 10$	$202 \pm 10$
$\Gamma_1$ (MeV)	$4.1 \pm 0.15$	$4.2 \pm 0.1$	$4.1 \pm 0.1$	$4.0 \pm 0.1$	$4.7 \pm 0.2$
$E_1$ (MeV)	$16.75 \pm 0.05$	$16.7 \pm 0.05$	$16.7 \pm 0.05$	$16.65 \pm 0.05$	$16.5 \pm 0.05$

TABLE 3

Integrated cross sections (the notation used is defined in the text)

	Rb	Sr	$^{89}\text{Y}$	$^{90}\text{Zr}$	$^{93}\text{Nb}$
$\sigma_0$ (MeV · b)	$1.14 \pm 0.06$	$1.42 \pm 0.07$	$1.36 \pm 0.07$	$1.26 \pm 0.07$	$1.33 \pm 0.07$
$\frac{\sigma_0}{0.06 NZ A^{-1}}$	$0.915 \pm 0.05$	$1.09 \pm 0.05$	$1.04 \pm 0.05$	$0.95 \pm 0.05$	$0.97 \pm 0.05$
$\sigma_{-1}$ (mb)	$67 \pm 4$	$80 \pm 5$	$77 \pm 5$	$71 \pm 5$	$79 \pm 5$
$\sigma_{-2}$ (mb · MeV $^{-1}$ )	$4 \pm 0.2$	$4.6 \pm 0.2$	$4.4 \pm 0.2$	$4 \pm 0.2$	$4.3 \pm 0.2$
$E_{th}$ (MeV)	24	27	27	26	24

(over)

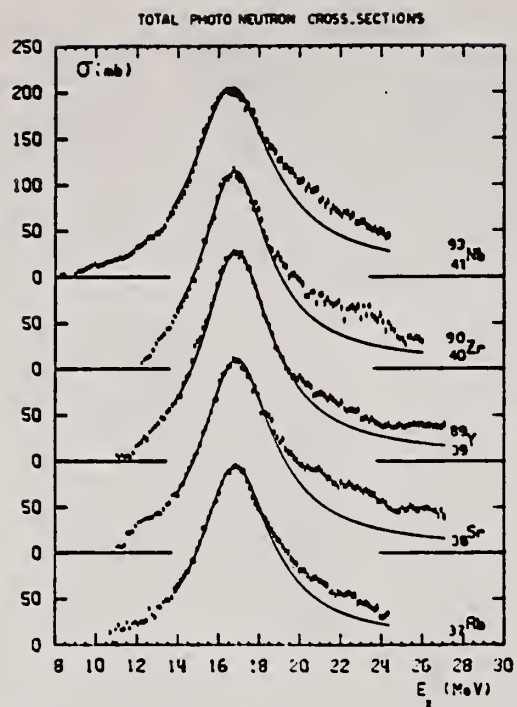


Fig. 6. Total photoneutron cross sections  $\sigma_T$  of Rb, Sr,  $^{89}\text{Y}$ ,  $^{90}\text{Zr}$  and  $^{93}\text{Nb}$  and best one Lorentz line fit corresponding to parameters given in table 1.



METHOD	REF. NO.	
	71 Um 1	hmg

REACTION	RESULT	EXCITATION ENERGY	SOURCE		DETECTOR		ANGLE
			TYPE	RANGE	TYPE	RANGE	
P,G	ABX	9-10	D	2-3	SCD-D		0
				(2.3-3.0)			

The  $^{88}\text{Sr}(\rho, \gamma)^{88}\text{Y}$  and  $^{88}\text{Y}(\rho, \gamma)^{88}\text{Zr}$  reactions have been investigated in the energy range  $E_p = 2.3$  to 3.0 MeV. Excitation functions for the transition to the ground state, with a total resolution of 2 keV, were determined for each reaction over this energy region. Using thick targets and both a single Ge(Li) detector and a Ge(Li) detector incorporated into a pair spectrometer, total summed spectra for the 700-keV region were obtained. The average total cross section of  $^{88}\text{Sr}(\rho, \gamma)^{88}\text{Y}$  and  $^{88}\text{Y}(\rho, \gamma)^{88}\text{Zr}$  was  $12 \pm 5 \mu\text{b}$  and  $17 \pm 7 \mu\text{b}$ , respectively. These total summed spectra, which represent the total  $\gamma$ -ray yield in this region, have been examined for a possible dependence of the intensity on the  $J^\pi$  of the final state. The data suggest such a  $J$ -dependence hypothesis, but detailed theoretical analysis of the  $^{88}\text{Sr}(\rho, \gamma)^{88}\text{Y}$  reaction does not completely agree with experiment. A spectrum from a Ge(Li) detector in coincidence with a NaI(Tl) detector was accumulated for the  $^{88}\text{Sr}(\rho, \gamma)^{88}\text{Y}$  reaction. The decay scheme of the states of  $^{88}\text{Y}$  up to an excitation energy of 3.621 MeV was determined and the implications about spins and parities are consistent with accepted assignments.

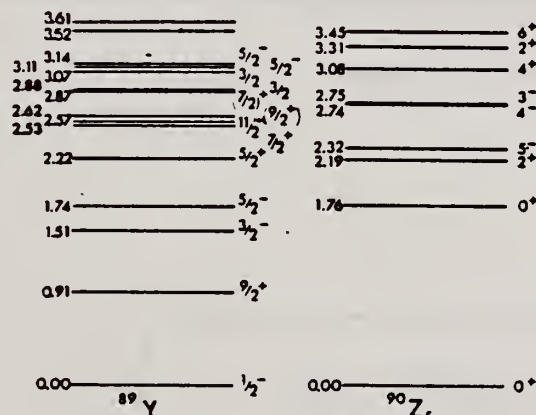


FIG. 1. Presently accepted level schemes for  $^{88}\text{Y}$  and  $^{90}\text{Zr}$  taken from the data of Van Patter (Ref. 8) and Ball (Ref. 9), respectively.

- <sup>8</sup>D. M. Van Patter, Bull. Am. Phys. Soc. 15, 573 (1970).  
<sup>9</sup>J. B. Ball, Bull. Am. Phys. Soc. 15, 574 (1970).

[over]

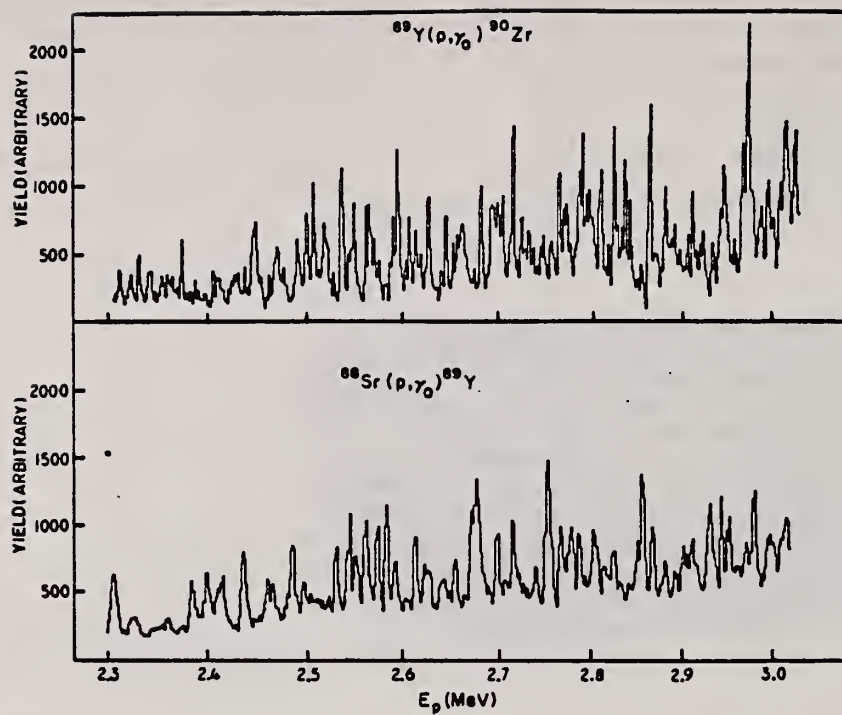


FIG. 2. Excitation functions for  $^{88}\text{Sr}(p,\gamma)^{89}\text{Y}$  and  $^{89}\text{Y}(p,\gamma)^{90}\text{Zr}$  over the energy region  $E_p = 2.3$  to 3.0 MeV.

REF. H.J. Askin, J.K.F. Allen, R. Hicks, R.J. Petty  
and M.N. Thompson  
PIGNS-72, 359 (1972) Sendai

ELEM. SYM.	A	Z
Zr	90	40

METHOD	REF. NO.	
	72As 10	hvm

REACTION	RESULT	EXCITATION ENERGY	SOURCE		DETECTOR		ANGLE
			TYPE	RANGE	TYPE	RANGE	
G,P	SPC	13- 30	C	35	SCD-D		90
G,XN	ABX	11- 28	C	11- 28	BF3-I		4PI
G,XN	SPC	12- 15	C	20- 24	SCI-D		4PI

Table 1. Features observed in photoproton and photoneutron measurements.

T=6 states observed in $^{90}\text{Zr}(\gamma, p)$ (MeV)	14.27	16.15	17.17	19.37	(20.5)*		
Structure observed in $^{90}\text{Zr}(\gamma, n)$ (MeV)		16.2	17.2	19.3	(20.5)	21.8	23.7

\*observed by protons decaying to 2nd excited state in  $^{89}\text{Y}$ .

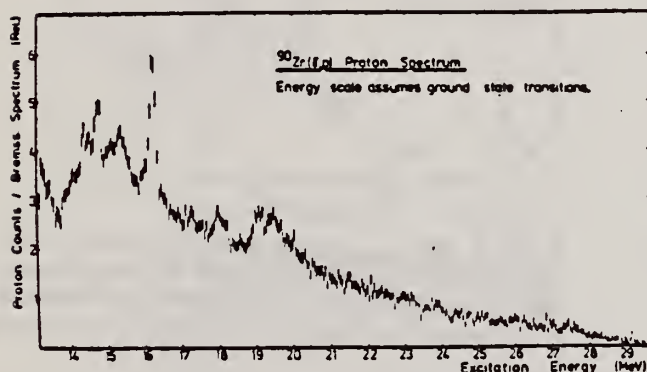


Fig. 2.  $^{90}\text{Zr}$  Photoproton spectrum.

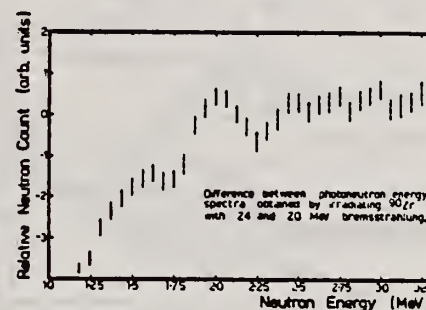


Fig. 4. Photoneutron spectrum from  $^{90}\text{Zr}$ .

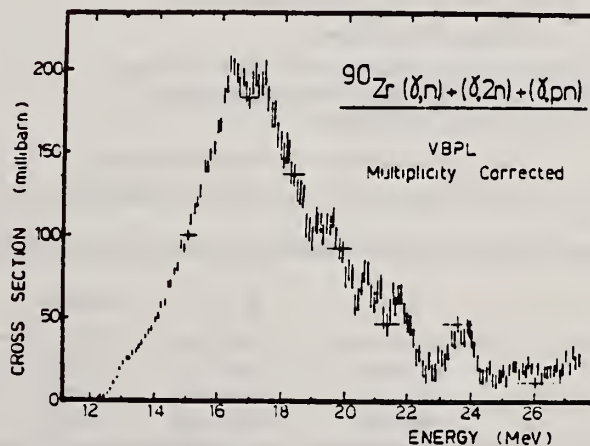


Fig. 3. Total photoneutron cross section of  $^{90}\text{Zr}$ . 359

REF.	S. Fukuda and Y. Torizuka Phys. Rev. Letters <u>29</u> , 1109 (1972)			ELEM. SYM.	A	Z
				Zr	90	40
METHOD				REF. NO. 72 Fu 6		hmg
REACTION	RESULT	EXCITATION ENERGY	SOURCE		DETECTOR	
			TYPE	RANGE	TYPE	RANGE
E, E/	FMF	7- 38	D	150-250	MAG-D	

Inelastic electron scattering from the giant dipole resonance region in <sup>90</sup>Zr was measured. In addition to the usual dipole resonance we have found new resonances at 14.0 MeV and around 28 MeV. The spins and parities and transition strengths of these states are discussed.

B(EL)

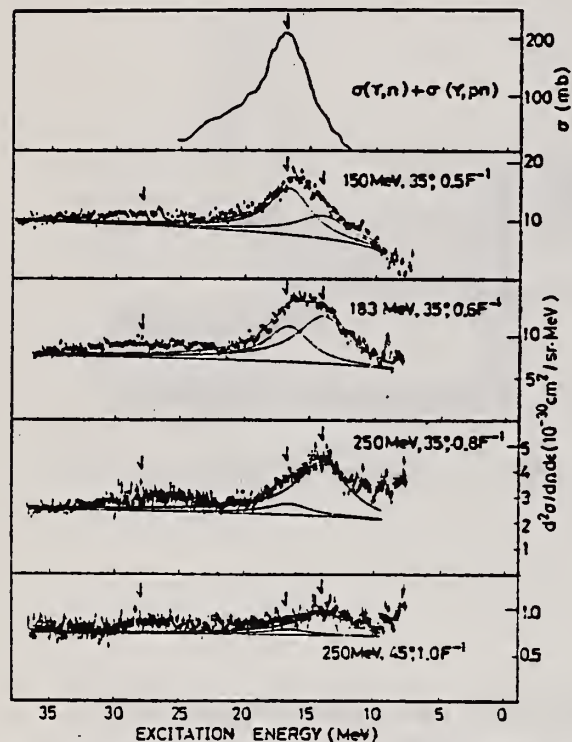


FIG 1. Spectra of photoreaction and electron scattering in <sup>90</sup>Zr. The arrows indicate the positions of the 14.0-, 16.65-, and 28-MeV peaks.

TABLE 1. B(E1), B(E2), and M<sub>fi</sub>, and energy-weighted sum-rule (EWSR) limits.

$E_x$ (MeV)	$J^\pi$	$P^a$	$E_x P^b$	(EWSR) <sup>b</sup>	$\frac{E_x P}{\text{EWSR}}$
16.65	1 <sup>-</sup>	17.0 ± 5.0	283 ± 86	264	1.07 ± 0.32
14.0	2 <sup>+</sup>	990 ± 300	13900 ± 4200	24900	0.56 ± 0.17
14.0	0 <sup>+</sup>	2050 ± 610	28700 ± 8500	28000	1.03 ± 0.3

<sup>a</sup>P is B(E1) in units e<sup>2</sup> F<sup>2</sup> for J<sup>π</sup> = 1<sup>-</sup>, B(E2) in e<sup>2</sup> F<sup>4</sup> for J<sup>π</sup> = 2<sup>+</sup>, and |M<sub>fi</sub>|<sup>2</sup> in F<sup>4</sup> for J<sup>π</sup> = 0<sup>+</sup>.

<sup>b</sup>Units are MeV times units of P.  
USC&NM-DC 26010-P64

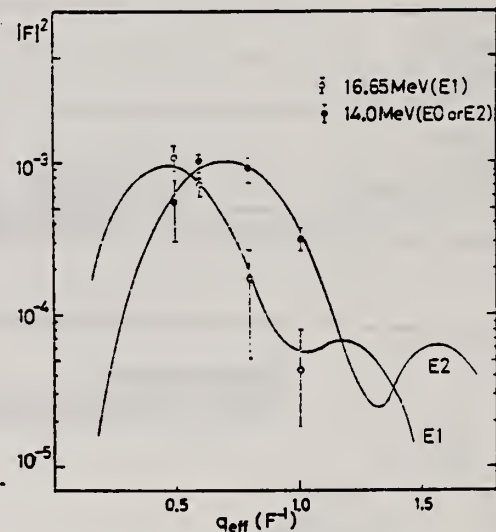


FIG. 2. The experimental form factors for the 14.0- and 16.65-MeV peaks are compared with the E2 and E1 form factors calculated with the DWBA code written by S. T. Tuan *et al.*, Nucl. Instrum. Methods 60, 70 (1968).



ELEM. SYM.	A	Z
Zr	90	40

METHOD	REF. NO.	
	72 Ha 9	hvm

REACTION	RESULT	EXCITATION ENERGY	SOURCE		DETECTOR		ANGLE
			TYPE	RANGE	TYPE	RANGE	
\$ P,G	ABX	13- 25	D	5- 17	NAI-D		DST

POLARIZED PROTONS

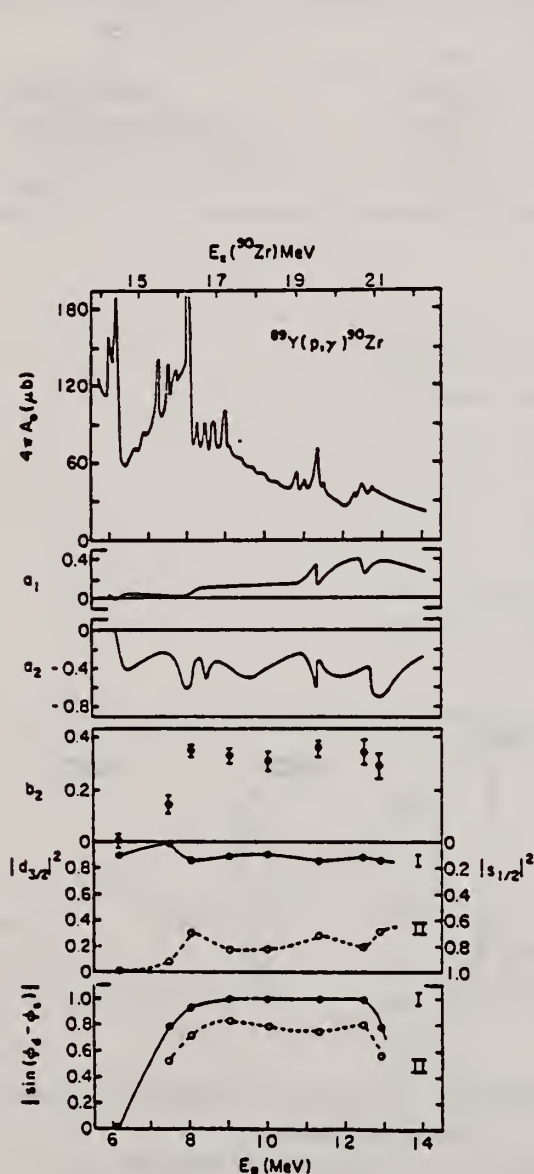


Fig. 7. Summary of the existing information on  $^{89}\text{Y}(p,\gamma)^{90}\text{Zr}$ . The two solutions for the proton channel are indicated by I and II.

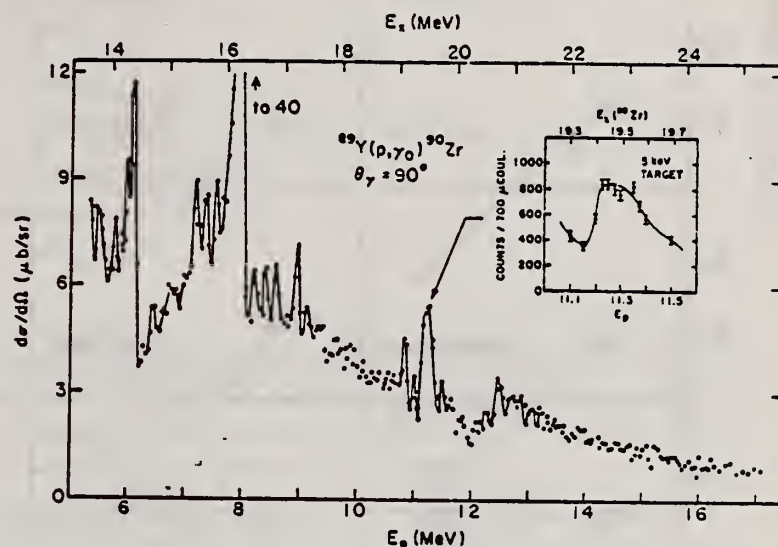


Fig. 4. The  $90^\circ$  yield from the unpolarized reaction  $^{89}\text{Y}(p,\gamma)^{90}\text{Zr}$

(over)



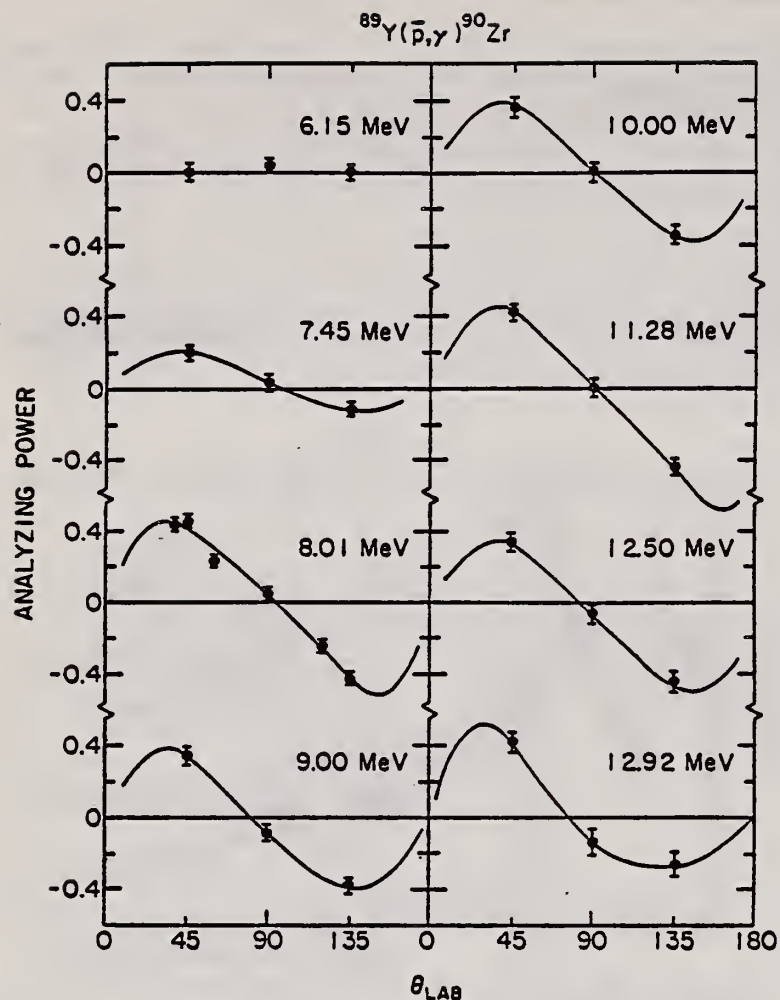


Fig. 6. Measured analyzing powers for the reaction  $^{89}\text{Y}(\bar{p},\gamma)^{90}\text{Zr}$  plotted vs. angle.

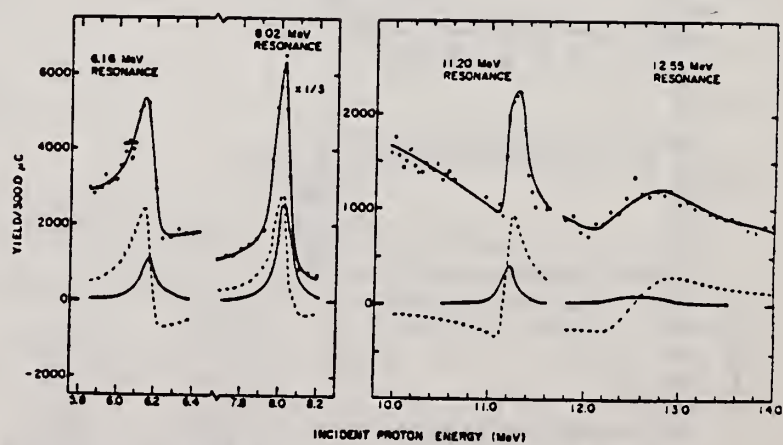


Fig. 5. Analysis of  $1^-$  analogue resonances in  $^{89}\text{Y}(\bar{p},\gamma)^{90}\text{Zr}$

METHOD					REF. NO.	
					72 Me 5	egf
REACTION	RESULT	EXCITATION ENERGY	SOURCE		DETECTOR	
			TYPE	RANGE	TYPE	RANGE
G,G	LFT	2	C		SCD-D	

2 = 2.186

TABLE 1

Widths of the 2.186 MeV level in  $^{90}\text{Zr}$  deduced from the various scattering experiments

Type of scatterer	$\Gamma_0^2/\Gamma$ (meV)	
	98°	127°
natural Zr metal	$4.90 \pm 0.20$	$4.96 \pm 0.23$
enr. $^{90}\text{ZrO}_2$ single scatt.	$4.61 \pm 0.19$	$4.90 \pm 0.21$
enr. $^{90}\text{ZrO}_2(^{27}\text{Al} + ^{90}\text{Zr})$ scatt.	$4.84 \pm 0.29$	$5.15 \pm 0.46$
average	$4.77 \pm 0.13$	$4.95 \pm 0.16$

TABLE 2

Comparison of the  $B(E2\uparrow)$  deduced from inelastic electron scattering and from resonance fluorescence experiments for the 2.186 MeV  $2^+$  state in  $^{90}\text{Zr}$ 

Method	$B(E2\uparrow)e^2 \cdot \text{fm}^4$
(e, e') <sup>a)</sup> hydrodyn. model	$830 \pm 19$
shell model	$1000 \pm 33$
( $\gamma, \gamma'$ ) present work	$608 \pm 35$
(e, e') <sup>b)</sup> hydrodyn. model	$440 \pm 20$
shell model	$440 \pm 30$

<sup>a)</sup> Ref. <sup>1)</sup>. (J. Bellicard et al., Nucl. Phys. A143 (1970) 213.<sup>b)</sup> M. T. Mills, private communication, Sept. 1971.

REF.

K. Shoda, M. Sugawara, T. Saito, H. Miyase, A. Suzuki, S. Oikawa,  
and J. Uegaki  
PICNS-72, 321 Sendai

ELEM. SYM.

A

Z

Zr

90

40

METHOD

REF. NO.

72 Sh 10

hvm

REACTION	RESULT	EXCITATION ENERGY	SOURCE		DETECTOR		ANGLE
			TYPE	RANGE	TYPE	RANGE	
E,P	SPC	16- 30	C	16- 30	MAG-D		UKN

I A STATES

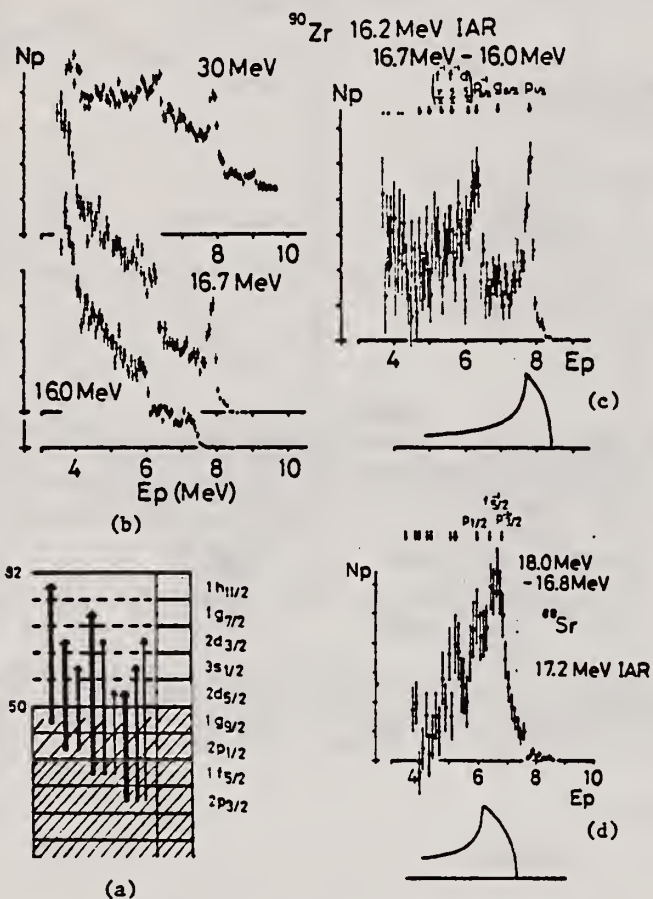


Fig. 7 (a): Shell model diagram of  $^{90}\text{Zr}$  and  $^{88}\text{Sr}$ .  
(b): Energy distributions of  $^{90}\text{Zr}(e,e'p)$ .  
(c): Energy distributions obtained from difference method. Residual states for 16.2 MeV IAR are shown by arrows.  
(d): Energy distributions obtained from difference method for  $^{88}\text{Sr}$ . Residual states for 17.2 MeV IAR are shown by arrows.

REF.

Y. Torizuka, Y. Kojima, T. Saito, K. Itoh, A. Nakada,  
S. Mitsunobu, M. Nagao, K. Hosoyama, S. Fukuda  
PICNS-72, p.171 Sendai

ELEM. SYM.

A

Z

Zr

90

40

METHOD

REF. NO.

72 To 6

hvm

REACTION	RESULT	EXCITATION ENERGY	SOURCE		DETECTOR		ANGLE
			TYPE	RANGE	TYPE	RANGE	
E,E/	FMF	0- 37	D	150-250	MAG-D		DST

LEVELS 14, 16.65

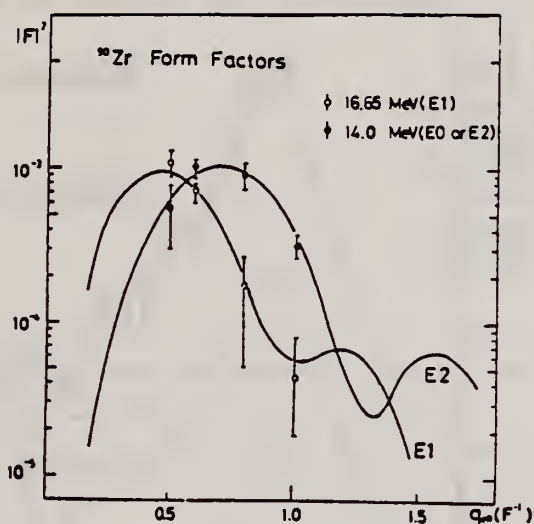


Fig. 5. The experimental form factors for the 14.0- and 16.65-MeV peaks are compared with the DWBA E2 and E1 form factors.

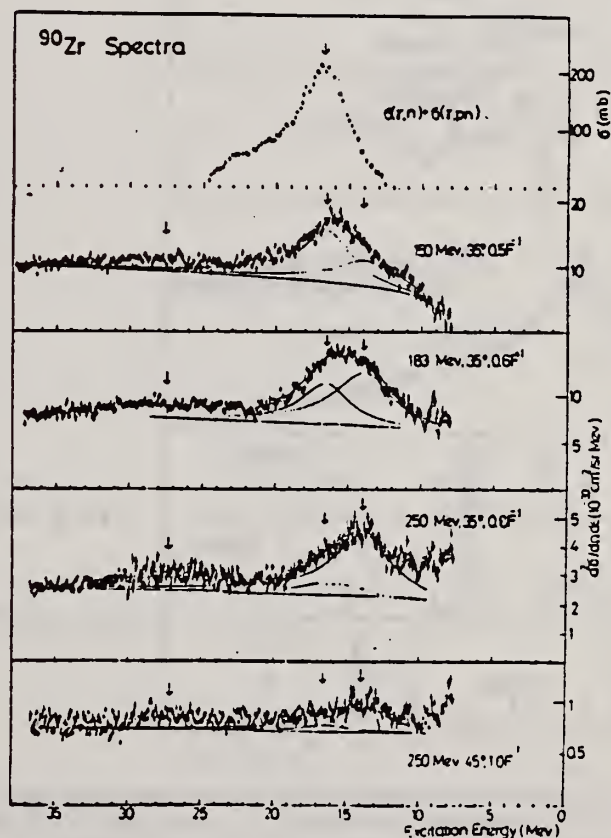


Fig. 4 The spectra of photoreaction and electron scattering



METHOD

REF. NO.

73 As 2

egf

REACTION	RESULT	EXCITATION ENERGY	SOURCE		DETECTOR		ANGLE
			TYPE	RANGE	TYPE	RANGE	
G,P		14- 29	C	31	SCD-D		90
G,XN	ABX	12- 28	C	12- 28	BF3-I		4PI*

\*N SPC GIVEN

588

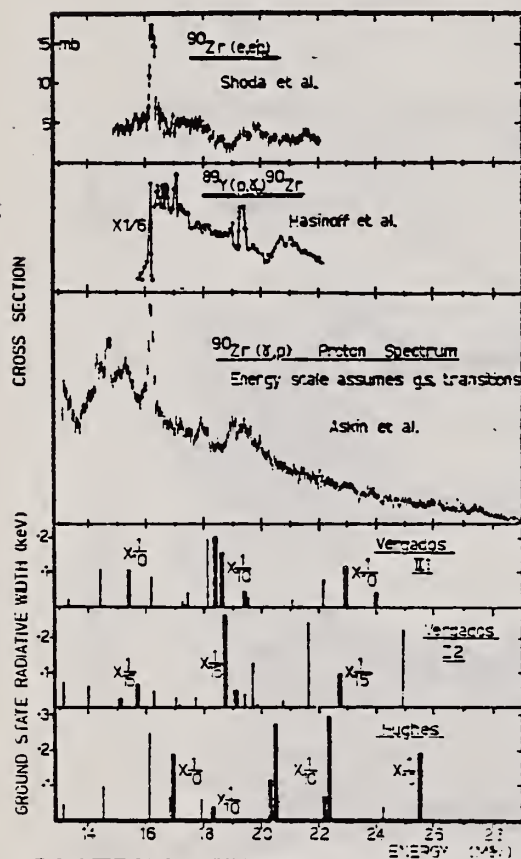


Fig. 3. Comparison of the presented  $^{90}\text{Zr}(\gamma, p)$  proton spectrum with the  $(e, e'p_0)$  data of Shoda <sup>6)</sup> and the  $(p, \gamma_0)$  measurement by Hasinoff *et al.* <sup>3)</sup>. Also shown are the results of calculations by Hughes and Fallieros <sup>3)</sup> and Vergados and Kuo <sup>4)</sup> of the excitations and ground state radiative widths of  $T_-$  states in  $^{90}\text{Zr}$ .

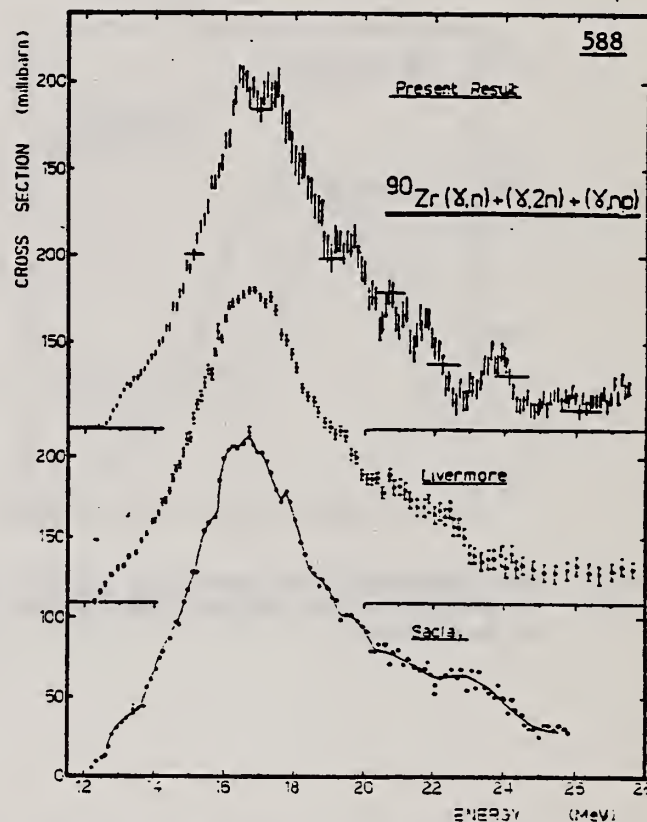


Fig. 4. The measured  $^{90}\text{Zr}$  photoneutron cross section and comparison with the work of Berman *et al.* <sup>19)</sup> at Livermore and the Saclay group <sup>20)</sup>.

(over)



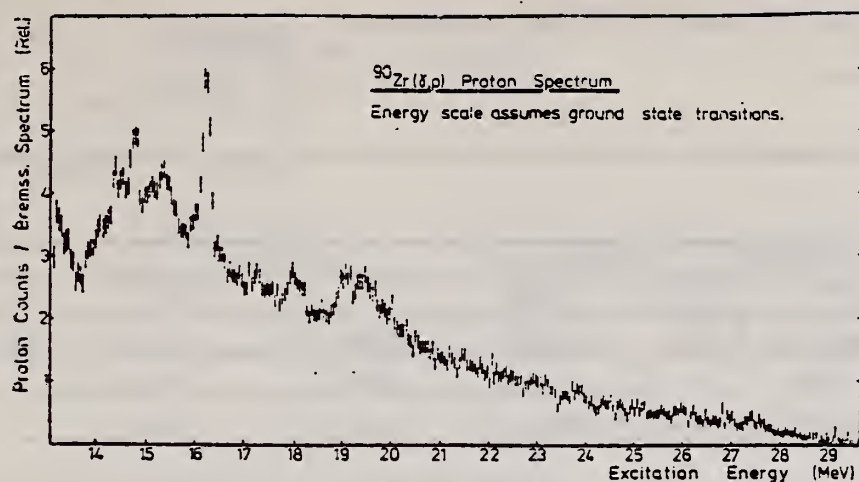


Fig. 2. The  $^{90}\text{Zr}(\gamma, p)$  proton spectrum.

TABLE I

$T = 6$ states observed in $^{90}\text{Zr}(\gamma, p)$ (MeV)	14.3	16.2	17.2	19.4	(20.7) <sup>a)</sup>		
Structure observed in $^{90}\text{Zr}(\gamma, n)$ (MeV)		16.2	17.2	19.4	20.7	21.8	23.7

<sup>a)</sup> Observed by protons decaying to excited residual states in  $^{89}\text{Y}$ .

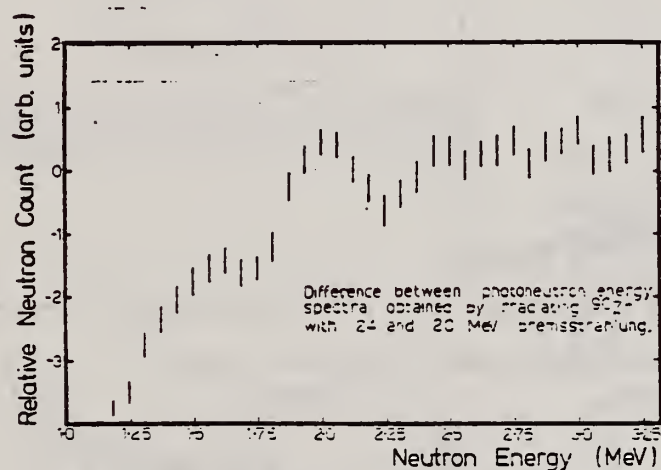


Fig. 5. Difference between the photoneutron energy spectrum measurements obtained using 24 and 20 MeV bremsstrahlung.

<sup>3</sup> T.A. Hughes et al., Nuclear isospin, ed. J.D. Anderson et al. (Academic Press, N.Y. 1969) p.109.

<sup>4</sup> J.D. Vergados et al., Phys. Lett. **35B** (1971) 93.

<sup>5</sup> M. Hasinoff et al., Phys. Lett. **30B** (1969) 337.

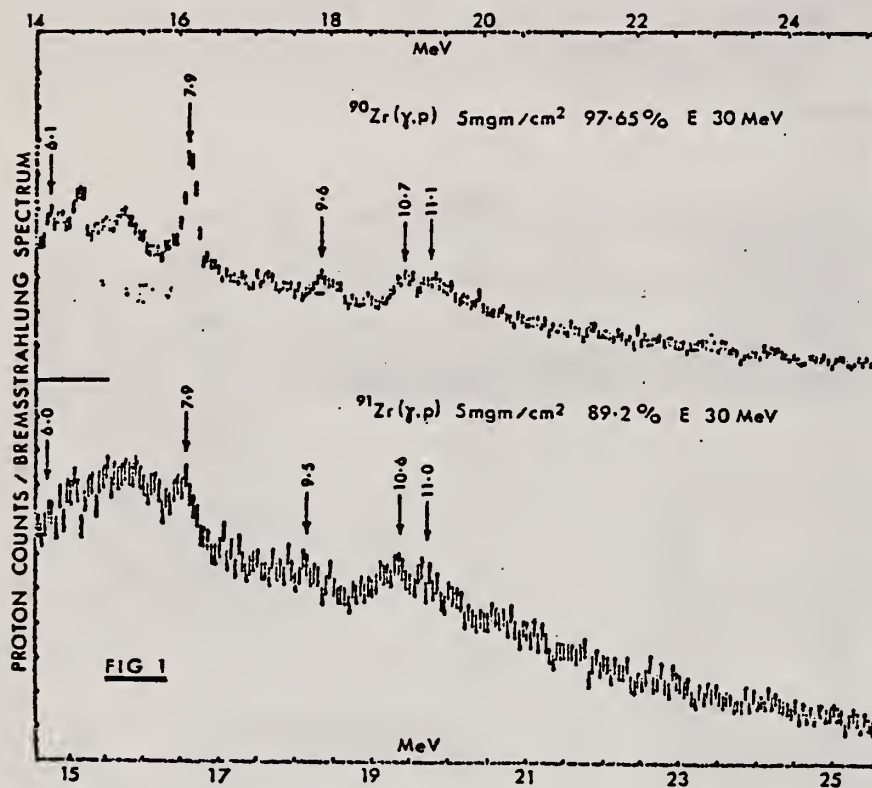
<sup>6</sup> K. Shoda et al., Phys. Rev. Lett. **23** (1969) 800.

<sup>19</sup> B.L. Berman et al., Phys. Rev. **162** (1967) 1098.

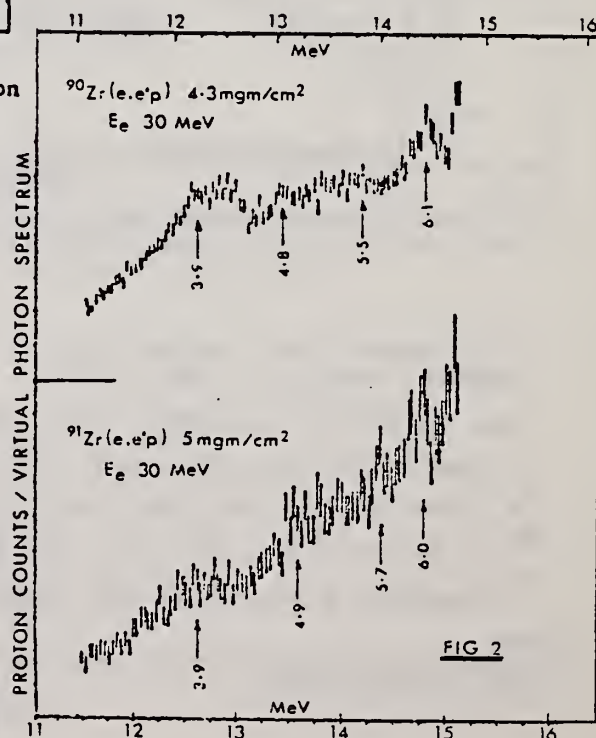
<sup>20</sup> A. Lepretre et al., Nucl. Phys. **A175** (1971) 609.

ELEM. SYM.	A	Z
Zr	90	40
REF. NO.		hmg
73 As 9		

REACTION	RESULT	EXCITATION ENERGY	SOURCE		DETECTOR		ANGLE
			TYPE	RANGE	TYPE	RANGE	
E, P	SPC	THR- 26	D	30	MAG-D		DST



Arrows show proton energies. Horizontal scales indicate excitation energies assuming ground state transitions.



REF. D. Brajnik, D. Jamnik, G. Kernel, M. Korun, U. Miklavzic,  
B. Pucelj and A. Stanovnik  
PICNS-73, Vol.I, p. 539 Asilomar

ELEM. SYM.	A	Z
Zr	90	40

METHOD

REF. NO.

73 Br 12

hmg

REACTION	RESULT	EXCITATION ENERGY	SOURCE		DETECTOR		ANGLE
			TYPE	RANGE	TYPE	RANGE	
G,P	ABX	8- 24	C	14- 24	SCD-D		DST
G,2N	ABX	21- 28	C	20- 28	ACT-I		UKN
G,NP	ABX	19- 28	C	20- 28	ACT-I		UKN

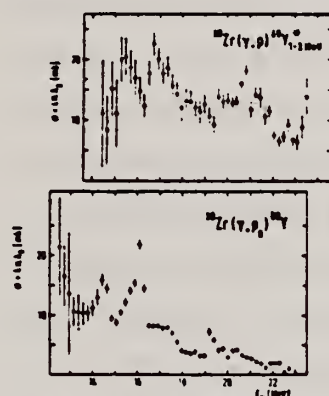


Fig.1. Cross section for the reaction  $^{90}\text{Zr}(\gamma,p)$  leaving the residual nucleus  $^{89}\text{Y}$  in excited states between 1 and 5 MeV (upper diagram). Photoproton cross section to the ground state of  $^{89}\text{Y}$  (lower diagram).

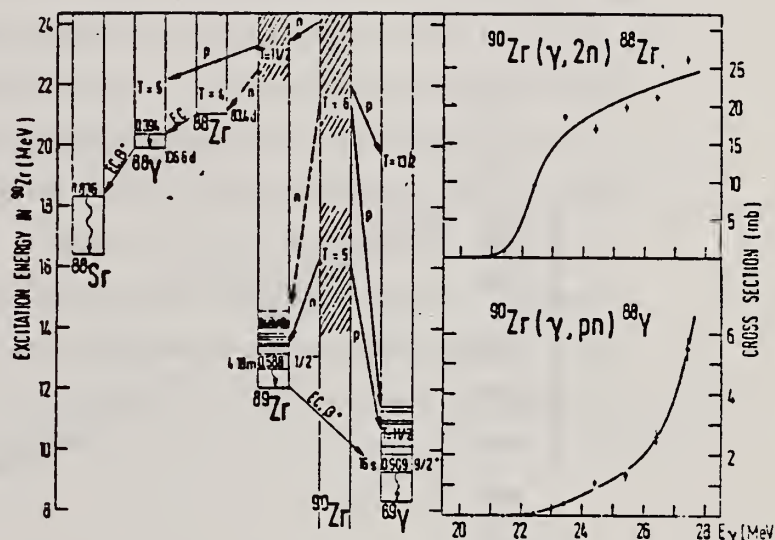


Fig.2. Cross sections for the reactions  $^{90}\text{Zr}(\gamma,2n)^{88}\text{Zr}$  and  $^{90}\text{Zr}(\gamma,pn)^{88}\text{Y}$ . The decay of the giant resonance is schematically shown in the left diagram.

REF.

F.E. Cecil, L.W. Fagg, W.L. Bendel, N. Ensslin, E.C. Jones, Jr.  
 PICNS-73, Vol. I, p. 699 Asilomar

ELEM. SYM.	A	Z
Zr	90	40
REF. NO.		
73 Ce 3		hmg

METHOD

REACTION	RESULT	EXCITATION ENERGY	SOURCE		DETECTOR		ANGLE
			TYPE	RANGE	TYPE	RANGE	
E, E/	LFT	9	D	37 - 61	MAG-D		180
		(9.1)					

Ground state M1 transition width =  $117 \pm 23$  eV.

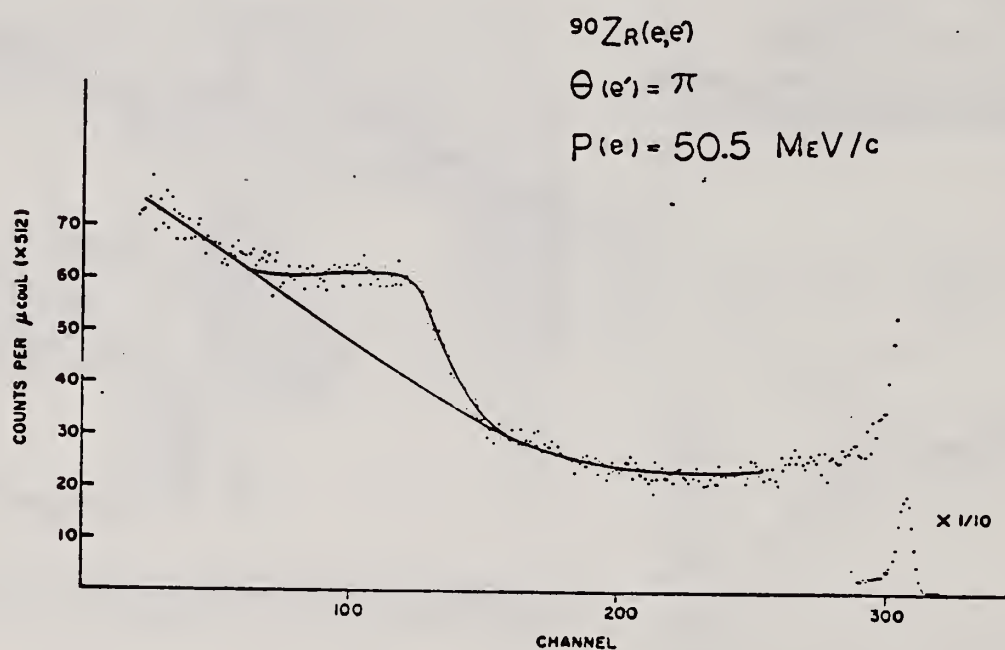


FIG 1

(over)



The giant magnetic dipole resonance recently observed in  $^{208}\text{Pb}$  <sup>1</sup> tends to confirm the explanation by Vergados <sup>2</sup> of the deviations from single particle calculations of numerous magnetic dipole measurements in the Lead region. A recent measurement <sup>3</sup> of the M1 width of the  $1+$  state in  $^{88}\text{Sr}$  similarly suggests the existence the giant M1 in  $^{90}\text{Zr}$ . This suggestion is supported by an assumed shell model structure of  $^{90}\text{Zr}$  of a closed  $1g_{9/2}$  neutron shell in the presence of an open  $1g_{7/2}$  shell. Within this assumption, the ground state M1 transition strength will be concentrated in the shell model configuration  $(g_{9/2}^{-1} - g_{7/2})^{1+}$ . In a recent search <sup>4,5</sup>, no evidence was found for such a state excited in inelastic proton scattering. As such a non-observance may be attributed to a Serber like nucleon-nucleon effective interaction, a subsequent search has been has been carried out using inelastic electron scattering at  $180^\circ$ .

In this experiment, a self supporting target of isotopically enriched  $^{90}\text{Zr}$ , of thickness  $66 \text{ mg/cm}^2$  was bombarded with electrons of 37, 50.5, and 60.5 MeV/c incident momentum from the NRL LINAC. The spectrum taken at 50.5 MeV/c is shown in figure 1. The broad peak centered around channel 110 in this figure is also evident in the 37 and 60.5 MeV/c data. This peak lies at an excitation energy of 9.1 MeV and is approximately 2.5 MeV FWHM. A preliminary analysis of the yields for this peak at the three bombarding momenta using the model described by Fagg et. al. <sup>6</sup> together with Coulomb distortion corrections <sup>7</sup> indicates the peak to be magnetic dipole in character. A tentative value of the ground state M1 transition width of this peak is then found to be  $117 \pm 23 \text{ eV}$ . In contrast, the predicted width of an M1 transition from the ground state of  $^{90}\text{Zr}$  to a  $1+$  state at 9.1 MeV whose shell model configuration is  $(g_{9/2}^{-1} - g_{7/2})$  is 50 eV. <sup>8</sup>



REACTION	RESULT	EXCITATION ENERGY	SOURCE		DETECTOR		ANGLE
			TYPE	RANGE	TYPE	RANGE	
P,G	ABX	13- 25	D	5- 17	NAI-D		DST

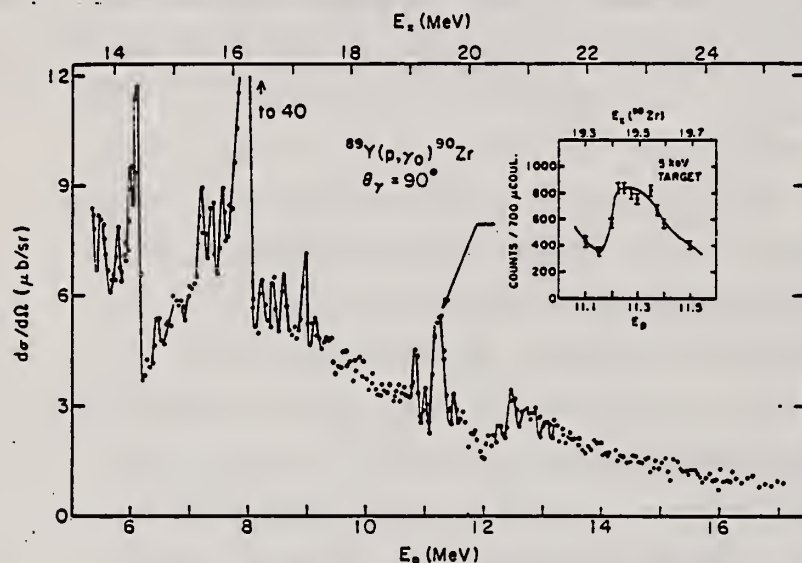


Fig. 3. Excitation curve for the reaction  $^{89}\text{Y}(p,\gamma)^{90}\text{Zr}$  at  $\theta_\gamma = 90^\circ$ . The solid lines indicate the sharp structures in the data. The insert shows the yield in the vicinity of the resonance at  $E_p = 11.30$  MeV measured with a thin target.

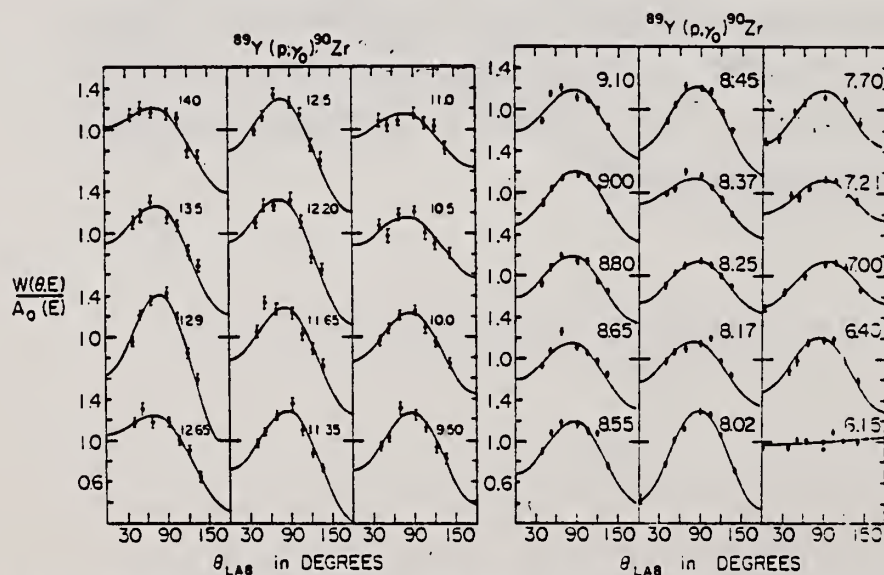


Fig. 4. Normalized angular distributions for the reaction  $^{89}\text{Y}(p,\gamma)^{90}\text{Zr}$ . The solid curves are least-square fits with Legendre polynomials up to  $P_2$ . The incident proton energy (in MeV) is listed in each case.

(over)

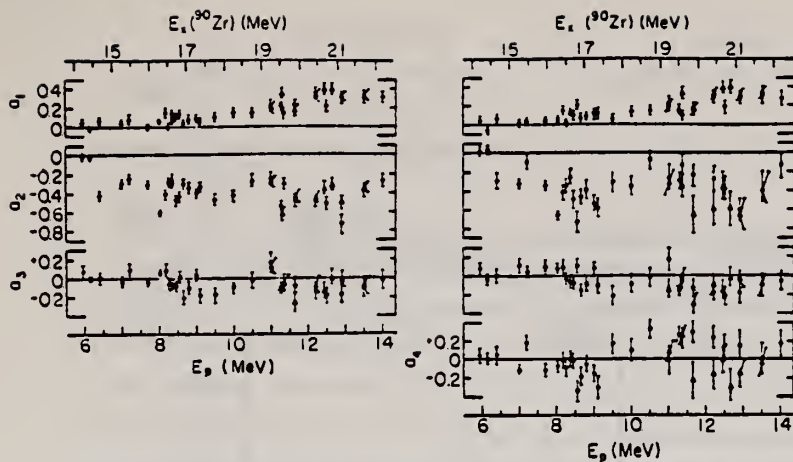


Fig. 6. Legendre polynomial coefficients obtained by fitting the  $^{89}\text{Y}(p, \gamma_0)^{90}\text{Zr}$  angular distributions shown in fig. 4 with the series  $W(\theta, E) = A_0[1 + \sum_{l=1}^N a_l(E)P_l(\cos \theta)]$  where  $N = 3, 4$ . The triangles represent data measured with a 120 keV thick target.

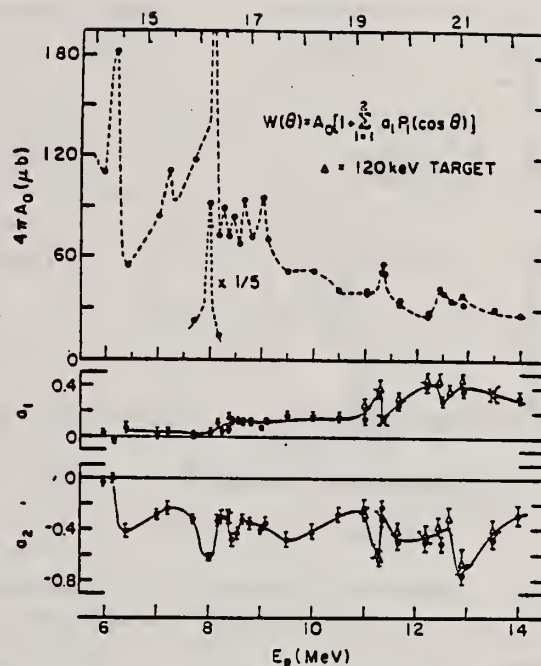


Fig. 5. Legendre polynomial coefficients obtained by fitting the  $^{89}\text{Y}(p, \gamma_0)^{90}\text{Zr}$  angular distributions shown in fig. 4 with the series  $W(\theta, E) = A_0[1 + \sum_{l=1}^N a_l(E)P_l(\cos \theta)]$ . The solid lines drawn through the  $a_1$  and  $a_2$  coefficients are visual fits which show the correlation between the structures observed in the  $A_0$ ,  $a_1$  and  $a_2$  curves. The scale for the total cross section ( $4\pi A_0$ ) should be multiplied by 0.8.

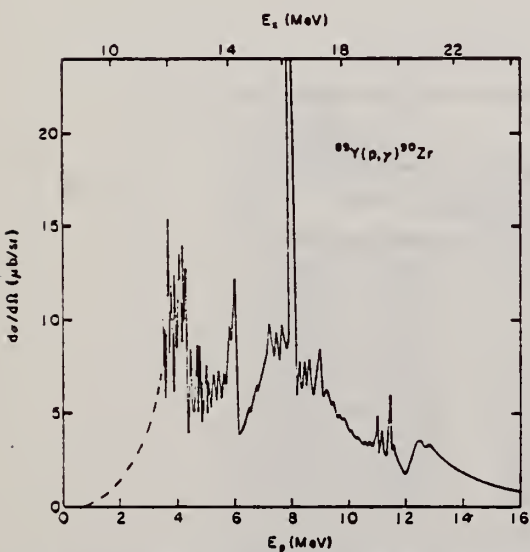


Fig. 14. Complete yield curve for the reaction  $^{89}\text{Y}(p, \gamma_0)^{90}\text{Zr}$  at  $\theta_g = 90^\circ$ . The curve below  $E_p = 5.40$  MeV is a symbolic representation of the data from ref. 23) which shows a great amount of fine structure.

- <sup>23</sup> E. Obst, F. Rauch, E. Rosle, Phys. Lett. 21 (1966) 50;  
E. Obst, F. Rauch and H.G. Wahsweiler, Nucl. Phys. A103 (1967) 17, 373

REF. Phan Xuan Ho, J. Bellicard, Ph. Leconte, I. Sick  
Nucl. Phys. **A210**, 189 (1973)

ELEM. SYM.	A	Z
Zr	90	40
REF. NO.		
73 Ho 4		egf

METHOD

REACTION	RESULT	EXCITATION ENERGY	SOURCE		DETECTOR		ANGLE
			TYPE	RANGE	TYPE	RANGE	
E, E/	FMF	2- 3	D	209	MAG-D		DST

2.19, 2.75, 3.08

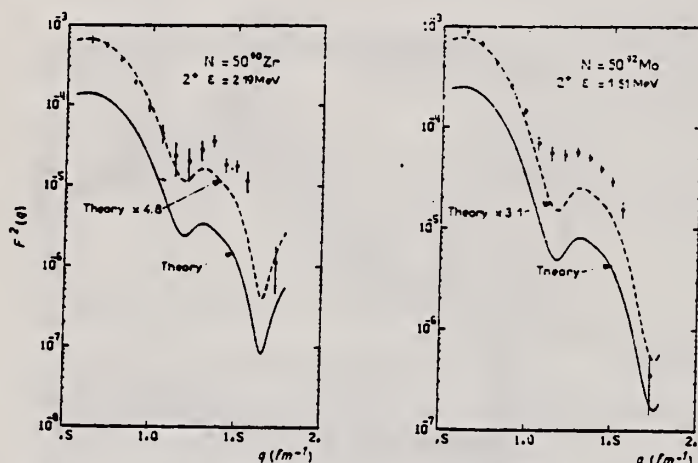


Fig. 5b. Squared inelastic form factor for 2<sup>+</sup> states of the N = 50 isotones.

TABLE 5  
Inelastic cross sections for E<sub>α</sub> = 209 MeV on <sup>90</sup>Zr

	θ (deg.)	(2 <sup>+</sup> )ε = 2.19 MeV dσ/dΩ(mb/sr)	(3 <sup>-</sup> )ε = 2.75 MeV dσ/dΩ(mb/sr)	(4 <sup>+</sup> )ε = 3.08 MeV dσ/dΩ(mb/sr)
(6 <sup>+</sup> ) 3.45 → -----	35	0.142 E-1 ± 0.170 E-2	0.220 E-1 ± 0.160 E-2	
(2 <sup>+</sup> ) 3.31 → -----	40	0.686 E-2 ± 0.490 E-3	0.139 E-1 ± 0.800 E-3	
	45	0.278 E-2 ± 0.170 E-3	0.846 E-2 ± 0.430 E-3	0.624 E-3 ± 0.176 E-3
(4 <sup>+</sup> ) 3.08 → =====	50	0.941 E-3 ± 0.610 E-4	0.443 E-2 ± 0.230 E-3	0.419 E-3 ± 0.580 E-4
	55	0.307 E-3 ± 0.360 E-4	0.221 E-2 ± 0.130 E-3	0.271 E-3 ± 0.350 E-4
(3 <sup>-</sup> ) 2.74 → =====	60	0.101 E-3 ± 0.250 E-4	0.984 E-3 ± 0.540 E-4	0.170 E-3 ± 0.240 E-4
	65	0.374 E-4 ± 0.165 E-4	0.346 E-3 ± 0.200 E-4	0.115 E-3 ± 0.150 E-4
	70	0.232 E-4 ± 0.100 E-4	0.102 E-3 ± 0.900 E-5	0.637 E-4 ± 0.820 E-5
(5 <sup>+</sup> ) 2.32 → =====	75	0.242 E-4 ± 0.640 E-5	0.242 E-4 ± 0.460 E-5	0.322 E-4 ± 0.450 E-5
(2 <sup>+</sup> ) 2.18 → =====	80	0.233 E-4 ± 0.350 E-5	0.199 E-4 ± 0.260 E-5	0.161 E-4 ± 0.220 E-5
	85	0.892 E-5 ± 0.163 E-5	0.220 E-4 ± 0.150 E-5	0.403 E-5 ± 0.950 E-6
	90	0.658 E-5 ± 0.104 E-5	0.216 E-4 ± 0.120 E-5	0.657 E-6 ± 0.353 E-6
	95	0.334 E-5 ± 0.950 E-6	0.174 E-4 ± 0.180 E-5	0.378 E-7 ± 0.193 E-7
(0 <sup>+</sup> ) 1.75 → -----	110	0.155 E-6 ± 0.900 E-7	0.509 E-5 ± 0.370 E-6	0.417 E-6 ± 0.238 E-6

Energy level diagram given by ref. <sup>24</sup>). Levels excited in our experiment are shown with solid lines, dashed lines correspond to other levels. The experimental values are normalized with the elastic cross sections calculated by a phase shift program using a 3-parameter Gaussian model. The parameters (c = 4.500, z = 2.530, w = 0.200) are obtained from ref. <sup>18</sup>).

(over)

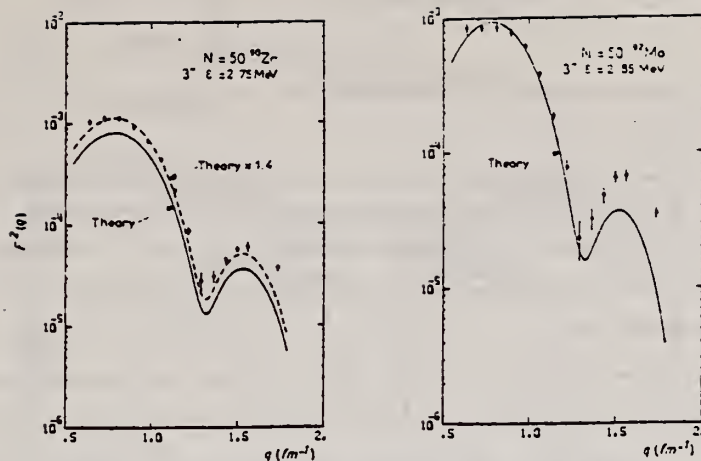


Fig. 6b. Squared inelastic form factor for  $3^-$  states of the  $N = 50$  isotones.

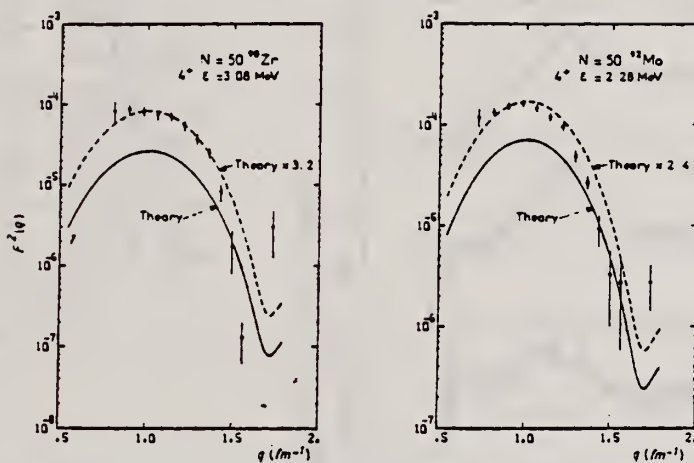


Fig. 7b. Squared inelastic form factor for  $4^+$  states of the  $N = 50$  isotones.

<sup>18</sup>Phan-Xuan Ho, J. Bellicard, A. Bussiere, M. Priou,  
Nucl. Phys. A179 (1972) 529.

<sup>24</sup>Nuclear Data Sheets B (1970).



REF.

Y. Torizuka, Y. Kojima, T. Saito, K. Itoh, A. Nakada,  
S. Mitsunobu, M. Nagao, K. Hosoyama, S. Fukuda, H. Miura  
PICNS-73, Vol. I, p.675 Asilomar

ELEM. SYM.

A

Z

Zr

90

40

METHOD

REF. NO.

73 To 1

hmg

REACTION	RESULT	EXCITATION ENERGY	SOURCE		DETECTOR		ANGLE
			TYPE	RANGE	TYPE	RANGE	
E, E/	FMF	5- 37	D	150-250	MAG-D		DST

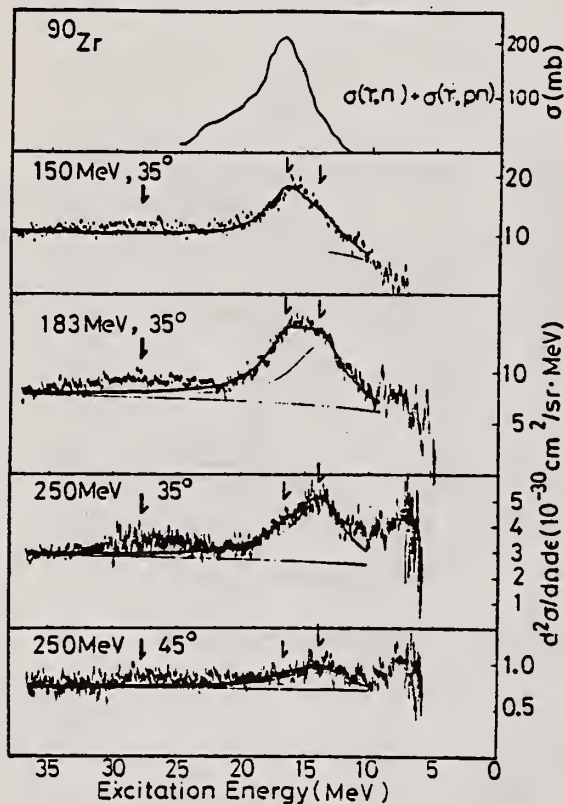


Fig. 5. Inelastic electron scattering spectra of  $^{90}\text{Zr}$  from 7 to 35 MeV. The photoreaction spectrum is shown for comparison. The arrows indicate the peaks at 14.0, 16.7, and 27 MeV.

Table III. The  $B(\text{EL})$ , monopole matrix elements (ME), and fractions of the energy-weighted sum rule (EWSR) for the giant resonances in  $^{90}\text{Zr}$ .

	$E_x$ (MeV)	$B(\text{EL})_{\text{or}}  \text{ME} ^2$	fraction of $T=0$ EWSR	fraction of $T=1$ EWSR
E2	14.0	$990 \text{ e}^2 \text{ fm}^4$	0.522	
	27.0	280.3	0.285	0.228
E0	14.0	$2050 \text{ fm}^4$	1.074	
	27.0	547.9	0.594	0.476
E1	16.65	$17.0 \text{ e}^2 \text{ fm}^2 *$		0.89

$$\cdot \sqrt{\langle r^2 \rangle} = 4.255 \text{ fm}$$

$$* B(\text{E1}) \text{ from } (\gamma, n) \text{ is } 18.8 \text{ e}^2 \text{ fm}^2$$

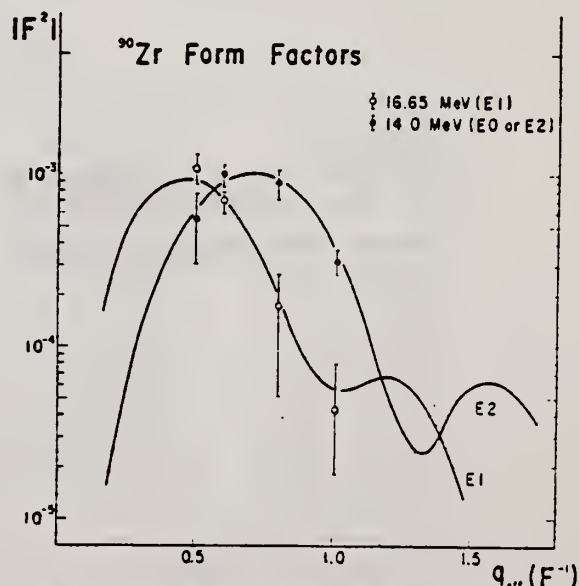


Fig. 6. The form factors for the 14.0- and 16.7-MeV states in  $^{90}\text{Zr}$ .

(over)



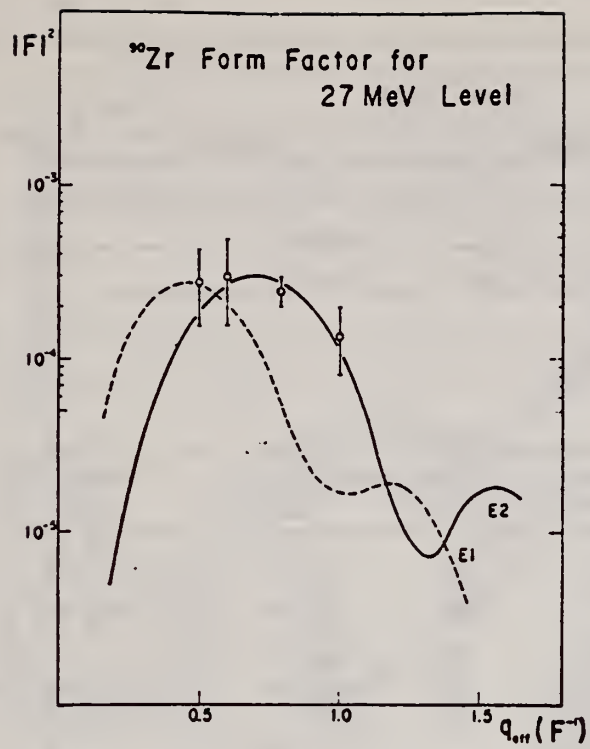


Fig. 8. The form factor for the 27-MeV state in  $^{90}\text{Zr}$ .

REF.

H.J. Askin, K.J.F. Allen, M.N. Thompson, K. Shoda, M. Sugawara,  
H. Miyase, and B.N. Sung  
Nucl. Phys. **A220**, 241 (1974)

ELEM. SYM.

A

Z

Zr

90

40

METHOD

REF. NO.

74 As 4

egf

Page 1 of 3

REACTION	RESULT	EXCITATION ENERGY	SOURCE		DETECTOR		ANGLE
			TYPE	RANGE	TYPE	RANGE	
G,P	SPC	8- 30	C	30	SCD-D		90
E,P	SPC	8- 30	D	20- 30	MAG-D		90

TABLE I  
Summary of results

Target	Proton energy $E_p$ (MeV)	Excitation energy (MeV)		Residual levels $^{90}\text{Y}$
		apparent	actual	
$^{90}\text{Zr}$	9.6	17.9	(19.4) <sup>a)</sup>	(1.5 MeV, $\frac{3}{2}^-$ ) <sup>a)</sup>
	11.1	19.4	19.4	g.s., $\frac{1}{2}^-$
	10.7	19.0	20.5-20.8	(1.74 MeV, $\frac{3}{2}^-$ ) <sup>a)</sup>
			(20.7) <sup>a)</sup>	
	12.5	20.8	20.8	g.s., $\frac{1}{2}^-$
	11.3	19.6	21.2-21.4	1.5 MeV, $\frac{3}{2}^-$ or 1.74 MeV, $\frac{3}{2}^-$
	10.2	18.5	(21.4) <sup>a)</sup>	(2.88 MeV, $\frac{3}{2}^-$ ) <sup>a)</sup>
$^{90}\text{Zr}$				$^{90}\text{Y}$ :
	9.5	18.2	19.7 <sup>b)</sup>	$\approx 1.5$ MeV <sup>b)</sup>
	11.0	19.7	(19.7-19.9) <sup>a)</sup>	g.s., $2^-$ or 0.2 MeV, $3^-$
	10.7	19.4	20.8-21.2	1.4-1.8
			(21.1) <sup>a)</sup>	(1.7) <sup>b)</sup>
	12.5	21.2	(21.2) <sup>a)</sup>	g.s., $2^-$ or 0.2 MeV, $3^-$
	11.3	20.0	21.5-21.8	1.5-1.8
	10.1	18.8	( $\approx 21.5$ ) <sup>a)</sup>	( $\approx 2.7$ MeV) <sup>a)</sup>

a) Most probable.

b) Consistent assignment.

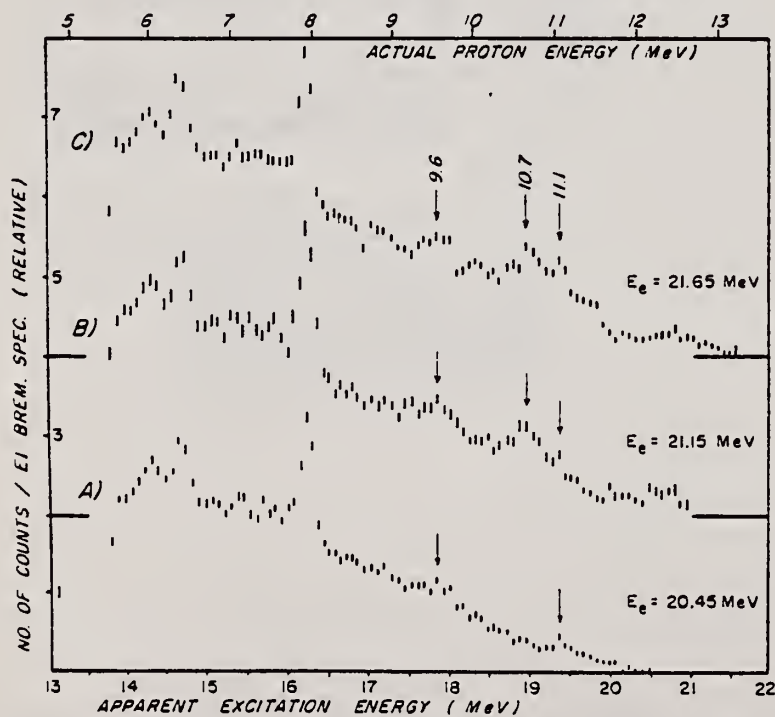


Fig. 3. The  $^{90}\text{Zr}(e, e'p)^{90}\text{Y}$  spectra: (a)  $E_e(\text{max}) = 20.45$  MeV; (b)  $E_e(\text{max}) = 21.15$  MeV; (c)  $E_e(\text{max}) = 21.65$  MeV.

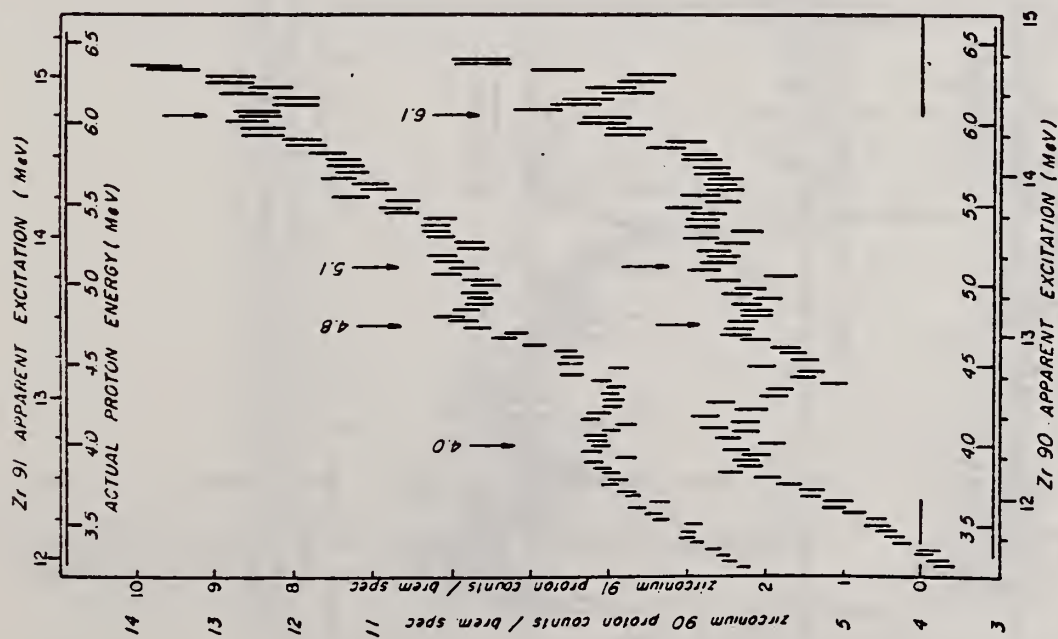


Fig. 1. The  $^{91}\text{Zr}(e, e'p)^{90}\text{Zr}$  proton spectrum (upper) and the  $^{90}\text{Zr}(e, e'p)^{89}\text{Zr}$  proton spectrum (lower). Bombarding electron energy  $E_e = 30$  MeV. Spectra are plotted with a common proton energy scale.

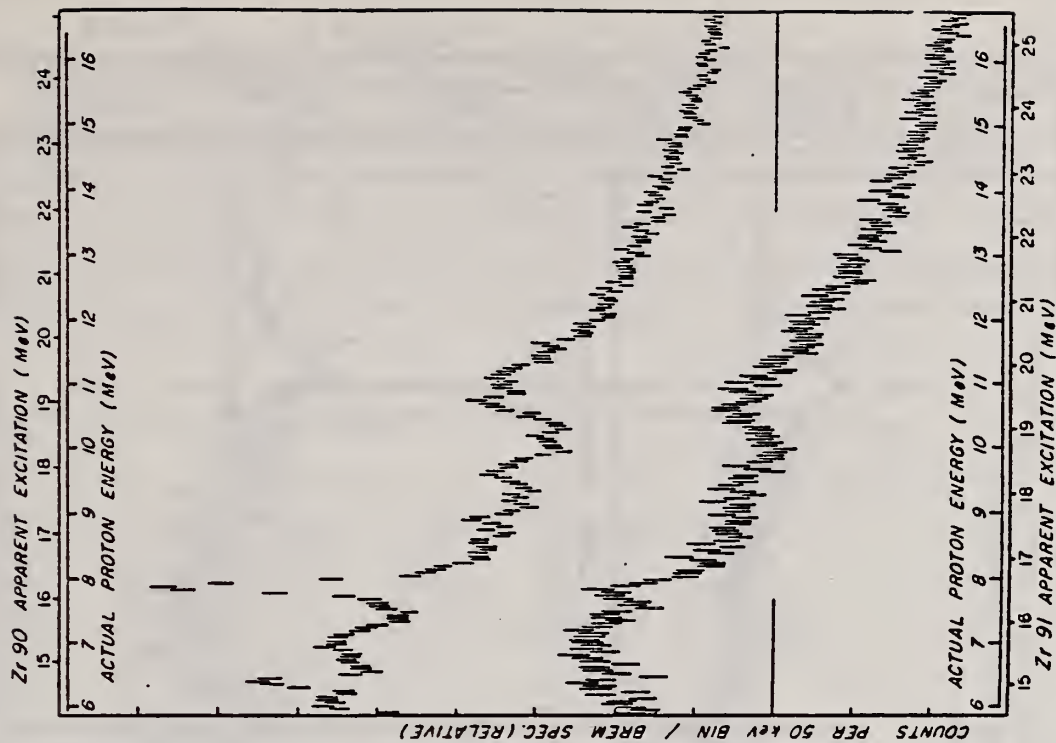


Fig. 2. The  $^{90}\text{Zr}(p, p)^{90}\text{Zr}$  proton spectrum (upper) and the  $^{91}\text{Zr}(p, p)^{90}\text{Zr}$  proton spectrum (lower). The  $E_e$  endpoint  $= 30$  MeV. Spectra are plotted with a common proton energy scale.

REF.

H.J. Askin, K.J.F. Allen, M.N. Thompson, K. Shoda, M. Sugawara,  
H. Miyase, and B.N. Sung  
Nucl. Phys. **A220**, 241 (1974)

ELEM. SYM.	A	Z
Zr	90	40
REF. NO.	74 As 4	
	egf	

METHOD

Page 3 of 3

REACTION	RESULT	EXCITATION ENERGY	SOURCE		DETECTOR		ANGLE
			TYPE	RANGE	TYPE	RANGE	

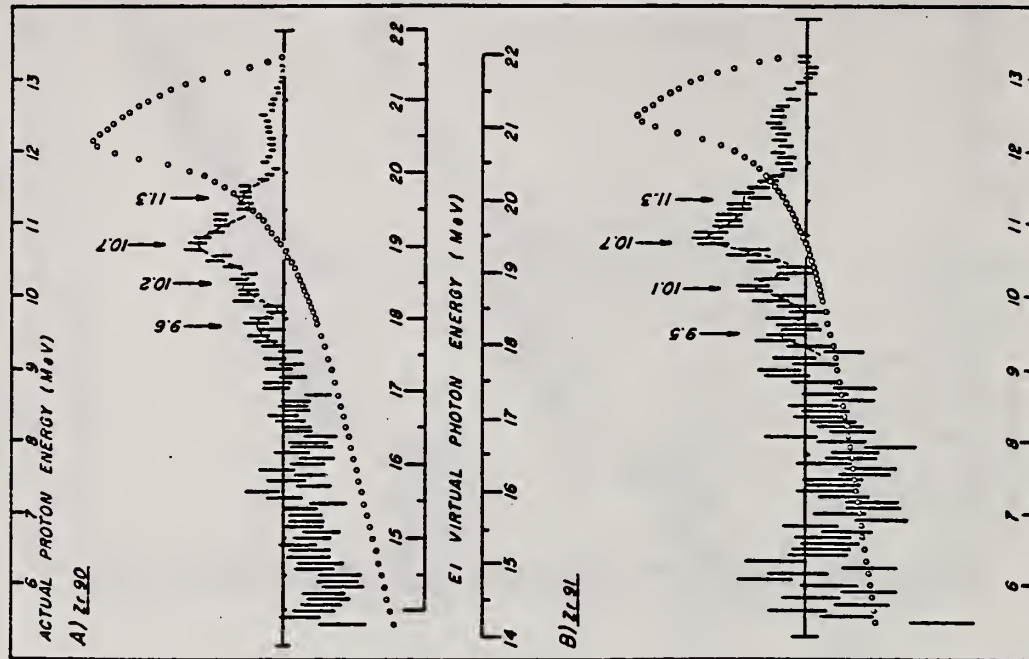


Fig. 7. Comparison of: (a) difference of  $^{90}\text{Zr}(e, e'p)^{99}\text{Y}$  proton spectra recorded with  $E_e(\text{max}) = 21.65$  MeV and  $20.45$  MeV and (b) difference of  $^{90}\text{Zr}(e, e'p)^{99}\text{Y}$  spectra recorded with  $E_e(\text{max}) = 22.15$  MeV and  $21.15$  MeV. Both proton difference spectra are plotted on a common proton energy scale. Corresponding E1 virtual photon difference spectra are superimposed.

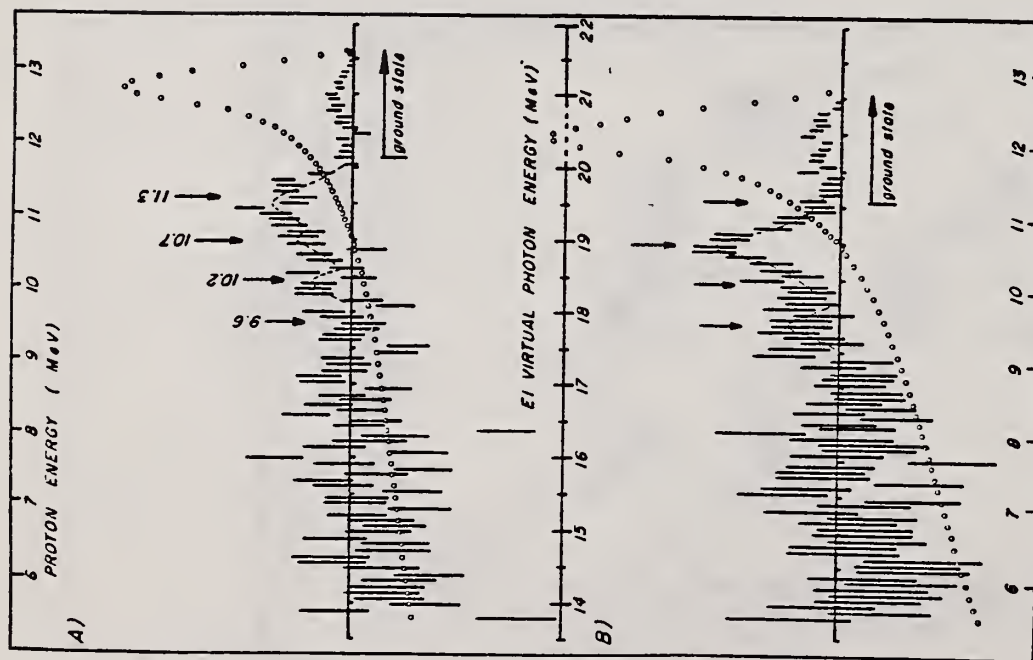


Fig. 5. Differences of  $^{90}\text{Zr}(e, e'p)^{99}\text{Y}$  proton spectra recorded with: (a)  $E_e(\text{max}) = 21.65$  MeV and  $E_e(\text{max}) = 21.15$  MeV; (b)  $E_e(\text{max}) = 20.45$  MeV and  $E_e(\text{max}) = 20.15$  MeV. The corresponding differences in the E1 virtual photon spectra are superimposed (circles).



METHOD

REF. NO.

74 Me 2

hmg

REACTION	RESULT	EXCITATION ENERGY	SOURCE		DETECTOR		ANGLE
			TYPE	RANGE	TYPE	RANGE	
G,G	LFT	2- 6	C	3- 6	SCD-D		DST

5 LEVELS 2-6 MEVTABLE II. Results of resonance-fluorescence experiments with  $^{90}\text{Zr}$ .

Level energy <sup>a</sup> (keV)	$I^\pi$	$\Gamma_0^2/\Gamma$ (meV)	$\Gamma_0/\Gamma$	$\Gamma_0$ (meV)	$\Gamma_0(\text{expt.})/\Gamma_0(\text{s.p.})$
2186	2 <sup>+</sup>	4.89 ± 0.28	1.00	4.89 ± 0.28	5.1
3308 ± 1	2 <sup>+</sup>	3.45 ± 0.60	0.75 ± 0.02	4.6 ± 0.8	0.6
3842 ± 1	2 <sup>+</sup>	24.0 ± 3.4	0.86 ± 0.02	28 ± 4	1.7
4580 ± 2	1 <sup>(-)</sup>	24.0 ± 4.0	0.5 ± 0.1 <sup>b</sup>	48 ± 13	3.7 × 10 <sup>-4</sup>
5504 ± 2	1 <sup>(-)</sup>	48 ± 17	0.6 ± 0.1	80 ± 32	3.5 × 10 <sup>-4</sup>
4120	2 <sup>+</sup>	0.3 ± 0.5			
4230	2 <sup>+</sup>	0.5 ± 0.9			
4680	2 <sup>+</sup>	<10			

<sup>a</sup> The energies listed for levels two to five are those determined in the present study. The last three energies are those reported in Ref. 4.<sup>b</sup> Reference 13.

TABLE I. Comparison of experimental and theoretical yield ratios.

Level energy (MeV)	$N_{sc}(98^\circ)/N_{sc}(127^\circ)$		
	Experiment	Theory	
		Spin 1	Spin 2
3.31	2.2 ± 0.6	} 0.74	} 2.08
3.84	2.0 ± 0.3		
4.58	0.7 ± 0.2		

4  
J.B. Ball, M.W. Johns, and K. Way, Nucl. Data A8, 407 (1970).13  
B. Seim, Ph.D. thesis, Johann Wolfgang Goethe-Universitaet, 1971 (unpublished).



METHOD

REF. NO.

74 Ra 3

egf

REACTION	RESULT	EXCITATION ENERGY	SOURCE		DETECTOR		ANGLE
			TYPE	RANGE	TYPE	RANGE	
P,G	ABX	13	D	4	SCD-D		55

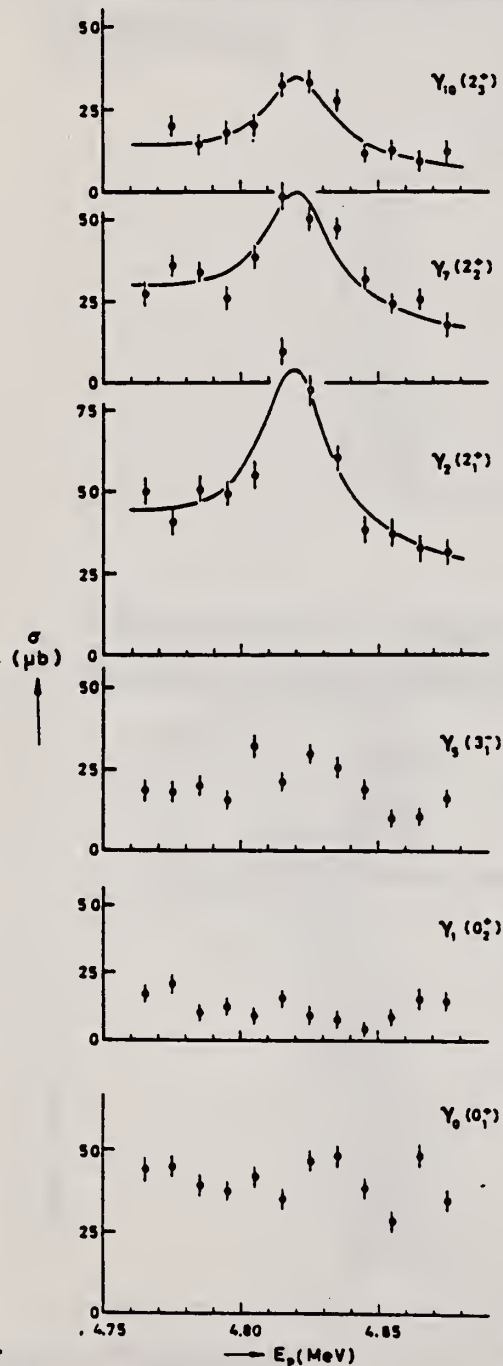
 $4=4.75-4.88$  MEV

Fig. 1. The  $^{89}\text{Y}(p, \gamma)^{90}\text{Zr}$  excitation functions obtained in the present experiment. The solid lines are Breit-Wigner curves (compare text).

Table 1  
Results for the  $\gamma$  decay of the ground state analog in  $^{90}\text{Zr}$ .

	$\gamma_2$	$\gamma_7$	$\gamma_{10}$
$E_\gamma$ (MeV) a)	10.92	9.80	9.26
$\sigma_\gamma$ ( $\mu\text{b}$ ) b)	$64 \pm 17$	$43 \pm 13$	$30 \pm 10$
$\Gamma$ (eV) c)	$15 \pm 4$	$10 \pm 3$	$7 \pm 3$
$\Gamma_\gamma^{\text{th}}$ (eV) d)	$\leq 4.4$	$\leq 3.2$	$\leq 2.9$
$\sigma_\gamma/E_\gamma^5$ ( $\mu\text{b}/\text{MeV}^5$ )	$41 \times 10^{-5}$	$47 \times 10^{-5}$	$44 \times 10^{-5}$
$\sigma_\gamma^{\text{c}}$ ( $\mu\text{b}$ ) e)	84	49	39

- a) Transition energy.  
b) Experimental resonance cross section.  
c) Experimental radiative width.  
d) Direct radiative width.  
e) Predicted compound resonance cross section.

REACTION	RESULT	EXCITATION ENERGY	SOURCE		DETECTOR		ANGLE
			TYPE	RANGE	TYPE	RANGE	
E, P	ABX	12- 24	D	12- 30	MAG-D		DST

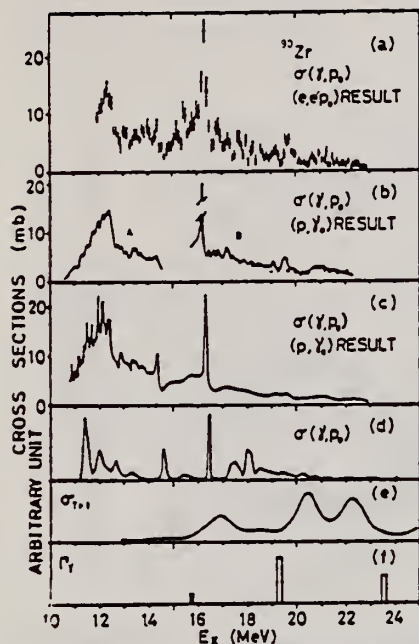


Fig. 11. Comparison of photon-proton cross sections of  $^{90}\text{Zr}$ . (a) Present result. (b) Curve A, ref. <sup>31</sup>); curve B, ref. <sup>32</sup>); open circles, ref. <sup>32</sup>). (c) Ref. <sup>4</sup>). (d), (e), (f) Theoretical estimates, refs. <sup>12, 14, 15</sup> respectively.

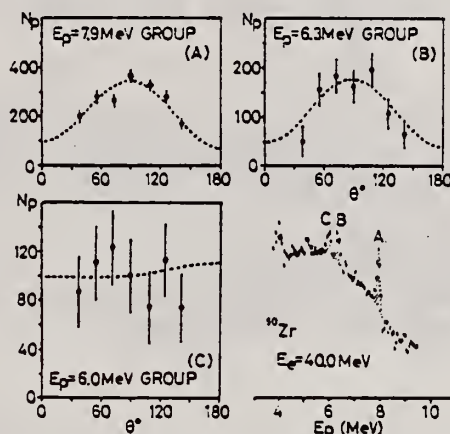


Fig. 14. Angular distributions of proton groups indicated by hatching in the proton spectrum which is summed over various angles. Both the dashed lines in the results of groups A and B are the results of  $(p, \gamma_0)$  for group A [ref. <sup>2</sup>]. The dashed line in the result of group C is the  $(p, \gamma_0)$  result of this group <sup>2</sup>.

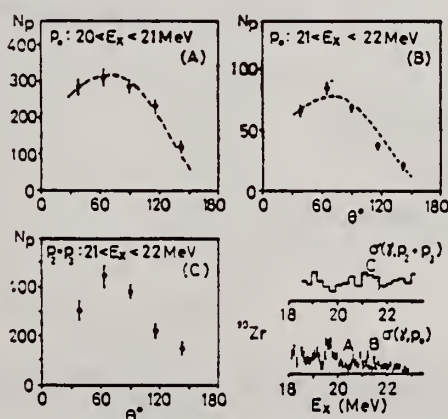


Fig. 15. Angular distributions of proton groups in the  $T+1$  coherent resonance region. The groups are indicated by hatching in the cross sections. The dashed line in the figure shows the result of  $(p, \gamma_0)$  in the corresponding regions <sup>3</sup>.

(over)

TABLE 5

The radiative width of the narrow E1 IAR obtained from the proton group in the proton spectra

Nucleus	$E_x$ (MeV)	$E_p$ (MeV)	$E_{\text{rel}}(J^\pi)$ (MeV)	$\Gamma_\gamma \frac{\Gamma_{p1}^{(a)}}{\Gamma}$ (eV)	$\Gamma_\gamma^{(a)}$ (eV)	$2(T+1) \frac{\Gamma_\gamma^{(a)}}{\Gamma_w}$	$2(T+1) \frac{\Gamma_\gamma^{(a)}}{\Gamma_{\text{p.p.}}}$	(p, $\gamma$ ) data $\Gamma_\gamma$ (eV)
$^{90}\text{Zr}$	14.5	6.0	0 ( $\frac{1}{2}^-$ )	26	26 <sup>b)</sup>	0.076		> 30 <sup>a)</sup>
	16.3	7.9	0 ( $\frac{1}{2}^-$ )	74				
	16.3	6.3	1.51 ( $\frac{1}{2}^-$ )	52	126 <sup>c)</sup>	0.26		> 60 <sup>a)</sup>
$^{89}\text{Y}$	13.0 <sup>d)</sup>	5.9	0 (0 <sup>+</sup> )	13	13 <sup>b)</sup>		0.13 <sup>f)</sup>	18 $\pm$ 3 <sup>b)</sup>
	14.5 <sup>e)</sup>	7.3	0 (0 <sup>+</sup> )	16	16 <sup>b)</sup>		0.14 <sup>f)</sup>	11 $\pm$ 2 <sup>b)</sup>
	15.9 <sup>e)</sup>	8.7	0 (0 <sup>+</sup> )	42	42 <sup>b)</sup>		0.68 <sup>f)</sup>	40 $\pm$ 8 <sup>b)</sup>
$^{88}\text{Sr}$	17.1	6.5	0 ( $\frac{1}{2}^-$ )	9.5				
	17.1	5.6	0.85 ( $\frac{1}{2}^-$ )	4.9	14 <sup>c)</sup>	0.029		
	17.3	6.7	0 ( $\frac{1}{2}^-$ )	30				
	17.3	5.9	0.85 ( $\frac{1}{2}^-$ )	18	48 <sup>c)</sup>	0.094		

The available data with the (p,  $\gamma$ ) experiment are shown in the last column.<sup>a)</sup> The errors may be  $\approx 30\%$  (for  $^{90}\text{Zr}$ ,  $^{88}\text{Sr}$ ) and  $\approx 50\%$  (for  $^{89}\text{Y}$ ) including the uncertainty of the process to separate the proton group.<sup>b)</sup>  $\Gamma_{p0}/\Gamma = 1$  was assumed.<sup>c)</sup>  $(\Gamma_{p0} + \Gamma_{p2})/\Gamma = 1$  was assumed.<sup>d)</sup>  $J^\pi = \frac{1}{2}^+$  was assigned as shown in table 3.<sup>e)</sup>  $J^\pi = \frac{3}{2}^+$  was assigned as shown in table 3.<sup>f)</sup> Correction was made for the spectroscopic factors on the ground state and the excited state with the data of the ( $\text{He}^3$ , d) and (d, p) reactions respectively.<sup>g)</sup> Ref. <sup>27)</sup>.<sup>h)</sup> Ref. <sup>6)</sup>.<sup>2</sup> J.L. Black et al., Phys. Lett. 11 (1964) 135; J.L. Black et al., Nucl. Phys. A92 (1967) 365.<sup>4</sup> W.M. Mason et al., Nucl. Phys. A135 (1969) 193.<sup>5</sup> M. Hasinoff et al., Phys. Lett. 30B (1969) 337.<sup>6</sup> P. Paul, nuclear structure studies using electron scattering and photo-reaction, ed. K. Shoda and H. Ui (Research report of Lab. Nucl. Sci. Tohoku Univ. vol. 5, 1972) p.343.<sup>12</sup> A. Piazza et al., Phys. Lett. 25B (1967) 579.<sup>14</sup> T.A. Hughes et al., Nuclear isospin, ed. J.D. Anderson et al. (Academic Press, New York, 1969) p.104.<sup>15</sup> J.D. Vergados et al., Phys. Lett. 35B (1971) 93.<sup>27</sup> J.L. Black et al., Nucl. Phys. A92 (1967) 365.<sup>31</sup> E. Obst et al., Phys. Lett. 21 (1966) 50.<sup>32</sup> P. Axel, et al., Phys. Rev. Lett. 19 (1967) 1343.

REF. K. Shoda, H. Miyase, M. Sugawara, T. Saito, S. Oikawa,  
A. Suzuki, J. Uegaki  
Nucl. Phys. A239, 397 (1975)

ELEM. SYM.	A	Z
Zr	90	40

METHOD	REF. NO.	
	75 Sh 4	egf

REACTION	RESULT	EXCITATION ENERGY	SOURCE		DETECTOR		ANGLE
			TYPE	RANGE	TYPE	RANGE	
E, p	ABX	14- 24	D	14- 25	MAG-D		90

E1 virtual photon spectrum used to obtain ( $\gamma$ , p) cross sections.

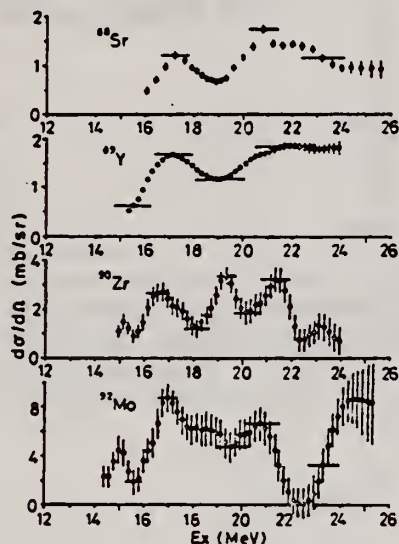


TABLE 2  
The parameters of the angular distributions determined by the least-squares fits with  
 $d\sigma/d\Omega = A[1 + B\sin^2\theta(1 - F\cos\theta)]$

	<sup>88</sup> Sr	<sup>90</sup> Zr	<sup>92</sup> Mo
$E_0$ (MeV)	21.5	22	20
$A$ (*)	1	2.04	6.67
$B$	0.59	0.69	0.057
$p$	0.59	0.47	2.3

\*) Relative value.

Fig. 3. Differential ( $\gamma$ , p) cross sections at  $\theta = 90^\circ$  analysed from (e, e'p) cross sections by the least structure method.

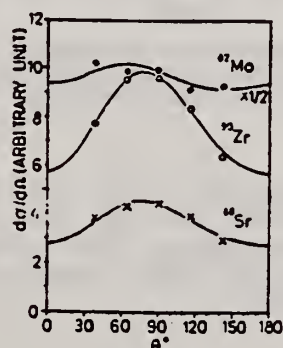


Fig. 4. Angular distributions of protons from the (e, e'p) reaction. The bombarding energies are 21.5, 22 and 20 MeV for <sup>88</sup>Sr, <sup>90</sup>Zr and <sup>92</sup>Mo respectively. The best fit curves obtained with eq. (7) are also shown.

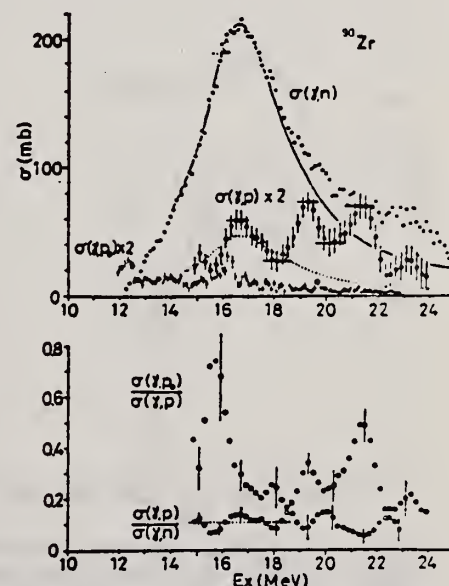


Fig. 7. The caption is the same as in fig. 5.

15

K. Shoda et al., Nucl.  
Phys. A221 (1974) 125

18

A. Lepretre et al., Nucl.  
Phys. A175 (1971) 609



REF.			R. P. Singhal, S. W. Brain, C. S. Curran, W. A. Gillespie, A. Johnston, E. W. Lees and A. G. Slight J. Phys. (London) <u>G1</u> , 588 (1975)			ELEM. SYM.	A	Z
						Zr	90	40
METHOD						REF. NO.		
						75 si 11		egf
REACTION	RESULT	EXCITATION ENERGY	SOURCE		DETECTOR		ANGLE	
			TYPE	RANGE	TYPE	RANGE		
E,E/	FMF	2- 6	D	53-112	MAG-D		DST	

13 STATES, 2.18-5.3

Figures 6, 7, and 8 also give form factors for other levels.

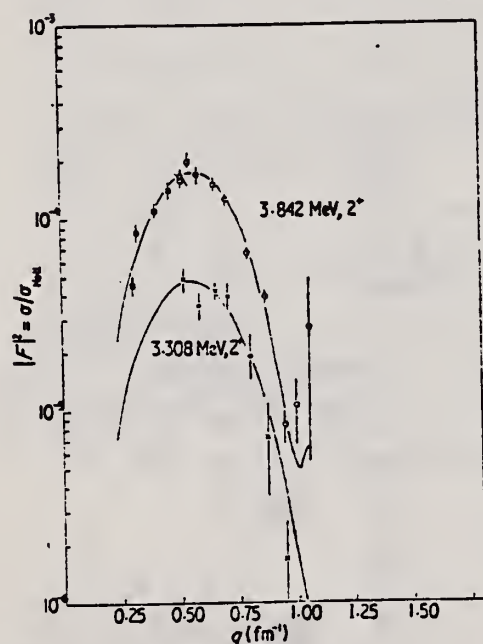


Figure 4. Inelastic form factors for the 3.842 MeV, 2<sup>+</sup> (□ and ○) and for the 3.308 MeV, 2<sup>+</sup> (×) levels. The data points □ are those of Bellicard *et al* (1970). The solid lines are the best fits to these levels with the model independent measurements of Metzger (1974) used as constraints (see text).

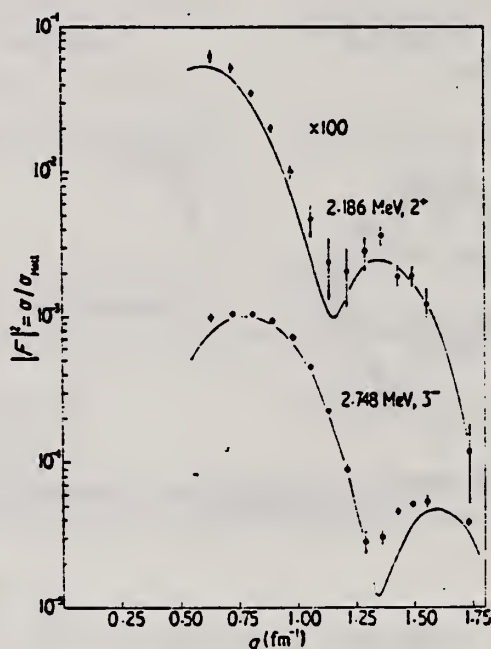


Figure 3. A comparison of the high momentum transfer data of Phan-Xuan-Ho *et al* (1973) with the extrapolation of the fits obtained in the present experiment to 209 MeV. The parameters of the fit are presented in table 3.

Bellicard *et al.*, Nucl. Phys. A143, 213 (1970).  
Metzger, Phys. Rev. C9, 1525 (1974).  
Phan-Xuan-Ho *et al.*, Nucl. Phys. A210, 189 (1973).  
Singhal *et al.*, Nucl. Phys. A218, 189 (1974).

(over)



Table 3. Results for the analysis of the present data using the Tassie model.

Excitation energy (MeV)	$J^\pi$	$\chi^2/D$	$c_{tr}$ (fm)	$t_{tr}$ (fm)	$R_{tr}$ (fm)	$B(EL \uparrow)$ ( $e^2 \text{fm}^{2L}$ )	$B(EL \uparrow)/B(EL \uparrow)_{\text{exp}}$
2.186 <sup>a</sup>	2 <sup>+</sup>	1.16	4.32	2.76	5.82 ± 0.11	673 ± 59	5.50 ± 0.48
2.319	5 <sup>-</sup>	0.79	3.19	2.31	6.75 ± 0.08	(2.12 ± 0.12) × 10 <sup>7b</sup>	8.37 ± 0.47
2.748	3 <sup>-</sup>	2.10 <sup>a</sup>	4.34	2.54	6.18 ± 0.28	8.74 ± 1.00 × 10 <sup>4</sup>	25.2 ± 2.9
3.077	4 <sup>+</sup>	1.03	4.33	2.15	6.15 ± 0.27	2.95 ± 0.80 × 10 <sup>5</sup>	3.32 ± 0.90
3.308	2 <sup>+</sup>	1.30	4.52	2.76 <sup>d</sup>	5.96	64	0.53
		0.94	4.06	3.22	6.13 ± 0.52	69 ± 18 <sup>a</sup>	0.56 ± 0.15
3.842	2 <sup>+</sup>	1.42	4.45	2.76	5.91	230	1.88
		1.18	4.75	2.15	5.58 ± 0.30	206 ± 36 <sup>a</sup>	1.68 ± 0.29
3.97	5 <sup>-</sup>	0.40	4.14	2.31 <sup>d</sup>	7.02 ± 0.60	2.62 ± 1.00 × 10 <sup>7</sup>	10.4 ± 4.0
4.07	4 <sup>+</sup> ?	0.40	3.15	2.15 <sup>d</sup>	5.56 ± 0.34	(4.0 ± 2.4) × 10 <sup>6</sup>	0.45 ± 0.27
	5 <sup>-</sup> ?	0.30	4.50	2.31 <sup>d</sup>	7.16 ± 0.30	(1.6 ± 0.9) × 10 <sup>7</sup>	6.4 ± 3.6
4.34	4 <sup>+</sup>	0.48	3.98	2.15 <sup>d</sup>	5.95 ± 0.16	1.50 ± 0.40 × 10 <sup>5</sup>	1.69 ± 0.45
4.47	4 <sup>+</sup>	0.98	4.93	2.15 <sup>d</sup>	6.53 ± 0.12	3.45 ± 0.65 × 10 <sup>5</sup>	3.87 ± 0.73
5.64	3 <sup>-</sup>	1.61	4.31	2.54 <sup>d</sup>	6.16 ± 0.09	6760 ± 950	1.95 ± 0.27
5.78	3 <sup>-</sup>	0.83	4.13	2.54 <sup>d</sup>	6.05 ± 0.13	1450 ± 220	0.42 ± 0.06
5.30 to 5.50 region	4 <sup>+</sup> ?	1.13	4.45	2.15 <sup>d</sup>	6.22 ± 0.35	3.1 ± 0.7 × 10 <sup>5</sup>	3.5 ± 0.8

<sup>a</sup> This is a re-analysis of the level and the numbers are very slightly different from those in Singhal *et al* (1974).

<sup>b</sup> The (n, n') point was treated as a datum point for the fit. See text.

<sup>c</sup> One datum point (Bellicard *et al* 1970) is contributing 15.2 to the  $\chi^2$  function.

<sup>d</sup>  $t_{tr}$  was fixed (see text).

<sup>e</sup> The ( $\gamma, \gamma'$ ) point was treated as a datum point for the fit. See text.

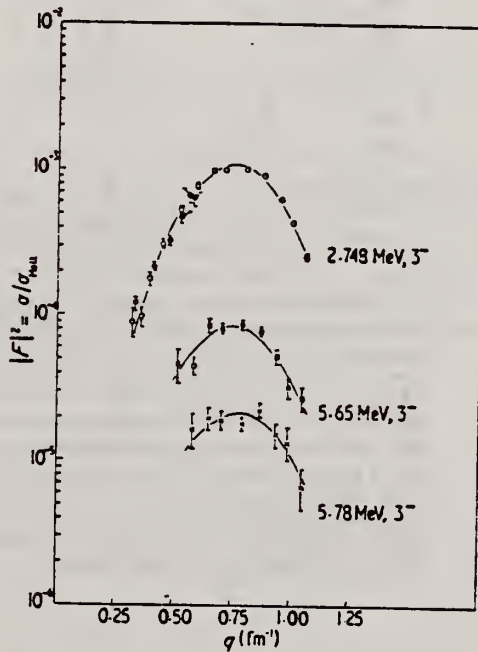


Figure 5. Inelastic form factors for the octupole transitions studied. The transitions shown are to the 2.748 MeV (● and ○), the 5.64 MeV (×) and to the 5.78 MeV (×) levels respectively. The solid circles for the 2.748 MeV level are data points taken from Bellicard *et al* (1970). Solid lines are the fits obtained by using the Tassie model.

REACTION	RESULT	EXCITATION ENERGY	SOURCE		DETECTOR		ANGLE
			TYPE	RANGE	TYPE	RANGE	
G,N	ABX	13- 30	C	13- 32	ACT-I		4PI <sup>1</sup>
G,2N	ABX	20- 31	C	13- 32	ACT-I		4PI
G,np	ABX	20- 31	C	13- 32	ACT-I		4PI

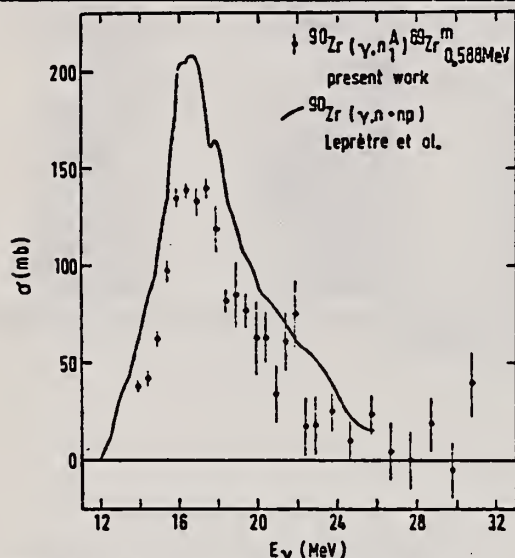


FIG. 12. The  $(\gamma, n_{1/2}^+)$  cross section represented by data points contains, in addition to the  $^{90}\text{Zr}(\gamma, n_{1/2}^+)^{89}\text{Zr}_{0.588}$  contribution, also contributions of all photoneutron cross sections involving those residual  $^{89}\text{Zr}$  states which subsequently decay to the first-excited state. For comparison the  $(\gamma, n + np)$  data of Leprêtre *et al.* (Ref. 6) (continuous curve) are also shown.

TABLE I. Integrated cross sections for various photonuclear reaction channels.

Reactions	Energy region of integration (MeV)	Integrated cross section (MeVmb)
$(\gamma, p_0)$	13-23.5	$79 \pm 7$
$(\gamma, p)_{0-3 \text{ MeV}}$	15-18	$35 \pm 4$
	15-23.5	$88 \pm 9$
$(\gamma, p)_{3-5 \text{ MeV}}$	17-23.5	$10 \pm 5$
$(\gamma, p)_{5-7 \text{ MeV}}$	18.5-23.5	$29 \pm 8$
$(\gamma, p_{\text{tot}})$	13-23.5	$206 \pm 19$
	13-18	$101 \pm 10$
$(\gamma, p_{1/2}^+)$	14-31.5	$35 \pm 5$
	14-23.5	$20 \pm 3$
	14-18	$5 \pm 1$
$(\gamma, n_{1/2}^+)$	14-31.5	$850 \pm 70$
$(\gamma, n)$	14-31.5	$1300 \pm 100$
$(\gamma, np)$	20-31	$14 \pm 6$
$(\gamma, 2n)$	21-31	$141 \pm 15$

# 1 ISOMER YIELD

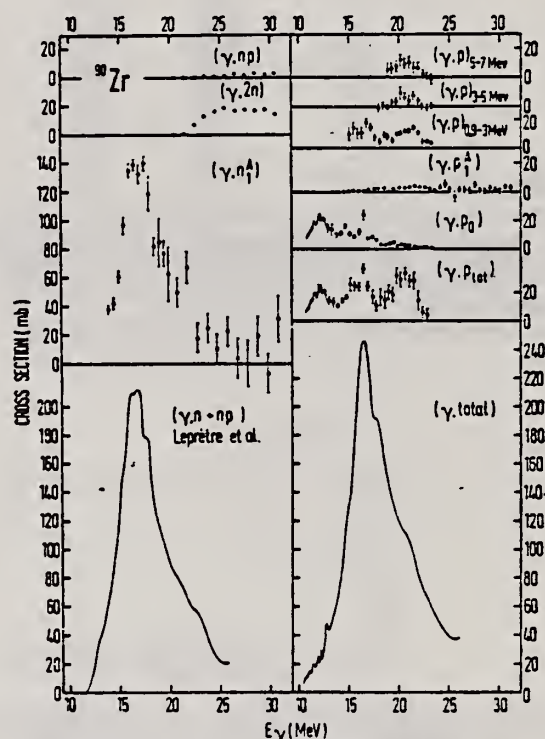


FIG. 14. Cross sections integrated over angles for processes studied in the present work (data points) are displayed with the exception of the total photoneutron cross section (solid curve in the bottom left corner of the diagram) for which the results of Leprêtre *et al.* (Ref. 6) are shown. The low-energy parts of the ground state and total photoproton cross sections are taken from Ref. 3 (solid curves). In the bottom right corner the sum of the total photoproton, the  $(\gamma, 2n)$  cross sections from the present experiment and  $(\gamma, n + np)$  cross section of Ref. 6, is displayed. It represents to a good accuracy the total photoabsorption cross section.

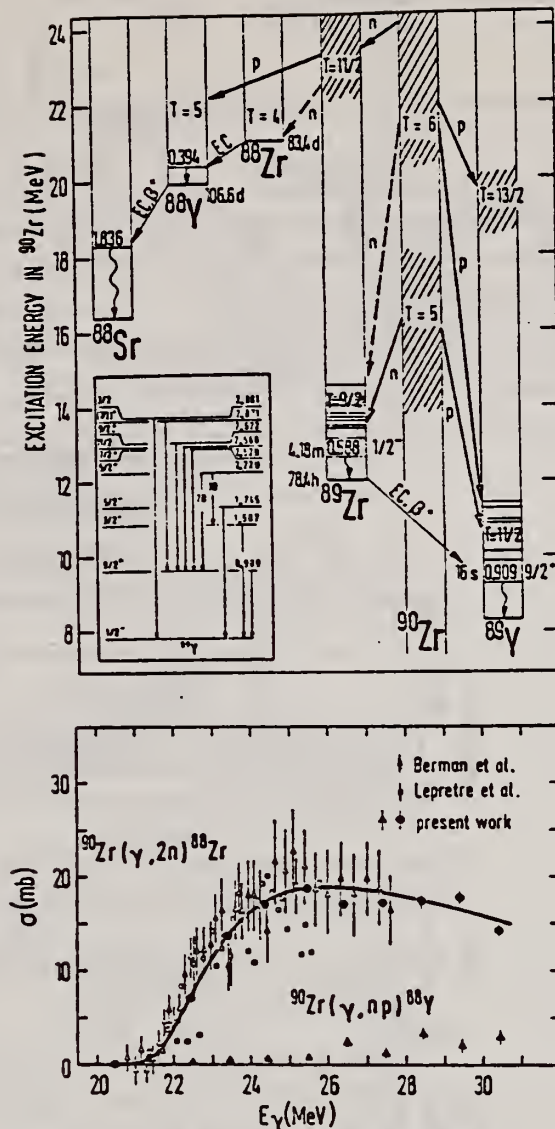


FIG. 13. Cross sections for the reactions  $^{90}\text{Zr}(\gamma, np)^{89}\text{Y}$  and  $^{90}\text{Zr}(\gamma, 2n)^{88}\text{Zr}$ . A comparison of present results for the cross section of the reaction  $^{90}\text{Zr}(\gamma, 2n)^{88}\text{Zr}$  with the data of Lepretre *et al.* (Ref. 6) and Berman *et al.* (Ref. 1) is given in the lower diagram. The solid line is drawn arbitrarily through data points of the present results. The decay scheme shows the decay modes used for the determination of the cross sections (upper diagram).

- <sup>1</sup>B. L. Berman, J. T. Caldwell, R. R. Harvey, M. A. Kelly, R. L. Bramblett, and S. C. Fultz, *Phys. Rev.* **162**, 1098 (1967).  
<sup>2</sup>P. Axel, D. M. Drake, S. Wheatstone, and S. S. Hanna, *Phys. Rev. Lett.* **19**, 1343 (1967).  
<sup>3</sup>W. M. Mason, G. Kernel, J. L. Black, and N. W. Tanner, *Nucl. Phys.* **A135**, 193 (1969).  
<sup>4</sup>K. Shoda, M. Sugawara, T. Saito, and H. Miyase, *Phys. Rev. Lett.* **23**, 800 (1969).  
<sup>5</sup>M. Hasinoff, G. A. Fisher, H. M. Kuan, and S. S. Hanna, *Phys. Lett.* **30B**, 337 (1969).  
<sup>6</sup>A. Lepretre, H. Beil, R. Bergère, P. Carlos, and A. Veyssiére, *Nucl. Phys.* **A175**, 609 (1971).  
<sup>7</sup>H. J. Askin, R. S. Hicks, K. J. F. Allen, R. J. Petty, and M. N. Thompson, *Nucl. Phys.* **A204**, 209 (1973).  
<sup>8</sup>M. Hasinoff, G. A. Fisher, and S. S. Hanna, *Nucl. Phys.* **A216**, 221 (1973).  
<sup>9</sup>K. Shoda, H. Miyase, M. Sugawara, T. Saito, S. Oikawa, A. Suzuki, and J. Uegaki, *Nucl. Phys.* **A239**, 397 (1975).  
<sup>10</sup>S. Fallieros, B. Goulard, and R. H. Venter, *Phys. Lett.* **19**, 398 (1965).  
<sup>11</sup>K. Shoda, M. Sugawara, T. Saito, and H. Miyase, *Nucl. Phys.* **A221**, 125 (1974).  
<sup>12</sup>S. S. Hanna, in *Nuclear Structure Studies Using Electron Scattering and Photoreactions*, Sendai, Japan, 1972, edited by K. Shoda and H. Ui (Tohoku University, Sendai, Japan, 1972), p. 453.  
<sup>13</sup>D. Brajnik, D. Jannik, G. Kernel, U. Miklavžic, and J. Snajder, *Nucl. Instrum.* **103**, 189 (1972).  
<sup>14</sup>J. Böhm, U. Miklavžic, B. Pucelj, J. Snajder, and M. Tiringier, *Nucl. Instrum.* (to be published).  
<sup>15</sup>D. Brajnik, D. Jannik, G. Kernel, U. Miklavžic, and A. Stanovnik, *Phys. Rev. C* **9**, 1901 (1974).  
<sup>16</sup>J. L. Black and N. W. Tanner, *Phys. Lett.* **11**, 135 (1964).



REACTION	RESULT	EXCITATION ENERGY	SOURCE		DETECTOR		ANGLE
			TYPE	RANGE	TYPE	RANGE	
G,P	ABX	8- 23	C	14- 24	SCD-D		DST <sup>1</sup>
G,P	ABX	13- 23	C	14- 24	SCD-D		DST <sup>2</sup>
G,P	ABX	14- 31	C	14- 32	ACT-I		4PI <sup>3</sup>

<sup>1</sup> TOT AND EXCIT STATE  
<sup>2</sup> GROUND STATE  
<sup>3</sup> ISOMER YIELD

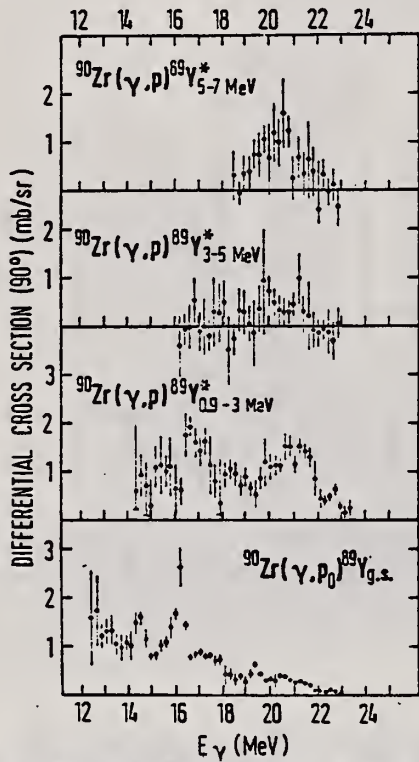


FIG. 3. Differential 90° cross section for the (γ,p<sub>0</sub>) reaction and differential summed cross sections for reactions involving various regions of excitations in the residual nucleus <sup>89</sup>Y.

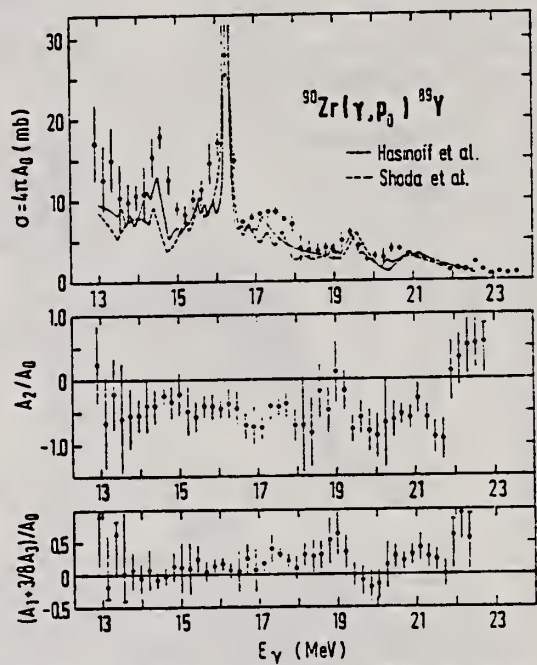


FIG. 4. Legendre polynomial coefficients for the angular distributions of protons in the reaction <sup>90</sup>Zr(γ,p<sub>0</sub>)<sup>89</sup>Y obtained from differential cross sections for the angles 30°, 90°, and 150° assuming an angular dependence of the form  $W(\theta) = \sum_{l=0}^3 A_l P_l(\cos\theta)$ . Cross sections for particular angles were determined from measured spectra by means of a least-squares-fit analysis (Ref. 13). On the top diagram present results for  $\sigma = 4\pi A_0$  (data points) are compared to the data of Refs. 11 and 8.

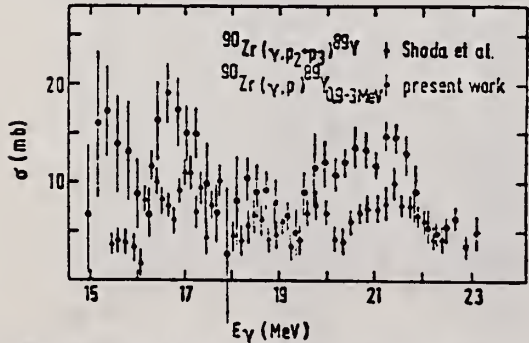


FIG. 8. A comparison of present results for the <sup>90</sup>Zr(γ,p)<sup>89</sup>Y<sub>0.3-3</sub> cross section with the data of Shoda et al. (Ref. 4).

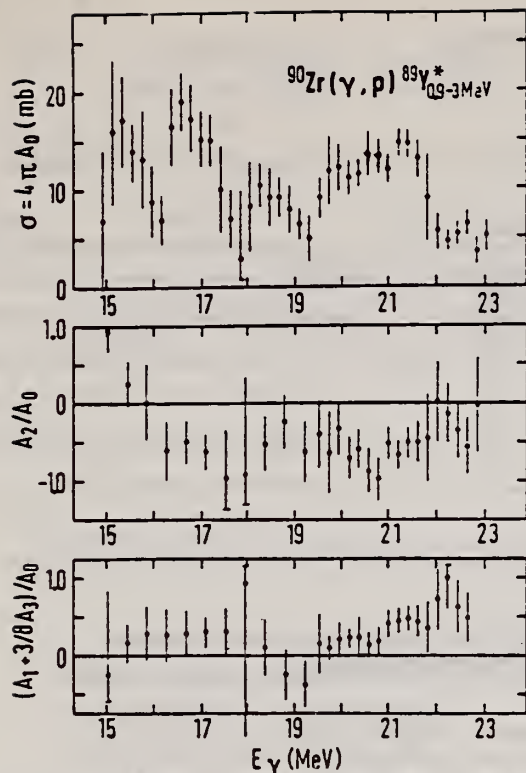


FIG. 6. Legendre polynomial coefficients for the angular distribution of protons in the reaction  $^{90}\text{Zr}(\gamma, p)^{89}\text{Y}^*$  involving excited states of  $^{89}\text{Y}$  with energies up to 3 MeV. See Fig. 4 for other details.

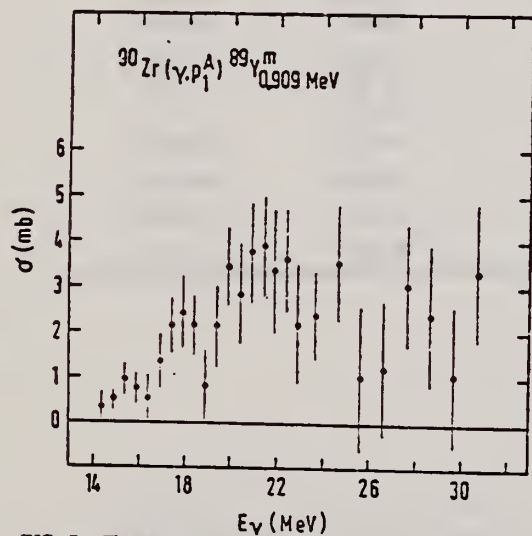


FIG. 7. The summed cross section  $(\gamma, p_1^i)$  for the  $^{90}\text{Zr}(\gamma, p)$  reactions leading to the 0.909 MeV first-excited isomeric state of  $^{89}\text{Y}$ . The cross section is obtained from a Penfold-Leiss analysis of the 0.909 MeV  $\gamma$ -ray activation yield. Here, besides the direct  $(\gamma, p_1)$  cross section, also contributions from states decaying to the 0.909 MeV state are contained. In particular,  $\sigma(\gamma, p_1^i)$  incorporates  $\sigma(\gamma, p_{5/2+7/2})$  and 70% of  $\sigma(\gamma, p_1)$ , involving  $^{89}\text{Y}$  states at 2.529, 2.568, 2.622, 2.871, and 2.220 MeV, respectively.

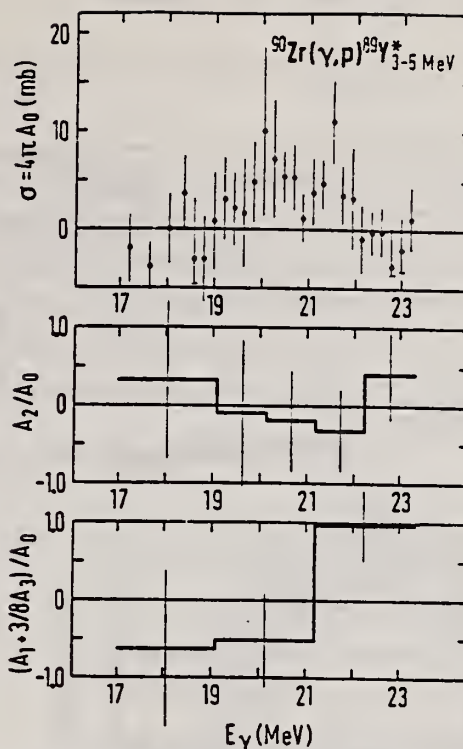


FIG. 9. Integrated cross section over angles and other Legendre polynomial coefficients for the photo-proton reaction channels leading to excited states in  $^{89}\text{Y}$  of energies 3-5 MeV (see Fig. 4 for other details).

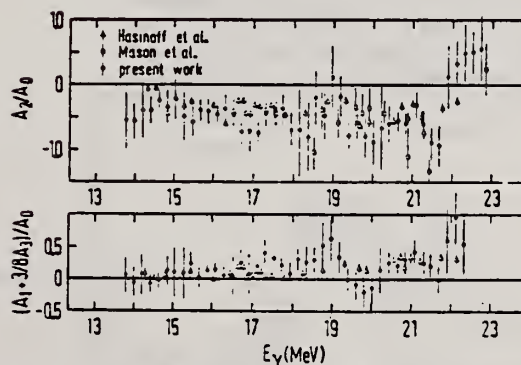


FIG. 5. A comparison of present results for the Legendre polynomial coefficients of the reaction  $^{90}\text{Zr}(\gamma, p)^{89}\text{Y}^*$  with the data of Refs. 3 and 8.



METHOD

REF. NO.

Page 5 of 5.

76 Br 5

hmg

REACTION	RESULT	EXCITATION ENERGY	SOURCE		DETECTOR		ANGLE
			TYPE	RANGE	TYPE	RANGE	

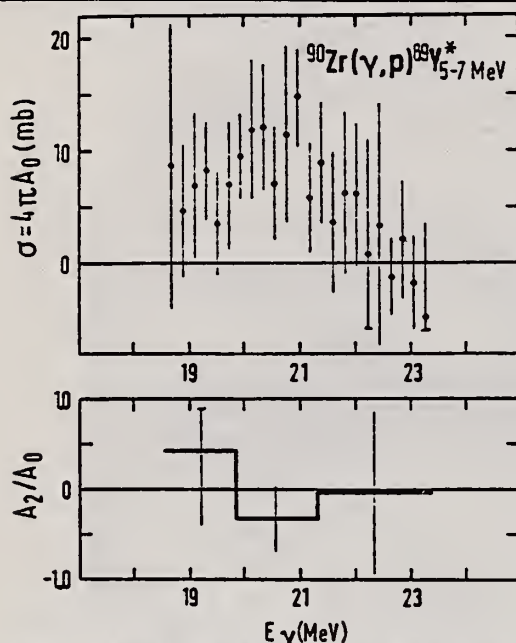


FIG. 10. Same as Fig. 9 for excitations of 5-7 MeV. Odd Legendre polynomial coefficients are not shown due to large errors.

TABLE I. Integrated cross sections for various photonuclear reaction channels.

Reactions	Energy region of integration (MeV)	Integrated cross section (MeV mb)
$(\gamma, p_0)$	13-23.5	$79 \pm 7$
$(\gamma, p)_{0.5-3 \text{ MeV}}$	15-18	$35 \pm 4$
	15-23.5	$88 \pm 9$
$(\gamma, p)_{3-5 \text{ MeV}}$	17-23.5	$10 \pm 5$
$(\gamma, p)_{5-7 \text{ MeV}}$	18.5-23.5	$29 \pm 8$
$(\gamma, p_{tot})$	13-23.5	$206 \pm 19$
	13-18	$101 \pm 10$
$(\gamma, p_1^{\frac{1}{2}})$	14-31.5	$35 \pm 5$
	14-23.5	$20 \pm 3$
	14-18	$5 \pm 1$
$(\gamma, n_1^{\frac{1}{2}})$	14-31.5	$850 \pm 70$
$(\gamma, n)$	14-31.5	$1300 \pm 100$
$(\gamma, n p)$	20-31	$14 \pm 6$
$(\gamma, 2n)$	21-31	$141 \pm 15$

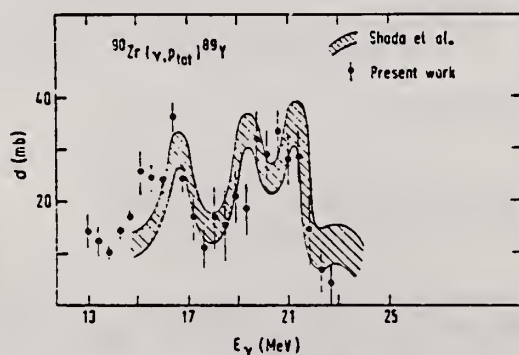


FIG. 11. Total photoproton cross section obtained by summing the contributions shown in Figs. 4, 6, 9, and 10 (data points) is compared to the corresponding data of Shoda *et al.* (Ref. 9). The shaded area represents experimental errors quoted in Ref. 9.

REF.

S. Fukuda and Y. Torizuka  
Phys. Lett. 62B, 146 (1976)

ELEM. SYM.	A	Z
Zr	90	40
REF. NO.		
76 Fu 1		egf

METHOD

REACTION	RESULT	EXCITATION ENERGY	SOURCE		DETECTOR		ANGLE
			TYPE	RANGE	TYPE	RANGE	
E, E/	FMF	6- 30	D	150-250	MAG-D		DST

## ANALYSIS FOR EO

The multipole expansion of the inelastic electron scattering continuum in  $^{90}\text{Zr}$  yields an E2-like structure which involves a giant monopole resonance at 17 MeV with a width of 4 MeV.

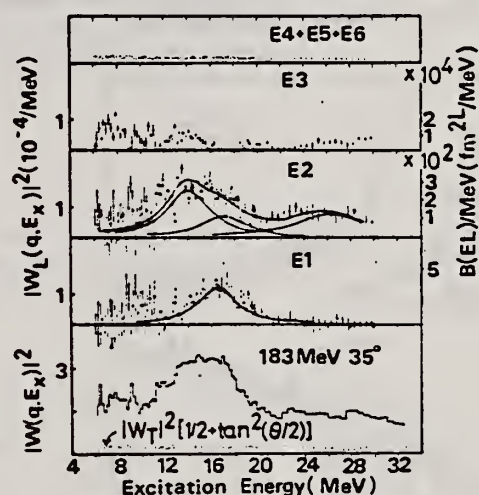


Fig. 1. Differential total form factor  $|W(q, E_X)|^2$  at 183 MeV  $35^\circ$ , transverse part  $|W_T|^2(1/2 + \tan^2\theta/2)$ , and  $|W_L(q, E_X)|^2$  corresponding to E1, E2, E3 and E4 + E5 + E6 are shown, where  $|W|^2$ ,  $|W_L|^2$ , and  $|W_T|^2$  are defined in ref. [16]. The scale at the right-hand side indicates  $B(EL)$  values in units of  $\text{fm}^2L/\text{MeV}$  and at the left-hand side form factors in units of  $10^{-4}/\text{MeV}$ .

Table 1  
 $B(EL)$  values in  $\text{fm}^2L$  and the percentages of the corresponding EWSR in  $^{90}\text{Zr}$ .

$E_X(\text{MeV})$	E1	E2	E3
6-10	$2.8 \pm 1.8$ (18 $\pm$ 12)% ( $T=1$ )	$(3.7 \pm 0.9) \times 10^3$ (11 $\pm$ 3)% ( $T=0$ )	$(4.2 \pm 0.4) \times 10^4$ (16 $\pm$ 1)% ( $T=0$ )
10-15	$7.3 \pm 1.1$ (28 $\pm$ 4)% ( $T=1$ )	$(10.9 \pm 0.6) \times 10^3$ (49 $\pm$ 3)% ( $T=0$ )	$(3.9 \pm 0.3) \times 10^4$ (24 $\pm$ 2)% ( $T=0$ )
15-20	$11.8 \pm 1.0$ (61 $\pm$ 5)% ( $T=1$ )	$(10.2 \pm 0.5) \times 10^3$ (64 $\pm$ 3)% ( $T=0$ )	$(0.9 \pm 0.2) \times 10^4$ (14 $\pm$ 4)% ( $T=0$ )
20-30	$2.7 \pm 1.4$ (17 $\pm$ 9)% ( $T=1$ )	$(12.5 \pm 0.7) \times 10^3$ (89 $\pm$ 5)% ( $T=1$ )	$(4.4 \pm 0.4) \times 10^4$ (34 $\pm$ 3)% ( $T=1$ )

ELEM. SYM.	A	Z
Zr	90	40

METHOD	REF. NO.	
	77 Di 2	hmg

REACTION	RESULT	EXCITATION ENERGY	SOURCE		DETECTOR		ANGLE
			TYPE	RANGE	TYPE	RANGE	
P,G	ABX	22- 35	C	14- 27	NAI-D		4PI

New detailed angular distribution measurements are presented for  $^{89}\text{Y}(p,\gamma_0)^{90}\text{Zr}$  above the giant dipole resonance ( $14\text{ MeV} \leq E_p \leq 27\text{ MeV}$ ), which show pronounced effects of higher multipoles. Direct-semidirect calculations provide a good description of the data by including E2 and E3 as well as E1 radiation. The sensitivity of the reaction to a  $T=1$  giant quadrupole resonance is demonstrated.

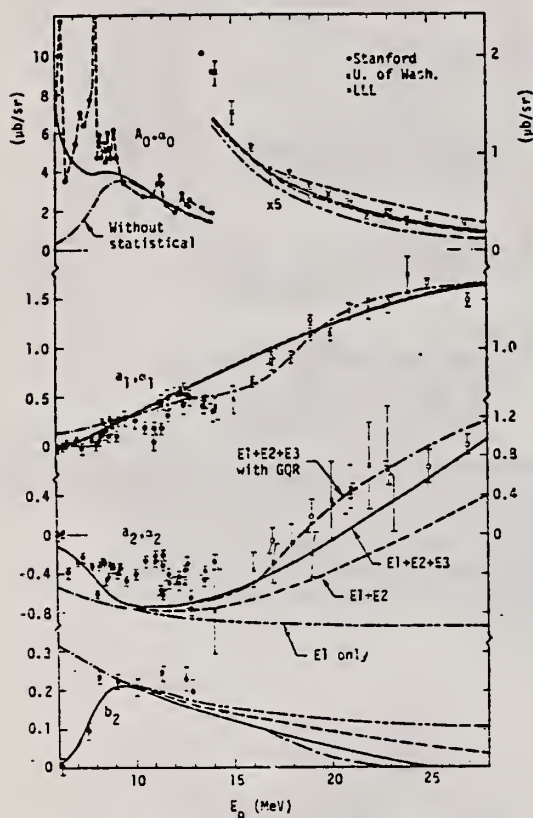


FIG. 1. Angular distribution coefficients for  $^{89}\text{Y}(p,\gamma_0)^{90}\text{Zr}$ . Crosses and open circles, present measurements of  $\alpha_i$  (see text); solid dots, previous measurements of  $A_0$ ,  $a_1$ , and  $b_2$  (Refs. 14 and 15) ( $A_0 \approx a_0$  and  $a_i \approx \alpha_i$  for  $E_p \leq 14\text{ MeV}$ ). The curves represent calculated  $\alpha_i$ ; the E1 curve includes both direct and semidirect (GDR); E2 and E3 are direct only, except where semidirect E2 (GQR) is indicated.

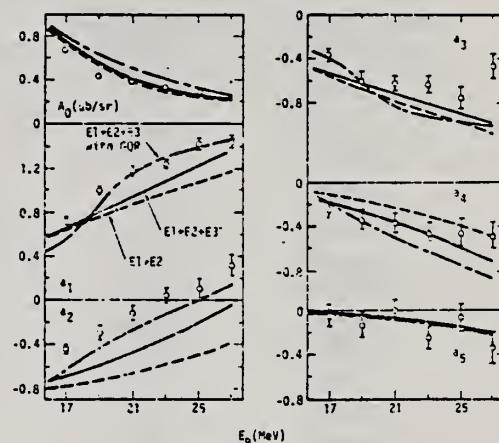


FIG. 2. Angular distribution coefficients extracted from LLL data. See text and Fig. 1 caption for significance of curves.

- 14 B. L. Berman et al., Phys. Rev. 162, 1098 (1967).
- 15 M. Hasinoff et al., Nucl. Phys. A216, 221 (1973).

METHOD

REF. NO.

78 Kn 7

rs

REACTION	RESULT	EXCITATION ENERGY	SOURCE		DETECTOR		ANGLE
			TYPE	RANGE	TYPE	RANGE	
E, E/	RLY	8-10	D	UKN	MAG-D		DST

M2 LEVELS

The location of the M2 giant resonance in  $^{28}\text{Si}$ ,  $^{90}\text{Zr}$  and  $^{208}\text{Pb}$ , predicted within the framework of the MSI-RPA particle-hole model, has been confirmed by high-resolution inelastic electron scattering ( $E_N \approx 44 A^{-1/3}$  MeV). The fragmented M2 strength distribution can only be described assuming a mass-dependent quenching of the intrinsic  $g_s$  factor. This has the consequence that the long sought M1 strength is much reduced in heavy nuclei, an effect which is supported experimentally.

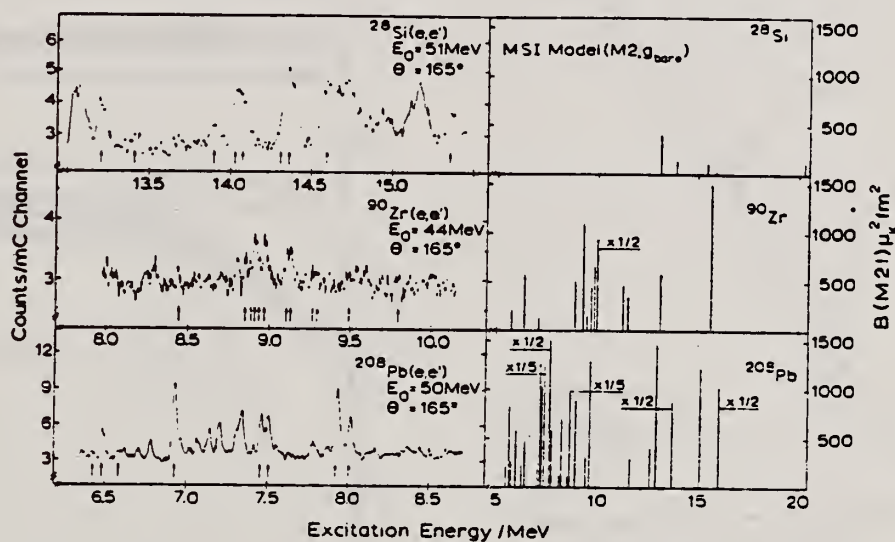


Fig. 1. The left part shows selected (e, e') spectra on  $^{28}\text{Si}$ ,  $^{90}\text{Zr}$  and  $^{208}\text{Pb}$  at various energies but all at  $\theta = 165^\circ$ . The  $2^-$  states are marked by arrows. The right part displays the model prediction for the M2 strength.



METHOD

REF. NO.

78 Ma 10

hg

REACTION	RESULT	EXCITATION ENERGY	SOURCE		DETECTOR		ANGLE
			TYPE	RANGE	TYPE	RANGE	
G,N	ABY	12-68	C	30-68	ACT		4PI
G,PN	ABY	20-68	C	30-68	ACT		4PI

Analysis is made of reactions interfering with photon activation analysis procedures.

The activation yield curves have been presented for a number of photonuclear reactions in the energy range from 30 to 68 MeV, in order to evaluate quantitatively the interferences due to competing reactions in multielement photon activation analysis. The general features of the yields as functions of both target mass number and excitation energy were elucidated from the data obtained, discussion being given on the results in terms of the reaction mechanism.

Simultaneous neutron activation due to appreciable neutron production from the converter and surrounding materials has also been studied, and, finally, the magnitudes of interferences in real multielement analysis were given in the form of their energy dependences.

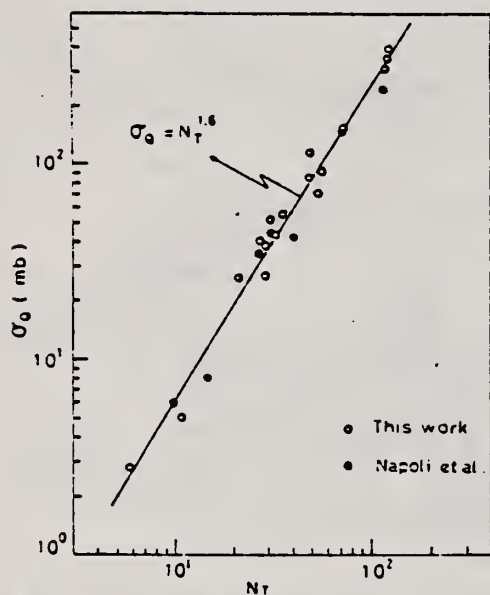


Fig. 2. Yield per equivalent quanta versus target neutron number.

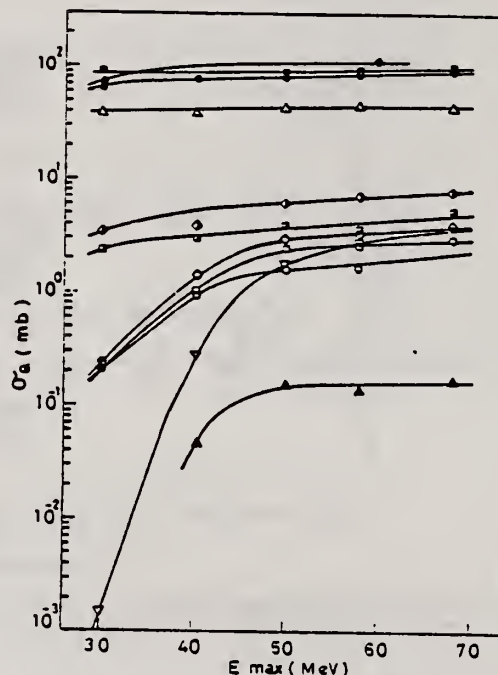


Fig. 7. Activation yield curves for the reactions on Y, Zr, Nb and Mo.  
 ◆  $^{89}\text{Y}(\gamma, n)^{88}\text{Y}$ , ●  $^{90}\text{Zr}(\gamma, n)^{89}\text{Zr}$ , ○  $^{90}\text{Zr}(\gamma, pn)^{88}\text{Y}$ ,  
 △  $^{93}\text{Nb}(\gamma, n)^{92m}\text{Nb}$ , ▲  $^{93}\text{Nb}(\gamma, xn)^{88}\text{Y}$ , ■  $^{100}\text{Mo}(\gamma, n)^{99}\text{Mo}$ ,  
 ◇  $^{97}\text{Mo}(\gamma, p)^{96}\text{Nb}$ , ▤  $^{96}\text{Mo}(\gamma, p)^{95m}\text{Nb}$ , ◊  $^{94}\text{Mo}(\gamma, pn)^{92m}\text{Nb}$ ,  
 □  $^{92}\text{Mo}(\gamma, 2n)^{90}\text{Mo}$ , ▽  $^{94}\text{Mo}(\gamma, xn)^{89}\text{Zr}$ .

(over)



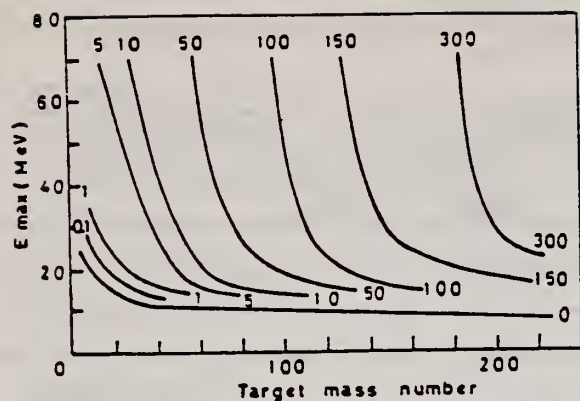


Fig. 9. Yields of the  $(\gamma, n)$  reactions as a function of bremsstrahlung maximum energy and target mass number. The numerical values in the figure are yields per equivalent quanta in mb.

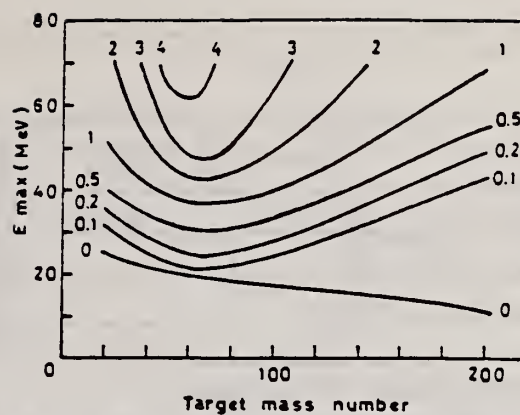


Fig. 11. Yields of the  $(\gamma, pn)$  reactions as a function of bremsstrahlung maximum energy and target mass number. The numerical values in the figure are yields per equivalent quanta in mb.

REF. D. Meuer, R. Frey, D.H.H. Hoffmann, A. Richter, E. Spamer, O. Titze, W. Knüpfner  
Nuc1. Phys. A349, 309 (1980)

ELEM. SYM.	A	Z
Zr	90	40
METHOD		
REF. NO.		
80 Me		hg

REACTION	RESULT	EXCITATION ENERGY	SOURCE		DETECTOR		ANGLE
			TYPE	RANGE	TYPE	RANGE	
E, E/	FMF	8-10	D	24-66	MAG-D		DST

Spectra shown in the paper

BML, 21 LEVELS

**Abstract:** High-resolution (FWHM = 30 keV) inelastic electron scattering on  $^{90}\text{Zr}$  at low momentum transfer ( $0.20 < q < 0.62 \text{ fm}^{-1}$ ) has been used to study magnetic transitions at excitation energies  $E_x = 8\text{--}10 \text{ MeV}$ . The experimental data were analyzed in the distorted-wave Born approximation (DWBA) with wave functions calculated in the random phase approximation (RPA). Three  $J^\pi = 1^+$  states have been identified  $E_x = 8.233, 9.000$  and  $9.371 \text{ MeV}$ . There is some indication of further very fragmented dipole strength and the upper limit for the total M1 strength in the investigated energy region is  $\Sigma B(M1) \uparrow \leq 2.5 \mu_N^2$ . It is much smaller than any theoretical prediction. Furthermore, a large number of  $2^-$  states has been observed, with the center of gravity located at  $E_x \approx 9 \text{ MeV}$ . These states carry a total strength of  $\Sigma B(M2) \uparrow = 1000 \mu_N^2 \cdot \text{fm}^2$ . Their strong fragmentation is in qualitative agreement with theoretical calculations, but the deduced strength is much smaller than theoretically predicted. In addition the distributions of spacings and radiative widths of the  $2^-$  states are consistent with a Wigner and a Porter-Thomas distribution, respectively.

E NUCLEAR REACTIONS  $^{90}\text{Zr}(e, e')$ ,  $E = 24\text{--}66 \text{ MeV}$ ; measured  $\sigma(E, \theta)$ .  $^{90}\text{Zr}$  deduced levels, transition strengths. Shell-model calculations.

TABLE 2

Levels observed in the present experiment and multipole assignment due to comparison with the theoretical calculations described in the text

$E_x \text{ (MeV)}$	$J^\pi$	$E_x \text{ (MeV)}$	$J^\pi$
7.774	$(1^+, 2^-)$	8.882	$2^-$
7.806	$(2^-)$	8.911	$2^-$
7.868	$(1^+, 2^-)$	8.934	$2^-$
7.907	$((3^-))$	8.971	$2^-$
7.996	$(3^-)$	9.000	$1^+$
8.032	$2^-$	9.061	$2^-$
8.113	$1^-(2^-)$	9.101	$2^-$
8.142	$1^+(2^-)$	9.127	$2^-$
8.233	$1^+$	9.150	$1^-(2^-)$
8.291	$2^-$	9.265	$2^-$
8.316	$(2^-)$	9.294	$2^-$
8.366	$(1^+)$	9.327	$2^-$
8.400	$(2^-)$	9.371	$1^+$
8.442	$2^-$	9.439	$1^+(2^-)$
8.494	$1^-(2^-)$	9.489	$2^-$
8.542	$2^-$	9.520	$(1^+, 2^-)$
8.602	$(1^+)$	9.541	$2^-$
8.627	$2^-$	9.601	$(1^-, 2^-)$
8.701	$(2^-)$	9.694	$2^-$
8.809	$(2^-)$	9.863	$(1^-, 2^-)$
8.853	$2^-$		

The excitation energies are uncertain to 3-10 keV and the number of parentheses around  $J^\pi$  values indicate the ambiguity in the assignments.

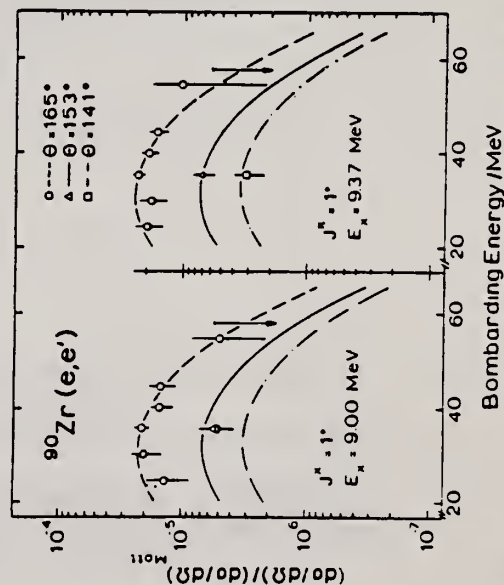


Fig. 7. Experimentally derived form factors for the two states at  $E_x = 9.000 \text{ MeV}$  and  $E_x = 9.371 \text{ MeV}$  compared to the shape of the theoretically predicted M1 form factor. This leads to a  $J^\pi = 1^+$  assignment.

(OVER)

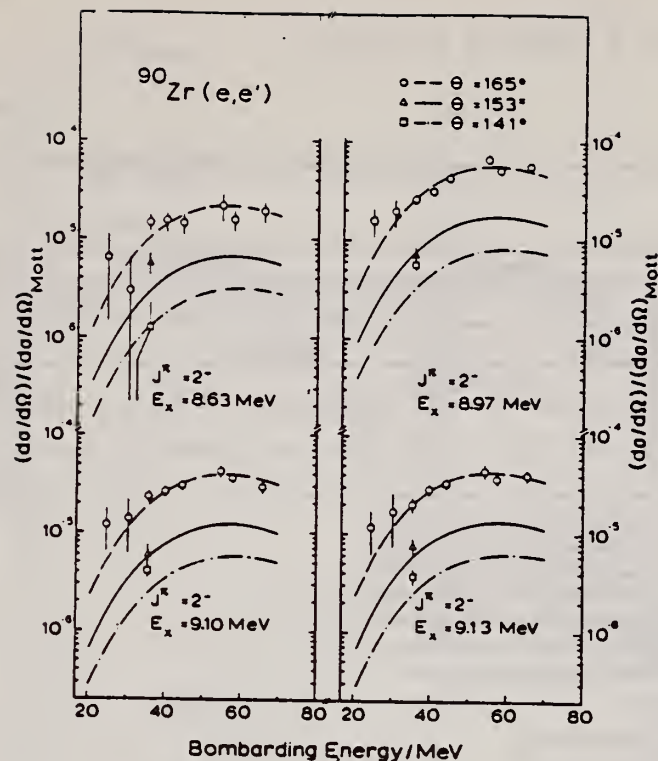


Fig. 8. Excitation function of four  $J^\pi = 2^-$  states. The experimental data are compared to MSI model calculations.

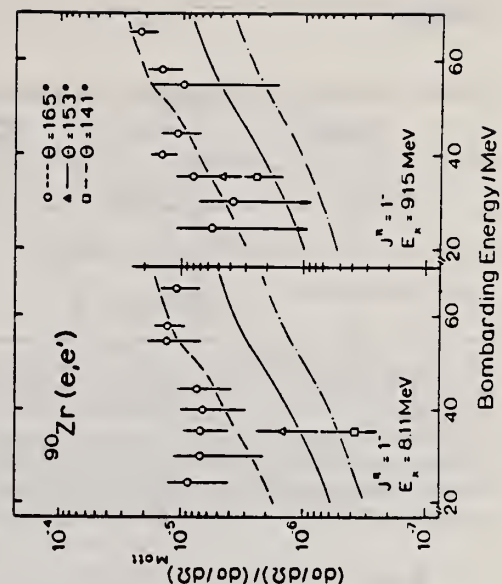


Fig. 10. Comparison between experimentally determined and calculated E1 form factors.

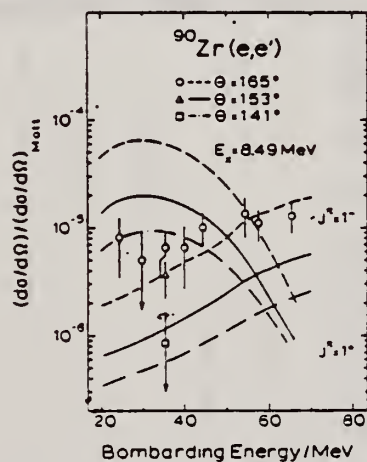


Fig. 11. Experimental form factor for the state at  $E_x = 8.494$  MeV compared to the different shapes of the theoretical form factor predictions for  $J^\pi = 1^-$  and  $J^\pi = 1^+$  states, respectively. The theoretical M1 form factor is scaled to obtain a ground-state radiative width of  $\Gamma^0_\gamma = 1.6$  eV as quoted in ref. <sup>42</sup>), obviously in disagreement with the experimental finding which is consistent with an E1 assignment to the transition.

ELEM. SYM.	A	Z
Zr	90	40
REF. NO.		.
80 Ra 3		hg

METHOD			SOURCE		DETECTOR		ANGLE
REACTION	RESULT	EXCITATION ENERGY	TYPE	RANGE	TYPE	RANGE	
A,G	ABX	15-19	D	9-13 (9.-12.5)	NAI-D		DST

The  $^{88}\text{Sr}(\alpha, \gamma_0)^{90}\text{Zr}$  reaction has been studied over the energy range  $9.0 \leq E_\alpha \leq 12.5$  MeV; there was no detectable yield below 9 MeV. Data were taken at three angles, thus making it possible to decompose the radiation into its  $E1$  and  $E2$  components. The  $E1$  yield, which is at least 85% of the total, shows a broad peak centered at an excitation energy of about 17 MeV. Utilizing Hauser-Feshbach calculations, the magnitude and shape of the  $E1$  yield is shown to be consistent with the  $E1$  capture proceeding entirely through the compound nucleus. The  $E2$  yield is small at the lower bombarding energies, but appears to be significant above about  $E(^{90}\text{Zr}^*) = 16.5$  MeV. Any observed  $E2$  cross section is shown to be much too large for the reaction to proceed mainly through the compound nucleus.

[NUCLEAR REACTIONS  $^{88}\text{Sr}(\alpha, \gamma_0)^{90}\text{Zr}$ ,  $9 \leq E_\alpha \leq 12.5$  MeV; measured  $E_\gamma$ ,  
 $d\sigma/d\Omega(\theta, E_\alpha)$ ; deduced  $\sigma_{E1}(\gamma, \alpha_0)$ ,  $\sigma_{E2}(\gamma, \alpha_0)$ .]

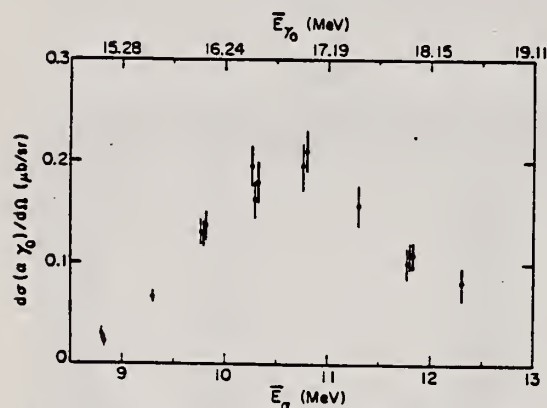


FIG. 3. Yield curve at  $90^\circ$ . The alpha energy is the mean energy in the target. Data are from different runs spread over about a year and the error bars indicate the estimated uncertainties in the absolute cross sections. The estimated errors in the relative cross sections, as far as angular distributions are concerned, are about one half of the absolute errors.

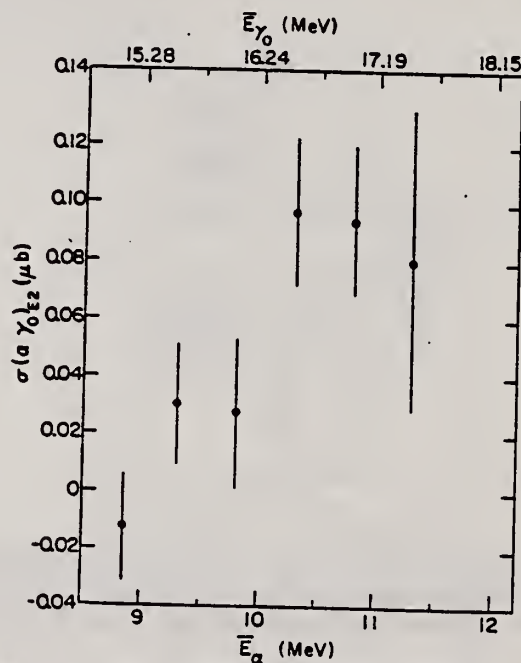


FIG. 4. Cross section for producing  $E2$  radiation.

(OVER)



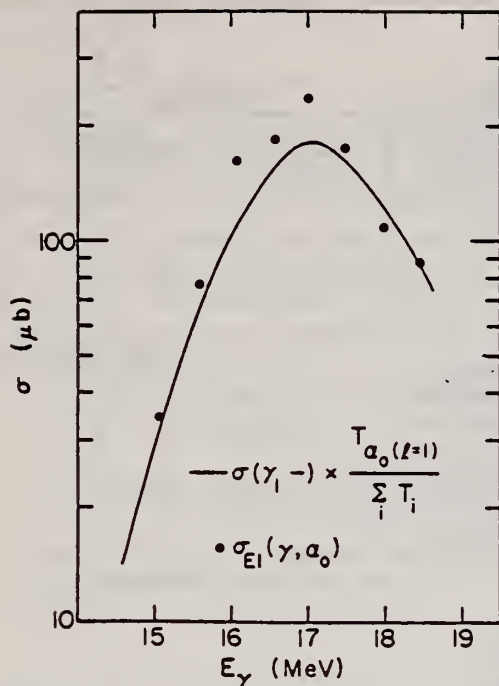


FIG. 5. Total  $E1$  absorption cross section calculated from the measured  $E1$  capture under the assumption that the entire reaction proceeds through the compound nucleus. Also shown is the measured total absorption given in Ref. 10.

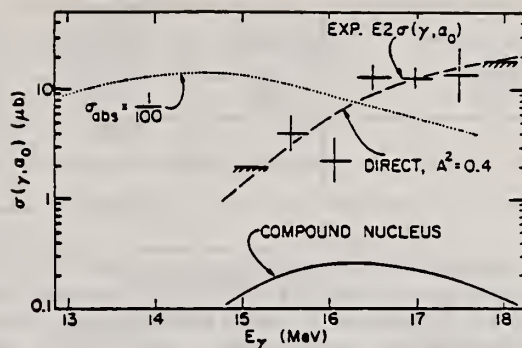


FIG. 6. Solid lines are the  $E2$   $(\gamma, \alpha_0)$  cross section, obtained from the observed  $E2$  capture by detailed balance. The cross hatching indicates an upper limit. Solid curve is the compound nucleus  $E2$   $(\gamma, \alpha_0)$  expected from a 4-MeV wide resonance centered at 14.5 MeV. The broken curve is that calculated for a direct reaction proceeding through a giant quadrupole state that has a 40%  $^{86}\text{Sr} + \alpha$  component. Dotted curve is the gamma-ray absorption cross section, divided by 100, expected for a 4-MeV wide resonance centered at 14.5 MeV.



METHOD

REACTION	RESULT	EXCITATION ENERGY	SOURCE		DETECTOR		ANGLE
			TYPE	RANGE	TYPE	RANGE	
E, $\alpha$	ABX	7-67	D	13-67	SPK-D		DST

The  $(e, \alpha)$  cross section in  $^{90}\text{Zr}$  has been measured at incident electron energies from 13.5 MeV to 66.5 MeV for  $\alpha$  particles between 6.9 and 16.8 MeV. The  $(\gamma, \alpha)$  cross section was deduced from it assuming both  $E1$  interaction and  $E2$  interaction. The angular distribution of the  $(\gamma, \alpha_0)$  cross section and an experiment using the bremsstrahlung plus electron beam make it clear that the  $E1$  interaction is dominant over all the present energy range. The  $(\gamma, \alpha)$  cross section extracted by using  $E1$  virtual photon spectra has a large bump above the excitation energy of 30 MeV in addition to a bump in the giant dipole resonance region. The  $(\gamma, \alpha_0)$  cross section also has a bump at the giant dipole resonance which exhausts most of the  $(\gamma, \alpha)$  cross section in that region. The compound nucleus model was used successfully to explain the bump at the giant dipole resonance. The cross section above 30 MeV is discussed in terms of the pre-equilibrium  $\alpha$  emission process combined with the quasi-deuteron model.

VIRT. PHOTON ANAL.

NUCLEAR REACTIONS  $^{90}\text{Zr}(e, \alpha)$ ,  $E_e = 13.5-66.5$  MeV; measured  $d\sigma(e, \alpha)/d\Omega$ , deduced  $d\sigma(\gamma, \alpha)/d\Omega$  and  $d\sigma(\gamma, \alpha_0)/d\Omega$ . Angular distributions;  $(\gamma, \alpha_0)$  at  $E_e = 17.5$  MeV and  $(e, \alpha)$  at  $E_e = 40.0$  MeV,  $\theta_\alpha = 45-135^\circ$ . Experiment using electron plus bremsstrahlung at  $E_e = 60.0$  MeV. Calculations, compound nucleus model, and pre-equilibrium exciton model combined with quasi-deuteron model.

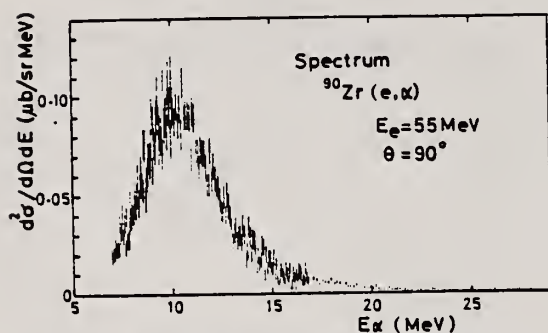


FIG. 4.  $(e, \alpha)$  energy spectrum of  $^{90}\text{Zr}$  at  $\theta = 90^\circ$ , for  $E_e = 55$  MeV. Alpha-particle energy was corrected for energy loss in half target thickness.

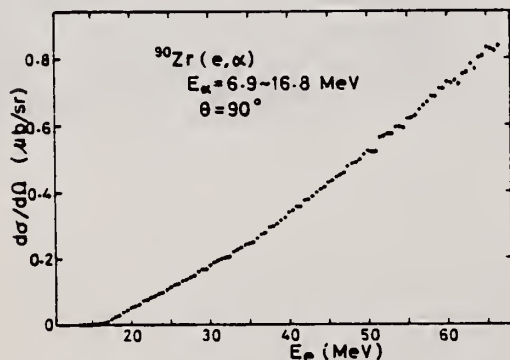


FIG. 5. Differential cross section of the  $(e, \alpha)$  reaction at  $\theta = 90^\circ$ .

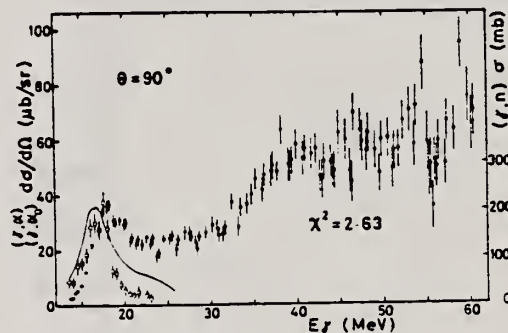


FIG. 6. Photoalpha differential cross section of  $^{90}\text{Zr}$  (closed points) analyzed from the  $(e, \alpha)$  cross section in Fig. 5 and  $^{90}\text{Zr}(\gamma, \alpha_0)$  differential cross section (open circles), at  $\theta = 90^\circ$ .  $E1$  interaction only was considered in these analyses. The value of  $\chi^2$  for the total  $(\gamma, \alpha)$  cross section was calculated for the cross section smoothed by eye. Solid line shows  $^{90}\text{Zr}(\gamma, n)$  cross section.

(OVER)

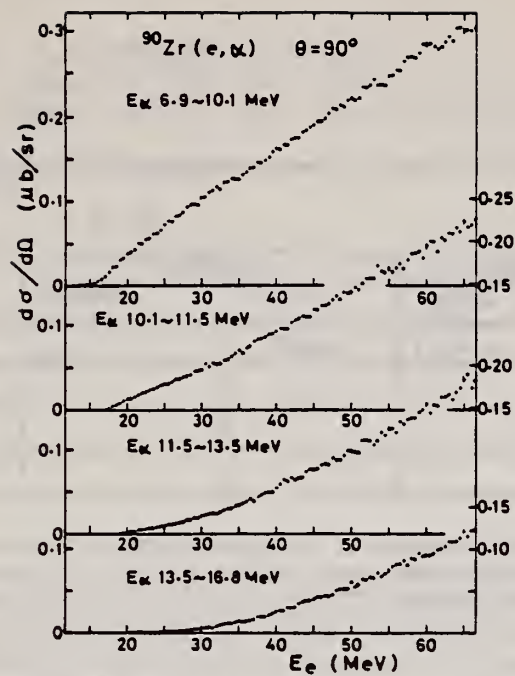


FIG. 9.  $^{90}\text{Zr}(e, \alpha)$  cross sections divided into four parts with particular  $\alpha$ -particle energies.

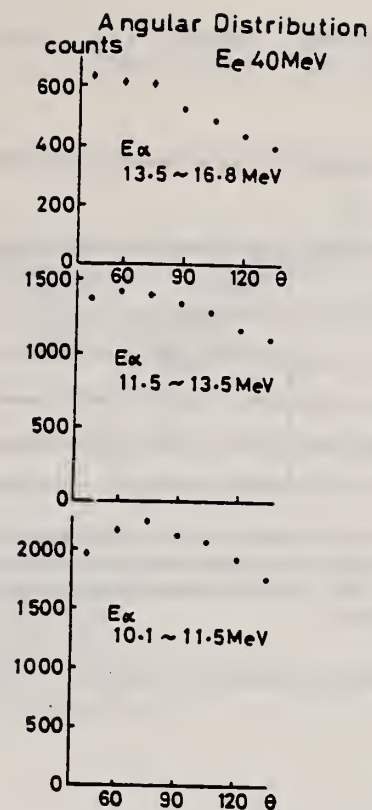


FIG. 13. Alpha-particle angular distributions at  $E_e = 40$  MeV.

REF. L.W. Fagg, W.L. Bendel, E.C. Jones, Jr.  
Phys. Rev. C26, 1304 (1982)

ELEM. SYM.	A	Z
Zr	90	40
REF. NO.		egf
82 Fa 2		

METHOD		SOURCE		DETECTOR		ANGLE
REACTION	RESULT	EXCITATION ENERGY	TYPE	RANGE	TYPE	RANGE
E, E/	ABX	0-12	D	37.61	MAG-D	
						180

Spectra of 37.2 and 60.6 MeV electrons scattered at 180° constitute evidence for very low observable *M1* transition strength and significant *M2* transition strength in the 9 MeV excitation energy region of <sup>90</sup>Zr. This is consistent with recent high resolution results of other workers at more forward angles.

NUCLEAR REACTIONS <sup>90</sup>Zr(*e, e'*), *E*<sub>0</sub> = 37.2, 60.6 MeV; measured *dσ/dΩ* at *θ* = 180°.

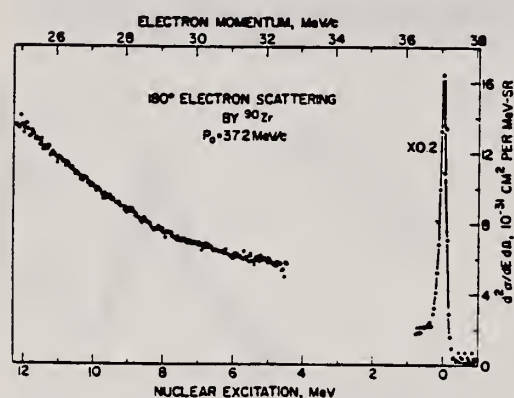


FIG. 1. Inelastic cross section spectrum of 37.2 MeV electrons scattered at 180° from <sup>90</sup>Zr.

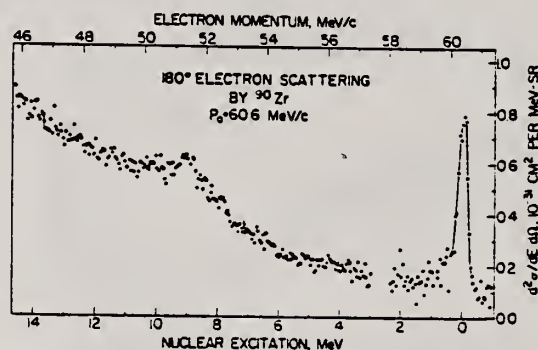


FIG. 2. Inelastic cross section spectrum of 60.6 MeV electrons scattered at 180° from <sup>90</sup>Zr.

REF. F.Z. Khien, N.K. Zui, N.T. An  
Yad. Fiz. 35, 257 (1982)  
Sov. J. Nucl. Phys. 35, 145 (1982)

ELEM. SYM.	A	Z
Zr	90	40

METHOD

REF. NO.	
82 Kh 2	egf

REACTION	RESULT	EXCITATION ENERGY	SOURCE		DETECTOR		ANGLE
			TYPE	RANGE	TYPE	RANGE	
G,N	NOX	12-14	C	14	ACT-I		4PI

# ISOMERIC RATIO

The method is developed for calculation of the isomeric ratio for the case of low excitation energy of the residual nucleus, and the isomeric ratio is measured in the  $(n, 2n)$  and  $(\gamma, n)$  reactions in the neutron-deficient nuclei  $^{110}\text{Mo}$ ,  $^{90}\text{Zr}$ ,  $^{86}\text{Sr}$ , and  $^{74}\text{Se}$ . The good agreement between the experimental and theoretical results on the  $(\gamma, n)$  reaction has confirmed the reliability of the characteristics of the residual nuclei, the transmission coefficients of the emitted neutrons, etc., used in the calculations. From study of the  $(n, 2n)$  reaction we have obtained values of the parameters of the spin dependence of the level density of the nucleus in the excitation-energy region  $\sim 14$  MeV.

PACS numbers: 25.20. + y, 25.40.Gr, 27.50. + e, 27.60. + j

TABLE III. Isomeric ratio in the  $(\gamma, n)$  reaction.

Target nucleus	$\alpha_{exp}$	$\alpha_{theor}$	Published data <sup>1)</sup>
$^{110}\text{Mo}$	$1.54 \pm 0.13$	1.36	$1.82 \pm 0.15$ (70) [9] $1.03 \pm 0.21$ (10) [10] $0.85 \pm 0.07$ (30) [15]
$^{90}\text{Zr}$	$1.52 \pm 0.04$	1.19	$0.50 \pm 0.15$ (30) [15]
$^{86}\text{Sr}$	$0.70 \pm 0.07$	0.56	$0.68 \pm 0.14$ (30) [15]
$^{74}\text{Se}$	$7.5 \pm 1.0$	$10.5^{+11}_{-8.5}$	

<sup>1)</sup>In parentheses we have given the values of the bremsstrahlung maximum energy.

<sup>2)</sup>In the calculations we used the  $^{74}\text{Se}$  level scheme of Ref. 2.

$I_p = 7/2^+$  and  $I_m = 1/2^+$ .

<sup>3)</sup>In the calculations we used the level scheme of  $^{74}\text{Se}$  in Ref. 3.

$I_p = 9/2^+$  and  $I_m = 3/2^+$ .





Zr  
A=91

Zr  
A=91

Zr  
A=91



Elem. Sym.	A	Z
Zr	91	40
Ref. No.		
55 Na 1		EGF

Method  $\text{BF}_3$  counters; 24 MeV Bremss; Betatron

Reaction	E or $\Delta E$	$E_0$	$\Gamma$	$\int \sigma dE$	$J\pi$	Notes
$(\gamma, xn)$	5.0-24	16.2	5.4	1.27 MeV-mb		<p><math>E_{th} = 7.2 \text{ MeV}; \sigma_{max} = 200 \text{ mb.}</math></p> <p>No Corrections.</p> <p>[NOTE: <u>Figure 3</u> - Ref 8: Katz, Baker, Montalbetti, Can. J. Phys. <u>31</u>, 250 (1953)]</p>

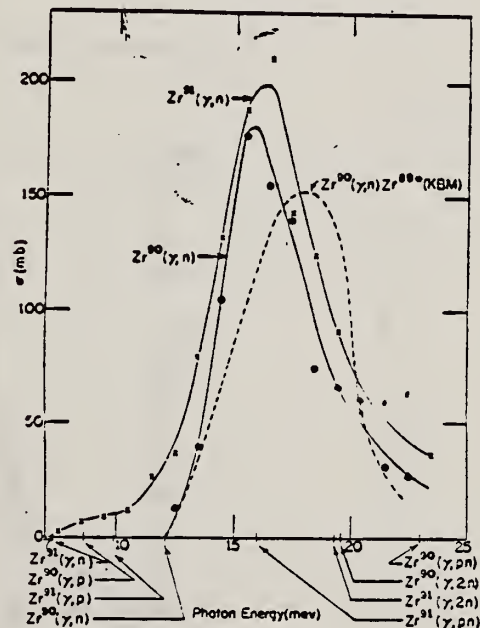


FIG. 3.  $(\gamma, n)$  cross sections for  $\text{Zr}^{90}$  and  $\text{Zr}^{91}$ . The ordinate scale is in millibarns ( $10^{-27} \text{ cm}^2$ ). The points shown are those calculated from the yield data. The solid curves are drawn to fit the points. The dashed curve is the cross section reported (see reference 5) for the production of the isomeric state of  $\text{Zr}^{90}$  by photon bombardment of natural Zr. The locations of the thresholds for various reactions in the two isotopes are indicated by the arrows.

Elem. Sym.	A	Z
Zr	91	40
Ref. No.		
56 Ye 2		EGF

Method 24 MeV betatron; 250r Victoreen in 3.75 cm Lucite; neutron detector

Reaction	E or $\Delta E$	$E_0$	$\Gamma$	$\int \sigma dE$	$J\pi$	Notes
$Zr^{91}(\gamma, xn)$	Bremss. 24	16.5	5.0 MeV	$\int_0^{23} = 1.22 \text{ MeV-b}$		

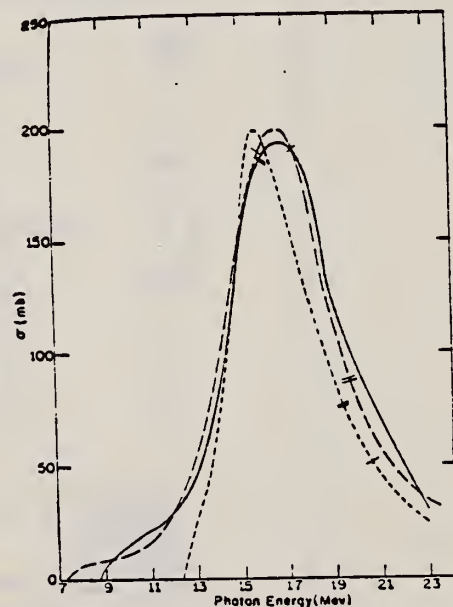


FIG. 5. Cross sections for the  $(\gamma, n)$  reactions in zirconium isotopes. Short dashes  $Zr^{90}$ , long dashes  $Zr^{91}$ , full curve  $Zr^{92}$ . The previously published  $Zr^{90}$  and  $Zr^{91}$  results have been recomputed, taking into account the present  $Zr^{92}$  measurements. The single and double slash marks on each curve represent the locations of the  $(\gamma, pn)$  and  $(\gamma, 2n)$  thresholds respectively. The units of the ordinate are  $10^{-27} \text{ cm}^2$ .

TABLE III. Parameters of giant-resonance cross-section curves for  $(\gamma, n)$  reactions in nuclei near 50 neutrons. Nuclides  $^{92}\text{As}^{75}$ ,  $^{91}\text{Nb}^{92}$ , and  $^{93}\text{Rh}^{102}$  from reference 4,  $^{90}\text{Zr}^{90}$  and  $^{91}\text{Zr}^{91}$  from reference 5 recomputed in present work. Neutron number is shown in column 2, location of peak cross-section value in column 3, peak cross-section value in column 4, half-height width of curve in column 5, and area under curve from threshold to 23 Mev in column 6.

Nuclide	N	$E_m$ (Mev)	$\sigma_m$ (millibarns)	$\Gamma$ (Mev)	$\int_{\text{thr}}^{23} \sigma dE$ (Mev-barns)
$^{92}\text{As}^{75}$	42	17.3	90.3	9.0	0.80
$^{91}\text{Nb}^{92}$	48	15.9	160	5.0	0.92
$^{93}\text{Rh}^{102}$	49	15.8	146	5.3	1.00
$^{90}\text{Zr}^{90}$	50	16.3	201	4.0	1.05
$^{91}\text{Zr}^{91}$	50	16.3	191	3.8	0.87
$^{92}\text{Zr}^{92}$	50	15.8	199	4.3	0.98
$^{93}\text{Zr}^{93}$	51	16.5	200	5.0	1.22
$^{94}\text{Zr}^{94}$	52	16.9	193	5.5	1.24
$^{95}\text{Nb}^{95}$	52	17.0	195	6.8	1.46
$^{96}\text{Rh}^{103}$	58	16.5	205	8.9	1.94

REF. S. C. Fultz, R. L. Bramblett, B. L. Berman, J. T. Caldwell,  
and M. A. Kelly  
Proc. Gatlinburg Conference 397 (1966)

ELEM. SYM.	A	Z
Zr	91	40
REF. NO.		
66 Fu 2		hmg

METHOD					REF. NO.	
					66 Fu 2	hmg
REACTION	RESULT	EXCITATION ENERGY	SOURCE		DETECTOR	
			TYPE	RANGE	TYPE	RANGE
G,XN	ABI	THR-30	D	THR-30	BF <sub>3</sub> -I	4PI
G,2N	ABI	THR-30	D	THR-30	BF <sub>3</sub> -I	4PI

TABLE 1

Integrated Cross Sections for Zirconium and Yttrium

Isotope	$E_{max}$ $a = \int \sigma_{tot} dE$ (MeV - barns)	$E_{max}$ $b = \int \sigma_{gamma} dE$ (MeV - barns)	b/a	$E_{max}$ (MeV)
<sup>90</sup> Zr	0.980	0.108	0.110	28
<sup>91</sup> Zr	1.078	0.202	0.187	30
<sup>92</sup> Zr	1.096	0.447	0.408	28
<sup>94</sup> Zr	1.041	0.577	0.554	30
<sup>89</sup> Y	0.991	0.095	0.096	28



ELEM. SYM.	A	Z
Zr	91	40
REF. NO.		
67 Be 2		hmg

METHOD

REACTION	RESULT	EXCITATION ENERGY	SOURCE		DETECTOR		ANGLE
			TYPE	RANGE	TYPE	RANGE	
G,N 7+	ABX	THR-30	D	THR-30	BF3-I		4PI
G,2N 8+	ABX	THR-30	D	THR-30	BF3-I		4PI

TABLE IV. Integrated cross sections.

Nucleus	$\sigma_{\text{int}}[(\gamma,n) + (\gamma,pn)]$ (MeV-b) <sup>a</sup>	$\sigma_{\text{int}}(\gamma,2n)$ (MeV-b) <sup>a</sup>	$E_{\gamma\text{max}}$ (MeV)	$\frac{\sigma_{\text{int}}(\gamma,2n)}{\sigma_{\text{int}}(\gamma, \text{total})^b}$	$(\frac{1}{2}\pi)\sigma_m\Gamma^*$ (MeV-b)	$0.06NZ/A$ (MeV-b)
$Y^{90}$	0.94	0.10	28	0.10	1.14	1.31
$Zr^{90}$	0.96	0.10	28	0.09	1.16	1.33
$Zr^{91}$	0.88	0.20	30	0.19	1.22	1.35
$Zr^{92}$	0.65	0.45	28	0.41	1.23	1.36
$Zr^{94}$	0.43	0.58	30	0.56 <sup>c</sup>	1.32	1.38

<sup>a</sup> All measured integrated cross-section values are given for an energy region from threshold to  $E_{\gamma\text{max}}$ . For the  $Zr^{91}$  and  $Zr^{92}$  cases, it was necessary to extrapolate the low-energy part of the total photoneutron cross section down to threshold; the error introduced in this process, however, is less than 0.5%.  
<sup>b</sup> The word "total" in this table refers to the total photoneutron cross section  $\sigma[(\gamma,n) + (\gamma,pn) + (\gamma,2n) + (\gamma,3n)]$ , and excludes the  $(\gamma,\gamma)$  and  $(\gamma,p)$  cross sections.  
<sup>c</sup> This value includes the contribution of  $\sigma_{\text{int}}(\gamma,3n)$ , which equals 0.03 MeV-b from threshold to 30 MeV.

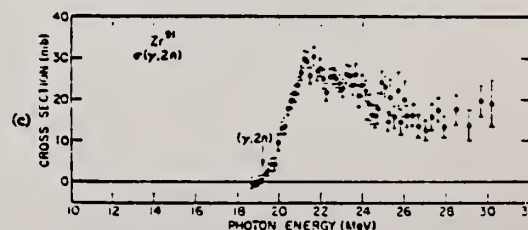
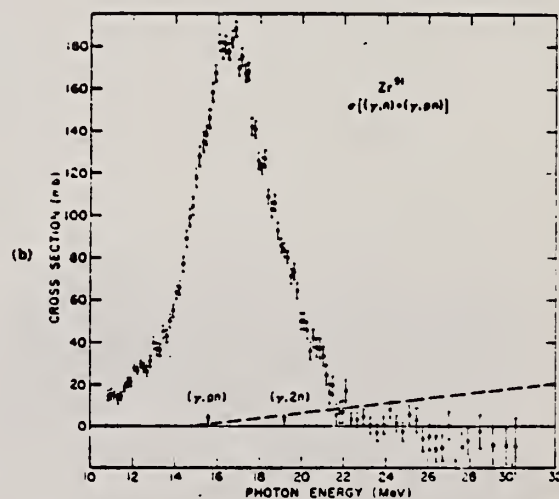
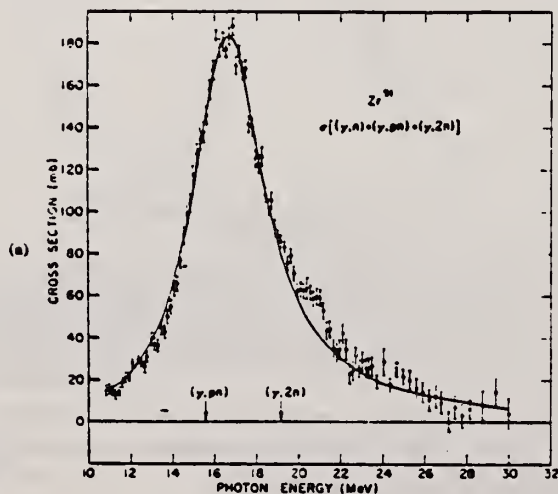


FIG. 10. (a) Total photoneutron cross section for  $Zr^{94}$ . (b) Single photoneutron cross section for  $Zr^{94}$ . (c) The  $(\gamma,2n)$  cross section for  $Zr^{94}$ .

REF. G. P. Antropov, I. E. Mitrofanov, A. I. Prokof'ev and V. S. Russkikh  
Izv. Akad. Nauk Fiz. 33, 700 (1969)  
Bull. Acad. Sci. USSR-Phys. 33, 645 (1969)

ELEM. SYM.	A	Z
Zr	91	40

METHOD

REF. NO.	
69 An 7	egf

REACTION	RESULT	EXCITATION ENERGY	SOURCE		DETECTOR		ANGLE
			TYPE	RANGE	TYPE	RANGE	
G,XN	ABX	12-23	C	12-23	BF3-I		4PI

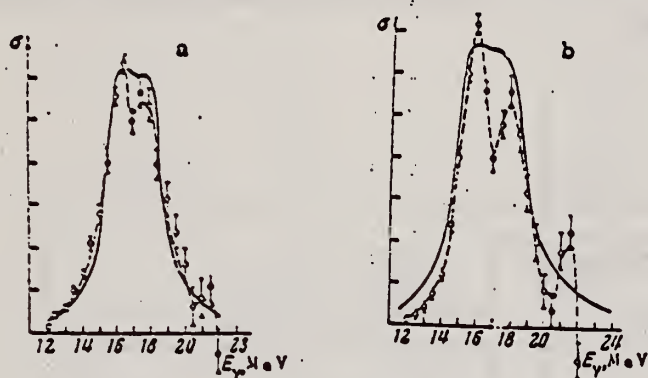


Fig.1. Cross section for the  $(\gamma, n)$  reaction in  $^{90}\text{Zr}$  (a) and  $^{91}\text{Zr}$  (b). The points and the dashed curve are experimental; the full curve is the sum of two Lorentz curves.

Table 1

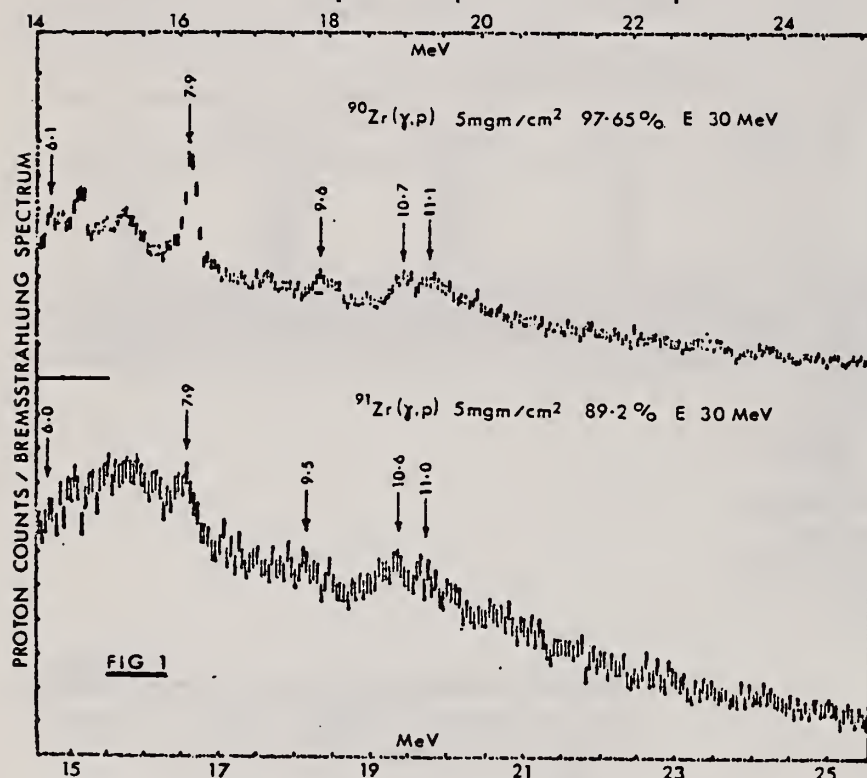
Nucleus	$0.06 NZ/A$	$\frac{22.5 \text{ MeV.}}{\int \sigma(E) dE}$	$\Gamma_{\text{exp.}}$ MeV	$\sigma_{\text{th}} 0.00225 A^{1/3}$
$^{90}\text{Zr}$	1.33	1.27	4.0	0.91
$^{91}\text{Zr}$	1.35	1.42	4.2	1.02

ELEM. SYM.	A	Z
Zr	91	40

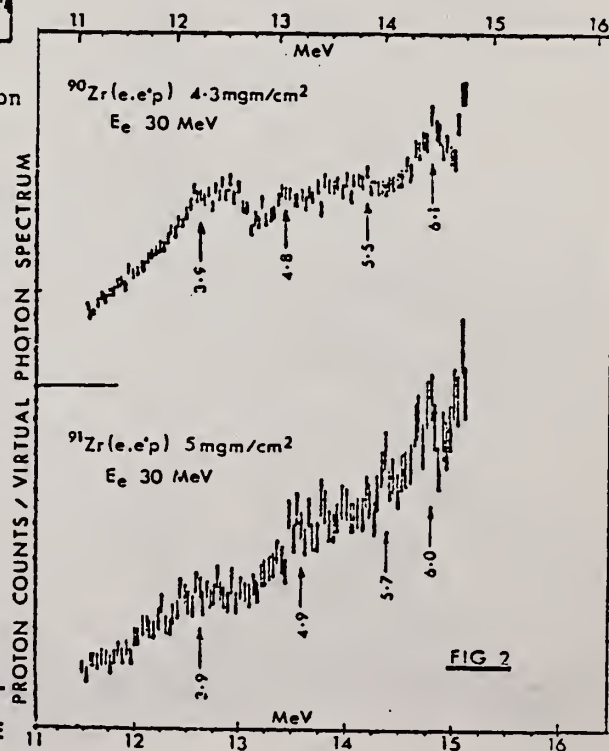
  

METHOD	REF. NO.	
	73 As 9	hmg

REACTION	RESULT	EXCITATION ENERGY	SOURCE		DETECTOR		ANGLE
			TYPE	RANGE	TYPE	RANGE	
E, P	SPC	THR- 26	D	30	MAG-D		DST



Arrows show proton energies. Horizontal scales indicate excitation energies assuming ground state transitions.



REF.

E.J. Winhold, B.H. Patrick, E.M. Bowey, and D.B. Gayther  
PICNS-73, Vol. I, p. 701 Asilomar

ELEM. SYM.	A	Z
Zr	91	40

METHOD	REF. NO.	
	73 W1 6	hmg

REACTION	RESULT	EXCITATION ENERGY	SOURCE		DETECTOR		ANGLE
			TYPE	RANGE	TYPE	RANGE	
G,N	ABX	7- 11	C	7- 11	TOF-D		130

PEAK AT 9.1 MEV

Table I

Reaction	Thres- hold (MeV)	Energy Range of Experiment (MeV)	Observed Peaks		
			Peak Energy (MeV)	$\frac{d\sigma}{d\omega}$ at peak (mb/ster.)	$4\pi \int_{\text{peak}} \left( \frac{d\sigma}{d\omega} \right)_{130^\circ} dE_\gamma$
$^{87}\text{Sr}(\gamma, n_0)$	8.44	9.4-11.1			(MeV-mb)
$^{87}\text{Sr}(\gamma, n_1)$	9.52	10.5-11.1			
$^{91}\text{Zr}(\gamma, n_0)$	7.19	7.8-10.3	9.1	1.2	20
$^{97}\text{No}(\gamma, n_0)$	6.82	7.6-9.2	8.1	0.3	3
$^{113}\text{Cd}(\gamma, n_0)$	6.54	7.4-9.3	7.7	0.9	7
$^{117}\text{Sn}(\gamma, n_0)$	6.94	7.6-8.8	7.8	2.5	20
$^{119}\text{Sn}(\gamma, n_0)$	6.48	7.1-9.0	7.8	1.6	18



REACTION	RESULT	EXCITATION ENERGY	SOURCE		DETECTOR		ANGLE
			TYPE	RANGE	TYPE	RANGE	
G,P	SPC	8- 30	C	30	SCD-D		90
E,P	SPC	8- 30	D	20- 30	MAG-D		90

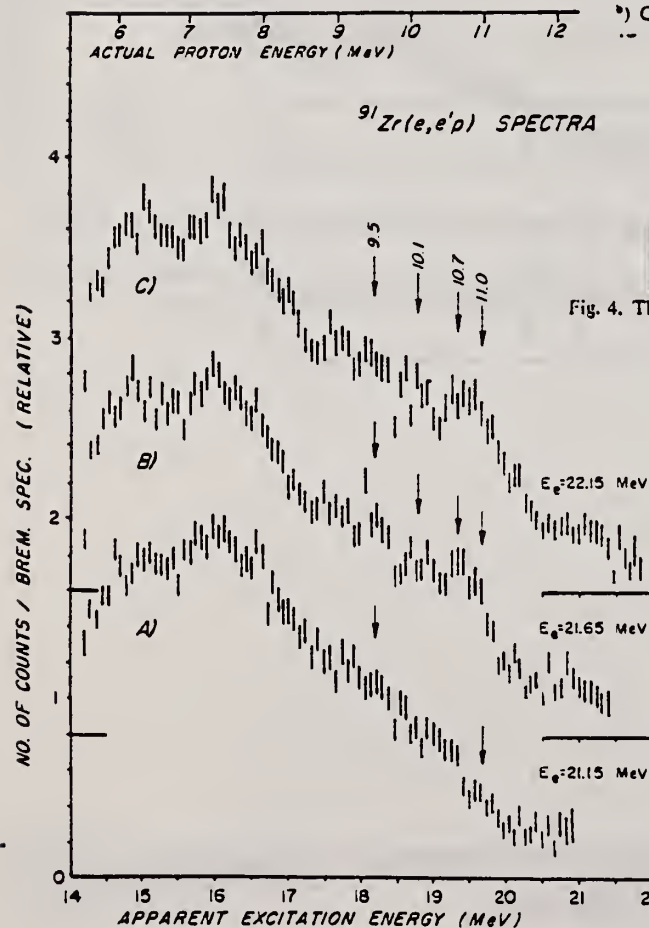
TABLE I

Summary of results

Target	Proton energy $E_p$ (MeV)	Excitation energy (MeV)		Residual levels $^{90}\text{Y}$
		apparent	actual	
$^{90}\text{Zr}$	9.6	17.9	(19.4) <sup>a)</sup>	(1.5 MeV, $\frac{1}{2}^-$ ) <sup>a)</sup>
	11.1	19.4	19.4	g.s., $\frac{1}{2}^-$
	10.7	19.0	20.5-20.8 (20.7) <sup>a)</sup>	(1.74 MeV, $\frac{1}{2}^-$ ) <sup>a)</sup>
	12.5	20.8	20.8	g.s., $\frac{1}{2}^-$
	11.3	19.6	21.2-21.4	1.5 MeV, $\frac{1}{2}^-$ or 1.74 MeV, $\frac{1}{2}^-$
	10.2	18.5	(21.4) <sup>a)</sup>	(2.88 MeV, $\frac{3}{2}^-$ ) <sup>a)</sup>
				$^{90}\text{Y}$ :
$^{91}\text{Zr}$	9.5	18.2	19.7 <sup>b)</sup>	$\approx 1.5$ MeV <sup>b)</sup>
	11.0	19.7	(19.7-19.9) <sup>a)</sup>	g.s., $2^-$ or 0.2 MeV, $3^-$
	10.7	19.4	20.8-21.2 (21.1) <sup>a)</sup>	1.4-1.8 (1.7) <sup>b)</sup>
	12.5	21.2	(21.2) <sup>a)</sup>	g.s., $2^-$ or 0.2 MeV, $3^-$
	11.3	20.0	21.5-21.8	1.5-1.8
	10.1	18.8	( $\approx 21.5$ ) <sup>a)</sup>	( $\approx 2.7$ MeV) <sup>a)</sup>

a) Most probable.

b) Consistent assignment.

Fig. 4. The  $^{91}\text{Zr}(e, e'p)^{90}\text{Y}$  spectra: (a)  $E_p(\text{max}) = 21.15$  MeV; (b)  $E_p(\text{max}) = 21.65$  MeV; (c)  $E_p(\text{max}) = 22.15$  MeV.



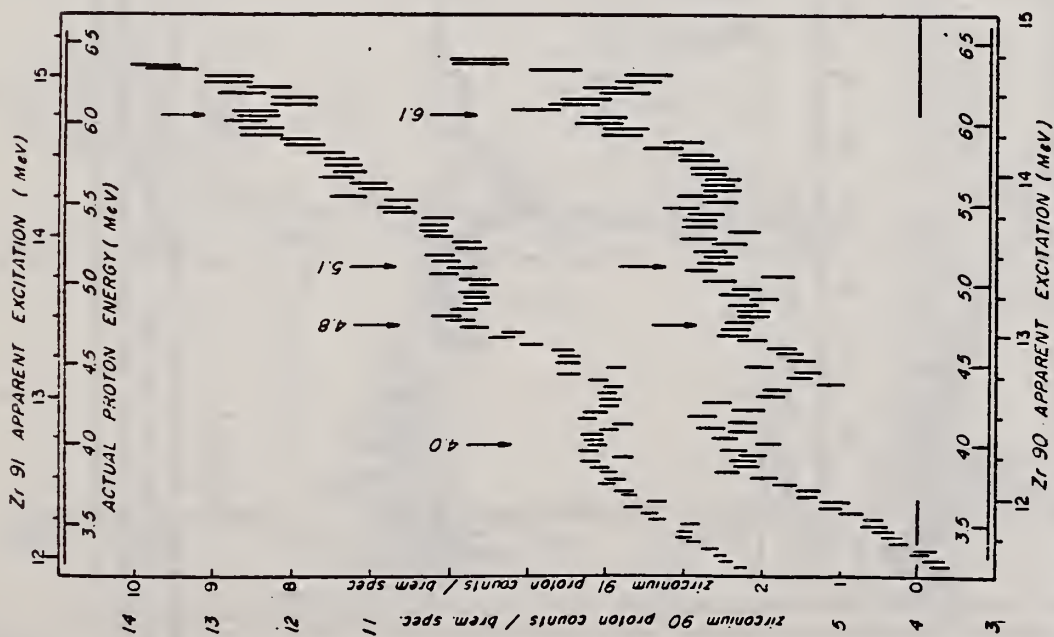


Fig. 1. The  $^{91}\text{Zr}(e,e'p)^{90}\text{Y}$  proton spectrum (upper) and the  $^{90}\text{Zr}(e,e'p)^{89}\text{Y}$  proton spectrum (lower). Bombarding electron energy  $E_0 = 30$  MeV. Spectra are plotted with a common proton energy scale.

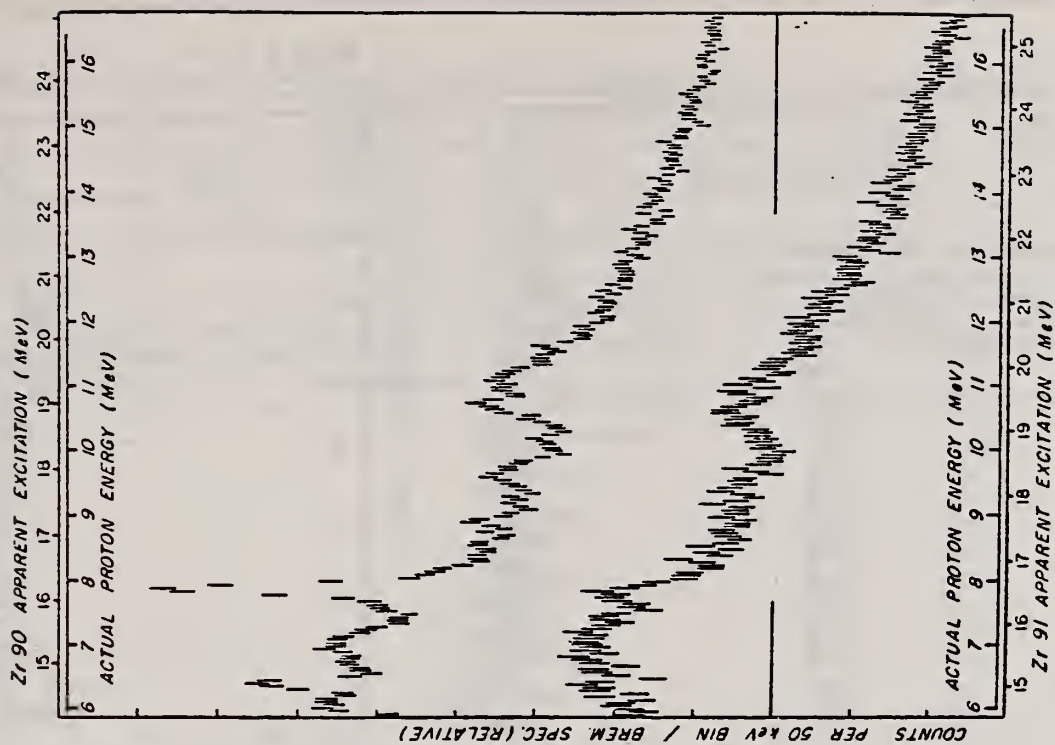


Fig. 2. The  $^{90}\text{Zr}(p,p)^{89}\text{Y}$  proton spectrum (upper) and the  $^{91}\text{Zr}(p,p)^{90}\text{Y}$  proton spectrum (lower). The  $E_0$  endpoint = 30 MeV. Spectra are plotted with a common proton energy scale.

METHOD

Page 3 of 3

REF. NO.	74 As 4	egf
----------	---------	-----

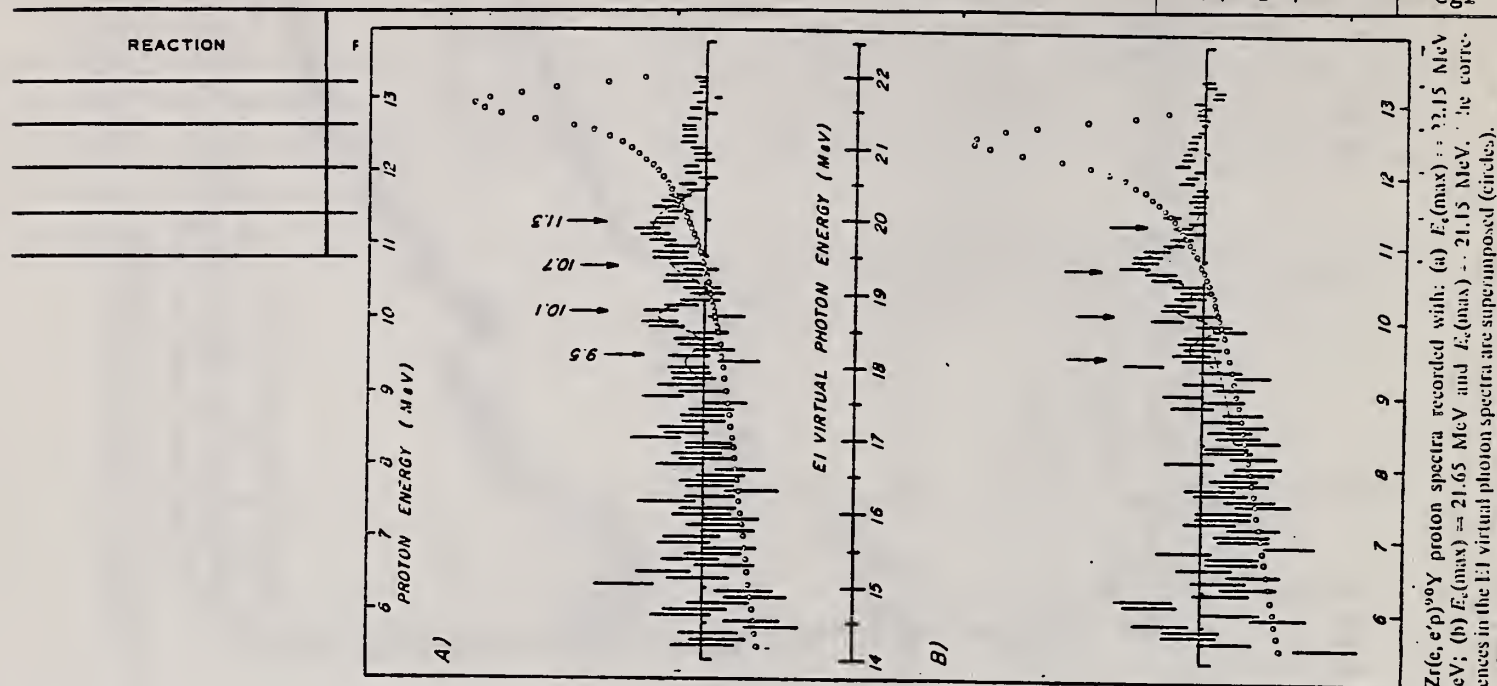


Fig. 6. Differences of  $^{91}\text{Zr}(e, e'p)^{90}\text{Y}$  proton spectra recorded with: (a)  $E_2(\text{max}) = 22.15$  MeV and  $E_2(\text{max}) = 21.65$  MeV; (b)  $E_2(\text{max}) = 21.65$  MeV and  $E_2(\text{max}) = 21.15$  MeV. The corresponding differences in the  $E_1$  virtual photon spectra are superimposed (circles).

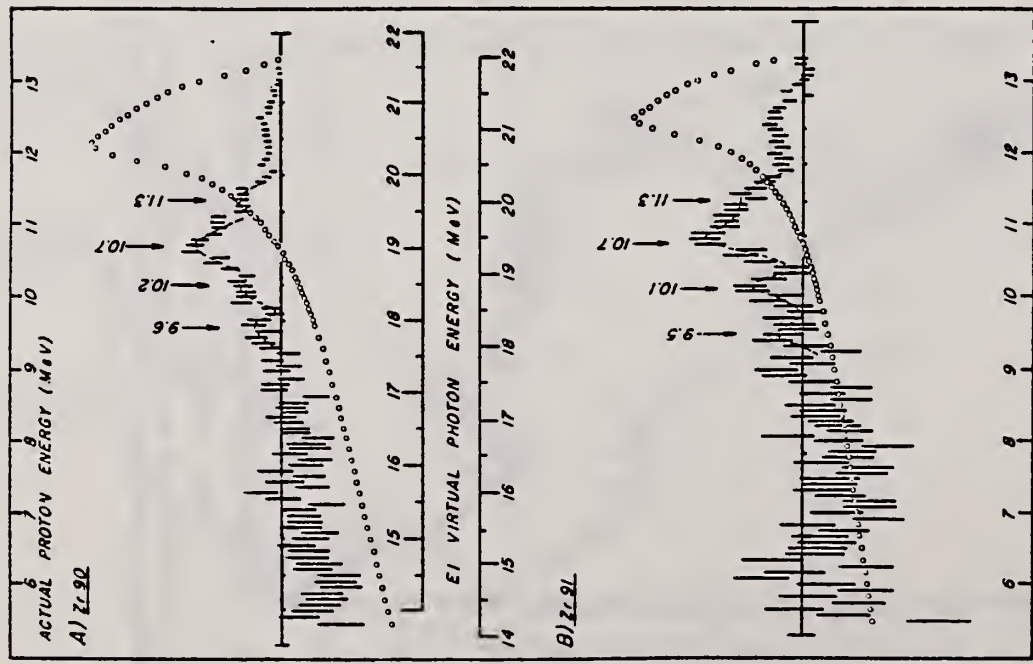


Fig. 7. Comparison of: (a) difference of  $^{90}\text{Zr}(e, e'p)^{89}\text{Y}$  proton spectra recorded with  $E_2(\text{max}) = 21.65$  MeV and  $20.45$  MeV and (b) difference of  $^{91}\text{Zr}(e, e'p)^{90}\text{Y}$  spectra recorded with  $E_2(\text{max}) = 22.15$  MeV and  $21.15$  MeV. Both proton difference spectra are plotted on a common proton energy scale. Corresponding  $E_1$  virtual photon difference spectra are superimposed.

## METHOD

REF. NO.

74 To 2

hmg

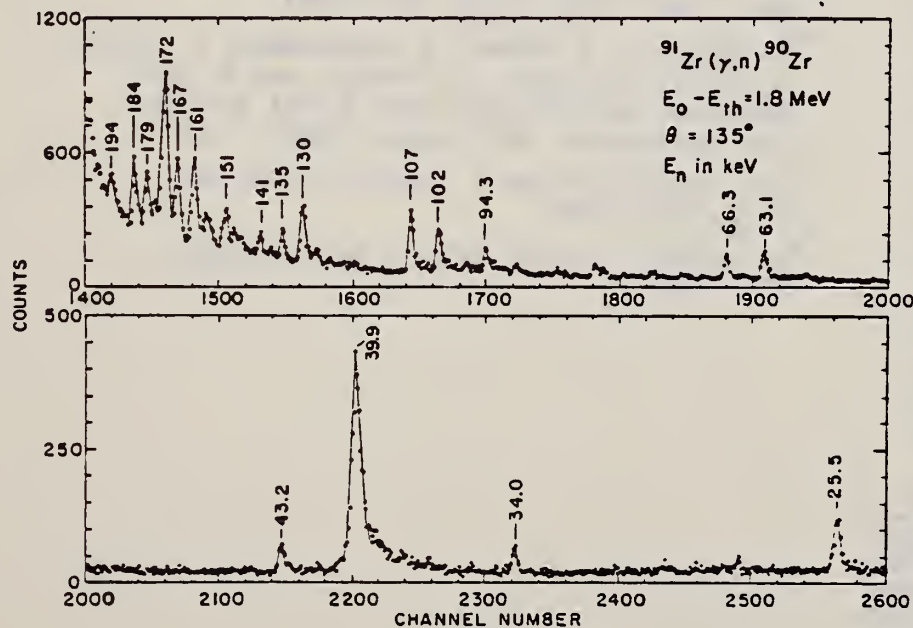
REACTION	RESULT	EXCITATION ENERGY	SOURCE		DETECTOR		ANGLE
			TYPE	RANGE	TYPE	RANGE	
G,N	LFT	7- 9	C	9	TOF-D		135

TABLE I.  $^{91}\text{Zr}(\gamma, n)^{90}\text{Zr}$  resonance parameters obtained from threshold photoneutron measurements at Argonne National Laboratory.  $j^\pi = \frac{1}{2}^+$  except as noted.

E (keV)	$E_n$ (RC) (keV)	$E_n$ (exp) (keV)	$\Gamma_{\gamma 0}$ (eV)
6.82	7.23	7.25	0.10
25.2	26.46	26.46	0.12
27.7	28.7	28.8	0.02
34.0 <sup>a</sup>	35.2	35.4	0.06
38.0	39.3	39.5	0.05
39.1 <sup>b</sup>	40.5	40.4	0.21
39.9 <sup>b</sup>	41.3	41.3	0.63
43.2	44.7	44.6	0.05
59.7	61.7	61.9	0.05
63.1	65.1	65.3	0.16
66.3	68.4	68.5	0.11
70.6	72.8	72.5	0.02
73.5	75.8	74.5	0.04
79.7	82.2	82.1	0.07
84.5 <sup>a</sup>	87.1	85.8	0.07
89.8	92.5	92.9	0.05
93.0 <sup>b</sup>	95.7	95.8	0.03
94.3 <sup>b</sup>	97.2	97.3	0.10
97.4	100.4	99.1	0.03
102.0	105.1	105.6	0.28
105.9	109.0	109.3	0.04
106.8	110.0	110.3	0.33
116.4	119.6	119.0	0.05
124.5	126.3	127.3	0.05
126.3 <sup>a</sup>	130.0	129.8	0.23
129.9	133.7	134.2	0.33
134.9	138.8	139.0	0.12
141.1	145.2	145.3	0.08
151.3	155.6	156.1	0.17
157.4	161.8	163.4	0.11
161.3	165.9	166.5	0.26
166.9	171.6	172.6	0.28
171.8	176.7	177.7	0.57
175.7	180.7	181.6	0.01
179.0	184.1	184.3	0.11
184.2	189.4	190.1	0.11
193.7 <sup>a</sup>	199.1	198.7	0.21
204.2	209.9	211.4	0.11
207.6	213.4	215.2	0.09
214.4	220.4	220.3	0.37

<sup>a</sup> An s-wave resonance;  $j^\pi = \frac{1}{2}^+$ .<sup>b</sup> Not well resolvedGamma ray widths correlate with  
neutron widths for p resonances.

3/2

FIG. 3. A portion of the threshold photoneutron spectrum of  $^{91}\text{Zr}$ . Prominent resonances are labeled with their energies in keV.



METHOD

REF. NO.	
77 Me 6	hmg

REACTION	RESULT	EXCITATION ENERGY	SOURCE		DETECTOR		ANGLE
			TYPE	RANGE	TYPE	RANGE	
G.G	LFT	1 - 5	C	1 - 5	SCD-D		DST
		(1.205-4.704)		(1.85-5.0)			

Using electron bremsstrahlung with up to 5-MeV end point energy, the resonant scattering of  $\gamma$  rays by an enriched sample of  $^{91}\text{Zr}$  has been studied. Substantial resonant scattering was observed from 14 levels. An additional 17 known levels were found to give rise to marginal peaks or to no observable scattering. In a few instances, the transition strengths corresponding to the resonance fluorescence yields could be compared with the results of other lifetime measurements and with the strengths expected under different assumptions concerning the nature of the levels involved.

14 LEVELS 1.2-4.7 MeV

TABLE II. Properties of the  $^{91}\text{Zr}$  levels studied with bremsstrahlung of energy  $\leq 5$  MeV.

$E_{\text{level}}^a$ (MeV)	$J_{\text{exc}}^b$	$\Gamma_0/\Gamma^c$	$g\Gamma_0^2/\Gamma^d$ (meV)
(1.205)	$\frac{1}{2}^+$	1.0	$0.07 \pm 0.11$
1.466 (1)	$\frac{5}{2}^+$	1.0	$1.3 \pm 0.4$
1.882 (1)	$\frac{7}{2}^+$	1.0	$8.0 \pm 1.1$
2.042 (1)	$\frac{3}{2}^+$	1.0	$27.3 \pm 2.6$
2.132 (1)	$\frac{9}{2}^+$	1.0	$6.3 \pm 0.9$
(2.190)	$\frac{5}{2}^-$	1.0	$0.5 \pm 0.5$
(2.201)	$\frac{7}{2}^-$	1.0	$1.5 \pm 0.8$
2.367 (1)	$(\frac{5}{2}, \frac{1}{2})^-$	1.0	$6.5 \pm 0.1$
(2.557)	$\frac{1}{2}^+$	0.8	$0.8 \pm 0.6$
2.577 (2)	$(\frac{5}{2})^-$	1.0	$3.6 \pm 0.9$
(2.641)	$(\frac{3}{2})^-$	1.0	$4 \pm 2$
2.694 (1)	$(\frac{5}{2})^-$	1.0	$24 \pm 4$
(2.776)	$(\frac{3}{2})^-$	1.0	$4 \pm 3$
2.811 (1)	$(\frac{7}{2})^-$	0.78	$23 \pm 4$
3.108 (3)	$\frac{9}{2}^+$		$8 \pm 3$
(3.235)	$\frac{1}{2}^-, \frac{3}{2}^-$		$1 \pm 3$
(3.317)	$\frac{7}{2}^+, \frac{9}{2}^+$		$3 \pm 3$
3.476 (1)	$\frac{1}{2}^-, \frac{3}{2}^-$	1.0	$90 \pm 10$
3.576 (1)	$\frac{1}{2}^-, \frac{3}{2}^-$		$40 \pm 7$
3.681 (3)	$(\frac{3}{2})^+$	1.0	$46 \pm 18^*$
3.704 (3)			$25 \pm 9$
4.322 (2)	$\frac{1}{2}^-, \frac{3}{2}^-$		$70 \pm 30$
(4.674)	$\frac{1}{2}^+, \frac{3}{2}^-$		$50 \pm 30$
(4.704)			$80 \pm 40$

<sup>a</sup>For weak excitations, the energies, given in parentheses, were taken from the literature (Refs. 2, 3, 5, 17, and 18). For well-defined excitations, the energies determined in the  $(\gamma, \gamma)$  experiments are listed, with the uncertainties in units of the last digits given in parentheses.

<sup>b</sup>From Refs. 5 and 18.

<sup>c</sup>Based on Refs. 2, 16, and 17.

<sup>d</sup>Results of the  $(\gamma, \gamma)$  experiments described in this paper.

\*The larger error reflects the fact that a contribution from the 3.684-MeV level in  $^{13}\text{C}$  had to be subtracted.

- <sup>2</sup>J.E. Glenn, H.W. Baer, and J.J. Kraushaar, Nucl. Phys. A165, 533 (1970)
- <sup>3</sup>A. Graue, L.H. Herland, K.J. Lervik, J.T. Nesse, and E.R. Cosman, Nucl. Phys. A187, 141 (1972)
- <sup>5</sup>H.P. Blok, L. Hulstman, E.J. Kaptein, and J. Blok, Nucl. Phys. A273, 142 (1976)
- <sup>16</sup>C. Borcea, E.R. Cosman, W. Duennweber, E. Grosse, M. Maier, K. Pingel, D. Proetel, and P. von Brentano, Annual report, Max Planck Institut fuer Kernphysik, 1970 (unpublished), p.52
- <sup>17</sup>S.S. Glickstein and G. Tessler, Phys. Rev. C 10, 173 (1974)
- <sup>18</sup>H. Verheul and W.B. Ewbank, Nucl. Data B8, 477 (1972)

Zr  
A=92

Zr  
A=92

Zr  
A=92





Elem. Sym.	A	Z
Zr	92	40
Ref. No.		
56 Ye 2		EGF

Method 24 MeV betatron; 250r Victoreen in 3.75 cm Lucite; neutron detector

Reaction	E or $\Delta E$	$E_0$	$\Gamma$	$\int \sigma dE$	$J\pi$	Notes
$Zr^{92}(\gamma, xn)$	Bremss. 24	16.9	5.5 MeV	$\int_0^{23} = 1.24 \text{ MeV-b}$		

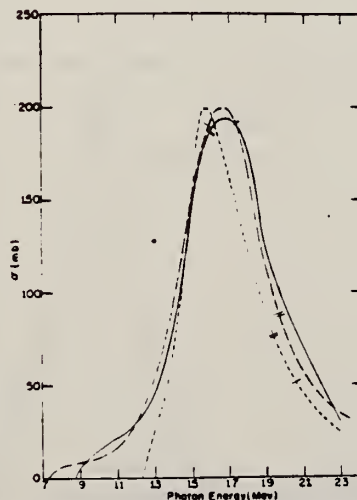


FIG. 5. Cross sections for the  $(\gamma, n)$  reactions in zirconium isotopes. Short dashes  $Zr^{90}$ , long dashes  $Zr^{91}$ , full curve  $Zr^{92}$ . The previously published  $Zr^{90}$  and  $Zr^{91}$  results have been recomputed, taking into account the present  $Zr^{92}$  measurements. The single and double slash marks on each curve represent the locations of the  $(\gamma, pn)$  and  $(\gamma, 2n)$  thresholds respectively. The units of the ordinate are  $10^{-27} \text{ cm}^2$ .

TABLE III. Parameters of giant-resonance cross-section curves for  $(\gamma, n)$  reactions in nuclei near 50 neutrons. Nuclides  $^{115}\text{As}$ ,  $^{115}\text{Nb}$ , and  $^{103}\text{Rh}$  from reference 4,  $^{90}\text{Zr}$  and  $^{91}\text{Zr}$  from reference 5 recomputed in present work. Neutron number is shown in column 2, location of peak cross-section value in column 3, peak cross-section value in column 4, half-height width of curve in column 5, and area under curve from threshold to 23 MeV in column 6.

Nuclide	N	$E_n$ (MeV)	$\sigma_m$ (millibarns)	$\Gamma$ (MeV)	$\int_0^{23} \sigma dE$ (MeV-barns)
$^{115}\text{As}$	42	17.3	90.3	9.0	0.80
$^{115}\text{Nb}$	48	15.9	160	5.0	0.92
$^{103}\text{Rh}$	49	15.8	146	5.3	1.00
$^{90}\text{Zr}$	50	16.3	201	4.0	1.05
$^{91}\text{Zr}$	50	16.3	191	3.8	0.87
$^{90}\text{Zr}$	50	15.8	199	4.3	0.98
$^{91}\text{Zr}$	51	16.5	200	5.0	1.22
$^{92}\text{Zr}$	52	16.9	193	5.5	1.24
$^{115}\text{Nb}$	52	17.0	195	6.8	1.46
$^{103}\text{Rh}$	58	16.5	205	8.9	1.94

REF. S. C. Fultz, R. L. Bramblett, B. L. Berman, and J. T. Caldwell  
and M. A. Kelly  
Proc. Gatlinburg Conference 397 (1966)

ELEM. SYM.	A	Z
Zr	92	40

METHOD	REF. NO.
	66 Fu 2 hmg

REACTION	RESULT	EXCITATION ENERGY	SOURCE		DETECTOR		ANGLE
			TYPE	RANGE	TYPE	RANGE	
G,XN	ABI	THR-28	D	THR-28	BF3-I		4PI
G,2N	ABI	THR-28	D	THR-28	BF3-I		4PI

TABLE I

Integrated Cross Sections for Zirconium and Yttrium

Isotope	$E_{max}$	$E_{max}$	b/a	$E_{max}$ (MeV)
	$a = \int \sigma_{int} dE$ (MeV - barns)	$b = \int \sigma_{T20} dE$ (MeV - barns)		
<sup>90</sup> Zr	0.980	0.108	0.110	28
<sup>91</sup> Zr	1.078	0.202	0.187	30
<sup>92</sup> Zr	1.096	0.447	0.408	28
<sup>94</sup> Zr	1.041	0.577	0.554	30
<sup>89</sup> Y	0.991	0.095	0.096	28

REF. B.L. Berman, J.T. Caldwell, R.R. Harvey, M.A. Kelly, R.L. Bramblett,  
and S.C. Fultz  
Phys. Rev. 162, 1098 (1967)

ELEM. SYM.	A	Z
Zr	92	40
REF. NO.		hmg
67 Be 2		

REACTION	RESULT	EXCITATION ENERGY	SOURCE		DETECTOR		ANGLE
			TYPE	RANGE	TYPE	RANGE	
G, N <u>11+</u>	ABX	THR-28	D	THR-28	BF3-I		4PI
G, 2N <u>10</u>	ABX	THR-28	D	THR-28	BF3-I		4PI

TABLE IV. Integrated cross sections.

Nucleus	$\sigma_{\text{int}}[(\gamma, n) + (\gamma, pn)]$ (McV-b) <sup>a</sup>	$\sigma_{\text{int}}(\gamma, 2n)$ (McV-b) <sup>a</sup>	$E_{\gamma, \text{max}}$ (McV)	$\frac{\sigma_{\text{int}}(\gamma, 2n)}{\sigma_{\text{int}}(\gamma, \text{total})}^b$	$(\frac{1}{2}\pi)\sigma_{\text{int}}\Gamma$ (McV-b)	$0.06NZ/A$ (McV-b)
$\text{Y}^{89}$	0.94	0.10	28	0.10	1.14	1.31
$\text{Zr}^{90}$	0.96	0.10	28	0.09	1.16	1.33
$\text{Zr}^{91}$	0.88	0.20	30	0.19	1.22	1.35
$\text{Zr}^{92}$	0.65	0.45	28	0.41	1.23	1.36
$\text{Zr}^{94}$	0.43	0.58	30	0.56 <sup>c</sup>	1.32	1.38

<sup>a</sup> All measured integrated cross-section values are given for an energy region from threshold to  $E_{\gamma, \text{max}}$ . For the  $\text{Zr}^{92}$  and  $\text{Zr}^{94}$  cases, it was necessary to extrapolate the low-energy part of the total photoneutron cross section down to threshold; the error introduced in this process, however, is less than 0.5%.  
<sup>b</sup> The word "total" in this table refers to the total photoneutron cross section  $\sigma[(\gamma, n) + (\gamma, pn) + (\gamma, 2n) + (\gamma, 3n)]$ , and excludes the  $(\gamma, \gamma)$  and  $(\gamma, p)$  cross sections.  
<sup>c</sup> This value includes the contribution of  $\sigma_{\text{int}}(\gamma, 3n)$ , which equals 0.03 McV-b from threshold to 30 MeV.

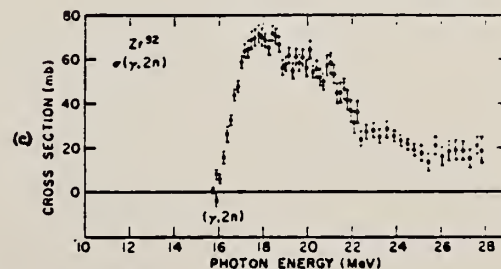
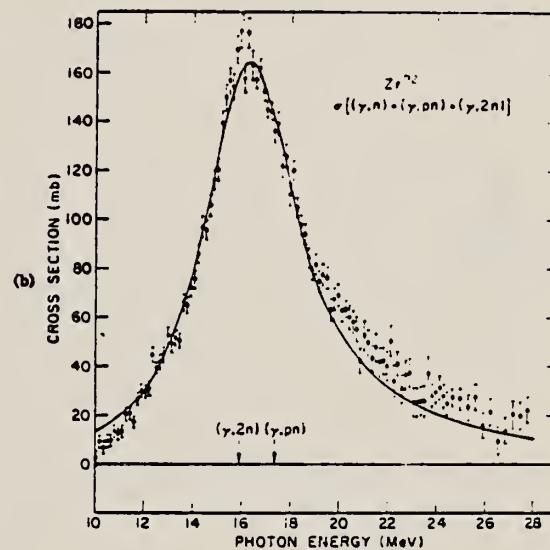
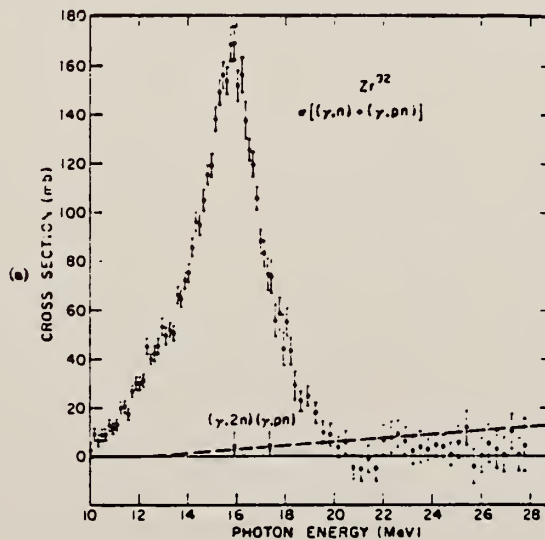


FIG. 11. (a) Total photoneutron cross section for  $\text{Zr}^{92}$ . (b) Single photoneutron cross section for  $\text{Zr}^{92}$ . (c) The  $(\gamma, 2n)$  cross section for  $\text{Zr}^{92}$ .





Zr  
A=94

Zr  
A=94

Zr  
A=94



REF. S. C. Fultz, R. L. Bramblett, B. L. Berman, J. T. Caldwell,  
and M. A. Kelly  
Proc. Gatlinburg Conference 397 (1966)

ELEM. SYM.	A	Z
Zr	94	40

METHOD					REF. NO.	
					66 Fu 2	hmg
REACTION	RESULT	EXCITATION ENERGY	SOURCE		DETECTOR	
			TYPE	RANGE	TYPE	RANGE
G,XN	ABI	THR-30	D	THR-30	BF3-I	4PI
G,2N	ABI	THR-30	D	THR-30	BF3-I	4PI

TABLE 1

Integrated Cross Sections for Zirconium and Yttrium

Isotope	$E_{max}$	$E_{max}$	b/a	$E_{max}$
	$a = \int \sigma_{tot} dE$ (MeV - barns)	$b = \int \sigma_{r,2n} dE$ (MeV - barns)		
<sup>90</sup> Zr	0.980	0.108	0.110	28
<sup>91</sup> Zr	1.078	0.202	0.187	30
<sup>92</sup> Zr	1.096	0.447	0.408	28
<sup>94</sup> Zr	1.041	0.577	0.554	30
<sup>89</sup> Y	0.991	0.095	0.096	28

ELEM. SYM.	A	Z
Zr	94	40
METHOD		REF. NO.
67 Be 2		hmg

REACTION	RESULT	EXCITATION ENERGY	SOURCE		DETECTOR		ANGLE
			TYPE	RANGE	TYPE	RANGE	
G, N 12	ABX	THR-30	D	THR-30	BF3-I		4PI
G, 2N 14	ABX	THR-30	D	THR-30	BF3-I		4PI

TABLE IV. Integrated cross sections.

Nucleus	$\sigma_{int}[(\gamma, n) + (\gamma, pn)]$ (MeV-b) <sup>a</sup>	$\sigma_{int}(\gamma, 2n)$ (MeV-b) <sup>a</sup>	$E_{\gamma max}$ (MeV)	$\frac{\sigma_{int}(\gamma, 2n)}{\sigma_{int}(\gamma, total)^b}$	$(\frac{1}{2}\pi)\sigma_{n\Gamma}$ (MeV-b)	$0.06NZ/A$ (MeV-b)
$Y^{88}$	0.94	0.10	28	0.10	1.14	1.31
$Zr^{90}$	0.96	0.10	28	0.09	1.16	1.33
$Zr^{91}$	0.88	0.20	30	0.19	1.22	1.35
$Zr^{92}$	0.65	0.45	28	0.41	1.23	1.36
$Zr^{94}$	0.43	0.58	30	0.56 <sup>c</sup>	1.32	1.38

<sup>a</sup> All measured integrated cross-section values are given for an energy region from threshold to  $E_{\gamma max}$ . For the  $Zr^{91}$  and  $Zr^{92}$  cases, it was necessary to extrapolate the low-energy part of the total photoneutron cross section down to threshold: the error introduced in this process, however, is less than 0.5%.  
<sup>b</sup> The word "total" in this table refers to the total photoneutron cross section  $\sigma[(\gamma, n) + (\gamma, pn) + (\gamma, 2n) + (\gamma, 3n)]$ , and excludes the  $(\gamma, \gamma)$  and  $(\gamma, p)$  cross sections.  
<sup>c</sup> This value includes the contribution of  $\sigma_{int}(\gamma, 3n)$ , which equals 0.03 MeV-b from threshold to 30 MeV.

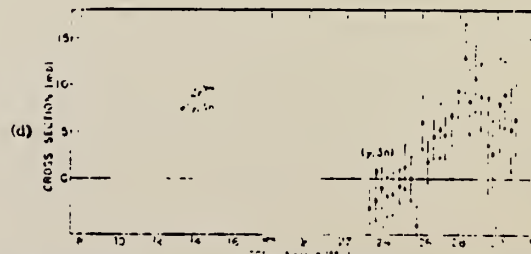
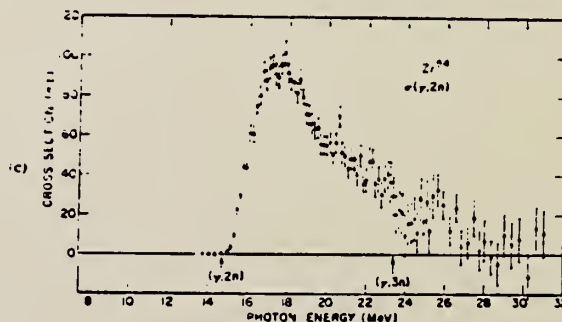
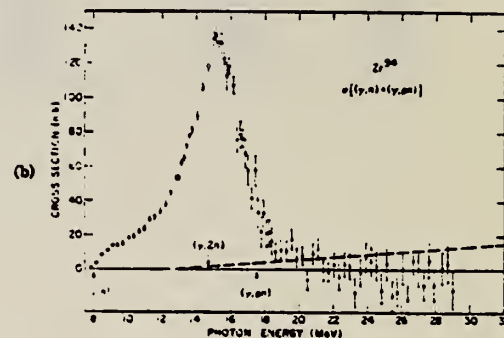
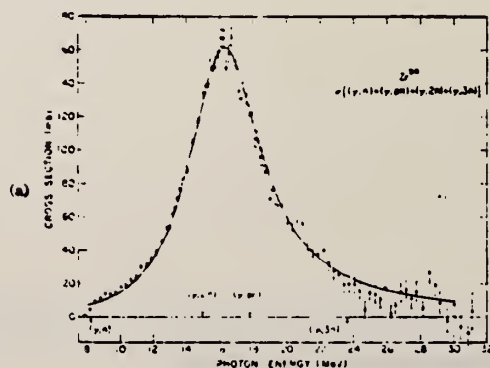


FIG. 12. (a) Total photoneutron cross section  $\sigma[(\gamma, n) + (\gamma, pn) + (\gamma, 2n) + (\gamma, 3n)]$  for  $Zr^{90}$ . (b) Single photoneutron cross section for  $Zr^{90}$ . (c) The  $(\gamma, 2n)$  cross section for  $Zr^{94}$ . (d) The  $(\gamma, 3n)$  cross section for  $Zr^{94}$ .

## NIOBIUM

Z=41

Niobium is a metallic element closely associated with tantalum in ores and in properties; it was named in 1844 by the German chemist Heinrich Rose after the goddess Niobe, daughter of Tantalus. It was first discovered in 1801 in a New England mineral by the British chemist Charles Hatchett, who called the element columbium. By international agreement in 1949, chemists established the name niobium but the name columbium persisted strongly in the U.S. metallurgical industry.





ELEM. SYM.	A	Z
Nb	93	41
REF. NO.		NVB
58 Ch 2		

Betatron					REF. NO.		NVB
					58 Ch 2		
REACTION	RESULT	EXCITATION ENERGY	SOURCE		DETECTOR		ANGLE
			TYPE	RANGE	TYPE	RANGE	
G, N	RLY	THR	C	THR	BF3-I		4PI

TABLE I  
MEASURED PHOTONEUTRON THRESHOLDS

THRESHOLD

Reaction	Measured Q value, Mev.	Other Q values, Mev.	Method	Reference
Nb <sup>93</sup> ( $\gamma$ , n)Nb <sup>92</sup>	8.86 $\pm$ 0.05	8.70 $\pm$ 0.20 8.69 $\pm$ 0.40	Threshold Mass data	Sher <i>et al.</i> (1951) Wapstra (1955)

See 58 Ka 1 for cross sections.

ELEM. SIM.	93	41
Nb	93	41
REF. NO.	58 Ka 1	NVB

METHOD Betatron; neutron cross section; BF<sub>3</sub> counters; ion chamber monitor

REACTION	RESULT	EXCITATION ENERGY	SOURCE		DETECTOR		ANGLE
			TYPE	RANGE	TYPE	RANGE	
G, XN	ABX	9-22	C	9-22	BF <sub>3</sub> -I		4PI

Таблица 2

Пороги испускания фотонейтронов

Изотоп	$E_n$ , Мэв	$E_{th}$ , Мэв	Изотоп	$E_n$ , Мэв	$E_{th}$ , Мэв
V <sup>51</sup>	11.16	20.5	Lu <sup>139</sup>	8.81	16.1
Mn <sup>55</sup>	10.14	19.2	Pr <sup>141</sup>	9.46	17.6
Co <sup>59</sup>	10.44	18.6	Tb <sup>159</sup>	8.16	14.8
As <sup>75</sup>	10.24	18.1	Ho <sup>165</sup>	8.10	14.6
Y <sup>89</sup>	11.82	20.7	Tm <sup>169</sup>	8.00	14.7
Nb <sup>93</sup>	8.86	17.1	Lu <sup>175</sup>	7.77	14.2
Rh <sup>103</sup>	9.46	16.8	Ta <sup>181</sup>	7.66	13.8
J <sup>127</sup>	9.14	16.2	Au <sup>197</sup>	7.96	13.3
Cs <sup>133</sup>	9.11	16.5	Bi <sup>209</sup>	7.43	14.5

# THRESHOLDS

не приведены, поскольку они превышают 22 мэв во всех случаях, кроме золота, для которого  $E_{th}=21$  Мэв. Свойства сечений  $\sigma_c(\gamma)$  сведены в табл. 3.

Таблица 1

Изотоп	$E_{th}$ , Мэв	$\sigma_n(E_\gamma)$ , барн	$E_n$ , Мэв	$\sigma_n$ , Мэв-барн	$\gamma(22)$ , 10 <sup>3</sup> нейтрон/100 р-мэв
V <sup>51</sup>	18.4	0.062	5.2	0.33	1.62
Mn <sup>55</sup>	20.2	0.060	7.0	0.39	2.01
Co <sup>59</sup>	18.3	0.068	6.3	0.44	2.30
As <sup>75</sup>	16.4	0.090	9.5	0.74	4.25
Y <sup>89</sup>	17.1	0.172	5.2	0.93	5.33
Nb <sup>93</sup>	18.0	0.156	7.5	1.17	6.80
Rh <sup>103</sup>	17.5	0.160	9.4	1.40	8.28
J <sup>127</sup>	15.2	0.273	6.8	1.76	11.9
Cs <sup>133</sup>	16.5	0.238	7.7	1.59	10.7
La <sup>139</sup>	15.5	0.325	3.8	1.55	11.2
Pr <sup>141</sup>	15.0	0.320	4.9	1.93	13.1
Tb <sup>159</sup>	15.6	0.274	9.8	2.49	18.1
Ho <sup>165</sup>	13.5	0.305	8.9	2.52	18.7
Tm <sup>169</sup>	16.4	0.250	8.4	1.91	14.9
Lu <sup>175</sup>	16.0	0.225	8.4	1.90	23.0
Ta <sup>181</sup>	14.5	0.380	8.5	3.15	22.0
Au <sup>197</sup>	13.8	0.475	4.7	3.04	22.6
Bi <sup>209</sup>	13.2	0.455	5.9	2.89	23.2

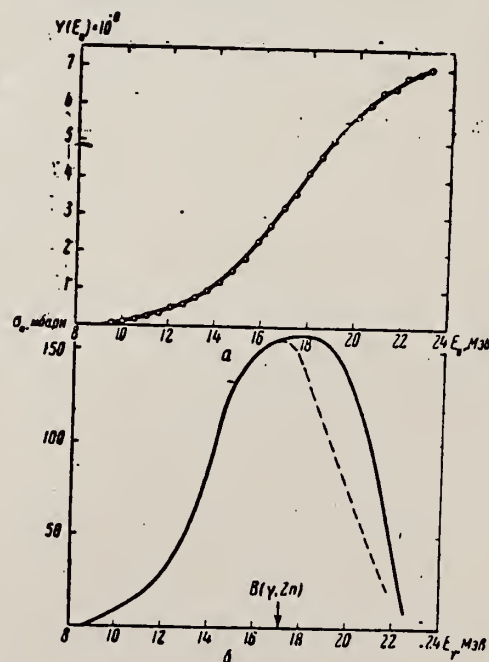


Рис. 6.

a — Выход фотонейтронов для Nb; б —  $\sigma_n(E_\gamma)$   
и  $\sigma_c(\gamma)$  для Nb

Ref. E. Silva, J. Goldemberg, P.B. Smith, L. Marquez  
Il Nuovo Cimento 2, 17 (1958)

Elem. Sym.	A	Z
Nb	93	41
Ref. No.		
58 Si 2		EH

Method 22 MeV Betatron; activation; NaI.

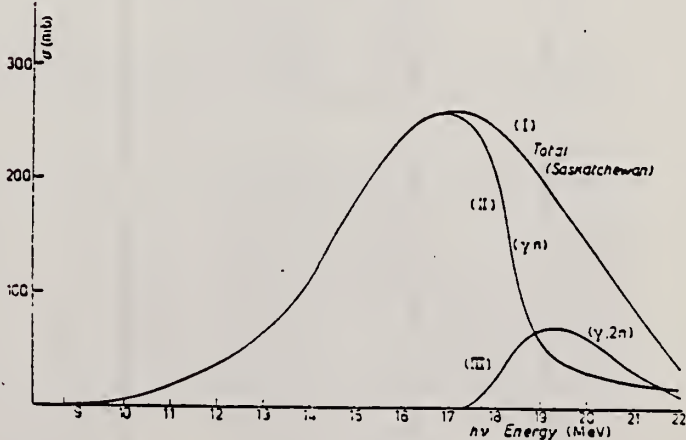
Reaction	E or ΔE	E <sub>0</sub>	Γ	∫σdE	Jπ	Notes
(γ,n)	8-22	~ 17		1.25 MeV-b		
						

Fig. 3.

Ref. M.E. Toms, J. McElhinney  
Phys. Rev. 111, 561 (1958)

Elem. Sym.	A	Z
Nb	93	41

Method Betatron; alpha yield; nuclear emulsion

Ref. No.	
58 To 2	NVB

Reaction	E or $\Delta E$	$E_0$	$\Gamma$	$\int \sigma dE$	$J\pi$	Notes
Nb <sup>93</sup> ( $\gamma, \alpha$ )	Bremss. 22					Yield = $0.5 \times 10^4$ alpha/mole/roentgen

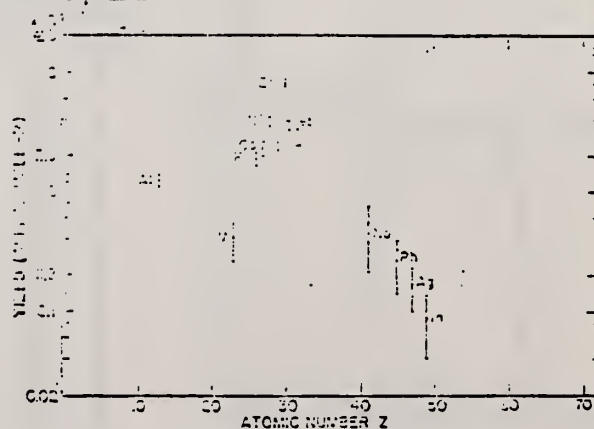


FIG. 8. Photo-alpha yields plotted against atomic numbers for the exposures of the survey.



Method Stanford Mark II accelerator; virtual and real photon spectrum from electrons; magnetic spectrum; KI scintillator crystals.

Ref. No.	JHH
60 Ba 5	

Reaction	E or $\Delta E$	$E_0$	$\Gamma$	$\int \sigma dE$	$J\pi$	Notes
----------	-----------------	-------	----------	------------------	--------	-------

$\text{Nb}^{93}(\gamma, p)$	$E_{e^-} = \leq 40$			$\int_0^{40} = 230 \pm 25\% \text{ MeVmb}$		$\int \sigma dE$ from calculated real and virtual photon spectrum.
-----------------------------	---------------------	--	--	--	--	--

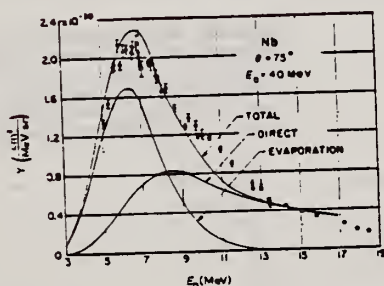


Fig. 8. Energy distribution of protons from Nb. The curves are calculated distributions arbitrarily normalized.

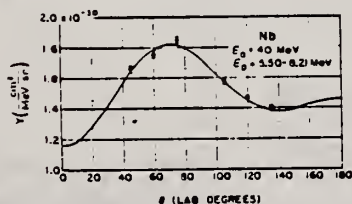


Fig. 9. Angular distribution of protons from Nb. The curve is a plot of the expression  $(1.31 - 0.15 \cos \theta + 0.41 \sin^2 \theta + 0.63 \cos \theta \sin^2 \theta) \times 10^{-28}$ , which is a four-parameter least-squares fit to the data.

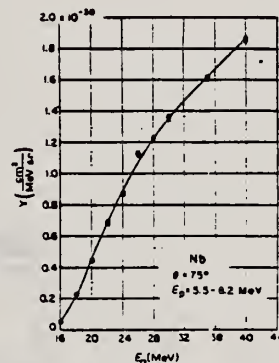


Fig. 14. Excitation of a group of protons from Nb as a function of primary electron energy. The curve was drawn arbitrarily.

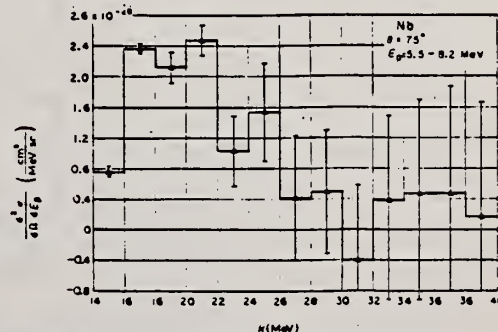


Fig. 17. Differential cross section for producing protons from Nb as a function of photon energy. The histogram was driven by a photon-difference analysis of Fig. 14.

METHOD Linac; proton spectrum; angular distribution; magnetic spectrometer

REF. NO.

60 Ba 6

NVB

REACTION	RESULT	EXCITATION ENERGY	SOURCE		DETECTOR		ANGLE
			TYPE	RANGE	TYPE	RANGE	
G,P	SPC	17-40	C	10-40	MAG-D	5-18	DST

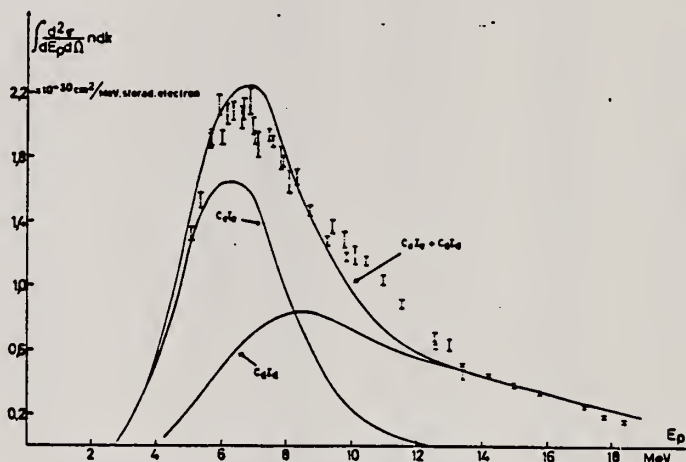


FIG. 2. — Distribution d'énergie.  $E_0 = 40$  MeV,  $\theta = 75^\circ$ .  
 $C_p I_e$  = distribution des protons évaporés.  $C_p I_d$  = distribution des protons directs.

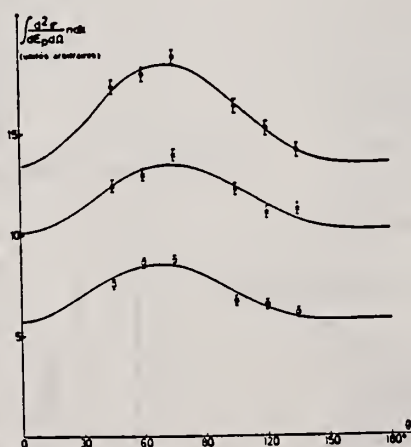


FIG. 3. — Distributions angulaires.  $E_0 = 40$  MeV.  
x  $E_p = 5.05 - 6.55$  MeV;  
+  $0.28 \sin^2 \theta (1 + 0.80 \cos \theta)$ ;  
O  $E_p = 5.75 - 7.15$  MeV;  
+  $0.31 \sin^2 \theta (1 + 0.99 \cos \theta)$ ;  
square  $E_p = 7.05 - 8.45$  MeV;  
+  $0.37 \sin^2 \theta (1 + 1.29 \cos \theta)$

de photons réels  $n_r$  (produits par le rayonnement de freinage dans l'émetteur secondaire, les fenêtres et la cible) et du nombre de photons virtuels  $n_v$  dans la cible. Il a été tenu compte de  $n_r$  et de  $n_v$  dans le calcul de  $n(E_0, k)$ . Pour le calcul de  $n_v$  on a supposé qu'on avait des transitions  $E_1$ .

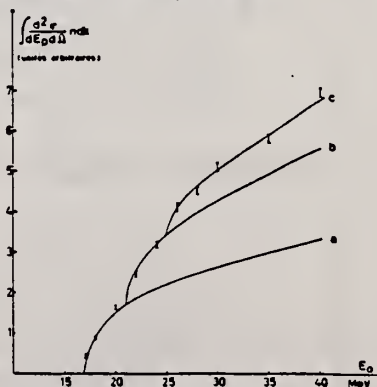


FIG. 4. — Fonction d'excitation.  $\theta = 75^\circ$ .  
a = isochromate de 17 MeV;  
b = somme d'isochromates de 17 et 21 MeV;  
c = somme d'isochromates de 17, 21 et 25 MeV;

METHOD				REF. NO.	
Betatron; neutron threshold; ion chamber				60 Ge 3	
REACTION	RESULT	EXCITATION ENERGY	SOURCE		ANGLE
			TYPE	RANGE	
G,N	NØX	THR	C THR	BF3-I	4 PI

THRESHOLD

TABLE I. Summary and comparison of neutron separation energies inferred from present threshold measurements with values predicted from mass data and reaction energies. All energies are expressed in the center-of-mass system in Mev.

Reaction	No. runs	Present results	Other results	Method	Reference
$Nb^{93}(\gamma,n)Nb^{92}$	2	$8.78 \pm 0.06$	$\geq 8.61 \pm 0.52$	mass data	m
			$8.86 \pm 0.05$	$Q(\alpha)$ threshold	n f

= Henry E. Duckworth, *Mass Spectroscopy* (Cambridge University Press, New York, 1958), p. 177.  
= L. J. Lidofsky, *Revs. Modern Phys.* 29, 773 (1957).

Method Monoergic  $\gamma$ 's from thermal n-capture; activation

Ref. No.	JHH
61 We 1	

Reaction	E or $\Delta E$	$E_0$	$\Gamma$	$\int \sigma dE$	$J\pi$	Notes
$(\gamma, n)$	8.997 9.30 9.73					<p>Measurement of 0.930 MeV <math>\gamma</math> from decay of Nb<sup>92</sup>.</p> <p>Data in Table II (millibarns), Fig. 6</p> <p><math>E_{\gamma}</math> thresh. = <math>8.99 \pm 0.04</math> MeV.</p>

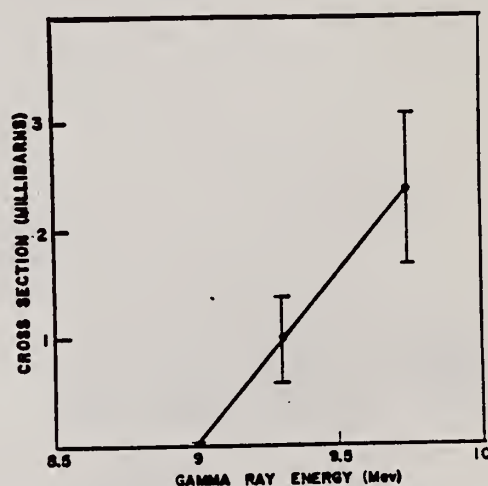


FIG. 6. Cross section vs energy Nb<sup>92</sup>( $\gamma, n$ )Nb<sup>92</sup>(10 day). The line indicates a possible extrapolation to threshold.

TABLE II. Summary of measured cross sections.

$\gamma$ -ray source Reaction \ Energy (Mev)	Co 7.49	Fe 7.64	Al 7.73	Cu 7.91	Cl 8.56	Ni 8.997	Fe 9.30	Cr 9.72	Fe 10.16	N 10.83
Ta <sup>181</sup> ( $\gamma, n$ )Ta <sup>180m</sup>	0 $\pm$ 0.05	0.5 $\pm$ 1	4.8 $\pm$ 1.6	14 $\pm$ 5	32 $\pm$ 16	44 $\pm$ 15	...	83 $\pm$ 33	...	120 $\pm$ 48
Au <sup>197</sup> ( $\gamma, n$ )Au <sup>196</sup>	...	...	...	0 $\pm$ 2	34 $\pm$ 17	44 $\pm$ 11	64 $\pm$ 30	80 $\pm$ 30	...	...
Ho <sup>165</sup> ( $\gamma, n$ )Ho <sup>164</sup>	...	...	...	0 $\pm$ 0.1	29 $\pm$ 15	30 $\pm$ 18	46 $\pm$ 21	86 $\pm$ 31	...	260 $\pm$ 93
Nb <sup>92</sup> ( $\gamma, n$ )Nb <sup>92</sup>	...	...	...	...	...	0.008 $\pm$ 0.005	1.0 $\pm$ 0.4	2.4 $\pm$ 0.7	...	...
Ag <sup>107</sup> ( $\gamma, n$ )Ag <sup>106</sup>	...	...	...	...	...	0 $\pm$ 0.1	...	4.4 $\pm$ 1.5	22 $\pm$ 16	23 $\pm$ 7.5



Elem. Sym.	A	Z
Nb	93	41
Ref. No.		
63 Mi 5		NVB

Method Betatron; proton yield; angular distribution; scintillator;  
ion chamber

Reaction	E or ΔE	E <sub>0</sub>	Γ	∫σdE	Jπ	Notes
Nb <sup>93</sup> (γ, xp)	Bremss. 22					Angular distribution: $Y(\theta) = a + b \sin^2\theta (1 + p \cos \theta)^2$ where $a = 23 \pm 8$ ; $b = 71 \pm 13$ ; $p = 0.1 \pm 0.1$ ; and $b/a = 3.0 \pm 1.2$ .  Yield ( $E_p > 8$ MeV): $(2.8 \pm 0.7) \cdot 10^5$ protons/mole-r.  Yield ( $3.7 < E_p < 14$ ): $(21 \pm 2) \cdot 10^5$

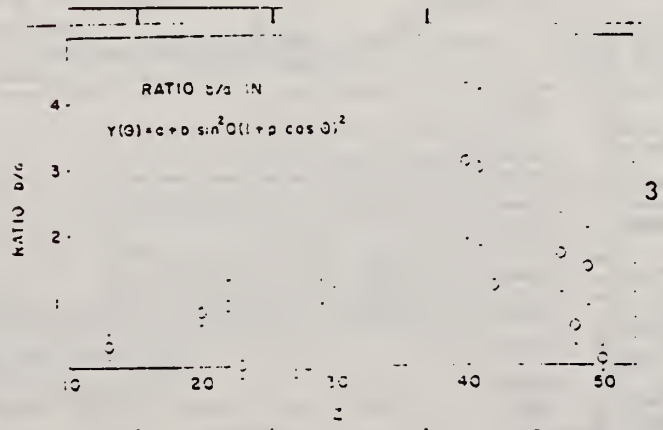
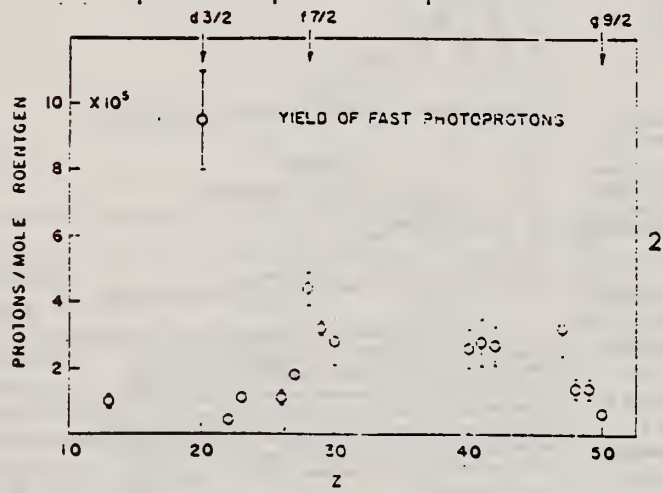


Fig. 2. The yields of fast photoprotons ( $E_p > 8$  MeV) obtained from targets of various elements which irradiated with 22 MeV bremsstrahlung. The target thicknesses range from 2.1 to 57.2 g/cm<sup>2</sup> (about 8 MeV for protons). The errors noted are statistical.

Fig. 3. The anisotropy coefficient  $b/a$  for fast photoprotons ( $E_p > 8$  MeV) from elements. The errors noted are statistical.

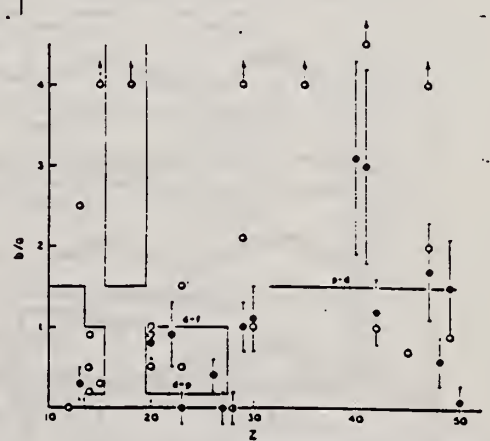


Fig. 4. The values of the fast photoproton anisotropy coefficient  $b/a$  found by the present authors (●) and other workers (○) in the region of the periodic table  $10 < Z < 50$ . Arrows indicate out-of-scale points. The references to the results of other workers are given in Table II. The denominations are explained in the text.



Method 30 MeV Synchrotron; emulsions

Ref. No.	JHH
63 Os 1	

Reaction	E or ΔE	E <sub>0</sub>	Γ	∫σdE	Jπ	Notes
(γ,p)	19.5 23.5 27.5			Relative yields: (E <sub>p</sub> ≥ 3 MeV)  1.00 ± 0.04 1.58 ± 0.04 2.22 ± 0.10		Measured yields > by factor of 10 than statistical theory including effects of nuclear pair correlation predicts.

FIG. 4. Dependence of photoproton yield Y<sub>p</sub> and photo-neutron yield Y<sub>n</sub> from Nb<sup>93</sup> on E<sub>γmax</sub>. For Y<sub>p</sub>: x—present work, o—[6], •—[7]; the yields have been multiplied by the factor 5. For Y<sub>n</sub>: x and o—measured in [11] and [12], respectively; the smooth curve was obtained in [10].

FIG. 3. Angular distributions of photoprotons from Nb<sup>93</sup> for E<sub>γmax</sub> = 19.5 MeV (a), 23.5 MeV (b), and 27.5 MeV (c). The histograms are the experimental results. The smooth curves represent distributions of the forms I(θ) = a + b sin<sup>2</sup> θ and I(θ) = a + b sin<sup>2</sup> θ + c sin<sup>2</sup> θ cos θ. The parameters a, b, and c obtained by least squares are given in Table II.

FIG. 2. Energy distributions of photoprotons from Nb<sup>93</sup> for E<sub>γmax</sub> = 19.5 MeV (a), 23.5 MeV (b), and 27.5 MeV (c). The histograms are the experimental spectra. The dashed histogram in Fig. 2b is the photoproton spectrum of Mo<sup>93</sup>. The smooth curves are spectra computed from the evaporation model for level density ω, taking account of pair correlations. The dashed curve in Fig. 2b is the same, neglecting pair correlations. Arrows indicate the maximum possible proton energy E<sub>pmax</sub> = E<sub>γmax</sub> - B<sub>p0</sub>.

Table II. Angular distribution parameters obtained by least squares

E <sub>γmax</sub> MeV	19.5			23.5			27.5				
	a	b	b/a	a	b	b/a	a	b	c	b/c	c/a
All protons	90.0 ± 5.1	65.1 ± 7.3	0.75 ± 0.18	63.7 ± 4.7	34.4 ± 6.5	0.54 ± 0.15	75.1 ± 5.3	21.3 ± 6.8	—	0.28 ± 0.11	—
>3 MeV	28.5 ± 3.2	8.5 ± 4.4	0.32 ± 0.20	22.1 ± 2.8	3.0 ± 2.7	0.14 ± 0.13	25.4 ± 2.8	—3.1 ± 3.8	—	—0.12 ± 0.14	—
3–6 MeV	29.9 ± 3.9	37.3 ± 5.6	1.25 ± 0.34	31.1 ± 3.3	28.2 ± 4.9	0.84 ± 0.25	35.5 ± 3.2	12.8 ± 4.5	—	0.36 ± 0.17	—
6–10 MeV	3.8 ± 1.3	—0.7 ± 1.7	—0.19 ± 0.53	10.5 ± 1.8	5.2 ± 2.5	0.49 ± 0.33	14.3 ± 2.2	11.6 ± 3.2	10.6 ± 3.1	0.81 ± 0.34	0.74 ± 0.22
>10 MeV	—	—	—	—	—	—	8.4 ± 1.6	6.1 ± 2.2	2.2 ± 1.1	0.72 ± 0.39	0.26 ± 0.29
10–12 MeV	—	—	—	—	—	—	5.9 ± 1.3	5.8 ± 2.1	7.8 ± 1.9	10.9 ± 0.58	1.31 ± 0.39
>12 MeV	—	—	—	—	—	—	—	—	—	—	—

METHOD

Betatron

REF. NO.

64 Sc 1

JOC

REACTION	RESULT	EXCITATION ENERGY	SOURCE		DETECTOR		ANGLE
			TYPE	RANGE	TYPE	RANGE	
G, A	SPC	THR - 33	C	33	SCD	6-14	90

ABS YIELD

TABELLE 1  
Meßdaten und Ergebnisse

	Ti	Ni	Cu	Nb
Targetdicke (mg/cm <sup>2</sup> )	2.08	1.52	9.90	8.87
Bestrahlungsdauer (h)	52.5	55.5	18.0	84.5
Registrierte Teilchenanzahl (4 ≤ E <sub>x</sub> ≤ 12.6 MeV)	1861	2376	2333	1987
Lage des Maximums E <sub>max</sub> der Energieverteilung (MeV)	6.4	8.2	8.5	11
Halbwertsbreite des Maximums (MeV)	2.8	2.8	4.0	3.5
Mittlerer Energieverlust im Target bei E <sub>x</sub> = E <sub>max</sub> (MeV)	0.4	0.25	1.7	1.1
Ausbeute in μb/MeV *)	22 ± 3.5	45 ± 7	23 ± 3.5	5.5 ± 0.8

\*) Vgl. Bemerkung \*) in Tabelle 2.

TABELLE 2  
Vergleich der Ergebnisse verschiedener Autoren

E <sub>x</sub> (MeV)	Ti	Ni	Cu	Nb
<b>Ausbeute (10<sup>3</sup> × N<sub>0</sub>/Mol. r)</b>				
Boulègue 31		58.7	50.8	
Diese Arbeit *) 32.5	48 ± 7	98 ± 15	50 ± 7.5	12 ± 1.8
Toms und McElhinney 21.5		39.4	26	4.6 b)
<b>Relative Ausbeute</b>				
Boulègue 31		1	0.87	
Kregar und Povh 30		1	0.54	
Diese Arbeit 32.5	0.49 ± 0.08	1	0.51 ± 0.08	0.12 ± 0.02
Toms und McElhinney 21.5		1	0.66	0.12 b)

\*) Die Fehlerangaben beinhalten auch die Unsicherheit in der Absolutmessung der Intensität des γ-Strahles.

b) Dieser Wert wurde aus nur 14 beobachteten Ereignissen bestimmt.

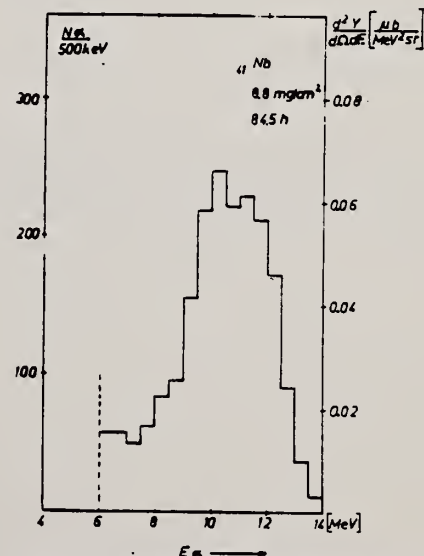


Abb. 1. Die erhaltenen Energie-Spektren der Photoalphateilchen aus Ti, Ni, Cu und Nb.

REF.				ELEM. SYM.		A	Z
K. Schlupmann, R. Wendling Naturwissenschaften <u>16</u> , 380 (1964)				Nb		93	41
METHOD				REF. NO.			
Betatron				64 Sc 3			NVB
REACTION	RESULT	EXCITATION ENERGY	SOURCE		DETECTOR		ANGLE
			TYPE	RANGE	TYPE	RANGE	
G,XP	SPC		C	32	SCI-D	2-15	90

ABY

$$\left(\frac{dY}{d\Omega}\right)_{90^\circ} = 18 \frac{\mu\text{b}}{\text{MeV-ster}} \pm 25\%$$

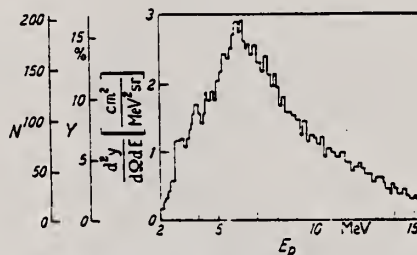


Fig. 1. Energieverteilung der bei dem Prozeß  $^{92}\text{Nb}(\gamma, p)^{91}\text{Zr}$  entstehenden Protonen.

REF.

W. B. Walters and J. P. Hummel  
Phys. Rev. 150, 867 (1966)

ELEM. SYM.

Nb

93

41

METHOD

Betatron

REF. NO.

66 Wa 1

JDM

REACTION	RESULT	EXCITATION ENERGY	SOURCE		DETECTOR		ANGLE
			TYPE	RANGE	TYPE	RANGE	
G,2P4N	RLY	THR-280	C	150,280	ACT-I		4PI

Measured isomeric yield ratios.

TABLE IV. Summary of the results for the photoproduction of the  $Y^{97}$  isomers (spins  $\frac{1}{2}$  and  $\frac{3}{2}$ ).

Target isotope and spin	Bremsstrahlung energy (MeV)	Fraction of yield to high-spin isomer
$Y^{97}$ ( $I = \frac{1}{2}$ )	150	$0.42 \pm 0.05$
	280	$0.42 \pm 0.05$
$Nb^{97}$ ( $I = \frac{3}{2}$ )	150	$0.71 \pm 0.13$
	280	$0.69 \pm 0.13$



REF.

R. R. Hurst and D. J. Donahue  
Nucl. Phys. A91, 365 (1967)

ELEM. SYM.	A	Z
Nb	93	41

METHOD	REF. NO.	
Neutron capture gamma rays	67 Hu 1	EGF

REACTION	RESULT	EXCITATION ENERGY	SOURCE		DETECTOR		ANGLE
			TYPE	RANGE	TYPE	RANGE	
G,N	ABX	9-11	D	9-11	BF3-I		4PI

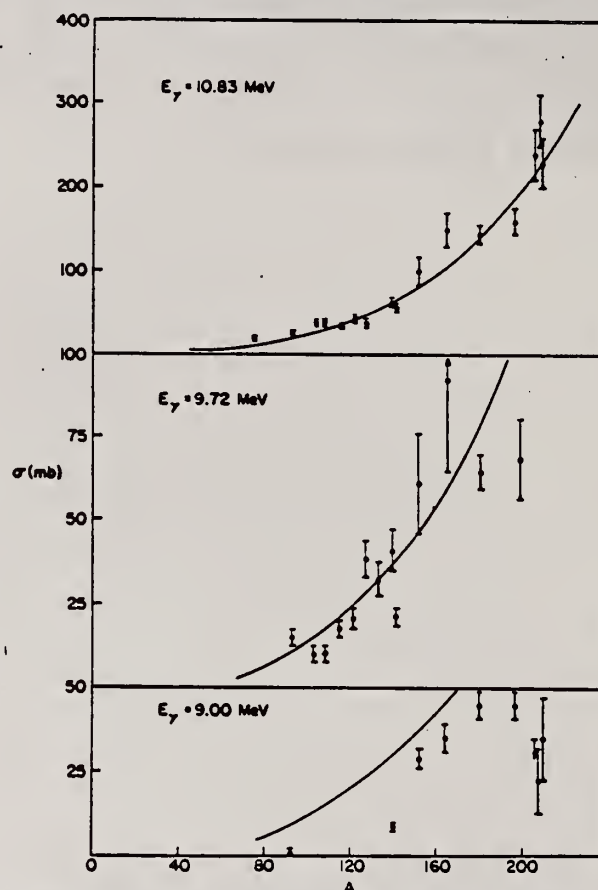


TABLE I  
Photoneutron cross sections (mb)

Target	7.72 MeV	9.00 MeV	9.72 MeV	10.83 MeV
<sup>58</sup> Co				9.0 ± 0.8
<sup>76</sup> As				20.4 ± 1.7
<sup>62</sup> Nb		0.53 ± 0.10	14.6 ± 2.2	25.8 ± 2.1
<sup>103</sup> Rh			10.6 ± 1.7	38.8 ± 3.1
<sup>107</sup> Ag			10.0 ± 1.5	37.6 ± 2.9
<sup>109</sup> Ag			17.1 ± 2.6	33.3 ± 2.7
<sup>118</sup> fn			20.7 ± 3.1	42.5 ± 3.6
<sup>121</sup> Sb			38.7 ± 5.8	38.8 ± 3.1
<sup>123</sup> Sb			31.7 ± 4.8	52.5 ± 3.8
<sup>127</sup> I			40.8 ± 6.5	63.0 ± 5.0
<sup>132</sup> Cs		8.61 ± 0.86	21.5 ± 3.2	58.3 ± 4.1
<sup>138</sup> La			61.3 ± 14.7	102 ± 18
<sup>141</sup> Pr		28.9 ± 3.2	92.2 ± 27.6	150 ± 20
<sup>161</sup> Eu			65.0 ± 5.5	146 ± 12
<sup>163</sup> Eu			68.4 ± 13.5	160 ± 15
<sup>168</sup> Ho		35.6 ± 4.3		238 ± 29
<sup>181</sup> Ta	4.14 ± 0.36	45.4 ± 3.7		280 ± 31
<sup>187</sup> Au		44.5 ± 3.6		226 ± 27
<sup>208</sup> Pb		< 34.3		
<sup>208</sup> Pb		22.6 ± 11.3		
<sup>209</sup> Bi		36.1 ± 12.0		

Fig. 1. Cross section (in mb) versus mass number of the target for gamma-ray energies of 9.00, 9.72 and 10.83 MeV. The solid lines are plots of eq. (1) in the text.



METHOD					REF. NO.		EGF
					67 Hu 2		
REACTION	RESULT	EXCITATION ENERGY	SOURCE		DETECTOR		ANGLE
			TYPE	RANGE	TYPE	RANGE	
G,N	ABY	THR-22	C	22	THR	4-	DST

YIELD AT  $E_0 = 22 \text{ MeV}$   
 $^{28}\text{Si} (n,p)$  ACTIVATION BY PHOTONEUTRONS

FIG. 3. The yields of fast photoneutrons from various elements as measured in the present work and by Baker. The present results have been normalized to Baker's measurements for lead.

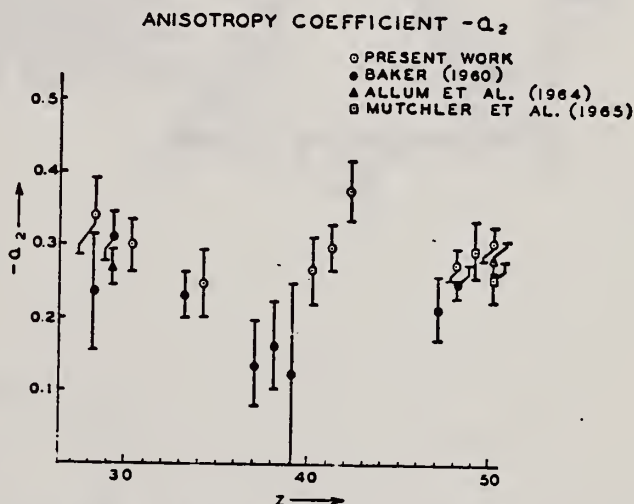
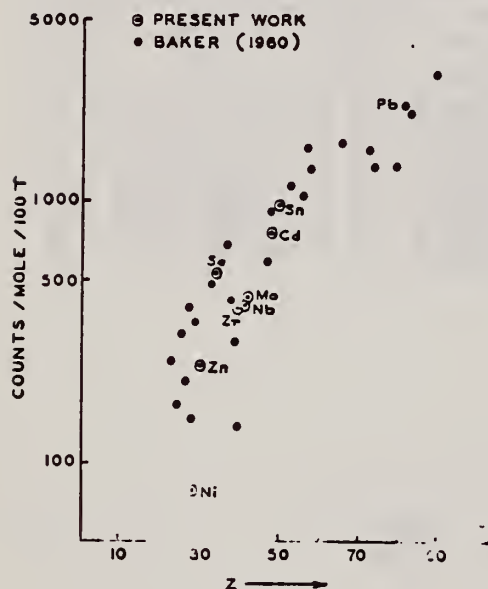


FIG. 2. The anisotropy coefficients  $a_2$ , in the formula  $W(\theta) = a_0(1 + a_1P_1 + a_2P_2)$ , obtained in the present work, and those obtained by other workers in the same part of the Periodic Table.

TABLE I

Element	$a_0^*$	$a_1$	$a_2$
Nickel	77 (1.0±0.05)	0.14±0.04	-0.34±0.04
Zinc	236 (1.0±0.04)	0.06±0.03	-0.30±0.04
Selenium	525 (1.0±0.05)	0.10±0.04	-0.25±0.05
Zirconium	380 (1.0±0.05)	0.03±0.04	-0.27±0.05
Niobium	392 (1.0±0.03)	0.01±0.02	-0.30±0.03
Molybdenum	410 (1.0±0.03)	0.05±0.03	-0.41±0.04
Cadmium	755 (1.0±0.02)	0.05±0.01	-0.28±0.02
Tin	935 (1.0±0.02)	0.08±0.02	-0.30±0.02
Lead	2274 (1.0±0.02)	0.06±0.02	-0.48±0.02

\*For comparison purposes the experimental value of  $a_0$  for Pb has been normalized to coincide with that obtained by Baker and McNeill (1961) and is the yield per mole per 100 roentgen. All other values of  $a_0$  have also been quoted with the same normalization.

REF.

G. Kraft and R. Kosiek  
Natur., Heft 13, 337 (1967)

ELEM. SYM.

A

Z

Nb

93

41

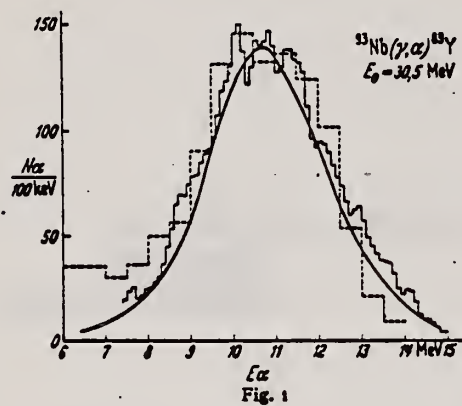
METHOD

REF. NO.

67 Kr 1

EGF

REACTION	RESULT	EXCITATION ENERGY	SOURCE		DETECTOR		ANGLE
			TYPE	RANGE	TYPE	RANGE	
G, A	SPC	2-31	C	31	SCD-D	6-15	90
				(30.5)			



REF.	N. G. Shevchenko, N. G. Afanas'ev, G. A. Savitskii, V. M. Khvastunov, V. D. Kovalev, A. S. Omelaenko, and I. S. Gul'karov J. Nucl. Phys. (USSR) <u>5</u> , 948 (1967) Sov. J. Nucl. Phys. <u>5</u> , 676 (1967)			ELEM. SYM.	A	Z	
				Nb	93	41	
METHOD				REF. NO.			
				67 Sh 1		HMG	
REACTION	RESULT	EXCITATION ENERGY	SOURCE		DETECTOR		ANGLE
			TYPE	RANGE	TYPE	RANGE	
E, E/	FMF	2-3	D	225	MAG-D		DST
		(2.5)					

G-WIDTH, J-PI

Table IV  
Absolute differential cross section for inelastic scattering of electrons with  
energy  $225 \pm 1$  MeV by  $\text{Nb}^{93}$  with excitation of levels at  $2.2 \pm 0.2$  MeV

$\theta$ , deg	Cross section, $\text{cm}^2/\text{sr}$	$\theta$ , deg	Cross section, $\text{cm}^2/\text{sr}$	$\theta$ , deg	Cross section, $\text{cm}^2/\text{sr}$
30	$(0.245 \pm 0.040) \cdot 10^{-28}$	57	$(5.89 \pm 0.53) \cdot 10^{-31}$	82	$(4.07 \pm 0.76) \cdot 10^{-33}$
40	$(1.54 \pm 1.14) \cdot 10^{-29}$	60	$(4.09 \pm 0.82) \cdot 10^{-31}$	84	$(3.23 \pm 0.72) \cdot 10^{-33}$
43	$(1.00 \pm 0.08) \cdot 10^{-29}$	65	$(3.11 \pm 0.37) \cdot 10^{-31}$	85	$(2.25 \pm 0.59) \cdot 10^{-33}$
45	$(8.54 \pm 0.65) \cdot 10^{-30}$	67	$(2.42 \pm 0.276) \cdot 10^{-31}$	87	$(2.97 \pm 0.48) \cdot 10^{-33}$
47	$(8.10 \pm 0.43) \cdot 10^{-30}$	67	$(2.42 \pm 0.276) \cdot 10^{-31}$	90	$(2.82 \pm 0.52) \cdot 10^{-33}$
50	$(2.94 \pm 0.26) \cdot 10^{-30}$	70	$(2.25 \pm 0.29) \cdot 10^{-31}$	95	$(2.06 \pm 0.37) \cdot 10^{-33}$
52	$(2.86 \pm 0.29) \cdot 10^{-30}$	75	$(1.08 \pm 0.18) \cdot 10^{-31}$	95	$(1.45 \pm 0.31) \cdot 10^{-33}$
55	$(1.37 \pm 0.12) \cdot 10^{-30}$	80	$(4.95 \pm 0.97) \cdot 10^{-32}$		

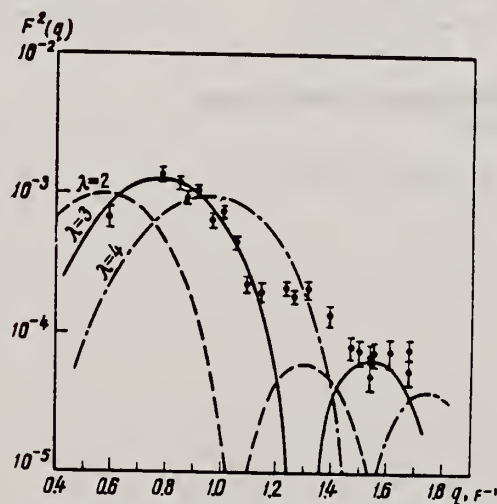


Fig. 6. Squared form factor as a function of momentum transfer for the  $2.2 \pm 0.2$  MeV inelastic peak from  $\text{Nb}^{93}$ . The curves are calculated in the Born approximation for different values of multipolarity  $\lambda$ .

REF. G. Kraft, R. Kosiek, R. Mundhenke and J. Winter  
Nucl. Phys. A118, 25 (1968)

ELEM. SYM.	A	Z
Nb	93	41

METHOD

REF. NO.	
68 Kr 2	egf

REACTION	RESULT	EXCITATION ENERGY	SOURCE		DETECTOR		ANGLE
			TYPE	RANGE	TYPE	RANGE	
G,A	ABX	THR-33	C	33 (32.5)	SCD-D	7-14	90

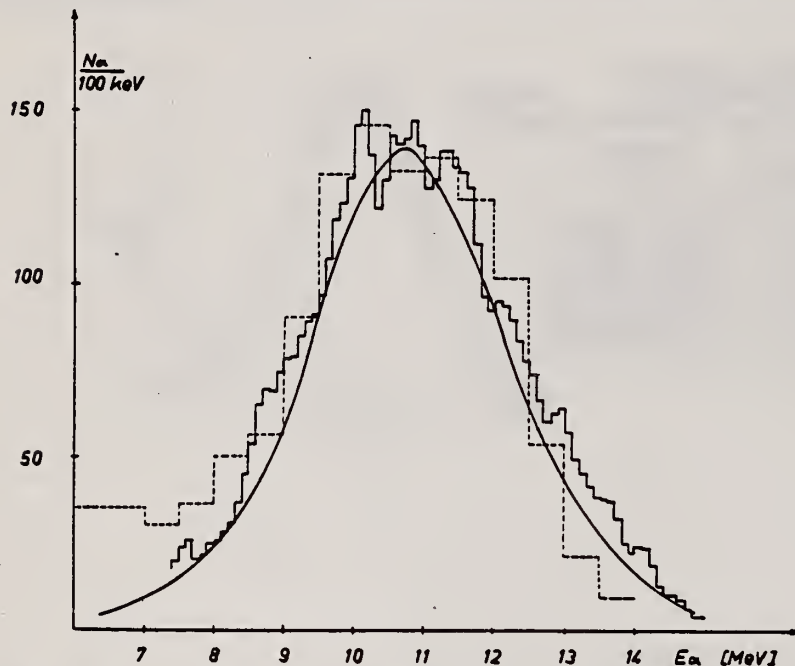


Fig. 4. Histogram: energy distribution of  $\alpha$ -particles from Nb. Dashed histogram: results of Scheer *et al.*<sup>2</sup>). Curve: statistical-model calculation.

<sup>2</sup>J. A. Scheer, K. Schlüpmann and F. Triantafyllidis,  
Nucl. Phys. 56, 113 (1964).



REF. N.V. Goncharov, A.I. Derebchinskii, O.P. Konovalov, S.G. Tonapetyan,  
and V.M. Khvorostyan  
Yad. Fiz. 14, 31 (1971)  
Sov. J. Nucl. Phys. 14, 18 (1972)

ELEM. SYM.	A	Z
Nb	93	41
REF. NO.		hmg
71 Go 2		

METHOD

REACTION	RESULT	EXCITATION ENERGY	SOURCE		DETECTOR		ANGLE
			TYPE	RANGE	TYPE	RANGE	
G, PI+	RLY	150-500	C	500	GCH-D		DST

# PI-/PI+ YIELD RATIO

Measurements are reported of the relative yield of  $\pi^+$  mesons and the  $\pi^-/\pi^+$  yield ratio for mesons with energy  $40 \pm 10$  MeV emitted in the angular range  $\theta_{lab} = 50-160^\circ$  in photon-induced reactions with  $E_{max} = 500$  MeV with light and medium nuclei. The charged  $\pi$ -meson detector was a 34-cm Freon bubble chamber with a tube for the beam. The  $\pi^-/\pi^+$  yield ratio for  $He^4$ ,  $Li^7$ ,  $C^{12}$ ,  $Si^{28}$ ,  $S^{32}$ ,  $Ca^{40}$ , and  $Nb^{93}$  was found to be respectively  $0.94 \pm 0.14$ ,  $2.15 \pm 0.31$ ,  $1.22 \pm 0.21$ ,  $1.25 \pm 0.15$ ,  $1.0 \pm 0.13$ ,  $1.11 \pm 0.13$ , and  $1.53 \pm 0.25$ . It was established that the  $\pi^+$ -meson yield follows a  $ZA^{-1/3}$  law.

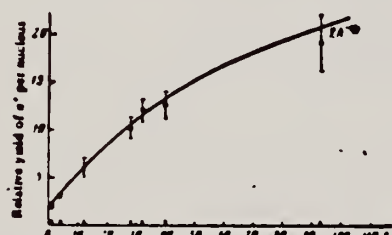
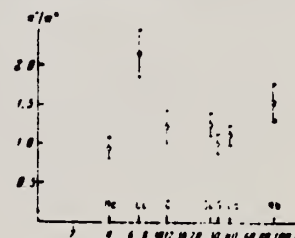


FIG. 2. Relative yield of  $\pi^+$  mesons per nucleus as a function of mass number A.

FIG. 3.  $\pi^-/\pi^+$  yield ratio as a function of mass number A.





METHOD

REF. NO.

71 Le 1

egf

REACTION	RESULT	EXCITATION ENERGY	SOURCE		DETECTOR		ANGLE
			TYPE	RANGE	TYPE	RANGE	
G,N 369	ABX	9-24	D	9-24	MOD-I		4PI
G,2N 370+	ABX	16-24	D	9-24	MOD-I		4PI

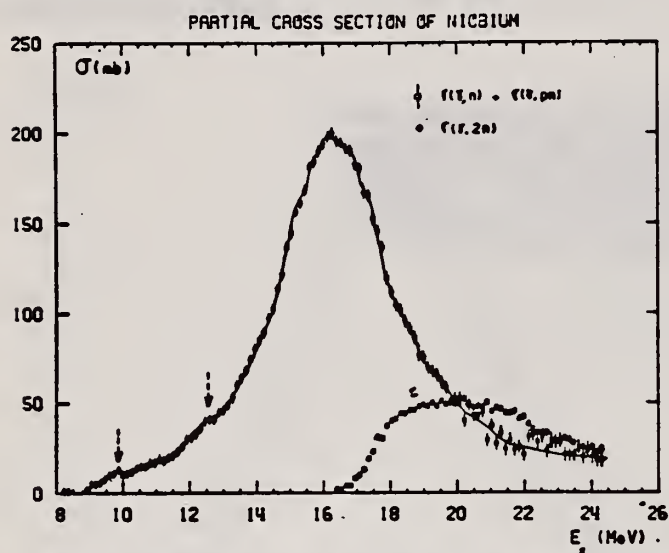


Fig. 5. Partial photoneutron cross sections  $\sigma(\gamma, n)$  and  $\sigma(\gamma, 2n)$  of  $^{93}\text{Nb}$ .

TABLE I  
Lorentz line parameters corresponding to fits shown in fig. 6.

	Rb	Sr	$^{89}\text{Y}$	$^{90}\text{Zr}$	$^{93}\text{Nb}$
$\sigma_0$ (mb)	$192 \pm 10$	$207 \pm 10$	$225 \pm 10$	$211 \pm 10$	$202 \pm 10$
$\Gamma_1$ (MeV)	$4.1 \pm 0.15$	$4.2 \pm 0.1$	$4.1 \pm 0.1$	$4.0 \pm 0.1$	$4.7 \pm 0.2$
$E_1$ (MeV)	$16.75 \pm 0.05$	$16.7 \pm 0.05$	$16.7 \pm 0.05$	$16.65 \pm 0.05$	$16.5 \pm 0.05$

TABLE 3  
Integrated cross sections (the notation used is defined in the text)

	Rb	Sr	$^{89}\text{Y}$	$^{90}\text{Zr}$	$^{93}\text{Nb}$
$\sigma_0$ (MeV · b)	$1.14 \pm 0.06$	$1.42 \pm 0.07$	$1.36 \pm 0.07$	$1.26 \pm 0.07$	$1.33 \pm 0.07$
$\frac{\sigma_0}{0.06 NZ A^{-1}}$	$0.915 \pm 0.05$	$1.09 \pm 0.05$	$1.04 \pm 0.05$	$0.95 \pm 0.05$	$0.97 \pm 0.05$
$\sigma_{-1}$ (mb)	$67 \pm 4$	$80 \pm 5$	$77 \pm 5$	$71 \pm 5$	$79 \pm 5$
$\sigma_{-2}$ (mb · MeV $^{-1}$ )	$4 \pm 0.2$	$4.6 \pm 0.2$	$4.4 \pm 0.2$	$4 \pm 0.2$	$4.8 \pm 0.2$
$E_M$ (MeV)	24	27	27	26	24

(over)

U.S. DEPARTMENT OF COMMERCE  
NATIONAL BUREAU OF STANDARDS

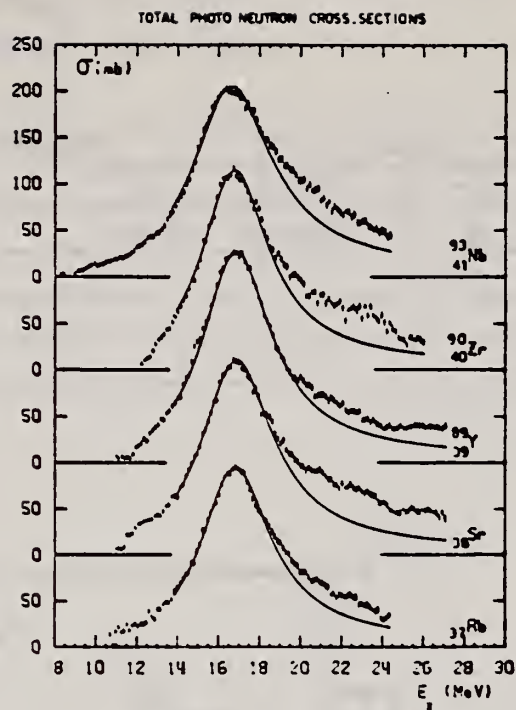


Fig. 6. Total photoneutron cross sections  $\sigma_T$  of Rb, Sr,  $^{89}\text{Y}$ ,  $^{90}\text{Zr}$  and  $^{93}\text{Nb}$  and best one Lorentz line fit corresponding to parameters given in table I.

Tatsuya Saito  
Nippon Kagaku Zasshi 92, 164 (1971)

Nb

93

41

## METHOD

REF. NO.

71 Sa 1

egf

REACTION	RESULT	EXCITATION ENERGY	SOURCE		DETECTOR		ANGLE
			TYPE	RANGE	TYPE	RANGE	
G,N	ABY	8-68	C	10-68	ACT-I		4PI

Nippon Kagaku Zasshi, 92, 164~168(1971)

The Yields of Radioactivities Induced by  $(\gamma, n)$  Reactions  
with Bremsstrahlung up to 68 MeV

by Tatsuya SAITO

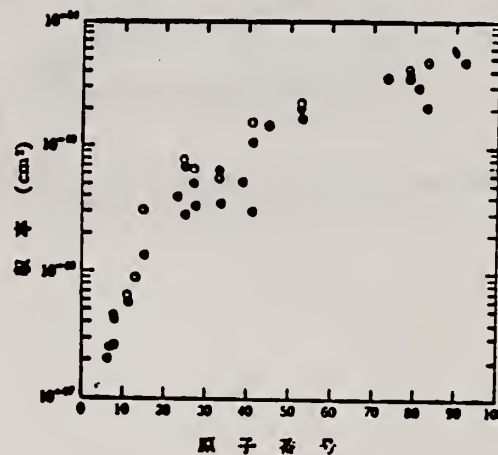
The  $(\gamma, n)$  yields of 12 target nuclides have been measured at 10, 13, 16, 30, 45 and 68 MeV bremsstrahlung by observing the induced activities.

The energy dependence of the yields has been investigated extensively in the same way as in the previous work at 20 MeV bremsstrahlung.

In the case of heavy nuclides, the yields rise greatly as a function of maximum bombarding energy up to 20 MeV, and rise gradually from 20 MeV up to 68 MeV. However, in the case of light nuclides, the yields rise greatly up to 30 MeV, because the neutron separation energies of light ones are larger than those of heavy ones, and the bremsstrahlung spectrum covers the giant resonance and so the yields rise gradually from 30 MeV up to 68 MeV.

The yields have approximately been estimated from the parameter of the giant resonance, that is the peak cross section and the half width, in order to compare with the experimental data. As a result, the experimental data of light nuclides and heavy ones are nearly in agreement with the estimated data of Nathans et al., Johns et al. and Montalbetti et al., but those of medium weight ones are relatively lower values.

Department of Chemistry, Faculty of Science, Tohoku University;  
Katahira-cho, Sendai-shi, Japan



●: 実験値, ⊕: Johns ら,  
⊙: Nathans ら, ○: Montalbetti ら  
図 4  $(\gamma, n)$  反応の収率の比較

ELEM. STM.	A	Z
Nb	93	41
METHOD	REF. NO.	
	73 Ba 20	egf

REACTION	RESULT	EXCITATION ENERGY	SOURCE		DETECTOR		ANGLE
			TYPE	RANGE	TYPE	RANGE	
G,N	NOX	THR- 27	C	10- 27	BF3-I		4PI

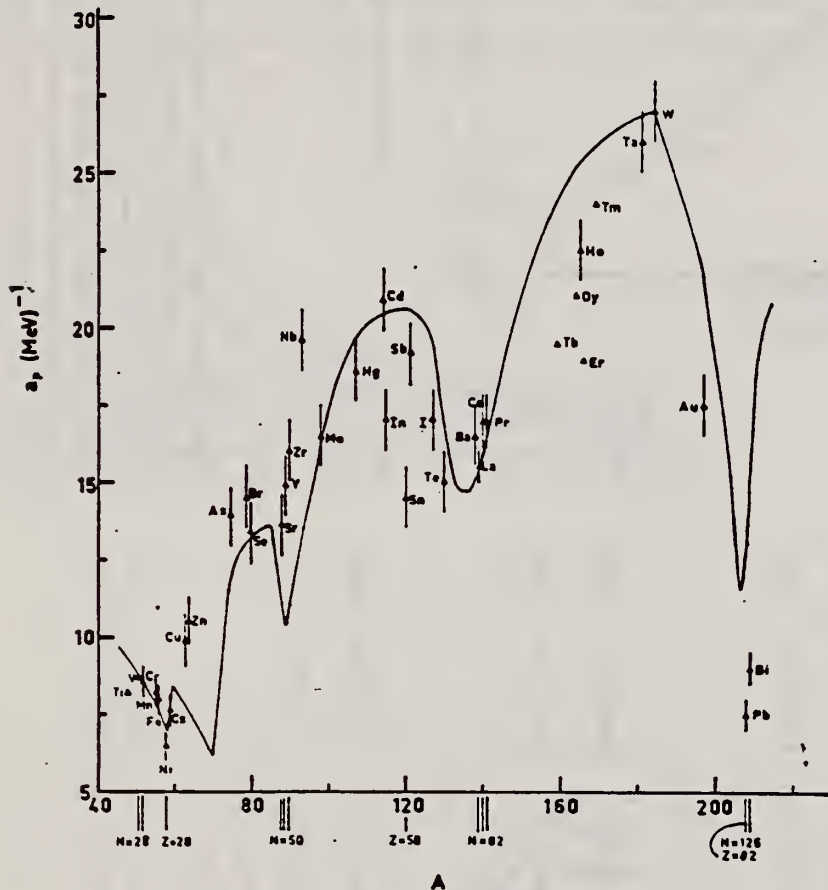


Fig. 12. Experimental values of the level density parameter  $a_p$  (Fermi gas formula plus pairing correction) versus atomic number  $A$ . The continuous curve is a least-squares fit to the data of a theoretical calculation from Newton <sup>13</sup>).

- 1 H. Baba and S. Baba, Japan Atomic Energy Research Institute report JAERI-1183 (1969).
- 2 H. Baba, Nucl. Phys. A159, 625 (1970).
- 15 T.D. Newton, Can. J. Phys. 34, 804 (1956).

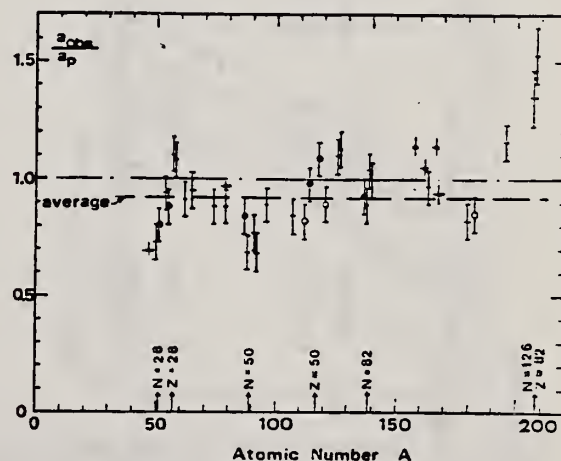


Fig. 15. Ratio  $a_{obs}/a_p$  versus atomic number  $A$ . Here  $a_{obs}$  is the level density parameter taken from the neutron resonance work of refs. <sup>1,2</sup>, and  $a_p$  is the level density parameter derived from the present  $(\gamma, n)$  work. Filled circles represent points where nuclei in the neutron resonance and in the  $(\gamma, n)$  experiment were the same. Open circles represent points where the respective nuclei were approximately matched. Triangles represent points which are based on measurement of neutron mean energies at two bremsstrahlung energies only.

(over)



TABLE 3 (continued)

Target	N (residual nucleus) <sup>a)</sup>	Goodness of fit <sup>b)</sup>	$\bar{E}_a(24)$ (MeV) <sup>c)</sup>	T (MeV) <sup>d)</sup>	$a_p$ (MeV <sup>-1/2</sup> ) <sup>e)</sup>	$a_{obs}$ (MeV <sup>-1/2</sup> )	$a_{obs}/a_p$
		no	p.c.				
Y	49 100%	G	G	1.30	14.9- <sup>88</sup> Y	10.17- <sup>90</sup> Y	0.68
Zr	49 52%	F	F	1.28	16.0- <sup>90</sup> Zr	12.2- <sup>91</sup> Zr	0.77
	50 11%						
	51 17%						
	53 17%						
	55 3%						
Nb	51 100%	F	F	1.28	19.6- <sup>92</sup> Nb	13.15- <sup>94</sup> Nb	0.68
Mo	49 16%	G	G	1.27	16.5- <sup>92</sup> Mo	14.7- <sup>97</sup> Mo	0.89
	51 9%						
	52 16%						
	53 17%						
	54 10%						
	55 24%						
	57 8%						
Ag	59 51%	V.P.	F	1.27	18.6- <sup>107</sup> Ag	15.61- <sup>108</sup> Ag	0.84
	61 49%						
Cd	57 1%	V.P.	F	1.24	20.9- <sup>111</sup> Cd	17.0- <sup>112</sup> Cd	0.82
	61 12%						
	62 13%						
	63 24%						
	64 12%						
	65 29%						
	67 8%						
In	63 4%	V.P.	F	1.26	17.0- <sup>114</sup> In	16.66- <sup>114</sup> In	0.98
	65 96%						
Sn	65 14%	V.P.	V.P.	1.38	14.5- <sup>116</sup> Sn	15.9- <sup>116</sup> Sn	1.09
(Z = 50)	66 8%						
	67 24%						
	68 9%						
	69 33%						
	71 5%						
	73 6%						
Sb	69 57%	V.P.	P	1.2	19.2- <sup>121</sup> Sb	17.0- <sup>121</sup> Sb	0.89
	71 43%						
Te	69 2%	V.P.	F	1.36	15.0- <sup>127</sup> Te	17.0- <sup>127</sup> Te	1.13
	71 5%						
	72 7%						
	73 19%						
	75 32%						
	77 34%						
I	73 100%	F	G	1.23	17.0- <sup>126</sup> I	17.02- <sup>126</sup> I	1.00

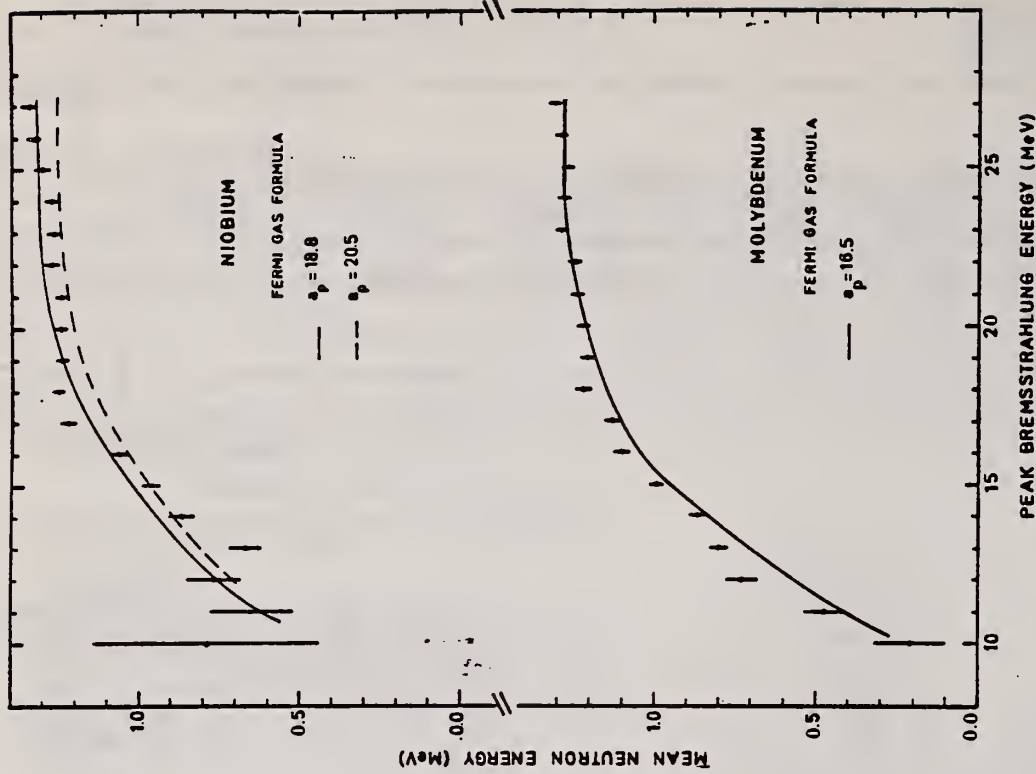


Fig. 8. Same as fig. 5, for niobium and molybdenum.

- <sup>a)</sup> Neutron numbers and abundances of respective residual nuclei in ( $\gamma$ , n) experiments.  
<sup>b)</sup> These give an assessment of the goodness of fit of a calculated  $\bar{E}_a$  versus  $E_0$  curve to the observed data, using the Fermi gas level density formula both without and with pairing corrections.  
<sup>c)</sup> Bremsstrahlung photon mean energies  $\bar{E}_a$  for peak bremsstrahlung energy  $E_0 = 24$  MeV.  
<sup>d)</sup> Nuclear temperature from fit with constant-temperature formula.  
<sup>e)</sup> Level density parameter  $a_p$  derived from the present ( $\gamma$ , n) experiment, using a Fermi gas formula plus pairing correction, and corresponding residual nucleus (the atomic weight shown is the weighted average of atomic weights of the respective isotopes present).  
<sup>f)</sup> As column 7, but using data on n-resonance absorption from refs. 1, 2).  
<sup>g)</sup> Measurements of  $\bar{E}_a(E_0)$  for these nuclei were made only for  $E_0 = 21, 23$  and 24 MeV.



REF. N.V. Goncharov, A.I. Derebchinskii, O.G. Kononov,  
S.G. Tonapetyan, and V.M. Khvorostyan  
Yad. Fiz. 17, 242 (1973)  
Sov. J. Nucl. Phys. 17, 124 (1973)

ELEM. SYM.	A	Z
Nb	93	41
REF. NO.		
73 Go 5		
hmg		

REACTION	RESULT	EXCITATION ENERGY	SOURCE		DETECTOR		ANGLE
			TYPE	RANGE	TYPE	RANGE	
G,PI+	ABY	170-400	C	400	BBL-D		90
G,PI-	ABY	170-400	C	400	BBL-D		90
G,P	ABY	76-400	C	400	BBL-D		90

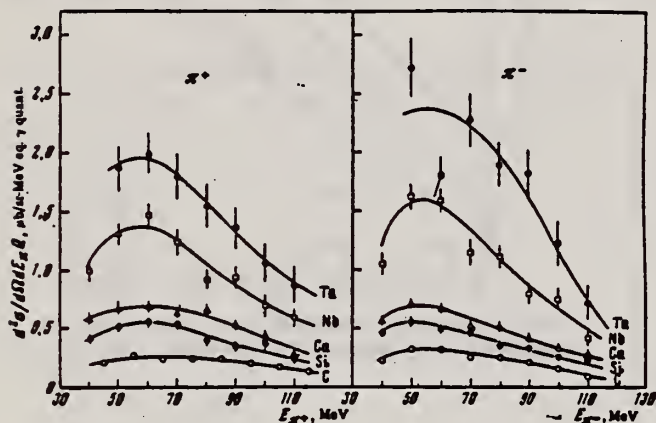


FIG. 2. Energy spectra of  $\pi^+$  and  $\pi^-$  mesons,  $E_{\gamma}^{\max} = 400$  MeV,  $\theta_{\text{lab}} = (90 \pm 7)^\circ$ .

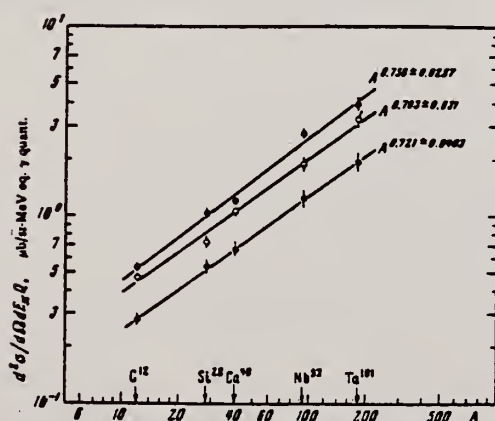


FIG. 4. Charged pion yield vs. the mass number of the nucleus:  $\bullet$ — $E_{\pi} = 105 \pm 10$  MeV,  $\circ$ — $E_{\pi} = 85 \pm 10$  MeV,  $\circ$ — $E_{\pi} = 65 \pm 10$  MeV.

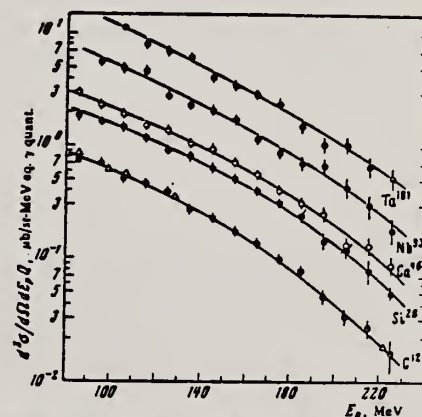


FIG. 3. Energy spectra of protons,  $E_{\gamma}^{\max} = 400$  MeV,  $\theta_{\text{lab}} = (90 \pm 7)^\circ$ . Circles—present data, triangles—from [18].

18P. Dougan, W. Stiefeler, LUSY Preprint, 1001-1003, 1970.

(over)

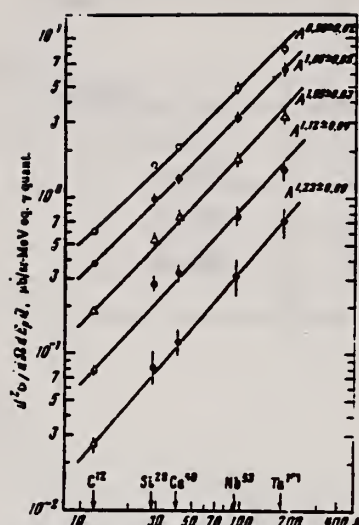


FIG. 5. Proton yields vs. mass number of the nucleus:  $\circ$ — $E_p = 100 \pm 10$  MeV,  $\bullet$ — $E_p = 125 \pm 15$  MeV,  $\Delta$ — $E_p = 155 \pm 15$  MeV,  $\square$ — $E_p = 185 \pm 15$  MeV,  $\circ$ — $E_p = 215 \pm 15$  MeV.

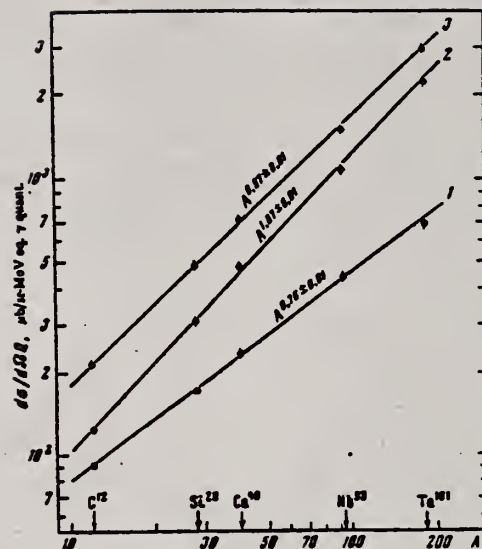


FIG. 6. Pion yield (1), proton yield (2), and summary pion and proton yield (3) vs. the mass number of the nucleus.

REF.

S. Sugiyama and T. Tomimasu  
PICNS-73, Vol.I, p. 563 Asilomar

ELEM. SYM.

A

Z

Nb

93

41

METHOD

REF. NO.

73 Su 12

hmg

REACTION	RESULT	EXCITATION ENERGY	SOURCE		DETECTOR		ANGLE
			TYPE	RANGE	TYPE	RANGE	
G,MU-T	ABX	10- 26	C	18, 26	MGP-D		4PI

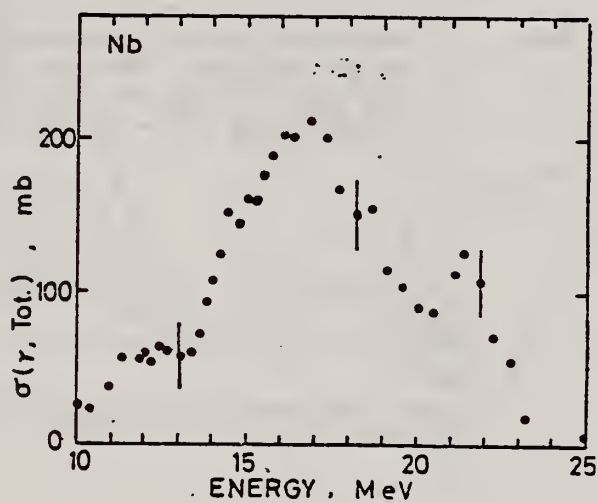


Fig. 2

Total photonuclear cross section for Nb

REF.	P. David, J. Debrus, F. Lubke, H. Mommsen, R. Schoenmackers, and G. Stein Nucl. Phys. <u>A221</u> , 145 (1974)				ELEM. SYM.	A	Z
					Nb	93	41
METHOD					REF. NO.		
					74 Da 2		egf
REACTION	RESULT	EXCITATION ENERGY	SOURCE		DETECTOR		ANGLE
			TYPE	RANGE	TYPE	RANGE	
G,A	ABY	10-450	C	450	TEL-D		90

Data measured for p,t, and He3, but not given in paper.

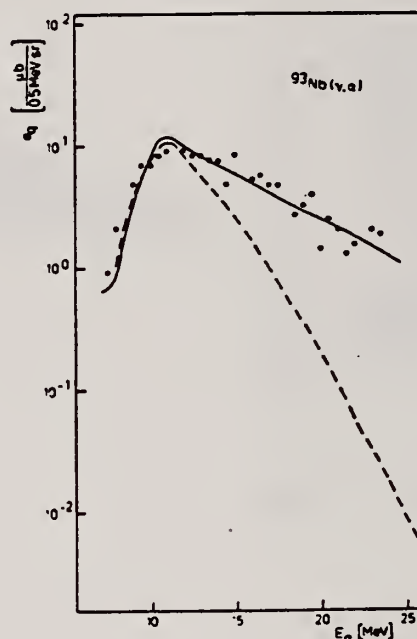


Fig. 7. Experimental data with statistical model calculations for the reaction  $^{93}\text{Nb}(\gamma, \alpha)$ . Broken line for  $E_{\gamma}^{\text{max}} = 50$  MeV (calculation). Full line for  $E_{\gamma}^{\text{max}} = 450$  MeV (fit).

TABLE 4

The integrated absorption cross sections and the percentage values of compound nucleus formation

$\Delta E_{\gamma}$ (MeV)	50-150	150-250	250-350	350-450	$\frac{\int \sigma_{\gamma \text{ tot}} dE_{\gamma}}{\int \sigma_{c\gamma} dE_{\gamma}^*)}$ (b · MeV)	$\sigma_{c\gamma}/\sigma_{\gamma \text{ tot}}$ (%)
$^{27}\text{Al}$ $\sigma_{\gamma \text{ tot}}$	6	10	15	12	4.3	
$\sigma_{\gamma \text{ tot}} = \sigma_{c\gamma}$	6.2		7.6		2.9	69
$^{40}\text{Ca}$ $\sigma_{\gamma \text{ tot}}$	8	15	22	17	6.2	
$\sigma_{c\gamma}$	7.2		10.1		3.75	60
$^{51}\text{V}$ $\sigma_{\gamma \text{ tot}}$	11	19	27	22	7.9	
$\sigma_{c\gamma}$	13		0.01		1.3	16.5
$^{93}\text{Nb}$ $\sigma_{\gamma \text{ tot}}$	19	35	50	39	15.3	
$\sigma_{c\gamma}$	5.8		5.9		2.3	15
$^{107}\text{Ag}$ $\sigma_{\gamma \text{ tot}}$	22	40	58	47	16.7	
$\sigma_{c\gamma}$	15		7.6		3.81	23

The  $\sigma_{\gamma \text{ tot}}$  values (in mb) used in the evaporation calculation in the  $\gamma$ -energy range  $E_{\gamma} = 50$ –450 MeV and corresponding best fit values  $\sigma'_{\gamma \text{ tot}}$  are given. The formation cross section of the compound nucleus  $\sigma_{c\gamma}$  is assumed to be equal to  $\sigma_{\gamma \text{ tot}}$  or  $\sigma'_{\gamma \text{ tot}}$ .

<sup>a)</sup>  $E_{\gamma} = 50$ –450 MeV.



METHOD	REF. NO.	hmg
	75 To 4	

REACTION	RESULT	EXCITATION ENERGY	SOURCE		DETECTOR		ANGLE
			TYPE	RANGE	TYPE	RANGE	
G,PI+	ABY	150-400	C	300,400	BBL-D		90
G,PI-	ABY	150-400	C	300,400	BBL-D		90
G,P	ABY	86-400	C	300,400	BBL-D		90

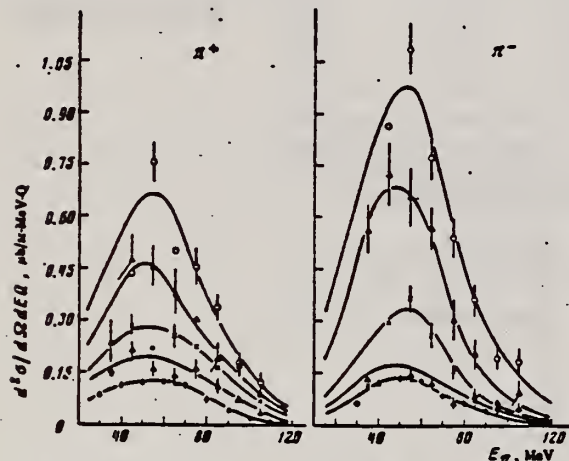


FIG. 1. Energy spectra of  $\pi^+$  and  $\pi^-$  mesons.  $E_{\pi}^{\max} = 300$  MeV,  $\theta_{\text{lab}} = 90 \pm 7^\circ$ . Points:  $\circ$ — $^{12}\text{C}$ ,  $\triangle$ — $^{28}\text{Si}$ ,  $\times$ — $^{40}\text{Ca}$ ,  $\diamond$ — $^{93}\text{Nb}$ ,  $\circ$ — $^{181}\text{Ta}$ .

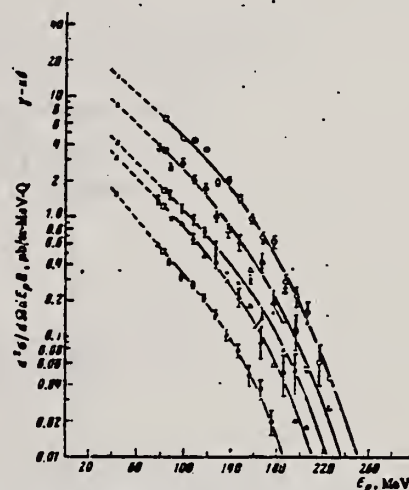


FIG. 3. Energy spectra of protons,  $E_p^{\max} = 300$  MeV,  $\theta_{\text{lab}} = 90 \pm 7^\circ$ . Points:  $\circ$ — $^{12}\text{C}$ ,  $\triangle$ — $^{28}\text{Si}$ ,  $\times$ — $^{40}\text{Ca}$ ,  $\diamond$ — $^{93}\text{Nb}$ ,  $\circ$ — $^{181}\text{Ta}$ ,  $\square$ —data from ref. 5,  $\bullet$ —data from ref. 6.

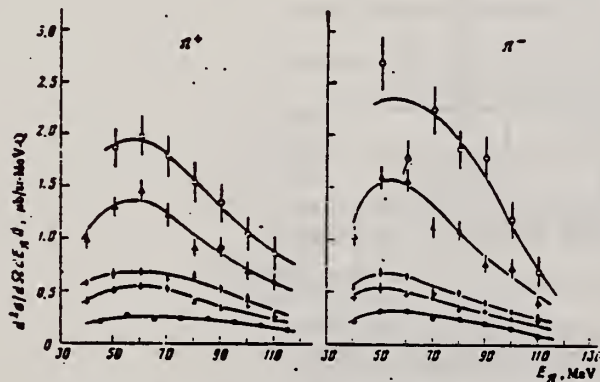


FIG. 2. Energy spectra of  $\pi^+$  and  $\pi^-$  mesons.  $E_{\pi}^{\max} = 400$  MeV,  $\theta_{\text{lab}} = 90 \pm 7^\circ$ . The points are the same as in Fig. 1.

FIG. 5. Dependence of yields of  $\pi$  mesons 1, protons 2, and the sum of  $\pi$ -meson and proton yields 4 as a function of mass number of the nucleus. The dashed line 3 is the theory. Points:  $\square$ —experimental differential cross sections for pions of all signs,  $\triangle$ —differential cross sections for protons emitted at the same angle  $\theta_{\text{lab}} = 90^\circ$ ,  $\circ$ —combined values of these differential cross sections. The statistical errors are shown.

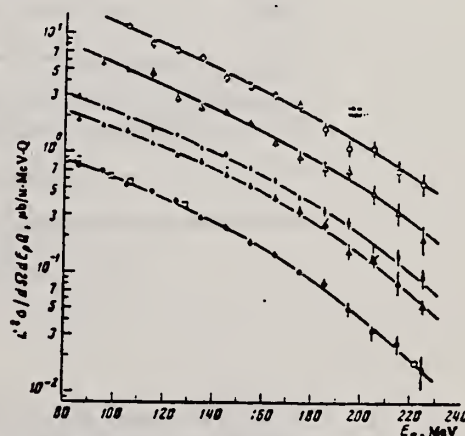
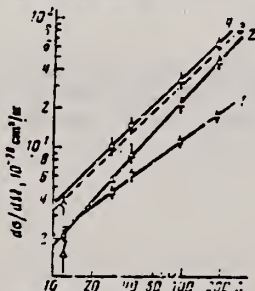


FIG. 4. Energy spectra of protons,  $E_p^{\max} = 400$  MeV,  $\theta_{\text{lab}} = 90 \pm 7^\circ$ . The points are the same as in Fig. 1;  $\square$ —data from ref. 7.

- 5 P.C.Murray et al., Phys.Rev. 94, 764 (54).
- 6 C.Levinthal et al., Phys.Rev. 82, 822 (51).
- 7 P.Dougan et al., LUSY Prep.1002 (1970).



ELEM. SYM.	A	Z
Nb	93	41
REF. NO.		
78 Be 2		rs

REACTION	RESULT	EXCITATION ENERGY	SOURCE		DETECTOR		ANGLE
			TYPE	RANGE	TYPE	RANGE	
G,G	LFT	1- 6	D	4- 6	SCD-D		DST

[illegible]

Fig. 3. Decay scheme of the 6465 keV level of  $^{91}\text{Nb}$  showing level energies and relative intensities normalized so that the intensity of the ground-state transition is taken to be 100. The level spins are those obtained by combining the results of the present work (table 1) and those reported in refs. <sup>3, 7</sup>.

TABLE 1  
 $\gamma$ -line energies  $E_\gamma$ , level energies  $E_i$  of  $^{93}\text{Nb}$ , angular distribution coefficients  $A$  and spins  $J^\pi$

Present work					Refs. <sup>3, 7</sup> ) <sup>a)</sup>	
$E_\gamma$ ( $\pm 3$ keV)	intensity	$A$ (exp)	$E_i$ ( $\pm 3$ keV)	$J^\pi$	$E_i$	$J^\pi$
5516	$280 \pm 5$	$0.06 \pm 0.04$	949	$\frac{13}{2}^+$	949.6	$\frac{13}{2}^+$
5486	$2 \pm 2$		979	$\frac{9}{2}^-, \frac{11}{2}^-, \frac{13}{2}^+$	979	$\frac{11}{2}^+$
5384	$47 \pm 2$	$0.02 \pm 0.07$	1081	$\frac{9}{2}^-, \frac{11}{2}^-, \frac{13}{2}^+$	1082.5	$\frac{9}{2}^+$
5168	$30 \pm 2$	$0.14 \pm 0.08$	1297	$\frac{9}{2}^-, \frac{13}{2}^+$	1297.8	$\frac{9}{2}^+$
4979	$12 \pm 3$		1486	$\frac{9}{2}^-, \frac{11}{2}^-, \frac{13}{2}^+$	1484	$\frac{9}{2}^-, \frac{11}{2}^-, \frac{13}{2}^+$
4971	$26 \pm 1$		1494	$\frac{9}{2}^-, \frac{11}{2}^-, \frac{13}{2}^+$	1491	$\frac{9}{2}^-, \frac{11}{2}^-, \frac{13}{2}^+$
4783	$31 \pm 1$		1682	$\frac{9}{2}^-, \frac{11}{2}^-, \frac{13}{2}^+$	1682.6	$\frac{9}{2}^-, \frac{11}{2}^-, \frac{13}{2}^+$
4514	$32 \pm 3$	$-0.19 \pm 0.12$	1951	$\frac{11}{2}^+$	1950.5	$\frac{11}{2}^+$
4095	$80 \pm 25$	$0.07 \pm 0.10$	2370	$\frac{9}{2}^-, \frac{13}{2}^+$	2360 <sup>b)</sup>	
3626	$80 \pm 25$	$-0.17 \pm 0.11$	2839	$\frac{11}{2}^+$	2810 <sup>b)</sup>	
6465	$100 \pm 2$	$0.04 \pm 0.05$	6465	$\frac{11}{2}^+$		

The spins  $J^\pi$  are based either on the values of  $A$  or on the assumption that the resonance level is deexcited by dipole transitions.

<sup>a)</sup> Only those levels of refs. <sup>3, 7</sup>) are listed which were also observed in the present work.

<sup>b)</sup> The reported energy uncertainty of these levels is  $\pm 20$  keV.

<sup>3</sup>I. J. van Heerden, W. R. McMurray and R. Saayman,  
 Z. Phys. **260** (1973) 9

<sup>7</sup>D. C. Kocher, Nucl. Data **B8** (1972) 527

TABLE 3  
 Values of  $R_T$ ,  $R$ ,  $\delta$ ,  $\sigma_e$ ,  $\Gamma_0/\Gamma$  and  $\Gamma_0$  of the 6465 keV level in  $^{93}\text{Nb}$

$R_T$ <sup>a)</sup>	$R$ <sup>b)</sup>	$\delta$ <sup>c)</sup> (eV)	$\sigma_e$ <sup>d)</sup> (mb)	$\Gamma_0/\Gamma$	$\Gamma$ (meV)
$1.022 \pm 0.011$	$0.004 \pm 0.003$	$6 \pm 2$	$1.6 \pm 0.7$	$0.12 \pm 0.03$	$38 \pm 17$

<sup>a)</sup>  $R_T$  is the ratio of scattering cross sections at  $T = 78^\circ\text{K}$  and room temperature  $T = 293^\circ\text{K}$  given for a  $13 \text{ g.cm}^2$  thick scatterer placed at an angle of  $60^\circ$  and a detector angle of  $135^\circ$  with respect to the incident beam.

<sup>b)</sup>  $R$  is the self-absorption ratio and is given for the same scatterer-detector geometry as that of  $R_T$  and for an absorber thickness of  $18.4 \text{ g.cm}^2$ .

<sup>c)</sup>  $\delta$  is the energy separation between the peak of the incident  $\gamma$ -line and the peak of the resonance level.

<sup>d)</sup>  $\sigma_e$  is the elastic scattering cross section.

METHOD

REF. NO.	
78 Fi 7	hg

REACTION	RESULT	EXCITATION ENERGY	SOURCE		DETECTOR		ANGLE
			TYPE	RANGE	TYPE	RANGE	
G,P	NOX	45-85	C	60-100	MAG-D		DST

Experimental data on the  $(\gamma, p)$  reaction at  $E_\gamma = 60-100$  MeV for targets in the range  $A = 7-93$  are compared with predictions based on a single-particle knock-out mechanism using shell model wavefunctions. The results show that this mechanism is more important than has generally been believed

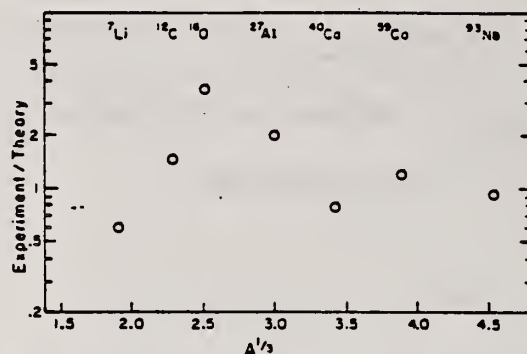


Fig. 2. The ratio of the measured photoproton emission populating low-lying states to the single-particle direct knock-out predictions is shown as a function of nuclear mass  $A$  for 80 MeV bremsstrahlung. Errors in the ratio, due to uncertainties in our calculations, are estimated to be a factor of  $\approx 1.5$ . Errors in the experimental data are negligible.

ELEM. SYM.	A	Z
NB	93	41
REF. NO.		hg
78 Ma 10		

REACTION	RESULT	EXCITATION ENERGY	SOURCE		DETECTOR		ANGLE
			TYPE	RANGE	TYPE	RANGE	
G,N	ABY	9-68	C	30-68	ACT		4PI
G,AN	ABY	13-68	C	30-68	ACT		4PI

Analysis is made of reactions interfering with photon activation analysis procedures.

The activation yield curves have been presented for a number of photonuclear reactions in the energy range from 30 to 68 MeV, in order to evaluate quantitatively the interferences due to competing reactions in multielement photon activation analysis. The general features of the yields as functions of both target mass number and excitation energy were elucidated from the data obtained, discussion being given on the results in terms of the reaction mechanism. Simultaneous neutron activation due to appreciable neutron production from the converter and surrounding materials has also been studied, and, finally, the magnitudes of interferences in real multielement analysis were given in the form of their energy dependences.

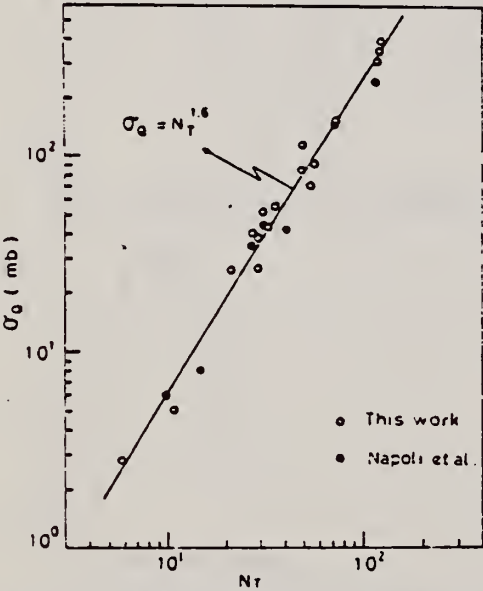


Fig. 2. Yield per equivalent quanta versus target neutron number.

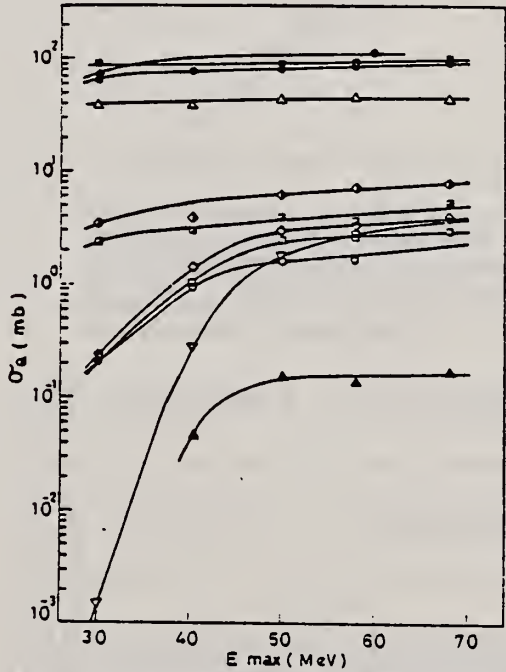


Fig. 7. Activation yield curves for the reactions on Y, Zr, Nb and Mo.  
◆ <sup>89</sup>Y(γ, n)<sup>88</sup>Y, ● <sup>90</sup>Zr(γ, n)<sup>89</sup>Zr, ○ <sup>90</sup>Zr(γ, pn)<sup>89</sup>Y,  
△ <sup>93</sup>Nb(γ, n)<sup>92m</sup>Nb, ▲ <sup>93</sup>Nb(γ, xn)<sup>88</sup>Y, ▣ <sup>100</sup>Mo(γ, n)<sup>99</sup>Mo,  
◊ <sup>97</sup>Mo(γ, p)<sup>96</sup>Nb, ▤ <sup>96</sup>Mo(γ, p)<sup>95m</sup>Nb, ◇ <sup>94</sup>Mo(γ, pn)<sup>92m</sup>Nb,  
□ <sup>92</sup>Mo(γ, 2n)<sup>90</sup>Mo, ▽ <sup>94</sup>Mo(γ, xn)<sup>89</sup>Zr.

(over)

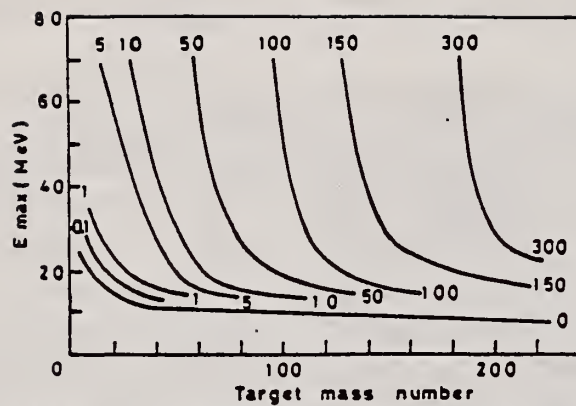


Fig. 9. Yields of the  $(\gamma, n)$  reactions as a function of bremsstrahlung maximum energy and target mass number. The numerical values in the figure are yields per equivalent quanta in mb.



ELEM. SYM.	A	Z
Nb	93	41

REF. NO.	egf
81 Va 2	

REACTION	RESULT	EXCITATION ENERGY	SOURCE		DETECTOR		ANGLE
			TYPE	RANGE	TYPE	RANGE	
\$G, SPL	ABY	THR*4	C	4*	ACT-I		4PI

The charge distribution of residual nuclei has been studied in the disintegration of  $^{93}\text{Nb}$  by bremsstrahlung with  $E_{\gamma, \text{max}} = 4.5 \text{ GeV}$ . Identification of the residual nuclei and determination of their yields were carried out by detecting the induced activity by means of a semiconductor  $\text{Ge(Li)}$  detector. Study of the charge distribution of isobars and comparison of the data obtained with the results of hadron-nucleus reactions permitted us to determine some regularities of the nuclear disintegration and to predict the probability of formation of residual nuclei which are hard to measure by the activation method. For quantitative estimates of the yields of the reaction products we used the five-parameter Rudstam formula. The nature and properties of the isobar and mass yields are discussed in comparison with calculations in terms of a two-step cascade-evaporative model.

\*4.5 GEV 39 FINAL Z,A

PACS numbers: 25.20. + y, 27.60. + j

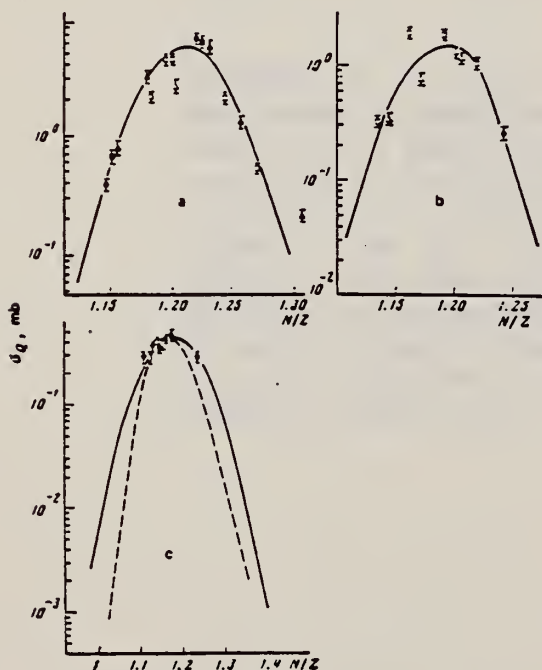


FIG. 1. Curves of the charge distribution of products of the reaction  $\text{Nb} + \gamma$  for the following mass intervals: a) 90-84, b) 83-75, c) 74-65. Points:  $\bullet$ -Nb,  $\blacksquare$ -Zr,  $\blacktriangle$ -Y,  $\circ$ -Sr,  $\square$ -Rb,  $\Delta$ -Br,  $\nabla$ -Se,  $\diamond$ -As,  $\circ$ -Ga,  $\times$ -Zn,  $\nabla$ -Co; c) calculation with the cascade-evaporative model<sup>4</sup> for the reaction  $\text{Mo} + p$  (in relative units); the dashed curve is for a proton energy 1800 MeV.

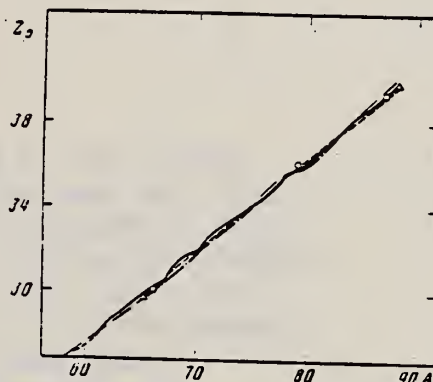


FIG. 2. Most probable charge of the charge distribution, as a function of the mass number of the product. Calculations of the cascade-evaporative model<sup>13</sup> for the reaction  $\text{Nb} + p$  with the following proton energies: 462 MeV (solid curve), 944 MeV (dashed curve), 1844 MeV (dot-dash curve). Points:  $\circ$ -data of the present work,  $\Delta$ -data of Ref. 13.

Residual nucleus	Type of yield	$\sigma_{\text{exp}}$ , mb (experiment)	$\sigma_{\text{calc}}$ , mb (theory)	$\sigma_{\text{exp}} / \sigma_{\text{calc}}$
$^{93}\text{Nb}$	C	$5.8 \pm 1.0$	5.10	9.56
$^{92}\text{Nb}$	C	$0.8 \pm 0.5$	7.16	0.91
$^{91}\text{Nb}$	C	$1.7 \pm 0.5$	5.98	0.90
$^{90}\text{Nb}$	C	$0.12 \pm 0.1$	2.08	0.17
$^{89}\text{Nb}$	C	$0.39 \pm 0.07$	0.63	0.57
$^{88}\text{Nb}$	C	$6.72 \pm 0.7$	5.63	1.31
$^{87}\text{Nb}$	C	$1.15 \pm 0.1$	1.63	0.97
$^{86}\text{Nb}$	C	$2.27 \pm 0.4$	2.18	1.03
$^{85}\text{Nb}$	C	$0.7 \pm 0.07$	0.77	0.90
$^{84}\text{Nb}$	C	$0.21 \pm 0.02$	0.22	0.94
$^{83}\text{Nb}$	C	$0.19 \pm 0.02$	1.17	0.85
$^{82}\text{Nb}$	C	$0.8 \pm 0.17$	2.29	1.19
$^{81}\text{Nb}$	C	$1.7 \pm 0.6$	3.99	0.95
$^{80}\text{Nb}$	C	$1.96 \pm 0.12$	2.18	2.44
$^{79}\text{Nb}$	C	$2.07 \pm 0.11$	0.85	0.93
$^{78}\text{Nb}$	C	$1.99 \pm 0.1$	2.12	1.13
$^{77}\text{Nb}$	C	$3.16 \pm 0.55$	0.90	2.32
$^{76}\text{Nb}$	C	$2.19 \pm 0.3$	0.89	2.11
$^{75}\text{Nb}$	C	$2.08 \pm 0.21$	0.99	2.11
$^{74}\text{Nb}$	C	$0.52 \pm 0.05$	0.77	0.65
$^{73}\text{Nb}$	C	$2.1 \pm 0.1$	1.37	1.06
$^{72}\text{Nb}$	C	$1.63 \pm 0.15$	0.33	1.33
$^{71}\text{Nb}$	C	$1.97 \pm 0.19$	1.06	1.83
$^{70}\text{Nb}$	C	$0.33 \pm 0.15$	0.33	1.03
$^{69}\text{Nb}$	C	$1.18 \pm 0.29$	0.82	1.43
$^{68}\text{Nb}$	C	$0.78 \pm 0.30$	0.36	0.85
$^{67}\text{Nb}$	C	$0.36 \pm 0.05$	0.67	1.00
$^{66}\text{Nb}$	C	$1.21 \pm 0.13$	0.36	1.07
$^{65}\text{Nb}$	C	$0.38 \pm 0.08$	0.13	2.36
$^{64}\text{Nb}$	C	$0.30 \pm 0.03$	0.21	1.40
$^{63}\text{Nb}$	C	$0.59 \pm 0.06$	0.39	0.87
$^{62}\text{Nb}$	C	$0.34 \pm 0.08$	0.35	1.06
$^{61}\text{Nb}$	C	$0.42 \pm 0.02$	0.23	1.83
$^{60}\text{Nb}$	C	$0.29 \pm 0.03$	0.23	2.15
$^{59}\text{Nb}$	C	$0.13 \pm 0.05$	0.09	1.89
$^{58}\text{Nb}$	C	$0.49 \pm 0.12$	0.09	4.6
$^{57}\text{Nb}$	C	$0.64 \pm 0.16$	0.05	10.5
$^{56}\text{Nb}$	C	$0.12 \pm 0.05$	0.05	2.4
$^{55}\text{Nb}$	C	$0.11 \pm 0.05$	0.09	15.8



## MOLYBDENUM

Z=42

*Molybdos* is the term first applied by the Greeks and Romans to describe minerals that were soft and lead-like in appearance. The word molybdenum itself was first introduced around 1816. Native molybdenum disulfide is a soft black mineral that looks like graphite. Up until the later part of the eighteenth century, both were sold under the same name: Molybdan, or molybdenum. The German writers called molybdenite "Wasserbley," a name suggestive of lead. Molybdenite was first identified by the Swedish chemist, Karl Wilhelm Scheele in 1778.



REF. Sven A. E. Johansson Phys. Rev. <u>97</u> , 434-43 (1955)			Mo		42
METHOD Synchrotron; ZnS counter; ion chamber			REF. NO. 55 Jo 1		NVB
REACTION	RESULT	EXCITATION ENERGY	SOURCE		ANGLE
			TYPE	RANGE	
G,P	RLY	THR - 65	C 65	SCI-D	14 - +

TABLE I. Target thickness and the constants  $a$  and  $b$  in the angular distribution curve  $a + (\sin\theta + b \sin\theta \cos\theta)^2$ .

Element	Target thickness mg/cm <sup>2</sup>	$a$	$b$
Carbon	182	0.32	0.80
Aluminum	274	0.58	1.35
Nickel	352	0.94	1.45
Molybdenum	295	0.62	2.00

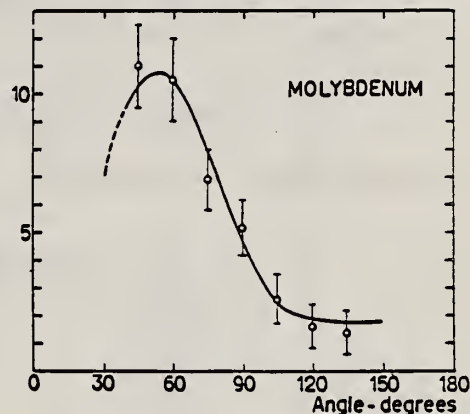


FIG. 5. The angular distributions of protons with an energy above 14 Mev.

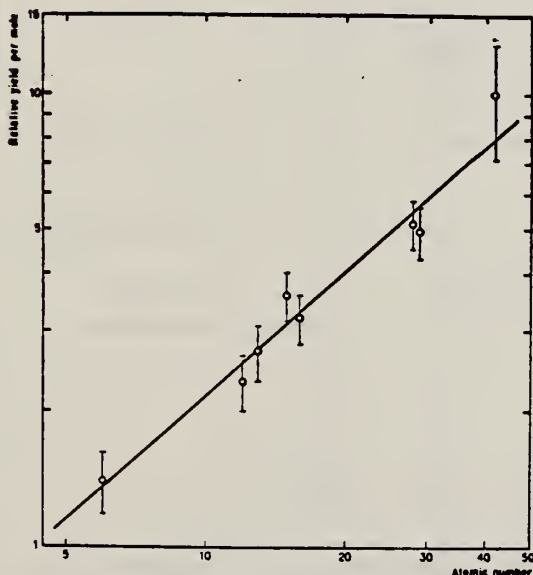


FIG. 10. The relative yield per mole for protons above 14 Mev as a function of the atomic number.



Ref.

K. Reibel, A.K. Mann  
 Phys. Rev. 118, 701 (1960)

Elem. Sym.

A

Z

Mo

42

Method

$\gamma$ 's from  $r^{19}(p,\gamma)$  reaction; protons from Vande Graaff; Ea 1.

Ref. No.

60 Re 1

JHH

Reaction	E or $\Delta E$	$E_0$	$\Gamma$	$\int \sigma dE$	$J\pi$	Notes
$(\gamma,\gamma)$	$E_\gamma \sim 7$					$\langle \sigma \rangle (E_p = 2.05 \text{ MeV}) = 1.4 \pm 0.2 \text{ mb}$

Method Betatron; proton yield; angular distribution; scintillator;  
ion chamber

Ref. No.	
63 M1 5	NVB

Reaction	E or ΔE	E <sub>0</sub>	Γ	∫σdE	Jπ	Notes
Mo(γ, xp)	Bremss. 22					<p>Angular distribution: <math display="block">Y(\theta) = a + b \sin^2 \theta (1 + p \cos \theta)^2</math> where <math>a = 46 \pm 10</math>; <math>b = 55 \pm 15</math>; <math>p = 0.2 \pm 0.2</math> and <math>b/a = 1.2 \pm 0.4</math>.</p> <p>Yield (<math>E_p &gt; 8</math> MeV): <math>(2.7 \pm 0.6) 10^5</math> protons/mole-r.</p> <p>Yield (<math>3.7 &lt; E_p &lt; 14</math>): <math>(26 \pm 3) 10^5</math></p>
<div><div><p>43/2      17/2      99/2</p><p>YIELD OF FAST PHOTOPROTONS</p></div><div><p>RATIO b/a IN <math>Y(\theta) = a + b \sin^2 \theta (1 + p \cos \theta)^2</math></p><p>RATIO b/a</p></div></div>						
<p>FIG. 2. The yields of fast photoprotons (<math>E_p &gt; 8</math> MeV) obtained from targets of various elements when irradiated with 22 MeV bremsstrahlung. The target thicknesses range from 351 to 572 are uniform 8 MeV for protons. The errors noted are statistical.</p> <p>FIG. 3. The anisotropy coefficient <math>b/a</math> for fast photoprotons (<math>E_p &gt; 8</math> MeV) from elements. The errors noted are statistical.</p> <div><p>FIG. 4. The values of the fast photoproton anisotropy coefficient <math>b/a</math> found by the present authors (●) and other workers (○) in the region of the periodic table <math>10 &lt; Z &lt; 50</math>. Arrows indicate out-of-scale points. The references to the results of other workers are given in Table II. The demarcations are explained in the text.</p></div>						

ELEM. SYM.	A	Z
Mo		42
REF. NO.		
66 Be 3		
JDM		

METHOO

Nuclear Resonance Scattering using N,G reactions.

REACTION	RESULT	EXCITATION ENERGY	SOURCE		DETECTOR		ANGLE
			TYPE	RANGE	TYPE	RANGE	
G,G	RLX	5 - 10	D	5 - 10	NAI-D	5 - 10	135

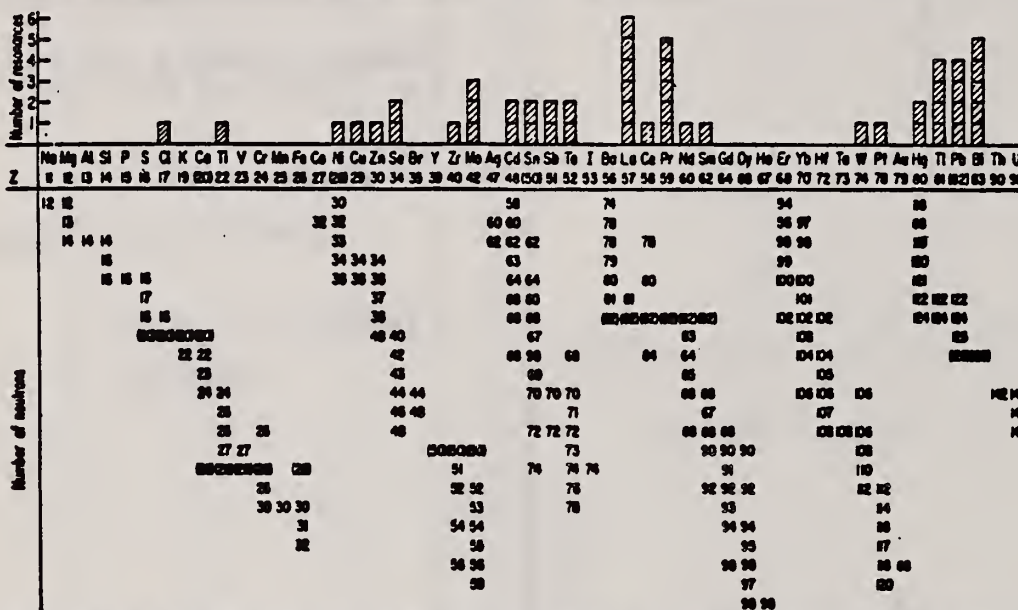


Fig. 3. Histogram of distribution of observed resonances among the different targets. The atomic number is given directly beneath the chemical symbol followed by the neutron numbers of the naturally occurring isotopes. Magic numbers are shown in brackets.

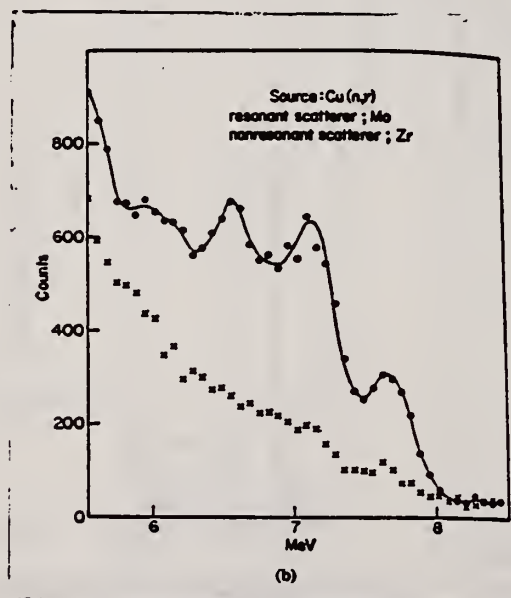


Fig.1.(b) Complex scattered spectrum from Mo excited by Cu capture rays (with Zr background).

TABLE III. List of effective cross sections.

Scatterer	Energy (MeV)	Gamma source	$\delta$ (mb)	Scatterer	Energy (MeV)	Gamma source	$\delta$ (mb)
Sm <sup>146</sup>	8.997	Ni	100	Su	7.01	Cu	110
Pr <sup>141</sup>	8.881	Cr	9	Nd	6.867	Co	30
La	8.532	Ni	6	Pr <sup>141</sup>	6.867	Co	3
Te	8.532	Ni	3 <sup>a</sup>	La	6.7	Ag	...
Cu	8.499	Cr	24	La	6.54	Co	12
Zr	8.496	Se	3050	Cd	6.474	Hg	110
Zn	8.119	Ni	13	Mo	6.44	Hg	25 <sup>a</sup>
Se	7.817	Ni	50	La	6.413	Ti	72
Se	7.76	K	90	Mo	6.413	Ti	10
Sb	7.67	V	...	Ti	6.413	Ti	25
Cd	7.64	Fe	40 <sup>a</sup>	W	6.3	Ti	...
Ni	7.64	Fe	7 <sup>a</sup>	Sb	6.31	Hg	6 <sup>a</sup>
Pr <sup>141</sup>	7.64	Fe	12 <sup>a</sup>	Ti	6.31	Hg	2 <sup>a</sup>
Ti	7.64	Fe	370 <sup>a</sup>	La	6.27	Ag	75
La	7.634	Cu	7	Pb <sup>208</sup>	6.15	Gd	...
Mo	7.634	Cu	11	Te	5.8	Ni	...
Bi <sup>209</sup>	7.634	Cu	4	La	6.12	Cl	35
Te	7.528	Ni	66 <sup>a</sup>	Pr <sup>141</sup>	6.12	Cl	110
Bi <sup>209</sup>	7.416	Se	100	Pt	5.99	Hg	40 <sup>a</sup>
Bi <sup>209</sup>	7.300	As	80 <sup>a</sup>	Ti	5.99	Hg	5 <sup>a</sup>
Pb <sup>208</sup>	7.285	Fe	4100	Pb <sup>208</sup>	5.9	Sr	...
Cl	7.285	Fe	34	Ce	5.646	Co	17
Pr <sup>141</sup>	7.185	Se	80	Bi <sup>209</sup>	5.646	Co	55
Ti	7.16	Cu	120	Pb <sup>208</sup>	5.53	Ag	70
La	7.15	Mn	50	Hg	5.44	Hg	75 <sup>a</sup>
Bi <sup>209</sup>	7.149	Ti	2000	Hg	4.903	Co	385

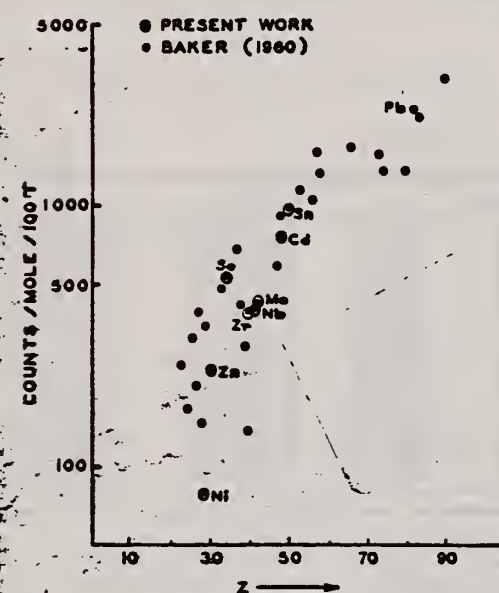
<sup>a</sup> High-energy component of a complex spectrum.  
<sup>b</sup> A broad scattered spectrum with no observable peak structure.  
<sup>c</sup> There are actually two lines of energies 7.647 and 7.633 MeV having equal intensities in the iron capture gamma spectrum. The cross section has therefore been corrected, although there is no possibility at present of deciding which line is responsible for each resonance.  
<sup>d</sup> Is probably an independent level in the complex spectrum of Ni  $\gamma$  rays on Te.  
<sup>e</sup> Rough estimate.  
<sup>f</sup> May be inelastic component from 7.528 level in Te.  
<sup>g</sup> The relative line intensities in this case are due to Groshov and co-workers.  
<sup>h</sup> No line is known for the source at this energy.  
<sup>i</sup> Difficult to resolve among the many source lines present at this energy.



REACTION	RESULT	EXCITATION ENERGY	SOURCE		DETECTOR		ANGLE
			TYPE	RANGE	TYPE	RANGE	
G,N	ABY	THR-22	C	22	THR	4-	DST

YIELD AT  $E_0 = 22$  MeV  
 $^{28}\text{Si}(n,p)$  ACTIVATION BY PHOTONEUTRONS

FIG. 3. The yields of fast photoneutrons from various elements as measured in the present work and by Baker. The present results have been normalized to Baker's measurements for lead.



ANISOTROPY COEFFICIENT  $-Q_2$

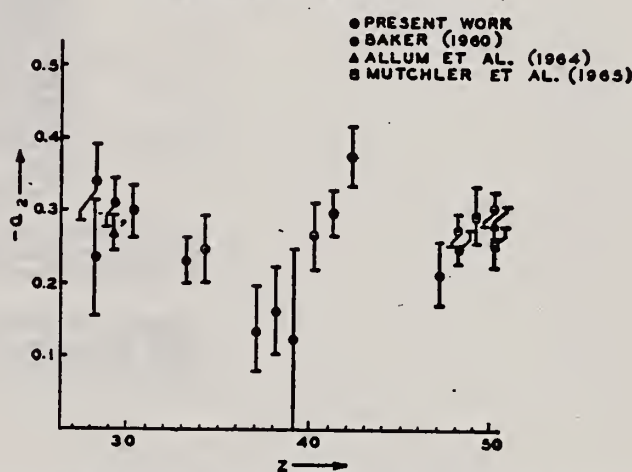


FIG. 2. The anisotropy coefficients  $a_2$  in the formula  $W(\theta) = a_0(1 + a_1P_1 + a_2P_2)$ , obtained in the present work, and those obtained by other workers in the same part of the Periodic Table.

TABLE I

Element	$a_0^*$	$a_1$	$a_2$
Nickel	77 (1.0±0.05)	0.14±0.04	-0.34±0.06
Zinc	236 (1.0±0.04)	0.06±0.03	-0.30±0.04
Selenium	525 (1.0±0.05)	0.10±0.04	-0.25±0.05
Zirconium	380 (1.0±0.05)	0.03±0.04	-0.27±0.05
Niobium	392 (1.0±0.03)	0.04±0.02	-0.30±0.03
Molybdenum	410 (1.0±0.03)	0.05±0.03	-0.41±0.04
Cadmium	755 (1.0±0.02)	0.05±0.01	-0.28±0.02
Tin	955 (1.0±0.02)	0.03±0.02	-0.30±0.02
Lead	2274 (1.0±0.02)	0.06±0.02	-0.48±0.02

\*For comparison purposes the experimental value of  $a_0$  for Pb has been normalized to coincide with that obtained by Baker and McNeill (1961) and is the yield per mole per 100 roentgen. All other values of  $a_0$  have also been quoted with the same normalization.

REF. J. W. Jury, J. S. Hewitt, and K. G. McNeill  
Can. J. Phys. 46, 1823 (1968)

ELEM. SYM. A Z  
Mo 42

METHOD REF. NO.  
68 Ju 1 EGF

REACTION	RESULT	EXCITATION ENERGY	SOURCE		DETECTOR		ANGLE
			TYPE	RANGE	TYPE	RANGE	
G,N	NOX	THR-22	C	22	THR	5-	DST

$$W(\theta) = a_0 + a_1 P_1 + a_2 P_2$$

TABLE I

Target element	Z	Energy	$a_0^*$	$a_1/a_0$	$a_2/a_0$
Vanadium	23	32	640 ± 50	0.11 ± 0.10	-0.09 ± 0.11
Chromium	24	22	365 ± 39	0.02 ± 0.08	0.00 ± 0.10
Manganese	25	22	450 ± 33	0.07 ± 0.05	-0.11 ± 0.06
Bromine	35	27	874 ± 54	0.05 ± 0.06	-0.15 ± 0.08
Molybdenum	42	22	610 ± 60	0.09 ± 0.05	-0.35 ± 0.06
Ruthenium	44	27	1100 ± 25	0.12 ± 0.02	-0.29 ± 0.03
Rhodium	45	27	1270 ± 47	0.06 ± 0.03	-0.14 ± 0.03
Palladium	46	27	1350 ± 29	0.26 ± 0.02	-0.12 ± 0.02
Antimony	51	27	2140 ± 62	0.04 ± 0.08	-0.25 ± 0.11
Lanthanum	57	27	1940 ± 70	0.12 ± 0.10	-0.52 ± 0.14
Praseodymium	59	30	1800 ± 58	0.20 ± 0.08	-0.40 ± 0.09
Platinum	78	27	2600 ± 52	0.17 ± 0.02	-0.15 ± 0.03
Lead	82	22	2274 ± 59	0.08 ± 0.08	-0.46 ± 0.09

\*The yield per mole per 100 r was normalized to a yield of 2274 for the lead sample at the same energy.



## METHOD

REF. NO.

71 Co 2

egf

REACTION	RESULT	EXCITATION ENERGY	SOURCE		DETECTOR		ANGLE
			TYPE	RANGE	TYPE	RANGE	
G,XN	ABI	36-64	C	10-64	BF3-I		4PI

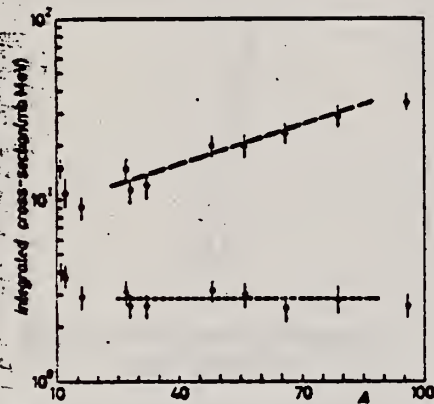
FAST N YIELD

Fig. 2.

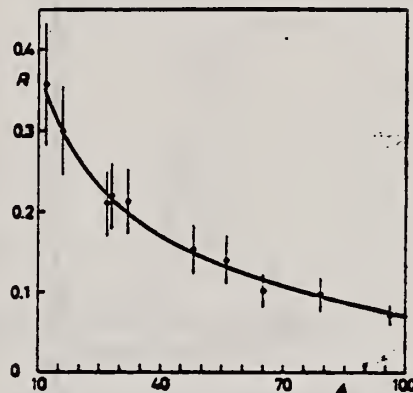


Fig. 3.

Fig. 2. - Experimental photoneutron cross-sections integrated over photon energy between 36 and 64 MeV and divided by  $NZ/A$  are plotted as a function of the mass number. Black dots are total cross-sections not corrected for neutron multiplicity; open circles represent fast neutron cross-sections (see text). The dashed lines are drawn only to guide the eye.

Fig. 3. - The ratio between fast and total photoneutron integrated cross-sections as a function of the mass number  $A$ . The solid line represents a fit of the ratios calculated for some nuclei by taking into account the theoretical neutron energy spectra given by GARRINI and ALLEN (1) and the efficiencies of our detector (see Fig. 1).

REF.

T. Mathasiri and S. A. E. Johansson  
Nucl. Phys. A167, 97 (1971)

ELEM. SYM.

A

Z

Mo

42

METHOD

REF. NO.

71 Me 1

egf

REACTION

RESULT

EXCITATION  
ENERGY

SOURCE

TYPE

RANGE

DETECTOR

TYPE

RANGE

ANGLE

 $G, F$ 

ABY

THR-900

C

300-900

FRG-I

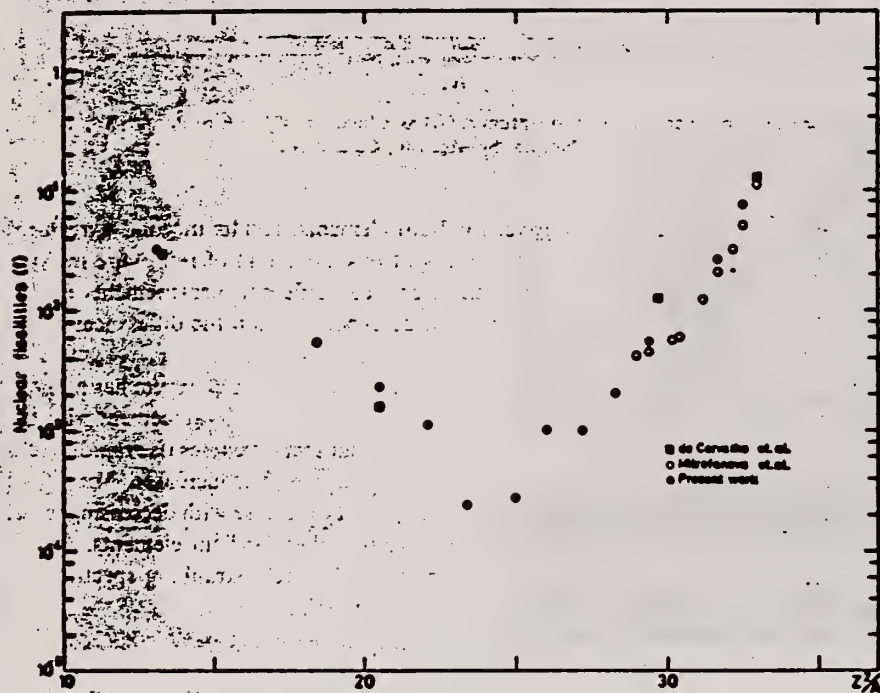
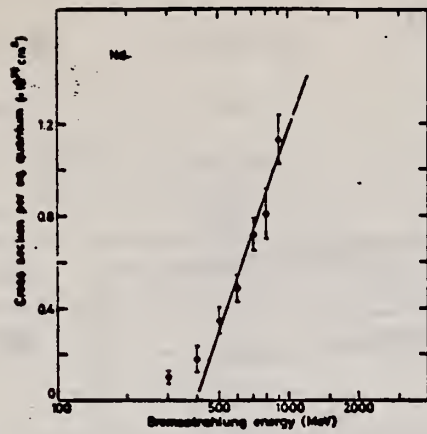
 $4\pi$ Fig. 2. Nuclear fissionities as a function of  $Z^2/A$ .

TABLE I

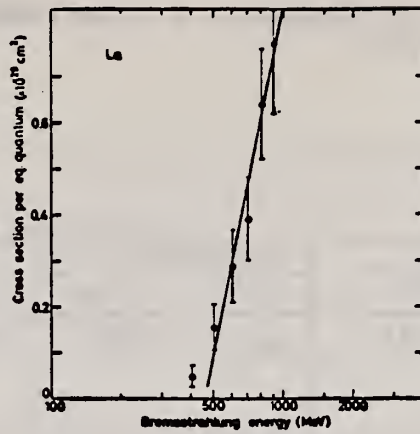
The constant fission cross sections above the threshold

Element	$\sigma_f$ (cm <sup>2</sup> )	Element	$\sigma_f$ (cm <sup>2</sup> )
Pb	$(5.0 \pm 0.2) \times 10^{-27}$	La	$(1.1 \pm 0.1) \times 10^{-29}$
Au	$(1.7 \pm 0.1) \times 10^{-27}$	Sn	$(4.3 \pm 1.1) \times 10^{-29}$
Ta	$(3.3 \pm 0.2) \times 10^{-28}$	Ag	$(8.4 \pm 2.0) \times 10^{-29}$
Yb	$(1.2 \pm 0.2) \times 10^{-28}$	Mo	$(1.7 \pm 0.4) \times 10^{-28}$
Ho	$(5.5 \pm 0.3) \times 10^{-29}$	Cu	$(6.6 \pm 1.2) \times 10^{-28}$
Gd	$(5.3 \pm 0.8) \times 10^{-29}$	Ni	$(5.8 \pm 0.1) \times 10^{-28}$
Nd	$(1.3 \pm 0.2) \times 10^{-29}$		

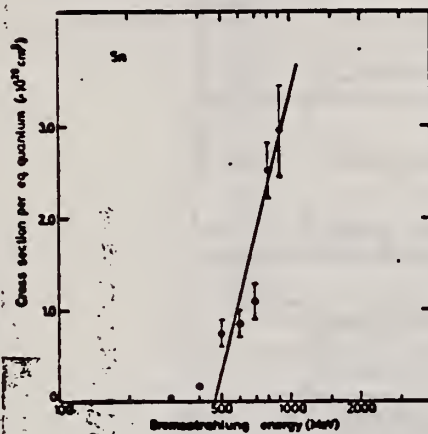
[over]



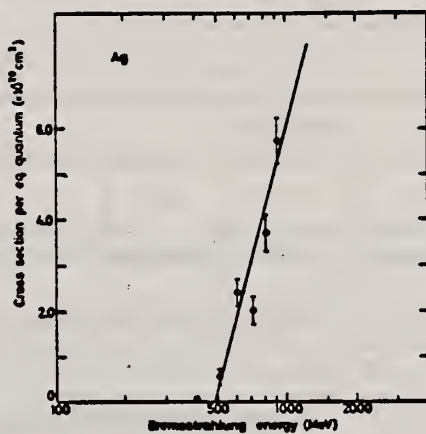
(g)



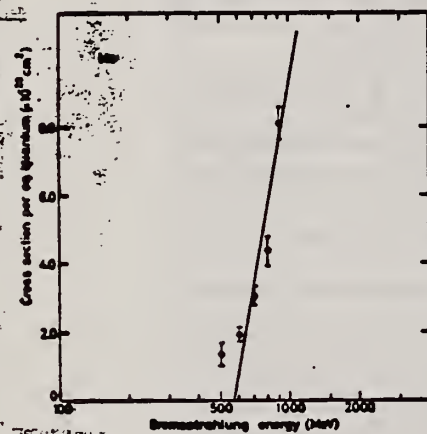
(h)



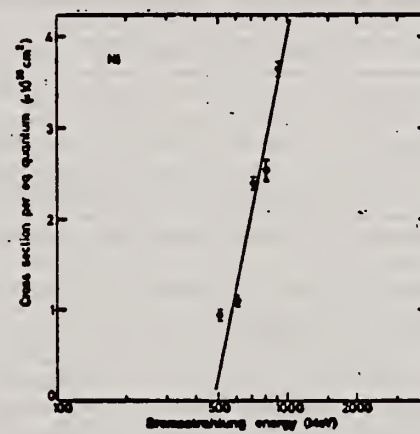
(i)



(j)



(k)



(l)

Fig. 1. Cross sections per equivalent quantum  $\sigma_q(E)$  as a function of  $\log E$ .

METHOD

REF. NO.

72 Ko 8

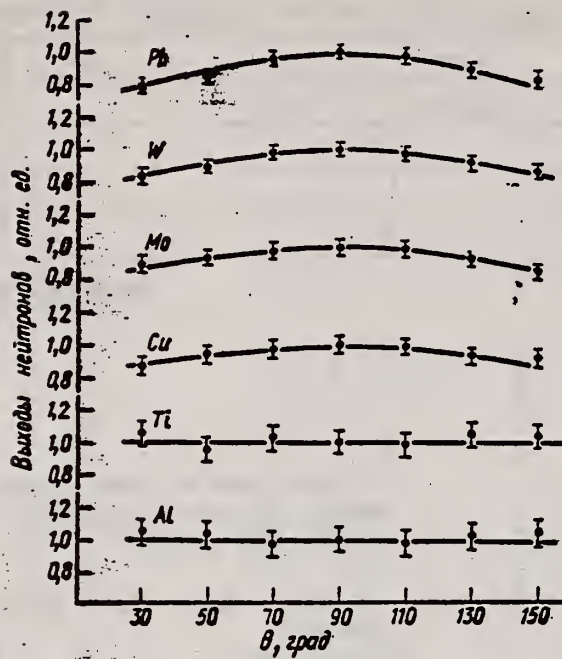
hmg

REACTION	RESULT	EXCITATION ENERGY	SOURCE		DETECTOR		ANGLE
			TYPE	RANGE	TYPE	RANGE	
G,N	NOX	6- 22	G	22	THR-I		DST

Мат-ри-аль	Энер-гия элек-трон. Мэв	Детек-тор	Угол, град							В/А
			30	50	70	90	110	130	150	
Al	22,5	P <sup>31</sup> (n, p)	1,05±0,08	1,03±0,08	0,97±0,08	1,0±0,08	0,98±0,08	1,02±0,08	1,04±0,08	Изотроп-ное
	22,5	Al <sup>27</sup> (n, p)	0,90±0,15	0,95±0,15	1,02±0,15	1,00±0,14	0,96±0,13	1,07±0,13	1,01±0,13	»
Ti	22,5	P <sup>31</sup> (n, p)	1,04±0,07	0,96±0,07	1,03±0,07	1,00±0,07	0,98±0,07	1,05±0,07	1,03±0,07	»
	22,5	Al <sup>27</sup> (n, p)	1,06±0,13	0,94±0,13	1,04±0,12	1,00±0,12	0,95±0,11	0,98±0,11	1,02±0,10	»
Ca	12,8	P <sup>31</sup> (n, p)	0,97±0,10	1,04±0,10	1,02±0,10	1,00±0,10	1,01±0,10	0,90±0,10	0,96±0,10	»
	17,0	P <sup>31</sup> (n, p)	1,03±0,07	0,97±0,07	1,00±0,07	1,00±0,07	1,06±0,07	0,95±0,07	0,88±0,07	»
	22,5	P <sup>31</sup> (n, p)	0,87±0,05	0,94±0,05	0,97±0,05	1,00±0,05	0,99±0,05	0,93±0,05	0,91±0,05	0,18±0,04
	22,5	Al <sup>27</sup> (n, p)	0,75±0,09	0,86±0,07	0,93±0,06	1,00±0,05	1,02±0,05	0,94±0,04	0,90±0,04	0,28±0,06
Mo	22,5	P <sup>31</sup> (n, p)	0,90±0,05	0,93±0,05	0,98±0,05	1,00±0,05	0,99±0,05	0,92±0,05	0,84±0,05	0,21±0,04
	22,5	Al <sup>27</sup> (n, p)	0,80±0,08	0,95±0,08	0,95±0,07	1,00±0,06	0,94±0,05	0,83±0,04	0,72±0,04	0,44±0,08
	22,5	Al <sup>27</sup> (n, α)	0,72±0,08	0,84±0,08	0,89±0,08	1,00±0,08	0,95±0,08	0,87±0,08	0,63±0,08	0,78±0,18
W	22,5	P <sup>31</sup> (n, p)	0,85±0,04	0,90±0,04	0,98±0,04	1,00±0,04	0,98±0,04	0,92±0,04	0,87±0,04	0,25±0,04
	22,5	Al <sup>27</sup> (n, p)	0,78±0,06	0,84±0,06	0,89±0,05	1,00±0,05	0,97±0,04	0,86±0,04	0,75±0,04	0,54±0,06
Pb	22,5	P <sup>31</sup> (n, p)	0,79±0,04	0,85±0,04	0,96±0,04	1,00±0,04	0,98±0,04	0,88±0,04	0,84±0,04	0,36±0,03
	22,5	Al <sup>27</sup> (n, p)	0,70±0,09	0,81±0,08	0,94±0,07	1,00±0,06	0,94±0,06	0,80±0,05	0,69±0,05	0,69±0,12

(over)





Угловое распределение быстрых фотонейтронов из Al, Ti, Cu, Mo, W, Pb, облучаемых электронами с энергией 22,5 Мэв. Детектор  $^{235}\text{Si}$ .



REF. R.F. Barrett, J.R. Birkelund, B.J. Thomas, K.S. Lam, and H.H. Thies Nucl. Phys. <u>A210</u> , 355 (1973)			ELEM. SYM.	A	Z
			Mo		42
METHOD			REF. NO.		
			73 Ba 20		egf
REACTION	RESULT	EXCITATION ENERGY	SOURCE		ANGLE
			TYPE	RANGE	
G,N	NOX	THR- 27	C	10- 27	4PI

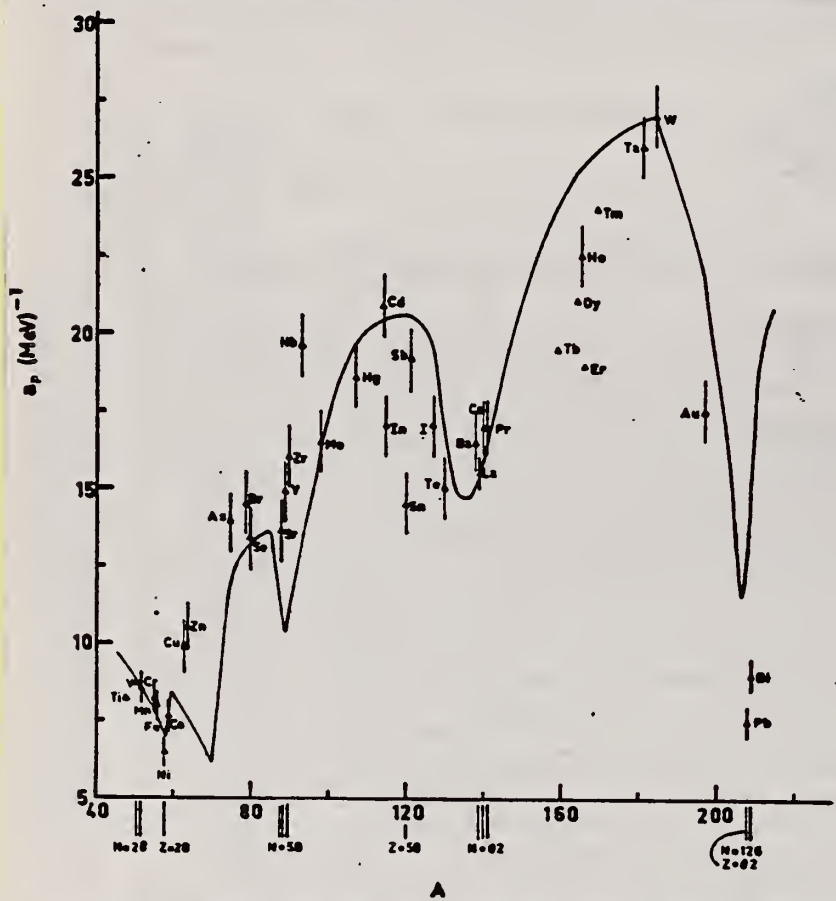


Fig. 12. Experimental values of the level density parameter  $a_p$  (Fermi gas formula plus pairing correction) versus atomic number  $A$ . The continuous curve is a least-squares fit to the data of a theoretical calculation from Newton <sup>1,2</sup>.

- 1 H. Baba and S. Baba, Japan Atomic Energy Research Institute report JAERI-1183 (1969).
- 2 H. Baba, Nucl. Phys. A159, 625 (1970).
- 15 T.D. Newton, Can. J. Phys. 34, 804 (1956).

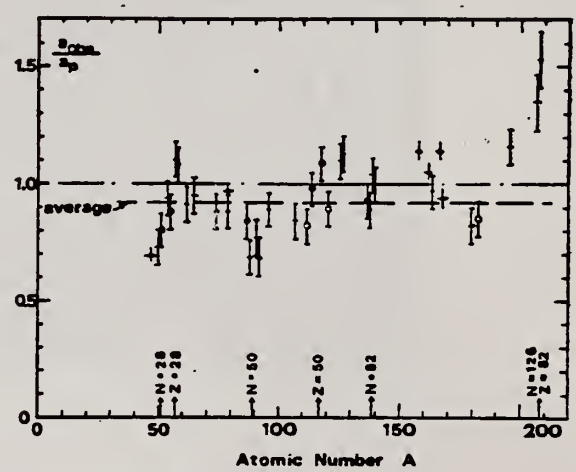


Fig. 15. Ratio  $a_{ave}/a_p$  versus atomic number  $A$ . Here  $a_{ave}$  is the level density parameter taken from the neutron resonance work of refs. <sup>1,2</sup>, and  $a_p$  is the level density parameter derived from the present  $(\gamma, n)$  work. Filled circles represent points where nuclei in the neutron resonance and in the  $(\gamma, n)$  experiment were the same. Open circles represent points where the respective nuclei were approximately matched. Triangles represent points which are based on measurement of neutron mean energies at two bremsstrahlung energies only.

(over)

TABLE 3 (continued)

Target	$N$ (residual nucleus) <sup>a)</sup>	Goodness of fit <sup>b)</sup> no. p.c.	$\bar{E}_0(24)$ (MeV) <sup>c)</sup>	$T$ (MeV) <sup>d)</sup>	$a_p$ (MeV <sup>-1</sup> ) <sup>e)</sup>	$a_{nb}$ (MeV <sup>-1</sup> ) <sup>f)</sup>	$a_{nb}/a_p$
Y	49 100%	G	1.30		14.9- <sup>88</sup> Y	10.17- <sup>90</sup> Y	0.68
Zr	49 52%	F	1.28		16.0- <sup>99</sup> Zr	12.2- <sup>91</sup> Zr	0.77
	50 11%						
	51 17%						
	53 17%						
	55 3%						
Nb	51 100%	F	1.28		19.6- <sup>92</sup> Nb	13.15- <sup>94</sup> Nb	0.68
Mo	49 16%	G	1.27		16.5- <sup>99</sup> Mo	14.7- <sup>97</sup> Mo	0.89
	51 9%						
	52 16%						
	53 17%						
	54 10%						
	55 24%						
	57 8%						
Ag	59 51%	V.P.	1.27	0.55	18.6- <sup>107</sup> Ag	15.61- <sup>108</sup> Ag	0.84
	61 49%						
Cd	57 1%	V.P.	1.24	0.54	20.9- <sup>111,4</sup> Cd	17.0- <sup>112</sup> Cd	0.82
	61 12%						
	62 13%						
	63 24%						
	64 12%						
	65 29%						
	67 8%						
In	63 4%	V.P.	1.26	0.57	17.0- <sup>114</sup> In	16.66- <sup>114</sup> In	0.98
	65 96%						
Sn	65 14%	V.P.	1.38	0.73	14.5- <sup>118</sup> Sn	15.9- <sup>118</sup> Sn	1.09
(Z = 50)	66 8%						
	67 24%						
	68 9%						
	69 33%						
	71 5%						
	73 6%						
Sb	69 57%	V.P.	1.2	0.68	19.2- <sup>121</sup> Sb	17.0- <sup>121</sup> Sb	0.89
	71 43%						
Te	69 2%	V.P.	1.36	0.83	15.0- <sup>127</sup> Te	17.0- <sup>127</sup> Te	1.13
	71 5%						
	72 7%						
	73 19%						
	75 32%						
	77 34%						
I	73 100%	F	1.23	0.70	17.0- <sup>126</sup> I	17.02- <sup>126</sup> I	1.00

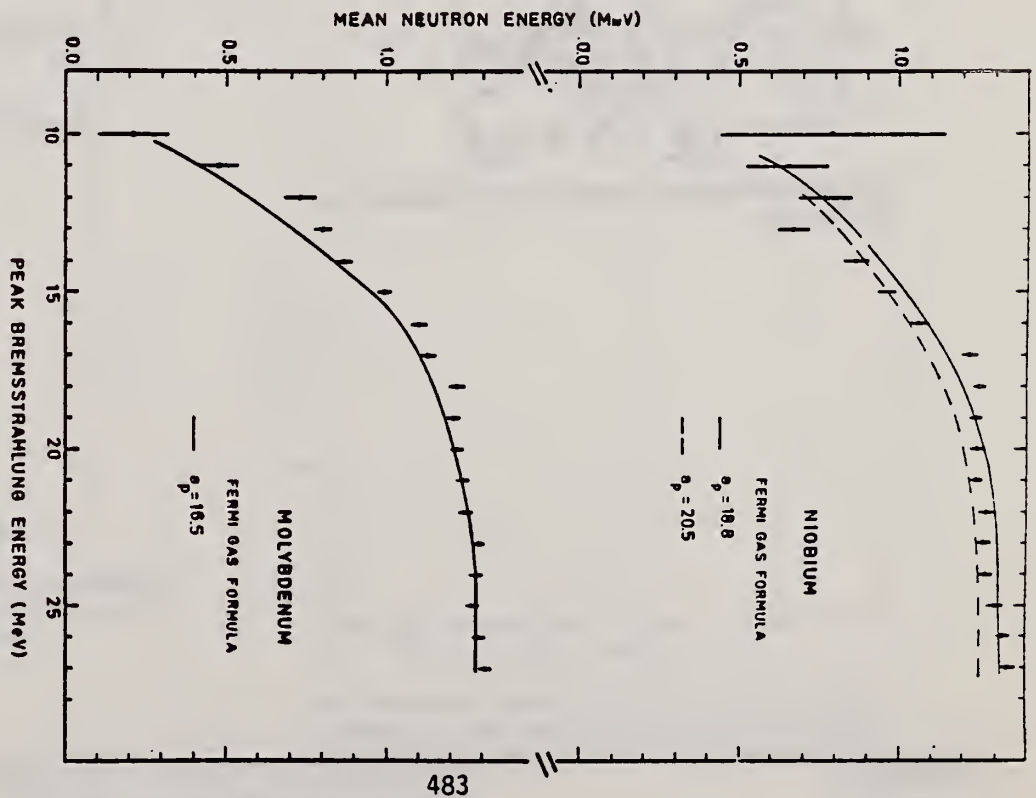


Fig. 8. Same as fig. 5, for niobium and molybdenum.

<sup>a)</sup> Neutron numbers and abundances of respective residual nuclei in  $(\gamma, n)$  experiments.

<sup>b)</sup> These give an assessment of the goodness of fit of a calculated  $\bar{E}_0$  versus  $E_0$  curve to the observed data, using the Fermi gas level density formula both without and with pairing corrections.

<sup>c)</sup> Bremsstrahlung photon neutron mean energies  $\bar{E}_0$  for peak bremsstrahlung energy  $E_0 = 24$  MeV.

<sup>d)</sup> Nuclear temperature from fit with constant-temperature formula.

<sup>e)</sup> Level density parameter  $a_p$  derived from the present  $(\gamma, n)$  experiment, using a Fermi gas formula plus pairing correction, and corresponding residual nucleus (the atomic weight shown is the weighted average of atomic weights of the respective isotopes present).

<sup>f)</sup> As column 7, but using data on n-resonance absorption from refs. 1, 2).

<sup>g)</sup> Measurements of  $\bar{E}_0(E_0)$  for these nuclei were made only for  $E_0 = 21, 23$  and 24 MeV.

REF. V.G. Vlasenko, V.A. Gol'dshtein, A.V. Mitrofanova, V.I. Noga,  
Yu.N. Ranuuk, V.I. Startsev, P.V. Sorokin, Yu.N. Telegin  
Yad. Fiz. 23, 504 (1976)  
Sov. J. Nucl. Phys. 23, 265 (1976)

ELEM. SYM.	A	Z
Mo		42
REF. NO.		
76 V1 1		hmg

METHOD

REACTION	RESULT	EXCITATION ENERGY	SOURCE		DETECTOR		ANGLE
			TYPE	RANGE	TYPE	RANGE	
E, E/	ABX	100-500	D	1* 2	MAG-D		DST

Inelastic electron scattering has been used to measure the total hadronic cross sections for absorption of photons with energy 150-500 MeV by nuclei of C, Al, Ni, Mo, and W. The results obtained are compared with calculations carried out in the impulse approximation.

\*E IN GEV, 1.2, 1.36

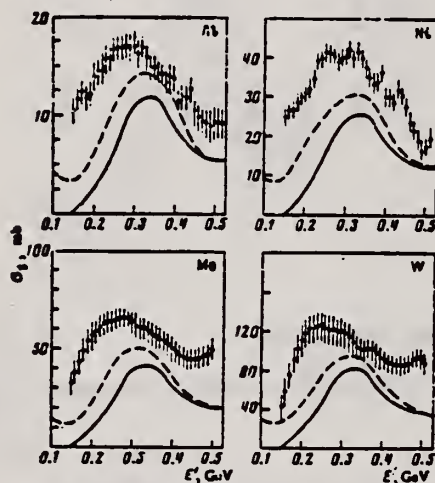


FIG. 5. Total hadronic cross sections for absorption of photons by nuclei.

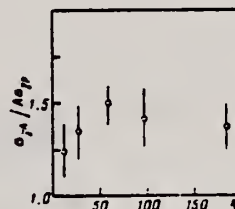


FIG. 6. The ratio  $\sigma_{T,A}/A\sigma_{T,p}$  as a function of  $A$  for  $k=0.32$  GeV.

REACTION	RESULT	EXCITATION ENERGY	SOURCE		DETECTOR		ANGLE
			TYPE	RANGE	TYPE	RANGE	
G, NA24	ABY	THR-999	C	400-999	ACT-I		4PI

999=1 GEV

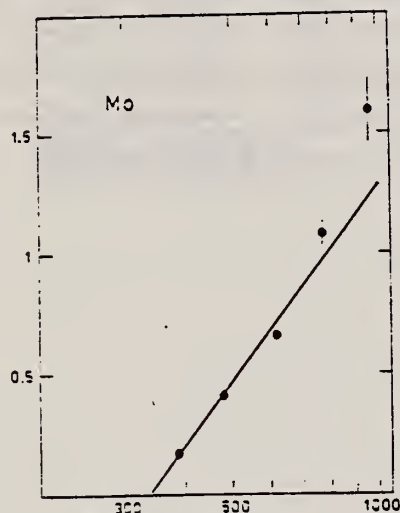


Fig. 1a-j. Bremsstrahlung energy (MeV)

Fig. 1a-j. The measured yield as a function of bremsstrahlung end point energy. The error bars give the statistical errors in the numbers of  $\gamma$ -quanta detected. The solid lines are fitted to the yield points with the least-squares method. The yield from Cu (Fig. 1a) is measured in [1] and has been recalculated using the monitor curve of [5]

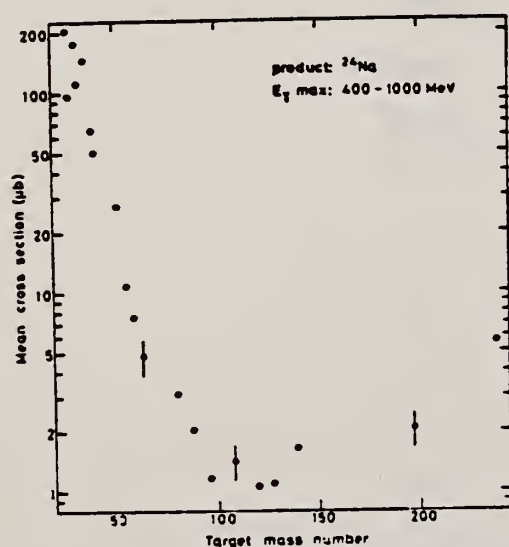


Fig. 2. The mean cross section in the energy range 400 to 1000 MeV calculated from the yields of Figure 1 in this work and of Figures 1 to 6 in [1]. The error bars in some points

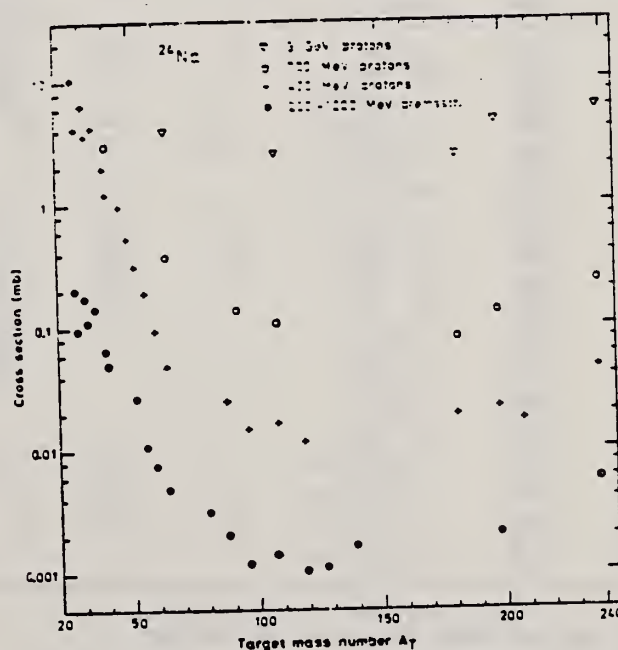


Fig. 4. Mean cross sections of the present work and of [1] (●) compared with the cross sections in proton irradiations: + 400 MeV from [4], ○ 700 MeV from [16] and an extrapolated value from [17], ▽ 3 GeV from [18]



REF. M. Schumacher, F. Smend, W. Mückenheim, P. Rullhusen, H.G. Börner  
Z. Phys. A300, 193 (1981)

ELEM. SYM.	A	Z
Mo		42
REF. NO.		egf
81 Sc 6		

METHOD					
REACTION	RESULT	EXCITATION ENERGY	SOURCE		ANGLE
			TYPE	RANGE	
G, G	ABX	7.7		7.7	90

Elastic scattering by nuclei in the range of mass numbers between 64 and 238 has been studied with monochromatic photons in the energy range between 2 and 8 MeV. These photons were provided either by a Ti( $n, \gamma$ ) source installed in the tangential through channel of the Grenoble high flux reactor, or by  $^{24}\text{Na}$  and  $^{56}\text{Co}$  sources produced by deuteron bombardment of Al or Fe at the Göttingen cyclotron. The photoexcitation of 23 nuclear levels has been observed and the decay properties and groundstate widths of the majority of these levels have been determined. For the lead scattering target the coherent elastic differential cross section has been studied in detail. There is evidence that below the photo-neutron threshold the elastic scattering via virtual photoexcitation of the nucleus can be approximated by extrapolating the real part of the Giant Dipole Resonance amplitude along a Lorentzian curve. Coulomb corrections to Delbrück scattering seem to play a small role at 6.5 MeV.

6.759, 7.168 MEV

Table 4. Properties of levels observed by photoexcitation.  $(d\sigma/d\Omega)^{\text{NRF}}$ : experimental differential cross section per identified isotope or element for resonance scattering through  $\Theta = 90^\circ$ .  $I^\pi$ : spin-parity of excited level;  $W(\Theta)$ : angular correlation function;  $g = (2I_{\text{ex}} + 1)/(2I_{\text{g}} + 1)$ ;  $\Gamma_0$ : radiative groundstate transition width,  $\Gamma$ : total level width. Errors in the last digits are given in parentheses

Isotope	$E_\gamma$ (MeV)	$(d\sigma/d\Omega)^{\text{NRF}}$ ( $\mu\text{b/sr}$ )	$I^\pi$	$\Gamma_0/\Gamma^a$	$W(\Theta)g\Gamma_0^2/\Gamma$ (meV)	$\Gamma_0^c$ (meV)	$\Gamma_0^d$ (meV)
$^{238}\text{U}$	2.754	13 (4)	(1)	0.77	0.145	0.084	-
$^{238}\text{U}$	3.254	421 (5)	$1^-$	0.24	0.83	1.5	0.52(15) <sup>d</sup>
$^{209}\text{Bi}$	6.555	2.1 (4) $\cdot 10^2$	-	-	0.74	0.74 <sup>b</sup>	-
$^{209}\text{Bi}$	7.168	1.7 (3) $\cdot 10^3$	$9/2^-^a$	1.00	710	786	820 (40) <sup>a</sup>
$^{203}\text{Tl}$	6.418	8.75(30) $\cdot 10^3$	$1/2^+$	0.28	30	102	82 (15) <sup>a</sup>
Tl	6.759	7 (3)	-	-	-	-	-
Hg	6.555	68 (17)	-	-	-	-	-
$^{186}\text{W}$	6.418	5.2 (3) $\cdot 10^2$	$1^-^a$	0.32	1.75	2.4	-
$^{184}\text{W}$	6.555	9.8 (10) $\cdot 10^2$	(1)	0.52	3.44	2.9	-
$^{184}\text{W}$	6.759	46 (10)	(1)	0.58	0.17	0.13	-
$^{181}\text{Ta}$	3.010	174 (17)	-	0.72	0.42	0.59	-
$^{181}\text{Ta}$	6.418	62 (4)	-	0.73	0.2	0.27 <sup>c</sup>	-
$^{181}\text{Ta}$	6.759	4.8 (12)	-	-	0.018	0.018 <sup>b</sup>	-
$^{165}\text{Ho}$	6.418	10.3 (30)	-	-	0.035	0.035 <sup>b</sup>	-
$^{165}\text{Ho}$	6.759	5.6 (14)	-	-	0.021	0.021 <sup>b</sup>	-
Nd	2.754	2.6 (5)	-	-	-	-	-
Nd	3.254	14.0 (10)	-	-	-	-	-
Ce	6.759	13.4 (10)	-	-	-	-	-
$^{121}\text{Sb}$	3.452	2.20 (5) $\cdot 10^3$	-	0.60	2.9	4.9 <sup>b</sup>	-
$^{100}\text{Mo}$	6.418	1.53 (4) $\cdot 10^4$	$1^-^a$	0.88	52	26	25 (8) <sup>a</sup>
$^{94}\text{Mo}$	6.555	4.4 (4) $\cdot 10^3$	(1)	0.33	15	21	-
Mo	6.759	6.2 (15)	-	-	-	-	-
Mo	7.168	8.2 (26) $\cdot 10^2$	-	-	-	-	-

<sup>a</sup> [11] <sup>b</sup>  $W(\Theta)g\Gamma_0/\Gamma = 1$  assumed <sup>c</sup>  $W(\Theta)g = 1$  assumed

<sup>d</sup> [28] (a small correction has been applied to the data of [28])

<sup>e</sup> Upper limits in case not all the transitions to lower levels were observed

<sup>f</sup> Present work

<sup>g</sup> Previous work

(OVER)



**Table 2.** Elastic differential cross sections  $d\sigma/d\Omega$  ( $\theta=90^\circ$ ) in  $\mu\text{b}\cdot\text{sr}$  measured with the  $\text{Ti}(n,\gamma)$  source and compared with theoretical predictions.  $n$ : predicted number of levels in a  $\Delta E=25$  eV interval at 6.5 MeV. Errors in the last digits are given in parentheses

Scattering target	6.418 MeV		6.555 MeV		6.759 MeV		7.168 MeV		$n$
	exp.	th.	exp.	th.	exp.	th.	exp.	th.	
$^{238}\text{U}$	23 (12)	10.3	-	-	-	-	-	-	45
$^{209}\text{Bi}$	-	-	219(39) <sup>b,c</sup>	8.0	12 (4)	7.4	$1.5(3) \cdot 10^5$ <sup>b,c</sup>	5.7	0.1
$^{208}\text{Pb}$	7.0(15)	8.6	-	-	6.5(11)	7.4	-	-	0.05
$^{205}\text{Tl}$	2586 (92) <sup>a,c</sup>	7.5	-	-	13 (3) <sup>b</sup>	6.0	-	-	0.4
$^{201}\text{Hg}$	12 (3)	7.8	74(17) <sup>b</sup>	6.5	6.7(15)	6.4	-	-	3.4
$^{208}\text{W}$	159 (10) <sup>a,c</sup>	6.6	306(33) <sup>a,c</sup>	6.3	20 (2) <sup>a,c</sup>	5.6	-	-	13
$^{181}\text{Ta}$	68 (4) <sup>a,c</sup>	6.3	-	-	10.1(12) <sup>b,c</sup>	5.3	-	-	28
$^{165}\text{Ho}$	15 (3) <sup>b</sup>	4.7	-	-	9.5(14) <sup>b</sup>	3.9	-	-	18
$^{140}\text{Ce}$	4.1(21)	4.1	-	-	17 (1) <sup>b,c</sup>	3.6	-	-	0.04
$^{116}\text{Sn}$	4.2(13)	3.0	-	-	2.5 (5)	2.7	-	-	1.9
$^{98}\text{Mo}$	1,474 (44) <sup>a,c</sup>	2.5	407(39) <sup>a,c</sup>	2.5	8.5(15) <sup>b,c</sup>	2.3	817(258) <sup>b,c</sup>	2.0	0.5
$^{64}\text{Zn}$	2.4 (8)	1.6	-	-	1.8 (5)	1.5	-	-	0.3

<sup>a</sup> Transitions to excited states observed

<sup>b</sup> Photoexcitation identified from size of differential cross section

<sup>c</sup> Photoexcitation reported in [11]



11b  
A=92

11b  
A=92

11b  
A=92



REF. A. El Sioufi, P. Erdos and P. Stoll  
Helv. Phys. Acta 30, 265 (1957)

ELEM. SYM.	A	Z
Mo	92	42

METHOD

REF. NO.  
57 El 1  
egf

REACTION	RESULT	EXCITATION ENERGY	SOURCE		DETECTOR		ANGLE
			TYPE	RANGE	TYPE	RANGE	
G,NP	ABI	19- 30	C	32	ACT-I		4PI

Tabelle 1.  
Zusammenstellung der gem. W. Q.

Reaktion	Q-Wert MeV	MeV barn	Verhältnis der Querschnitte
$\text{Zn}^{66}(\gamma, np)\text{Cu}^{66})$	18,65	0,02	$\frac{\sigma \text{Zn}^{66}(\gamma, p)}{\sigma \text{Zn}^{66}(\gamma, np)} = 3,6 \pm 0,5$
$\text{Zn}^{66}(\gamma, p)\text{Cu}^{67\text{**}})$	10,01	0,08	
$\text{Zn}^{66}(\gamma, 2n)\text{Zn}^{64}$	20,82	0,08	$\frac{\sigma \text{Zn}^{66}(\gamma, np)}{\sigma \text{Zn}^{66}(\gamma, 2n)} = 0,25$
$\text{Mo}^{92}(\gamma, np)\text{Nb}^{90}$	19,5	0,02	
$\text{Mo}^{92}(\gamma, p)\text{Nb}^{91}$		0,09	$\frac{\sigma \text{Mo}^{92}(\gamma, p)}{\sigma \text{Mo}^{92}(\gamma, np)} = 4,5$
*) $\sigma_{\text{max}}$ : 5,3 mb bei $E_{\gamma} = 27 \pm 0,5$ MeV $\Gamma = 3,7$ MeV.			
**) $\sigma_{\text{max}}$ : 11,5 mb bei $E_{\gamma} = 22 \pm 0,5$ MeV $\Gamma = 6,4$ MeV.			



REF.

A. Hofmann, P. Stoll  
 Helv. Phys. Acta 31, 591 (1958)

ELEM. SYM.	A	Z
Mo	92	42
REF. NO.		
58 Ho 1		egf

METHOD

REACTION	RESULT	EXCITATION ENERGY	SOURCE		DETECTOR		ANGLE
			TYPE	RANGE	TYPE	RANGE	
G, NP	ABI	19- 32	C	32	ACT-I		4PI

( $\gamma$ ,np) yields include ( $\gamma$ ,d).

Tabelle I

Reaktion	Q-Wert MeV	I.W.Q. $\bar{\sigma}$ MeV barn	$\sigma_{\max}$ mb	$E_{\max}$ MeV	$\Gamma$ MeV
Ca <sup>40</sup> ( $\gamma$ , pn) K <sup>38</sup>	-24,3	0,005	2,4	30 $\pm$ 1	2,1
Zn <sup>64</sup> ( $\gamma$ , pn) Cu <sup>63</sup>	-18,36	0,03			
Zn <sup>66</sup> ( $\gamma$ , pn) Cu <sup>64</sup>	-18,65	0,031	7,2	28 $\pm$ 1	4
Zn <sup>68</sup> ( $\gamma$ , p) Cu <sup>67</sup>	-10,01	0,19	11,4	22,7 $\pm$ 1	6
Sc <sup>40</sup> ( $\gamma$ , pn) As <sup>76</sup>	-20,43	0,02			
Zn <sup>64</sup> ( $\gamma$ , 2n) Zn <sup>62</sup>	-20,82	0,08			
Mo <sup>92</sup> ( $\gamma$ , pn) Nb <sup>90</sup>	-19,5	0,02			
Sb <sup>123</sup> ( $\gamma$ , pn) Sn <sup>121</sup>	-18,2	0,0006			

Method Betatron; neutron yield; radioactivity; r-chamber

Ref. No.	
59 Mu 2	NVB

Reaction	E or $\Delta E$	$E_0$	$\Gamma$	$\int \sigma dE$	$J\pi$	Notes
$\text{Mo}^{92}(\gamma, n)$	Bremss. 0-25	16.0	2.7 MeV	1.48 MeV-b		

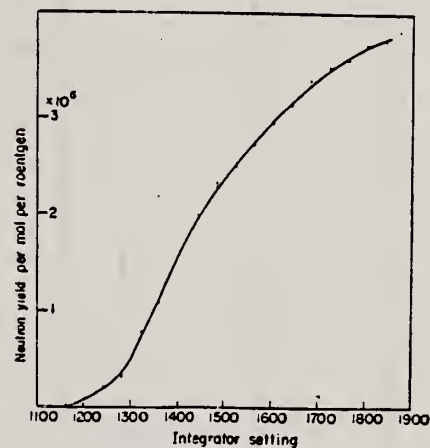
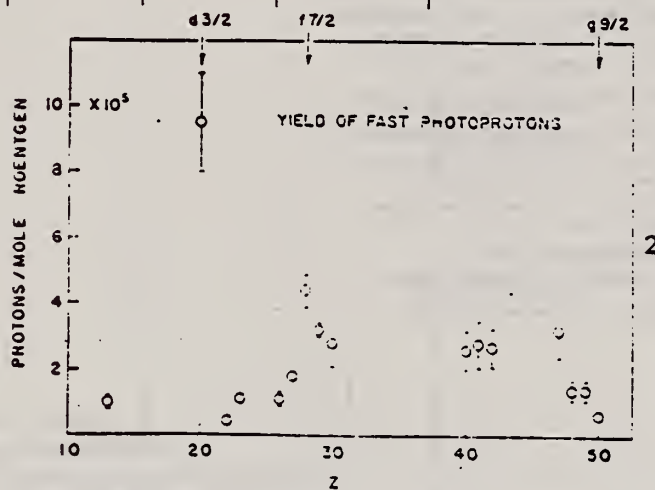


Fig. 4-2. Activation curve for  $\text{Mo}^{92}(\gamma, n)\text{Mo}^{91}$ .

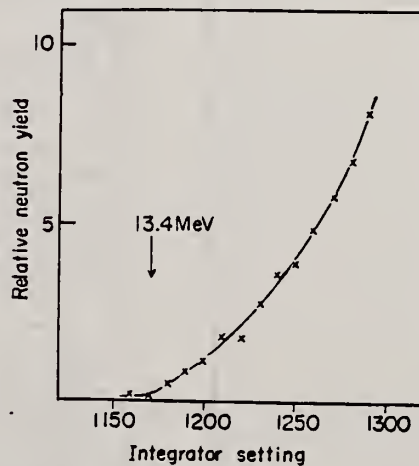


Fig. 3-2. Activation curve near threshold for  $\text{Mo}^{92}(\gamma, n)\text{Mo}^{91}$ .

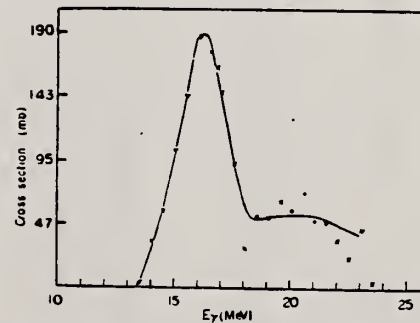


Fig. 5-2. Cross section curve for  $\text{Mo}^{92}(\gamma, n)\text{Mo}^{91}$ .

Ref. J.H. Carver, G.E. Coote, T.R. Sherwood  
Nuclear Phys. 55, 449 (1962)

Elem. Sym.	A	Z
Mo	92	42
Ref. No. 62 Ca 1		
JHH		

Method 30 MeV electron synchrotron; activation; NaI

Reaction	E or ΔE	E <sub>0</sub>	Γ	∫σdE	Jπ	Notes																																																																																																																																																															
Mo <sup>92</sup> (γ,n)	Bremss. 30																																																																																																																																																																				
<p>1) J. E. Hulsberg and E. Vandenberg, Phys. Rev. <u>122</u> (1960) 1305</p> <p>2) T. Ericson, Advances in Physics, <u>2</u> (1960) 425</p> <p>3) D. L. Allan, Nuclear Physics <u>24</u> (1961) 274</p> <p>4) C. T. Eibson, Phys. Rev. <u>114</u> (1959) 179</p> <p>5) C. T. Eibson, Phys. Rev. <u>122</u> (1961) 1235</p> <p>6) T. Ericson, Nuclear Physics <u>11</u> (1959) 481</p> <p>7) J. H. Carver and C. A. Jones, Nuclear Physics <u>13</u> (1960) 184</p> <p>8) A. C. Douglas and E. MacDonald, Nuclear Physics <u>11</u> (1959) 388</p> <p>9) T. Ericson and V. A. Scutarski, Nuclear Physics <u>2</u> (1958) 284</p> <p>10) L. Katz, L. Fessenden and H. Mosby, Can. J. Phys. <u>30</u> (1952) 474</p> <p>11) L. Katz, E. G. Baker and E. Montalbetti, Can. J. Phys. <u>31</u> (1953) 29</p> <p>12) E. Silva and J. Goldemberg, An. Acad. Brasil Ciencias <u>28</u> (1956) 275</p> <p>13) J. H. Carver and D. C. Penelope, Phys. Rev. <u>120</u> (1960) 2155</p> <p>14) J. H. Blatt and V. F. Weisskopf, "Theoretical Nuclear Physics" New York: Wiley (1952)</p> <p>15) E. H. Vogner, L. L. Marston and E. L. Heath, U.S. Atomic Energy Commission Report T20-16770 (1958)</p> <p>16) Nuclear Data Sheets, National Research Council, Washington (1960, up to and including Set 5)</p> <p>17) E. Vandenberg and J. E. Hulsberg, Phys. Rev. <u>122</u> (1960) 1313</p> <p>18) E. Weigold and E. Glover, Nuclear Physics (in press)</p> <p>19) E. J. Le Comte and D. W. Lang, Nuclear Physics <u>11</u> (1959) 32</p> <p>20) T. D. Horton, Can. J. Phys. <u>34</u> (1956) 804</p> <p>21) D. W. Lang, Nuclear Physics <u>26</u> (1961) 434</p> <p>22) H. E. Ross, "Internal Conversion Coefficients", Amsterdam: North Holland Publishing Co. (1958)</p> <p>23) J. Goldemberg and L. Katz, Phys. Rev. <u>80</u> (1953) 308</p>																																																																																																																																																																					
<p>TABLE 1 Isomeric Ratios from (γ,n) reactions</p> <table><tr><th rowspan="2">Target Nucleus</th><th rowspan="2">J<sub>π</sub></th><th colspan="4">Residual Nucleus</th><th rowspan="2">Isomer ratio: <math>\frac{I_2}{I_1} = \frac{Y_2}{Y_1 + Y_2}</math></th><th rowspan="2">σ</th></tr><tr><th>Ground state</th><th>Metastable state</th><th>Spin</th><th>Half-life</th></tr><tr><td>Ce<sup>139</sup></td><td>7/2<sup>+</sup></td><td>Ce<sup>138</sup></td><td>2<sup>+</sup></td><td>71.34</td><td>5<sup>+</sup></td><td>9.2h</td><td>0.44 ± 0.02</td><td>3.2 ± 0.2</td></tr><tr><td>Ce<sup>140</sup></td><td>0<sup>+</sup></td><td>Ce<sup>139</sup></td><td>1/2<sup>+</sup></td><td>82m</td><td>7/2<sup>+</sup></td><td>49a</td><td>0.48 ± 0.07</td><td>2.0 ± 0.5</td></tr><tr><td>Pr<sup>141</sup></td><td>3/2<sup>+</sup></td><td>Pr<sup>140</sup></td><td>1<sup>+</sup></td><td>10m</td><td>5<sup>+</sup></td><td>4.4h</td><td>0.32 ± 0.02</td><td>6.5 ± 1.0</td></tr><tr><td>Pr<sup>142</sup></td><td>0<sup>+</sup></td><td>Pr<sup>141</sup></td><td>9/2<sup>+</sup></td><td>64d</td><td>1/2<sup>+</sup></td><td>70m</td><td>0.56 ± 0.07</td><td>2.2 ± 0.4</td></tr><tr><td>Zr<sup>90</sup></td><td>0<sup>+</sup></td><td>Zr<sup>89</sup></td><td>9/2<sup>+</sup></td><td>77h</td><td>1/2<sup>+</sup></td><td>4.4a</td><td>0.55 ± 0.10</td><td>2.0 ± 0.7</td></tr><tr><td>La<sup>138</sup></td><td>0<sup>+</sup></td><td>La<sup>137</sup></td><td>9/2<sup>+</sup></td><td>15.7a</td><td>1/2<sup>+</sup></td><td>16a</td><td>0.46 ± 0.04</td><td>6 ± 2</td></tr><tr><td>Ag<sup>107</sup></td><td>1/2<sup>+</sup></td><td>Ag<sup>106</sup></td><td>1<sup>+</sup></td><td>24m</td><td>6</td><td>4.34</td><td>0.04 ± 0.02</td><td>2.0 ± 0.5</td></tr><tr><td>In<sup>115</sup></td><td>9/2<sup>+</sup></td><td>In<sup>112</sup></td><td>1<sup>+</sup></td><td>14.5a</td><td>4<sup>+</sup></td><td>20.7m</td><td>0.8 ± 0.1</td><td>3.1 ± 0.7</td></tr><tr><td>Cd<sup>116</sup></td><td>0<sup>+</sup></td><td>Cd<sup>115</sup></td><td>1/2<sup>+</sup></td><td>53h</td><td>11/2<sup>+</sup></td><td>43a</td><td>≤ 0.2</td><td>≤ 3</td></tr><tr><td>Ce<sup>140</sup></td><td>0<sup>+</sup></td><td>Ce<sup>139</sup></td><td>5/2<sup>+</sup></td><td>160d</td><td>11/2<sup>+</sup></td><td>55a</td><td>0.08 ± 0.01</td><td>2.5 ± 0.2</td></tr><tr><td>Hg<sup>198</sup></td><td>0<sup>+</sup></td><td>Hg<sup>197</sup></td><td>1/2<sup>+</sup></td><td>65h</td><td>15/2<sup>+</sup></td><td>24m</td><td>0.05 ± 0.01</td><td>5.4 ± 0.5</td></tr></table> <table><tr><th colspan="8">Previous work</th></tr><tr><th>Target</th><th>J<sub>π</sub></th><th>Residual Nucleus</th><th>Ground state</th><th>Metastable state</th><th>Spin</th><th>Half-life</th><th>Isomer ratio</th></tr><tr><td>Pr<sup>141</sup> (10)</td><td>3/2<sup>+</sup></td><td>Pr<sup>140</sup></td><td>1<sup>+</sup></td><td>10m</td><td>5<sup>+</sup></td><td>4.4h</td><td>0.55</td></tr><tr><td>Pr<sup>142</sup> (12)</td><td>0<sup>+</sup></td><td>Pr<sup>141</sup></td><td>9/2<sup>+</sup></td><td>64d</td><td>1/2<sup>+</sup></td><td>70m</td><td>0.5</td></tr><tr><td>Zr<sup>90</sup> (11)</td><td>0<sup>+</sup></td><td>Zr<sup>89</sup></td><td>9/2<sup>+</sup></td><td>77h</td><td>1/2<sup>+</sup></td><td>4.4a</td><td>0.44 ± 0.06</td></tr><tr><td>In<sup>115</sup> (23)</td><td>9/2<sup>+</sup></td><td>In<sup>112</sup></td><td>1<sup>+</sup></td><td>14.5a</td><td>4<sup>+</sup></td><td>20.7m</td><td>0.85</td></tr></table> <p>The yields, Y<sub>1</sub> and Y<sub>2</sub>, are for (γ,n) reactions ending in the isomeric or ground states. The yield Y<sub>2</sub> is for the metastable state.</p>							Target Nucleus	J <sub>π</sub>	Residual Nucleus				Isomer ratio: $\frac{I_2}{I_1} = \frac{Y_2}{Y_1 + Y_2}$	σ	Ground state	Metastable state	Spin	Half-life	Ce <sup>139</sup>	7/2 <sup>+</sup>	Ce <sup>138</sup>	2 <sup>+</sup>	71.34	5 <sup>+</sup>	9.2h	0.44 ± 0.02	3.2 ± 0.2	Ce <sup>140</sup>	0 <sup>+</sup>	Ce <sup>139</sup>	1/2 <sup>+</sup>	82m	7/2 <sup>+</sup>	49a	0.48 ± 0.07	2.0 ± 0.5	Pr <sup>141</sup>	3/2 <sup>+</sup>	Pr <sup>140</sup>	1 <sup>+</sup>	10m	5 <sup>+</sup>	4.4h	0.32 ± 0.02	6.5 ± 1.0	Pr <sup>142</sup>	0 <sup>+</sup>	Pr <sup>141</sup>	9/2 <sup>+</sup>	64d	1/2 <sup>+</sup>	70m	0.56 ± 0.07	2.2 ± 0.4	Zr <sup>90</sup>	0 <sup>+</sup>	Zr <sup>89</sup>	9/2 <sup>+</sup>	77h	1/2 <sup>+</sup>	4.4a	0.55 ± 0.10	2.0 ± 0.7	La <sup>138</sup>	0 <sup>+</sup>	La <sup>137</sup>	9/2 <sup>+</sup>	15.7a	1/2 <sup>+</sup>	16a	0.46 ± 0.04	6 ± 2	Ag <sup>107</sup>	1/2 <sup>+</sup>	Ag <sup>106</sup>	1 <sup>+</sup>	24m	6	4.34	0.04 ± 0.02	2.0 ± 0.5	In <sup>115</sup>	9/2 <sup>+</sup>	In <sup>112</sup>	1 <sup>+</sup>	14.5a	4 <sup>+</sup>	20.7m	0.8 ± 0.1	3.1 ± 0.7	Cd <sup>116</sup>	0 <sup>+</sup>	Cd <sup>115</sup>	1/2 <sup>+</sup>	53h	11/2 <sup>+</sup>	43a	≤ 0.2	≤ 3	Ce <sup>140</sup>	0 <sup>+</sup>	Ce <sup>139</sup>	5/2 <sup>+</sup>	160d	11/2 <sup>+</sup>	55a	0.08 ± 0.01	2.5 ± 0.2	Hg <sup>198</sup>	0 <sup>+</sup>	Hg <sup>197</sup>	1/2 <sup>+</sup>	65h	15/2 <sup>+</sup>	24m	0.05 ± 0.01	5.4 ± 0.5	Previous work								Target	J <sub>π</sub>	Residual Nucleus	Ground state	Metastable state	Spin	Half-life	Isomer ratio	Pr <sup>141</sup> (10)	3/2 <sup>+</sup>	Pr <sup>140</sup>	1 <sup>+</sup>	10m	5 <sup>+</sup>	4.4h	0.55	Pr <sup>142</sup> (12)	0 <sup>+</sup>	Pr <sup>141</sup>	9/2 <sup>+</sup>	64d	1/2 <sup>+</sup>	70m	0.5	Zr <sup>90</sup> (11)	0 <sup>+</sup>	Zr <sup>89</sup>	9/2 <sup>+</sup>	77h	1/2 <sup>+</sup>	4.4a	0.44 ± 0.06	In <sup>115</sup> (23)	9/2 <sup>+</sup>	In <sup>112</sup>	1 <sup>+</sup>	14.5a	4 <sup>+</sup>	20.7m	0.85
Target Nucleus	J <sub>π</sub>	Residual Nucleus				Isomer ratio: $\frac{I_2}{I_1} = \frac{Y_2}{Y_1 + Y_2}$			σ																																																																																																																																																												
		Ground state	Metastable state	Spin	Half-life																																																																																																																																																																
Ce <sup>139</sup>	7/2 <sup>+</sup>	Ce <sup>138</sup>	2 <sup>+</sup>	71.34	5 <sup>+</sup>	9.2h	0.44 ± 0.02	3.2 ± 0.2																																																																																																																																																													
Ce <sup>140</sup>	0 <sup>+</sup>	Ce <sup>139</sup>	1/2 <sup>+</sup>	82m	7/2 <sup>+</sup>	49a	0.48 ± 0.07	2.0 ± 0.5																																																																																																																																																													
Pr <sup>141</sup>	3/2 <sup>+</sup>	Pr <sup>140</sup>	1 <sup>+</sup>	10m	5 <sup>+</sup>	4.4h	0.32 ± 0.02	6.5 ± 1.0																																																																																																																																																													
Pr <sup>142</sup>	0 <sup>+</sup>	Pr <sup>141</sup>	9/2 <sup>+</sup>	64d	1/2 <sup>+</sup>	70m	0.56 ± 0.07	2.2 ± 0.4																																																																																																																																																													
Zr <sup>90</sup>	0 <sup>+</sup>	Zr <sup>89</sup>	9/2 <sup>+</sup>	77h	1/2 <sup>+</sup>	4.4a	0.55 ± 0.10	2.0 ± 0.7																																																																																																																																																													
La <sup>138</sup>	0 <sup>+</sup>	La <sup>137</sup>	9/2 <sup>+</sup>	15.7a	1/2 <sup>+</sup>	16a	0.46 ± 0.04	6 ± 2																																																																																																																																																													
Ag <sup>107</sup>	1/2 <sup>+</sup>	Ag <sup>106</sup>	1 <sup>+</sup>	24m	6	4.34	0.04 ± 0.02	2.0 ± 0.5																																																																																																																																																													
In <sup>115</sup>	9/2 <sup>+</sup>	In <sup>112</sup>	1 <sup>+</sup>	14.5a	4 <sup>+</sup>	20.7m	0.8 ± 0.1	3.1 ± 0.7																																																																																																																																																													
Cd <sup>116</sup>	0 <sup>+</sup>	Cd <sup>115</sup>	1/2 <sup>+</sup>	53h	11/2 <sup>+</sup>	43a	≤ 0.2	≤ 3																																																																																																																																																													
Ce <sup>140</sup>	0 <sup>+</sup>	Ce <sup>139</sup>	5/2 <sup>+</sup>	160d	11/2 <sup>+</sup>	55a	0.08 ± 0.01	2.5 ± 0.2																																																																																																																																																													
Hg <sup>198</sup>	0 <sup>+</sup>	Hg <sup>197</sup>	1/2 <sup>+</sup>	65h	15/2 <sup>+</sup>	24m	0.05 ± 0.01	5.4 ± 0.5																																																																																																																																																													
Previous work																																																																																																																																																																					
Target	J <sub>π</sub>	Residual Nucleus	Ground state	Metastable state	Spin	Half-life	Isomer ratio																																																																																																																																																														
Pr <sup>141</sup> (10)	3/2 <sup>+</sup>	Pr <sup>140</sup>	1 <sup>+</sup>	10m	5 <sup>+</sup>	4.4h	0.55																																																																																																																																																														
Pr <sup>142</sup> (12)	0 <sup>+</sup>	Pr <sup>141</sup>	9/2 <sup>+</sup>	64d	1/2 <sup>+</sup>	70m	0.5																																																																																																																																																														
Zr <sup>90</sup> (11)	0 <sup>+</sup>	Zr <sup>89</sup>	9/2 <sup>+</sup>	77h	1/2 <sup>+</sup>	4.4a	0.44 ± 0.06																																																																																																																																																														
In <sup>115</sup> (23)	9/2 <sup>+</sup>	In <sup>112</sup>	1 <sup>+</sup>	14.5a	4 <sup>+</sup>	20.7m	0.85																																																																																																																																																														

Ref. W.E. Del Bianco, W.E. Stephens  
Phys. Rev. 126, 709 (1962)

Elem. Sym.	A	Z
Mo	92	42

Method Electrostatic generator,  $H^3(p,\gamma)He^4$  reaction; activation of positron emitter; 2 NaI in coincidence.

Ref. No.	
62 De 1	JHH

Reaction	E or $\Delta E$	$E_0$	$\Gamma$	$\int \sigma dE$	$J\pi$	Notes
$(\gamma, n)$	20.48					$\sigma(\gamma, n) = 35.4 \pm 2.3$ mb (branch leaving $Mo^{91}$ nucleus in ground state).

ELEM. SYM.	A	Z
Mo	92	42
REF. NO.		JOC
64 Ge 1		

METHOD  
Betatron; ion chamber monitor

REACTION	RESULT	EXCITATION ENERGY	SOURCE		DETECTOR		ANGLE
			TYPE	RANGE	TYPE	RANGE	
1) G,N	ABX	THR - 22	C	THR - 33	ACT-I		4 PI
2) G,2N	ABX	THR - 33	C	THR - 33	ACT-I		4 PI
3) G,NP	ABX	THR - 33	C	THR - 33	ACT-I		4 PI

2) MIXED WITH G,NP  
3) MIXED WITH G,2N

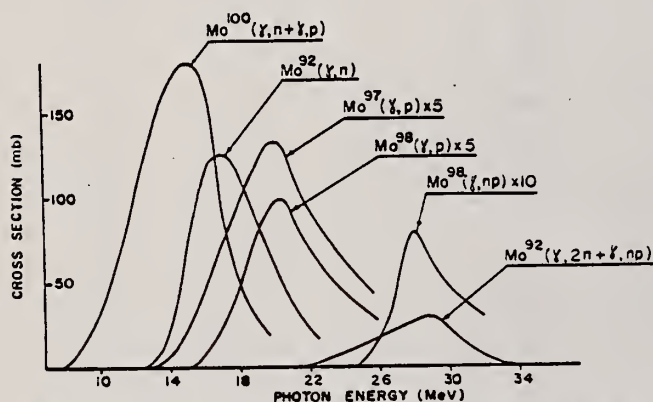


Fig. 2. Cross sections for photoreactions in molybdenum isotopes.

TABLE 2  
Reaction parameters

Reaction	Peak energy (MeV)	$\int \sigma dE$ (MeV · mb)
Mo <sup>100</sup> ( $\gamma$ , n + $\gamma$ , p)	15	1110 ± 200
Mo <sup>92</sup> ( $\gamma$ , n)	17	750 ± 70
Mo <sup>97</sup> ( $\gamma$ , p)	20	215 ± 50
Mo <sup>98</sup> ( $\gamma$ , p)	20	140 ± 15
Mo <sup>98</sup> ( $\gamma$ , np)	23	30 ± 10
Mo <sup>92</sup> ( $\gamma$ , np + $\gamma$ , 2n)	29	160 ± 25



REF. S. Costa, F. Ferrero, S. Ferroni, L. Pasquallini and E. Silva - also  
Istituto Nazionale di Fisica Nucleare - Sezione di Torino  
Nuclear Phys. 72, 158 (1965)

ELEM. SYM.	A	Z
Mo	92	42
REF. NO.		
65 Co 1		EGF

METHOD				REF. NO.		
				65 Co 1		EGF
REACTION	RESULT	EXCITATION ENERGY	SOURCE		DETECTOR	
			TYPE	RANGE	TYPE	RANGE
G,N	RLX	THR - 70	C	12 - 70	ACT-I	4PI

Measured isomer production ratio.  
Spin cut off < 1.5

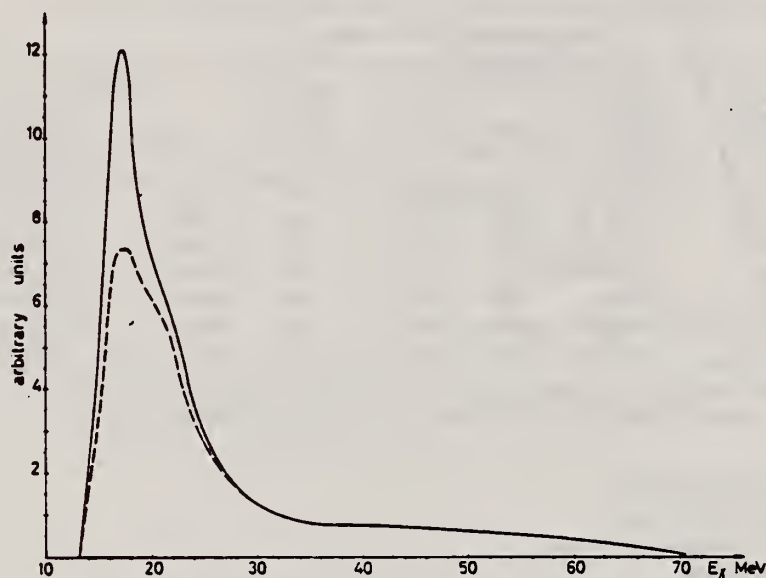


Fig. 3. ( $\gamma, n$ ) reaction in  $^{96}\text{Mo}$ , total (solid line) and  $\frac{1}{2}^-$  state (dashed line) cross sections.

TABLE I  
Spins and half-lives of isomeric states

Target nucleus	Spin of isomeric states	Half-life	Modes of decay (used for detection)	Detection method
$^{40}\text{K}$	$0^+$	0.95 sec	$\beta^+$ (100 %)	$\gamma$ - $\gamma$ fast-slow coincidence (resolving time 0.2 and 2 $\mu\text{sec}$ )
$J = \frac{1}{2}$	$3^+$	7.7 min	$\beta^+$ (> 99 %)	$\gamma$ - $\gamma$ coincidence
$^{90}\text{Zr}$	$\frac{1}{2}^-$	4.3 min	$\gamma$ (93 %) $\beta^+$ (1.7 %)	NaI (well type) spectrometer centered on the 0.588 MeV $\gamma$ ray line $\gamma$ - $\gamma$ coincidence
$J = 0$	$\frac{1}{2}^+$	79 h	$\beta^+$ (30 %)	$\gamma$ - $\gamma$ coincidence
$^{96}\text{Mo}$	$\frac{1}{2}^-$	66 sec	$\gamma$ (57 %) $\beta^+$ (38 %)	NaI (well type) spectrometer centered on the 0.658 MeV $\gamma$ ray line $\gamma$ - $\gamma$ coincidence
$J = 0$	$\frac{1}{2}^+$	16 min	$\beta^+$ (94 %)	$\gamma$ - $\gamma$ coincidence

METHOD

REF. NO.

68 Ge 1

egf

REACTION	RESULT	EXCITATION ENERGY	SOURCE		DETECTOR		ANGLE
			TYPE	RANGE	TYPE	RANGE	
G,N	ABX	12-26	C	THR-26	ACT-I		4PI

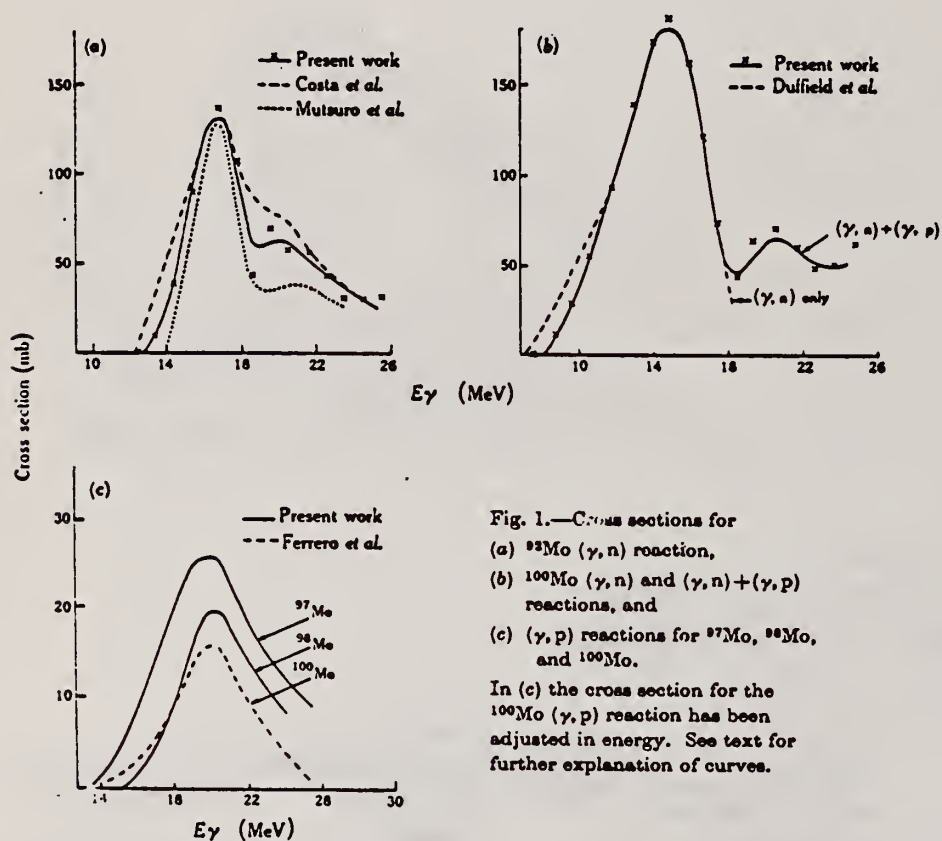


Fig. 1.—Cross sections for  
(a)  $^{98}\text{Mo}(\gamma, n)$  reaction,  
(b)  $^{100}\text{Mo}(\gamma, n)$  and  $(\gamma, n) + (\gamma, p)$   
reactions, and  
(c)  $(\gamma, p)$  reactions for  $^{97}\text{Mo}$ ,  $^{98}\text{Mo}$ ,  
and  $^{100}\text{Mo}$ .

In (c) the cross section for the  
 $^{100}\text{Mo}(\gamma, p)$  reaction has been  
adjusted in energy. See text for  
further explanation of curves.

REF. Y. Oka, T. Kato and A. Yamadera  
Bull. Chem. Soc. Japan 41, 1606 (1968)

ELEM. SYM.	A	Z
Mo	92	42

METHOD

REF. NO.

68 Ok 2

egf

REACTION	RESULT	EXCITATION ENERGY	SOURCE		DETECTOR		ANGLE
			TYPE	RANGE	TYPE	RANGE	
G,N	ABY	THR-20	C	20	ACT- I		4PI

ISOMERIC YIELD

TABLE 1. THE PARTICULARS OF THE ( $\gamma$ ,n) REACTION PRODUCTS AND THE DATA OBTAINED WITH 20 MeV BREMSSTRAHLUNG

Nuclide		Half-life of product (sec)	Gamma-ray determined			Limit of detection ( $\mu$ g)	Yield ( $\text{mol}^{-1} \cdot \text{R}^{-1}$ )
Parent (Natural abundance, %)	Residual		Energy (MeV)	Branching ratio (%)	Photopeak activity (cpm/mg) <sup>a)</sup>		
<sup>24</sup> Mg(78.60)	<sup>23</sup> Mg	9.9	0.511	200	$2.04 \times 10^6$	0.49	$8.1 \times 10^6$
<sup>76</sup> Ge(7.67)	<sup>75m</sup> Ge	48	0.139	100	$6.37 \times 10^6$	1.6	$1.1 \times 10^6$
<sup>78</sup> Se(23.52)	<sup>77m</sup> Se	17	0.162	100	$1.82 \times 10^6$	0.55	$1.2 \times 10^6$
<sup>98</sup> Mo(15.86)	<sup>91m</sup> Mo	65	0.650	57	$2.22 \times 10^6$	4.5	$2.7 \times 10^6$
<sup>140</sup> Ce(88.48)	<sup>139m</sup> Ce	58	0.745	100	$1.06 \times 10^6$	0.95	$1.3 \times 10^6$
<sup>142</sup> Nd(27.13)	<sup>141m</sup> Nd	64	0.760	100	$3.19 \times 10^6$	3.1	$1.4 \times 10^6$
<sup>159</sup> Tb(100)	<sup>158m</sup> Tb	11	0.111	100	$2.56 \times 10^6$	3.8	$2.2 \times 10^6$

a) The value corrected at the end of one-minute irradiation with the dose rate of  $10^7$  R/min; Counting geometry is 20% with a 3"dia.  $\times$  3"NaI(Tl) detector.

REF.

K. Shoda, M. Sugawara, T. Saito & H. Miyase  
 PICNS-69 Proceedings of the Conference on Nuclear Isospin.  
 Asilomar-Pacific Grove, California 1969 (Academic Press,  
 New York & London 1969)p.125.

ELEM. SYM.	A	Z
Mo	92	42
REF. NO.		
69 Sh 6		egf

METHOD

REACTION	RESULT	EXCITATION ENERGY	SOURCE		DETECTOR		ANGLE
			TYPE	RANGE	TYPE	RANGE	
E, P	SPC	11-18	D	20	D	20	UKN

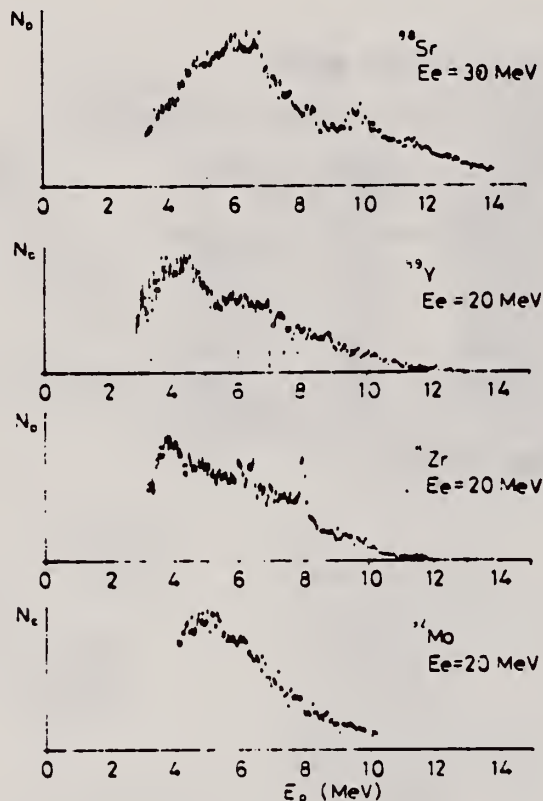


Fig. 1. Energy distributions of photoprotons. Vertical broken lines and solid lines indicate the position of  $p_0$  corresponding to the ground IAS and electric dipole IAS (2-4) respectively.



REF. B.S. Ishkhanov, I.M. Kapitonov, E.V. Lazutin, I.M. Piskarev,  
and O.P. Shevchenko  
Yad. Fiz. 11, 702 (1970)  
Sov. J. Nucl. Phys. 11, 394 (1970)

ELEM. SYM.	A	Z
Mo	92	42

METHOD

REF. NO.	
70 Is 1	hmg

REACTION	RESULT	EXCITATION ENERGY	SOURCE		DETECTOR		ANGLE
			TYPE	RANGE	TYPE	RANGE	
G, XN	ABX	THR-30	C	THR-30	BF3-I		4PI

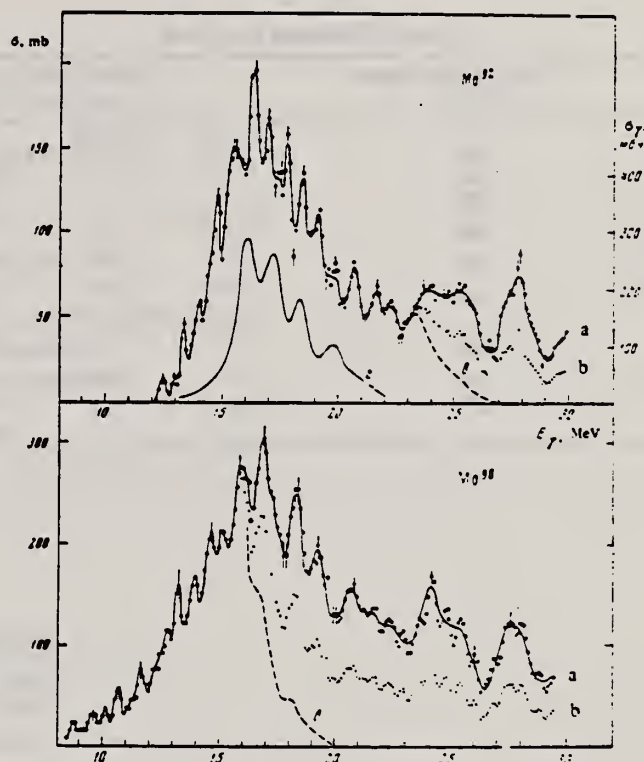
WE used the 35-MeV betatron of our institute to investigate photoneutron reactions on the isotopes  $\text{Mo}^{92}$  and  $\text{Mo}^{98}$ . The yield curves of the reactions  $(\gamma, \text{Tn})$  were measured in the energy range from 7 to 30 MeV in steps of 100 keV. The targets were prepared from metallic Mo. The content of the investigated isotopes was not less than 97%. The use of a highly efficient neutron detector ( $\epsilon \approx 45\%$ ) and of a multichannel method of measurements has made it possible to obtain the yield curves with high accuracy (0.1% in the region 25–30 MeV) and to observe, for the first time, the intermediate structure of the giant resonance on the isotopes of Mo. The statistical reduction of the experimental information and the determination of the cross sections of the photoneutron reactions was carried out in accordance with a program prepared by the Computational Center of the Moscow State University<sup>[1]</sup>.

The obtained cross section of the reactions  $\sigma(\gamma, \text{Tn}) = \sigma(\gamma, n) + 2\sigma(\gamma, 2n) + \sigma(\gamma, np)$  are shown in the figure, from which it is seen that approximately 15 resonances are observed in each cross section.

The widths of the giant resonances in the reaction  $(\gamma, \text{Tn})$  on  $\text{Mo}^{92}$  and  $\text{Mo}^{98}$  are 5 and 7 MeV respectively (curves a in the figure). After taking into account the multiplicity in accordance with the data of<sup>[2]</sup> for this region of nuclei, the cross sections obtained were  $\sigma_n = \sigma(\gamma, n) + \sigma(\gamma, 2n) + \sigma(\gamma, np)$  (curves b). The widths of these cross sections for  $\text{Mo}^{92}$  and  $\text{Mo}^{98}$  are the same and equal 5 MeV. The curves c correspond to the cross sections  $\sigma(\gamma, n) + \sigma(\gamma, np)$ . The widths for them are 5 and 3.5 MeV respectively for  $\text{Mo}^{92}$  and  $\text{Mo}^{98}$ .

The widths  $\sigma_n$  of the integral cross sections of the reactions for  $\text{Mo}^{92}$  and  $\text{Mo}^{98}$  are  $1.29 \pm 0.13$  and  $2.0 \pm 0.2$  MeV-b. The integral cross section  $\sigma_n$  increases with increasing  $N - Z$  for isotopes of a given element. It is interesting to note, however, that in the case of Mo the increase of  $\sigma_n$  and of the width of the giant resonance is due to the cross section of the reaction  $(\gamma, 2n)$ . Thus, for  $\text{Mo}^{92}$  we have  $\sigma(\gamma, 2n) = 0.17 \pm 0.02$  MeV-b, whereas for  $\text{Mo}^{98}$  we have  $\sigma(\gamma, 2n) = 0.83 \pm 0.08$  MeV-b, i.e., the cross section of the reaction  $(\gamma, 2n)$  increases by almost five times. Such a sharp increase of the cross section of the reaction  $\text{Mo}^{98}(\gamma, 2n)$  is connected with the low threshold of the  $(\gamma, 2n)$  reaction, namely  $E_{\text{Mo}^{98}}^{\text{thr}}(\gamma, 2n) = 15.5$  MeV. For comparison, we point out that  $E_{\text{Mo}^{92}}^{\text{thr}}(\gamma, 2n) = 22.8$  MeV.

For the reaction  $(\gamma, n) + (\gamma, np)$ , the integral cross sections for  $\text{Mo}^{92}$  and  $\text{Mo}^{98}$  are respectively  $1.12 \pm 0.11$  and  $1.10 \pm 0.11$  MeV-b.



Effective cross sections for  $\text{Mo}^{92}$  and  $\text{Mo}^{98}$ : a —  $\sigma(\gamma, \text{Tn})$ ; b —  $\sigma(\gamma, n) + \sigma(\gamma, 2n) + \sigma(\gamma, np)$ ; c —  $\sigma(\gamma, n) + \sigma(\gamma, np)$ ; d — total-absorption cross section  $\sigma_\gamma$ , obtained in<sup>[3]</sup> for  $\text{Mo}^{94}$  (right-hand scale).

There are at present no published data on the structure of the photoneutron cross sections on the Mo isotopes. Such general characteristics of the giant resonance as the position and magnitude of the integral cross section are known only for the reaction  $\text{Mo}^{92}(\gamma, n)^{[3-5]}$ . Even these results, however, are highly contradictory. Thus, data on the width of the giant resonance, obtained in<sup>[3]</sup>, exceed the data of<sup>[4]</sup> by a factor of 2.

In conclusion, let us compare the experimental results obtained by us with the calculations performed on the basis of the collective dynamic theory<sup>[6]</sup>. The photodisintegration of the  $\text{Mo}^{94}$  was calculated within the framework of this theory, and the result is shown in the figure (curve d). We see that the theoretical calculation agrees only roughly with the experimental data. The experimentally measured cross sections re-



ELEM. SYM.	A	Z
Mo	92	42
REF. NO.		
70 Wa 3		egf

METHOD			SOURCE		DETECTOR		ANGLE
REACTION	RESULT	EXCITATION ENERGY	TYPE	RANGE	TYPE	RANGE	
G,2N	RLY	THR-305	C	150-305	ACT-I		4PI
G,pn	RLY	THR-305	C	150-305	ACT-I		4PI

TABLE 1  
Summary of measured yield ratios

Target	Bremsstrahlung energy (MeV)	Measured yield ratio
natural Cr	150	$^{48}\text{Cr}/^{48}\text{V} = 0.043 \pm 0.002$
	250	$0.047 \pm 0.009$
	305	$0.042 \pm 0.002$
enriched $^{52}\text{Cr}$	250	$0.025 \pm 0.005$
natural Fe	250	$^{52}\text{Fe}/^{52}\text{Mn} = 0.037 \pm 0.003$
enriched $^{56}\text{Fe}$	250	$0.024 \pm 0.005$
		$^{52}\text{Mn}/(^{52}\text{Mn} + ^{55}\text{Mn}) = 0.47 \pm 0.02$
natural Y	150	$^{87}\text{Y}/^{87}\text{Sr} = 12.9 \pm 1.6$
natural Mo	150	$^{90}\text{Mo}/^{90}\text{Nb} = 0.41 \pm 0.05$
	280	$0.49 \pm 0.05$

TABLE 2  
Summary of experimental and theoretical ratios of ( $\gamma$ , 2n) to ( $\gamma$ , pn) yields

Target isotope	Bremsstrahlung energy (MeV)	Experimental ( $\gamma$ , 2n)/( $\gamma$ , pn) yield ratio	Calculated ( $\gamma$ , 2n)/( $\gamma$ , pn) yield ratio
$^{50}\text{Cr}$	250	$0.095 \pm 0.025$	0.14
$^{54}\text{Fe}$	250	$0.10 \pm 0.03$	0.07
$^{89}\text{Y}$	150	$7.4 \pm 1.0$	6.7
$^{92}\text{Mo}$	150	$0.41 \pm 0.05$	0.15
	280	$0.49 \pm 0.05$	0.16

REF.

P. E. Haustein and A. F. Voigt  
J. inorg. nucl. Chem. 33, 289 (1971)

ELEM. SYM.

A

Z

Mo

92

42

METHOD

REF. NO.

71 Ha 2

egf

REACTION	RESULT	EXCITATION ENERGY	SOURCE		DETECTOR		ANGLE
			TYPE	RANGE	TYPE	RANGE	
G,N	RLY	13-70	C	70	ACT-I		4PI

Isomer ratio = (yield to low spin state)/(yield to high spin state)

ISOMER RATIOTable 2. Isomer ratio measurements for  $^{91}\text{Mo}$ ,  $^{137}\text{Ce}$ , and  $^{141}\text{Nd}$ 

Reaction	Isomer ratio	$I^\pi$ Target	$I^\pi$ Ground state	$I^\pi$ Isomer	Threshold (MeV)	$41A^{-1/2}$ (MeV)
$^{91}\text{Mo}(\gamma, n)^{90}\text{Mo}$	$1.92 \pm 0.15$	$0^+$	$9/2^+$	$1/2^-$	13.13	16.60
$^{91}\text{Mo}(\gamma, 3n)^{88}\text{Mo}$	$1.59 \pm 0.16$	$0^+$			30.72	16.52
$^{137}\text{Ce}(\gamma, n)^{136}\text{Ce}$	3.1	$0^+$	$3/2^+$	$11/2^+$	10.31	15.30
$^{137}\text{Ce}(\gamma, 3n)^{134}\text{Ce}$	$1.10 \pm 0.12$	$0^+$			26.34	15.26
$^{141}\text{Nd}(\gamma, n)^{140}\text{Nd}$	$5.2 \pm 0.3$	$0^+$	$3/2^+$	$11/2^+$	9.79	15.22
$^{141}\text{Nd}(\gamma, 3n)^{138}\text{Nd}$	$1.80 \pm 0.25$	$0^+$			23.67	15.17

REF.

ELEM. SYM.	A	Z
Mo	92	42
REF. NO.		hvm
72 Ho 6		

METHOD

REACTION	RESULT	EXCITATION ENERGY	SOURCE		DETECTOR		ANGLE
			TYPE	RANGE	TYPE	RANGE	
E, E/	ABX	1, 2	D	209	MAG-D		DST

1=1.51, 2=2.85 MEV

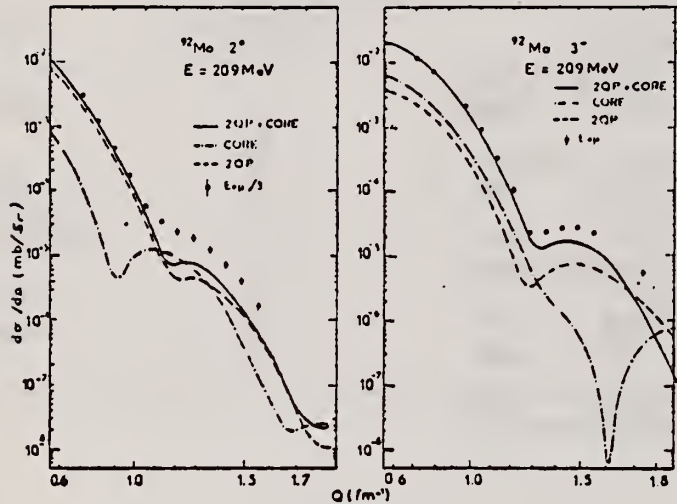


Fig. 5

Phan Xuan Ho, J. B. Bellicard, Ph. Leconte and I. Sick  
J. Phys. (Paris) Colloq. 5, 167 (1972)

Mo

92

42

METHOD

REF. NO.

72 Ho 10

egf

REACTION	RESULT	EXCITATION ENERGY	SOURCE		DETECTOR		ANGLE
			TYPE	RANGE	TYPE	RANGE	
E, E/	ABX	1, 2	D	209	MAG-D		DST

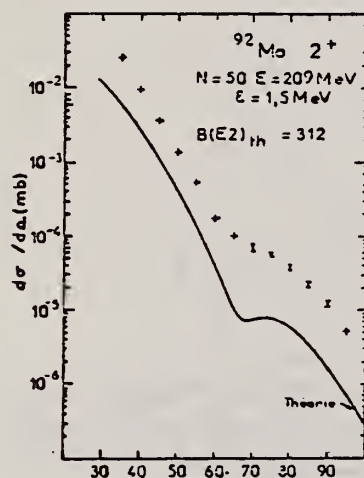
1.5, 2.85 MEV

Fig. 1

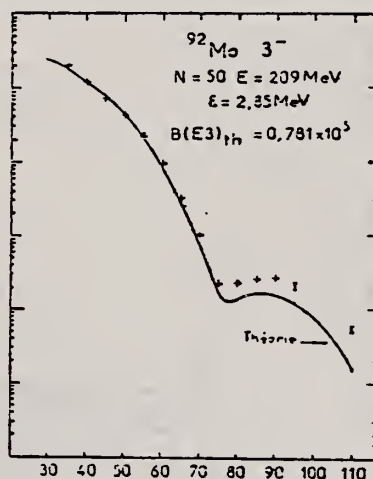


Fig. 2

REF. R. Bergere, H. Beil, P. Carlos, A. Lepretre, A. Veyssiere  
PICNS-73, Vol. I, p. 525 Asilomar

ELEM. SYM.	A	Z
Mo	92	42
REF. NO.		73 Be 10
		hmg

METHOD

REACTION	RESULT	EXCITATION ENERGY	SOURCE		DETECTOR		ANGLE
			TYPE	RANGE	TYPE	RANGE	
G, SN	ABX	12- 28	D	12- 28	BF3-I		4PI

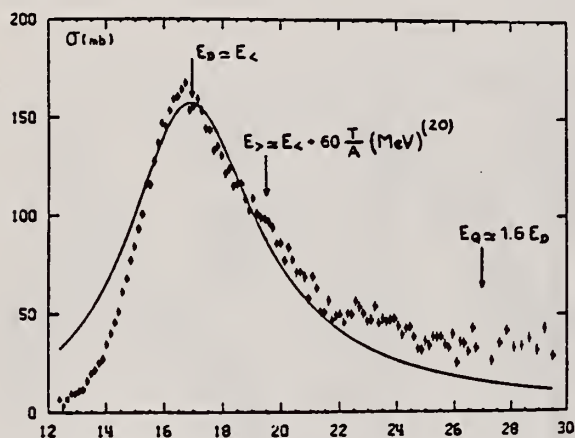


Fig. 14 Total  $\sigma(\gamma, n) + \sigma(\gamma, pn) + \sigma(\gamma, 2n)$  cross section of  $^{92}\text{Mo}$ .

Table I

Isotopes	$^{92}\text{Mo}$	$^{94}\text{Mo}$	$^{96}\text{Mo}$	$^{98}\text{Mo}$	$^{100}\text{Mo}$
$\sigma_{\text{on}}$	0.83	0.98	1.08	1.11	1.08

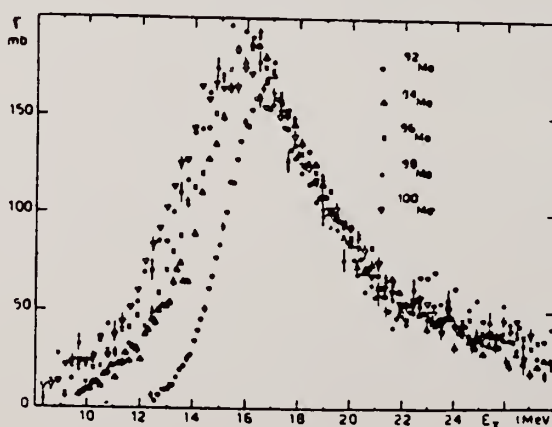


Fig. 15 Comparison of the total photoneutron cross sections of  $^{92}\text{Mo}$ ,  $^{94}\text{Mo}$ ,  $^{96}\text{Mo}$ ,  $^{98}\text{Mo}$  and  $^{100}\text{Mo}$



METHOD

REF. NO.

73 Ho 4

egf

REACTION	RESULT	EXCITATION ENERGY	SOURCE		DETECTOR		ANGLE
			TYPE	RANGE	TYPE	RANGE	
E, E/	FMF	1- 3	D	209	MAG-D		DST

1.51, 2.28, 2.85

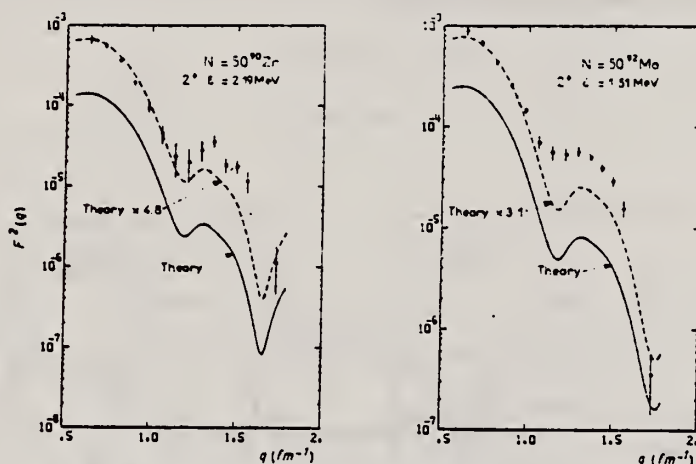


Fig. 5b. Squared inelastic form factor for 2<sup>+</sup> states of the N = 50 isotones.

TABLE 6  
Inelastic cross sections for E<sub>α</sub> = 209 MeV on <sup>92</sup>Mo

	θ (deg.)	(2 <sup>+</sup> )ε = 1.51 MeV da/dΩ(mb/sr)	(3 <sup>-</sup> )ε = 2.85 MeV da/dΩ(mb/sr)	(4 <sup>+</sup> )ε = 2.28 MeV da/dΩ(mb/sr)
(3 <sup>-</sup> ) 3.57 → —————	35	0.209 E-1 ± 0.220 E-2	0.197 E-1 ± 0.220 E-2	
(2 <sup>+</sup> ) 3.09 → —————	40	0.916 E-2 ± 0.630 E-3	0.114 E-1 ± 0.700 E-3	0.161 E-2 ± 0.300 E-3
	45	0.363 E-2 ± 0.200 E-3	0.708 E-2 ± 0.440 E-3	0.112 E-2 ± 0.100 E-3
(3 <sup>-</sup> ) 2.85 → —————	50	0.139 E-2 ± 0.800 E-4	0.418 E-2 ± 0.230 E-3	0.829 E-3 ± 0.630 E-4
	55	0.533 E-3 ± 0.400 E-4	0.221 E-2 ± 0.140 E-3	0.593 E-3 ± 0.410 E-4
(6 <sup>+</sup> ) 2.61 → - - - - -	60	0.175 E-3 ± 0.250 E-4	0.957 E-3 ± 0.470 E-4	0.367 E-3 ± 0.280 E-4
(5 <sup>-</sup> ) 2.52 → - - - - -	65	0.996 E-4 ± 0.153 E-4	0.330 E-3 ± 0.220 E-4	0.215 E-3 ± 0.130 E-4
(4 <sup>+</sup> ) 2.28 → —————	70	0.697 E-4 ± 0.880 E-5	0.100 E-3 ± 0.120 E-4	0.124 E-3 ± 0.110 E-4
	75	0.549 E-4 ± 0.560 E-5	0.223 E-4 ± 0.710 E-5	0.469 E-4 ± 0.600 E-5
	80	0.362 E-4 ± 0.280 E-5	0.232 E-4 ± 0.400 E-5	0.193 E-4 ± 0.250 E-5
	85	0.214 E-4 ± 0.170 E-5	0.260 E-4 ± 0.330 E-5	0.509 E-5 ± 0.169 E-5
	90	0.122 E-4 ± 0.130 E-5	0.270 E-4 ± 0.250 E-5	0.137 E-5 ± 0.940 E-6
(2 <sup>+</sup> ) 1.51 → —————	95	0.501 E-5 ± 0.900 E-6	0.215 E-4 ± 0.220 E-5	0.877 E-6 ± 0.687 E-6
	110	0.546 E-7 ± 0.325 E-7	0.536 E-5 ± 0.440 E-6	0.422 E-6 ± 0.210 E-6

Energy level diagram given by ref. <sup>24</sup>). Levels excited in our experiment are shown with solid lines, dashed lines correspond to other levels. The experimental values are normalized with the elastic cross sections calculated by a phase shift program using a 3-parameter Gaussian model. The parameters (c = 4.610, z = 2.520, w = 0.190) are obtained from ref. <sup>18</sup>).

(over)

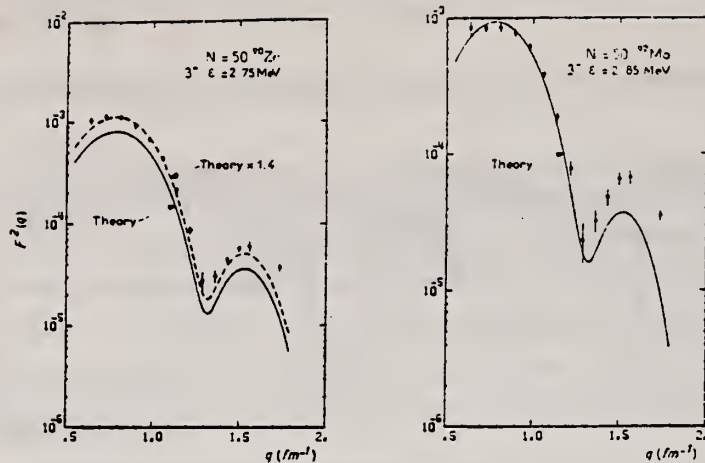


Fig. 6b. Squared inelastic form factor for  $3^-$  states of the  $N = 50$  isotones.

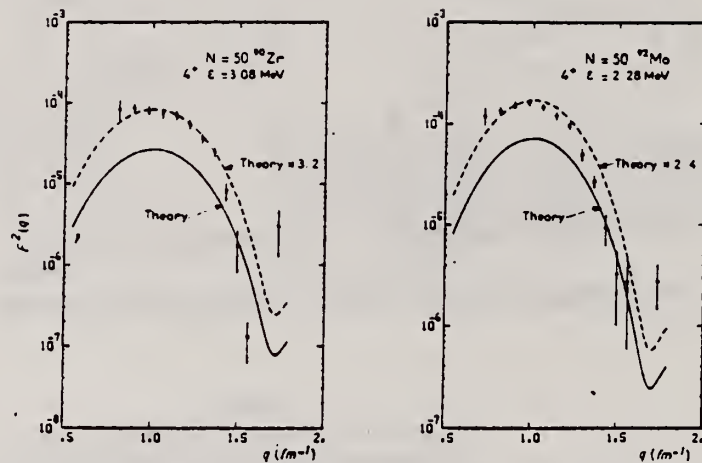


Fig. 7b. Squared inelastic form factor for  $4^+$  states of the  $N = 50$  isotones.

<sup>18</sup> Phan-Xuan Ho, J. Bellicard, A. Bussiere, M. Priou,  
Nucl. Phys. A179 (1972) 529.

<sup>24</sup> Nuclear Data Sheets B (1970).

REF.		H. Beil, R. Bergere, P. Carlos, A. Lepretre, A. De Miniac, and A. Veyssiere Nucl. Phys. <u>A227</u> , 427 (1974)				ELEM. SYM.		A	Z
						Mo		92	42
METHOD						REF. NO.			
						74 Be 3		egf	
REACTION	RESULT	EXCITATION ENERGY	SOURCE		DETECTOR		ANGLE		
			TYPE	RANGE	TYPE	RANGE			
G,N *	ABX	12- 30	D	12- 30	BF3-I		4PI		
G,2N **	ABX	22- 30	D	22- 30	BF3-I		4PI		

\* 693  
\*\* 694+

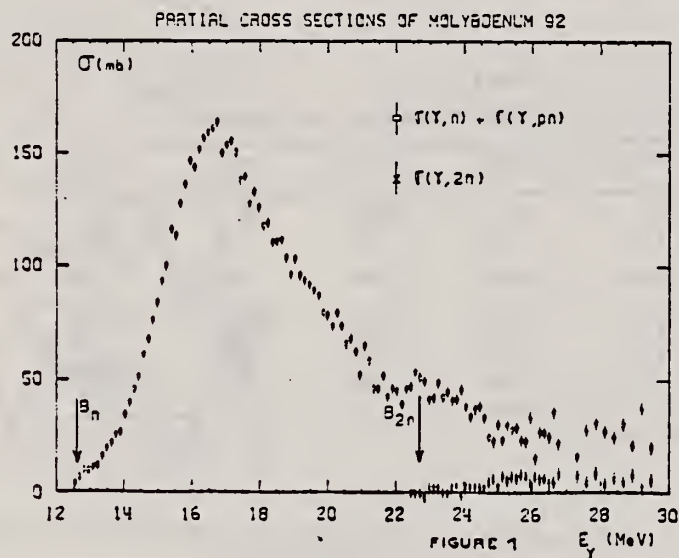


Fig. 1. Partial photoneutron cross sections  $\sigma(\gamma, n) + \sigma(\gamma, pn)$  and  $\sigma(\gamma, 2n)$  of  $^{92}\text{Mo}$ . Arrows  $B_n$  and  $B_{2n}$  indicate theoretical threshold values for  $(\gamma, n)$  and  $(\gamma, 2n)$  reactions respectively.

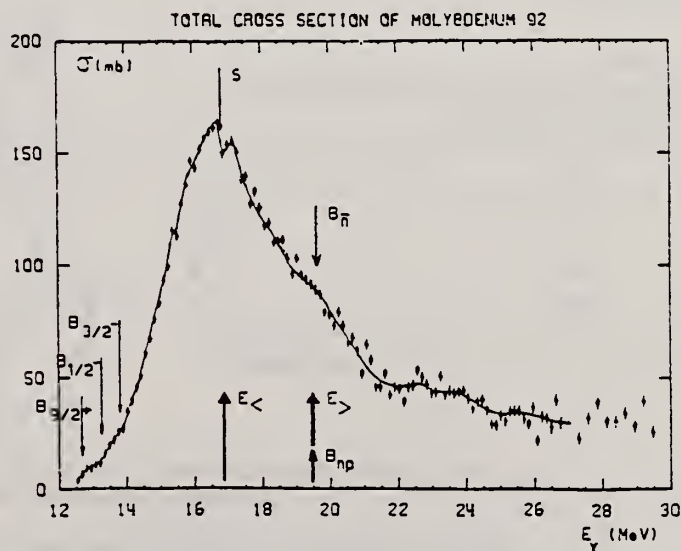


Fig. 7. Total photoneutron cross section  $\sigma_{\gamma,n}(E)$  of  $^{92}\text{Mo}$ . The solid line is merely to guide the eye.

(over)

TABLE 3

Lorentz line parameters  $E_1$ ,  $\sigma_1$  and  $\Gamma_1$  corresponding to the best single Lorentz line fits to the experimental  $\sigma_{T,n}(E)$  curves shown in fig. 12

	$E_1$ (MeV)	$\sigma_1$ (mb)	$\Gamma_1$ (MeV)
$^{92}\text{Mo}$	$16.9 \pm 0.1$	$154 \pm 10$	$5.4 \pm 0.2$
$^{94}\text{Mo}$	$16.4 \pm 0.1$	$184 \pm 10$	$5.7 \pm 0.2$
$^{96}\text{Mo}$	$16.2 \pm 0.1$	$184 \pm 10$	$6.3 \pm 0.2$
$^{98}\text{Mo}$	$15.8 \pm 0.1$	$189 \pm 15$	$6.0 \pm 0.2$
$^{100}\text{Mo}$	$15.7 \pm 0.1$	$170 \pm 10$	$7.9 \pm 0.2$

TABLE 4

Integrated photoneutron cross sections and sum rules of the Mo isotopes

Nucleus	$^{92}\text{Mo}$	$^{94}\text{Mo}$	$^{96}\text{Mo}$	$^{98}\text{Mo}$	$^{100}\text{Mo}$
$E_M$ (MeV)	29	29	29.5	29	28.5
$\sigma_{0n}$ (MeV · b)	1.10	1.37	1.53	1.60	1.53
$\frac{\sigma_{0n}}{0.06 N Z A^{-1}}$	0.804	0.98	1.08	1.11	1.08
$\sigma_{-1n}$ (mb)	60	79.3	89.2	95.4	95.4
$\sigma_{-1n} A^{-\frac{1}{3}}$ (mb)	0.145	0.186	0.203	0.211	0.206
$\sigma_{-2n}$ (mb · MeV $^{-1}$ )	3.3	4.8	5.1	6.0	6.1
$\sigma_{-2n} A^{-\frac{1}{3}}$ ( $\mu\text{b} \cdot \text{MeV}^{-1}$ )	1.77	2.48	2.55	2.91	2.86

The notation used is defined in the text.



REF. K. Shoda, H. Miyase, M. Sugawara, T. Saito, S. Oikawa,  
A. Suzuki, J. Uegaki  
Nucl. Phys. A239, 397 (1975)

ELEM. SYM.	A	Z
Mo	92	42
REF. NO.		egf
75 Sh 4		

METHOD					REF. NO.		
					75 Sh 4	egf	
REACTION	RESULT	EXCITATION ENERGY	SOURCE		DETECTOR		ANGLE
			TYPE	RANGE	TYPE	RANGE	
E,P	ABX	14- 26	D	14- 25	MAG-D		90

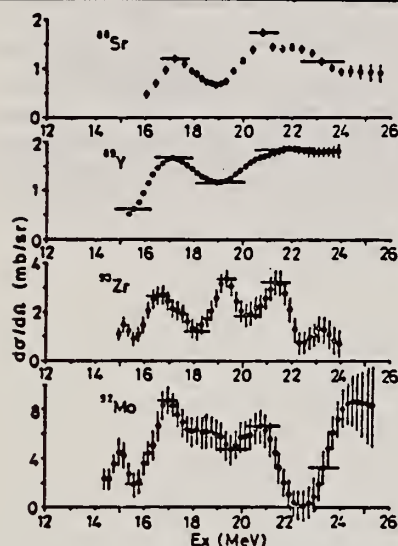


Fig. 3. Differential ( $\gamma$ , p) cross sections at  $\theta = 90^\circ$  analysed from (e, e'p) cross sections by the least structure method.

El virtual photon spectrum used to obtain ( $\gamma$ , p) cross sections.

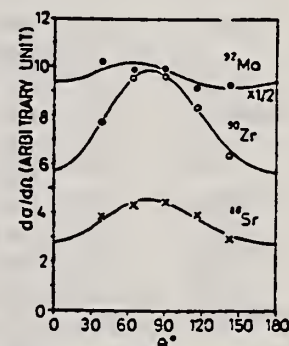


Fig. 4. Angular distributions of protons from the (e, e'p) reaction. The bombarding energies are 21.5, 22 and 20 MeV for  $^{88}\text{Sr}$ ,  $^{90}\text{Zr}$  and  $^{92}\text{Mo}$  respectively. The best fit curves obtained with eq. (7) are also shown.

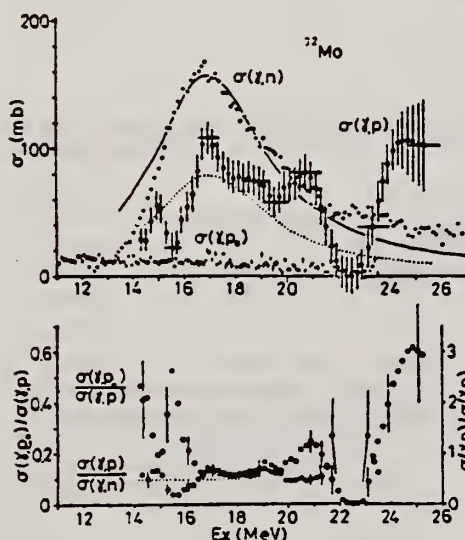


Fig. 5. Upper figure: open circles,  $\sigma(\gamma, p)$ ; closed circles,  $\sigma(\gamma, n)$  [ref. <sup>18</sup>]; closed points,  $\sigma(\gamma, p_0)$  [ref. <sup>18</sup>]; solid line, Lorentz line fit to the  $T_{<}$  region of  $\sigma(\gamma, n)$  [ref. <sup>18</sup>]; dotted line, Lorentz line fit to the  $T_{<}$  region of  $\sigma(\gamma, p)$  with  $\Gamma_i$  and  $E_R$  equal to those of  $\sigma(\gamma, n)$ . Lower figure: ratio between cross sections. Dotted line: constant for  $\sigma(\gamma, p)/\sigma(\gamma, n)$  determined around  $T_{<}$  GDR.

Fig. 5. Upper figure: open circles,  $\sigma(\gamma, p)$ ; closed circles,  $\sigma(\gamma, n)$  [ref. <sup>18</sup>]; closed points,  $\sigma(\gamma, p_0)$  [ref. <sup>18</sup>]; solid line, Lorentz line fit to the  $T_{<}$  region of  $\sigma(\gamma, n)$  [ref. <sup>18</sup>]; dotted line, Lorentz line fit to the  $T_{<}$  region of  $\sigma(\gamma, p)$  with  $\Gamma_i$  and  $E_R$  equal to those of  $\sigma(\gamma, n)$ . Lower figure: ratio between cross sections. Dotted line: constant for  $\sigma(\gamma, p)/\sigma(\gamma, n)$  determined around  $T_{<}$  GDR.

<sup>a</sup>) Relative value.

TABLE 2

The parameters of the angular distributions determined by the least-squares fits with  $d\sigma/d\Omega = A[1 + B\sin^2\theta(1 - \rho\cos\theta)]$

	$^{88}\text{Sr}$	$^{90}\text{Zr}$	$^{92}\text{Mo}$
$E_a$ (MeV)	21.5	22	20
$A^a$	1	2.04	6.67
$B$	0.59	0.69	0.057
$\rho$	0.59	0.47	2.3

<sup>15</sup> K. Shoda et al., Nucl. Phys. A221 (1974) 125

<sup>18</sup> A. Lepretre et al., Nucl. Phys. A175 (1971) 609



REF.

H. Bartsch, K. Huber, U. Kneissl, H. Krieger  
Nucl. Phys. A256, 243 (1976)

ELEM. SYM.	A	Z
Mo	92	42
REF. NO.		egf
76 Ba 1		

METHOD

REACTION	RESULT	EXCITATION ENERGY	SOURCE		DETECTOR		ANGLE
			TYPE	RANGE	TYPE	RANGE	
G, N	RLY	THR-UKN	C	UKN	SCD-D		4PI

TABLE I  
Experimental and theoretical results

ISOMER RATIO

Process	Target-spin	$E_\gamma$ (keV)	$T_{1/2}$	Spin high	Spin low	$R_{exp} = \frac{\sigma_{high}}{\sigma_{low}}$	SCOP (%)
$^{181}\text{Ta}(\gamma, 3n)$	$\frac{7}{2}^+$	93	2.2 h 9.31 min. 8.15 h	$7^-$	$1^+$	$0.51 \pm 0.09$	$3.6 \pm 0.2$
$^{142}\text{Nd}(\gamma, n)$	$0^+$	755 1100-1300, 145	63 s 2.5 h	$\frac{7}{2}^-$	$\frac{1}{2}^+$	$0.055 \pm 0.006$ $0.19 \pm 0.01^*)$	$2.20 \pm 0.06$
$^{92}\text{Mo}(\gamma, n)$	$0^+$	652.9 1208, 1508, 1581, 1637	66 s 15.49 min	$\frac{1}{2}^+$	$\frac{1}{2}^-$	$1.03 \pm 0.21$ $0.85 \pm 0.07^*)$ $1.92 \pm 0.15^*)$	$5.03 \pm 0.75$ $4 \pm \frac{1}{2}$
$^{100}\text{Mo}(\gamma, n)$	$0^+$	97.3 140.5	$16.8 \mu\text{s}$ 66.02 h	$\frac{1}{2}^+$	$\frac{1}{2}^+$	$0.85 \pm 0.24$	$1.72 \pm 0.25$
$^{108}\text{Pd}(\gamma, n)$	$0^+$	214.5 115	22 s 850 ns	$\frac{7}{2}^-$	$\frac{1}{2}^+$	$0.5 \pm 0.2$	$3.4 \pm 0.5$
$^{110}\text{Pd}(\gamma, n)$	$0^+$	188 113 87.7	4.7 min 390 ns 13.47 h	$\frac{7}{2}^-$ $\frac{7}{2}^-$ $\frac{1}{2}^+$	$\frac{1}{2}^+$ $\frac{1}{2}^+$ $\frac{1}{2}^+$	$0.11 \pm 0.02$ $0.41 \pm 0.09$ $3.2 \pm 0.7$	$3.14 \pm 0.15$ $3.0 \pm 0.25$ $3.3 \pm 0.4$
$^{89}\text{Y}(\gamma, n)$	$\frac{1}{2}^-$	231.7 442.3 392.5	14.2 ms  $300 \mu\text{s}$	$8^+$	$1^+$	$0.056 \pm 0.008$	

\*) Ref. <sup>14</sup>). \*) Ref. <sup>15</sup>).<sup>14</sup> P.E. Haustein et al., J. Inorg. Nucl. Chem. 33, 289 (1971)<sup>15</sup> J.H. Carver et al., Nucl. Phys. 37, 449 (1962)

ELEM. SYM.	A	Z
Mo	92	42
REF. NO.		
77 Me 2		hmg

METHOD			REF. NO.		
			77 Me 2		hmg
REACTION	RESULT	EXCITATION ENERGY	SOURCE		ANGLE
			TYPE	RANGE	
G,G	LFT	1- 5	C	2- 6	DST
		(1.509-4.634)		(2.0-5.1)	

Levels in  $^{92}\text{Mo}$  at 1.509 ( $2^+$ ), 3.091 ( $2^+$ ), 3.925 ( $2^+$ ), 3.942, and 4.634 MeV have been excited by bremsstrahlung. Based on the angular distributions of the resonantly scattered  $\gamma$  lines, spin one can be unambiguously assigned to the 3.942- and 4.634-MeV levels. The lifetimes deduced from the scattering yields are compared with the results of two sets of Doppler shift attenuation experiments which had been analyzed using different theories for the attenuation factor  $F(\tau)$ .

5 STATES 1.509-4.634

TABLE II. Comparison of the lifetimes derived for the  $^{92}\text{Mo}$  states from the resonance fluorescence experiments with DSAM results.

$E_{\text{Level}}$ (MeV)	Resonance fluorescence	Mean lifetimes (fs)	
		Doppler shift attenuation Winterbon $F(\tau)$	Blaugrund $F(\tau)$
1.509	$582 \pm 37$	$520^{+120}_{-70}^b$	$420^{+80}_{-50}^b$
3.091	$46.3 \pm 4.0$	$50^{+5}_{-4}^b$	$31^{+3}_{-3}^c$
3.925	$15.3 \pm 3.6$	$24^{+23}_{-15}^b$	$29^{+23}_{-17}^c$
3.942	$16.5 \pm 2.5$	$14^{+15}_{-4}^b$	$30^{+23}_{-17}^c$

<sup>a</sup> Energies according to Ref. 3 (rounded off).

<sup>b</sup> Ref. 1.

<sup>c</sup> Ref. 3.

TABLE I. Properties of the  $^{92}\text{Mo}$  levels excited with bremsstrahlung of energy  $\leq 5.1$  MeV.

$E_{\text{Level}}$ (MeV)	$J^\pi$	$\Gamma_0/\Gamma$	$\Gamma_0^2/\Gamma$ (meV)	$\Gamma_0$ (meV)	$\Gamma$ (meV)
1.509(1)	$2^+$	1	$1.13 \pm 0.07$	$1.13 \pm 0.07$	$1.13 \pm 0.07$
3.092(2)	$2^+$	$0.82(2)^b$	$9.3 \pm 0.6$	$11.3 \pm 0.8$	$13.8 \pm 1.2$
3.925(2)	$2^+$	$0.65(5)^b$	$18 \pm 3$	$28 \pm 5$	$43 \pm 10$
3.944(2)	$1^a$	$1^b$	$40 \pm 6$	$\begin{cases} 40 \pm 6 \\ 60 \pm 20^c \end{cases}$	$40 \pm 6$
4.634(2)	$1^a$	$0.59 \pm 0.19^d$	$86 \pm 13$	$145 \pm 40^c$	$250 \pm 110$

<sup>a</sup> Energies deduced from the resonance fluorescence data.

<sup>b</sup> Combining the results of Refs. 3 and 10.

<sup>c</sup> From a self-absorption experiment.

<sup>d</sup> From a comparison of columns 4 and 5.

<sup>1</sup> R. Doerr, F. Rauch, et al., Proc. Int. Conf. on Nucl. Struc. and Spectroscopy, Amsterdam, 1974, ed. by H.P. Blok and A.E.L. Dieperink (Scholar's Press, Amsterdam, 1974), Vol.1, p.130.

<sup>3</sup> C.T. Papadopoulos et al., Nucl. Phys. A254, 93 (1975).

<sup>10</sup> R. Doerr et al., Jahresbericht 1973 (IKF-32), Inst. fur Kernphysik, Frankfurt/Main (unpublished) p.22.

REF. H. Bartsch, K. Huber, U. Kneissl and H. Krieger  
Z. Physik A285, 273 (1978)

ELEM. SYM.	A	Z
Mo	92	42

METHOD

REF. NO.  
78 Ba 11

hmg  
11/17/80

REACTION	RESULT	EXCITATION ENERGY	SOURCE		DETECTOR		ANGLE
			TYPE	RANGE	TYPE	RANGE	
G,NPG	LFT	*123(122.6)	C	20,40	SCD-D	---	135

Short-lived isomers in the nuclei  $^{90,92}\text{Nb}$ ,  $^{99}\text{Mo}$ ,  $^{98,100,101}\text{Tc}$  and  $^{101}\text{Ru}$  populated in photonuclear reactions were studied by pulsed beam techniques. Energy and half-life of the  $\gamma$ -rays deexciting the isomeric levels were measured by recording energy-time spectra. The delayed  $\gamma$ -rays and K X-rays were detected by means of an intrinsic Ge-detector of high resolution. From the measured intensity ratios internal conversion coefficients were determined. The multipolarities of the isomeric transitions could be deduced in most cases. A classification of the observed isomers has been tried on the basis of the obtained experimental results and most recent literature data.

\*KeV, Isomer LFT

Table I. Experimental results. E: energy,  $T_{1/2}$ : half-life,  $I_{rel}$ : relative intensity, L: multipolarity, H: hindrance factor

Line	E [keV]	$T_{1/2}$ [ $\mu\text{s}$ ]	$T_{1/2}$ [ $\mu\text{s}$ ] (weighted average)	$I_{rel}$	$\alpha_K$	Intensity ratios	L	H
$^{90}\text{Nb}$ K X-rays	—	—	—	1	—	—	—	—
123	$122.6 \pm 0.2$	$63 \pm 2$	—	2.5	$0.56 \pm 0.22$	—	E2	120
$^{92}\text{Nb}$ K X-rays	—	—	—	1	—	—	—	—
90	$90.4 \pm 0.2$	$5.9 \pm 0.2$	—	10.3	$0.14 \pm 0.01$	—	E1	$1.5 \cdot 10^7$
$^{99}\text{Mo}$ K X-rays	—	$15.2 \pm 0.4$	$15.5 \pm 0.2$	1	—	—	—	—
98	$97.8 \pm 0.1$	$15.6 \pm 0.2$	—	0.95	$1.45 \pm 0.27$	—	E2	20
138	$137.7 \pm 0.2$	$0.79 \pm 0.09$	$0.76 \pm 0.06$	1	—	$I_{430}/I_{138} =$	M1	—
449	$449.2 \pm 0.2$	$0.74 \pm 0.08$	—	0.97	—	$0.97 \pm 0.08$	(M2)	(37)
$^{98}\text{Tc}$ K X-rays	—	$14.8 \pm 0.5$	$14.6 \pm 0.4$	1	—	—	—	—
22	$21.8 \pm 0.2$	$16.4 \pm 2.7$	from X, 43	0.036	—	$I_{43}/I_{22} =$	E1 + 1% M2	$10^7$
26	—	—	—	—	—	$5.1 \pm 0.5$	(E2)	—
43	$43.5 \pm 0.2$	$14.4 \pm 0.5$	—	0.18	—	—	M1	—
$^{100}\text{Tc}$ K X-rays	—	$8.2 \pm 0.7$	$8.2 \pm 0.3$	1	—	—	—	—
29	$28.7 \pm 0.3$	—	from X, 172	0.027	—	$I_{172}/I_{29} =$	E2	1
172	$172.3 \pm 0.3$	$8.2 \pm 0.3$	—	2.2	—	$82 \pm 40$	(M1, E2)	—
$^{101}\text{Tc}$ K X-rays	—	—	—	1	—	—	—	—
192	$192.0 \pm 0.3$	$636 \pm 8$	—	5.0	$0.26 \pm 0.06$	—	M2	560
$^{101}\text{Ru}$ K X-rays	—	$16.1 \pm 3.9$	$17.5 \pm 0.4$	1	—	—	—	—
220	$220.7 \pm 0.2$	$17.4 \pm 0.5$	from 220, 306	7.5	—	$I_{306}/I_{220} =$	M2	28
306	$306.6 \pm 0.3$	$17.7 \pm 0.6$	—	9.1	—	$1.2 \pm 0.1$	—	—



ELEM. SYM.	A	Z
Mo	92	42

METHOD	REF. NO.	
	78 Ma 10	hg

REACTION	RESULT	EXCITATION ENERGY	SOURCE		DETECTOR		ANGLE
			TYPE	RANGE	TYPE	RANGE	
G,2N	ABY	23-68	C	30-68	ACT - I		4PI

Analysis is made of reactions interfering with photon activation analysis procedures.

The activation yield curves have been presented for a number of photonuclear reactions in the energy range from 30 to 68 MeV, in order to evaluate quantitatively the interferences due to competing reactions in multielement photon activation analysis. The general features of the yields as functions of both target mass number and excitation energy were elucidated from the data obtained, discussion being given on the results in terms of the reaction mechanism.

Simultaneous neutron activation due to appreciable neutron production from the converter and surrounding materials has also been studied, and, finally, the magnitudes of interferences in real multielement analysis were given in the form of their energy dependences.

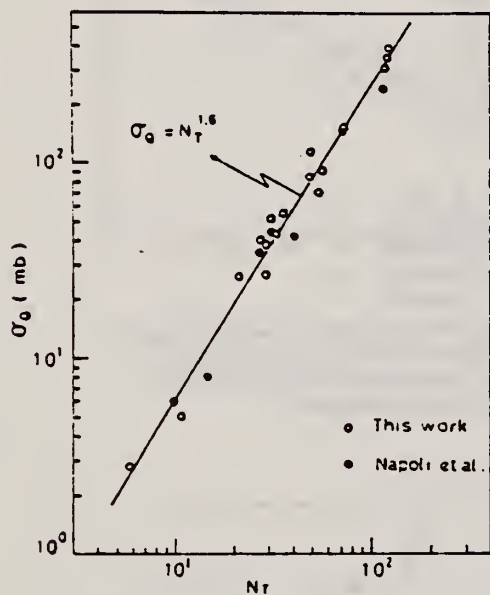


Fig. 2. Yield per equivalent quanta versus target neutron number.

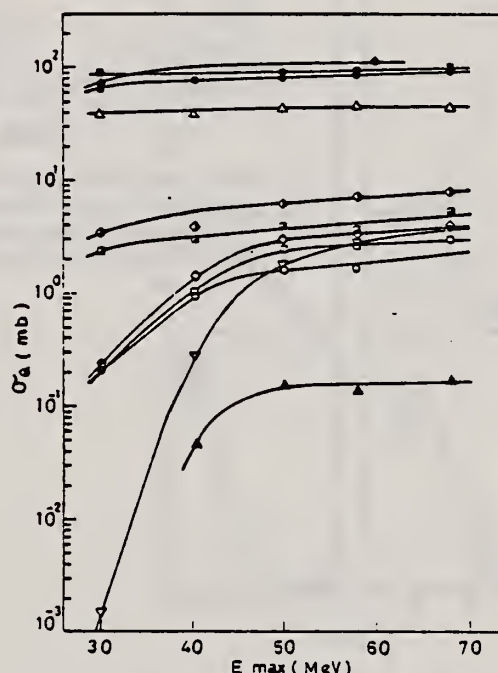


Fig. 7. Activation yield curves for the reactions on Y, Zr, Nb and Mo.

◆  $^{89}\text{Y}(\gamma, n)^{88}\text{Y}$ ,    ●  $^{90}\text{Zr}(\gamma, n)^{89}\text{Zr}$ ,    ○  $^{90}\text{Zr}(\gamma, pn)^{88}\text{Y}$ ,  
 △  $^{93}\text{Nb}(\gamma, n)^{92m}\text{Nb}$ ,    ▲  $^{93}\text{Nb}(\gamma, xn)^{88}\text{Y}$ ,    ■  $^{100}\text{Mo}(\gamma, n)^{99}\text{Mo}$ ,  
 ◇  $^{97}\text{Mo}(\gamma, p)^{96}\text{Nb}$ ,    ▤  $^{96}\text{Mo}(\gamma, p)^{95m}\text{Nb}$ ,    ◊  $^{94}\text{Mo}(\gamma, pn)^{92m}\text{Nb}$ ,  
 □  $^{92}\text{Mo}(\gamma, 2n)^{90}\text{Mo}$ ,    ▽  $^{94}\text{Mo}(\gamma, xn)^{89}\text{Zr}$ .

REF.

J.J. Murphy, II, D.M. Skopik, J. Asai, and J. Uegaki  
Phys. Rev. C 18, 736 (1978)

ELEM. SYM.

A

Z

Mo

92

42

METHOD

REF. NO.

78 Mu 9

hg

REACTION	RESULT	EXCITATION ENERGY	SOURCE		DETECTOR		ANGLE
			TYPE	RANGE	TYPE	RANGE	
E,A	ABX	5-100	D	100	MAG-D		DST

$\alpha$  particles from the electrodisintegration of seven nuclei with Z between 29 and 79 have been observed. Energy spectra at 50° in the laboratory for six nuclei and angular distributions for five nuclei are reported. The cross sections exhibit a broad peak whose magnitude decreases with increasing Z; the energy of the peak increases as Z increases. Angular distributions at the highest energies measured become increasingly forward peaked suggesting a direct-reaction process.

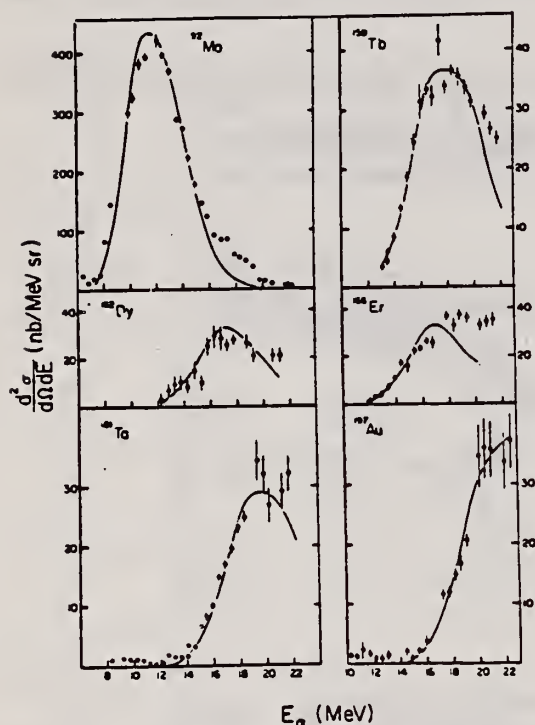


FIG. 2. The  $\alpha$ -particle energy spectra at 50° in the laboratory for the four new nuclei studied as well as for two nuclei in which additional data have been obtained. The solid curves are the evaporation model fits described in text.

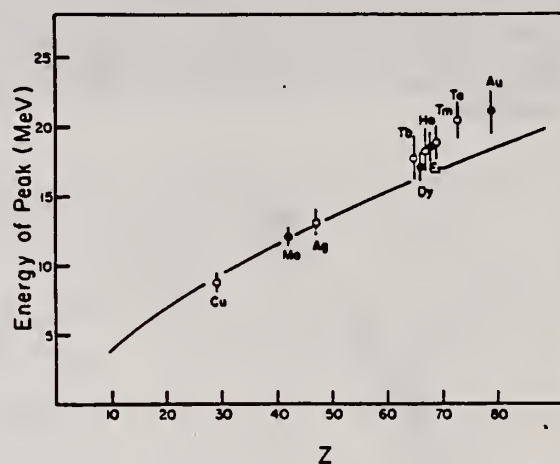


FIG. 3. Energy of the cross section peak as a function of Z. The solid line is the energy of the classical Coulomb barrier. The closed circles are the current work; the open circles are from Ref. 1.

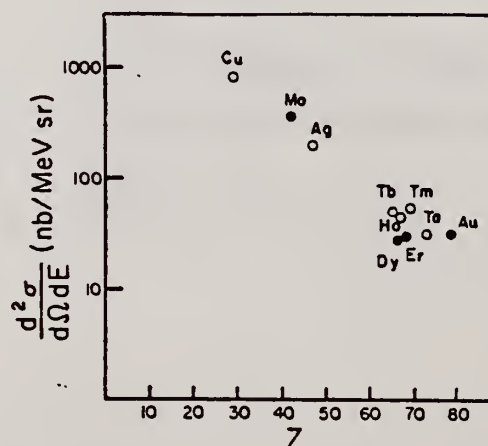


FIG. 4. Magnitude of cross section peak as a function of Z. The closed circles are the current work; the open circles are from Ref. 1.

<sup>1</sup>J.J. Murphy, II, H.J. Gehrhardt, and D.M. Skopik, Nucl. Phys. A277, 69 (1977)



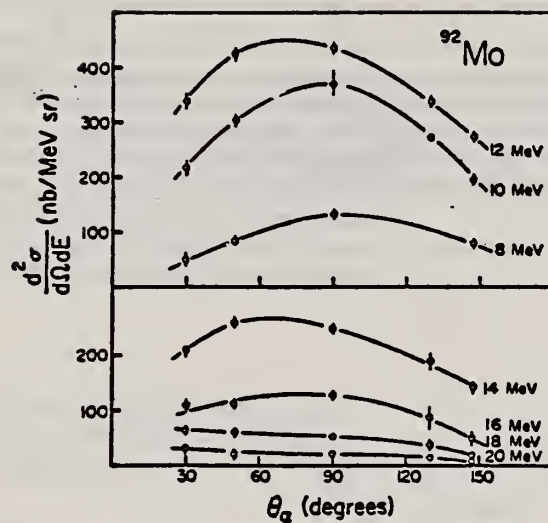


FIG. 5. Angular distributions for molybdenum. Errors are statistical; curves are to guide the eye. Increased forward peaking with increasing energy is taken as evidence for the importance of the direct process at higher energies.

REF.	A. G. Flowers, D. Branford, J. C. McGeorge, A. C. Shotter, P. Thorley C. H. Zimmerman, R. O. Owens, J. S. Pringle Phys. Rev. Lett. <u>43</u> , 323 (1979)	ELEM. SYM.	A	Z
		Mo	92	42
METHOD		REF. NO.		
		79F12		hg

REACTION	RESULT	EXCITATION ENERGY	SOURCE		DETECTOR		ANGLE
			TYPE	RANGE	TYPE	RANGE	
E,A	SPC	UKN	D	120	MAG-D		30

This paper presents energy spectra of  $\alpha$  particles emitted following the bombardment of  $^{27}\text{Al}$ ,  $^{nat}\text{Ni}$ ,  $^{92}\text{Mo}$ ,  $^{94}\text{Mo}$ , and  $^{197}\text{Au}$  with 120-MeV electrons, together with  $\alpha$ -particle angular distributions from  $^{197}\text{Au}$  and  $^{nat}\text{Ni}$  for  $E_\alpha = 30$  and 50 MeV. The data are compared with preequilibrium exciton-model and statistical-model calculations. It is concluded that few-step processes are dominant in the production of  $\alpha$  particles with energies above 20 MeV.

# PREEQUILIB A EMISS

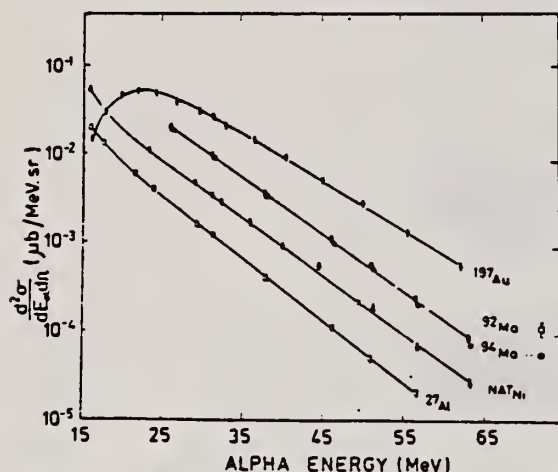


FIG. 1.  $\alpha$ -particle energy spectra at  $\theta_\alpha = 30^\circ$ , for  $E_e = 120$  MeV. Errors shown are the sum of statistical and systematic contributions. The solid lines are a guide to the eye.

TABLE I. Temperatures corresponding to the pre-equilibrium component of the  $(e, \alpha)$  reaction, derived from energy spectra at  $\theta_\alpha = 30^\circ$  for  $E_e = 120$  MeV.

Target	Temperature <sup>a</sup> (MeV)
$^{27}\text{Al}$	5.3
$^{nat}\text{Ni}$	5.5
$^{68}\text{Zn}$	5.4
$^{92}\text{Mo}$	5.6
$^{94}\text{Mo}$	5.4
$^{197}\text{Au}$	6.1

<sup>a</sup>Error is  $\pm 0.2$  MeV.

REF. T.J. Bowles, R.J. Holt, H.E. Jackson, R.M. Laszewski, R.D. McKeown,  
A.M. Nathan, J.R. Specht  
Phys. Rev. C24, 1940 (1981)

ELEM. SYM.	A	Z
Mo	92	42

REF. NO.	hg
81 Bo 5	

METHOD				REF. NO.	
				81 Bo 5	

REACTION	RESULT	EXCITATION ENERGY	SOURCE		DETECTOR		ANGLE
			TYPE	RANGE	TYPE	RANGE	
G,G	ABX	15-23	D	15-23	NAI-D		90

Quasimonochromatic photons have been used to measure elastic and inelastic photon scattering cross sections in the giant dipole resonance region of  $^{52}\text{Cr}$ , Fe,  $^{60}\text{Ni}$ ,  $^{92}\text{Mo}$ , and  $^{96}\text{Mo}$  in an experiment in which the elastic and inelastic scattering are resolved. The elastic scattering cross sections show clear evidence for isospin splitting of the giant dipole resonance. The inelastic scattering to low-lying vibrational levels, which is a measure of the coupling between the giant dipole resonance and collective surface vibrations, is in qualitative agreement with the predictions of the dynamic collective model. However, when examined in detail, this model does not provide an adequate description of the scattering data.

NUCLEAR REACTIONS  $^{52}\text{Cr}$ , Fe,  $^{60}\text{Ni}$ ,  $^{92,96}\text{Mo}$  ( $\gamma, \gamma'$ ),  $14 \leq E_\gamma \leq 22$  MeV; measured  $E_\gamma$ ,  $E_{\gamma'}$ ,  $d\sigma/d\Omega$  for  $\gamma_0, \gamma_1$ . Compared to DCM predictions. Tagged photons.

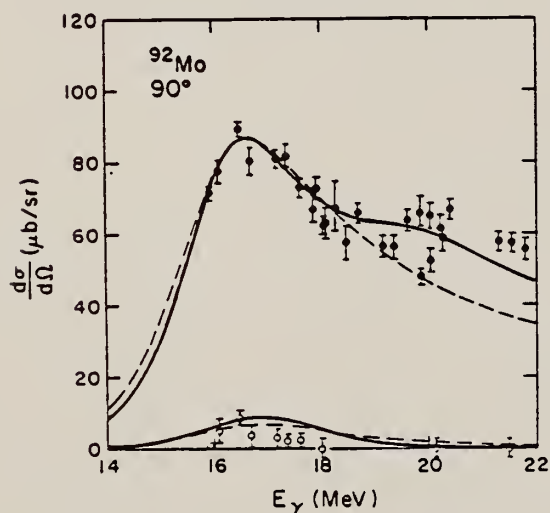


FIG. 5. Elastic (closed circles) and inelastic (open circles) scattering cross sections at  $\theta=90^\circ$  on  $^{92}\text{Mo}$ . The error bars represent statistical uncertainties only. The solid (dashed) lines are DCM calculations for the elastic and inelastic cross sections including (not including) the effect of isospin splitting.

REF. F.Z. Khien, N.K. Zui, N.T. An  
Yad. Fiz. 35, 257 (1982)  
Sov. J. Nucl. Phys. 35, 145 (1982)

ELEM. SYM.	A	Z
Mo	92	42

METHOD	REF. NO.	
	82 Kh 2	egf

REACTION	RESULT	EXCITATION ENERGY	SOURCE		DETECTOR		ANGLE
			TYPE	RANGE	TYPE	RANGE	
G,N	NOX	13-14	C	14	ACT-I		4PI

### ISOMERIC RATIO

The method is developed for calculation of the isomeric ratio for the case of low excitation energy of the residual nucleus, and the isomeric ratio is measured in the  $(n, 2n)$  and  $(\gamma, n)$  reactions in the neutron-deficient nuclei  $^{92}\text{Mo}$ ,  $^{90}\text{Zr}$ ,  $^{88}\text{Sr}$ , and  $^{74}\text{Se}$ . The good agreement between the experimental and theoretical results on the  $(\gamma, n)$  reaction has confirmed the reliability of the characteristics of the residual nuclei, the transmission coefficients of the emitted neutrons, etc., used in the calculations. From study of the  $(n, 2n)$  reaction we have obtained values of the parameters of the spin dependence of the level density of the nucleus in the excitation-energy region  $\sim 14$  MeV.

PACS numbers: 25.20. + y, 25.40.Gr, 27.50. + e, 27.60. + j

TABLE III. Isomeric ratio in the  $(\gamma, n)$  reaction.

Target nucleus	$\alpha_{\text{exp}}$	$\alpha_{\text{theor}}$	Published data <sup>1)</sup>
$^{92}\text{Mo}$	$1.54 \pm 0.15$	1.36	$1.82 \pm 0.15$ (70) [9] $1.03 \pm 0.21$ (10) [10] $0.85 \pm 0.07$ (30) [15]
$^{90}\text{Zr}$	$1.52 \pm 0.04$	1.49	$0.50 \pm 0.15$ (30) [15]
$^{88}\text{Sr}$	$0.70 \pm 0.07$	0.86	$0.68 \pm 0.14$ (30) [15]
$^{74}\text{Se}$	$7.5 \pm 1.0$	$(0.5^{+1.1}_{-0.8})$	

<sup>1)</sup>In parentheses we have given the values of the bremsstrahlung maximum energy.

<sup>2)</sup>In the calculations we used the  $^{74}\text{Se}$  level scheme of Ref. 2,  $I_f = 7/2^+$  and  $I_m = 1/2^+$ .

<sup>3)</sup>In the calculations we used the level scheme of  $^{74}\text{Se}$  in Ref. 3,  $I_f = 9/2^+$  and  $I_m = 3/2^+$ .

110  
A=94

110  
A=94

110  
A=94





REF. P. E. Haustein and A. F. Voigt  
J. inorg. nucl. Chem. 33, 289 (1971)

ELEM. SYM.	A	Z
Mo	94	42

METHOD	REF. NO.	
	71 Ha 2	egf

REACTION	RESULT	EXCITATION ENERGY	SOURCE		DETECTOR		ANGLE
			TYPE	RANGE	TYPE	RANGE	
G, 3N	RLY	31-70	C	70	ACT-I		4PI

Isomer ratio = (yield to low spin state)/(yield to high spin state)

ISOMER RATIO

Table 2. Isomer ratio measurements for  $^{94}\text{Mo}$ ,  $^{137}\text{Ce}$ , and  $^{141}\text{Nd}$

Reaction	Isomer ratio	$I^\pi$ Target	$I^\pi$ Ground state	$I^\pi$ Isomer	Threshold (MeV)	$41A^{-1/3}$ (MeV)
$^{94}\text{Mo}(\gamma, n)^{94}\text{Mo}$	$1.92 \pm 0.15$	$0^+$	$9/2^+$	$1/2^-$	13.13	16.60
$^{94}\text{Mo}(\gamma, 3n)^{91}\text{Mo}$	$1.59 \pm 0.16$	$0^+$			30.72	16.52
$^{137}\text{Ce}(\gamma, n)^{137}\text{Ce}$	3.1	$0^+$	$3/2^+$	$11/2^+$	10.31	15.30
$^{137}\text{Ce}(\gamma, 3n)^{134}\text{Ce}$	$1.10 \pm 0.12$	$0^+$			26.34	15.26
$^{141}\text{Nd}(\gamma, n)^{141}\text{Nd}$	$5.2 \pm 0.3$	$0^+$	$3/2^+$	$11/2^+$	9.79	15.22
$^{141}\text{Nd}(\gamma, 3n)^{138}\text{Nd}$	$1.80 \pm 0.25$	$0^+$			23.67	15.17

ELEM. SYM.	A	Z
Mo	94	42
REF. NO.		hmg
73 Be 10		

METHOD			SOURCE		DETECTOR		ANGLE
REACTION	RESULT	EXCITATION ENERGY	TYPE	RANGE	TYPE	RANGE	
G <sub>p</sub> SN	ABX	9- 28	D	9- 28	BF3-I		4PT

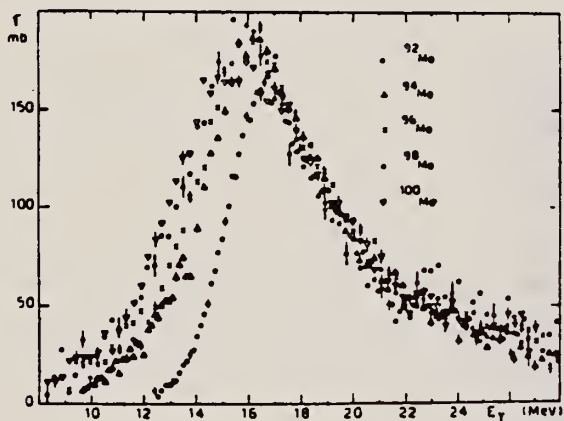


Fig. 15 Comparison of the total photoneutron cross sections of <sup>92</sup>Mo <sup>94</sup>Mo <sup>96</sup>Mo <sup>98</sup>Mo and <sup>100</sup>Mo

Table I

Isotopes	<sup>92</sup> Mo	<sup>94</sup> Mo	<sup>96</sup> Mo	<sup>98</sup> Mo	<sup>100</sup> Mo
σ <sub>on</sub>	0.83	0.98	1.08	1.11	1.08

REF.	H. Beil, R. Bergere, P. Carlos, A. Lepretre, A. De Miniac, and A. Veyssiere Nucl. Phys. <u>A227</u> , 427 (1974)					ELEM. SYM.	A	Z
						Mo	94	42
METHOD						REF. NO.		
						74 Be 3		egf
REACTION	RESULT	EXCITATION ENERGY	SOURCE		DETECTOR		ANGLE	
			TYPE	RANGE	TYPE	RANGE		
* G,N	ABX	9- 28	D	9- 28	BF3-I		4PI	
** G,2N	ABX	15- 28	D	15- 28	BF3-I		4PI	
							* <u>696+</u>	
PARTIAL CROSS SECTIONS OF MOLYBDENUM 94							** <u>697+</u>	

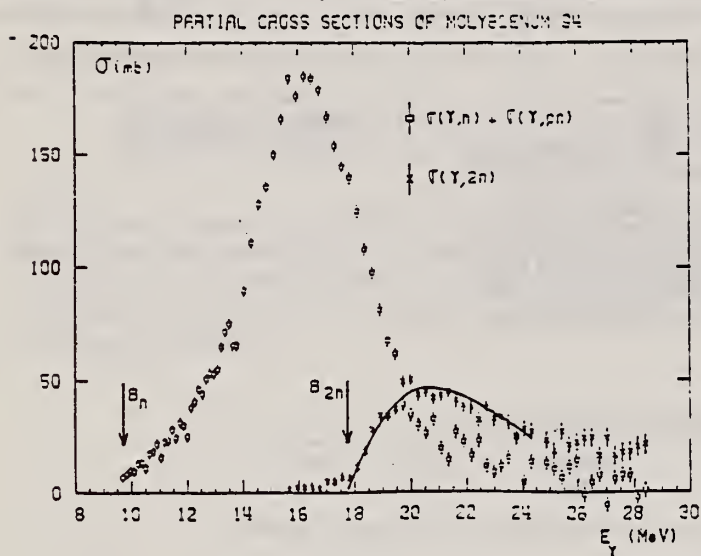


Fig. 2. Same as fig. 1, for <sup>94</sup>Mo.

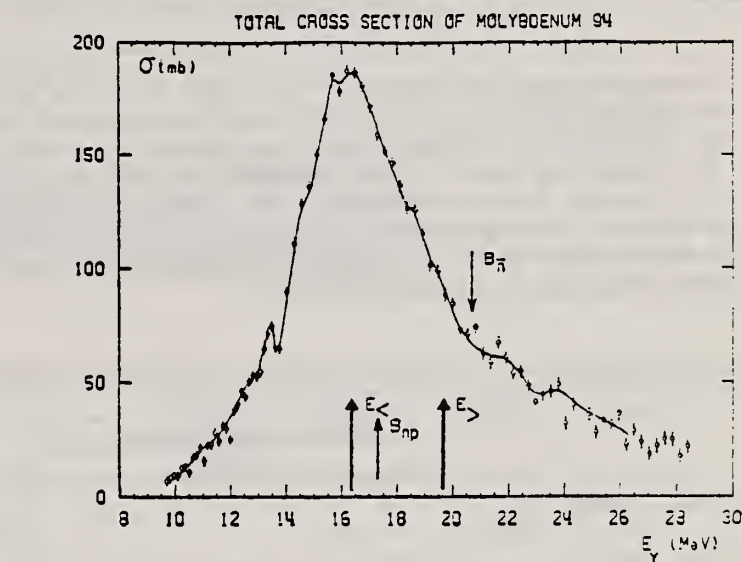


Fig. 8. Same as fig. 7, for <sup>94</sup>Mo.

TABLE 3

Lorentz line parameters  $E_1$ ,  $\sigma_1$  and  $\Gamma_1$  corresponding to the best single Lorentz line fits to the experimental  $\sigma_{T,a}(E)$  curves shown in fig. 12

	$E_1$ (MeV)	$\sigma_1$ (mb)	$\Gamma_1$ (MeV)
<sup>92</sup> Mo	$16.9 \pm 0.1$	$154 \pm 10$	$5.4 \pm 0.2$
<sup>94</sup> Mo	$16.4 \pm 0.1$	$184 \pm 10$	$5.7 \pm 0.2$
<sup>96</sup> Mo	$16.2 \pm 0.1$	$184 \pm 10$	$6.3 \pm 0.2$
<sup>98</sup> Mo	$15.8 \pm 0.1$	$189 \pm 15$	$6.0 \pm 0.2$
<sup>100</sup> Mo	$15.7 \pm 0.1$	$170 \pm 10$	$7.9 \pm 0.2$

TABLE 4

Integrated photoneutron cross sections and sum rules of the Mo isotopes

Nucleus	<sup>92</sup> Mo	<sup>94</sup> Mo	<sup>96</sup> Mo	<sup>98</sup> Mo	<sup>100</sup> Mo
$E_M$ (MeV)	29	29	29.5	29	28.5
$\sigma_{0n}$ (MeV · b)	1.10	1.37	1.53	1.60	1.55
$\sigma_{0n}$	0.804	0.98	1.08	1.11	1.08
$0.06 NZA^{-1}$					
$\sigma_{-1n}$ (mb)	60	79.3	89.2	95.4	95.4
$\sigma_{-1n} A^{-1/3}$ (mb)	0.145	0.186	0.203	0.211	0.210
$\sigma_{-2n}$ (mb · MeV <sup>-1</sup> )	3.3	4.8	5.1	6.0	6.1
$\sigma_{-2n} A^{-1/3}$ (μb · MeV <sup>-1</sup> )	1.77	2.48	2.55	2.91	2.86

REF. H. Bartsch, K. Huber, U. Kneisß and H. Krieger  
Z. Physik A285, 273 (1978)

ELEM. SYM.	A	Z
Mo	94	42

METHOD

REF. NO.

78 Ba 11

hmg  
11/17/80

REACTION	RESULT	EXCITATION ENERGY	SOURCE		DETECTOR		ANGLE
			TYPE	RANGE	TYPE	RANGE	
G,NPG	LFT	*91(90.4)	C	20,40	SCD-D	---	135

\*KeV, Isomer LFT

Short-lived isomers in the nuclei  $^{90,92}\text{Nb}$ ,  $^{99}\text{Mo}$ ,  $^{98,100,101}\text{Tc}$  and  $^{101}\text{Ru}$  populated in photonuclear reactions were studied by pulsed beam techniques. Energy and half-life of the  $\gamma$ -rays deexciting the isomeric levels were measured by recording energy-time spectra. The delayed  $\gamma$ -rays and K X-rays were detected by means of an intrinsic Ge-detector of high resolution. From the measured intensity ratios internal conversion coefficients were determined. The multipolarities of the isomeric transitions could be deduced in most cases. A classification of the observed isomers has been tried on the basis of the obtained experimental results and most recent literature data.

Table 1. Experimental results. E: energy,  $T_{1/2}$ : half-life,  $I_{rel}$ : relative intensity, L: multipolarity, H: hindrance factor

Line	E [keV]	$T_{1/2}$ [ $\mu\text{s}$ ]	$T_{1/2}$ [ $\mu\text{s}$ ] (weighted average)	$I_{rel}$	$a_K$	Intensity ratios	L	H
$^{90}\text{Nb}$ K X-rays	—	—	—	1	—	—	—	—
123	$122.6 \pm 0.2$	$63 \pm 2$	—	2.5	$0.56 \pm 0.22$	—	E2	120
$^{92}\text{Nb}$ K X-rays	—	—	—	1	—	—	—	—
90	$90.4 \pm 0.2$	$5.9 \pm 0.2$	—	10.3	$0.14 \pm 0.01$	—	E1	$1.5 \cdot 10^7$
$^{99}\text{Mo}$ K X-rays	—	$15.2 \pm 0.4$	$15.5 \pm 0.2$	1	—	—	—	—
98	$97.8 \pm 0.1$	$15.6 \pm 0.2$	—	0.95	$1.45 \pm 0.27$	—	E2	20
138	$137.7 \pm 0.2$	$0.79 \pm 0.09$	$0.76 \pm 0.06$	1	—	$I_{430}/I_{138} =$	M1	—
449	$449.2 \pm 0.2$	$0.74 \pm 0.08$	—	0.97	—	$0.97 \pm 0.08$	(M2)	(37)
$^{98}\text{Tc}$ K X-rays	—	$14.8 \pm 0.5$	$14.6 \pm 0.4$	1	—	—	—	—
22	$21.8 \pm 0.2$	$16.4 \pm 2.7$	from	0.036	—	$I_{43}/I_{12} =$	E1 + 1% M2	$10^7$
26	—	—	X, 43	—	—	$5.1 \pm 0.5$	(E2)	—
43	$43.5 \pm 0.2$	$14.4 \pm 0.5$	—	0.18	—	—	M1	—
$^{100}\text{Tc}$ K X-rays	—	$8.2 \pm 0.7$	$8.2 \pm 0.3$	1	—	—	—	—
29	$28.7 \pm 0.3$	—	from	0.027	—	$I_{172}/I_{29} =$	E2	1
172	$172.3 \pm 0.3$	$8.2 \pm 0.3$	X, 172	2.2	—	$82 \pm 40$	(M1, E2)	—
$^{101}\text{Tc}$ K X-rays	—	—	—	1	—	—	—	—
192	$192.0 \pm 0.3$	$636 \pm 8$	—	5.0	$0.26 \pm 0.06$	—	M2	560
$^{101}\text{Ru}$ K X-rays	—	$16.1 \pm 3.9$	$17.5 \pm 0.4$	1	—	—	—	—
220	$220.7 \pm 0.2$	$17.4 \pm 0.5$	from	7.5	—	$I_{306}/I_{220} =$	M2	28
306	$306.6 \pm 0.3$	$17.7 \pm 0.6$	220, 306	9.1	—	$1.2 \pm 0.1$	—	—



METHOD

REF. NO.

78 Ma 10

hg

REACTION	RESULT	EXCITATION ENERGY	SOURCE		DETECTOR		ANGLE
			TYPE	RANGE	TYPE	RANGE	
G,PN	ABY	17-68	C	30-68	ACT - I		4PI
G,AN	ABY	14-68	C	30-68	ACT - I		4PI

Analysis is made of reactions interfering with photon activation analysis procedures.

(G,PN) TO NB-92M

(G,AN) TO ZR-89M

The activation yield curves have been presented for a number of photonuclear reactions in the energy range from 30 to 68 MeV, in order to evaluate quantitatively the interferences due to competing reactions in multielement photon activation analysis. The general features of the yields as functions of both target mass number and excitation energy were elucidated from the data obtained, discussion being given on the results in terms of the reaction mechanism.

Simultaneous neutron activation due to appreciable neutron production from the converter and surrounding materials has also been studied, and, finally, the magnitudes of interferences in real multielement analysis were given in the form of their energy dependences.

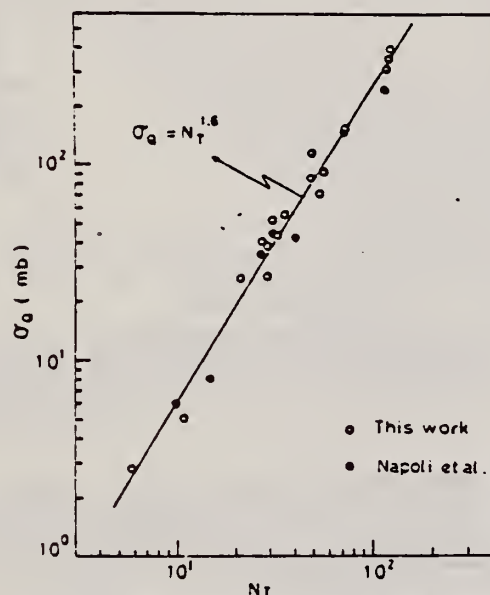


Fig. 2. Yield per equivalent quanta versus target neutron number.

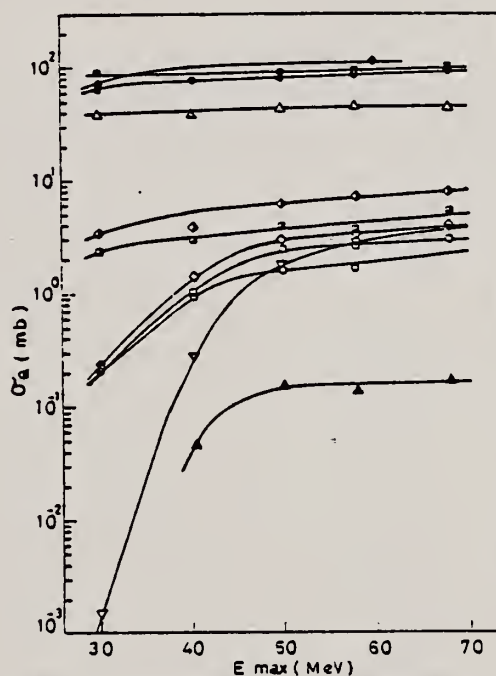


Fig. 7. Activation yield curves for the reactions on Y, Zr, Nb and Mo.  
 ◆  $^{89}\text{Y}(\gamma, n)^{88}\text{Y}$ , ●  $^{90}\text{Zr}(\gamma, n)^{89}\text{Zr}$ , ○  $^{90}\text{Zr}(\gamma, pn)^{88}\text{Y}$ ,  
 △  $^{93}\text{Nb}(\gamma, n)^{92\text{m}}\text{Nb}$ , ▲  $^{93}\text{Nb}(\gamma, xn)^{88}\text{Y}$ , ■  $^{100}\text{Mo}(\gamma, n)^{99}\text{Mo}$ ,  
 ◇  $^{97}\text{Mo}(\gamma, p)^{96}\text{Nb}$ , ▤  $^{96}\text{Mo}(\gamma, p)^{95\text{m}}\text{Nb}$ , ◊  $^{94}\text{Mo}(\gamma, pn)^{92\text{m}}\text{Nb}$ ,  
 □  $^{92}\text{Mo}(\gamma, 2n)^{90}\text{Mo}$ , ▽  $^{94}\text{Mo}(\gamma, xn)^{89}\text{Zr}$ .

(over)

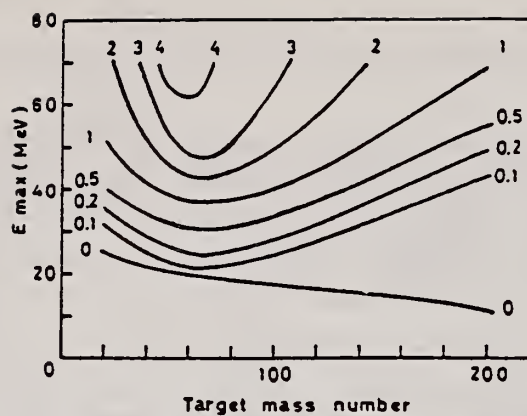


Fig. 11. Yields of the  $(\gamma, pn)$  reactions as a function of bremsstrahlung maximum energy and target mass number. The numerical values in the figure are yields per equivalent quanta in mb.

METHOD					REF. NO.	
					79F12	hg
REACTION	RESULT	EXCITATION ENERGY	SOURCE		DETECTOR	
			TYPE	RANGE	TYPE	RANGE
E,A	SPC	UKN	D	120	MAG-D	

This paper presents energy spectra of  $\alpha$  particles emitted following the bombardment of  $^{27}\text{Al}$ ,  $^{nat}\text{Ni}$ ,  $^{92}\text{Mo}$ ,  $^{94}\text{Mo}$ , and  $^{197}\text{Au}$  with 120-MeV electrons, together with  $\alpha$ -particle angular distributions from  $^{197}\text{Au}$  and  $^{nat}\text{Ni}$  for  $E_\alpha = 30$  and 50 MeV. The data are compared with preequilibrium exciton-model and statistical-model calculations. It is concluded that few-step processes are dominant in the production of  $\alpha$  particles with energies above 20 MeV.

PREEQUILIB A EMISS

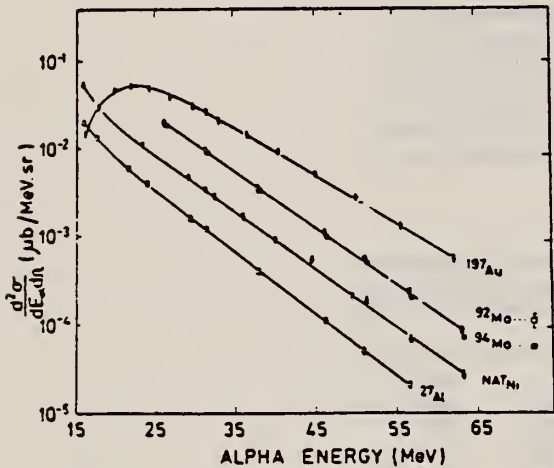


FIG. 1.  $\alpha$ -particle energy spectra at  $\theta_\alpha = 30^\circ$ , for  $E_e = 120$  MeV. Errors shown are the sum of statistical and systematic contributions. The solid lines are a guide to the eye.

TABLE I. Temperatures corresponding to the pre-equilibrium component of the  $(e,\alpha)$  reaction, derived from energy spectra at  $\theta_\alpha = 30^\circ$  for  $E_e = 120$  MeV.

Target	Temperature <sup>a</sup> (MeV)
$^{27}\text{Al}$	5.3
$^{nat}\text{Ni}$	5.5
$^{68}\text{Zn}$	5.4
$^{92}\text{Mo}$	5.6
$^{94}\text{Mo}$	5.4
$^{197}\text{Au}$	6.1

<sup>a</sup>Error is  $\pm 0.2$  MeV.

REF. M. Schumacher, F. Smend, W. Mückenheim, P. Rullhusen, H.G. Börner  
Z. Phys. A300, 193 (1981)

ELEM. SYM.	A	Z
Mo	94	42
REF. NO.		
81 Sc 6		egf

METHOD					REF. NO. 81 Sc 6		egf
REACTION	RESULT	EXCITATION ENERGY	SOURCE		DETECTOR		ANGLE
			TYPE	RANGE	TYPE	RANGE	
G,G	ABX	6		6	SCD-D		90

Elastic scattering by nuclei in the range of mass numbers between 64 and 238 has been studied with monochromatic photons in the energy range between 2 and 8 MeV. These photons were provided either by a  $Ti(n, \gamma)$  source installed in the tangential through channel of the Grenoble high flux reactor, or by  $^{24}Na$  and  $^{56}Co$  sources produced by deuteron bombardment of Al or Fe at the Göttingen cyclotron. The photoexcitation of 23 nuclear levels has been observed and the decay properties and groundstate widths of the majority of these levels have been determined. For the lead scattering target the coherent elastic differential cross section has been studied in detail. There is evidence that below the photo-neutron threshold the elastic scattering via virtual photoexcitation of the nucleus can be approximated by extrapolating the real part of the Giant Dipole Resonance amplitude along a Lorentzian curve. Coulomb corrections to Delbrück scattering seem to play a small role at 6.5 MeV.

6.555 MEV

Table 4. Properties of levels observed by photoexcitation.  $(d\sigma/d\Omega)^{NRF}$ : experimental differential cross section per identified isotope or element for resonance scattering through  $\Theta = 90^\circ$ .  $I^\pi$ : spin-parity of excited level;  $W(\Theta)$ : angular correlation function;  $g = (2I_{ex} + 1)/(2I_g + 1)$ ;  $\Gamma_0$ : radiative groundstate transition width,  $\Gamma$ : total level width. Errors in the last digits are given in parentheses

Isotope	$E_x$ (MeV)	$(d\sigma/d\Omega)^{NRF}$ ( $\mu b/sr$ )	$I^\pi$	$\Gamma_0/\Gamma^a$	$W(\Theta)g\Gamma_0^2/\Gamma$ (meV)	$\Gamma_0^f$ (meV)	$\Gamma_0^g$ (meV)
$^{238}U$	2.754	13 (4)	(1)	0.77	0.145	0.084	-
$^{238}U$	3.254	421 (5)	$1^-$	0.24	0.83	1.5	0.52(15) <sup>d</sup>
$^{209}Bi$	6.555	2.1 (4) $\cdot 10^2$	-	-	0.74	0.74 <sup>b</sup>	-
$^{209}Bi$	7.168	1.7 (3) $\cdot 10^3$	$9/2^{+*}$	1.00	710	786	820 (40) <sup>e</sup>
$^{203}Tl$	6.418	8.75(30) $\cdot 10^3$	$1/2^+$	0.28	30	102	82 (15) <sup>e</sup>
Tl	6.759	7 (3)	-	-	-	-	-
Hg	6.555	68 (17)	-	-	-	-	-
$^{186}W$	6.418	5.2 (3) $\cdot 10^2$	$1^{-*}$	0.32	1.75	2.4	-
$^{184}W$	6.555	9.8 (10) $\cdot 10^2$	(1)	0.52	3.44	2.9	-
$^{184}W$	6.759	46 (10)	(1)	0.58	0.17	0.13	-
$^{181}Ta$	3.010	174 (17)	-	0.72	0.42	0.59	-
$^{181}Ta$	6.418	62 (4)	-	0.73	0.2	0.27 <sup>c</sup>	-
$^{181}Ta$	6.759	4.8 (12)	-	-	0.018	0.018 <sup>b</sup>	-
$^{163}Ho$	6.418	10.3 (30)	-	-	0.035	0.035 <sup>b</sup>	-
$^{163}Ho$	6.759	5.6 (14)	-	-	0.021	0.021 <sup>b</sup>	-
Nd	2.754	2.6 (5)	-	-	-	-	-
Nd	3.254	14.0 (10)	-	-	-	-	-
Ce	6.759	13.4 (10)	-	-	-	-	-
$^{121}Sb$	3.452	2.20 (5) $\cdot 10^3$	-	0.60	2.9	4.9 <sup>b</sup>	-
$^{100}Mo$	6.418	1.53 (4) $\cdot 10^4$	$1^{-*}$	0.88	52	26	25 (8) <sup>e</sup>
$^{94}Mo$	6.555	4.4 (4) $\cdot 10^3$	(1)	0.33	15	21	-
Mo	6.759	6.2 (15)	-	-	-	-	-
Mo	7.168	8.2 (26) $\cdot 10^2$	-	-	-	-	-

<sup>a</sup> [11] <sup>b</sup>  $W(\Theta)g\Gamma_0/\Gamma = 1$  assumed <sup>c</sup>  $W(\Theta)g = 1$  assumed

<sup>d</sup> [28] (a small correction has been applied to the data of [28])

<sup>e</sup> Upper limits in case not all the transitions to lower levels were observed

<sup>f</sup> Present work

<sup>g</sup> Previous work

11b  
A=95

11b  
A=95

11c  
A=95





REF.

H. Langhoff, R. Cesareo and A. Flammersfeld  
Z. Physik 205, 1 (1967)

ELEM. SYM.

A

Z

Mo

95

42

METHOD

REF. NO.

67 La 3

egf

REACTION	RESULT	EXCITATION ENERGY	SOURCE		DETECTOR		ANGLE
			TYPE	RANGE	TYPE	RANGE	
G,G	LFT	1	D	1	NAI-D	0-1	DST
		(766 keV)					

Lifetime  $2.9 \pm 1.6$   
 $1.0$  psec. $1=0.766$  MEV

$$W(\theta) = 1 + A_2 P_2(\cos\theta) \quad A_2 = 0.5 \begin{matrix} +0.3 \\ -0.2 \end{matrix}$$



110  
A=96

110  
A=96

110  
A=96



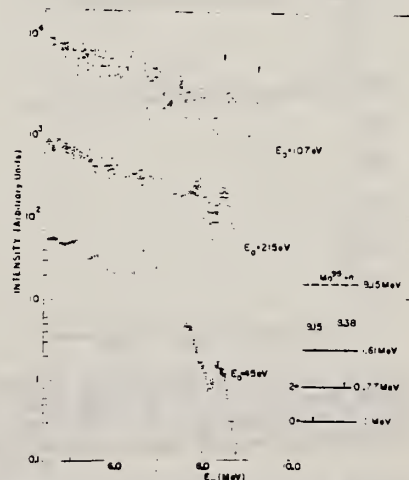


Elem. Sym.	A	Z
Mo	96	42
Ref. No.		62Ja1
		BC

Method

reactor, Argonne fast chopper - NaI(Tl)

Reaction	E or $\Delta E$	$E_0$	$\Gamma$	$\int \sigma dE$	$J^\pi$	Notes
$\text{Mo}^{95}(n, \gamma)\text{Mo}^{96}$	$E_n$ up to 700 eV.	107 eV			$1^-$	<p>Resonance due to capture of p wave neutron; E1 transition</p> <p>Capture of <math>\gamma</math>-ray spectrum studied in order to identify individual resonances due to p wave neutron capture.</p> <p>Detector at <math>90^\circ</math></p>



METHOD

REF. NO.

69 An 6

egf

REACTION	RESULT	EXCITATION ENERGY	SOURCE		DETECTOR		ANGLE
			TYPE	RANGE	TYPE	RANGE	
G,P	ABY	106-999	C	700,999	TEL-D	97-230	DST
G,D	ABY	113-999	C	700,999	TEL-D	97-205	DST

999 = 1.2 GEV

### Summary

The cross-sections of the  $(\gamma, p)$   $(\gamma, d)$  reactions were investigated.  $\text{Li}^7$ ,  $\text{Be}^9$ ,  $\text{C}^{12}$ ,  $\text{Si}^{28}$ ,  $\text{Cu}^{63}$ ,  $\text{Mo}^{96}$  and  $\text{Ta}^{181}$  targets were irradiated with the bremsstrahlung of 700 and 1200 MeV maximum energy from the Kharkov PhTI Ac. Sci. UkrSSR linear accelerator. The photo-protons and deuterons were detected by the scintillation telescope at  $30^\circ$ ,  $60^\circ$ , and  $120^\circ$  with the beam. Possible mechanisms of the proton and deuteron photoproduction are discussed. The qualitative agreement of  $A$  dependence of the cross-sections is observed with a suggestion on the meson mechanism for these reactions.

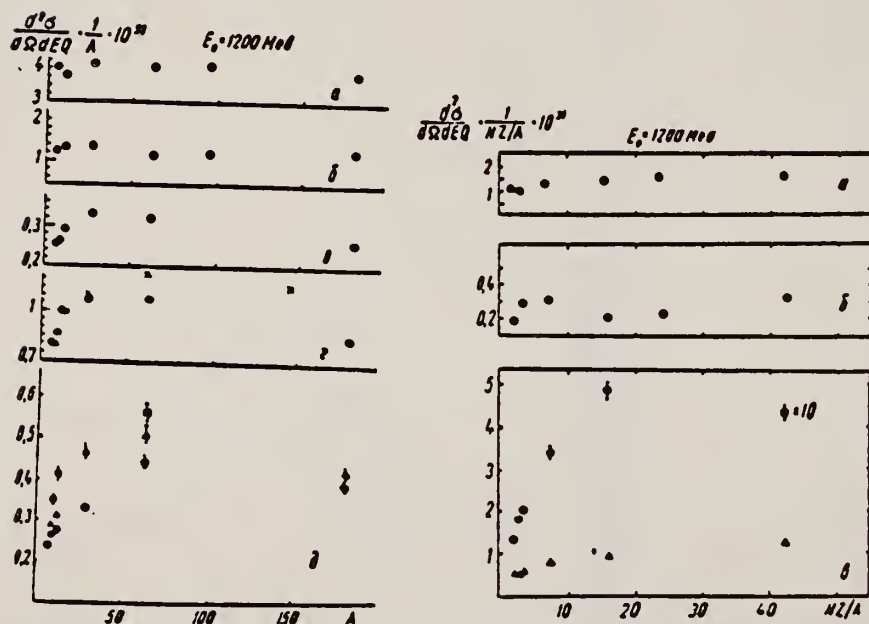


Рис. 1. Залежність перерізу  $(\gamma, p)$ -реакції від  $A$ :  $a$  —  $\theta = 30^\circ$ ,  $E_\gamma = 97$  Mev;  $b$  —  $E_\gamma = 205$  Mev;  $c$  —  $\theta = 60^\circ$ ,  $E_\gamma = 230$  Mev;  $z$  —  $E_\gamma = 157$  Mev ( $\times$  — дані [3]);  $d$  —  $\theta = 120^\circ$ ,  $\bigcirc$  —  $E_\gamma = 120$  Mev,  $\Delta$  —  $E_\gamma = 157$  Mev,  $\square$  —  $E_\gamma = 230$  Mev. Абсолютне значення перерізу наведено при енергії протонів  $E_p = 120$  Mev. Інші дані нормовані до перерізу для  $\text{Li}^7$  при  $E_p = 120$  Mev.

Рис. 2. Залежність перерізу  $(\gamma, d)$ -реакції від  $NZ/A$ :  $a$  —  $\theta = 30^\circ$ ,  $E_d = 97$  Mev;  $b$  —  $\theta = 30^\circ$ ,  $E_d = 205$  Mev;  $c$  —  $\theta = 60^\circ$ ,  $E_d = 97$  Mev,  $\bigcirc$  —  $\theta = 120^\circ$ ,  $E_d = 97$  Mev (перерізи наведені в одиницях  $10^{-32}$  см<sup>2</sup>/стер · Mev · Q).

METHOD

REF. NO.

69 Be 7

hmg

REACTION	RESULT	EXCITATION ENERGY	SOURCE		DETECTOR		ANGLE
			TYPE	RANGE	TYPE	RANGE	
G,G	LFT	6.0	D	6.0	D		DST
		(6.41,6.44)		(6.41,6.44)			(90,135)

Self-Absorption.

6.41, 6.44 MEV

Results of determination of the resonance-level parameters

Source-scatterer	$E_{\gamma}$ , MeV	$\langle \sigma_{pp} \rangle$ , mb	$\Gamma_{\gamma 0}$ , eV	D, keV	Reference
Pb - $Zn^{64}$	7.38	33±4.5	0.58±0.12	53.70±0.13	This work
Ti - $Mo^{96}$	6.413	11.2 ±1.4	0.11±0.02	8.68±1.57	"
Ti - $La^{139}$	6.413	16.04±2.10	0.28±0.05	8.03±1.42	"
Ti - $Bi^{209}$	7.15	1200±230	0.32±0.07	1.84±0.40	"
	6.996	1560	-	-	[1]
	7.15	2600±800	0.42±0.14	-	[3]
Ti - $Cu^{65}$	6.07	423±108	0.34±0.06	99.1±17.4	This work
	6.07	440±130	0.36±0.07	-	[5]
Ti - $Cu^{63}$	6.07	215 ± 71	0.18±0.04	57.14±12.70	This work
	6.07	200 ± 50	0.16±0.03	-	[6]
	8.50	22 ± 7	0.25±0.08	130±40	This work
Cr - $Cu^{63}$	8.499	35	75	-	[1]
	8.50	19 ± 6	0.28±0.09	-	[6]
	8.50	36 ± 9	0.47±0.10	21.36±4.54	This work
Cr - $Cu^{65}$	8.499	80	10.5	-	[1]
	8.50	42 ± 13	0.94±0.29	-	[6]
	7.01	1150±240	0.15±0.04	0.44±0.12	This work
Cu - $Sn^{117}$	7.01	1000	-	-	[1]
	7.01	1200±400	0.3 ± 0.3	-	[5]
Hg - $Mo^{96}$	6.44	201±37	0.12±0.04	0.23±3.07	This work

REF. R. Bergere, H. Beil, P. Carlos, A. Lepretre, A. Veyssiere  
PICNS-73, Vol. I, p. 525 Asilomar

ELEM. SYM.	A	Z
Mo	96	42

METHOD

REF. NO.

73 Be 10

hmg

REACTION	RESULT	EXCITATION ENERGY	SOURCE		DETECTOR		ANGLE
			TYPE	RANGE	TYPE	RANGE	
G, SN	ABX	9- 28	D	9- 28	BF3-I		4PI

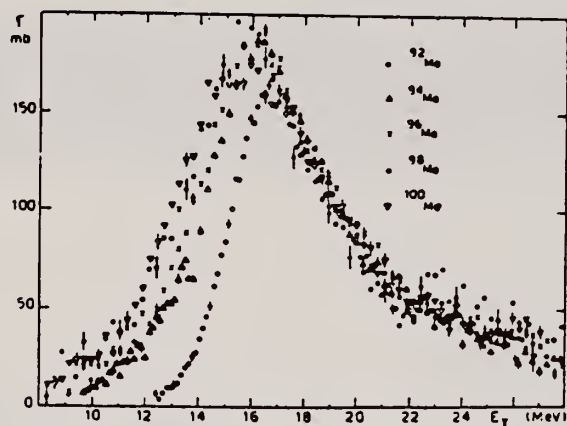


Fig. 15 Comparison of the total photoneutron cross sections of  $^{92}\text{Mo}$   $^{94}\text{Mo}$   $^{96}\text{Mo}$   $^{98}\text{Mo}$  and  $^{100}\text{Mo}$

Table I

Isotopes	$^{92}\text{Mo}$	$^{94}\text{Mo}$	$^{96}\text{Mo}$	$^{98}\text{Mo}$	$^{100}\text{Mo}$
$\sigma_{\text{on}}$	0.83	0.98	1.08	1.11	1.08



REF.	H. Beil, R. Bergere, P. Carlos, A. Lepretre, A. De Miniac, and A. Veyssiere Nucl. Phys. <u>A227</u> , 427 (1974)	ELEM. SYM.	Mo	96	42
METHOD		REF. NO.	74 Be 3		egf

REACTION	RESULT	EXCITATION ENERGY	SOURCE		DETECTOR		ANGLE
			TYPE	RANGE	TYPE	RANGE	
* G,N	ABX	9- 28	D	9- 28	BF3-I		4PI
** G,2N	ABX	16- 28	D	16- 28	BF3-I		4PI
*** G,3N	ABX	26- 29	D	26- 29	BF3-I		4PI

\*699 +  
\*\*700  
\*\*\*701+

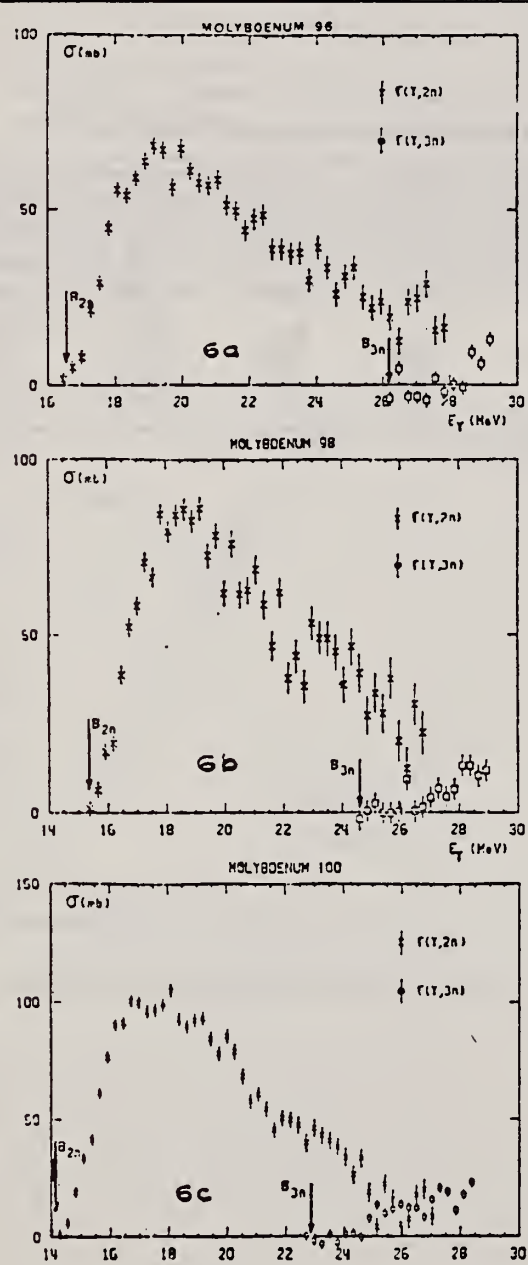


Fig. 6. Partial photonuclear cross sections  $\sigma(\gamma, 2n)$  and  $\sigma(\gamma, 3n)$  of  $^{96}\text{Mo}$ ,  $^{98}\text{Mo}$  and  $^{100}\text{Mo}$ . Arrows indicate theoretical threshold values given in table 2.

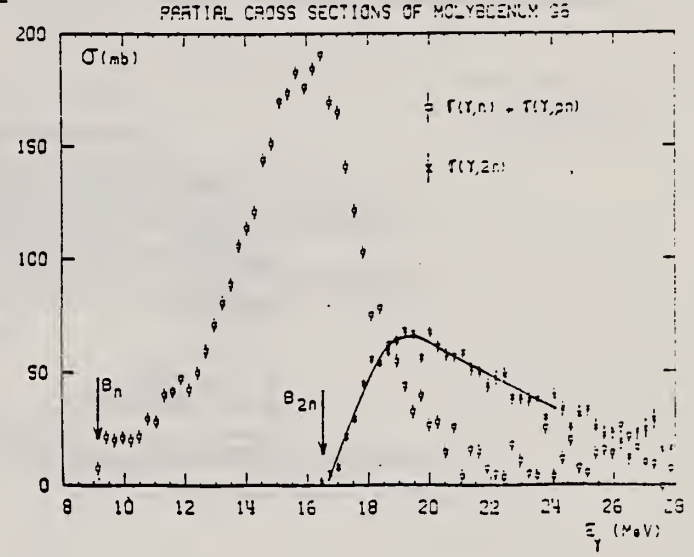


Fig. 3. Same as fig. 1, for  $^{96}\text{Mo}$ .

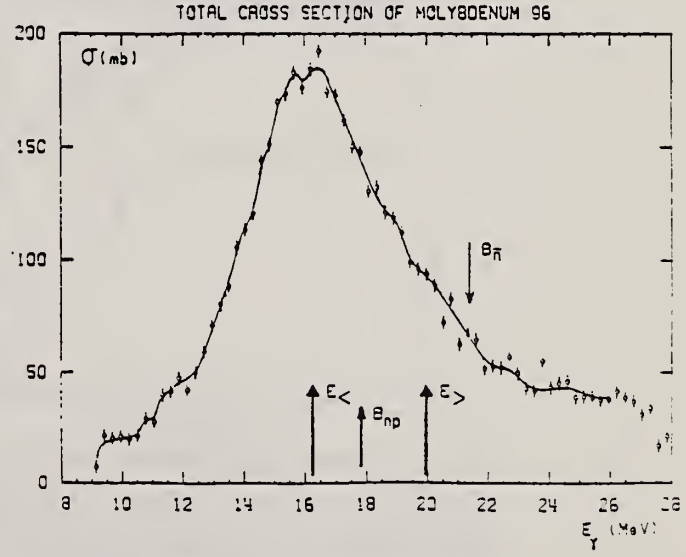


Fig. 9. Same as fig. 7, for  $^{96}\text{Mo}$ .

(over)



TABLE 3

Lorentz line parameters  $E_1$ ,  $\sigma_1$  and  $\Gamma_1$  corresponding to the best single Lorentz line fits to the experimental  $\sigma_{T,n}(E)$  curves shown in fig. 12

	$E_1$ (MeV)	$\sigma_1$ (mb)	$\Gamma_1$ (MeV)
$^{92}\text{Mo}$	$16.9 \pm 0.1$	$154 \pm 10$	$5.4 \pm 0.2$
$^{94}\text{Mo}$	$16.4 \pm 0.1$	$184 \pm 10$	$5.7 \pm 0.2$
$^{96}\text{Mo}$	$16.2 \pm 0.1$	$184 \pm 10$	$6.3 \pm 0.2$
$^{98}\text{Mo}$	$15.8 \pm 0.1$	$189 \pm 15$	$6.0 \pm 0.2$
$^{100}\text{Mo}$	$15.7 \pm 0.1$	$170 \pm 10$	$7.9 \pm 0.2$

TABLE 4

Integrated photoneutron cross sections and sum rules of the Mo isotopes

Nucleus	$^{92}\text{Mo}$	$^{94}\text{Mo}$	$^{96}\text{Mo}$	$^{98}\text{Mo}$	$^{100}\text{Mo}$
$E_M$ (MeV)	29	29	29.5	29	28.5
$\sigma_{0n}$ (MeV · b)	1.10	1.37	1.53	1.60	1.58
$\frac{\sigma_{0n}}{0.06 N Z A^{-1}}$	0.804	0.98	1.03	1.11	1.03
$\sigma_{-1n}$ (mb)	60	79.3	89.2	95.4	95.4
$\sigma_{-1n} A^{-\frac{1}{2}}$ (mb)	0.145	0.186	0.203	0.211	0.206
$\sigma_{-2n}$ (mb · MeV $^{-1}$ )	3.3	4.8	5.1	6.0	6.1
$\sigma_{-2n} A^{-\frac{1}{2}}$ ( $\mu\text{b} \cdot \text{MeV}^{-1}$ )	1.77	2.48	2.55	2.91	2.86

The notation used is defined in the text.

ELEM. SYM.	A	Z
Mo	96	42
REF. NO.		
78 Ma 10		hg

METHOD			SOURCE		DETECTOR		ANGLE
REACTION	RESULT	EXCITATION ENERGY	TYPE	RANGE	TYPE	RANGE	
G,P	ABY	9-68	C	30-68	ACT -I		4PI

Analysis is made of reactions interfering with  
photon activation analysis procedures.

TO NB-95M

The activation yield curves have been presented for a number of photonuclear reactions in the energy range from 30 to 68 MeV, in order to evaluate quantitatively the interferences due to competing reactions in multielement photon activation analysis. The general features of the yields as functions of both target mass number and excitation energy were elucidated from the data obtained, discussion being given on the results in terms of the reaction mechanism.

Simultaneous neutron activation due to appreciable neutron production from the converter and surrounding materials has also been studied, and, finally, the magnitudes of interferences in real multielement analysis were given in the form of their energy dependences.

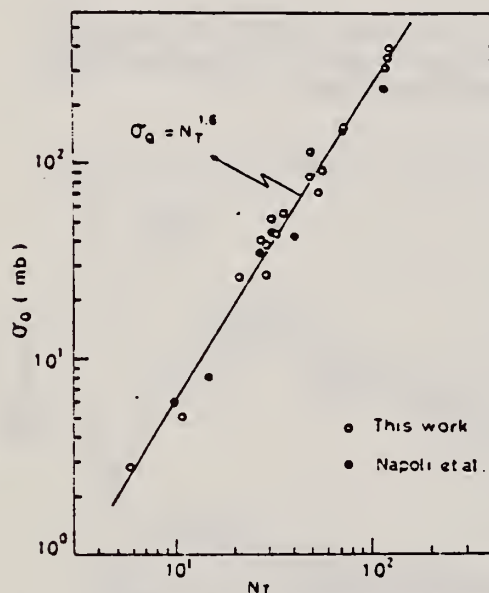


Fig. 2. Yield per equivalent quanta versus target neutron number.

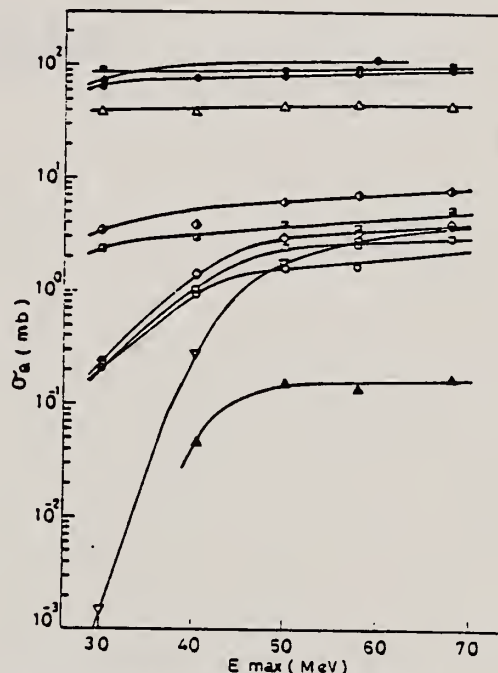


Fig. 7. Activation yield curves for the reactions on Y, Zr, Nb and Mo.  
 ◆  $^{89}\text{Y}(\gamma, n)^{88}\text{Y}$ , ●  $^{90}\text{Zr}(\gamma, n)^{89}\text{Zr}$ , ○  $^{90}\text{Zr}(\gamma, pn)^{88}\text{Y}$ ,  
 △  $^{93}\text{Nb}(\gamma, n)^{92m}\text{Nb}$ , ▲  $^{93}\text{Nb}(\gamma, xn)^{88}\text{Y}$ , ■  $^{100}\text{Mo}(\gamma, n)^{99}\text{Mo}$ ,  
 ◇  $^{97}\text{Mo}(\gamma, p)^{96}\text{Nb}$ , ▤  $^{96}\text{Mo}(\gamma, p)^{95m}\text{Nb}$ , ◇  $^{94}\text{Mo}(\gamma, pn)^{92m}\text{Nb}$ ,  
 □  $^{92}\text{Mo}(\gamma, 2n)^{90}\text{Mo}$ , ▽  $^{94}\text{Mo}(\gamma, xn)^{89}\text{Zr}$ .

(over)

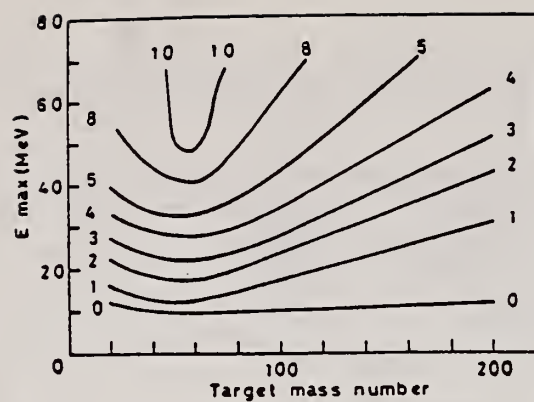


Fig. 10. Yields of the  $(\gamma, p)$  reactions as a function of bremsstrahlung maximum energy and target mass number. The numerical values in the figure are yields per equivalent quanta in mb.

REF. T.J. Rowles, R.J. Holt, H.E. Jackson, R.M. Laszewski, R.D. McKeown,  
A.M. Nathan, J.R. Specht  
Phys. Rev. C24, 1940 (1981)

ELEM. SYM.	A	Z
Mo	96	42
REF. NO.		
81 Bo 5		hg

METHOD

REACTION	RESULT	EXCITATION ENERGY	SOURCE		DETECTOR		ANGLE
			TYPE	RANGE	TYPE	RANGE	
G, G	ABX	14-23	D	14-23	NAI-D		90

Quasimonochromatic photons have been used to measure elastic and inelastic photon scattering cross sections in the giant dipole resonance region of  $^{52}\text{Cr}$ , Fe,  $^{60}\text{Ni}$ ,  $^{92}\text{Mo}$ , and  $^{96}\text{Mo}$  in an experiment in which the elastic and inelastic scattering are resolved. The elastic scattering cross sections show clear evidence for isospin splitting of the giant dipole resonance. The inelastic scattering to low-lying vibrational levels, which is a measure of the coupling between the giant dipole resonance and collective surface vibrations, is in qualitative agreement with the predictions of the dynamic collective model. However, when examined in detail, this model does not provide an adequate description of the scattering data.

NUCLEAR REACTIONS  $^{52}\text{Cr}$ , Fe,  $^{60}\text{Ni}$ ,  $^{92,96}\text{Mo}$  ( $\gamma, \gamma'$ ),  $14 \leq E_\gamma \leq 22$  MeV; measured  $E_\gamma$ ,  $E_{\gamma'}$ ,  $d\sigma/d\Omega$  for  $\gamma_0, \gamma_1$ . Compared to DCM predictions. Tagged photons.

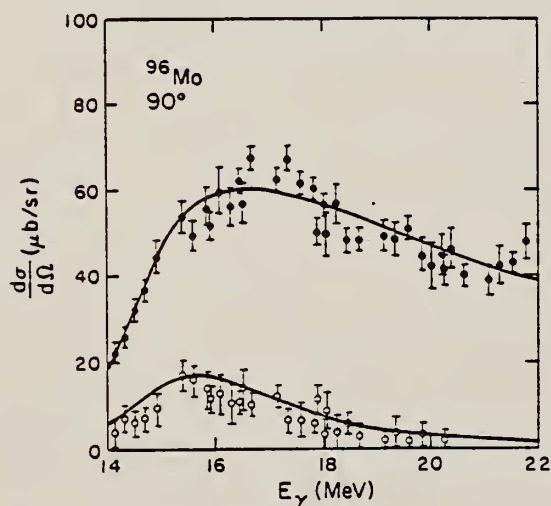


FIG. 4. Elastic (closed circles) and inelastic (open circles) scattering cross sections at  $\theta=90^\circ$  on  $^{96}\text{Mo}$ . The error bars represent statistical uncertainties only. The solid lines are the DCM calculations for the elastic and inelastic cross sections. The curves corresponding to calculations with and without isospin splitting are indistinguishable.





ib  
A=97

ib  
A=97

ib  
A=97



REACTION	RESULT	EXCITATION ENERGY	SOURCE		DETECTOR		ANGLE
			TYPE	RANGE	TYPE	RANGE	
G,p	ABX	THR - 26	C	THR - 33	ACT - I		4 PI

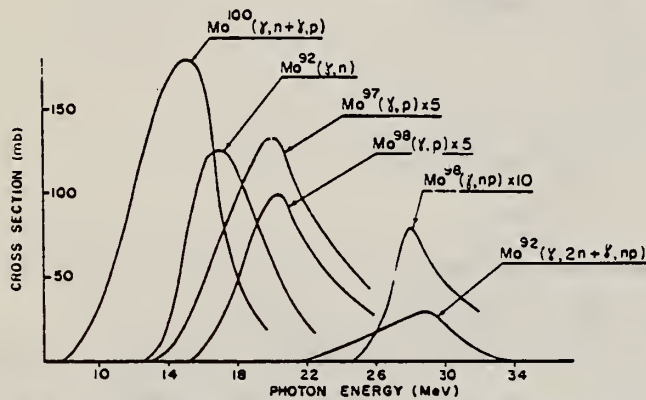


Fig. 2. Cross sections for photoreactions in molybdenum isotopes.

TABLE 2  
Reaction parameters

Reaction	Peak energy (MeV)	$\int \sigma dE$ (MeV · mb)
$Mo^{100}(\gamma, n-\gamma, p)$	15	$1110 \pm 200$
$Mo^{92}(\gamma, n)$	17	$750 \pm 70$
$Mo^{97}(\gamma, p)$	20	$215 \pm 50$
$Mo^{98}(\gamma, p)$	20	$140 \pm 15$
$Mo^{98}(\gamma, np)$	23	$30 \pm 10$
$Mo^{92}(\gamma, np-\gamma, 2n)$	29	$160 \pm 25$

REACTION	RESULT	EXCITATION ENERGY	SOURCE		DETECTOR		ANGLE
			TYPE	RANGE	TYPE	RANGE	
G,P	ABX	13-26	C	THR-26	ACT-I		4PI

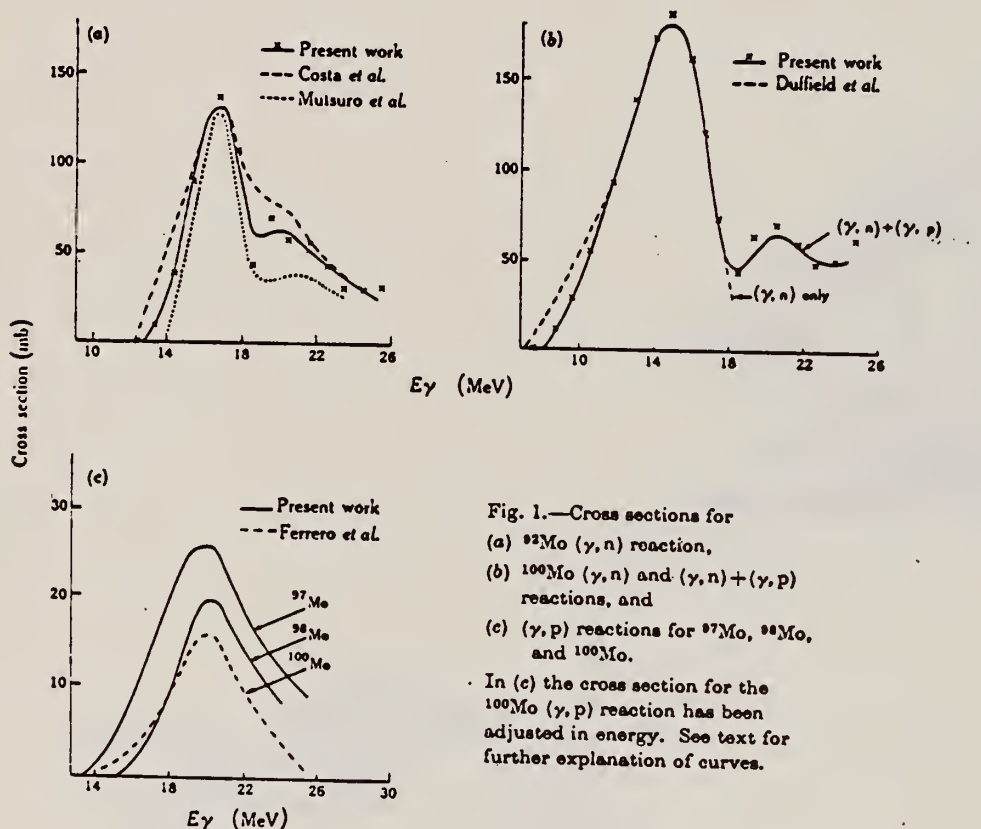


Fig. 1.—Cross sections for  
(a)  $^{92}\text{Mo}(\gamma, n)$  reaction,  
(b)  $^{100}\text{Mo}(\gamma, n)$  and  $(\gamma, n) + (\gamma, p)$   
reactions, and  
(c)  $(\gamma, p)$  reactions for  $^{97}\text{Mo}$ ,  $^{98}\text{Mo}$ ,  
and  $^{100}\text{Mo}$ .

In (c) the cross section for the  
 $^{100}\text{Mo}(\gamma, p)$  reaction has been  
adjusted in energy. See text for  
further explanation of curves.

ELEM. SYM.	A	Z
Mo	97	42

METHOD	REF. NO.	
	73 W1 6	hmg

REACTION	RESULT	EXCITATION ENERGY	SOURCE		DETECTOR		ANGLE
			TYPE	RANGE	TYPE	RANGE	
G,N	ABX	6- 10	G	7- 10	TOF-D		130

PEAK AT 8.1 MEV

Table I

Reaction	Thres- hold (MeV)	Energy Range of Experiment (MeV)	Observed Peaks		
			Peak Energy (MeV)	$\frac{d\sigma}{d\omega}$ at peak (mb/ster.)	$4\pi \int \left( \frac{d\sigma}{d\omega} \right)_{130^\circ} dE_\gamma$ peak
$^{87}\text{Sr}(\gamma, n_0)$	8.44	9.4-11.1	.		(MeV-mb)
$^{87}\text{Sr}(\gamma, n_1)$	9.52	10.5-11.1			
$^{91}\text{Zr}(\gamma, n_0)$	7.19	7.8-10.3	9.1	1.2	20
$^{97}\text{Nb}(\gamma, n_0)$	6.82	7.8-9.2	8.1	0.3	3
$^{113}\text{Cd}(\gamma, n_0)$	6.54	7.4-9.3	7.7	0.9	7
$^{117}\text{Sn}(\gamma, n_0)$	6.94	7.6-8.8	7.8	2.5	20
$^{119}\text{Sn}(\gamma, n_0)$	6.48	7.1-9.0	7.8	1.6	18



METHOD					REF. NO.		hg
					78 Ma 10		
REACTION	RESULT	EXCITATION ENERGY	SOURCE		DETECTOR		ANGLE
			TYPE	RANGE	TYPE	RANGE	
G,P	ABY	9-68	C	30-68	ACT - I		4PI

Analysis is made of reactions interfering with photon activation analysis procedures.

The activation yield curves have been presented for a number of photonuclear reactions in the energy range from 30 to 68 MeV, in order to evaluate quantitatively the interferences due to competing reactions in multielement photon activation analysis. The general features of the yields as functions of both target mass number and excitation energy were elucidated from the data obtained, discussion being given on the results in terms of the reaction mechanism.

Simultaneous neutron activation due to appreciable neutron production from the converter and surrounding materials has also been studied, and, finally, the magnitudes of interferences in real multielement analysis were given in the form of their energy dependences.

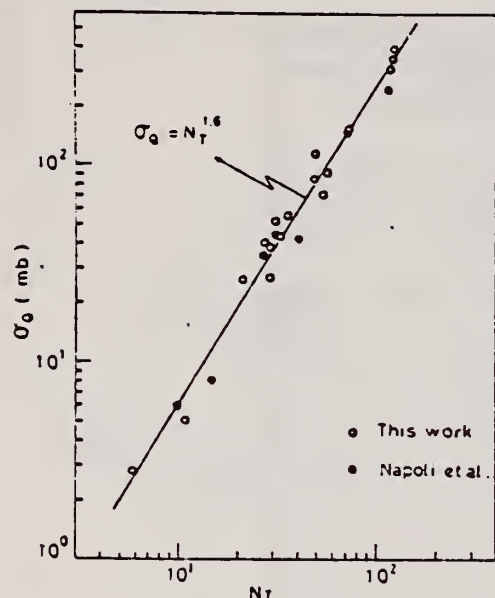


Fig. 2. Yield per equivalent quanta versus target neutron number.

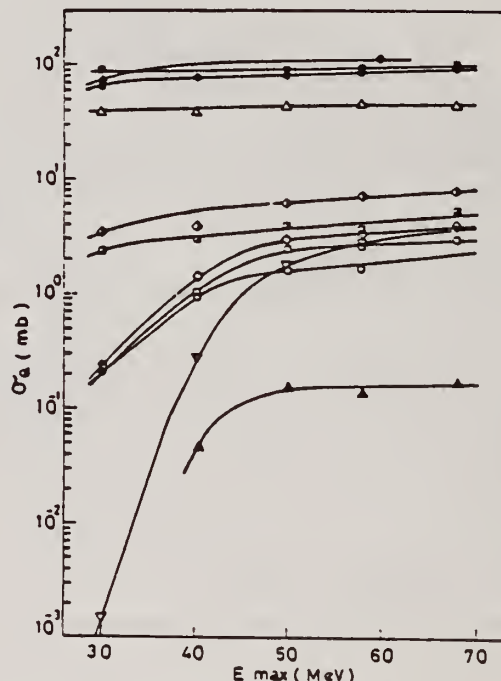


Fig. 7. Activation yield curves for the reactions on Y, Zr, Nb and Mo.

◆  $^{89}\text{Y}(\gamma, n)^{88}\text{Y}$ ,    ●  $^{90}\text{Zr}(\gamma, n)^{89}\text{Zr}$ ,    ○  $^{90}\text{Zr}(\gamma, pn)^{88}\text{Y}$ ,  
 △  $^{93}\text{Nb}(\gamma, n)^{92m}\text{Nb}$ ,    ▲  $^{93}\text{Nb}(\gamma, xn)^{88}\text{Y}$ ,    ■  $^{100}\text{Mo}(\gamma, n)^{99}\text{Mo}$ ,  
 ◇  $^{97}\text{Mo}(\gamma, p)^{96}\text{Nb}$ ,    ▤  $^{96}\text{Mo}(\gamma, p)^{95m}\text{Nb}$ ,    ◊  $^{94}\text{Mo}(\gamma, pn)^{92m}\text{Nb}$ ,  
 □  $^{92}\text{Mo}(\gamma, 2n)^{90}\text{Mo}$ ,    ▽  $^{94}\text{Mo}(\gamma, xn)^{89}\text{Zr}$ .

(over)

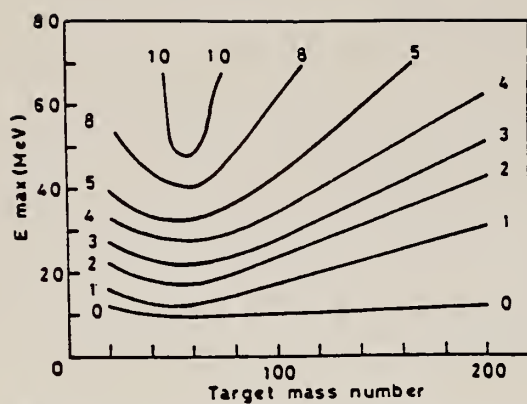


Fig. 10. Yields of the  $(\gamma, p)$  reactions as a function of bremsstrahlung maximum energy and target mass number. The numerical values in the figure are yields per equivalent quanta in mb.



1b  
A=98

1b  
A=98

1b  
A=98





REF. A. El Sioufi, P. Erdos and P. Stoll  
Helv. Phys. Acta 30, 265 (1957)

ELEM. SYM.	A	Z
Mo	98	42

METHOD				REF. NO.	
				57 B1 1	egf
REACTION	RESULT	EXCITATION ENERGY	SOURCE		ANGLE
			TYPE	RANGE	
G,P	ABI	10- 30	C	32	4PI

Tabelle 1.  
Zusammenstellung der gem. W. Q.

Reaktion	Q-Wert MeV	MeV barn	Verhältnis der Querschnitte
$Zn^{66}(\gamma, np)Cu^{64*}$	18,65	0,02	$\frac{\sigma_{Zn^{66}(\gamma, p)}}{\sigma_{Zn^{66}(\gamma, np)}} = 3,6 \pm 0,5$
$Zn^{66}(\gamma, p)Cu^{67**})^6$	10,01	0,08	
$Zn^{66}(\gamma, 2n)Zn^{64}$	20,82	0,03	$\frac{\sigma_{Zn^{66}(\gamma, np)}}{\sigma_{Zn^{66}(\gamma, 2n)}} = 0,25$
$Mo^{92}(\gamma, np)Nb^{90}$	19,5	0,02	
$Mo^{92}(\gamma, p)Nb^{91}$		0,09	$\frac{\sigma_{Mo^{92}(\gamma, p)}}{\sigma_{Mo^{92}(\gamma, np)}} = 4,5$
*) $\sigma_{max}$ : 5,3 mb bei $E_\gamma = 27 \pm 0,5$ MeV $\Gamma = 3,7$ MeV.			
**) $\sigma_{max}$ : 11,5 mb bei $E_\gamma = 22 \pm 0,5$ MeV $\Gamma = 6,4$ MeV.			

## METHOD

Betatron; ion chamber monitor

## REF. NO.

64 Ge 1

JOC

REACTION	RESULT	EXCITATION ENERGY	SOURCE		DETECTOR		ANGLE
			TYPE	RANGE	TYPE	RANGE	
G,P	ABX	THR - 26	C	THR-33	ACT - I		4 PI
G,NP	ABX	THR - 32	C	THR-33	ACT - I		4 PI

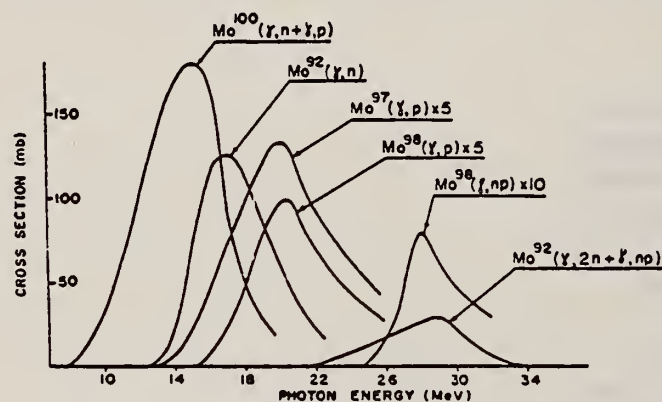


Fig. 2. Cross sections for photoreactions in molybdenum isotopes.

TABLE 2  
Reaction parameters

Reaction	Peak energy (MeV)	$\int \sigma dE$ (MeV · mb)
$\text{Mo}^{100}(\gamma, n + \gamma, p)$	15	$1110 \pm 200$
$\text{Mo}^{92}(\gamma, n)$	17	$750 \pm 70$
$\text{Mo}^{97}(\gamma, p)$	20	$215 \pm 50$
$\text{Mo}^{98}(\gamma, p)$	20	$140 \pm 15$
$\text{Mo}^{98}(\gamma, np)$	28	$30 \pm 10$
$\text{Mo}^{92}(\gamma, np - \gamma, 2n)$	29	$160 \pm 25$

METHOD						REF. NO.	
						68 Ge 1	egf
REACTION	RESULT	EXCITATION ENERGY	SOURCE		DETECTOR		ANGLE
			TYPE	RANGE	TYPE	RANGE	
G,P	ABX	13-26	C	THR-26	ACT-I		4PI

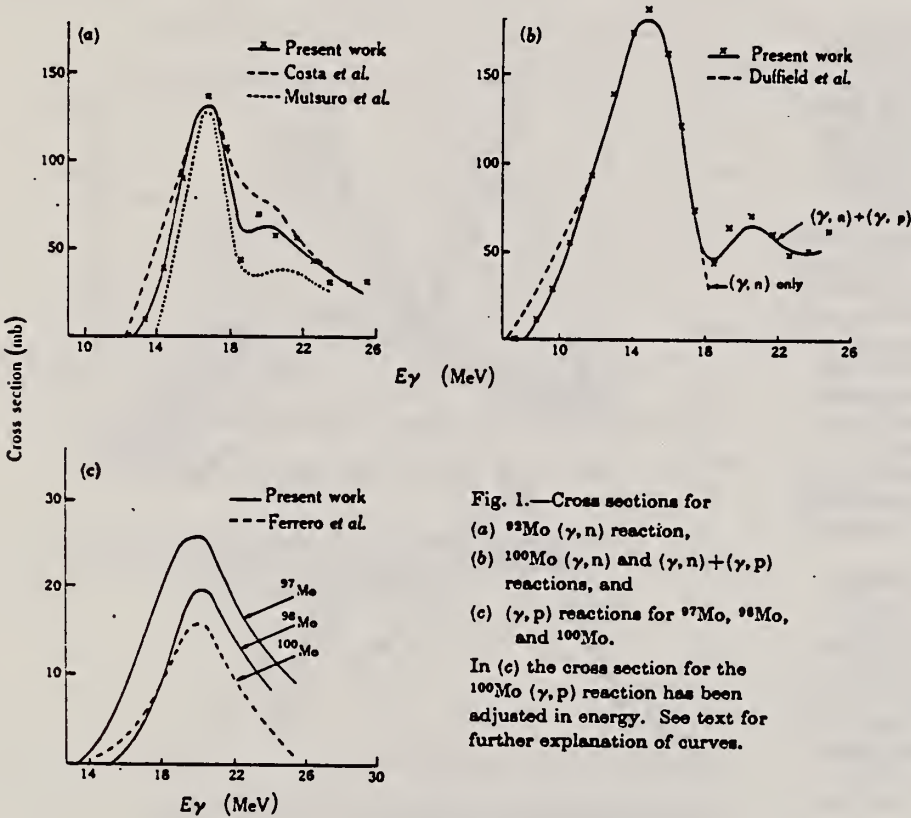


Fig. 1.—Cross sections for  
(a)  $^{93}\text{Mo}(\gamma, n)$  reaction,  
(b)  $^{100}\text{Mo}(\gamma, n)$  and  $(\gamma, n) + (\gamma, p)$   
reactions, and  
(c)  $(\gamma, p)$  reactions for  $^{97}\text{Mo}$ ,  $^{98}\text{Mo}$ ,  
and  $^{100}\text{Mo}$ .  
In (c) the cross section for the  
 $^{100}\text{Mo}(\gamma, p)$  reaction has been  
adjusted in energy. See text for  
further explanation of curves.

REF.	B.S. Ishkhanov, I.M. Kapitonov, E.V. Lazutin, I.M. Piskarev, and O.P. Shevchenko				ELEM. SYM.	A	Z
	Yad. Fiz. <u>11</u> , 702 (1970)				Mo	98	42
	Sov. J. Nucl. Phys. <u>11</u> , 394 (1970)						
METHOD					REF. NO.		
					70 Is 1		hmg
REACTION	RESULT	EXCITATION ENERGY	SOURCE		DETECTOR		ANGLE
			TYPE	RANGE	TYPE	RANGE	
G,XN	ABX	THR-30	C	THR-30	BF3-I		4PI

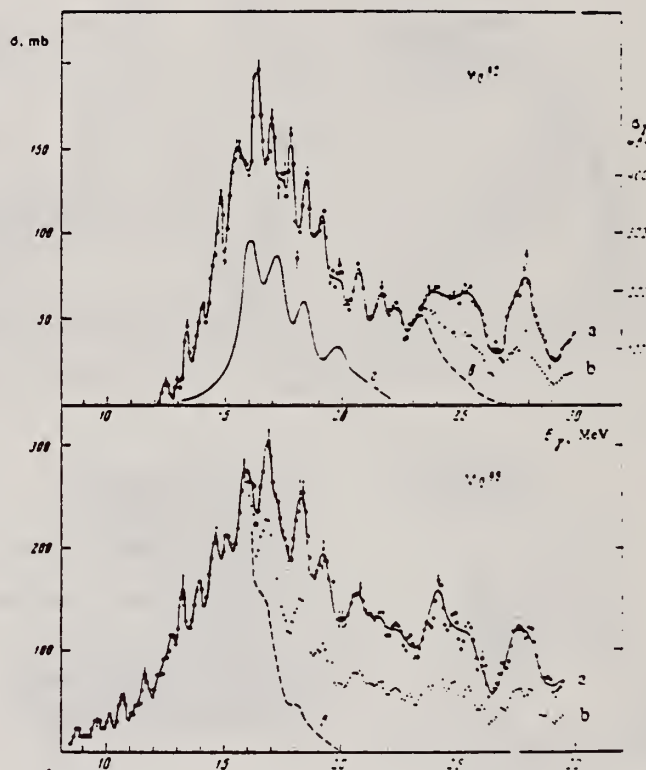
WE used the 35-MeV betatron of our institute to investigate photoneutron reactions on the isotopes  $\text{Mo}^{92}$  and  $\text{Mo}^{98}$ . The yield curves of the reactions  $(\gamma, \text{Tn})$  were measured in the energy range from 7 to 30 MeV in steps of 100 keV. The targets were prepared from metallic Mo. The content of the investigated isotopes was not less than 97%. The use of a highly efficient neutron detector ( $\epsilon \approx 45\%$ ) and of a multichannel method of measurements has made it possible to obtain the yield curves with high accuracy (0.1% in the region 25–30 MeV) and to observe, for the first time, the intermediate structure of the giant resonance on the isotopes of Mo. The statistical reduction of the experimental information and the determination of the cross sections of the photoneutron reactions was carried out in accordance with a program prepared by the Computational Center of the Moscow State University<sup>[1]</sup>.

The obtained cross section of the reactions  $\sigma(\gamma, \text{Tn}) = \sigma(\gamma, n) + 2\sigma(\gamma, 2n) + \sigma(\gamma, np)$  are shown in the figure, from which it is seen that approximately 15 resonances are observed in each cross section.

The widths of the giant resonances in the reaction  $(\gamma, \text{Tn})$  on  $\text{Mo}^{92}$  and  $\text{Mo}^{98}$  are 5 and 7 MeV respectively (curves a in the figure). After taking into account the multiplicity in accordance with the data of<sup>[2]</sup> for this region of nuclei, the cross sections obtained were  $\sigma_n = \sigma(\gamma, n) + \sigma(\gamma, 2n) + \sigma(\gamma, np)$  (curves b). The widths of these cross sections for  $\text{Mo}^{92}$  and  $\text{Mo}^{98}$  are the same and equal 5 MeV. The curves c correspond to the cross sections  $\sigma(\gamma, n) + \sigma(\gamma, np)$ . The widths for them are 5 and 3.5 MeV respectively for  $\text{Mo}^{92}$  and  $\text{Mo}^{98}$ .

The widths  $\sigma_n$  of the integral cross sections of the reactions for  $\text{Mo}^{92}$  and  $\text{Mo}^{98}$  are  $1.29 \pm 0.13$  and  $2.0 \pm 0.2$  MeV-b. The integral cross section  $\sigma_n$  increases with increasing  $N - Z$  for isotopes of a given element. It is interesting to note, however, that in the case of Mo the increase of  $\sigma_n$  and of the width of the giant resonance is due to the cross section of the reaction  $(\gamma, 2n)$ . Thus, for  $\text{Mo}^{92}$  we have  $\sigma(\gamma, 2n) = 0.17 \pm 0.02$  MeV-b, whereas for  $\text{Mo}^{98}$  we have  $\sigma(\gamma, 2n) = 0.83 \pm 0.08$  MeV-b, i.e., the cross section of the reaction  $(\gamma, 2n)$  increases by almost five times. Such a sharp increase of the cross section of the reaction  $\text{Mo}^{98}(\gamma, 2n)$  is connected with the low threshold of the  $(\gamma, 2n)$  reaction, namely  $E_{\text{Mo}^{98}}^{\text{thr}}(\gamma, 2n) = 15.5$  MeV. For comparison, we point out that  $E_{\text{Mo}^{92}}^{\text{thr}}(\gamma, 2n) = 22.8$  MeV.

For the reaction  $(\gamma, n) + (\gamma, np)$ , the integral cross sections for  $\text{Mo}^{92}$  and  $\text{Mo}^{98}$  are respectively  $1.12 \pm 0.11$  and  $1.10 \pm 0.11$  MeV-b.



Effective cross sections for  $\text{Mo}^{92}$  and  $\text{Mo}^{98}$ : a —  $\sigma(\gamma, \text{Tn})$ ; b —  $\sigma(\gamma, n) + \sigma(\gamma, 2n) + \sigma(\gamma, np)$ ; c —  $\sigma(\gamma, n) + \sigma(\gamma, np)$ ; d — total-absorption cross section  $\sigma_\gamma$ , obtained in<sup>[3]</sup> for  $\text{Mo}^{94}$  (right-hand scale).

There are at present no published data on the structure of the photoneutron cross sections on the Mo isotopes. Such general characteristics of the giant resonance as the position and magnitude of the integral cross section are known only for the reaction  $\text{Mo}^{92}(\gamma, n)^{[3-5]}$ . Even these results, however, are highly contradictory. Thus, data on the width of the giant resonance, obtained in<sup>[3]</sup>, exceed the data of<sup>[4]</sup> by a factor of 2.

In conclusion, let us compare the experimental results obtained by us with the calculations performed on the basis of the collective dynamic theory<sup>[6]</sup>. The photodisintegration of the  $\text{Mo}^{94}$  was calculated within the framework of this theory, and the result is shown in the figure (curve d). We see that the theoretical calculation agrees only roughly with the experimental data. The experimentally measured cross sections re-



REF. R. Bergere, H. Beil, P. Carlos, A. Lepretre, A. Veyssiere  
 PICNS-73, Vol.I, p.525 Asilomar

ELEM. SYM.	A	Z
Mo	98	42
REF. NO.		
73 Be 10		hmg

METHOD

REACTION	RESULT	EXCITATION ENERGY	SOURCE		DETECTOR		ANGLE
			TYPE	RANGE	TYPE	RANGE	
G,SN	ABX	8- 28	D	8- 28	BF3-I		4PI

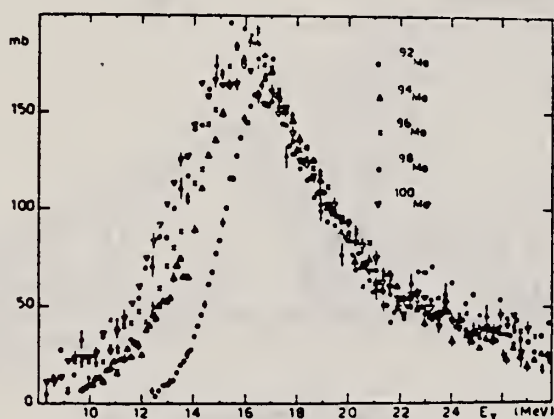


Fig. 15 Comparison of the total photoneutron cross sections of <sup>92</sup>Mo <sup>94</sup>Mo <sup>96</sup>Mo <sup>98</sup>Mo and <sup>100</sup>Mo

Table I

Isotopes	<sup>92</sup> Mo	<sup>94</sup> Mo	<sup>96</sup> Mo	<sup>98</sup> Mo	<sup>100</sup> Mo
σ <sub>on</sub>	0.83	0.98	1.08	1.11	1.08



METHOD

REF. NO.

74 Be 3

egf

REACTION	RESULT	EXCITATION ENERGY	SOURCE		DETECTOR		ANGLE
			TYPE	RANGE	TYPE	RANGE	
* G,N	ABX	8- 28	D	8- 28	BF3-I		4PI
** G,2N	ABX	15- 28	D	15- 28	BF3-I		4PI
*** G,3N	ABX	24- 29	D	24- 29	BF3-I		4PI

\*703 +  
\*\*704  
\*\*\*705+

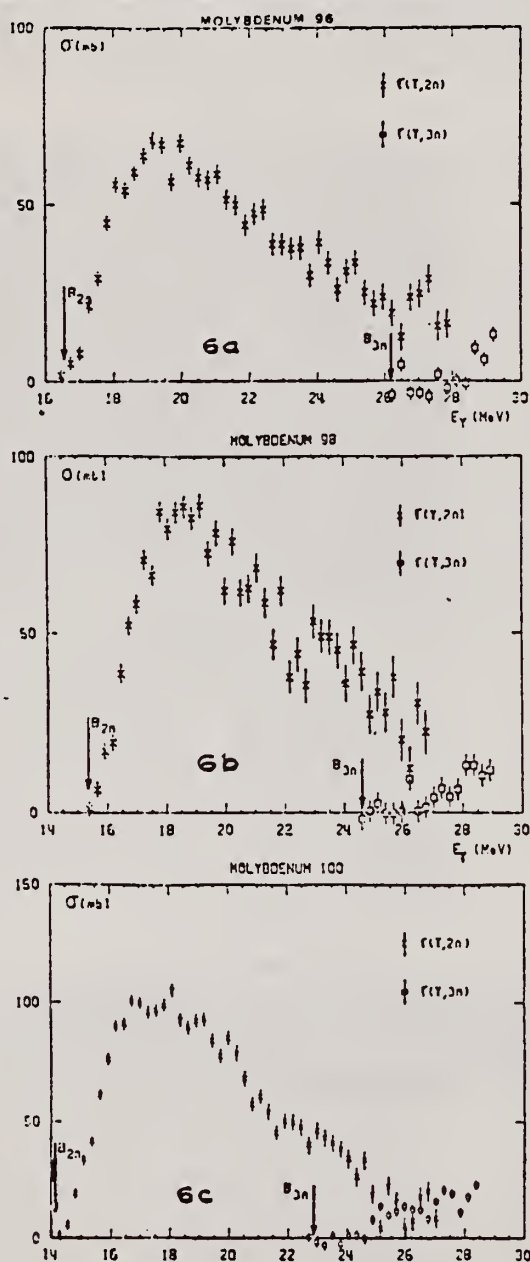


Fig. 6. Partial photoneutron cross sections  $\sigma(\gamma, 2n)$  and  $\sigma(\gamma, 3n)$  of  $^{96}\text{Mo}$ ,  $^{98}\text{Mo}$  and  $^{100}\text{Mo}$ . Arrows indicate theoretical threshold values given in table 2.

PARTIAL CROSS SECTIONS OF MOLYBDENUM 98

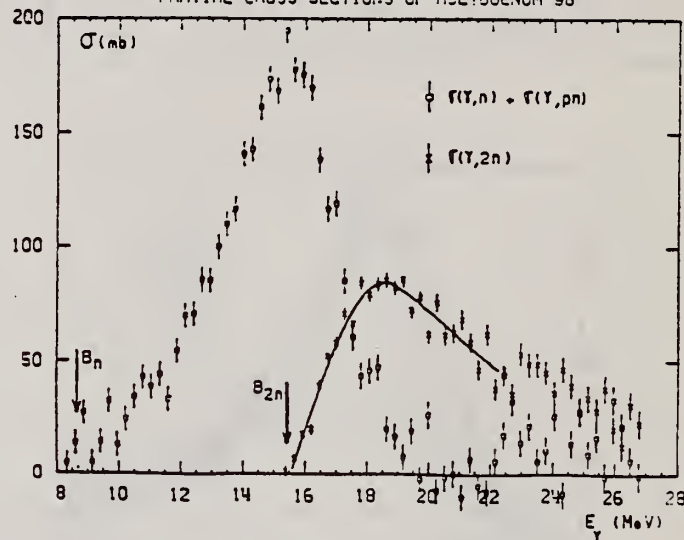


Fig. 4. Same as fig. 1, for  $^{98}\text{Mo}$ .

TOTAL CROSS SECTION OF MOLYBDENUM 98

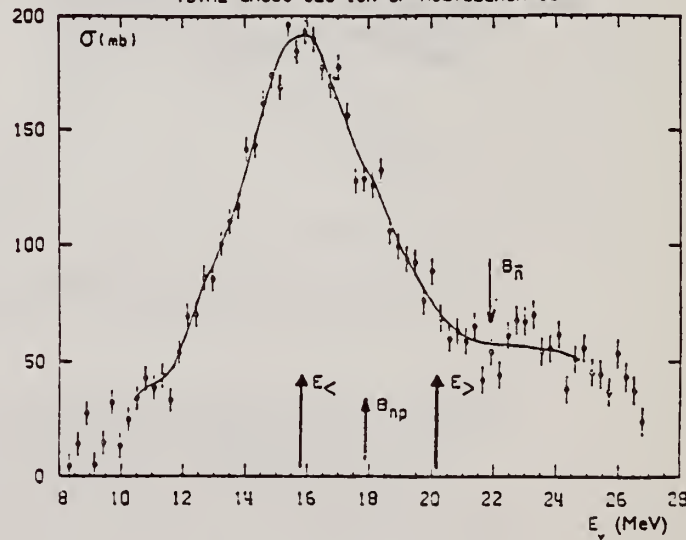


Fig. 10. Same as fig. 7, for  $^{98}\text{Mo}$ .

(over)

TABLE 3

Lorentz line parameters  $E_1$ ,  $\sigma_1$  and  $\Gamma_1$  corresponding to the best single Lorentz line fits to the experimental  $\sigma_{T,n}(E)$  curves shown in fig. 12

	$E_1$ (MeV)	$\sigma_1$ (mb)	$\Gamma_1$ (MeV)
$^{92}\text{Mo}$	$16.9 \pm 0.1$	$154 \pm 10$	$5.4 \pm 0.2$
$^{94}\text{Mo}$	$16.4 \pm 0.1$	$184 \pm 10$	$5.7 \pm 0.2$
$^{96}\text{Mo}$	$16.2 \pm 0.1$	$184 \pm 10$	$6.3 \pm 0.2$
$^{98}\text{Mo}$	$15.8 \pm 0.1$	$189 \pm 15$	$6.0 \pm 0.2$
$^{100}\text{Mo}$	$15.7 \pm 0.1$	$170 \pm 10$	$7.9 \pm 0.2$

TABLE 4

Integrated photoneutron cross sections and sum rules of the Mo isotopes

Nucleus	$^{92}\text{Mo}$	$^{94}\text{Mo}$	$^{96}\text{Mo}$	$^{98}\text{Mo}$	$^{100}\text{Mo}$
$E_M$ (MeV)	29	29	29.5	29	28.5
$\sigma_{0n}$ (MeV · b)	1.10	1.37	1.53	1.60	1.58
$\sigma_{0n}$	0.804	0.98	1.08	1.11	1.08
$0.06 N Z A^{-1}$					
$\sigma_{-1n}$ (mb)	60	79.3	89.2	95.4	95.4
$\sigma_{-1n} A^{-\frac{1}{2}}$ (mb)	0.145	0.186	0.203	0.211	0.206
$\sigma_{-2n}$ (mb · MeV $^{-1}$ )	3.3	4.8	5.1	6.0	6.1
$\sigma_{-2n} A^{-\frac{1}{2}}$ ( $\mu\text{b} \cdot \text{MeV}^{-1}$ )	1.77	2.48	2.55	2.91	2.86

The notation used is defined in the text.



Mo  
A=100

Mo  
A=100

Mo  
A=100





Elem. Sym.	A	Z
Mo	100	42
Ref. No. 57 Fe 3		NVB

Method Betatron; proton yield; radioactivity; ion chamber

Reaction	E or $\Delta E$	$E_0$	$\Gamma$	$\int \sigma dE$	$J\pi$	Notes
$\text{Mo}^{100}(\gamma, p)$	Bremss. 14-30			$\int_{14}^{30} = 0.10 \pm 0.2$ MeV-b		

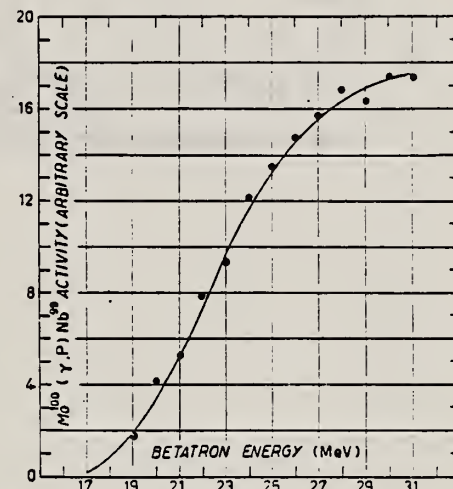


Fig. 1.

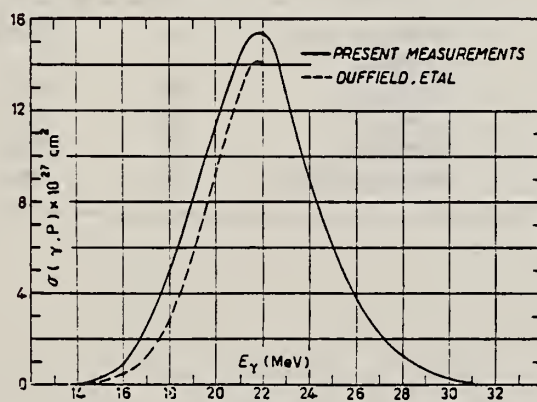


Fig. 2.

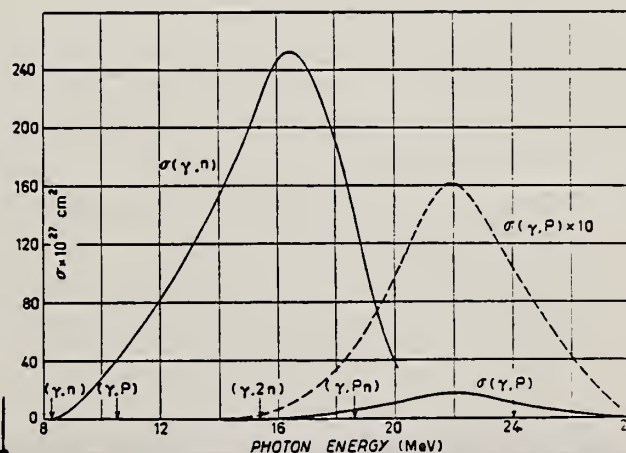


Fig. 3.

METHOD					REF. NO.	
Betatron; ion chamber monitor					64 Ge 1 JOC	

REACTION	RESULT	EXCITATION ENERGY	SOURCE		DETECTOR		ANGLE
			TYPE	RANGE	TYPE	RANGE	
1) G,N	ABX	THR - 20	C	THR-33	ACT - I		4 PI
2) G,P	ABX	THR - 20	C	THR-33	ACT - I		4 PI

- 1) MIXED WITH G,P
- 2) MIXED WITH G,N

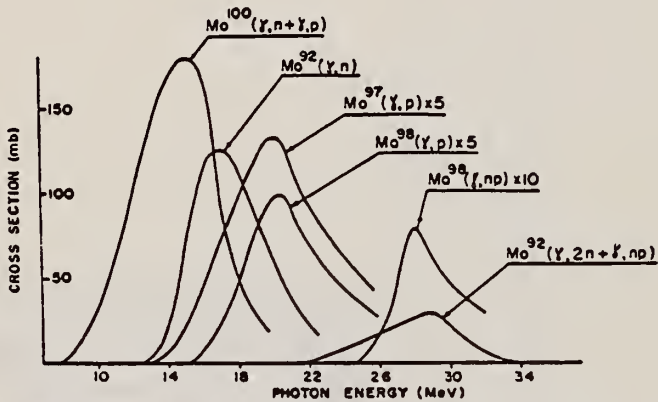


Fig. 2. Cross sections for photoreactions in molybdenum isotopes-

TABLE 2  
Reaction parameters

Reaction	Peak energy (MeV)	$\int \sigma dE$ (MeV · mb)
Mo <sup>100</sup> ( $\gamma$ , n + $\gamma$ , p)	15	1110 ± 200
Mo <sup>92</sup> ( $\gamma$ , n)	17	750 ± 70
Mo <sup>97</sup> ( $\gamma$ , p)	20	215 ± 50
Mo <sup>98</sup> ( $\gamma$ , p)	20	140 ± 15
Mo <sup>98</sup> ( $\gamma$ , np)	28	30 ± 10
Mo <sup>92</sup> ( $\gamma$ , np + $\gamma$ , 2n)	29	160 ± 25

METHOD

REF. NO.

68 Ge 1

egf

REACTION	RESULT	EXCITATION ENERGY	SOURCE		DETECTOR		ANGLE
			TYPE	RANGE	TYPE	RANGE	
$G, N+P$	ABX	7-26	C	THR-26	ACT-I		4PI

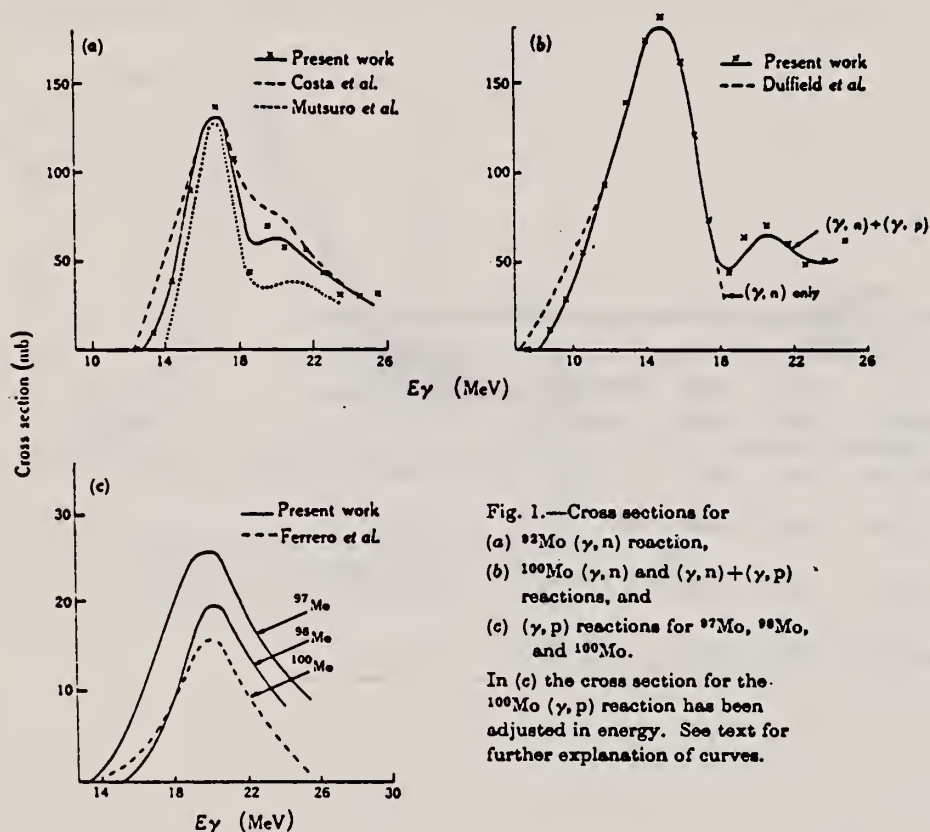


Fig. 1.—Cross sections for  
(a)  $^{92}\text{Mo} (\gamma, n)$  reaction,  
(b)  $^{100}\text{Mo} (\gamma, n)$  and  $(\gamma, n) + (\gamma, p)$   
reactions, and  
(c)  $(\gamma, p)$  reactions for  $^{92}\text{Mo}$ ,  $^{98}\text{Mo}$ ,  
and  $^{100}\text{Mo}$ .

In (c) the cross section for the  
 $^{100}\text{Mo} (\gamma, p)$  reaction has been  
adjusted in energy. See text for  
further explanation of curves.

METHOD

REF. NO.

71 Mo 2

egf

REACTION	RESULT	EXCITATION ENERGY	SOURCE		DETECTOR		ANGLE
			TYPE	RANGE	TYPE	RANGE	
G,G/	LFT	6	D	6,8	SCD-D		DST

6.418 MEV

Table 1

Summary of the experimental and theoretical decay properties of the resonance levels excited by nuclear photo-excitation.

Scatterer	Transition $1^- \rightarrow 2^+$ (keV)	$A$ ( $1^- \rightarrow 2^+$ )	$\Gamma_\gamma$ (meV)	$\Gamma(M2)$ ( $\mu$ eV)	$\Gamma(M2)$ (W.u.)	$\delta^2(M2/E1)$ ( $\times 10^3$ )	$\delta^2(M2/E1)$ Weisskopf estimate ( $\times 10^6$ )
$^{74}\text{Ge}$	6018 → 2200	$0.14 \pm 0.04$	$120 \pm 15$	190	0.89	$17 \begin{smallmatrix} +23 \\ -12 \end{smallmatrix}$	3.2
$^{100}\text{Mo}$	6418 → 1064	$0.20 \pm 0.08$	$50 \pm 45$	110	0.079	$46 \begin{smallmatrix} +53 \\ -33 \end{smallmatrix}$	6.3
$^{112}\text{Cd}$	7632 → 617	$0.09 \pm 0.02$	$86 \pm 15$	36	0.006	$3.6 \begin{smallmatrix} +4.5 \\ -2.7 \end{smallmatrix}$	10.8
$^{186}\text{W}$	6418 → 122	$-0.011 \pm 0.014$	$46 \pm 35$	110	0.023	$9.0 \begin{smallmatrix} +5.4 \\ -4.1 \end{smallmatrix}$	8.7

REF. R. Bergere, H. Beil, P. Carlos, A. Lepretre, A. Veyssiere  
 PIGNS-73, Vol.I, p.525 Asilomar

ELEM. SYM.	A	Z
Mo	100	42
REF. NO.		
73 Be 10		hmg

METHOD					REF. NO.	
					73 Be 10	
REACTION	RESULT	EXCITATION ENERGY	SOURCE		DETECTOR	
			TYPE	RANGE	TYPE	RANGE
G, SN	ABX	8- 28	D	8- 28	BF3-I	4PI

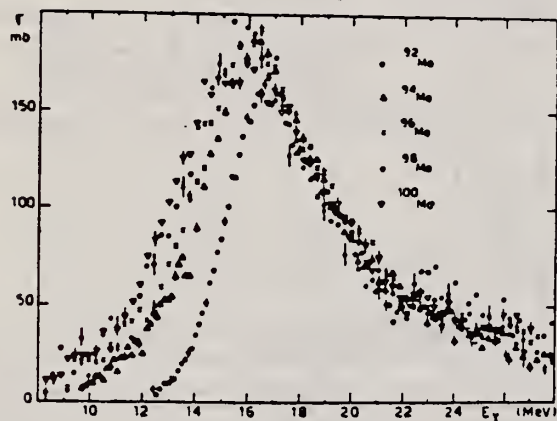


Fig. 15 Comparison of the total photoneutron cross sections of  $^{92}\text{Mo}$ ,  $^{94}\text{Mo}$ ,  $^{96}\text{Mo}$ ,  $^{98}\text{Mo}$  and  $^{100}\text{Mo}$

Table I

Isotopes	$^{92}\text{Mo}$	$^{94}\text{Mo}$	$^{96}\text{Mo}$	$^{98}\text{Mo}$	$^{100}\text{Mo}$
$\sigma_{\text{on}}$	0.83	0.98	1.08	1.11	1.08



REF.				ELEM. SYM.		A	Z
R. Moreh, A. Wolf, O. Shahal, J. Tenenbaum, A. Nof Nucl. Phys. <u>A217</u> , 477 (1973)				Mo		100	42
METHOD				REF. NO.			
				73 Mo 12			egf
REACTION	RESULT	EXCITATION ENERGY	SOURCE		DETECTOR		ANGLE
			TYPE	RANGE	TYPE	RANGE	
G,G	LFT	5- 8	D	5- 8	SCD-D		DST

Fig. 2. Decay scheme of four resonance levels in <sup>100</sup>Mo showing the relative intensities for de-excitation to low-lying levels. Most probable spins and parities for some levels assigned from angular distribution results are given. Parentheses indicate uncertainties.

Fig. 2. Decay scheme of four resonance levels in <sup>100</sup>Mo showing the relative intensities for de-excitation to low-lying levels. Most probable spins and parities for some levels assigned from angular distribution results are given. Parentheses indicate uncertainties.

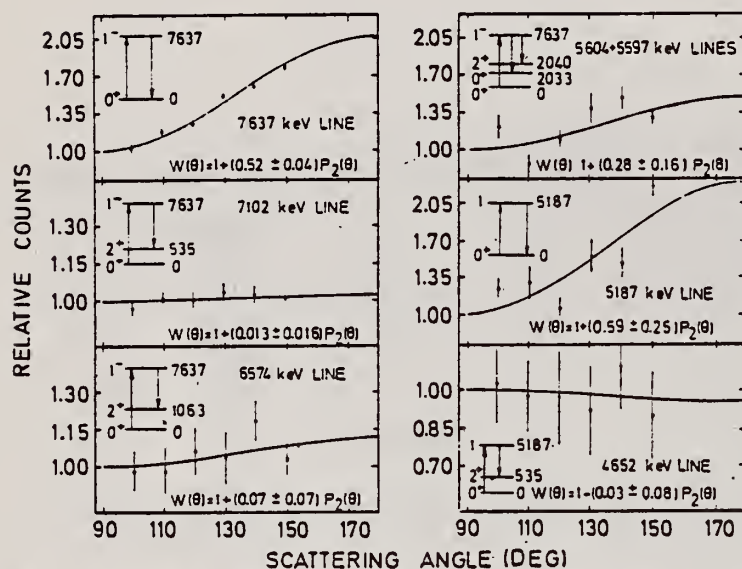


Fig. 3. Angular distributions of the elastic and some inelastic transitions de-exciting the 7637 keV level in <sup>100</sup>Mo as measured using a 20 cm<sup>3</sup> Ge(Li) detector. The solid lines have the form  $W(\theta) = 1 + AP_2(\cos \theta)$  and are least square fits to the experimental distributions. In each case the corresponding  $\gamma\gamma$  cascade is indicated.

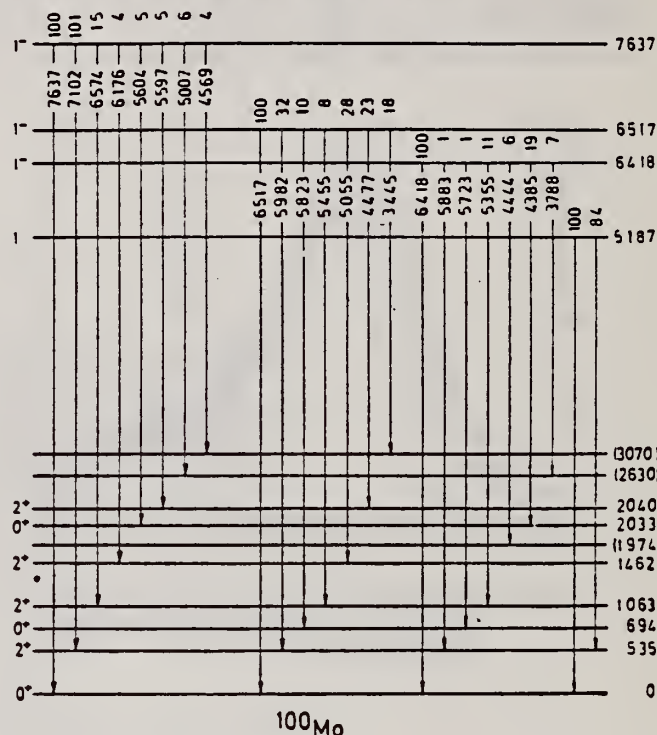


TABLE 6  
Summary of the parameters of the resonance levels in <sup>100</sup>Mo

Energy (keV)	(n, $\gamma$ ) source	$\Gamma_0$ (meV)	$\Gamma$ (meV)	$\langle\sigma_r\rangle$ (mb)	$\delta$ ( $\pm V$ )
6418	Ti	$25 \pm 8$	$50 \pm 35$	$150 \pm 15$	$4.7 \pm 0.3$
6517	V	$72 \pm 48$	$180 \pm 100$	$110 \pm 30$	$12.8 \pm 1.2$
7637	Cu	$40 \pm 5$	$140 \pm 40$	$98 \pm 15$	$4.5 \pm 0.5$

REF.

H. Beil, R. Bergere, P. Carlos, A. Lepretre, A. De Miniac, and  
A. Veyssiere  
Nucl. Phys. **A227**, 427 (1974)

ELEM. SYM.

A

Z

Mo

100

42

METHOD

REF. NO.

74 Be 3

egf

REACTION	RESULT	EXCITATION ENERGY	SOURCE		DETECTOR		ANGLE
			TYPE	RANGE	TYPE	RANGE	
* G,N	ABX	8- 27	D	8- 27	BF3-I		4PI
** G,2N	ABX	14- 27	D	14- 27	BF3-I		4PI
*** G,3N	ABX	21- 28	D	21- 28	BF3-I		4PI

\*707 +  
\*\*708  
\*\*\*709+

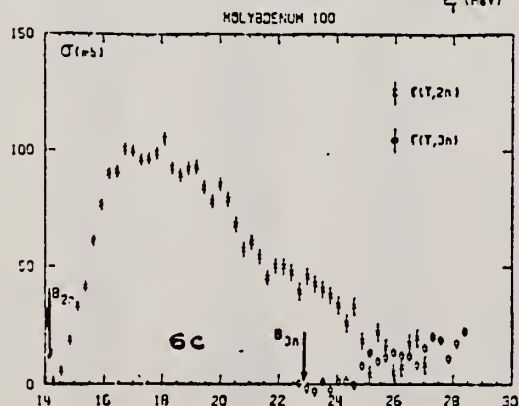
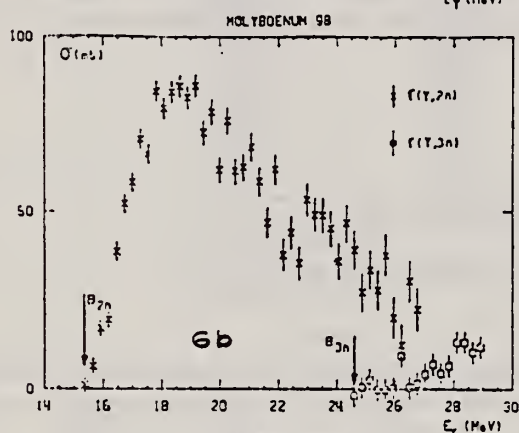
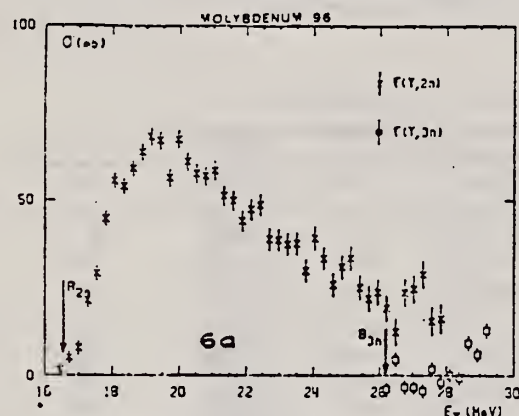


Fig. 6. Partial photoneutron cross sections  $\sigma(\gamma, 2n)$  and  $\sigma(\gamma, 3n)$  of  $^{96}\text{Mo}$ ,  $^{98}\text{Mo}$  and  $^{100}\text{Mo}$ .  
Arrows indicate theoretical threshold values given in table 2.

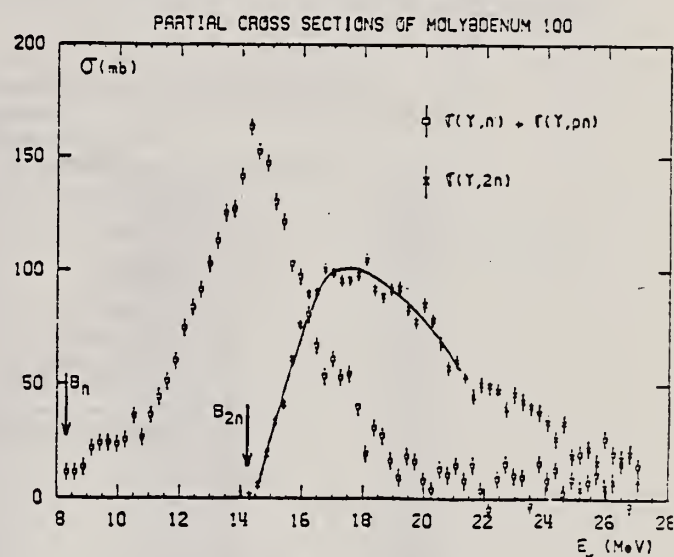


Fig. 5. Same as fig. 1, for  $^{100}\text{Mo}$ .

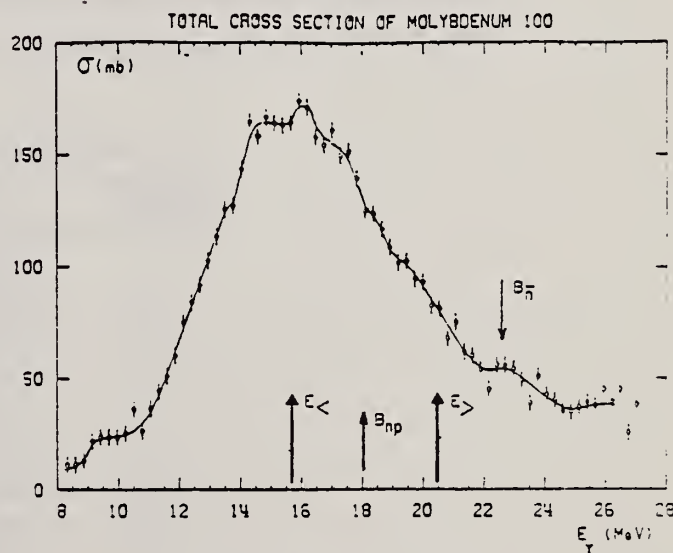


Fig. 11. Same as fig. 7, for  $^{100}\text{Mo}$ .

(over)

TABLE 3

Lorentz line parameters  $E_1$ ,  $\sigma_1$  and  $\Gamma_1$  corresponding to the best single Lorentz line fits to the experimental  $\sigma_{T,n}(E)$  curves shown in fig. 12

	$E_1$ (MeV)	$\sigma_1$ (mb)	$\Gamma_1$ (MeV)
$^{92}\text{Mo}$	$16.9 \pm 0.1$	$154 \pm 10$	$5.4 \pm 0.2$
$^{94}\text{Mo}$	$16.4 \pm 0.1$	$184 \pm 10$	$5.7 \pm 0.2$
$^{96}\text{Mo}$	$16.2 \pm 0.1$	$184 \pm 10$	$6.3 \pm 0.2$
$^{98}\text{Mo}$	$15.8 \pm 0.1$	$189 \pm 15$	$6.0 \pm 0.2$
$^{100}\text{Mo}$	$15.7 \pm 0.1$	$170 \pm 10$	$7.9 \pm 0.2$

TABLE 4

Integrated photoneutron cross sections and sum rules of the Mo isotopes

Nucleus	$^{92}\text{Mo}$	$^{94}\text{Mo}$	$^{96}\text{Mo}$	$^{98}\text{Mo}$	$^{100}\text{Mo}$
$E_M$ (MeV)	29	29	29.5	29	23.5
$\sigma_{0n}$ (MeV · b)	1.10	1.37	1.53	1.60	1.53
$\sigma_{0n}$ $0.06 N Z A^{-1}$	0.804	0.93	1.03	1.11	1.03
$\sigma_{-1n}$ (mb)	60	79.3	89.2	95.4	95.4
$\sigma_{-1n} A^{-1}$ (mb)	0.145	0.186	0.203	0.211	0.206
$\sigma_{-2n}$ (mb · MeV $^{-1}$ )	3.3	4.8	5.1	6.0	6.1
$\sigma_{-2n} A^{-1}$ ( $\mu\text{b} \cdot \text{MeV}^{-1}$ )	1.77	2.48	2.55	2.91	2.86

The notation used is defined in the text.

## METHOD

REF. NO.

74 Wo 2

egf

REACTION	RESULT	EXCITATION ENERGY	SOURCE		DETECTOR		ANGLE
			TYPE	RANGE	TYPE	RANGE	
\$ G,G	LFT	6- 8	D	6- 8	SCD-D		DST

 $\delta$  = Doppler width

6.418, 7.637

TABLE 4

Upper limit of  $\Gamma_0/\Gamma$ , the temperature variation ratio  $R_T$ , and the self-absorption ratio  $R$ 

Scatterer ( $\gamma$ -source)	$E_0$ (MeV)	$\Gamma_0/\Gamma$ ( $\pm 15\%$ )	$R_T$ <sup>a)</sup>	$R(\%)$ <sup>b)</sup>
<sup>63</sup> Cu(Ti)	6.556	0.80	0.94 $\pm$ 0.02	1.1 $\pm$ 0.5
<sup>69</sup> Ga(Cu)	7.306	0.52	1.035 $\pm$ 0.004	3.5 $\pm$ 0.5
<sup>100</sup> Mo(Cu)	7.637	0.28	1.043 $\pm$ 0.007	0.8 $\pm$ 0.3
<sup>100</sup> Mo(Ti)	6.418	0.85	1.032 $\pm$ 0.003	0.6 $\pm$ 0.3
<sup>118</sup> Sn(Cu)	6.988	0.84	1.020 $\pm$ 0.009	5.7 $\pm$ 0.2
<sup>126</sup> Te(Cu)	7.915	0.4 $\pm$ 0.1	0.95 $\pm$ 0.05	6 $\pm$ 5
<sup>130</sup> Te(Cu)	7.637	0.45 $\pm$ 0.10	0.84 $\pm$ 0.05	0.9 $\pm$ 1.5
<sup>139</sup> La(Cu)	7.637	0.55	0.95 $\pm$ 0.01	2.2 $\pm$ 0.3
<sup>139</sup> La(Ti)	6.418	0.78	0.968 $\pm$ 0.008	6.4 $\pm$ 0.8
<sup>141</sup> Pr(Cu)	7.915	0.25	1.02 $\pm$ 0.01	0.9 $\pm$ 0.9
<sup>141</sup> Pr(Cu)	7.252	0.51	1.005 $\pm$ 0.003	5.9 $\pm$ 0.4
<sup>144</sup> Nd(Cu)	7.915	0.27	0.89 $\pm$ 0.05	< 0.5
<sup>186</sup> W(Ti)	6.418	0.31	1.030 $\pm$ 0.004	< 0.5
<sup>203</sup> Tl(Ti)	6.418	0.28	1.03 $\pm$ 0.01	1.6 $\pm$ 0.3
<sup>203</sup> Tl(Cu)	7.252	0.58	1.02 $\pm$ 0.01	1.6 $\pm$ 0.7
<sup>209</sup> Bi(Cu)	7.637	1.00	1.00 $\pm$ 0.02	2 $\pm$ 1
<sup>209</sup> Bi(Ti)	7.168	1.00	0.971 $\pm$ 0.005	28.0 $\pm$ 0.6

<sup>a)</sup> The values of  $R_T$  are given for 10 g/cm<sup>2</sup> thick scatterers placed at an angle of 60° and a detector angle of 135°.<sup>b)</sup> The values of  $R$  are given for the same scatterer-detector geometry as that of  $R_T$  and a 20 g/cm<sup>2</sup> thick absorber.

TABLE 7

Summary of  $\Gamma$ ,  $\Gamma_0$  and  $\delta$  of resonance levels measured in the present work and in earlier works <sup>8, 16, 17)</sup>

Isotope	Energy (MeV)	$\Gamma$ (meV)	$\Gamma_0$ (meV)	$\delta$ (eV)	Ground state transition
<sup>63</sup> Cu	6.556	70 $\pm$ 10	28 $\pm$ 15	11.2 $\pm$ 0.8	
<sup>69</sup> Ga <sup>a)</sup>	7.306	105 $\pm$ 40	48 $\pm$ 7	6.2 $\pm$ 0.5	E1
<sup>100</sup> Mo <sup>c)</sup>	7.637	140 $\pm$ 40	40 $\pm$ 5	4.5 $\pm$ 0.5	E1
<sup>100</sup> Mo <sup>c)</sup>	6.418	50 $\pm$ 35	25 $\pm$ 8	4.25 $\pm$ 0.25	E1
<sup>118</sup> Sn	6.988	152 $\pm$ 5	128 $\pm$ 3	5.5 $\pm$ 0.5	E1
<sup>126</sup> Te	7.915	12 $\pm$ 6	5 $\pm$ 2	11 $\pm$ 2	M1
<sup>130</sup> Te	7.637	60 $\pm$ 30	30 $\pm$ 10	15 $\pm$ 2	E1
<sup>139</sup> La <sup>b)</sup>	7.637	170 $\pm$ 40	47 $\pm$ 6	10.5 $\pm$ 0.5	E1
<sup>139</sup> La <sup>b)</sup>	6.418	85 $\pm$ 15	67 $\pm$ 8	9.5 $\pm$ 0.5	E1
<sup>141</sup> Pr <sup>b)</sup>	7.915	7 $\pm$ 3	2 $\pm$ 1	6.6 $\pm$ 1.0	M1
<sup>141</sup> Pr <sup>b)</sup>	7.252	290 $\pm$ 30	110 $\pm$ 10	6.4 $\pm$ 0.5	E1
<sup>144</sup> Nd <sup>b)</sup>	7.915	30 $\pm$ 10	8 $\pm$ 3	14.0 $\pm$ 0.5	M1
<sup>186</sup> W	6.418	46 $\pm$ 35	6 $\pm$ 3	1 $\pm$ 1	E1
<sup>203</sup> Tl <sup>b)</sup>	6.418	350 $\pm$ 60	82 $\pm$ 15	0.5 $\pm$ 0.5	
<sup>203</sup> Tl <sup>b)</sup>	7.252	50 $\pm$ 30	25 $\pm$ 6	5.2 $\pm$ 1.5	M1
<sup>209</sup> Bi	7.637	> 500	> 30		
<sup>209</sup> Bi <sup>b)</sup>	7.168	820 $\pm$ 40	820 $\pm$ 40	5.8 $\pm$ 0.8	E1

<sup>a)</sup> Ref. <sup>16)</sup>.<sup>b)</sup> Ref. <sup>8)</sup>.<sup>c)</sup> Ref. <sup>17)</sup>.

(over)



TABLE 6  
Values of  $A_2$ ,  $N_{\parallel}/N_{\perp}$ , spins, and mixing amplitudes  $x$

Scatterer ( $\gamma$ -source)	$E_0$ (MeV)	$A_2$	$N_{\parallel}/N_{\perp}$	$J_0^{\pi}$	$J^{\pi}$	$J_f^{\pi}$	$x$
$^{63}\text{Cu}(\text{Ti})$	6.556	0		$\frac{3}{2}^-$	$\frac{1}{2}^-$	$\frac{3}{2}^-$	0
$^{69}\text{Ga}(\text{Cu})$	7.306	$0.14 \pm 0.01$	$1.046 \pm 0.022$	$\frac{3}{2}^-$	$\frac{3}{2}^+$	$\frac{3}{2}^-$	0
$^{100}\text{Mo}(\text{Cu})$	7.637	$0.49 \pm 0.05$	$1.17 \pm 0.05$	$0^+$	$1^-$	$0^+$	0
$^{100}\text{Mo}(\text{Cu})$	7.102 <sup>a)</sup>	$0.013 \pm 0.016$		$0^+$	$1^-$	$2^-$	$-0.06 \pm 0.02$ <sup>b)</sup>
$^{100}\text{Mo}(\text{Ti})$	6.418	$0.52 \pm 0.02$	$1.15 \pm 0.03$	$0^+$	$1^-$	$0^+$	0
$^{100}\text{Mo}(\text{Ti})$	5.355 <sup>a)</sup>	$0.19 \pm 0.08$		$0^+$	$1^-$	$2^-$	$0.21 \pm 0.12$ <sup>b)</sup>
$^{118}\text{Sn}(\text{Cu})$	6.988	$0.48 \pm 0.02$	$1.12 \pm 0.05$	$0^+$	$1^-$	$0^+$	0
$^{126}\text{Te}(\text{Cu})$	7.915	$0.46 \pm 0.11$	$0.86 \pm 0.10$	$0^+$	$1^+$	$0^+$	0
$^{130}\text{Te}(\text{Cu})$	7.637	$0.48 \pm 0.04$	$1.12 \pm 0.04$	$0^+$	$1^-$	$0^+$	0
$^{139}\text{La}(\text{Cu})$	7.637	$0.16 \pm 0.02$	$1.024 \pm 0.015$	$\frac{1}{2}^+$	$\frac{1}{2}^-$	$\frac{1}{2}^+$	0
$^{139}\text{La}(\text{Ti})$	6.418	$0.093 \pm 0.004$	$1.018 \pm 0.006$	$\frac{1}{2}^+$	$\frac{1}{2}^-$	$\frac{1}{2}^+$	0
$^{141}\text{Pr}(\text{Cu})$	7.915	$0.41 \pm 0.06$	$0.94 \pm 0.03$	$\frac{1}{2}^+$	$\frac{1}{2}^-$	$\frac{1}{2}^+$	$0.26^{+0.13}_{-0.09}$
$^{141}\text{Pr}(\text{Cu})$	7.252	$0.23 \pm 0.06$	$1.03 \pm 0.02$	$\frac{1}{2}^+$	$\frac{1}{2}^-$	$\frac{1}{2}^+$	0
$^{144}\text{Nd}(\text{Cu})$	7.915	$0.50 \pm 0.03$	$0.92 \pm 0.09$	$0^+$	$1^+$	$0^+$	0
$^{186}\text{W}(\text{Ti})$	6.418	$0.49 \pm 0.05$	$1.15 \pm 0.06$	$0^+$	$1^-$	$0^+$	0
$^{186}\text{W}(\text{Ti})$	6.296 <sup>a)</sup>	$-0.011 \pm 0.014$		$0^+$	$1^-$	$2^+$	$-0.10 \pm 0.05$ <sup>c)</sup>
$^{203}\text{Ti}(\text{Ti})$	6.418	0	$1.01 \pm 0.01$	$\frac{1}{2}^+$	$\frac{1}{2}^-$	$\frac{1}{2}^-$	0
$^{203}\text{Ti}(\text{Cu})$	7.252	$0.71 \pm 0.08$	$0.90 \pm 0.02$	$\frac{1}{2}^+$	$\frac{1}{2}^+$	$\frac{1}{2}^+$	$-0.25 \pm 0.05$
$^{203}\text{Ti}(\text{Cu})$	7.047 <sup>a)</sup>	$-0.69 \pm 0.03$		$\frac{1}{2}^+$	$\frac{1}{2}^+$	$\frac{1}{2}^+$	$0.33 \pm 0.04$
$^{209}\text{Bi}(\text{Cu})$	7.637	$0.24 \pm 0.04$		$\frac{1}{2}^+$	$\frac{1}{2}^+$	$\frac{1}{2}^+$	
$^{209}\text{Bi}(\text{Ti})$	7.168	$0.20 \pm 0.02$	$1.040 \pm 0.015$	$\frac{1}{2}^+$	$\frac{1}{2}^+$	$\frac{1}{2}^+$	

Errors refer to one standard deviation.

<sup>a)</sup> Inelastic transitions.

<sup>b)</sup> Ref. <sup>17)</sup>.

<sup>c)</sup> Ref. <sup>15)</sup>.

TABLE 8  
Values of  $\Gamma$ ,  $D$ ,  $k_{E1}$  and  $k_{M1}$

E1 transitions					M1 transitions				
scatterer ( $\gamma$ -source)	$E_0 \rightarrow E_f$ (MeV)	$\Gamma_f$ (meV)	$D$ (eV)	$k_{E1}$ ( $10^{-10} \text{ MeV}^{-1/2}$ )	scatterer ( $\gamma$ -source)	$E_0 \rightarrow E_f$ (MeV)	$\Gamma_f$ (meV)	$D$ (eV)	$k_{M1}$ ( $10^{-10} \text{ MeV}^{-1/2}$ )
$^{62}\text{Ni}(\text{Fe})$ <sup>a)</sup>	7.646		12300		$^{126}\text{Te}(\text{Cu})$	7.915		260	
	$\rightarrow 1.172$	24		0.5		$\rightarrow 0.666$	2.3		23
$^{69}\text{Ga}(\text{Cu})$	7.306		660		$^{141}\text{Pr}(\text{Cu})$	$\rightarrow 1.421$	1.7		
	$\rightarrow 0.572$	3.2		1.0		7.915		90	
	$\rightarrow 0.872$	2.7		0.9		$\rightarrow 1.298$	1.3		30
$^{100}\text{Mo}(\text{Cu})$	7.637		670			$\rightarrow 1.437$	0.8		32
	$\rightarrow 0.535$	40		7.7		$\rightarrow 1.580$	1.4		31
	$\rightarrow 1.063$	5.7		1.4		$\rightarrow 1.655$	1.0		32
	$\rightarrow 1.461$	1.4		0.4	$^{141}\text{Pr}(\text{Fe})$ <sup>c)</sup>	7.632		170	
$^{112}\text{Cd}(\text{Fe})$ <sup>b)</sup>	7.632		350			$\rightarrow 0.145$	5.6		78
	$\rightarrow 0.617$	11		4		$\rightarrow 1.130$	6.4		100
	$\rightarrow 1.223$	7.3		3.4		$\rightarrow 1.293$	0.4		9
	$\rightarrow 1.429$	2		1		$\rightarrow 1.437$	5.6		140
	$\rightarrow 1.468$	1.7		0.9		$\rightarrow 1.451$	6.8		170
$^{130}\text{Te}(\text{Cu})$	7.637		360			$\rightarrow 1.532$	1.1		10
	$\rightarrow 0.837$	16		5.5	$^{144}\text{Nd}(\text{Cu})$	7.915		380	
	$\rightarrow 1.589$	18		8.8		$\rightarrow 0.697$	13		21
$^{139}\text{La}(\text{Cu})$	7.637		190			$\rightarrow 1.041$	2.7		22
	$\rightarrow 1.384$	3		2.5	$^{203}\text{Ti}(\text{Cu})$	$\rightarrow 1.564$	6.2		14
	$\rightarrow 1.538$	3		2.7		7.252		1200	
$^{141}\text{Pr}(\text{Cu})$	7.252		220			$\rightarrow 0.205$	4		3
	$\rightarrow 0.146$	82		38					
	$\rightarrow 1.120$	8.6		6.5					
$^{186}\text{W}(\text{Cu})$	6.418		110						
	$\rightarrow 0.122$	12		14					

The values of  $D$  refer to an excitation energy  $E_0$ .

<sup>a)</sup> Ref. <sup>1)</sup>.

<sup>b)</sup> Ref. <sup>29)</sup>.

<sup>c)</sup> Ref. <sup>30)</sup>.



H. Bartsch, K. Huber, U. Kneissl, H. Krieger  
Nucl. Phys. A256, 243 (1976)

ELEM. SYM.	A	Z
Mo	100	42
REF. NO.		
76 Ba 1		egf

METHOD

REACTION	RESULT	EXCITATION ENERGY	SOURCE		DETECTOR		ANGLE
			TYPE	RANGE	TYPE	RANGE	
G,N	RLY	THR-UKN	C	UKN	SCD-D		4PI

ISOMER RATIO

TABLE I  
Experimental and theoretical results

Process	Target-spin	$E_\gamma$ (keV)	$T_{1/2}$	Spin high	Spin low	$R_{exp} = \frac{\sigma_{high}}{\sigma_{low}}$	SCOP (h)
$^{181}\text{Ta}(\gamma, 3n)$	$\frac{1}{2}^+$	93	2.2 h 9.31 min 8.15 h	$7^-$	$1^+$	$0.51 \pm 0.09$	$3.6 \pm 0.2$
$^{142}\text{Nd}(\gamma, n)$	$0^+$	755 1100-1300, 145	63 s 2.5 h	$\frac{1}{2}^-$	$\frac{3}{2}^+$	$0.055 \pm 0.006$ $0.19 \pm 0.01^*)$	$2.20 \pm 0.06$
$^{92}\text{Mo}(\gamma, n)$	$0^+$	652.9 1208, 1508, 1581, 1637	66 s 15.49 min	$\frac{3}{2}^+$	$\frac{1}{2}^-$	$1.03 \pm 0.21$ $0.85 \pm 0.07^*)$ $1.92 \pm 0.15^*)$	$5.03 \pm 0.75$ $4 \pm \frac{1}{2}$
$^{100}\text{Mo}(\gamma, n)$	$0^+$	97.3 140.5	$16.8 \mu\text{s}$ 66.02 h	$\frac{3}{2}^+$	$\frac{1}{2}^+$	$0.85 \pm 0.24$	$1.72 \pm 0.25$
$^{108}\text{Pd}(\gamma, n)$	$0^+$	214.5 115	22 s 850 ns	$\frac{1}{2}^-$	$\frac{1}{2}^+$	$0.5 \pm 0.2$	$3.4 \pm 0.5$
$^{110}\text{Pd}(\gamma, n)$	$0^+$	188 113 87.7	4.7 min 390 ns 13.47 h	$\frac{1}{2}^-$ $\frac{1}{2}^-$ $\frac{1}{2}^+$	$\frac{1}{2}^+$ $\frac{1}{2}^+$ $\frac{1}{2}^+$	$0.11 \pm 0.02$ $0.41 \pm 0.09$ $3.2 \pm 0.7$	$3.14 \pm 0.15$ $3.0 \pm 0.25$ $3.3 \pm 0.4$
$^{89}\text{Y}(\gamma, n)$	$\frac{1}{2}^-$	231.7 442.3 392.5	14.2 ms  $300 \mu\text{s}$	$8^+$	$1^+$	$0.056 \pm 0.008$	

<sup>a)</sup> Ref. <sup>14)</sup>.    <sup>b)</sup> Ref. <sup>15)</sup>.

<sup>14)</sup> P.E. Hausteing et al., J. Inorg. Nucl. Chem. 33, 289 (1971)

<sup>15)</sup> J.H. Carver et al., Nucl. Phys. 37, 449 (1962)

REF.	H. Bartsch, K. Huber, U. Kneissl and H. Krieger Z. Physik <u>A285</u> , 273 (1978)	ELEM. SYM.	A	Z
		Mo	100	42
METHOD		REF. NO.	78 Ba 11	hmg 11/17/80

REACTION	RESULT	EXCITATION ENERGY	SOURCE		DETECTOR		ANGLE
			TYPE	RANGE	TYPE	RANGE	
G, NG	LFT	98(97,8)*450(499.2)	C	20,40	SCD-D	---	135

Short-lived isomers in the nuclei  $^{90,92}\text{Nb}$ ,  $^{99}\text{Mo}$ ,  $^{98,100,101}\text{Tc}$  and  $^{101}\text{Ru}$  populated in photonuclear reactions were studied by pulsed beam techniques. Energy and half-life of the  $\gamma$ -rays deexciting the isomeric levels were measured by recording energy-time spectra. The delayed  $\gamma$ -rays and K X-rays were detected by means of an intrinsic Ge-detector of high resolution. From the measured intensity ratios internal conversion coefficients were determined. The multipolarities of the isomeric transitions could be deduced in most cases. A classification of the observed isomers has been tried on the basis of the obtained experimental results and most recent literature data.

\*KeV, Isomer LFT

Table 1. Experimental results.  $E$ : energy,  $T_{1/2}$ : half-life,  $I_{rel}$ : relative intensity,  $L$ : multipolarity,  $H$ : hindrance factor

Line	$E$ [keV]	$T_{1/2}$ [ $\mu\text{s}$ ]	$T_{1/2}$ [ $\mu\text{s}$ ] (weighted average)	$I_{rel}$	$\alpha_K$	Intensity ratios	$L$	$H$
$^{90}\text{Nb}$ K X-rays	—	—	—	1	—	—	—	—
123	$122.6 \pm 0.2$	$63 \pm 2$	—	2.5	$0.56 \pm 0.22$	—	E2	120
$^{92}\text{Nb}$ K X-rays	—	—	—	1	—	—	—	—
90	$90.4 \pm 0.2$	$5.9 \pm 0.2$	—	10.3	$0.14 \pm 0.01$	—	E1	$1.5 \cdot 10^7$
$^{99}\text{Mo}$ K X-rays	—	$15.2 \pm 0.4$	$15.5 \pm 0.2$	1	—	—	—	—
98	$97.8 \pm 0.1$	$15.6 \pm 0.2$	—	0.95	$1.45 \pm 0.27$	—	E2	20
138	$137.7 \pm 0.2$	$0.79 \pm 0.09$	$0.76 \pm 0.06$	1	—	$I_{430}/I_{138} =$	M1	—
449	$449.2 \pm 0.2$	$0.74 \pm 0.08$	—	0.97	—	$0.97 \pm 0.08$	(M2)	(37)
$^{98}\text{Tc}$ K X-rays	—	$14.8 \pm 0.5$	$14.6 \pm 0.4$	1	—	—	—	—
22	$21.8 \pm 0.2$	$16.4 \pm 2.7$	from	0.036	—	$I_{43}/I_{22} =$	E1 + 1% M2	$10^7$
26	—	—	X, 43	—	—	$5.1 \pm 0.5$	(E2)	—
43	$43.5 \pm 0.2$	$14.4 \pm 0.5$	—	0.18	—	—	M1	—
$^{100}\text{Tc}$ K X-rays	—	$8.2 \pm 0.7$	$8.2 \pm 0.3$	1	—	—	—	—
29	$28.7 \pm 0.3$	—	from	0.027	—	$I_{172}/I_{29} =$	E2	1
172	$172.3 \pm 0.3$	$8.2 \pm 0.3$	X, 172	2.2	—	$82 \pm 40$	(M1, E2)	—
$^{101}\text{Tc}$ K X-rays	—	—	—	1	—	—	—	—
192	$192.0 \pm 0.3$	$636 \pm 8$	—	5.0	$0.26 \pm 0.06$	—	M2	560
$^{101}\text{Ru}$ K X-rays	—	$16.1 \pm 3.9$	$17.5 \pm 0.4$	1	—	—	—	—
220	$220.7 \pm 0.2$	$17.4 \pm 0.5$	from	7.5	—	$I_{306}/I_{220} =$	M2	28
306	$306.6 \pm 0.3$	$17.7 \pm 0.6$	220, 306	9.1	—	$1.2 \pm 0.1$	—	—

ELEM. SYM.	A	Z
Mo	100	42

METHOD					REF. NO.	
					78 Ba 14	hg
REACTION	RESULT	EXCITATION ENERGY	SOURCE		DETECTOR	
			TYPE	RANGE	TYPE	RANGE
G,N	RLY	8-65	C	65	SCD-D	4PI

Isomeric cross section ratios were measured for the photonuclear reactions  $^{100}\text{Mo}(\gamma, n)$   $^{99\text{m}, \text{m}_2, \text{s}}\text{Mo}$  and  $^{102}\text{Ru}(\gamma, p)$   $^{101\text{m}, \text{s}}\text{Tc}$ . Using the Huizenga-Vandenbosch-method spin cut-off parameters were deduced. The applicability of this statistical procedure is discussed. A systematic analysis of all known  $(\gamma, x n)$  isomeric ratio-measurements shows a linear correlation between derived spin cut-off parameters and the mean value of the spins of the isomeric pair.

# ISOMER YIELD, DE-EX G

Table 1. Experimental and theoretical results

Process	Targetspin (h)	$E_\gamma$ (keV)	$t_{1/2}$	Spin high (h)	Spin low (h)	$R_{\text{exp}}$	SCOP(h)
$^{100}\text{Mo}(\gamma, n)$	0 <sup>+</sup>	449.2	760 ns	11/2 <sup>-</sup>	5/2 <sup>+</sup>	0.11 ± 0.02	4.3 ± 0.4
		137.7		11/2 <sup>-</sup>	1/2 <sup>+</sup>	0.10 ± 0.02	4.3 ± 0.4
		97.8		5/2 <sup>-</sup>	1/2 <sup>+</sup>	0.94 ± 0.25	1.8 ± 0.3
$^{102}\text{Ru}(\gamma, p)$	0 <sup>+</sup>	191.9	636 μs	9/2 <sup>+</sup>	1/2 <sup>-</sup>	1.33 ± 0.30	1.65 ± 0.35
		306.6					

$$R_{\text{exp}} = \frac{Y_{\text{high spin}}}{Y_{\text{low spin}}}$$

METHOD					REF. NO.	
					78 Ma 10	hg
REACTION	RESULT	EXCITATION ENERGY	SOURCE		DETECTOR	
			TYPE	RANGE	TYPE	RANGE
G,N	ABY	8-68	C	30-68	ACT - I	4PI

Analysis is made of reactions interfering with photon activation analysis procedures.

The activation yield curves have been presented for a number of photonuclear reactions in the energy range from 30 to 68 MeV, in order to evaluate quantitatively the interferences due to competing reactions in multielement photon activation analysis. The general features of the yields as functions of both target mass number and excitation energy were elucidated from the data obtained, discussion being given on the results in terms of the reaction mechanism.

Simultaneous neutron activation due to appreciable neutron production from the converter and surrounding materials has also been studied, and, finally, the magnitudes of interferences in real multielement analysis were given in the form of their energy dependences.

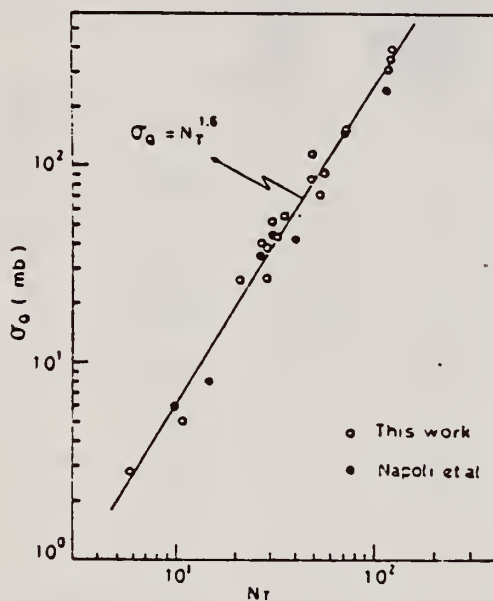


Fig. 2. Yield per equivalent quanta versus target neutron number.

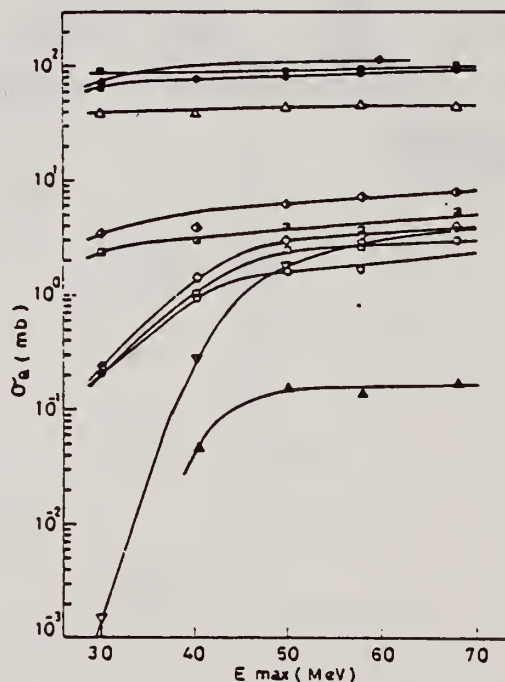


Fig. 7. Activation yield curves for the reactions on Y, Zr, Nb and Mo.  
 ◆  $^{89}\text{Y}(\gamma, n)^{88}\text{Y}$ , ●  $^{90}\text{Zr}(\gamma, n)^{89}\text{Zr}$ , ○  $^{90}\text{Zr}(\gamma, pn)^{88}\text{Y}$ ,  
 △  $^{93}\text{Nb}(\gamma, n)^{92m}\text{Nb}$ , ▲  $^{93}\text{Nb}(\gamma, xn)^{88}\text{Y}$ , ■  $^{100}\text{Mo}(\gamma, n)^{99}\text{Mo}$ ,  
 ◇  $^{97}\text{Mo}(\gamma, p)^{96}\text{Nb}$ , ▽  $^{96}\text{Mo}(\gamma, p)^{95m}\text{Nb}$ , ◊  $^{94}\text{Mo}(\gamma, pn)^{92m}\text{Nb}$ ,  
 □  $^{92}\text{Mo}(\gamma, 2n)^{90}\text{Mo}$ , ▽  $^{94}\text{Mo}(\gamma, xn)^{89}\text{Zr}$ .

(over)



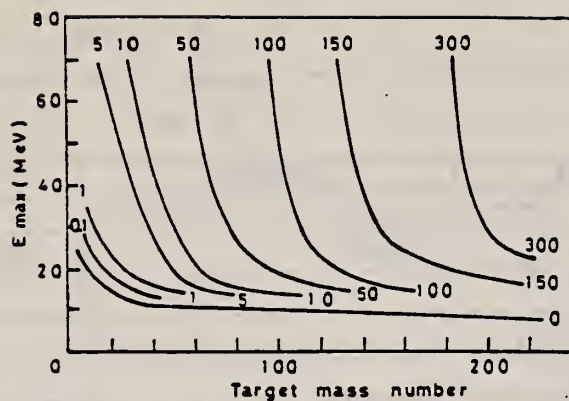


Fig. 9. Yields of the  $(\gamma, n)$  reactions as a function of bremsstrahlung maximum energy and target mass number. The numerical values in the figure are yields per equivalent quanta in mb.



ELEM. SYM.	A	Z
Mo	100	42
REF. NO.		
81 Sc 6		egf

METHOD					
REACTION	RESULT	EXCITATION ENERGY	SOURCE		ANGLE
			TYPE	RANGE	
G,G	ABX	6		6	SCD-D

6.418 MEV

Elastic scattering by nuclei in the range of mass numbers between 64 and 238 has been studied with monochromatic photons in the energy range between 2 and 8 MeV. These photons were provided either by a  $Ti(n,\gamma)$  source installed in the tangential through channel of the Grenoble high flux reactor, or by  $^{24}Na$  and  $^{56}Co$  sources produced by deuteron bombardment of Al or Fe at the Göttingen cyclotron. The photoexcitation of 23 nuclear levels has been observed and the decay properties and groundstate widths of the majority of these levels have been determined. For the lead scattering target the coherent elastic differential cross section has been studied in detail. There is evidence that below the photo-neutron threshold the elastic scattering via virtual photoexcitation of the nucleus can be approximated by extrapolating the real part of the Giant Dipole Resonance amplitude along a Lorentzian curve. Coulomb corrections to Delbrück scattering seem to play a small role at 6.5 MeV.

**Table 4.** Properties of levels observed by photoexcitation.  $(d\sigma/d\Omega)^{NRF}$ : experimental differential cross section per identified isotope or element for resonance scattering through  $\theta = 90^\circ$ .  $I^\pi$ : spin-parity of excited level;  $W(\theta)$ : angular correlation function;  $g = (2I_{\pi\pi} + 1)/(2I_\pi + 1)$ ;  $\Gamma_0$ : radiative groundstate transition width,  $\Gamma$ : total level width. Errors in the last digits are given in parentheses

Isotope	$E_\gamma$ (MeV)	$(d\sigma/d\Omega)^{NRF}$ ( $\mu b/sr$ )	$I^\pi$	$\Gamma_0/\Gamma^a$	$W(\theta)g\Gamma_0^2/\Gamma$ (meV)	$\Gamma_0^f$ (meV)	$\Gamma_0^g$ (meV)
$^{238}U$	2.754	13 (4)	(1)	0.77	0.145	0.084	-
$^{238}U$	3.254	421 (5)	$1^-$	0.24	0.83	1.5	0.52(15) <sup>d</sup>
$^{209}Bi$	6.555	2.1 (4) $\cdot 10^2$	-	-	0.74	0.74 <sup>b</sup>	-
$^{209}Bi$	7.168	1.7 (3) $\cdot 10^3$	$9/2^{+*}$	1.00	710	786	820 (40) <sup>a</sup>
$^{203}Tl$	6.418	8.75(30) $\cdot 10^3$	$1/2^+$	0.28	30	102	82 (15) <sup>a</sup>
Tl	6.759	7 (3)	-	-	-	-	-
Hg	6.555	68 (17)	-	-	-	-	-
$^{186}W$	6.418	5.2 (3) $\cdot 10^2$	$1^-$	0.32	1.75	2.4	-
$^{184}W$	6.555	9.8 (10) $\cdot 10^2$	(1)	0.52	3.44	2.9	-
$^{184}W$	6.759	46 (10)	(1)	0.58	0.17	0.13	-
$^{181}Ta$	3.010	174 (17)	-	0.72	0.42	0.59	-
$^{181}Ta$	6.418	62 (4)	-	0.73	0.2	0.27 <sup>c</sup>	-
$^{181}Ta$	6.759	4.8 (12)	-	-	0.018	0.018 <sup>b</sup>	-
$^{165}Ho$	6.418	10.3 (30)	-	-	0.035	0.035 <sup>b</sup>	-
$^{165}Ho$	6.759	5.6 (14)	-	-	0.021	0.021 <sup>b</sup>	-
Nd	2.754	2.6 (5)	-	-	-	-	-
Nd	3.254	14.0 (10)	-	-	-	-	-
Ce	6.759	13.4 (10)	-	-	-	-	-
$^{121}Sb$	3.452	2.20 (5) $\cdot 10^3$	-	0.60	2.9	4.9 <sup>b</sup>	-
$^{100}Mo$	6.418	1.53 (4) $\cdot 10^4$	$1^-$	0.88	52	26	25 (8) <sup>a</sup>
$^{94}Mo$	6.555	4.4 (4) $\cdot 10^3$	(1)	0.33	15	21	-
Mo	6.759	6.2 (15)	-	-	-	-	-
Mo	7.168	8.2 (26) $\cdot 10^2$	-	-	-	-	-

<sup>a</sup> [11] <sup>b</sup>  $W(\theta)g\Gamma_0/\Gamma = 1$  assumed <sup>c</sup>  $W(\theta)g = 1$  assumed

<sup>d</sup> [28] (a small correction has been applied to the data of [28])

<sup>e</sup> Upper limits in case not all the transitions to lower levels were observed

<sup>f</sup> Present work

<sup>g</sup> Previous work

## RUTHENIUM

~~Z=44~~

Ruthenium, the last of the platinum metals to be discovered, was found in the insoluble residues arising from the refining of the extensive alluvial deposits of native platinum found in the Ural Mountain region of Russia. G. W. Osann announced in 1828 that he found three new elements in the residues; he called them pluran, ruthen, and polin. His work, discredited by the great Berzelius, later was a stimulus to the real discovery of ruthenium in 1844 by K. K. Klaus from the University of Kazan. This Russian chemist showed that Osann's ruthenium oxide was very impure but did contain a small amount of a new metal. Klaus adopted the name ruthenium, a latinized name for Russia, partly for patriotic reasons and partly in recognition of the earlier work of Osann.



REF. J. W. Jury, J. S. Hewitt, and K. G. McNeill  
Can. J. Phys. 46, 1323 (1968)

ELEM. SYM.	A	Z
Ru		44
REF. NO.		EGF
68 Ju 1		

METHOD			SOURCE		DETECTOR		ANGLE
REACTION	RESULT	EXCITATION ENERGY	TYPE	RANGE	TYPE	RANGE	
G,N	NOX	THR-27	C	27	THR	5-	DST

$$W(\theta) = a_0 + a_1 P_1 + a_2 P_2$$

TABLE I

Target element	Z	Energy	$a_0^*$	$a_1/a_0$	$a_2/a_0$
Vanadium	23	32	640 ± 50	0.11 ± 0.10	-0.09 ± 0.11
Chromium	24	22	365 ± 39	0.02 ± 0.08	0.00 ± 0.10
Manganese	25	22	450 ± 33	0.07 ± 0.05	-0.11 ± 0.06
Bromine	35	27	874 ± 54	0.05 ± 0.06	-0.15 ± 0.08
Molybdenum	42	22	610 ± 60	0.09 ± 0.05	-0.35 ± 0.06
Ruthenium	44	27	1100 ± 25	0.12 ± 0.02	-0.29 ± 0.03
Rhodium	45	27	1270 ± 47	0.06 ± 0.03	-0.14 ± 0.03
Palladium	46	27	1350 ± 29	0.26 ± 0.02	-0.12 ± 0.02
Antimony	51	27	2140 ± 62	0.04 ± 0.08	-0.25 ± 0.11
Lanthanum	57	27	1940 ± 70	0.12 ± 0.10	-0.52 ± 0.14
Praseodymium	59	30	1800 ± 58	0.20 ± 0.08	-0.40 ± 0.09
Platinum	78	27	2600 ± 52	0.17 ± 0.02	-0.15 ± 0.03
Lead	82	22	2274 ± 59	0.08 ± 0.08	-0.46 ± 0.09

\*The yield per mole per 100 r was normalized to a yield of 2274 for the lead sample at the same energy.





Pu  
A=99

Pu  
A=99

Pu  
A=99



ELEM. SYM.	A	Z
Ru	99	44
REF. NO.		hmg
78 Ba 11		1/17/80

METHOD

REACTION	RESULT	EXCITATION ENERGY	SOURCE		DETECTOR		ANGLE
			TYPE	RANGE	TYPE	RANGE	
G, PG	LFT	22(21.8)*44(43.5)	C	20,40	SCD-D	---	135

Short-lived isomers in the nuclei  $^{90,92}\text{Nb}$ ,  $^{99}\text{Mo}$ ,  $^{98,100,101}\text{Tc}$  and  $^{101}\text{Ru}$  populated in photonuclear reactions were studied by pulsed beam techniques. Energy and half-life of the  $\gamma$ -rays deexciting the isomeric levels were measured by recording energy-time spectra. The delayed  $\gamma$ -rays and K X-rays were detected by means of an intrinsic Ge-detector of high resolution. From the measured intensity ratios internal conversion coefficients were determined. The multipolarities of the isomeric transitions could be deduced in most cases. A classification of the observed isomers has been tried on the basis of the obtained experimental results and most recent literature data.

\*KeV, Isomer LFT

Table 1. Experimental results. E: energy,  $T_{1/2}$ : half-life,  $I_{rel}$ : relative intensity, L: multipolarity, H: hindrance factor

Line	E [keV]	$T_{1/2}$ [ $\mu$ s]	$T_{1/2}$ [ $\mu$ s] (weighted average)	$I_{rel}$	$a_K$	Intensity ratios	L	H
$^{90}\text{Nb}$ K X-rays	—	—	—	1	—	—	—	—
123	$122.6 \pm 0.2$	$63 \pm 2$	—	2.5	$0.56 \pm 0.22$	—	E2	120
$^{92}\text{Nb}$ K X-rays	—	—	—	1	—	—	—	—
90	$90.4 \pm 0.2$	$5.9 \pm 0.2$	—	10.3	$0.14 \pm 0.01$	—	E1	$1.5 \cdot 10^7$
$^{99}\text{Mo}$ K X-rays	—	$15.2 \pm 0.4$	$15.5 \pm 0.2$	1	—	—	—	—
98	$97.8 \pm 0.1$	$15.6 \pm 0.2$	—	0.95	$1.45 \pm 0.27$	—	E2	20
138	$137.7 \pm 0.2$	$0.79 \pm 0.09$	$0.76 \pm 0.06$	1	—	$I_{430}/I_{138} =$	M1	—
449	$449.2 \pm 0.2$	$0.74 \pm 0.08$	—	0.97	—	$0.97 \pm 0.08$	(M2)	(37)
$^{98}\text{Tc}$ K X-rays	—	$14.8 \pm 0.5$	$14.6 \pm 0.4$	1	—	—	—	—
22	$21.8 \pm 0.2$	$16.4 \pm 2.7$	from	0.036	—	$I_{43}/I_{22} =$	E1 + 1% M2	$10^7$
26	—	—	X, 43	—	—	$5.1 \pm 0.5$	(E2)	—
43	$43.5 \pm 0.2$	$14.4 \pm 0.5$	—	0.18	—	—	M1	—
$^{100}\text{Tc}$ K X-rays	—	$8.2 \pm 0.7$	$8.2 \pm 0.3$	1	—	—	—	—
29	$28.7 \pm 0.3$	—	from	0.027	—	$I_{172}/I_{29} =$	E2	1
172	$172.3 \pm 0.3$	$8.2 \pm 0.3$	X, 172	2.2	—	$82 \pm 40$	(M1, E2)	—
$^{101}\text{Tc}$ K X-rays	—	—	—	1	—	—	—	—
192	$192.0 \pm 0.3$	$636 \pm 8$	—	5.0	$0.26 \pm 0.06$	—	M2	560
$^{101}\text{Ru}$ K X-rays	—	$16.1 \pm 3.9$	$17.5 \pm 0.4$	1	—	—	—	—
220	$220.7 \pm 0.2$	$17.4 \pm 0.5$	from	7.5	—	$I_{306}/I_{220} =$	M2	28
306	$306.6 \pm 0.3$	$17.7 \pm 0.6$	220, 306	9.1	—	$1.2 \pm 0.1$	—	—



Ru  
A=101

Ru  
A=101

Ru  
A=101





METHOD

REF. NO.

78 Ba 11

hmg  
11/17/80

REACTION	RESULT	EXCITATION ENERGY	SOURCE		DETECTOR		ANGLE
			TYPE	RANGE	TYPE	RANGE	
G, PG	LFT	29(28.7)*173(172.3)	C	20,40	SCD-D	---	135

\*KeV, Isomer LFT

Short-lived isomers in the nuclei  $^{90,92}\text{Nb}$ ,  $^{99}\text{Mo}$ ,  $^{98,100,101}\text{Tc}$  and  $^{101}\text{Ru}$  populated in photonuclear reactions were studied by pulsed beam techniques. Energy and half-life of the  $\gamma$ -rays deexciting the isomeric levels were measured by recording energy-time spectra. The delayed  $\gamma$ -rays and K X-rays were detected by means of an intrinsic Ge-detector of high resolution. From the measured intensity ratios internal conversion coefficients were determined. The multipolarities of the isomeric transitions could be deduced in most cases. A classification of the observed isomers has been tried on the basis of the obtained experimental results and most recent literature data.

Table 1. Experimental results. E: energy,  $T_{1/2}$ : half-life,  $I_{rel}$ : relative intensity, L: multipolarity, H: hindrance factor

Line	E [keV]	$T_{1/2}$ [ $\mu$ s]	$T_{1/2}$ [ $\mu$ s] (weighted average)	$I_{rel}$	$\alpha_E$	Intensity ratios	L	H
$^{90}\text{Nb}$ K X-rays	—	—	—	1	—	—	—	—
123	$122.6 \pm 0.2$	$63 \pm 2$	—	2.5	$0.56 \pm 0.22$	—	E2	120
$^{92}\text{Nb}$ K X-rays	—	—	—	1	—	—	—	—
90	$90.4 \pm 0.2$	$5.9 \pm 0.2$	—	10.3	$0.14 \pm 0.01$	—	E1	$1.5 \cdot 10^7$
$^{98}\text{Mo}$ K X-rays	—	$15.2 \pm 0.4$	$15.5 \pm 0.2$	1	—	—	—	—
98	$97.8 \pm 0.1$	$15.6 \pm 0.2$	—	0.95	$1.45 \pm 0.27$	—	E2	20
138	$137.7 \pm 0.2$	$0.79 \pm 0.09$	$0.76 \pm 0.06$	1	—	$I_{450}/I_{138} =$	M1	—
449	$449.2 \pm 0.2$	$0.74 \pm 0.08$	—	0.97	—	$0.97 \pm 0.08$	(M2).	(37)
$^{98}\text{Tc}$ K X-rays	—	$14.8 \pm 0.5$	$14.6 \pm 0.4$	1	—	—	—	—
22	$21.8 \pm 0.2$	$16.4 \pm 2.7$	from	0.036	—	$I_{43}/I_{22} =$	E1 + 1% M2	$10^7$
26	—	—	X, 43	—	—	$5.1 \pm 0.5$	(E2)	—
43	$43.5 \pm 0.2$	$14.4 \pm 0.5$	—	0.18	—	—	M1	—
$^{100}\text{Tc}$ K X-rays	—	$8.2 \pm 0.7$	$8.2 \pm 0.3$	1	—	—	—	—
29	$28.7 \pm 0.3$	—	from	0.027	—	$I_{172}/I_{29} =$	E2	1
172	$172.3 \pm 0.3$	$8.2 \pm 0.3$	X, 172	2.2	—	$82 \pm 40$	(M1, E2)	—
$^{101}\text{Tc}$ K X-rays	—	—	—	1	—	—	—	—
192	$192.0 \pm 0.3$	$636 \pm 8$	—	5.0	$0.26 \pm 0.06$	—	M2	560
$^{101}\text{Ru}$ K X-rays	—	$16.1 \pm 3.9$	$17.5 \pm 0.4$	1	—	—	—	—
220	$220.7 \pm 0.2$	$17.4 \pm 0.5$	from	7.5	—	$I_{306}/I_{220} =$	M2	28
306	$306.6 \pm 0.3$	$17.7 \pm 0.6$	220, 306	9.1	—	$1.2 \pm 0.1$	—	—



PU  
A=102

PU  
A=102

PU  
A=102





METHOD

REF. NO.

78 Ba 11

hmg  
11/17/80

REACTION	RESULT	EXCITATION ENERGY	SOURCE		DETECTOR		ANGLE
			TYPE	RANGE	TYPE	RANGE	
G <sub>e</sub> NG	LFT	221(220.7)*307	(306.6) C	20,40	SCD-D	---	135

Short-lived isomers in the nuclei  $^{90,92}\text{Nb}$ ,  $^{99}\text{Mo}$ ,  $^{98,100,101}\text{Tc}$  and  $^{101}\text{Ru}$  populated in photonuclear reactions were studied by pulsed beam techniques. Energy and half-life of the  $\gamma$ -rays deexciting the isomeric levels were measured by recording energy-time spectra. The delayed  $\gamma$ -rays and K X-rays were detected by means of an intrinsic Ge-detector of high resolution. From the measured intensity ratios internal conversion coefficients were determined. The multipolarities of the isomeric transitions could be deduced in most cases. A classification of the observed isomers has been tried on the basis of the obtained experimental results and most recent literature data.

\*KeV, Isomer LFT

Table 1. Experimental results. E: energy,  $T_{1/2}$ : half-life,  $I_{rel}$ : relative intensity, L: multipolarity, H: hindrance factor

Line	E [keV]	$T_{1/2}$ [ $\mu$ s]	$T_{1/2}$ [ $\mu$ s] (weighted average)	$I_{rel}$	$a_K$	Intensity ratios	L	H
$^{90}\text{Nb}$ K X-rays	—	—	—	1	—	—	—	—
123	$122.6 \pm 0.2$	$63 \pm 2$	—	2.5	$0.56 \pm 0.22$	—	E2	120
$^{92}\text{Nb}$ K X-rays	—	—	—	1	—	—	—	—
90	$90.4 \pm 0.2$	$5.9 \pm 0.2$	—	10.3	$0.14 \pm 0.01$	—	E1	$1.5 \cdot 10^7$
$^{99}\text{Mo}$ K X-rays	—	—	—	1	—	—	—	—
98	$97.8 \pm 0.1$	$15.2 \pm 0.4$	$15.5 \pm 0.2$	0.95	$1.45 \pm 0.27$	—	E2	20
138	$137.7 \pm 0.2$	$0.79 \pm 0.09$	$0.76 \pm 0.06$	1	—	$I_{430}/I_{138} =$	M1	—
449	$449.2 \pm 0.2$	$0.74 \pm 0.08$	—	0.97	—	$0.97 \pm 0.08$	(M2)	(37)
$^{99}\text{Tc}$ K X-rays	—	—	—	1	—	—	—	—
22	$21.8 \pm 0.2$	$14.8 \pm 0.5$	$14.6 \pm 0.4$	0.036	—	$I_{43}/I_{22} =$	E1 + 1% M2	$10^7$
26	—	—	from X, 43	—	—	$5.1 \pm 0.5$	(E2)	—
43	$43.5 \pm 0.2$	$14.4 \pm 0.5$	—	0.18	—	—	M1	—
$^{100}\text{Tc}$ K X-rays	—	—	—	1	—	—	—	—
29	$28.7 \pm 0.3$	$8.2 \pm 0.7$	$8.2 \pm 0.3$	0.027	—	$I_{172}/I_{29} =$	E2	1
172	$172.3 \pm 0.3$	$8.2 \pm 0.3$	from X, 172	2.2	—	$82 \pm 40$	(M1, E2)	—
$^{101}\text{Tc}$ K X-rays	—	—	—	1	—	—	—	—
192	$192.0 \pm 0.3$	$636 \pm 8$	—	5.0	$0.26 \pm 0.06$	—	M2	560
$^{101}\text{Ru}$ K X-rays	—	—	—	1	—	—	—	—
220	$220.7 \pm 0.2$	$16.1 \pm 3.9$	$17.5 \pm 0.4$	7.5	—	$I_{306}/I_{220} =$	M2	28
306	$306.6 \pm 0.3$	$17.4 \pm 0.5$	from 220, 306	9.1	—	$1.2 \pm 0.1$	—	—

METHOD					REF. NO.		
					78 Ba 14		hg
REACTION	RESULT	EXCITATION ENERGY	SOURCE		DETECTOR		ANGLE
			TYPE	RANGE	TYPE	RANGE	
G,P	RLY	9-65	C	65	SCD-D		4PI

Isomeric cross section ratios were measured for the photonuclear reactions  $^{100}\text{Mo}(\gamma, n)$   $^{99\text{m}, \text{m}_2, \text{s}}\text{Mo}$  and  $^{102}\text{Ru}(\gamma, p)$   $^{101\text{m}, \text{s}}\text{Tc}$ . Using the Huizenga-Vandenbosch-method spin cut-off parameters were deduced. The applicability of this statistical procedure is discussed. A systematic analysis of all known  $(\gamma, xn)$  isomeric ratio-measurements shows a linear correlation between derived spin cut-off parameters and the mean value of the spins of the isomeric pair.

# ISOMER YIELD, DE-EX G

Table 1. Experimental and theoretical results

Process	Targetspin (h)	$E_\gamma$ (keV)	$t_{1/2}$	Spin high (h)	Spin low (h)	$R_{exp}$	SCOP(h)
$^{100}\text{Mo}(\gamma, n)$	$0^+$	449.2	760 ns	$11/2^-$	$5/2^+$	$0.11 \pm 0.02$	$4.3 \pm 0.4$
		137.7		$11/2^-$	$1/2^+$	$0.10 \pm 0.02$	$4.3 \pm 0.4$
		97.8		$5/2^-$	$1/2^+$	$0.94 \pm 0.25$	$1.8 \pm 0.3$
$^{102}\text{Ru}(\gamma, p)$	$0^+$	191.9	636 $\mu\text{s}$	$9/2^+$	$1/2^-$	$1.33 \pm 0.30$	$1.65 \pm 0.35$
		306.6					

$$R_{exp} = \frac{Y_{\text{high spin}}}{Y_{\text{low spin}}}$$

RHODIUM  
Z=45

Rhodium was discovered in 1803-04 by W. H. Wollaston (1766-1828) while working in London. He was investigating methods to improve the technology for the refining and fabrication of platinum. Some 7000 ounces of native platinum from South America had been dissolved in aqua regia to remove the platinum. Wollaston discovered the new element when he decomposed the substance precipitated by the addition of mercurous cyanide. He choose the name rhodium (from the Greek *rhodon*, rose) in recognition of the beautiful color of the chloro salt and its aqueous solutions.

PH  
A=103

PH  
A=103



Method Synchrotron; proton yield, spectrum; angular distribution;  
nuclear emulsion; ion chamber.

Ref. No.	NVB
56 Da 2	

Reaction	E or $\Delta E$	$E_0$	$\Gamma$	$\int \sigma dE$	$J\pi$	Notes
$\text{Rh}^{103}(\gamma, xp)$	70					Yield = $2.6 \times 10^5$ protons(up to 16 MeV)/r-mole $\pm 30\%$ for 70 MeV Bremss.

FIG. 4. The calculated energy distribution (smooth curve marked total) contains both evaporated and direct protons in a 1 to 1 ratio. The separate distributions are also shown. A constant nuclear temperature of 1.0 Mev. was used for the evaporated proton energy distribution.

FIG. 5. The angular distributions of photoprotons of various energies from rhodium. Standard deviations are shown. The smooth curves were calculated from equation (1b).



ELEM. SYM.	A	Z
Rh	103	45
REF. NO.		NVB
58 Ch 2		

Betatron

REACTION	RESULT	EXCITATION ENERGY	SOURCE		DETECTOR		ANGLE
			TYPE	RANGE	TYPE	RANGE	
G, N	RLY	THR	C	THR	BF3-I		4PI

See 58 Ka 1 for cross sections.

THRESHOLD

TABLE I  
MEASURED PHOTONEUTRON THRESHOLDS

Reaction	Measured Q value, Mev.	Other Q values, Mev.	Method	Reference
$Rh^{103}(\gamma, n)Rh^{102}$	$0.46 \pm 0.08$	$9.35 \pm 0.20$	Threshold	Sher <i>et al.</i> (1951)
		$0.45 \pm 0.30$	{ Mass data Q- value	Duckworth (unpublished)
				Kochendorfer and Farmer (1954)
		$9.41 \pm 0.34$	{ Mass data Q+ value	Duckworth (unpublished)
				Kochendorfer and Farmer (1954)

METHOD	REACTION	RESULT	EXCITATION ENERGY	SOURCE		DETECTOR		ANGLE
				TYPE	RANGE	TYPE	RANGE	
Betatron; neutron cross section; BF <sub>3</sub> counters; ion chamber monitor	G, XN	ABX	9-22	C	9-22	BF <sub>3</sub> -I		4PI

REF. NO.  
58 Ka 1  
NVB

Таблица 2

Пороги испускания фотонейтронов

Изотоп	$B_n$ , Мэв	$B_{nn}$ , Мэв	Изотоп	$B_n$ , Мэв	$B_{nn}$ , Мэв
V <sup>51</sup>	11.16	20.5	La <sup>139</sup>	8.81	16.1
Mn <sup>55</sup>	10.14	19.2	Pr <sup>141</sup>	9.46	17.6
Co <sup>59</sup>	10.44	18.6	Tb <sup>159</sup>	8.16	14.8
As <sup>75</sup>	10.24	18.1	Ho <sup>165</sup>	8.10	14.6
Y <sup>89</sup>	11.82	20.7	Tm <sup>169</sup>	8.00	14.7
Nb <sup>93</sup>	8.86	17.1	Lu <sup>175</sup>	7.77	14.2
Rh <sup>103</sup>	9.46	16.8	Ta <sup>181</sup>	7.66	13.8
J <sup>127</sup>	9.14	16.2	Au <sup>197</sup>	7.96	13.3
Cs <sup>133</sup>	9.11	16.5	Bi <sup>209</sup>	7.43	14.5

# THRESHOLDS

не приведены, поскольку они превышают 22 Мэв во всех случаях, кроме золота, для которого  $B_{nn}=21$  Мэв. Свойства сечений  $\sigma_c(\gamma)$  сведены в табл. 3.

Таблица 1

Изотоп	$B_{nn}$ , Мэв	$\sigma_n(E_\gamma)$ , барн	$T$ , Мэв	$\sigma_n$ , Мэв · барн	$\gamma(22)$ , 10 <sup>6</sup> нейтрон/100 р · моль
V <sup>51</sup>	18.4	0.062	5.2	0.33	1.62
Mn <sup>55</sup>	20.2	0.060	7.0	0.39	2.01
Co <sup>59</sup>	18.3	0.068	6.3	0.44	2.30
As <sup>75</sup>	16.4	0.090	9.5	0.74	4.25
Y <sup>89</sup>	17.1	0.172	5.2	0.93	5.33
Nb <sup>93</sup>	18.0	0.156	7.5	1.17	6.80
Rh <sup>103</sup>	17.5	0.160	9.4	1.40	8.28
J <sup>127</sup>	15.2	0.273	6.8	1.76	11.9
Cs <sup>133</sup>	16.5	0.238	7.7	1.59	10.7
La <sup>139</sup>	15.5	0.325	3.8	1.55	11.2
Pr <sup>141</sup>	15.0	0.320	4.9	1.93	13.1
Tb <sup>159</sup>	15.6	0.274	9.8	2.49	18.1
Ho <sup>165</sup>	13.5	0.305	8.9	2.52	18.7
Tm <sup>169</sup>	16.4	0.250	8.4	1.91	14.9
Lu <sup>175</sup>	16.0	0.225	8.4	1.90	23.0
Ta <sup>181</sup>	14.5	0.380	8.5	3.15	22.0
Au <sup>197</sup>	13.8	0.475	4.7	3.04	22.6
Bi <sup>209</sup>	13.2	0.455	5.9	2.89	23.2

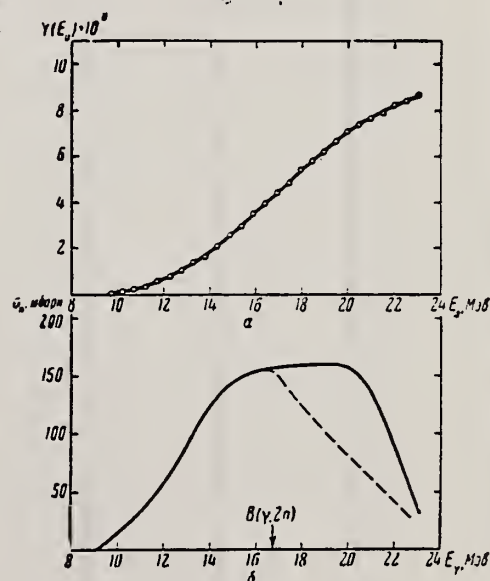


Рис. 7.

$\alpha$  — Выход фотонейтронов для Rh;  $\delta$  —  $\sigma_n(E_\gamma)$  и  $\sigma_c(\gamma)$  для Rh

Ref. M.E. Toms, J. McElhinney  
Phys. Rev. 111, 561 (1958)

Elem. Sym.	A	Z
Rh	103	45

Method Betatron; alpha spectrum; nuclear emulsion

Ref. No.	
58 To 2	NVB

Reaction	E or $\Delta E$	$E_0$	$\Gamma$	$\int \sigma dE$	$J\pi$	Notes
Rh <sup>103</sup> ( $\gamma, \alpha$ )	Bremss. 22					Yield = $0.3 \times 10^4$ alpha/mole/röntgen

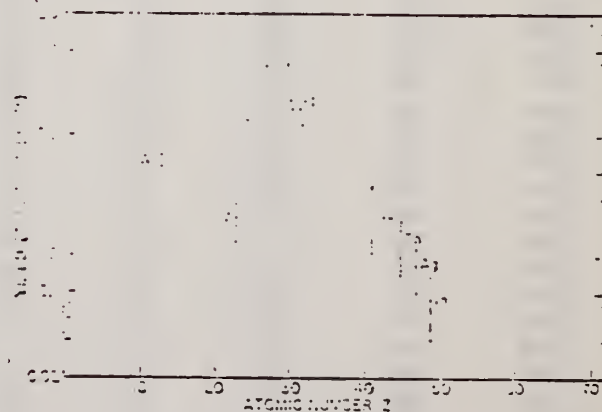


Fig. 8. Photo-alpha yields plotted against atomic numbers for the exposures of the survey.

REF.

N. Ikeda and K. Yoshihara  
Radioisotopes (Tokyo) 8, 24 (1959)

ELEM. SYM.

A

Z

Rh

103

45

METHOD

REF. NO.

59 Ik 1

EGF

REACTION	RESULT	EXCITATION ENERGY	SOURCE		DETECTOR		ANGLE
			TYPE	RANGE	TYPE	RANGE	
G,G/	ABX	1.3	D	1.3	ACT-I		4PI

Source was 10 kc  $^{60}\text{Co}$ .

Activation cross section  $3 \times 10^{-32} \text{ cm}^2$ .

Activation of 57m 40 keV state.

Method 24 MeV betatron; neutron yield;  $\text{BF}_3$  chamber, Lucite ionization chamber

Ref. No.	
59 Pa 2	EH

Reaction	E or $\Delta E$	$E_0$	$\Gamma$	$\int \sigma dE$	$J\pi$	Notes
$\text{Rh}^{103}(\gamma, n)$	Bremss.	14.5	3.4 MeV			$\sigma_a = 104 \text{ mb}$ $\sigma_b = 164 \text{ mb}$  $Q_0 = 2.1b$ compared to 2.2 b found in Coulomb excitation experiments of Heydenburg and Temmer [Phys. Rev. <u>95</u> , 861 (1954)].
	24	17	4.5 MeV			

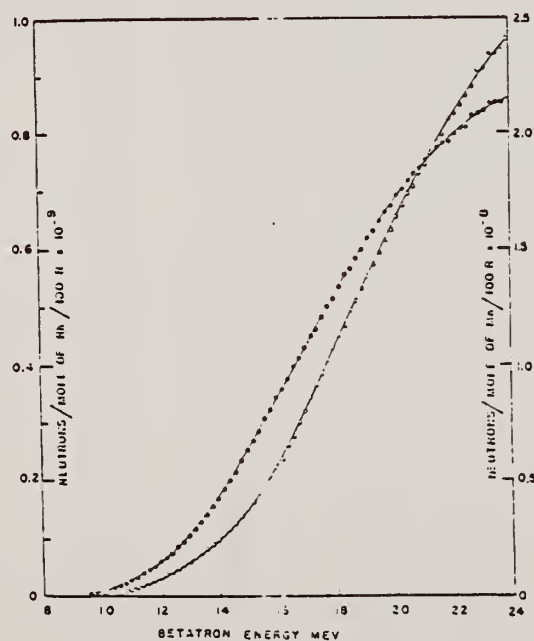


FIG. 1. Photon-neutron yield versus betatron energy.  $\circ$  manganese;  $\square$  rhodium.

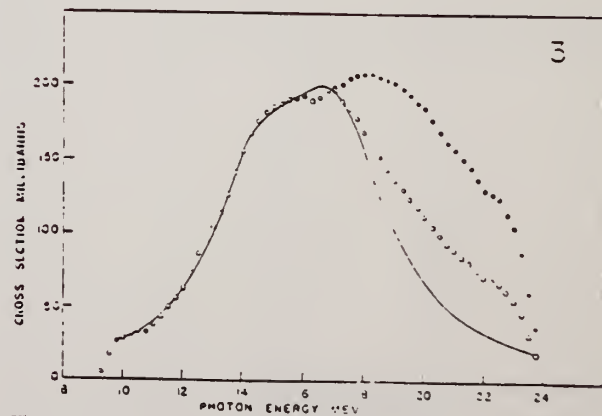


FIG. 2.  $\sigma_a = \sigma_b$  at  $E = 16.5$  MeV;  $\circ$  the resonance cross section  $\sigma_a$  and  $\sigma_b$  is calculated from the resonance curves whose parameters are given in the text.



Ref. O.V. Bogdankevich, L.E. Lazareva, A.M. Moiseev  
Zhur, Eksp. i Teoret. Fiz. 39, 1224 (1960)  
Soviet Phys. JETP 12, 853 (1961)

Elem. Sym.	A	Z
Rh	103	45
Ref. No.	60 Bo 2	JHH

Method 30-MeV synchrotron; activation

Reaction	E or $\Delta E$	$E_0$	$\Gamma$	$\int \sigma dE$	$J\pi$	Notes
$Rh^{103}(\gamma, \gamma^1)$ $Rh^{103m}$ Bremss.	5.9-25.5 ~ 20	9.3				In Table II, below, $(\gamma, \gamma^1)$ is compared with $n = (\gamma, n) + (\gamma, 2n)$ as measured by Parsons [Can. J. Phys. 37, 1344 (1959)].

Table II

E, Mev	$\sigma(\gamma, \gamma')$ , mb	$\sigma_n$ , mb	$\sigma(\gamma, \gamma')/\sigma_n$	E, Mev	$\sigma(\gamma, \gamma')$ , mb	$\sigma_n$ , mb	$\sigma(\gamma, \gamma')/\sigma_n$
5	1.8	—	—	12	0.6	62.1	0.01
7	8.5	—	—	14	1.2	155.2	~0.01
9.3	21.2	—	—	16	2.7	193.1	~0.01
9.35	21.1	10.3	2.04	18	6.1	169.0	0.04
9.5	14.8	17.2	0.86	19	9.2	136.2	0.07
9.75	4.4	25.2	0.18	20	10.3	111.0	0.09
10	2.6	27.6	0.09	21	8.7	87.9	0.10
11	1.0	37.2	0.03	22	4.4	71.7	0.06

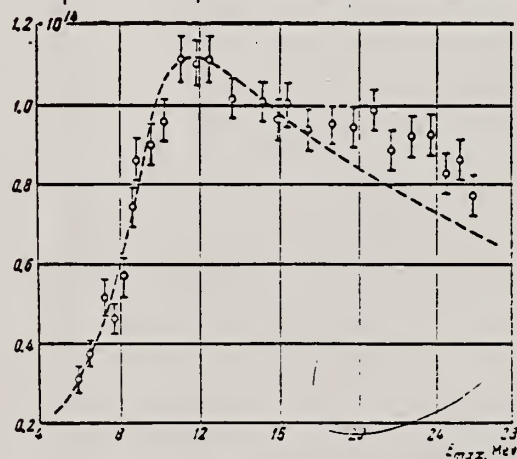


FIG. 1. Yield of the reaction  $Rh^{103}(\gamma, \gamma') Rh^{103m}$  at various maximum x-ray energies  $E_{max}$ . Ordinates — saturated activity per second per mole per ampere of ionization current of the absolute chamber. The dashed curve is the yield curve calculated under the assumption that the reaction cross section is zero at energies above 12.5 Mev.

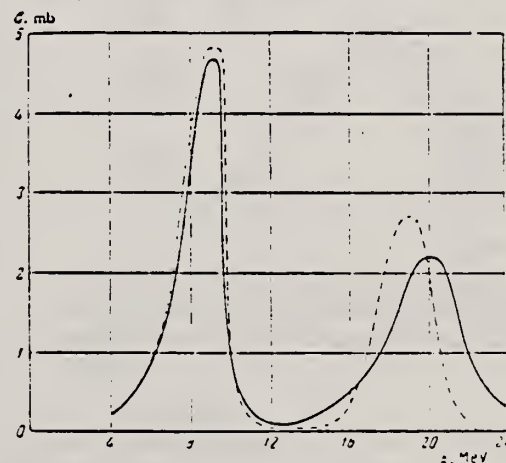


FIG. 2. Cross section of the reaction  $Rh^{103}(\gamma, \gamma') Rh^{103m}$ . Two versions of the calculation are given; other versions yield intermediate values.

REF. K.N. Geller, J. Halpern, E.G. Muirhead  
Phys. Rev. 118, 1302 (1960)

ELEM. SYM.	A	Z
Rh	103	45

METHOD	REF. NO.
Betatron; neutron threshold; ion chamber	60 Ge 3
	NVB

REACTION	RESULT	EXCITATION ENERGY	SOURCE		DETECTOR		ANGLE
			TYPE	RANGE	TYPE	RANGE	
G,N	NØX	THR	C	THR	BF3-I		4PI

THRESHOLD

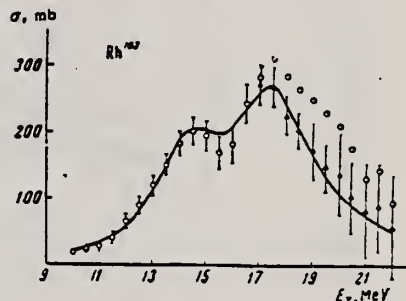
TABLE I. Summary and comparison of neutron separation energies inferred from present threshold measurements with values predicted from mass data and reaction energies. All energies are expressed in the center-of-mass system in Mev.

Reaction	No. runs	Present results	Other results	Method	Reference
$Rh^{103}(\gamma,n)Rh^{102}$	2	$9.307 \pm 0.032$	$9.40 \pm 0.33$	mass data	m
				$Q(\beta^+)$	n
			$9.46 \pm 0.30$	mass data	m
				$Q(\beta^-)$	n
			$9.46 \pm 0.08$	threshold	f

• Henry E. Duckworth, *Mass Spectroscopy* (Cambridge University Press, New York, 1958), p. 177.  
• L. J. Lidofsky, *Revs. Modern Phys.* 29, 773 (1957).

Elem. Sym.	A	Z
Rh	103	45
Ref. No.		62Bo1
		36

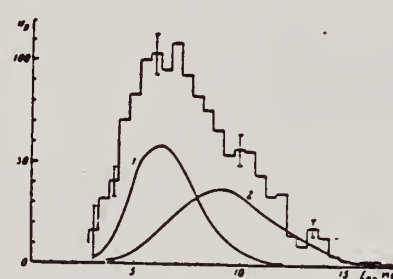
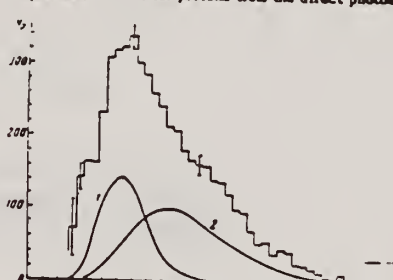
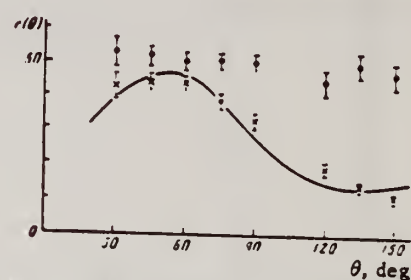
Method  
30 MeV Synchrotron - BF<sub>3</sub>

Reaction	E or ΔE	E <sub>0</sub>	Γ	∫σdE	Jπ	Notes																																																																
(γ,n) threshold	23 MeV	Fig.3 fitted with smooth curve which is superposition of 2 Lorentz lines - Data for Lorentz lines given in Table 1 ( $\sigma_{int} = \int \sigma_{\gamma} dE_{\gamma}$ )																																																																				
<p><math>E = R_1 - R_2/R_0</math>, <math>R_1</math> and <math>R_2</math> are axes of nuclear ellipsoid. <math>R_0</math> radius of sphere with volume equal to nuclear ellipsoid).</p> <div></div> <p>FIG. 3. Photoneutron production cross section of Rh<sup>103</sup>. Here and in the other graphs we denote the experimental values of <math>\sigma_n</math> by circles, the computed values of <math>\sigma_{\gamma}</math> by triangles.</p> <p>Table I</p> <table><tr><th></th><th>Ta<sup>181</sup></th><th>Rh<sup>103</sup></th><th>In<sup>115</sup></th><th></th><th>Ta<sup>181</sup></th><th>Rh<sup>103</sup></th><th>In<sup>115</sup></th></tr><tr><td><math>\sigma_1^{max}</math>, mb</td><td>350</td><td>150</td><td>166</td><td><math>\sigma_{int2}</math>, MeV.b</td><td>2.38</td><td>1.43</td><td>1.43</td></tr><tr><td><math>E_{01}</math>, MeV</td><td>12.4</td><td>14.25</td><td>14</td><td><math>\sigma_{int2}/\sigma_{int1}</math></td><td>1.8</td><td>2.0</td><td>1.8</td></tr><tr><td><math>\Gamma_1</math>, MeV</td><td>2.4</td><td>3.0</td><td>3.0</td><td><math>\sigma_{int}</math>, MeV.b</td><td>3.70</td><td>2.13</td><td>2.21</td></tr><tr><td><math>\sigma_{int1}</math>, MeV.b</td><td>1.32</td><td>0.706</td><td>0.78</td><td><math>\sigma_{int}/(0.058NZ/A)</math></td><td>1.46</td><td>1.44</td><td>1.36</td></tr><tr><td><math>\sigma_2^{max}</math>, mb</td><td>400</td><td>240</td><td>240</td><td><math>s</math></td><td>0.23</td><td>0.21</td><td>0.15</td></tr><tr><td><math>E_{02}</math>, MeV</td><td>15.5</td><td>17.5</td><td>16.25</td><td><math>s_0</math></td><td>0.22</td><td>0.20</td><td>0.14</td></tr><tr><td><math>\Gamma_2</math>, MeV</td><td>3.8</td><td>3.8</td><td>3.8</td><td><math>Q_0</math>, b</td><td>7.1±0.8</td><td>2.7±0.3</td><td>2.3±0.4</td></tr></table>								Ta <sup>181</sup>	Rh <sup>103</sup>	In <sup>115</sup>		Ta <sup>181</sup>	Rh <sup>103</sup>	In <sup>115</sup>	$\sigma_1^{max}$ , mb	350	150	166	$\sigma_{int2}$ , MeV.b	2.38	1.43	1.43	$E_{01}$ , MeV	12.4	14.25	14	$\sigma_{int2}/\sigma_{int1}$	1.8	2.0	1.8	$\Gamma_1$ , MeV	2.4	3.0	3.0	$\sigma_{int}$ , MeV.b	3.70	2.13	2.21	$\sigma_{int1}$ , MeV.b	1.32	0.706	0.78	$\sigma_{int}/(0.058NZ/A)$	1.46	1.44	1.36	$\sigma_2^{max}$ , mb	400	240	240	$s$	0.23	0.21	0.15	$E_{02}$ , MeV	15.5	17.5	16.25	$s_0$	0.22	0.20	0.14	$\Gamma_2$ , MeV	3.8	3.8	3.8	$Q_0$ , b	7.1±0.8	2.7±0.3	2.3±0.4
	Ta <sup>181</sup>	Rh <sup>103</sup>	In <sup>115</sup>		Ta <sup>181</sup>	Rh <sup>103</sup>	In <sup>115</sup>																																																															
$\sigma_1^{max}$ , mb	350	150	166	$\sigma_{int2}$ , MeV.b	2.38	1.43	1.43																																																															
$E_{01}$ , MeV	12.4	14.25	14	$\sigma_{int2}/\sigma_{int1}$	1.8	2.0	1.8																																																															
$\Gamma_1$ , MeV	2.4	3.0	3.0	$\sigma_{int}$ , MeV.b	3.70	2.13	2.21																																																															
$\sigma_{int1}$ , MeV.b	1.32	0.706	0.78	$\sigma_{int}/(0.058NZ/A)$	1.46	1.44	1.36																																																															
$\sigma_2^{max}$ , mb	400	240	240	$s$	0.23	0.21	0.15																																																															
$E_{02}$ , MeV	15.5	17.5	16.25	$s_0$	0.22	0.20	0.14																																																															
$\Gamma_2$ , MeV	3.8	3.8	3.8	$Q_0$ , b	7.1±0.8	2.7±0.3	2.3±0.4																																																															

Elem. Sym.	A	Z
Rh	103	45
Ref. No. 62Sh2		

Method

35 MeV Betatron ; nuclear emulsions

Reaction	E or ΔE	E <sub>o</sub>	Γ	∫σdE	J π	Notes																																																																																													
(γ, p)	E <sub>γmax</sub> = 22.5 33.5					<p>Angular distribution of photoprotons fitted to</p> $a \pm b \sin^2 \theta (1 + p \cos \theta)^2$ <p>where a, b and p are given in the article.</p> <p>Quadrupole absorption is estimated to be about 20%.</p>																																																																																													
<div>  <p>FIG. 1. Energy distribution of 1287 photoprotons from Rh for <math>E_{\gamma\max} = 22.5</math> MeV. Calculated spectra: curve 1 for evaporation; curve 2 for protons from the direct photoeffect.</p> </div> <div>  <p>FIG. 2. Energy distribution of 5222 photoprotons from Rh for <math>E_{\gamma\max} = 33.5</math> MeV. Same notation as in Fig. 1.</p> </div> <div>  <p>FIG. 6. Angular distributions of photoprotons from Rh for <math>E_{\gamma\max} = 33.5</math> MeV. <math>\circ - E_p = 3.25-9.25</math> MeV; <math>\times - E_p &gt; 9.25</math> MeV.</p> </div> <div> <p>Table I. Parameters of curves of <math>a + b \sin^2 \theta (1 + p \cos \theta)^2</math> and estimated contributions of E2 transitions</p> <table> <tr> <th>Element</th> <th>Z</th> <th><math>E_{\gamma\max}</math>, MeV</th> <th><math>E_p</math>, MeV</th> <th>a</th> <th>b</th> <th>p</th> <th>% E2/E1 + E2</th> </tr> <tr> <td rowspan="2">Rh</td> <td rowspan="2">45</td> <td>22.5</td> <td>3.25-9.25</td> <td>97</td> <td>0</td> <td>0</td> <td>0</td> </tr> <tr> <td></td> <td>&gt;9.25</td> <td>28</td> <td>19</td> <td>0.2</td> <td>~1</td> </tr> <tr> <td rowspan="2">Pt</td> <td rowspan="2">78</td> <td>33.5</td> <td>3.25-9.25</td> <td>49</td> <td>0</td> <td>0</td> <td>0</td> </tr> <tr> <td></td> <td>&gt;9.25</td> <td>14.5</td> <td>16</td> <td>1.2</td> <td>~20</td> </tr> <tr> <td rowspan="2">Pb</td> <td rowspan="2">82</td> <td>33.5</td> <td>7.25-14.25</td> <td>34.5</td> <td>15.5</td> <td>2.6</td> <td>~50</td> </tr> <tr> <td></td> <td>&gt;14.25</td> <td>3</td> <td>8</td> <td>3.8</td> <td>~75</td> </tr> <tr> <td rowspan="2"></td> <td rowspan="2"></td> <td>22.5</td> <td>&gt;5.25</td> <td>15.5</td> <td>13</td> <td>1.8</td> <td>~40</td> </tr> <tr> <td></td> <td>&gt;10.25</td> <td>6.5</td> <td>8</td> <td>2.2</td> <td>~50</td> </tr> </table> </div> <div> <p>Table II. Measured yields Y of photoprotons from Rh, Pt, and Pb, and estimates based on the evaporation model and on the direct photoeffect</p> <table> <tr> <th>Element</th> <th>Rh</th> <th>Pt</th> <th>Pb</th> </tr> <tr> <td><math>E_{\gamma\max}</math>, MeV</td> <td>22.5</td> <td>33.5</td> <td>33.5</td> <td>22.5</td> </tr> <tr> <td><math>Y_{\text{exp}}</math></td> <td><math>1.3 \cdot 10^6</math></td> <td><math>2.8 \cdot 10^6</math></td> <td><math>9.6 \cdot 10^6</math></td> <td><math>2.9 \cdot 10^6</math></td> </tr> <tr> <td>protons/mole-sec</td> <td></td> <td></td> <td></td> <td></td> </tr> <tr> <td><math>Y_{\text{exp}}/Y_{\text{evap}}</math></td> <td>~3</td> <td>~6</td> <td>~2000</td> <td>~1500</td> </tr> <tr> <td><math>Y_{\text{exp}}/Y_{\text{direct}}</math></td> <td>~3</td> <td>~4.5</td> <td>~20</td> <td>~11</td> </tr> </table> </div>							Element	Z	$E_{\gamma\max}$ , MeV	$E_p$ , MeV	a	b	p	% E2/E1 + E2	Rh	45	22.5	3.25-9.25	97	0	0	0		>9.25	28	19	0.2	~1	Pt	78	33.5	3.25-9.25	49	0	0	0		>9.25	14.5	16	1.2	~20	Pb	82	33.5	7.25-14.25	34.5	15.5	2.6	~50		>14.25	3	8	3.8	~75			22.5	>5.25	15.5	13	1.8	~40		>10.25	6.5	8	2.2	~50	Element	Rh	Pt	Pb	$E_{\gamma\max}$ , MeV	22.5	33.5	33.5	22.5	$Y_{\text{exp}}$	$1.3 \cdot 10^6$	$2.8 \cdot 10^6$	$9.6 \cdot 10^6$	$2.9 \cdot 10^6$	protons/mole-sec					$Y_{\text{exp}}/Y_{\text{evap}}$	~3	~6	~2000	~1500	$Y_{\text{exp}}/Y_{\text{direct}}$	~3	~4.5	~20	~11
Element	Z	$E_{\gamma\max}$ , MeV	$E_p$ , MeV	a	b	p	% E2/E1 + E2																																																																																												
Rh	45	22.5	3.25-9.25	97	0	0	0																																																																																												
			>9.25	28	19	0.2	~1																																																																																												
Pt	78	33.5	3.25-9.25	49	0	0	0																																																																																												
			>9.25	14.5	16	1.2	~20																																																																																												
Pb	82	33.5	7.25-14.25	34.5	15.5	2.6	~50																																																																																												
			>14.25	3	8	3.8	~75																																																																																												
		22.5	>5.25	15.5	13	1.8	~40																																																																																												
			>10.25	6.5	8	2.2	~50																																																																																												
Element	Rh	Pt	Pb																																																																																																
$E_{\gamma\max}$ , MeV	22.5	33.5	33.5	22.5																																																																																															
$Y_{\text{exp}}$	$1.3 \cdot 10^6$	$2.8 \cdot 10^6$	$9.6 \cdot 10^6$	$2.9 \cdot 10^6$																																																																																															
protons/mole-sec																																																																																																			
$Y_{\text{exp}}/Y_{\text{evap}}$	~3	~6	~2000	~1500																																																																																															
$Y_{\text{exp}}/Y_{\text{direct}}$	~3	~4.5	~20	~11																																																																																															



Method 35 - MeV betatron; emulsions

Ref. No.	JHH
62 Sh 4	

Reaction	E or ΔE	E <sub>0</sub>	Γ	∫σdE	Jπ	Notes
Rh <sup>103</sup> (γ,p)	Bremss. 22.5 33.5					Parameters a, b and p for $w(\theta) = a + b \sin^2\theta(1 + p \cos\theta)^2$ in Table I.

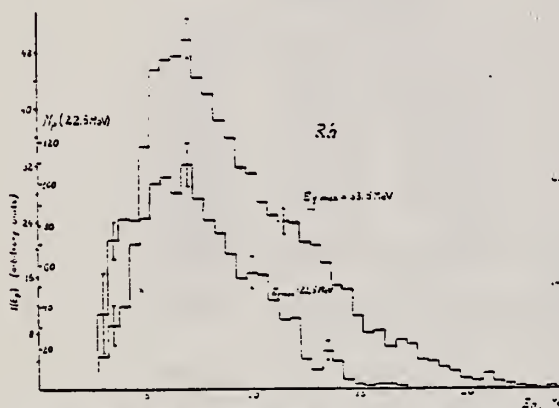


Fig. 2. Energy distributions of photoprotons from Rh<sup>103</sup> when irradiated with  $E_{\max} = 22.5$  or 33.5 MeV.  $N_p$  is the number of protons in the spectrum interval 0.5 MeV. Relative scale and  $E_p$  are chosen the same for all spectra in figs. 2-6. Statistical errors are given.

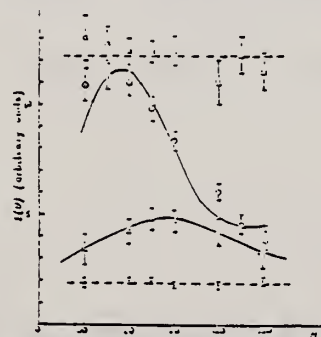


Fig. 3. Angular distributions of photoprotons from Rh<sup>103</sup>. Experimental points for irradiation with bremsstrahlung γ-spectrum with  $E_{\max} = 22.5$  MeV are designated by solid dots for  $E_p < 9.25$  MeV and by crosses for  $E_p > 9.25$  MeV. For the case of  $E_{\max} = 33.5$  MeV, squares denote  $E_p < 9.25$  MeV and circles circles  $E_p > 9.25$  MeV. Curves plotted through experimental points are described by expressions of the type (1); the coefficients for which are given in Table I.

Table I. Coefficients of expressions of type (1) for angular distributions of photoprotons from Rh<sup>103</sup> and Pt<sup>194</sup>. Coefficients are given in parentheses.

Element	Z	$E_{\max}$ (MeV)	$E_p$ (MeV)	a	b	p	Ref. (1)
Rh	45	22.5	0-9.25	1.0	0	0	0
			> 9.25	2.3	1.0	0.2	1
			0-9.25	12.2	0	0	0
Pt	78	22.5	0-9.25	4.5	0.7	1.2	0.0
			9.25-11.25	1.4	0.7	0.42	1
			> 11.25	2.9	4.4	0.02	1
W	74	33.5	0-9.25	1.5	1.2	1.2	0.0
			9.25-11.25	4.2	1.05	2.2	0.0
			> 11.25	0.5	1.2	1.5	0.0
Pt	78	33.5	0-9.25	0.5	0	0	0
			9.25-11.25	2.5	1.0	1.0	0.0
			> 11.25	2.2	0.5	1.0	0.0
Pb	82	33.5	0-9.25	1.2	0.05	0.4	0
			9.25-11.25	1.5	0.35	2.0	0.0
			> 11.25	0.53	0.5	1.4	0.0
Pt	78	22.5	0-9.25	0.6	1.0	0.4	0
			9.25-11.25	2.5	1.0	1.2	0.0
			> 11.25	1.4	0.05	2.0	0.0
Pb	82	22.5	0-9.25	1.1	0.5	2.0	0.0
			9.25-11.25	1.05	0.75	2.2	0.0
			> 11.25	1.0	1.2	1.2	0.0
Pb	82	33.5	0-9.25	1.15	0.65	2.0	0.0
			9.25-11.25	1.1	1.0	2.2	0.0
			> 11.25	1.1	1.0	2.2	0.0

Table 2. Measured photoproton yields and calculated yields for Rh<sup>103</sup> and Pt<sup>194</sup> by the use of expression (1) for bremsstrahlung.

Element	$E_{\max}$ (MeV)	$E_p$ (MeV)	Yield (10 <sup>4</sup> )	Yield (2)
Rh <sup>103</sup>	22.5	0-9.25	1.0	1.0
	33.5	0-9.25	1.0	1.0
Pt <sup>194</sup>	22.5	0-9.25	1.0	1.0
	33.5	0-9.25	1.0	1.0
W	22.5	0-9.25	1.0	1.0
	33.5	0-9.25	1.0	1.0
Pt	22.5	0-9.25	1.0	1.0
	33.5	0-9.25	1.0	1.0
Pb	22.5	0-9.25	1.0	1.0
	33.5	0-9.25	1.0	1.0

\* The same for Pt<sup>194</sup> and W.

## References

- 1) M. E. Toms and W. E. Stephens, Phys. Rev. 93 (1955) 926
- 2) M. M. Hoffman and A. G. W. Cameron, Phys. Rev. 92 (1953) 1154
- 3) W. C. Barber and V. J. Vanhise, Nuclear Physics 16 (1960) 561
- 4) M. E. Toms and W. E. Stephens, Phys. Rev. 92 (1953) 562
- 5) E. D. Stakimovskiy, JETP 33 (1960) 95
- 6) R. E. Taylor, Nuclear Physics 19 (1960) 453
- 7) A. G. W. Cameron, W. Harms and L. Katz, Phys. Rev. 83 (1951) 1204
- 8) V. G. Neudachin, V. G. Shevchenko and N. P. Yudin, Report at the Second All-Union Conf. for Nuclear Reactions at Low and Medium Energies, Moscow, 1960
- 9) E. D. Courant, Phys. Rev. 82 (1951) 703
- 10) V. V. Dzhansov, V. G. Shevchenko and N. P. Yudin, JETP 41 (1961) 1920



REF. B.S. Ishkanov, E.N. Kornienko, Yu.I. Sorokin, V.G. Shevchenko, B.A. Yur'ev Zhur. Eksp. i Teoret. Fiz. <u>45</u> , 38 (1963); Soviet Phys. JETP 18, 29 (1964)			ELEM. STM. A Rh 103 45				
METHOD Betatron; proton cross section; CsI; ion chamber			REF. NO. 63 Is 2 NVB				
REACTION	RESULT	EXCITATION ENERGY	SOURCE		DETECTOR		ANGLE
			TYPE	RANGE	TYPE	RANGE	
G, XP	ABX	13-32	C	14-32	SCI-D	3-+	DST
				(14.5-32.5)		(3.5-+)	

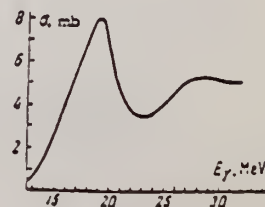
E peak       $\sigma$  peak      half width

19±0.5 MeV    8±1.5 mb    ~ 5.5 MeV

$$\int_{13}^{32} \sigma dE = 85 \pm 15 \text{ MeV-mb}$$

Discuss quadrupole resonance.

FIG. 3. Plot of the  $Rh^{103}(\gamma, p)$  reaction cross section against the energy  $E_{\gamma}$ .



REF. A. Veres Acta Phys. Acad. Sci. Hung. <u>16</u> , 261-73 (1963)			ELEM. S.Y.M.		
			Rh	103	45
METHOD Radioactive source			REF. NO. 63 Ve 2		NVB
REACTION	RESULT	EXCITATION ENERGY	SOURCE		ANGLE
			TYPE	RANGE	
G,G/	ABX	0-1	D	0-1	NAI-D

Activation by  $^{60}\text{Co}$  radiation.

ISOMERS

Таблица II  
Измеренные значения после облучения, сравниваемые с другими литературными данными

Элемент	Активность облучения после первого измерения (имп/мин.)	Актив. экстрп. в конце облуч. (имп/мин.)	Литературные данные		Данные измерений		$\sigma$ ( $10^{-28}\text{см}^2$ )	$\Gamma_{\text{уп}}$ ( $10^{-3}\text{эв}$ )
			$T_{1/2}$	$E$ (кэв)	$T_{1/2}$	$E$ (кэв)		
Se-77m	$3842 \pm 96$	5400	17,5 сек.	160	$18,1 \pm 1$ сек.	$160 \pm 10$	9,5	1,75
Sr-87m	$191 \pm 5$	200	2,8 ч.	390	$2,9 \pm 0,1$ ч.	$365 \pm 25$	0,85	0,2
Y-89m	$96 \pm 20$	170	16 сек.	910	$16,7 \pm 5$ сек.		0,08	0,02
Rh-103m	$28 \pm 5$	31	57 мин.	40	$58 \pm 2$ мин.	$20,5 \pm 0,5$	0,08	0,01
Ag-107m	$220 \pm 14$	250	44 сек.	93	$43,8 \pm 0,6$ сек.	$91 \pm 10$	0,8	0,2
Ag-109m			39 сек.	88				
Hf-179m	$80 \pm 18$	155	19 сек.	160; 215	$19 \pm 2$ сек.		1	0,2
Ir-191m	$90 \pm 20$	250	4,9 сек.	42; 130	$5 \pm 2$ сек.		5,6	1
Pt-195m	$90 \pm 9$	100	3,5 д.	31; 100; 130;	$3,5 \pm 0,2$ д.	$32 \pm 3$ $67,5 \pm 5$ $96 \pm 5$ $130 \pm 10$	0,2	0,04
Au-197m	$240 \pm 16$	520	7,2 сек.	130; 277; 407	$7,2 \pm 1$ сек.	68:130: $280 \pm 20$ $390 \pm 20$	0,07	0,01
Hg-199m	$9,6 \pm 3,2$		42 мин.	160; 370			0,005	0,001

Acta Phys. Hung. Tom. XVI. Fasc. 3.

METHOD

REF. NO.	
65 Kr 1	EGF

REACTION	RESULT	EXCITATION ENERGY	SOURCE		DETECTOR		ANGLE
			TYPE	RANGE	TYPE	RANGE	
G,2P	ABX	15-40	C	15-40	ACT-I		4PI
G,G/	RLY	7-18	C	7-18	ACT-I		4PI
E,E/	RLY	7-18	D	7-18	ACT-I		4PI

(Last two cards) E/G ISOMER YIELD

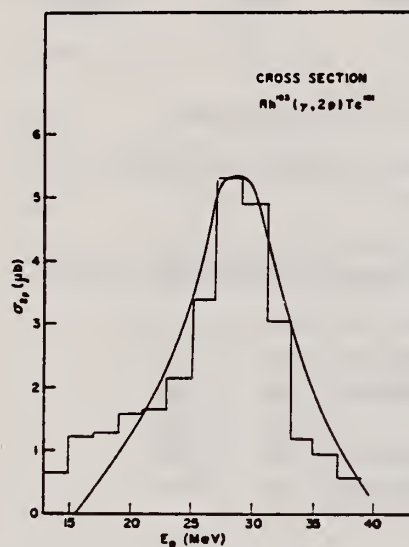


Fig. 4. Cross section for the reaction  $\text{Rh}^{103}(\gamma, 2p)\text{Tc}^{101}$ .

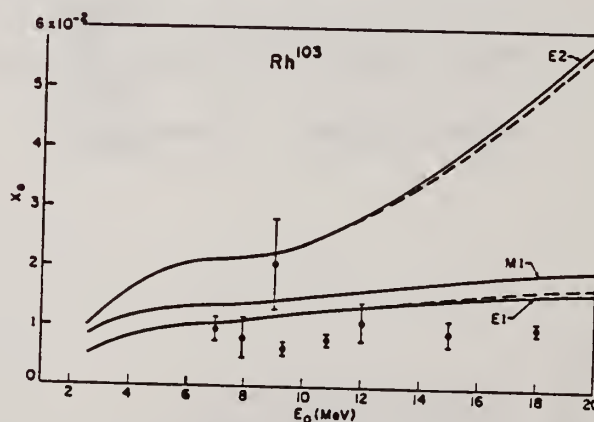


Fig. 5. Experimental results for the ratio of electron/photon yields in  $\text{Rh}^{103m}$  and the theoretical predictions under the assumptions that the cross section is made up entirely of either E1, M1, or E2 transitions (solid curves). The dashed curve lying near the E1 curve was computed under the assumption that the first peak in the cross section curve is E1 while the second peak is E2. The dashed curve lying near the E2 curve was computed under the assumption that the first peak is E2 and the second is E1.

METHOD	REF. NO.	
Neutron capture gamma rays	67 Hu 1	EGF

REACTION	RESULT	EXCITATION ENERGY	SOURCE		DETECTOR		ANGLE
			TYPE	RANGE	TYPE	RANGE	
G,N	ABX	10,11	D	10,11	BF3-I		4PI

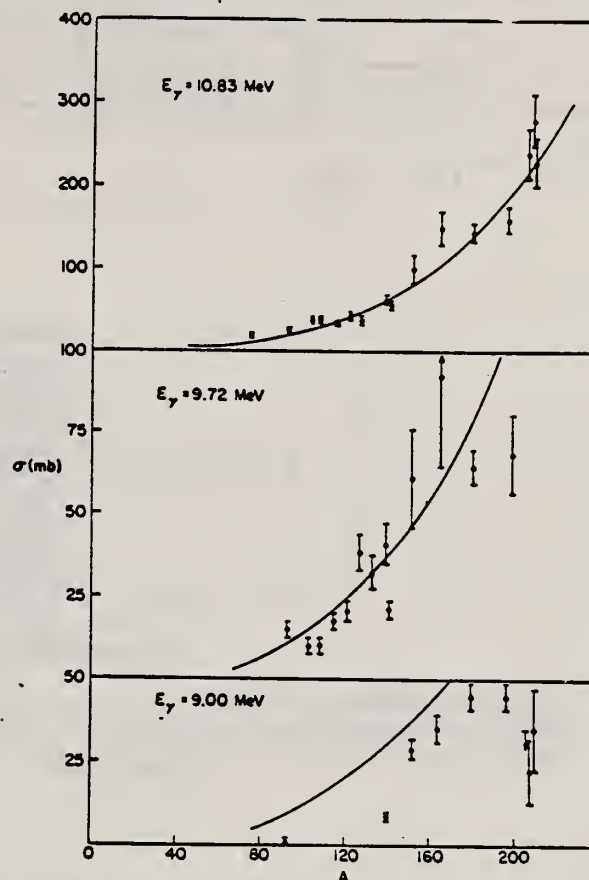


TABLE 1  
Photoneutron cross sections (mb)

Fig. 1. Cross section (in mb) versus mass number of the target for gamma-ray energies of 9.00, 9.72 and 10.83 MeV. The solid lines are plots of eq. (1) in the text.

Target	7.72 MeV	9.00 MeV	9.72 MeV	10.83 MeV
<sup>59</sup> Co				9.0 ± 0.8
<sup>75</sup> As				20.4 ± 1.7
<sup>82</sup> Nb		0.53 ± 0.10	14.6 ± 2.2	25.8 ± 2.1
<sup>103</sup> Rh			10.6 ± 1.7	38.8 ± 3.1
<sup>107</sup> Ag			10.0 ± 1.5	37.6 ± 2.9
<sup>109</sup> Ag			17.1 ± 2.6	33.3 ± 2.7
<sup>118</sup> In			20.7 ± 3.1	42.5 ± 3.6
<sup>121</sup> Sb			38.7 ± 5.8	38.8 ± 3.1
<sup>123</sup> Sb			31.7 ± 4.8	52.5 ± 3.8
<sup>127</sup> I			40.8 ± 6.5	63.0 ± 5.0
<sup>133</sup> Cs		8.61 ± 0.86	21.5 ± 3.2	58.3 ± 4.1
<sup>139</sup> La			61.3 ± 14.7	102 ± 18
<sup>141</sup> Pr		28.9 ± 3.2	92.2 ± 27.6	150 ± 20
<sup>151</sup> Eu			65.0 ± 5.5	146 ± 12
<sup>153</sup> Eu			68.4 ± 13.5	160 ± 15
<sup>165</sup> Ho		35.6 ± 4.3		238 ± 29
<sup>181</sup> Ta	4.14 ± 0.36	45.4 ± 3.7		280 ± 31
<sup>187</sup> Au		44.5 ± 3.6		226 ± 27
<sup>208</sup> Pb		< 34.3		
<sup>209</sup> Pb		22.6 ± 11.3		
<sup>209</sup> Bi		36.1 ± 12.0		

REF. J. W. Jury, J. S. Hewitt, and K. G. McNeill  
Can. J. Phys. 46, 1823 (1968)

ELEM. SYM.	A	Z
Rh	103	45

METHOD

REF. NO.  
68 Ju 1  
EGF

REACTION	RESULT	EXCITATION ENERGY	SOURCE		DETECTOR		ANGLE
			TYPE	RANGE	TYPE	RANGE	
G,N	NOX	THR-27	C	27	THR	5-	DST

$$W(\theta) = a_0 + a_1 P_1 + a_2 P_2$$

TABLE I

Target element	Z	Energy	$a_0^*$	$a_1/a_0$	$a_2/a_0$
Vanadium	23	32	$640 \pm 50$	$0.11 \pm 0.10$	$-0.09 \pm 0.11$
Chromium	24	22	$365 \pm 39$	$0.02 \pm 0.08$	$0.00 \pm 0.10$
Manganese	25	22	$450 \pm 33$	$0.07 \pm 0.05$	$-0.11 \pm 0.06$
Bromine	35	27	$874 \pm 54$	$0.05 \pm 0.06$	$-0.15 \pm 0.08$
Molybdenum	42	22	$610 \pm 60$	$0.09 \pm 0.05$	$-0.35 \pm 0.06$
Ruthenium	44	27	$1100 \pm 25$	$0.12 \pm 0.02$	$-0.29 \pm 0.03$
Rhodium	45	27	$1270 \pm 47$	$0.06 \pm 0.03$	$-0.14 \pm 0.03$
Palladium	46	27	$1350 \pm 29$	$0.26 \pm 0.02$	$-0.12 \pm 0.02$
Antimony	51	27	$2140 \pm 62$	$0.04 \pm 0.08$	$-0.25 \pm 0.11$
Lanthanum	57	27	$1940 \pm 70$	$0.12 \pm 0.10$	$-0.52 \pm 0.14$
Praseodymium	59	30	$1800 \pm 58$	$0.20 \pm 0.08$	$-0.40 \pm 0.09$
Platinum	78	27	$2600 \pm 52$	$0.17 \pm 0.02$	$-0.15 \pm 0.03$
Lead	82	22	$2274 \pm 59$	$0.08 \pm 0.08$	$-0.46 \pm 0.09$

\*The yield per mole per 100 r was normalized to a yield of 2274 for the lead sample at the same energy.



REF.			H. G. De Carvalho, V. Di Napoli, D. Margadonna, F. Salvetti and K. Tesch Nucl. Phys. <u>A126</u> , 505 (1969)			ELEM. SYM.	A	Z
						Rh	103	45
METHOD						REF. NO.		
						69 De 1		egf
REACTION	RESULT	EXCITATION ENERGY	SOURCE		DETECTOR		ANGLE	
			TYPE	RANGE	TYPE	RANGE		
G,N	ABY	THR-999	C	1-6	ACT-I		4PI	
				(1.0-5.5)				
G,2N	ABY	THR-999	C	2-6	ACT-I		4PI	
				(2.0-5.5)				

Yield per equivalent quantum.

999 = 5.5 GEV

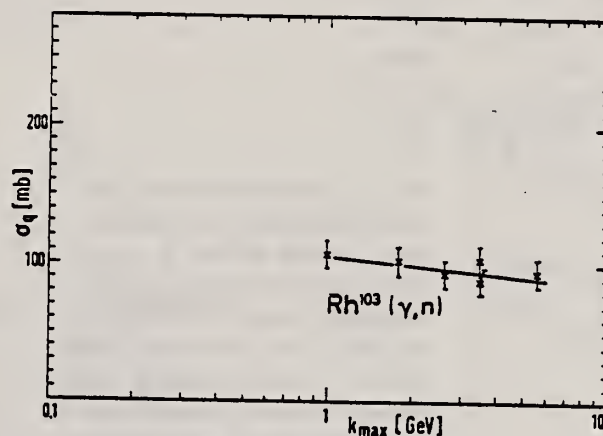


Fig. 2. See caption to fig. 1.

Cross sections per equivalent quantum for  $(\gamma, n)$  reactions as a function of the maximum bremsstrahlung energy. A straight line is adjusted to the experimental points by means of a least-squares fit. The indicated errors are due to the  $\gamma$ -ray spectroscopy. The dashed line gives the result of simple estimates.

In addition to the reactions mentioned above, we measured in the energy range 2-5.5 GeV, the following reactions:  $^{55}\text{Mn}(\gamma, n)$ ,  $^{55}\text{Mn}(\gamma, 3n)$ ,  $^{103}\text{Rh}(\gamma, 2n)$  and  $^{127}\text{I}(\gamma, 3n)$ . The resulting cross sections per equivalent quantum are 43 mb, 0.55 mb, 21 mb and 9.5 mb, respectively. Within the experimental error of 20 %, we found no variation of these cross sections with the maximum bremsstrahlung energy.

REACTION	RESULT	EXCITATION ENERGY	SOURCE		DETECTOR		ANGLE
			TYPE	RANGE	TYPE	RANGE	
G,N	ABY	9-900	C	400-900	ACT-I		4PI
G,2N	ABY	17-900	C	400-900	ACT-I		4PI
G,6p9n	ABY	THR-900	C	400-900	ACT-I		4PI

Yield = Cross section per equivalent quantum

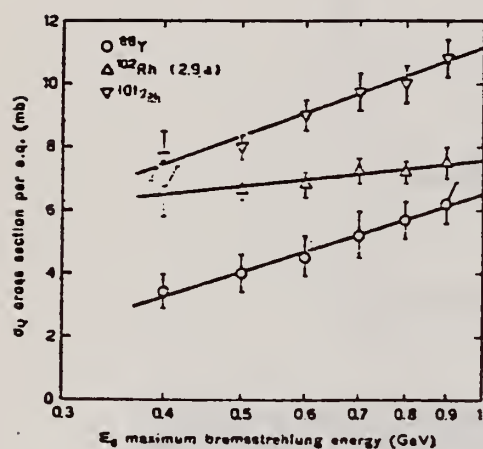


FIG. 7. - Behaviour of cross sections per equivalent quantum  $\sigma_q$ , as a function of  $\log_{10} E_0$  (maximum bremsstrahlung energy) for reactions  $^{102}\text{Rh}(\gamma, n)$ ,  $^{102}\text{Rh}(t, 2.9 y)$ ,  $^{102}\text{Rh}(\gamma, 2n)$ ,  $^{101}\text{Rh}$  and  $^{103}\text{Rh}(\gamma, 6p 9n)$ ,  $^{88}\text{Y}$ . The straight lines through the experimental points were obtained by using the least-squares method

TABLE III.

Bremsstrahlung energy $E_0$ (GeV)	$\sigma_q$ (mb)		
	$^{102}\text{Rh}(2.9 y)$	$^{101}\text{Rh}$	$^{88}\text{Y}$
0.4	$6.6 \pm 0.8$	$7.7 \pm 0.8$	$3.4 \pm 0.6$
0.5	$6.6 \pm 0.3$	$8.0 \pm 0.4$	$4.0 \pm 0.6$
0.6	$6.8 \pm 0.4$	$9.0 \pm 0.5$	$4.5 \pm 0.6$
0.7	$7.3 \pm 0.4$	$9.8 \pm 0.6$	$5.2 \pm 0.6$
0.8	$7.2 \pm 0.4$	$10.0 \pm 0.6$	$5.7 \pm 0.6$
0.9	$7.5 \pm 0.5$	$10.8 \pm 0.6$	$6.2 \pm 0.6$

L.E. Lazareva, A.I. Lepestkin, and V.I. Sidorov  
Yad. Fiz. 20, 242 (1974)  
Sov. J. Nucl. Phys. 20, 128 (1975)

ELEM. SYM.	A	Z
Rh	103	45

## METHOD

REF. NO.

74 La 5

hmg

REACTION	RESULT	EXCITATION ENERGY	SOURCE		DETECTOR		ANGLE
			TYPE	RANGE	TYPE	RANGE	
G, XN	SPC	8- 29	C	29	EMU-D		DST
				(28.5)			

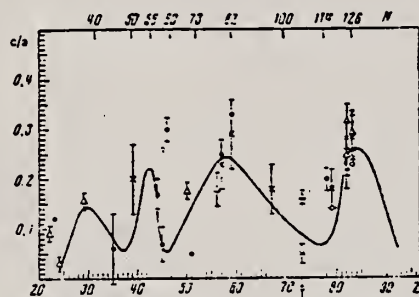


FIG. 2. Asymmetry coefficients  $c/a$  obtained for nuclei with various  $Z$  in the following studies: ref. 10 -  $E_{\gamma \text{ max}} = 25.5$  MeV,  $E_n > 7.4$  MeV (\*); ref. 11 -  $E_{\gamma \text{ max}} = 27-32$  MeV,  $E_n > 5$  MeV ( $\bullet$ ); ref. 12 -  $E_{\gamma \text{ max}} = 34$  MeV,  $E_n > 8$  MeV ( $\Delta$ ); ref. 13 -  $E_{\gamma \text{ max}} = 55$  MeV,  $E_n > 5$  MeV ( $\times$ ); present work -  $E_{\gamma \text{ max}} = 28.5$  MeV,  $E_n > 5$  MeV ( $\odot$ ). The smooth curve shows the coefficient  $b/a$  characterizing the photoneutron angular distribution anisotropy as a function of atomic number  $Z$ . (This has been converted from the curve given in ref. 11 and is for the distribution  $I(\theta) = a + b \sin^2 \theta + c \cos \theta$ , normalized at the points  $Z_0 = 82-83$ .)

<sup>11</sup> J.W. Jury, J.S. Hewitt, K.G. McNeill, Can. J. Phys. 46, 1823 (1968).

<sup>12</sup> F.R. Allum, T.W. Quirk, B.M. Spicer, Nucl. Phys. 53, 545 (1964).

<sup>13</sup> G.C. Reinhardt and W.D. Whitehead, Nucl. Phys. 30, 201 (1962).

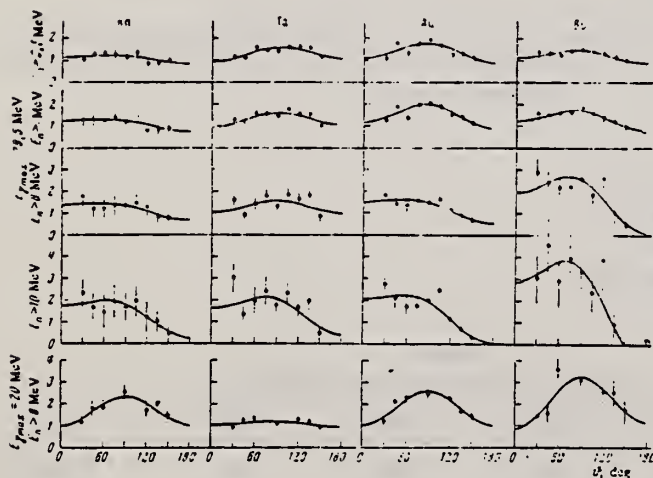


FIG. 1. Angular distributions of photoneutrons obtained in irradiation of Rh, Ta, Au, and Bi samples by bremsstrahlung with maximum energy  $E_{\gamma \text{ max}} = 28.5$  MeV. The curves were calculated from the experimental points by the method of least squares for a distribution of the form  $I(\theta) = a + b \sin^2 \theta + c \cos \theta$  and normalized ( $a = 1$ ). For comparison we have shown below the angular distributions of photoneutrons with energy  $E_n > 8$  MeV obtained in irradiation of the same samples by bremsstrahlung with  $E_{\gamma \text{ max}} = 20$  MeV.

(over)

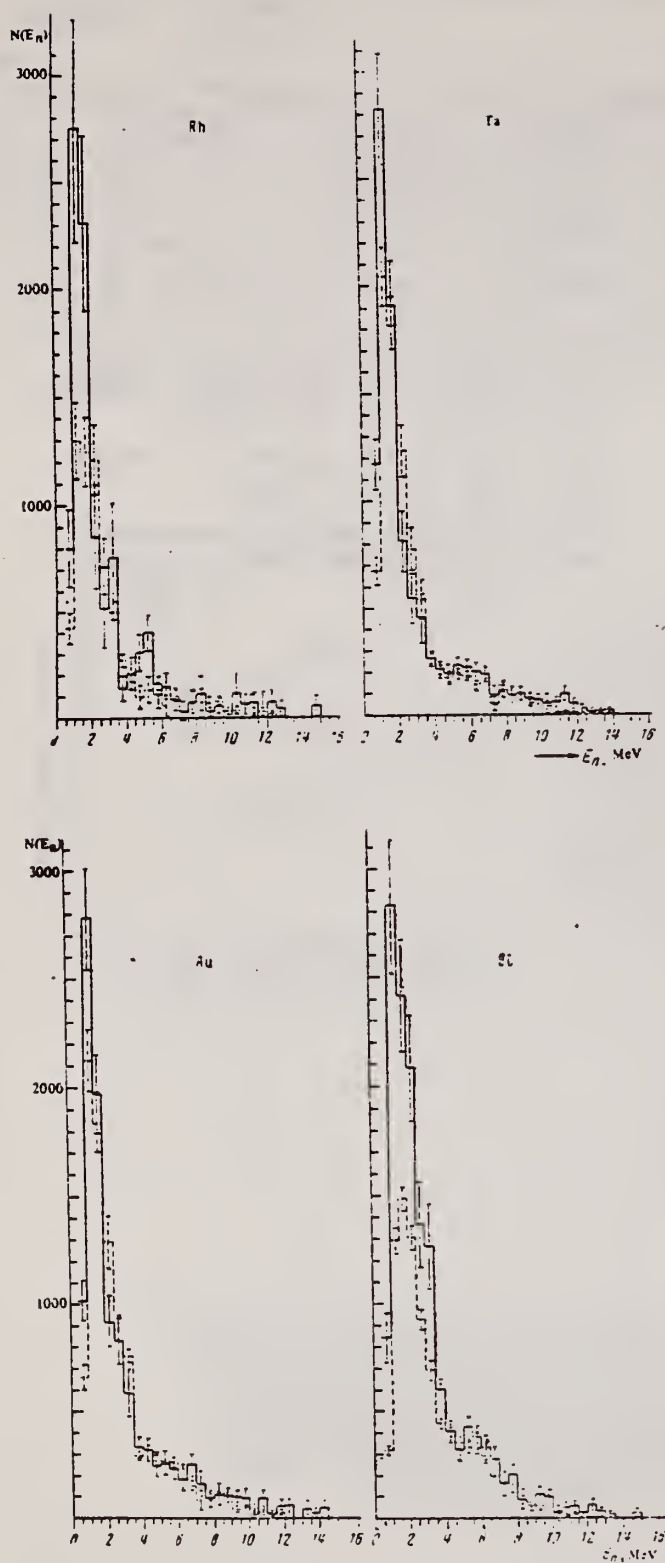
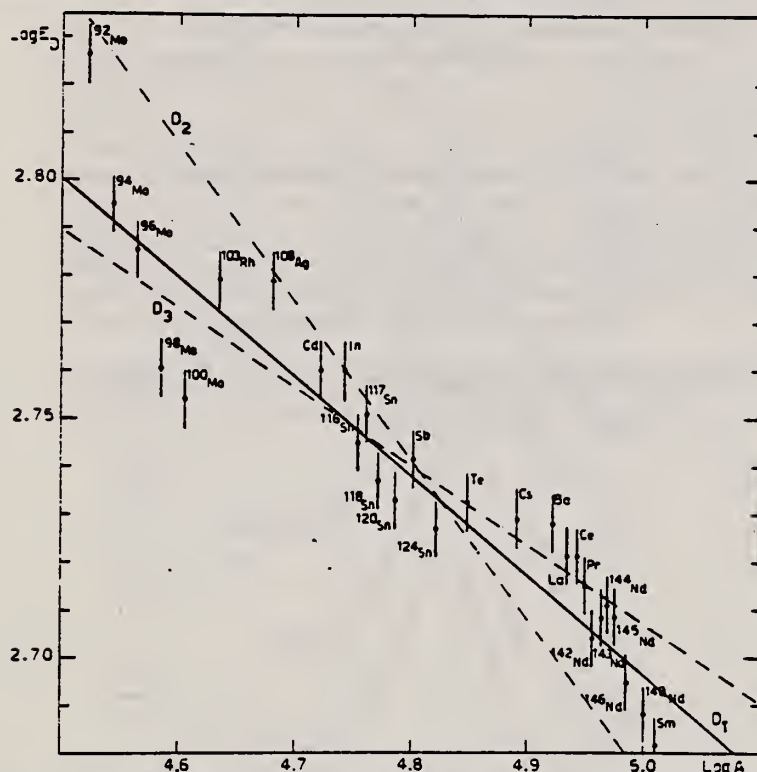


FIG. 3. Photoneutron energy spectra from Rh, Ta, Au, and Bi for  $\gamma$ -radiation of the samples by bremsstrahlung with maximum energy  $E_{\gamma \text{ max}} = 20$  (dashed line) and 28.5 (solid line) MeV for angles  $\theta$  with maximum neutron yield. For each nucleus the histograms given for  $E_{\gamma \text{ max}} = 20$  and 28.5 MeV have been combined in the interval  $E_n = 4 - 4.5$  MeV.



ELEM. SYM.	A	Z
Rh	103	45
REF. NO.		
74 Le 1		egf

REACTION	RESULT	EXCITATION ENERGY	SOURCE		DETECTOR		ANGLE
			TYPE	RANGE	TYPE	RANGE	
G,N	ABX	9- 24	D	9- 24	MOD-I		4PI
G,2N	ABX	16- 24	D	9- 24	MOD-I		4PI



617+  
618+

Fig. 13. Experimental results of the average energy  $E_D$  of the GDR versus the mass number  $A$  with the best fit  $E_D = 41.8 A^{-1/4.8}$  (line  $D_1$ ). Two fits with  $A^{-1/2}$  and  $A^{-1/3}$  laws are also shown as lines  $D_2$  and  $D_3$  respectively.

TABLE 7  
Lorentz line parameters for a two-Lorentz-line fit of the GDR of rhodium

$\sigma_1$ (mb)	$E_1$ (MeV)	$\Gamma_1$ (MeV)	$\sigma_2$ (mb)	$E_2$ (MeV)	$\Gamma_2$ (MeV)
88	15	$4.94 \pm 0.1$	126	17.05	$6.90 \pm 0.1$

Errors are the same as in table 4.

TABLE 6  
Lorentz line parameters for a single Lorentz line fit

	$^{103}_{45}\text{Rh}$	$^{106}_{46}\text{Pd}$	$^{107}_{47}\text{Ag}$	$^{108}_{48}\text{Cd}$	$^{115}_{49}\text{In}$
$\sigma_0$ (mb)	191	199	198	226	243
$\Gamma_0$ (MeV)	$7.4 \pm 0.1$	$7.1 \pm 0.1$	$7.7 \pm 0.1$	$6.3 \pm 0.1$	$6.1 \pm 0.1$
$E_0$ (MeV)	16.15	15.9	16.1	15.8	15.8

Errors are the same as in table 4.



$^{103}\text{Rh}$	Pd	Ag	Cd	$^{115}\text{In}$	$^{116}\text{Sn}$	$^{117}\text{Sn}$	$^{118}\text{Sn}$	$^{120}\text{Sn}$	$^{124}\text{Sn}$	Sb	Te	$^{133}\text{Cs}$
$E_M$ (MeV)	21.3	29.7	26.5	29.7	29.7	21.6	23	29.7	23	29.7	26	24.1
$\sigma_0$ (MeV · b)	1.75	1.90	1.75	2.1	1.86	1.57	1.69	2.14	1.62	2.1	2.05	2.15
$\sigma_0$ (0.06 NZ/A) (MeV · b)	1.53	1.59	1.65	1.69	1.71	1.72	1.73	1.75	1.79	1.78	1.85	1.93
$\sigma'_0$ (0.06 NZ/A)	1.45	1.50	1.35	1.39	1.29	1.25	1.25	1.34	1.17	1.39	1.37	1.38
$\sigma_{-1}$ (mb)	96	88.2	107	121	113	102	107	128	104	125	125	136.9
$\sigma_{-2}$ (mb · MeV $^{-1}$ )	6.2	6.6	6.8	7.4	7.15	6.80	7.0	8.1	6.9	7.9	7.9	9.05
$\sigma_{-1/41}$	0.212	0.215	0.200	0.220	0.203	0.181	0.188	0.220	0.171	0.210	0.198	0.205
$\sigma_{-3/41}$	$2.83 \times 10^{-3}$	$2.78 \times 10^{-3}$	$2.68 \times 10^{-3}$	$2.81 \times 10^{-3}$	$2.67 \times 10^{-3}$	$2.51 \times 10^{-3}$	$2.55 \times 10^{-3}$	$2.86 \times 10^{-3}$	$2.31 \times 10^{-3}$	$2.72 \times 10^{-3}$	$2.52 \times 10^{-3}$	$2.70 \times 10^{-3}$

The average errors  $\Delta\sigma_0$  and  $\Delta\sigma'_0$  are  $\pm 0.1$  MeV · mb.

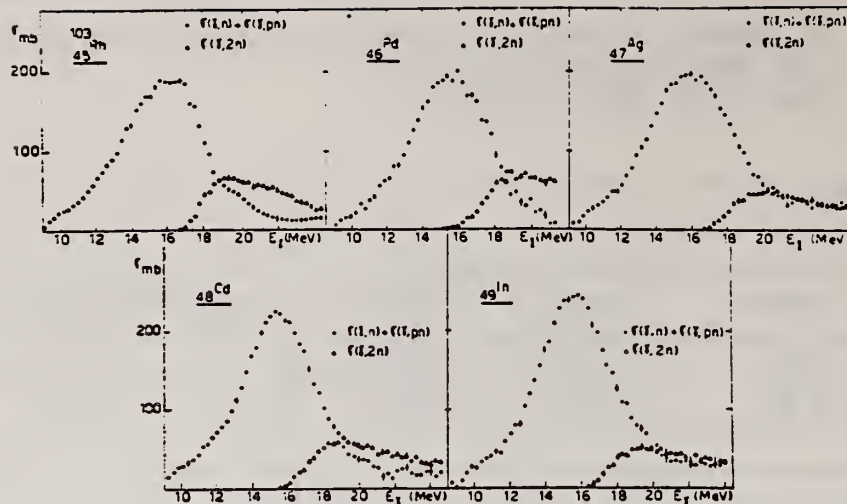


Fig. 7. Partial photoneutron cross sections [ $\sigma(\gamma, n) + \sigma(\gamma, np)$ ] and  $\sigma(\gamma, 2n)$  for  $_{45}\text{Rh}$ ,  $_{46}\text{Pd}$ ,  $_{47}\text{Ag}$ ,  $_{48}\text{Cd}$  and  $_{49}\text{In}$ .

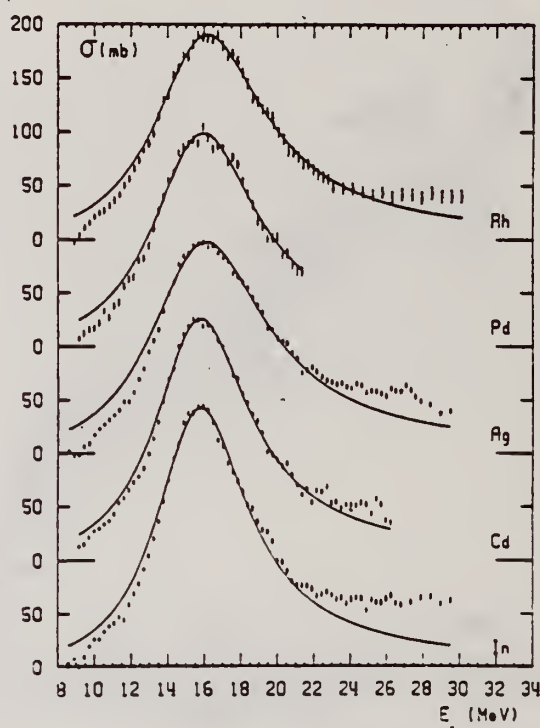


Fig. 8. Best single Lorentz line fit to  $\sigma_{\text{tot}}(\gamma, \text{tot}) = \sigma(\gamma, n) + \sigma(\gamma, np) + \sigma(\gamma, 2n)$  for  $_{45}\text{Rh}$ ,  $_{46}\text{Pd}$ ,  $_{47}\text{Ag}$ ,  $_{48}\text{Cd}$  and  $_{49}\text{In}$ .

REF. Y. Cauchois, H. Ben Abdelaziz, R. Khérouf, C. Schloesing-Möller  
J. Phys. G7, 1539 (1981)

ELEM. SYM.	A	Z
Rh	103	45
REF. NO.		
81 Ca 2		hg

METHOD

REACTION	RESULT	EXCITATION ENERGY	SOURCE		DETECTOR		ANGLE
			TYPE	RANGE	TYPE	RANGE	
G.G	LET	0.2 (.803, 1.277)	C	0 - 2	SCD-D		

.803, 1.277 MEV

**Abstract.** Lifetimes of 49 excited states below 1.65 MeV have been measured in <sup>24</sup>Mg, <sup>27</sup>Al, <sup>48</sup>Ti, <sup>58</sup>Ni, <sup>59</sup>Co, <sup>61,62</sup>Ni, <sup>63,65</sup>Cu, <sup>64,66,68</sup>Zn, <sup>75</sup>As, <sup>103</sup>Rh, <sup>113,115</sup>In, <sup>116,118,120</sup>Sn and <sup>121,123</sup>Sb by means of nuclear resonance fluorescence experiments. The levels are excited by bremsstrahlung x-ray photons. The self-absorption technique applied to suitable cases provides nuclear absorption cross sections, widths and lifetimes from which the x-ray spectral distributions are also obtained. Scattering experiments are performed for all other cases in order to obtain widths and lifetimes from these x-ray photon curves. The Compton effect in the sample is taken into account. Self-absorption provides  $g\Gamma_0$  from which  $\Gamma$  is deduced using adopted  $J^\pi$  and  $\Gamma_0/\Gamma$  values; scattering provides  $u = g(\Gamma_0^2/\Gamma)W(\theta)$  from which  $\Gamma$  is also deduced with  $J$ ,  $\Gamma_0/\Gamma$  and mixing ratios taken from the literature. Thanks to simultaneous determination of the x-ray spectra all the lifetimes as given by our programs with their statistical errors form an unusually coherent set of values.

NUCLEAR REACTIONS ( $\gamma, \gamma'$ ), bremsstrahlung excitation; natural isotopes: <sup>24</sup>Mg, <sup>27</sup>Al, <sup>48</sup>Ti, <sup>58</sup>Ni, <sup>59</sup>Co, <sup>61,62</sup>Ni, <sup>63,65</sup>Cu, <sup>64,66,68</sup>Zn, <sup>75</sup>As, <sup>103</sup>Rh, <sup>113,115</sup>In, <sup>116,118,120</sup>Sn and <sup>121,123</sup>Sb;  $E \approx 0.5-1.65$  MeV; measured  $g\Gamma_0$  or  $g(\Gamma_0^2/\Gamma)W(\theta)$ ; deduced  $T_{1/2}$ .

(OVER)

Tableau 3. Résultats des mesures des niveaux étudiés par diffusion.

Table 3. Results obtained using the diffusion method.

Isotope	Energie (keV)	$J^\pi$	$J^\pi_0$	$\Gamma_0/\Gamma$	$\delta$	$u = g(\Gamma_0^2/\Gamma)W(\theta)$ (meV)	$\tau$ (ps) ce travail	$\tau_{ref}$ (ps)	Références†
<sup>24</sup> Mg	1368,59(4)	2 <sup>+</sup>	0 <sup>+</sup>	1	E2	1,08(13)	1,76(21)	1,98(4)	Endt et van der Leun (1978)
<sup>27</sup> Al	1014,45(3)	$\frac{1}{2}^-$	$\frac{1}{2}^-$	0,971	+0,351(12)	0,186(13)	2,20(16)	2,12(8)	Endt et van der Leun (1978)
<sup>48</sup> Ti	983,512(3)	2 <sup>+</sup>	0 <sup>+</sup>	1	E2	0,282(23)	6,74(55)	6,1(13)	Been (1978)
<sup>58</sup> Ni	1454,45(15)	2 <sup>+</sup>	0 <sup>+</sup>	1	E2	2,11(26)	0,90(11)	0,92(3)	Kocher et Auble (1976)
<sup>59</sup> Co	1099,224(25)	$\frac{1}{2}^-$	$\frac{1}{2}^-$	1	(E2)	0,069(8)	4,79(55)	3,17(58)	Kim (1976)
<sup>59</sup> Co	1458,8(3)	$\frac{1}{2}^-$	$\frac{1}{2}^-$	0,91	(E2)	0,68(8)	1,17(14)	1,52(16)	Kim (1976)
<sup>59</sup> Co	1480,9(3)	$\frac{1}{2}^-$	$\frac{1}{2}^-$	0,8	<0,35 <sup>a</sup>	1,23(15)	0,254(31)	0,31(3)	Kim (1976)
<sup>61</sup> Ni	1185,7(6)	$\frac{1}{2}^-$	$\frac{1}{2}^-$	0,77(8) <sup>i</sup>	0,14 <sup>i</sup>	1,88(49)	0,21(5)	0,16(3)	Andreev <i>et al</i> (1974)
<sup>62</sup> Ni	1172,91(9)	2 <sup>+</sup>	0 <sup>+</sup>	1	E2	0,88(17)	2,15(42)	2,09(3)	Halbert (1979a)
<sup>63</sup> Cu	1327,00(7)	$\frac{1}{2}^-$	$\frac{1}{2}^-$	0,84	(E2)	1,04(14)	0,84(11)	0,88(4)	Auble (1979b)
<sup>63</sup> Cu	1412,05(4)	$\frac{1}{2}^-$	$\frac{1}{2}^-$	0,72	+0,61( $\frac{1}{2}$ – $\frac{3}{2}$ )	0,260(38)	1,90(28)	1,61(3)	Auble (1979b)
<sup>64</sup> Zn	991,54(7)	2 <sup>+</sup>	0 <sup>+</sup>	1	E2	0,640(54)	2,97(25)	2,60(13)	Halbert (1979b)
<sup>65</sup> Cu	1481,83(5)	$\frac{1}{2}^-$	$\frac{1}{2}^-$	0,85	(E2)	1,13(19)	0,79(13)	0,49(5)	Auble (1975a)
<sup>66</sup> Zn	1039,37(6)	2 <sup>+</sup>	0 <sup>+</sup>	1	E2	0,70(6)	2,71(23)	2,25(15)	Auble (1975b)
<sup>66</sup> Zn	1077,38(5)	2 <sup>+</sup>	0 <sup>+</sup>	1	E2	0,70(6)	2,71(23)	2,34(23)	Lewis (1975)
<sup>75</sup> As	572,5(10)	$\frac{1}{2}^-$	$\frac{1}{2}^-$	1 <sup>d</sup>	0,39 <sup>b</sup>	0,236(26)	4,14(46)	3,5(9)	Horen et Lewis (1975)
<sup>75</sup> As	823,0(10)	$\frac{1}{2}^-$	$\frac{1}{2}^-$	0,86 <sup>d</sup>	(E2)	0,214(22)	4,27(43)	3,5(3)	Robinson <i>et al</i> (1967)
<sup>75</sup> As	865,5(10)	$\frac{1}{2}^-$	$\frac{1}{2}^-$	0,83 <sup>d</sup>	— <sup>c</sup>	0,78(6)	0,863(68)	0,60(12)	Celliers <i>et al</i> (1977)
<sup>75</sup> As	1076,0(10)	$\frac{1}{2}^-$	$\frac{1}{2}^-$	0,94 <sup>d</sup>	0,38 <sup>d</sup>	1,97(13)	0,287(19)	0,32(7)	Celliers <i>et al</i> (1977)
<sup>75</sup> As	1128,5(10)	$\frac{1}{2}^-$	$\frac{1}{2}^-$	1	E1 <sup>d</sup>	0,224(24)	1,47(16)	—	
<sup>75</sup> As	1349,0(10)	$\frac{1}{2}^-$	$\frac{1}{2}^-$	0,67 <sup>d</sup>	0,20 <sup>d</sup>	1,61(29)	0,180(32)	0,12(3)	Wilson (1970)
<sup>75</sup> As	1370,0(10)	$\frac{1}{2}^-$	$\frac{1}{2}^-$	0,47 <sup>d</sup>	0,47 <sup>d</sup>	0,64(13)	0,218(44)	—	
<sup>103</sup> Rh	803,1(2)	$\frac{1}{2}^-$	$\frac{1}{2}^-$	0,70	M1	1,85(16)	0,174(15)	—	Harmatz (1979)
<sup>103</sup> Rh	1277,0(2)	$\frac{1}{2}^-$	$\frac{1}{2}^-$	0,75	–0,62(30) <sup>e</sup>	0,81(9)	0,87(10)	1,3(9)	Harmatz (1979)
<sup>113</sup> In	1177(1)	$\frac{1}{2}^-$	$\frac{1}{2}^-$	1	+0,5(2)	9,1(8)	0,086(8)	0,10(6)	Tuttle <i>et al</i> (1976)
<sup>113</sup> In	1510(1)	$\frac{1}{2}^-$	$\frac{1}{2}^-$	0,935	–0,5( $\frac{1}{2}$ – $\frac{3}{2}$ )	6,4(9)	0,071(10)	0,11( $\frac{1}{2}$ – $\frac{3}{2}$ )	Tuttle <i>et al</i> (1976)
<sup>113</sup> In	1077,7(10)	$\frac{1}{2}^-$	$\frac{1}{2}^-$	0,81 <sup>j</sup>	(E2)	0,159(24)	1,61(24)	1,23(7)	Tuttle <i>et al</i> (1976)
<sup>113</sup> In	1290,59(3)	$\frac{1}{2}^-$	$\frac{1}{2}^-$	0,98 <sup>j</sup>	(E2)	1,31(11)	0,66(6)	0,55(4)	Tuttle <i>et al</i> (1976)
<sup>113</sup> In	1448,78(3)	$\frac{1}{2}^-$	$\frac{1}{2}^-$	0,86	–8 <sup>f</sup>	0,90(11)	0,50(6)	0,52(20)	Tuttle <i>et al</i> (1976)
<sup>113</sup> In	1486,1(1)	$\frac{1}{2}^-$	$\frac{1}{2}^-$	0,787	–0,8 <sup>f</sup>	0,63(9)	0,63(9)	0,4(3)	Tuttle <i>et al</i> (1976)
<sup>113</sup> In	1497,2(4)	( $\frac{1}{2}^-$ )	( $\frac{1}{2}^-$ )	<1	(E2)	1,33(16)	<0,30(4)	—	
<sup>113</sup> In	1607,8(15)	( $\frac{1}{2}^-$ )	( $\frac{1}{2}^-$ )	≤1	(E2)	1,54(24)	≤0,26(4)	—	
<sup>116</sup> Sn	1293,54(2)	2 <sup>+</sup>	0 <sup>+</sup>	1	E2	3,58(37)	0,53(6)	0,522(14)	Carlson <i>et al</i> (1975)
<sup>116</sup> Sn	1229,64(4)	2 <sup>+</sup>	0 <sup>+</sup>	1	E2	2,75(28)	0,69(7)	0,67(2)	Carlson <i>et al</i> (1976)
<sup>120</sup> Sn	1171,6(2)	2 <sup>+</sup>	0 <sup>+</sup>	1	E2	1,83(16)	1,04(9)	0,91(2)	Kocher (1976)
<sup>121</sup> Sb	1023,5(10)	$\frac{1}{2}^-$	$\frac{1}{2}^-$	1	0,57  <sup>g</sup>	3,69(34)	0,228(21)	0,20(7) <sup>h</sup>	Tamura <i>et al</i> (1979)
<sup>121</sup> Sb	1105,5(10)	$\frac{1}{2}^-$	$\frac{1}{2}^-$	0,4	—	0,47(4)	0,42(4)	—	
<sup>121</sup> Sb	1142,5(10)	$\frac{1}{2}^-$	$\frac{1}{2}^-$	0,6	(E2)	0,85(8)	0,449(40)	0,41(8) <sup>h</sup>	Booth <i>et al</i> (1973)
<sup>121</sup> Sb	1384,0(10)	$\frac{1}{2}^-$	$\frac{1}{2}^-$	1	0,45  <sup>g</sup>	4,7(5)	0,092(10)	0,088(14) <sup>h</sup>	Booth <i>et al</i> (1973)
<sup>123</sup> Sb	1029,5(10)	$\frac{1}{2}^-$	$\frac{1}{2}^-$	1	0,57  <sup>g</sup>	2,96(27)	0,272(25)	0,26(4) <sup>h</sup>	Booth <i>et al</i> (1973)
<sup>123</sup> Sb	1086,5(10)	$\frac{1}{2}^-$	$\frac{1}{2}^-$	1	$\delta$   > 1,26 <sup>a</sup>	1,06(9)	0,67(6)	0,72(15) <sup>h</sup>	Booth <i>et al</i> (1973)

† Références pour les colonnes 3, 4, 5, 6 et 9 de chaque ligne, sauf indication appelée au bas de ce tableau. Pour les autres données se reporter au texte.

Remarque. Pour calculer  $\delta^2$  quand nous ne disposons que de  $B(E2)$ , pour un mélange (E2) + (M1), nous déduisons  $g\Gamma_0(E2) \propto B(E2)E_2^2$ ; en admettant  $W(\theta) = 1$  et connaissant  $\Gamma_0/\Gamma$ , notre détermination de  $u$  donne une première approximation de  $g\Gamma_0$  d'où une valeur de  $\delta^2 = (g\Gamma_0(E2))/(g\Gamma_0 - g\Gamma_0(E2))$  qui permet d'améliorer  $W(\theta)$  et  $g\Gamma_0$  de proche en proche.

<sup>a</sup> Swann (1971); <sup>b</sup> Robinson *et al* (1967); <sup>c</sup>  $W(\theta) = 0,99$  calculé d'après la formule de Celliers *et al* (1977); <sup>d</sup> Abbondanno *et al* (1978); <sup>e</sup> Sayer *et al* (1972); <sup>f</sup> Tuttle *et al* (1976); <sup>g</sup> d'après  $B(E2)$  de Barnes *et al* (1966); <sup>h</sup> calculé d'après Booth *et al* (1973); <sup>i</sup> Williams *et al* (1975); <sup>j</sup> Dietrich *et al* (1970).

## PALLADIUM

Z=46

William Wollaston first isolated palladium from crude platinum; in 1803 he announced the discovery by circulating an anonymous advertisement of the new metal for sale. Because of this unorthodox announcement, it was widely thought that the new metal was not an element but an alloy of platinum and mercury. A year later, however, Wollaston explained his source of the palladium along with an announcement of his discovery of yet another new element, rhodium.





REF.			ELEM. STM.		A	L	
P. Kneisel, A. Goldmann and H. v. Buttler Z. Physik <u>199</u> , 440 (1967)			Pd		46		
METHOD			REF. NO.				
Linac			67 Kn 1		JDM		
REACTION	RESULT	EXCITATION ENERGY	SOURCE		DETECTOR		ANGLE
			TYPE	RANGE	TYPE	RANGE	
G,T	RLY	THR-49	C	36,49	ACT-I		4PI

Tabelle. Zusammenstellung der Meßergebnisse

	$E_m = 36,2 \text{ MeV}$	$E_m = 49,2 \text{ MeV}$
$Y[\text{Ni}(\gamma, t)]/Y[\text{C}(\gamma, n)\text{C}^{11}]$	$(2,2 \pm 0,2) 10^{-3}$	$(4,6 \pm 0,4) 10^{-3}$
$Y[\text{Pd}(\gamma, t)]/Y[\text{C}(\gamma, n)\text{C}^{11}]$	—	$(6,1 \pm 1,0) 10^{-3}$
$\sigma_\gamma[\text{Ni}(\gamma, t)]$	$(4,0 \pm 0,4) \mu\text{barn}$	$(10,5 \pm 1,0) \mu\text{barn}$
$\sigma_\gamma[\text{Pd}(\gamma, t)]$	—	$(13,8 \pm 2,3) \mu\text{barn}$

REF. J. W. Jury, J. S. Hewitt, and K. G. McNeill  
Can. J. Phys. 46, 1823 (1968)

ELEM. SYM.	A	Z
Pd		46
REF. NO.		EGF
68 Ju 1		

METHOD			SOURCE		DETECTOR		ANGLE
REACTION	RESULT	EXCITATION ENERGY	TYPE	RANGE	TYPE	RANGE	
G,N	NOX	THR-27	C	27	THR	5-	DST

$$W(\theta) = a_0 + a_1 P_1 + a_2 P_2$$

TABLE I

Target element	Z	Energy	$a_0^*$	$a_1/a_0$	$a_2/a_0$
Vanadium	23	32	$640 \pm 50$	$0.11 \pm 0.10$	$-0.09 \pm 0.11$
Chromium	24	22	$565 \pm 39$	$0.02 \pm 0.08$	$0.00 \pm 0.10$
Manganese	25	22	$450 \pm 33$	$0.07 \pm 0.05$	$-0.11 \pm 0.06$
Bromine	35	27	$874 \pm 54$	$0.65 \pm 0.06$	$-0.15 \pm 0.08$
Molybdenum	42	22	$610 \pm 60$	$0.09 \pm 0.05$	$-0.55 \pm 0.06$
Ruthenium	44	27	$1100 \pm 25$	$0.12 \pm 0.02$	$-0.29 \pm 0.03$
Rhodium	45	27	$1270 \pm 47$	$0.06 \pm 0.03$	$-0.14 \pm 0.03$
Palladium	46	27	$1350 \pm 29$	$0.26 \pm 0.02$	$-0.12 \pm 0.02$
Antimony	51	27	$2140 \pm 62$	$0.04 \pm 0.08$	$-0.25 \pm 0.11$
Lanthanum	57	27	$1940 \pm 70$	$0.12 \pm 0.10$	$-0.52 \pm 0.14$
Praseodymium	59	30	$1800 \pm 58$	$0.20 \pm 0.08$	$-0.40 \pm 0.09$
Platinum	78	27	$2600 \pm 52$	$0.17 \pm 0.02$	$-0.15 \pm 0.03$
Lead	82	22	$2274 \pm 59$	$0.08 \pm 0.08$	$-0.46 \pm 0.09$

\*The yield per mole per 100 r was normalized to a yield of 2274 for the lead sample at the same energy.

REF. A. Lepretre, H. Beil, R. Bergere, P. Carlos, A. De Miniac,  
A. Veyssiere, and K. Kernbach  
Nucl. Phys. A219, 39 (1974)

ELEM. SYM.	A	Z
Pd		46
REF. NO.	74 Le 1	
	ezf	

METHOD			REF. NO.		
			74 Le 1		ezf
REACTION	RESULT	EXCITATION ENERGY	SOURCE		ANGLE
			TYPE	RANGE	
G,N	ABX	9- 22	D	9- 22	4PI
G,2N	ABX	15- 22	D	9- 22	4PI

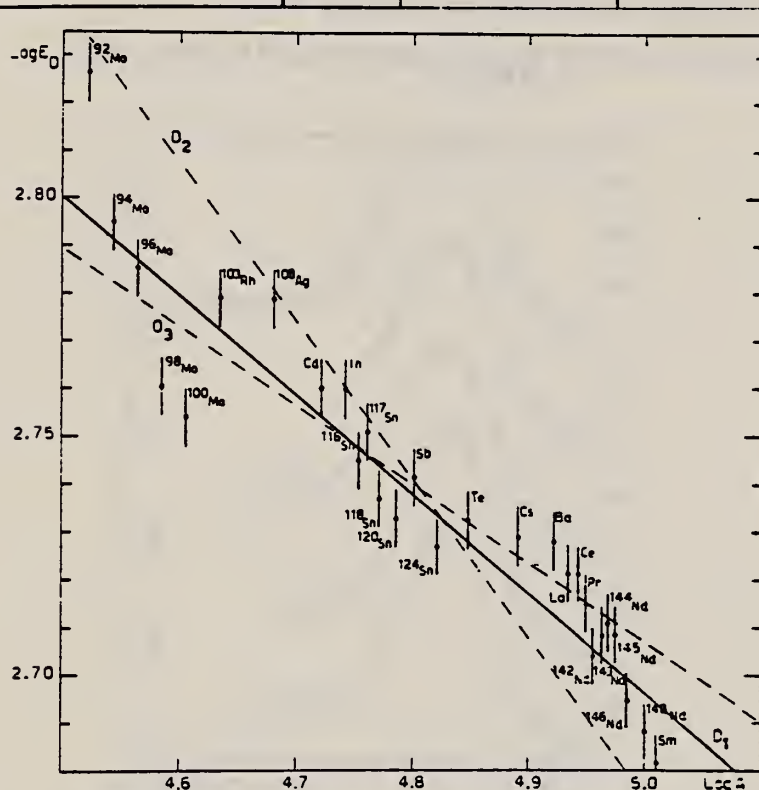


Fig. 13. Experimental results of the average energy  $E_D$  of the GDR versus the mass number  $A$  with the best fit  $E_D = 41.8 A^{-1/4.8}$  (line  $D_1$ ). Two fits with  $A^{-1/4}$  and  $A^{-1/5}$  laws are also shown as lines  $D_2$  and  $D_3$  respectively.

TABLE 6  
Lorentz line parameters for a single Lorentz line fit

	$^{103}_{43}\text{Rh}$	$^{46}_{46}\text{Pd}$	$^{47}_{47}\text{Ag}$	$^{48}_{48}\text{Cd}$	$^{115}_{49}\text{In}$
$\sigma_0$ (mb)	191	199	198	226	243
$\Gamma_0$ (MeV)	$7.4 \pm 0.1$	$7.1 \pm 0.1$	$7.7 \pm 0.1$	$6.3 \pm 0.1$	$6.1 \pm 0.1$
$E_0$ (MeV)	16.15	15.9	16.1	15.8	15.8

Errors are the same as in table 4.

(over)

TABLE II  
Integrated cross sections as defined in the text

	<sup>103</sup> Rh	Pd	Ag	Cd	<sup>113</sup> In	<sup>116</sup> Sn	<sup>117</sup> Sn	<sup>118</sup> Sn	<sup>119</sup> Sn	<sup>120</sup> Sn	<sup>124</sup> Sn	Sb	Te	<sup>123</sup> Cs
$E_n$ (MeV)	30	21.3	29.7	26.5	29.7	29.7	21.6	23	29.7	29.7	23	29.7	26	24.1
$\sigma_0$ (MeV · b)	1.75	1.38	1.90	1.75	2.1	1.86	1.57	1.69	2.14	2.14	1.62	2.1	2.05	2.15
$0.06 NZ/A$ (MeV · b)	1.53	1.567	1.59	1.65	1.69	1.71	1.72	1.73	1.75	1.75	1.79	1.78	1.85	1.93
$\sigma'_0/(0.06 NZ/A)$	1.45	1.41	1.50	1.35	1.39	1.29	1.25	1.25	1.34	1.34	1.17	1.39	1.37	1.38
$\sigma_{-1}$ (mb)	96	88.2	109	107	121	113	102	107	128	128	104	125	125	136.9
$\sigma_{-1}$ (mb · MeV <sup>-1</sup> )	6.2	5.8	6.6	6.8	7.4	7.15	6.80	7.0	8.1	8.1	6.9	7.9	7.9	9.05
$\sigma_{-1}/A$	0.212	0.175	0.215	0.200	0.220	0.203	0.181	0.188	0.220	0.220	0.171	0.210	0.198	0.205
$\sigma_{-1}/A$	$2.83 \times 10^{-3}$	$2.44 \times 10^{-3}$	$2.78 \times 10^{-3}$	$2.68 \times 10^{-3}$	$2.81 \times 10^{-3}$	$2.67 \times 10^{-3}$	$2.51 \times 10^{-3}$	$2.55 \times 10^{-3}$	$2.86 \times 10^{-3}$	$2.86 \times 10^{-3}$	$2.31 \times 10^{-3}$	$2.72 \times 10^{-3}$	$2.52 \times 10^{-3}$	$2.70 \times 10^{-3}$

The average errors  $\Delta\sigma_0$  and  $\Delta\sigma'_0$  are  $\pm 0.1$  MeV · mb.

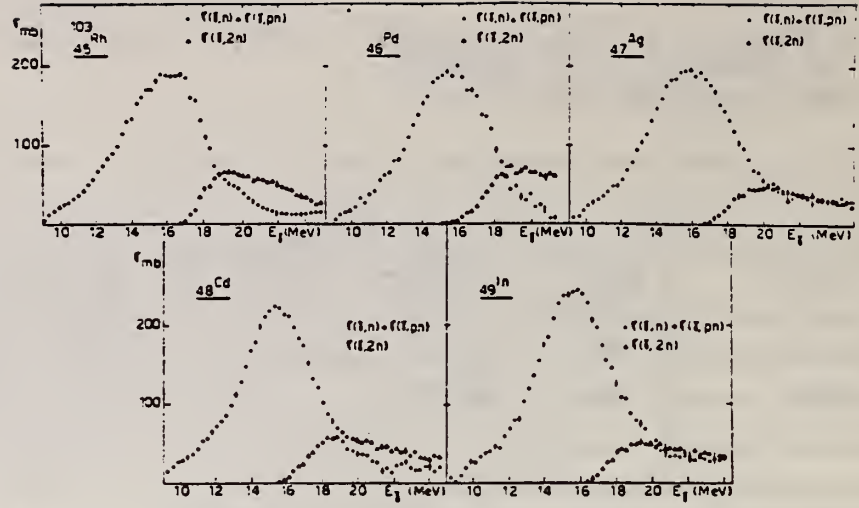


Fig. 7. Partial photoneutron cross sections [ $\sigma(\gamma, n) + \sigma(\gamma, np)$ ] and  $\sigma(\gamma, 2n)$  for <sup>45</sup>Rh, <sup>46</sup>Pd, <sup>47</sup>Ag, <sup>48</sup>Cd and <sup>49</sup>In.

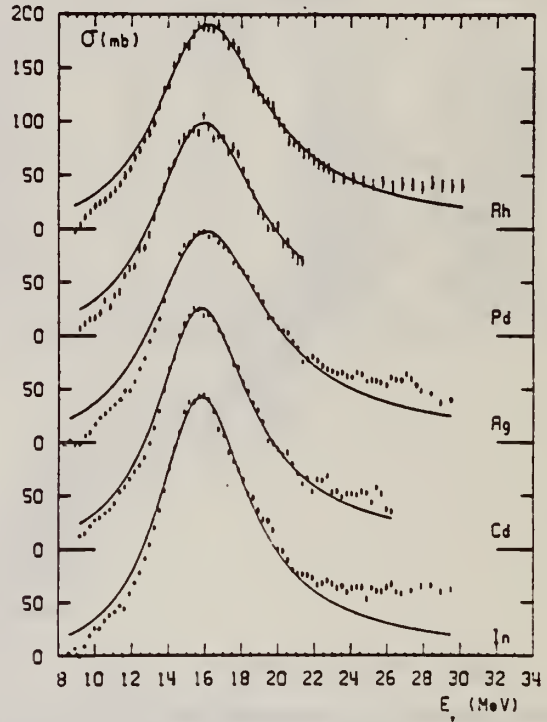


Fig. 8. Best single Lorentz line fit to  $\sigma_{tot}(\gamma, tot) = \sigma(\gamma, n) + \sigma(\gamma, np) + \sigma(\gamma, 2n)$  for <sup>45</sup>Rh, <sup>46</sup>Pd, <sup>47</sup>Ag, <sup>48</sup>Cd and <sup>49</sup>In.

Pd  
A=104

Pd  
A=104

Pd  
A=104





METHOD

REF. NO.

68 Ok 3

egf

REACTION	RESULT	EXCITATION ENERGY	SOURCE		DETECTOR		ANGLE
			TYPE	RANGE	TYPE	RANGE	
G, NP	ABY	THR-20	C	20	ACT-I		4PI

TABLE 2. THE YIELDS OF SOME ( $\gamma$ , pn) REACTIONS  
WITH 20 MeV BREMSSTRAHLUNG

Reaction	Half-life of product	Specific activity <sup>a)</sup> ( $\mu$ Ci/mg)	Yield ( $\text{mol}^{-1} \cdot \text{R}^{-1}$ )
$^{54}\text{Fe}(\gamma, \text{pn})^{54}\text{Mn}$	314 d	$2.5 \times 10^{-4}$	$3.6 \times 10^2$
$^{64}\text{Zn}(\gamma, \text{pn})^{64}\text{Cu}$	13 hr	$7.2 \times 10^{-3}$	$7.5 \times 10^3$
$^{104}\text{Pd}(\gamma, \text{pn})^{103}\text{Rh}$	210 d	$1.1 \times 10^{-4}$	$1.7 \times 10^3$

a) The value corrected at the end of 1 hr irradiation ( $9.4 \times 10^6$  R/min).



Pd  
A=105

Pd  
A=105

Pd  
A=105





Ref. F.R. Metzger  
Phys. Rev. 128, 2332 (1962)

Elem. Sym.	A	Z
Pd	105	46

Method Rh <sup>105</sup> source on ultra centrifuge rotor to compensate for Doppler shift; NaI.	Ref. No. 62 Me 1	JHH
--	---------------------	-----

Reaction	E or ΔE	E <sub>0</sub>	Γ	∫σdE	Jπ	Notes
Pd <sup>105</sup> (γ,γ)	319 keV	319 keV			7/2 <sup>+</sup>	<p>Spins 1/2 and 3/2 eliminated; spin 5/2 possible, but less probable than 7/2.</p> <p>E2/M1 mixing amplitude (I = 7/2) is S = -0.11.</p> <p>Gamma transition probability (I = 7/2) is <math>\tau_{\gamma} = (1.37 \pm 0.07) 10^{10} \text{ sec}^{-1}</math>.</p> <p><math>w(\theta) = 1 + (0.25 \pm 0.05) P_2(\cos \theta)</math>.</p>

REF.

Yu. K. Shubnyi, Yu. A. Lysikov  
Izv. Akad. Nauk SSSR Fiz. 35, 1651 (1971)

ELEM. SYM.	A	Z
Pd	105	46

METHOD

REF. NO.

71 Sh 6

egf

REACTION	RESULT	EXCITATION ENERGY	SOURCE		DETECTOR		ANGLE
			TYPE	RANGE	TYPE	RANGE	
G,G	LFT	1	D	1	NAI-D		UKN

 $6.9 \pm 1.0 \times 10^{-11} \text{ s}$ 1 = .319 MEV

Pd  
A=106

Pd  
A=106

Pd  
A=106



METHOD

REF. NO.

69 Da 1

egf

REACTION	RESULT	EXCITATION ENERGY	SOURCE		DETECTOR		ANGLE
			TYPE	RANGE	TYPE	RANGE	
G,G	ABY	1	D	1	NAI-D	0-1	120

$$d\sigma/d\Omega = 0.27 \pm 0.05 \text{ mb/sr.}$$

$$I = 5117 \text{ MEV}$$

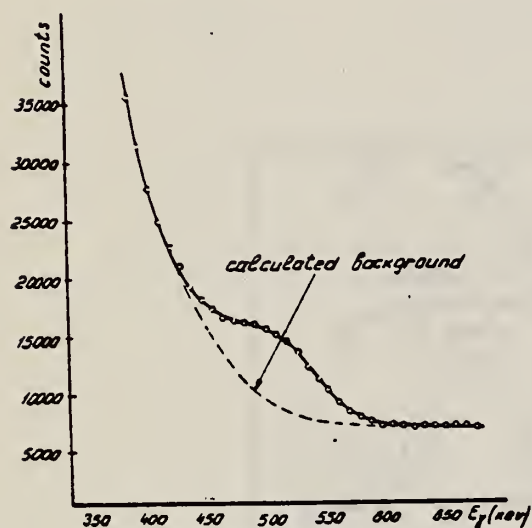


Fig. 1. Scintillation counter pulse spectrum of  $^{64}\text{Cu}$  annihilation radiation scattered at  $\theta = 120^\circ$  by palladium which includes the 511 keV  $\gamma$ -line corresponding to elastic processes (Rayleigh and resonant  $\gamma$ -ray scattering).



REF. K. Hosoyama, Y. Torizuka, Y. Kawazoe, H. Ui  
PICNS-72, 139 (1972) Sendai

ELEM. SYM.	A	Z
Pd	106	46

METHOD					REF. NO.	
					72 Ho 7	hvm
REACTION	RESULT	EXCITATION ENERGY	SOURCE		DETECTOR	
			TYPE	RANGE	TYPE	ANGLE
E, E/	FMP	0, 1	D	250	MAG-D	DST

$Q = .51; I = 1.13$  MEV

	$\frac{B(E2)}{B_{sp}(E2)}$	$\alpha_0$	$\alpha$	$Q_2(b)$	$\frac{B(E2)}{B_{sp}(E2)}$	$Q_2(b)$	
$^{114}\text{Cd}$	29	0.18	0.21	$-0.39 \pm 0.07$	34	$-0.38$	a)
					31.2	$-0.32 \pm 0.38$	b)
$^{106}\text{Pd}$	50	0.23	0.25	$-0.53 \pm 0.07$	48 $\pm 3$		c)
					42 $\pm 3$	$-0.458 \pm 0.059$	d)

- a) S.G. Steadman et al. NPA155 (1970) 1  
b) A.M. Kleinfield et al. NPA158 (1970) 81  
c) R.L. Robinson et al. NPA124 (1963) 553  
d) R. Beyer et al. P.R. 52 (1970) 1469

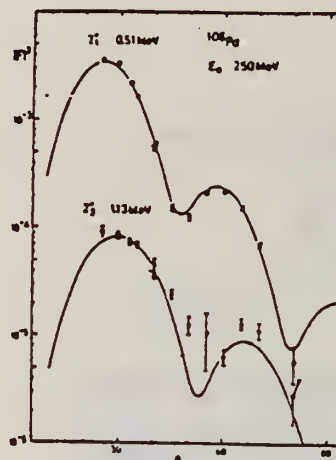


fig. 3

REF.

Y. Torizuka, Y. Kojima, T. Saito, K. Itoh, A. Nakada,  
S. Mitsunobu, M. Nagao, K. Hosoyama, S. Fukuda  
PICNS-72, p.171 Sendai

ELEM. SYM.

A

Z

Pd

106

46

METHOD

REF. NO.

72 To 6

hvm

REACTION	RESULT	EXCITATION ENERGY	SOURCE		DETECTOR		ANGLE
			TYPE	RANGE	TYPE	RANGE	
E,E/	SPC	0- 37	D	183	MAG-D		35

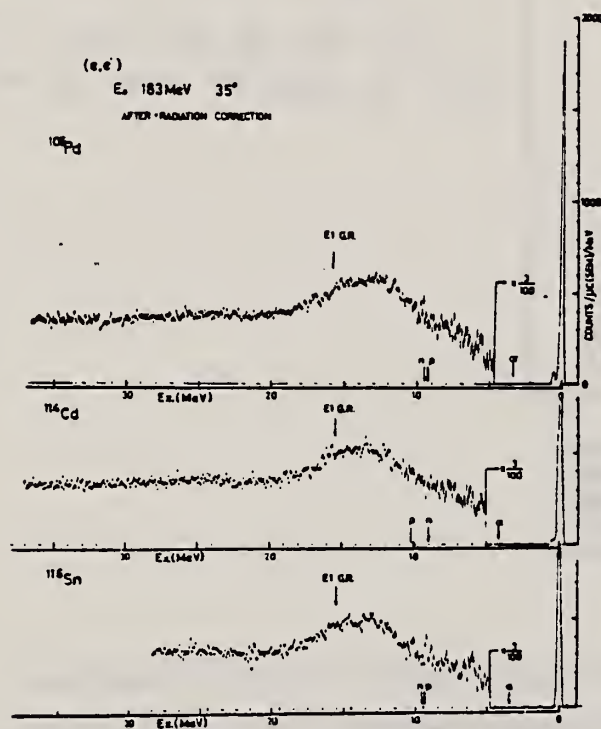


Fig. 6. Spectra of  $^{116}\text{Sn}$ ,  $^{114}\text{Cd}$  and  $^{106}\text{Pb}$  obtained at 183 MeV and 35°.

ELEM. SYM.	A	Z
Pd	106	46
REF. NO.		hmg
73 Ho 2		

REACTION	RESULT	EXCITATION ENERGY	SOURCE		DETECTOR		ANGLE
			TYPE	RANGE	TYPE	RANGE	
E, E/	FMF	0- 2	D	183,250	MAG-D		DST

LEVEL .51, 1.13 COMPLEX

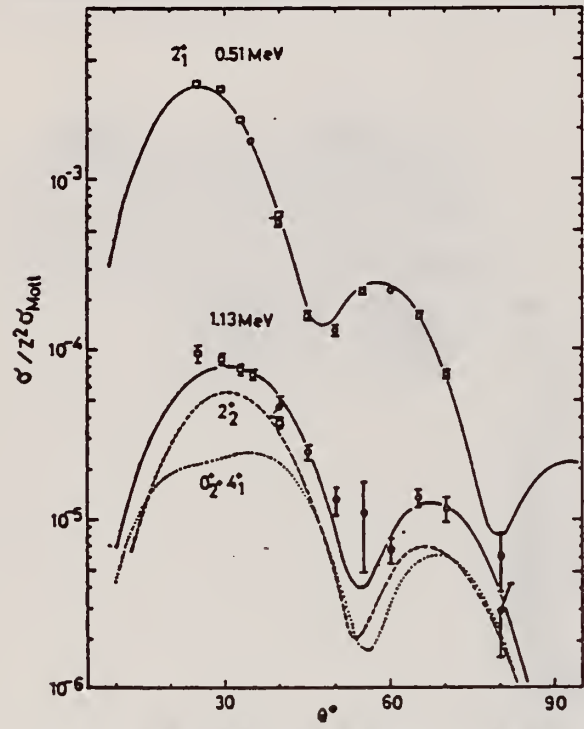


FIG. 1. Inelastic electron scattering form factors for the  $2_1^+$  and unresolved  $0_2^+$ ,  $2_2^+$ , and  $4_1^+$  levels in  $^{106}\text{Pd}$  at an incident energy of 250 MeV. The triplet form factors are compared with the sum of the  $0_2^+$  and  $4_1^+$  form factor (dotted line) and  $2_2^+$  form factor (dashed line).

TABLE II. Values of the radiative transition rates for the crossover and cascade transitions from the  $2_2^+$  state.

	$^{106}\text{Pd}$		$^{114}\text{Cd}$	
	Present	Experimental	Present	Experimental
$B(E2, 2_2^+ \rightarrow 2_1^+)$	$1.39^{+0.06}_{-0.14}$	$0.98 \pm 0.13^a$	$1.56^{+0.08}_{-0.13}$	$0.75 \pm 0.20^b$
$B(E2, 2_2^+ \rightarrow 0^+)$	$(0.92^{+0.32}_{-0.72}) \times 10^{-2}$	$(2.51^{+0.43}_{-0.33}) \times 10^{-2}^a$	$0.75^{+1.05}_{-0.33}$	$(1.6 \pm 0.3) \times 10^{-2}^b$

<sup>a</sup>Ref. 2.

<sup>b</sup>Ref. 6.

(over)

TABLE I. Values of  $c$ ,  $t$ ,  $\beta$ , and  $\alpha$  (the parameters of  $\rho_{tr}$ ),  $B(E2)$  in single-particle units, and the  $2_1^+$  state static quadrupole moment.

	$c$	$t$	$\beta$	$\alpha$	Present		Coulomb excitation	
					$\frac{B(E2)}{B_{sp}(E2)}$	$Q_2$ (b)	$\frac{B(E2)}{B_{sp}(E2)}$	$Q_2$ (b)
$^{106}\text{Pd}$	$0.97c_0^a$	$1.05t_0^b$	0.23	0.23	$50 \pm 5$	$-0.51 \pm 0.07$	$48 \pm 3^c$ $42 \pm 3^d$	$-0.458 \pm 0.059^d$
$^{114}\text{Cd}$	$0.95c_0^e$	$t = t_0^f$	0.18	0.19	$29 \pm 3$	$-0.36 \pm 0.07$	$31 \pm 2^g$ $34^h$	$-0.32 \pm 0.08^g$ $-0.38^h$
$^a c_0 = 5.14 \text{ fm.}$		$^c \text{Ref. 2.}$		$^e c_0 = 5.43 \text{ fm.}$		$^g \text{Ref. 3.}$		
$^b t_0 = 2.59 \text{ fm.}$		$^d \text{Ref. 5.}$		$^f t_0 = 2.50 \text{ fm.}$		$^h \text{Ref. 4.}$		

<sup>2</sup>R. L. Robinson et al., Nucl. Phys. A124, 553 (1969).

<sup>3</sup>S. G. Steadman et al., Nucl. Phys. A155, 1 (1970).

<sup>4</sup>A. M. Kleinfeld et al., Nucl. Phys. A158, 81 (1970).

<sup>5</sup>R. Beyer et al., Phys. Rev. C2, 1469 ('70).

<sup>6</sup>W. T. Milner et al., Nucl. Phys. A129, 687 ('69).





Pd

A=108

Pd

A=108

Pd

A=108



ELEM. SYM.	A	Z
Pd	108	46
REF. NO.		egf
69 De 2		

METHOD				REF. NO.		
				69 De 2		egf
REACTION	RESULT	EXCITATION ENERGY	SOURCE		DETECTOR	
			TYPE	RANGE	TYPE	RANGE
G,XN	ABX	9-25	C	9-25	BF3-I	4PI
G,P	ABX	9-25	C	9-25	ACT-I	4PI

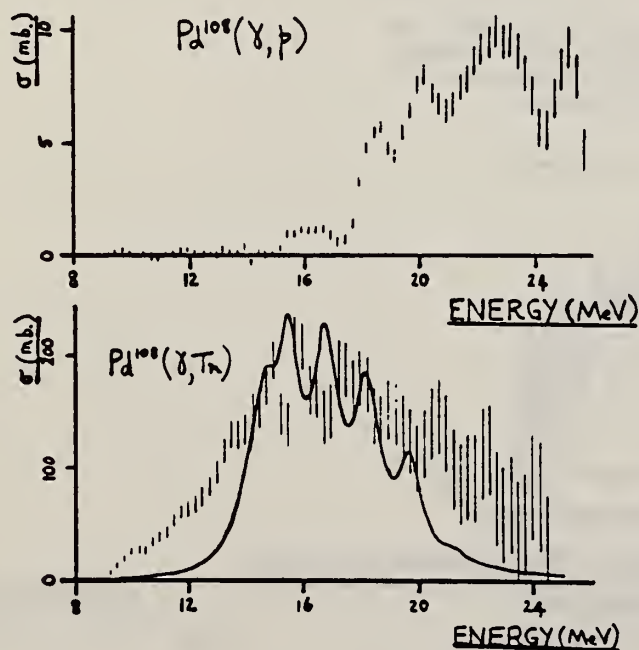
# VIBRATIONAL MODE SPLITTING OF THE $^{108}\text{Pd}$ GIANT DIPOLE RESONANCE

T. K. Deague, E. G. Muirhead and B. M. Spicer, School of Physics, University of Melbourne, Parkville, Victoria 3042, Australia

The  $^{108}\text{Pd}$  photoneutron production cross section, and the  $^{108}\text{Pd}(\gamma,p)^{107}\text{Rh}$  cross section have been measured by direct neutron detection, and by counting the 305 keV  $\gamma$ -ray in the residual  $^{107}\text{Rh}$ , respectively. Both cross sections were unfolded from yield curves by the method of Penfold and Leiss. Comparison was made to the neutron production cross section for the double weighting of the  $(\gamma,n)$  reaction. The two cross sections are shown in the figure.

The low energy spectrum of  $^{108}\text{Pd}$  is a good approximation to that of a spherical vibrator, the vibrations having comparatively large amplitude. Hence  $^{108}\text{Pd}$  is a good test for the dynamic collective model of the giant resonance (Huber, Danos, Weber and Greiner, Phys.Rev. 155 (1967) 1073), in which quadrupole surface vibrations are coupled to the giant dipole vibration. A fit to the predicted dipole spectrum, using Lorentz line shapes, is shown in the figure. Reasonable agreement is evident, although the theoretical peak at 16.75 MeV is not matched in the experiment. The additional strength at lower energies is attributed tentatively to single particle effects.

Fallieros, Goulard and Venter (Phys.Lett. 19 (1965) 398) have suggested that the giant dipole resonance should be split into two components with isospins  $T_0 (= N-Z/2)$  and  $T_0 + 1$ . In a sufficiently heavy nucleus, these components are represented by the  $(\gamma,n)$  and  $(\gamma,p)$  cross sections respectively. Accepting this break-up, the separation of the T-components in  $^{108}\text{Pd}$  is  $\sim 6$  MeV. The ratio of the strengths in the two components is 0.0235; this is to be compared with Macfarlane's estimate of this ratio (in "Isobaric Spin in Nuclear Physics", eds. J. D. Fox and D. Robson, Academic Press, 1966) of  $D/T_0$  where the dynamical factor,  $D$ , is less than unity.



METHOD

REF. NO.

69 De 5

egf

REACTION	RESULT	EXCITATION ENERGY	SOURCE		DETECTOR		ANGLE
			TYPE	RANGE	TYPE	RANGE	
G,XN	ABX	8-25	C	8-25	BF3-I		4PI
G,P	ABX	15-28	C	8-28	ACT-I		4PI

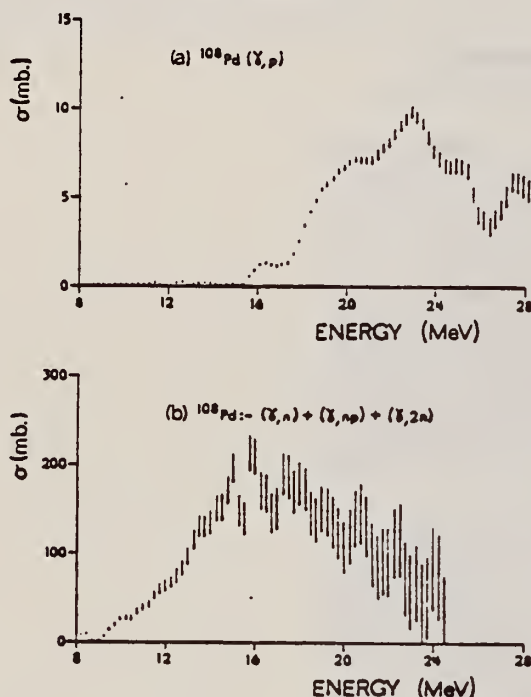


Fig. 2 (a) The  $(\gamma, p)$  cross section in  $^{108}\text{Pd}$ , obtained using an analysis bin width of 1.5 MeV. (b) The  $(\gamma, n) + (\gamma, np) + (\gamma, 2n)$  cross section in  $^{108}\text{Pd}$ , obtained using an analysis bin width of 0.5 MeV.

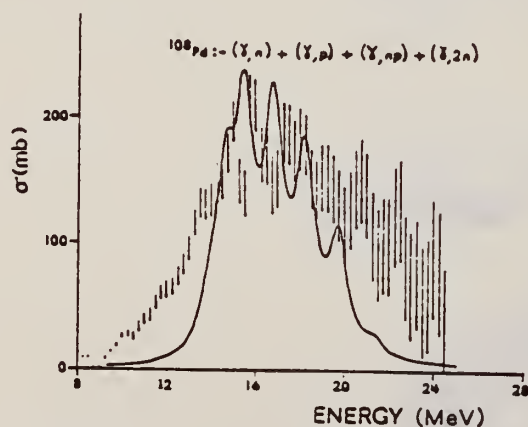


Fig. 3. The  $(\gamma, n) + (\gamma, p) + (\gamma, np) + (\gamma, 2n)$  cross section in  $^{108}\text{Pd}$ , obtained using an analysis bin width of 0.5 MeV, compared with a fit of Lorentz line shapes with widths 1.0 MeV, to the  $^{108}\text{Pd}$  dipole spectrum predicted by Huber <sup>6</sup>.

<sup>6</sup>M. G. Huber, private communication (1967)

[over]

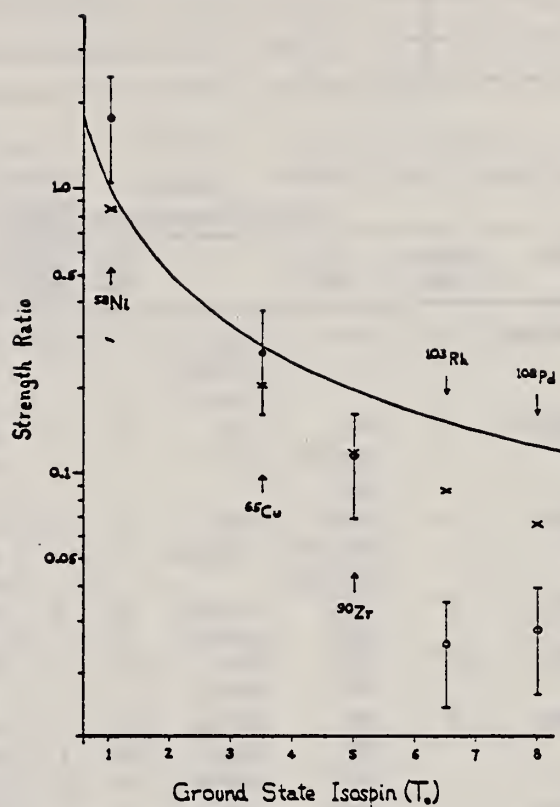


Fig. 7. The ratio, for five nuclei, of the "bremsstrahlung weighted" cross sections for proton and neutron production, respectively (circles with error bars), as a function of the ground state isospin,  $T_0$ . Crosses represent theoretical estimates of the relative strengths of the  $T_0 + 1$  and  $T_0$  giant dipole resonances. The continuous curve gives the "geometric factor",  $1/T_0$ .



H. Bartsch, K. Huber, U. Kneissl, H. Krieger  
Nucl. Phys. A256, 243 (1976)

Pd

108

46

## METHOD

REF. NO.

76 Ba 1

egf

REACTION	RESULT	EXCITATION ENERGY	SOURCE		DETECTOR		ANGLE
			TYPE	RANGE	TYPE	RANGE	
G, N	RLY	THR-UKN	C	UKN	SCD-D		4PI

ISOMER RATIO

TABLE 1  
Experimental and theoretical results

Process	Target- spin	$E_\gamma$ (keV)	$T_{1/2}$	Spin high	Spin low	$R_{exp} = \frac{\sigma_{high}}{\sigma_{low}}$	SCOP (%)
$^{181}\text{Ta}(\gamma, 3n)$	$\frac{1}{2}^+$	93	2.2 h 9.31 min 8.15 h	$7^-$	$1^+$	$0.51 \pm 0.09$	$3.6 \pm 0.2$
$^{142}\text{Nd}(\gamma, n)$	$0^+$	755 1100-1300, 145	63 s 2.5 h	$\frac{1}{2}^-$	$\frac{1}{2}^+$	$0.055 \pm 0.006$ $0.19 \pm 0.01^a)$	$2.20 \pm 0.06$
$^{92}\text{Mo}(\gamma, n)$	$0^+$	652.9 1208, 1508, 1581, 1637	66 s 15.49 min	$\frac{1}{2}^+$	$\frac{1}{2}^-$	$1.03 \pm 0.21$ $0.85 \pm 0.07^b)$ $1.92 \pm 0.15^a)$	$5.03 \pm 0.75$ $4 \pm 1$
$^{100}\text{Mo}(\gamma, n)$	$0^+$	97.3 140.5	16.8 $\mu\text{s}$ 66.02 h	$\frac{1}{2}^+$	$\frac{1}{2}^+$	$0.85 \pm 0.24$	$1.72 \pm 0.25$
$^{108}\text{Pd}(\gamma, n)$	$0^+$	214.5 115	22 s 850 ns	$\frac{1}{2}^-$	$\frac{1}{2}^+$	$0.5 \pm 0.2$	$3.4 \pm 0.5$
$^{110}\text{Pd}(\gamma, n)$	$0^+$	188 113 87.7	4.7 min 390 ns 13.47 h	$\frac{1}{2}^-$ $\frac{1}{2}^-$ $\frac{1}{2}^+$	$\frac{1}{2}^+$ $\frac{1}{2}^+$ $\frac{1}{2}^+$	$0.11 \pm 0.02$ $0.41 \pm 0.09$ $3.2 \pm 0.7$	$3.14 \pm 0.15$ $3.0 \pm 0.25$ $3.3 \pm 0.4$
$^{89}\text{Y}(\gamma, n)$	$\frac{1}{2}^-$	231.7 442.3 392.5	14.2 ms 300 $\mu\text{s}$	$8^+$	$1^+$	$0.056 \pm 0.008$	

<sup>a)</sup> Ref. <sup>14)</sup>. <sup>b)</sup> Ref. <sup>15)</sup>.

<sup>14)</sup> P.E. Haustein et al, J. Inorg. Nucl. Chem. 33, 289 (1971)

<sup>15)</sup> J.H. Carver et al., Nucl. Phys. 37, 449 (1962)

REF. R.G. Arthur, R.P. Singhal, S.W. Brain, W.A. Gillespie, A. Johnston, E.W. Lees and M.W.S. Macauley J. Phys. G4, 961 (1978)

ELEM. SYM.	A	Z
Pd	108	46
REF. NO.		rs
78 Ar 4		

METHOD

REACTION	RESULT	EXCITATION ENERGY	SOURCE		DETECTOR		ANGLE
			TYPE	RANGE	TYPE	RANGE	
E, E/	FMF	0-2	D	21-121	MAG-D		140

**Abstract.** The elastic electron-scattering form factor, and inelastic form factors for the  $2_1^+$  (0.434 MeV),  $2_2^+$  (0.931 MeV) and  $3^-$  (2.046 MeV) states in  $^{108}\text{Pd}$  were measured. The ground-state charge distribution parameters were obtained from a phase-shift analysis of the elastic form factor. Analysis of the  $2_1^+$  and  $2_2^+$  form factors in the anharmonic vibrator model yields the reduced transition probabilities and the  $2_1^+$  quadrupole moment ( $Q_{21}$ ) which is in excellent agreement with recent Coulomb reorientation measurements. The  $3^-$  form factor is well described by the assumption that this state is a pure octupole vibration.

**Comment:** Elastic & inelastic scattering data given in two tables.

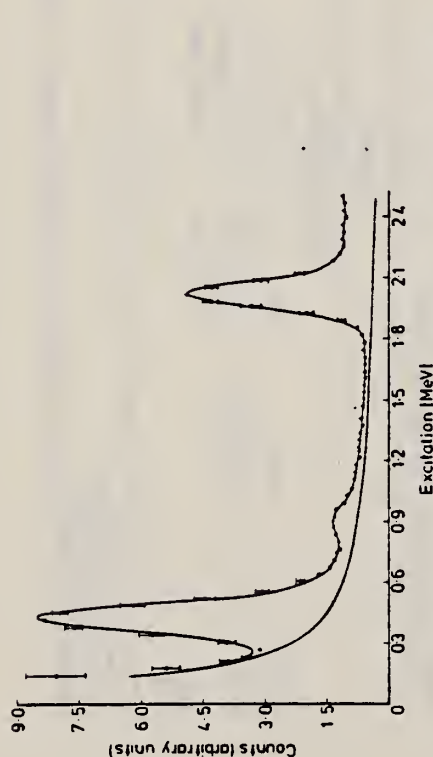


Figure 1.  $^{108}\text{Pd}$  inelastic spectrum at a momentum transfer value of  $0.75 \text{ fm}^{-1}$ . The full curve through the data points is the result of the line-shape analysis, and the underlying curve is the elastic radiation tail.

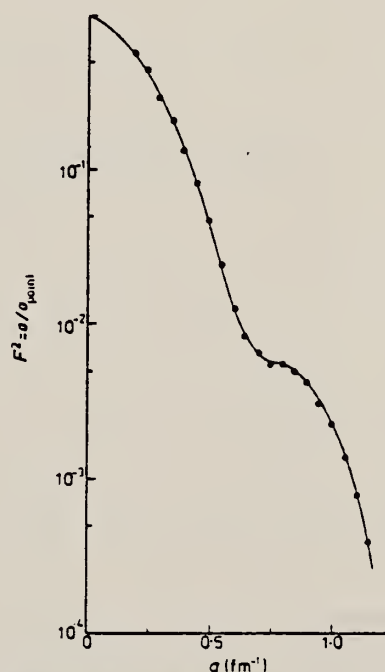


Figure 3.  $^{106}\text{Pd}$  elastic form factor. The full curve is the phase-shift best fit. The error bars are smaller than the data points.

(over)

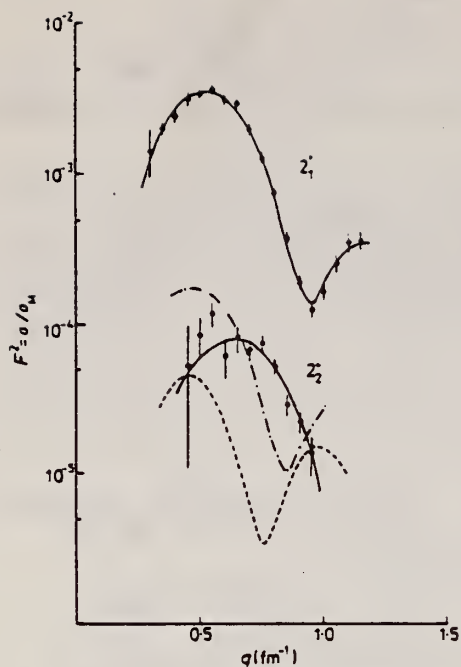


Figure 4.  $2_1^+$  and  $2_2^+$  form factors—anharmonic model fits. The fits to the  $2_2^+$  are respectively  $\cos \phi = -1$  (—),  $\cos \phi = +1$  (---) and pure harmonic two-phonon (----).

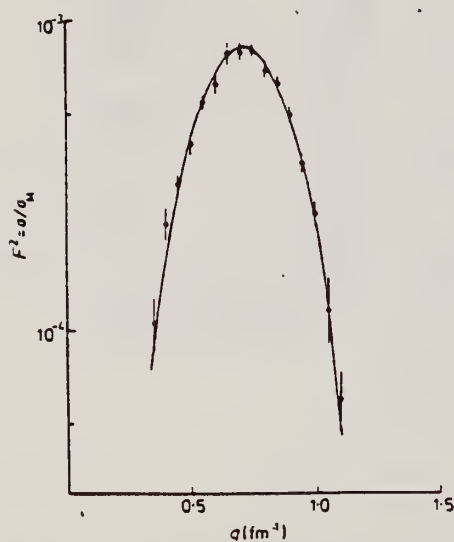


Figure 5.  $3_1^-$  form factor. The full curve is the best fit assuming the level to be a single octupole phonon vibration.

Table 4. Quadrupole moment and  $B(EL, 1)$  values.

$E_x$ (MeV)	$J^\pi$	$Q_2$ (e b)			$B(EL, 1)$ ( $e^2 \text{fm}^2$ )	
		(e, e')	Coulomb excitation		(e, e')	Coulomb excitation
			(i)	(ii)		
0.434	$2_1^+$	$-0.58 \pm 0.04$	$-0.58 \pm 0.13^a$	$-0.37 \pm 0.12^a$	$8049 \pm 290$	$7600 \pm 500^c$
0.931	$2_2^+$	$-0.51 \pm 0.06^c$	$-0.51 \pm 0.06^c$	$-0.30 \pm 0.06^c$	$58.2 \pm 9.6$	$7000 \pm 700^b$
2.046	$3_1^-$				$(11.3 \pm 1.5) \times 10^4$	$170 \pm 15^c$
						$(9.3 \pm 2.6) \times 10^4^d$

(i) Constructive interference.

(ii) Destructive interference.

<sup>a</sup> Robinson *et al* (1969), <sup>b</sup> Harper *et al* (1971), <sup>c</sup> Lutz *et al* (1972), <sup>d</sup> Hasselgren *et al* (1976).

Pd  
A=110

Pd  
A=110

Pd  
A=110





METHOD

REF. NO.

69 De 5

egf

REACTION	RESULT	EXCITATION ENERGY	SOURCE		DETECTOR		ANGLE
			TYPE	RANGE	TYPE	RANGE	
G,N	ABX	8-28	C	8-28	ACT-I		4PI

ISOMER YIELD ONLY

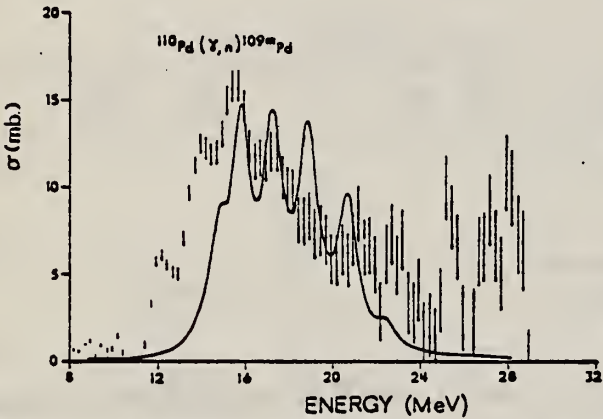


Fig. 4. The  $^{110}\text{Pd}(\gamma, n)^{109\text{m}}\text{Pd}$  cross section, obtained using an analysis bin width of 1.0 MeV, compared with a fit of Lorentz line shapes with widths 1.0 MeV, to the  $^{110}\text{Pd}$  dipole spectrum predicted by Huber <sup>6</sup>).

<sup>6</sup>M. G. Huber, private communication (1967).

REF.

S. Penner, J.W. Lightbody, Jr., S.P. Fivozinsky, H. Grannell,  
P.L. Hallowell, and M. Finn  
PICNS-72, 49 (1972) Sendai

ELEM. SYM.	A	Z
Pd	110	46

METHOD

REF. NO.

72 Pe 2

hvm

REACTION	RESULT	EXCITATION ENERGY	SOURCE		DETECTOR		ANGLE
			TYPE	RANGE	TYPE	RANGE	
E,E/	FMF	0, 0	D	40-110	MAG-D		128

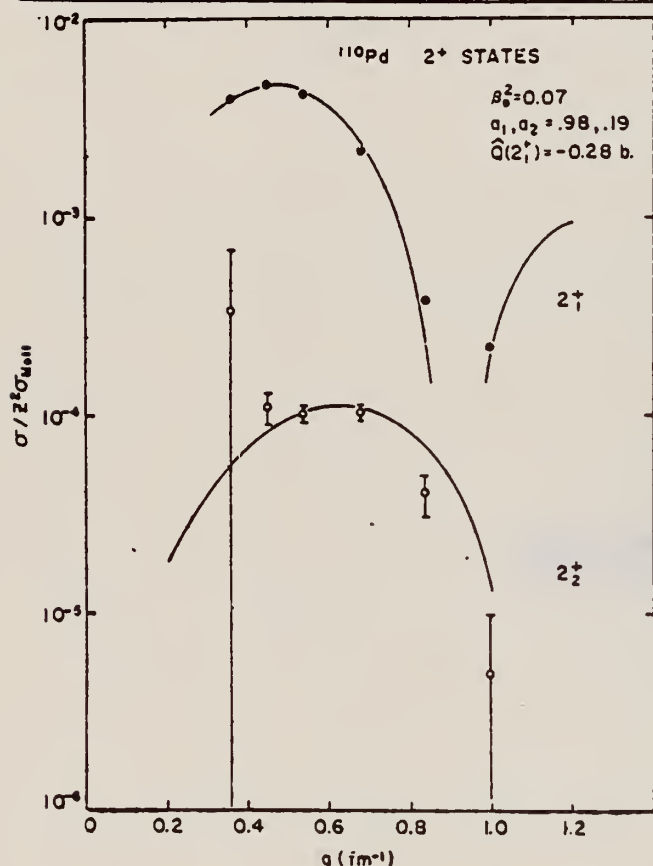


Fig. 2. Form factors for excitation of the first and second  $2^+$  states in  $^{110}\text{Pd}$ . The smooth curves are the best fits of the anharmonic vibrator model.

$Q = .374, Q = .81 \text{ MEV}$

Table 2. First Excited State Static Quadrupole Moments

Nucleus	Q, barns	
	electron scattering	reorientation effect
$^{48}\text{Ti}$	$-.177 \pm .008^b$	$-.22 \pm .08^c$ $-.135 \pm .082^d$ $-.38 \pm .13^e$
$^{52}\text{Cr}$	$-.082 \pm .016^a$	$-.07 \pm .13^f$
$^{60}\text{Ni}$	$-.104 \pm .018^b$	$0 \pm .13^g$
$^{64}\text{Zn}$	$-.135 \pm .016^b$	-
$^{70}\text{Zn}$	$-.21 \pm .03^b$	-
$^{110}\text{Pd}$	$-.28 \pm .03^a$	$(-.27 \text{ OR } -.48) \pm .05^h$ $(-.45 \text{ OR } -.72) \pm .12^i$
$^{114}\text{Cd}$	$-.29 \pm .03^a$	$-.32 \pm .08^j$
$^{118}\text{Sn}$	$-.14 \pm .03^a$	$+.09 \pm .13^k$

a) New preliminary values

b) From Ref. (1)

c) O. Hausser, et al., Nucl. Phys. A150, 417 (1970)

d) P.M.S. Lesser, et al., University of Rochester Annual Report, 1970 (unpublished)

e) N.V. deCastro-Faria, et al., Nucl. Phys. A174, 37 (1971)

f) D. Cline, University of Rochester Report UR-NSRL-40, 1971 (unpublished)

g) D. Cline, et al., Nucl. Phys. A133, 445 (1969)

h) R. Beyer, et al., Phys. Rev. C2, 1469 (1970)

i) R.P. Harper, et al., Nucl. Phys. A162, 161 (1971)

j) Z. Berant, et al., Phys. Rev. Letters 27, 110 (1971)

k) A.M. Kleinfeld, et al., Nucl. Phys. A154, 499 (1970)

REF.

H. Bartsch, K. Huber, U. Kneissl, H. Krieger  
Nucl. Phys. A256, 243 (1976)

ELEM. SYM.

A

Z

Pd

110

46

METHOD

REF. NO.

76 Ba 1

egf

REACTION	RESULT	EXCITATION ENERGY	SOURCE		DETECTOR		ANGLE
			TYPE	RANGE	TYPE	RANGE	
G, N	RLY	THR-UKN	C	UKN	SCD-D		4PI

ISOMER RATIOTABLE 1  
Experimental and theoretical results

Process	Target-spin	$E_\gamma$ (keV)	$T_{1/2}$	Spin high	Spin low	$R_{exp} = \frac{\sigma_{high}}{\sigma_{low}}$	SCOP ( $\bar{h}$ )
$^{181}\text{Ta}(\gamma, 3n)$	$\frac{1}{2}^+$	93	2.2 h 9.31 min 8.15 h	7 <sup>-</sup>	1 <sup>+</sup>	0.51 $\pm$ 0.09	3.6 $\pm$ 0.2
$^{142}\text{Nd}(\gamma, n)$	0 <sup>+</sup>	755 1100-1300, 145	63 s 2.5 h	$\frac{1}{2}^-$	$\frac{1}{2}^+$	0.055 $\pm$ 0.006 0.19 $\pm$ 0.01 <sup>a)</sup>	2.20 $\pm$ 0.06
$^{92}\text{Mo}(\gamma, n)$	0 <sup>+</sup>	652.9 1208, 1508, 1581, 1637	66 s 15.49 min	$\frac{1}{2}^+$	$\frac{1}{2}^-$	1.03 $\pm$ 0.21 0.85 $\pm$ 0.07 <sup>b)</sup> 1.92 $\pm$ 0.15 <sup>a)</sup>	5.03 $\pm$ 0.75 4 $\pm$ $\frac{1}{2}$
$^{100}\text{Mo}(\gamma, n)$	0 <sup>+</sup>	97.3 140.5	16.8 $\mu$ s 66.02 h	$\frac{1}{2}^+$	$\frac{1}{2}^+$	0.85 $\pm$ 0.24	1.72 $\pm$ 0.25
$^{108}\text{Pd}(\gamma, n)$	0 <sup>+</sup>	214.5 115	22 s 850 ns	$\frac{1}{2}^-$	$\frac{1}{2}^+$	0.5 $\pm$ 0.2	3.4 $\pm$ 0.5
$^{110}\text{Pd}(\gamma, n)$	0 <sup>+</sup>	188 113 87.7	4.7 min 390 ns 13.47 h	$\frac{1}{2}^-$ $\frac{1}{2}^-$ $\frac{1}{2}^+$	$\frac{1}{2}^+$ $\frac{1}{2}^+$ $\frac{1}{2}^+$	0.11 $\pm$ 0.02 0.41 $\pm$ 0.09 3.2 $\pm$ 0.7	3.14 $\pm$ 0.15 3.0 $\pm$ 0.25 3.3 $\pm$ 0.4
$^{89}\text{Y}(\gamma, n)$	$\frac{1}{2}^-$	231.7 442.3 392.5	14.2 ms 300 $\mu$ s	8 <sup>+</sup>	1 <sup>+</sup>	0.056 $\pm$ 0.008	

<sup>a)</sup> Ref. <sup>14)</sup>. <sup>b)</sup> Ref. <sup>15)</sup>.<sup>14</sup> P.E. Haustein et al., J. Inorg. Nucl. Chem. 33, 289 (1971)  
<sup>15</sup> J. H. Carver et al., Nucl. Phys. 37, 449 (1962)

REF.

J.W. Lightbody, Jr., S. Penner, S.P. Fivozinsky,  
P.W. Hallowell and Hall Crannell  
Phys. Rev. C14, 952 (1976)

ELEM. SYM.

A

Z

Pd

110

46

METHOD

REF. NO.

76 Li 5

hmg

REACTION	RESULT	EXCITATION ENERGY	SOURCE		DETECTOR		ANGLE
			TYPE	RANGE	TYPE	RANGE	
E, E/	FMF	0, 1	D	39-111	MAG-D		127
		(.374, .81)					

TABLE VI. Anharmonic vibrator model parameters.

LEVEL .374, .81

	$^{110}\text{Pd}$	$^{114}\text{Cd}$	$^{116}\text{Sn}$
$c_{11}$ (fm)	$5.169 \pm 0.022$	$5.214 \pm 0.021$	$5.446 \pm 0.048$
$x_{11}$ (fm)	$0.529 \pm 0.039$	$0.593 \pm 0.040$	$0.550 \pm 0.047$
$\beta_0$	$0.277 \pm 0.012$	$0.218 \pm 0.009$	$0.124 \pm 0.004$
$a$	$0.2011 \pm 0.0044$	$0.1749 \pm 0.0060$	$0.14 \pm 0.02^a$
$B(E2_1^+)$ ( $e^2\text{fm}^4$ )	$7966 \pm 682$	$5753 \pm 475$	$2288 \pm 148$
$\chi^2(Z_1^+)/ (N-P)$	1.3	1.5	1.2
$N-P$	3	3	4
$B(E2_2^+)$ ( $e^2\text{fm}^4$ )	$72.9 \pm 8.0$	$50.2 \pm 7.6$	$19.8^{+1.0}_{-1.1}$
$\chi^2(Z_2^+)/ (N-P)$	3.0	3.0	1.0
$N-P$	5	5	6

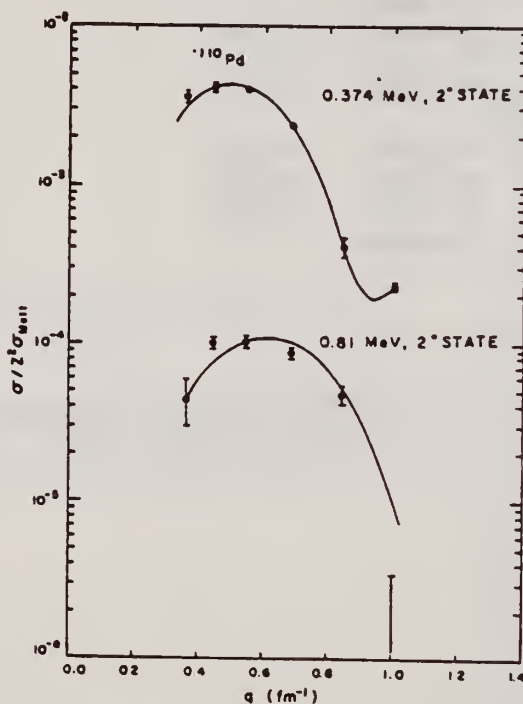
<sup>a</sup> Fit estimated by eye.

FIG. 5. Cross sections for  $^{110}\text{Pd}$  in units of  $Z^2 \sigma_{\text{Mott}}$  for the 0.374 and 0.81 MeV,  $\sigma_{\text{Mott}}$   $2^+$  states. The solid curves are fits based on the anharmonic vibrator model.

(over)



TABLE III. Ratios of inelastic scattering cross sections to  $Z^2\sigma_{\text{Mott}}$ .

<sup>52</sup> Cr				
E <sub>i</sub> (MeV)	θ (deg)	1.43 MeV, 2 <sup>+</sup> state		3.16 MeV, 2 <sup>+</sup> state
39.38	127.74	(0.90 ± 0.04)·03		(0.55 ± 0.55)·05
49.44	127.74	(0.159± 0.006)·02		(0.29 ± 0.07)·04
59.84	127.71	(0.26 ± 0.02)·02		(0.89 ± 0.30)·04
75.22	127.71	(0.265± 0.007)·02		(0.842± 0.012)·04
92.73	127.74	(0.222± 0.005)·02		(0.428± 0.052)·04
110.20	127.69	(0.97 ± 0.02)·03		(0.222± 0.044)·04
<sup>110</sup> Pd				
E <sub>i</sub> (MeV)	θ (deg)	0.374 MeV, 2 <sub>1</sub> <sup>+</sup> state		0.81 MeV, 2 <sub>1</sub> <sup>+</sup> state
39.38	127.74	(0.35 ± 0.03)·02		(0.45± 0.14)·04
49.44	127.74	(0.40 ± 0.02)·02		(0.10± 0.01)·03
59.84	127.71	(0.40 ± 0.02)·02		(0.10± 0.01)·03
75.22	127.71	(0.233± 0.003)·02		(0.86± 0.07)·04
92.73	127.74	(0.40 ± 0.05)·03		(0.48± 0.06)·04
110.20	127.69	(0.23± 0.01)·03		(0.17± 0.17)·05
<sup>114</sup> Cd				
E <sub>i</sub> (MeV)	θ (deg)	0.558 MeV, 2 <sub>1</sub> <sup>+</sup> state		1.208 MeV, 2 <sub>1</sub> <sup>+</sup> state
39.38	127.74	(0.20 ± 0.02)·02		(0.46± 0.07)·04
49.44	127.74	(0.28 ± 0.02)·02		(0.40± 0.06)·04
59.84	127.71	(0.220± 0.014)·02		(0.58± 0.11)·04
75.22	127.71	(0.118± 0.005)·02		(0.34± 0.04)·04
92.73	127.74	(0.204± 0.007)·03		(0.11± 0.04)·04
110.20	127.69	(0.155± 0.007)·03		(0.61± 0.35)·05
<sup>116</sup> Sn				
E <sub>i</sub> (MeV)	θ (deg)	1.294 MeV, 2 <sub>1</sub> <sup>+</sup> state	2.112 MeV, 2 <sub>1</sub> <sup>+</sup> state	2.266 MeV, 3 <sup>-</sup> state
39.38	127.74	(0.65± 0.04)·03	(0.68 ± 1.05)·05	(0.18 ± 0.02)·03
49.44	127.74	(0.88 ± 0.04)·03	(0.26 ± 0.69)·05	(0.40 ± 0.01)·03
59.84	127.71	(0.84 ± 0.03)·03	(0.21 ± 0.06)·04	(0.63 ± 0.02)·03
75.22	127.71	(0.36± 0.02)·03	(0.5 ± 7.4)·06	(0.84 ± 0.02)·03
75.02	127.81	(0.34 ± 0.02)·03	(0.47 ± 0.39)·05	(0.82 ± 0.01)·03
92.73	127.74	(0.50 ± 0.09)·04	(0 ± 0.19)·04	(0.60 ± 0.01)·03
110.20	127.69	(0.85 ± 0.10)·04	(0 ± 0.8)·05	(0.14 ± 0.01)·03









## DEFINITIONS OF ABBREVIATIONS AND SYMBOLS

Note: In this list definitions are given for various photoneutron reactions in which the following symbols are used: N, NL, nN, SN and XN. Corresponding definitions apply for reactions involving other nuclear particles where the symbols N (neutron) is replaced by, e.g. P, D, T, HE, A etc. Where unknown reactions result in the production of a specific radionuclide, the chemical symbol and mass number is listed as the reaction product, e.g. a G,NA22 reaction in <sup>59</sup>Co.

A	alpha particle		response function. Contrast with D = discrete.
ANAL	analysis		
ABI	absolute integrated cross-section data	CCH	cloud chamber
ABX	absolute cross-section data	CF	compared with
ABY	absolute yield data. Often means cross-section per equivalent quantum is listed.	CHRGD	charged
ACT	measurement of induced radio-activity of the target	CMPT	Compton
ASM	asymmetric, asymmetry	COIN COINC	coincidence, coincide
AVG	average	COH	coherent
BBL	bubble chamber	CK	Cerenkov
BEL B(EL)	reduced electric radiative transition probability	D	deuteron or discrete. When discrete, it is used to describe a photon source or a detector response function. Contrast with C = continuous.
BF3	BF <sub>3</sub> neutron counter with moderator e.g., Halpern detector, long counter	DLTE	energy loss
BML	reduced magnetic radiative transition probability, B(ML)	DLTQ	momentum transfer
BREAKS	levels located by "breaks" in the yield curve	DST	distribution
BRKUP	breakup	DT BAL	detailed balance
BRMS	bremsstrahlung	E	electron
BTW	between	E/	inelastically scattered electron
C	continuous. Used to describe a photon source or a detector	E+	positron
		EDST	energy distribution or spectrum
		E/N	used only to indicate a coincidence experiment as in (E,E/N).

N stands for any outgoing particle measured in coincidence with an inelastically scattered electron. Distinguish from eg., (E,N) which is used to represent an electron induced reaction when only the outgoing particle N is detected.

EMU emulsions (photographic plates)

EXCIT excited

F fission

FMF form factor

FM-1 inverse femtometers

FRAG fragment

G photon

G/ inelastically scattered photon

G-WIDTH gamma-ray transition width

HAD hadrons, hadron production

HE <sup>3</sup>He particle  
He3

INT interaction, integral, intensity

INC includes

ION ionization chamber

ISOB isobaric

ISM isomer

J multiplicity of particle defined by following symbol e.g. (G,PJN) with remark J = 2,3,5,7

JPI spin and parity of a nuclear state  
J-PI

K second multiplicity index, e.g. (G,JPKN) with both J & K positive integers greater than 1

KE kinetic energy

L may be an integer or zero that always follows a reaction product symbol. This is used to indicate transitions to specific states in the residual nuclide. When the letter is used as in (G,NL) the cross section given is that for the sum of transitions to two or more specific final states.

LFT excited state lifetime

LIM limit

LV,LVS level, levels

LQD liquid

MAG magnetic spectrometer

MEAS measurement(s)

MGC magnetic Compton spectrometer

MGP magnetic pair spectrometer

MOD moderated neutron detector not employing a BF<sub>3</sub> counter, e.g. rhodium foil, Szilard-Chalmers reaction, <sup>3</sup>He, <sup>6</sup>Li reactions, GD loaded liquid scintillator, etc.

MSP mass spectrometer

MULT multiple, multipole, multiplicity

MU-T used only in combination with G to indicate a total photon absorption cross section measurement, i.e. (G,MU-T)

N neutron (see also XN and SN). The notation (G,N) is used to indicate a reaction in which only a single neutron is emitted, i.e. the reaction that can, in many cases, be measured by observing the radioactive decay of the residual nuclide.



nN	where n is any integer. (G,nN) indicates the sum over all reaction cross sections in which n neutrons are emitted.	SN	sum of neutron producing reactions, $\sigma(\gamma,SN)=\sigma(\gamma,N) + \sigma(\gamma,NP) + \sigma(\gamma,2N) + \sigma(\gamma,3N) + \text{etc.}$
NAI	NaI(Tl) spectrometer	SPC	photon or particle energy spectrum
NEUT	neutron(s)	SPK	spark chamber
NOX	no cross-section data	SPL	spallation
P	proton (see also XP)	STAT	statistical
PART	particle(s)	SYM	symetric, symmetry
PHOT	photon(s)	T	triton
PI	pion, usually written as PI+, PI-, PIO to indicate charge	TEL	counter telescope
POL	polarized or polarization	THR	threshold for reaction or threshold detector, e.g., $^{29}\text{Si}(n,p)^{29}\text{Al}$ .
Q-SQUAR	momentum transfer squared ( $q^2$ )	TOF	time-of-flight detector
RCL	recoil	TRK	tracks of particles or fragments observed in solid materials (glass, mylar, etc.)
REL	relative	TRNS	transition
RLI	relative integrated cross-section data	UKN UNK	unknown
RLX	relative cross-section data	VIB	vibrational
RSP	reaction spectrometer	VIR PHOT	virtual photon(s)
RLY	relative yield data	XN	all neutrons, total neutron yield, $\sigma(\gamma,XN) = \sigma(\gamma,N) + 2\sigma(\gamma,2N) + 3\sigma(\gamma,3N) + \sigma(\gamma,NP) + \text{etc.}$
SCTD	scattered	XP	all protons, total proton yield $\sigma(\gamma,XP) = \sigma(\gamma,P) + \sigma(\gamma,NP) + 2\sigma(\gamma,2P) + \text{etc.}$
SCD	semiconductor (solid state) detector	XX XXX	reaction products defined in REMARKS
SCI	scintillator detector other than NaI, e.g., CsI, KI, organic (liquid or solid), stilbene, He	YLD	yield
SEP	separation		
SEP ISOTP	separated isotope used		
SIG	SIGMA (cross section)		

4PI	a $4\pi$ geometry was used or a method like radioactivity or a total absorption measurement		products was determined. The polarized particle is indicated in REMARKS.
999	energy defined in REMARKS	* or @	symbols used to indicate that the units associated with the numerals on one or both sides of the symbol in a specific column are not MeV. The units are defined in REMARKS.
\$	indicates the measurement involved beams or targets that were either polarized or aligned, or that the polarization of the reaction		

U.S. DEPT. OF COMM. <b>BIBLIOGRAPHIC DATA SHEET</b> (See instructions)		1. PUBLICATION OR REPORT NO.	2. Performing Organ. Report No.	3. Publication Date
4. TITLE AND SUBTITLE  Photonuclear Data-Abstract Sheets 1955-1982				
5. AUTHOR(S)  E.G. Fuller and Henry Gerstenberg				
6. PERFORMING ORGANIZATION (If joint or other than NBS, see instructions)  NATIONAL BUREAU OF STANDARDS DEPARTMENT OF COMMERCE WASHINGTON, D.C. 20234			7. Contract/Grant No.	
			8. Type of Report & Period Covered	
9. SPONSORING ORGANIZATION NAME AND COMPLETE ADDRESS (Street, City, State, ZIP)				
10. SUPPLEMENTARY NOTES  <input type="checkbox"/> Document describes a computer program; SF-185, FIPS Software Summary, is attached.				
11. ABSTRACT (A 200-word or less factual summary of most significant information. If document includes a significant bibliography or literature survey, mention it here)  These abstract sheets cover most classes of experimental photonuclear data leading to information of the electromagnetic matrix element between the ground and excited states of a given nucleus. This fifteen volume work contains nearly 7200 abstract sheets and covers 89 chemical elements from hydrogen through americium. It represents a twenty-seven year history of the study of electromagnetic interactions. The sheets are ordered by target element, target isotope, and by an assigned bibliographic reference code. Information is given on the type of measurement, excitation energies studied, source type and energies, detector type, and angular ranges covered in the measurement. For a given reference, the relevant figures and tables are mounted on a separate sheet for each nuclide studied.				
12. KEY WORDS (Six to twelve entries; alphabetical order; capitalize only proper names; and separate key words by semicolons) data-abstract sheets, elements, experimental, isotopes, nuclear physics, photonuclear reactions				
13. AVAILABILITY  <input type="checkbox"/> Unlimited <input checked="" type="checkbox"/> For Official Distribution, Do Not Release to NTIS <input type="checkbox"/> Order From Superintendent of Documents, U.S. Government Printing Office, Washington, D.C. 20402.  <input type="checkbox"/> Order From National Technical Information Service (NTIS), Springfield, VA. 22161			14. NO. OF PRINTED PAGES	
			15. Price	







